NASA TECHNICAL TRANSLATION

NASA TT F-315

NASA TT F-315

N65-23843
(ACCESSION NUMBER)
285
(PAGES)
(CODE)
(NASA CR OR TMX OR AD NUMBER)
1
(CATEGORY)

THE UPPER LAYERS OF THE ATMOSPHERE

by I. A. Khvostikov

Gidrometeorologicheskoye Izdatel'stvo,
Leningrad, 1964

GPO PRICE $ _____
CFSTI PRICE(S) $ 8.55
Hard copy (HC) 5
Microfiche (MF) 8 2.00

NATIONAL AERONAUTICS AND SPACE ADMINISTRATION • WASHINGTON, D. C. • MAY 1965

NASA TT F-315

THE UPPER LAYERS OF THE ATMOSPHERE

I. A. Khvostikov

Translation of "Vysokiye sloi atmosfery."
Gidrometeorologicheskoye Izdatel'stvo, Leningrad, 1964.

NATIONAL AERONAUTICS AND SPACE ADMINISTRATION

For sale by the Clearinghouse for Federal Scientific and Technical Information
Springfield, Virginia 22151 – Price $8.85

UDC 551.510.536

ANNOTATION

23843

This book contains an exposition of contemporary scientific knowledge of the upper layers of the atmosphere. Methods of measurement with the aid of rockets and artificial Earth satellites are examined, as well as meteoric acoustical and radio measurement methods, searchlight probes of the atmosphere and observations of optical phenomena of the day, twilight and night sky. Results are cited of studies of the structure and composition of the stratosphere and still higher layers, as well as the results of investigations of winds, tidal phenomena, vertical and turbulent movements and circulation of the upper layers of the atmosphere based on observations of ozone, atomic oxygen and water vapor. The theoretical treatment of some phenomena and some atmospheric processes (thermal conditions, air currents, diffusional distribution of gases and others) is presented. Considerable attention is given to the Earth-Sun problem, including questions of the effect of solar activity on atmospheric processes, to the structure of the upper layers of the atmosphere and to the connection between circulation processes and geomagnetic variations.

The book is intended for meteorologists, geophysicists and astronomers, and for engineering and technical personnel working in the fields of radiocommunication, aviation and jet engineering.

CONTENTS

	Page
Foreword	iv
Part I Structure and Composition of the Upper Layers of the Atmosphere	1
Chapter 1. Density and Pressure Measurement by the Meteor Method	1
1. The meteor method for study of the upper layers of the atmosphere	1
2. Investigation of meteors by radar	15
Chapter 2. Structure of the Atmosphere Determined by Observations of the Twilight Sky	35
3. Twilight observations method	35
4. Theory of the twilight method, including multiple light scattering	43
5. Limits of applicability of the twilight method for study of the atmosphere	50
Chapter 3. Searchlight Sounding of the Atmosphere	60
6. Sounding method	60
7. Measurement of air pressure and density in the stratosphere by the searchlight method of sounding the atmosphere	74
Chapter 4. Use of Rockets and Satellites for Measurement of Atmospheric Pressure and Density	85
8. Measurement of pressure and density by instruments carried aloft by rockets	85
9. Measurement of pressure and density of the upper layers of the atmosphere using artificial Earth satellites	122
10. Results of pressure and density measurement with rockets and satellites	134
11. Pressure and density variations	157
Chapter 5. Heat Regime of the Upper Layers of the Atmosphere	169
12. Indirect methods for temperature measurement in the upper layers of the atmosphere	169

Page

13. Study of the heat regime of the atmosphere by rockets and satellites 186

14. Principle patterns of the heat regime of the upper layers of the atmosphere 198

Chapter 6. Gas Composition of the Atmosphere 216

15. Model of a "mixed" atmosphere 216

16. Air samples. Use of mass spectrometer 224

17. Theory of diffuse separation of gases in the atmosphere 240

18. Change of molecular weight with height 251

19. Water vapor in the stratosphere 25[illegible]

Chapter 7. Aerosol Composition of the Atmosphere 265

20. Dust particles in the high layers of the atmosphere 265

21. Nacreous and noctilucent clouds 279

Part II Dynamics of the Upper Layers of the Atmosphere 300

Chapter 8. Methods of Wind Measurement in the Upper Layers of the Atmosphere 300

22. Drift of bodies freely floating in the atmosphere 301

23. Acoustic methods 308

24. Wind measurements using guided missiles 317

25. Falling spheres method 319

26. Wind measurements in the ionosphere 320

Chapter 9. Data on Air Currents 329

27. Wind in the stratosphere 329

28. Wind in the mesosphere 338

29. Wind in the thermosphere 369

30. Wind in the ionosphere 379

Page

Chapter 10. Vertical and Turbulent Air Movements in the Upper Layers of the Atmosphere 399

31. Convection in the ozonosphere 399

32. Wind turbulence as indicated by meteor data 405

33. Turbulent and vertical movements in the ionosphere 411

Chapter 11. Theory of Air Currents 418

34. Wind in the stratosphere 418

35. Air currents in the mesosphere and lower layers of the thermosphere 430

36. Meridional circulation in the stratosphere and mesosphere 439

37. Wind in the ionosphere 453

Chapter 12. Atmospheric Tides 462

38. Theory of atmospheric tides 462

39. Comparison of theory of tidal winds and observations 472

40. Wind in the ionosphere and geomagnetic field variations 482

Chapter 13. Atmospheric Circulation as Revealed by Observations of Ozone, Atomic Oxygen and Water Vapor 505

41. Ozone and atmospheric circulation 505

42. Atmospheric circulation as revealed by observations of water vapor in the stratosphere and atomic oxygen 509

References 514

FOREWORD

The present book examines the fundamentals of the physics of the upper atmosphere, of the greatest interest to the science of meteorology (structure, composition and dynamics). These problems are among the most important in this field. The author has attempted a thorough survey of investigational methods of the most varied nature, and of the theory of measurement methods, with technical examples of observation and data processing without which it would be difficult to evaluate the reliability of the results obtained. Special attention is given to the exposition of actual measurement data, the generalization of data, and their conclusions, although the latter are sometimes difficult to formulate. In this connection, the book devotes a good deal of space to the exposition, often detailed, of the factual content of many recent works (particularly those dealing with the International Geophysical Year). Such a method of exposition, making extensive use of primary and recent sources, (typical of many sections of this book) permitted illustration of the state of the problem.

The author details questions not fully covered in the literature. For example, some aspects of upper atmosphere investigations, using twilight sky phenomena, are not sufficiently covered in the monograph literature; in this book twilight sky methods and their results are adequately discussed. However, those problems which, although closely related to the basic theme of this book, are the subject of recent publications, are merely "cited" to avoid repetition. For example, in the chapters on the meteor method of studying the upper layers of the atmosphere, there are many references to books by V. G. Fesenkov (ref. 212), B. Yu. Levin (ref. 109), I. S. Astapovich (ref. 7), L. A. Katasev (ref. 79), Ye. L. Krinov (ref. 93), Ye. I. Fialko (ref. 221a), and B. Lovell (ref. 110). In other chapters, there are frequent references to the books by R. M. Gudi (ref. 44), S. G. Mitra (ref. 127) and R. L. F. Boyd and A. J. Siton (ref. 13), published in Russian, and especially to recent monographs by Soviet authors treating problems of the upper atmosphere, B. A. Mirtov (ref. 125), K. Ya. Kondrat'yev (refs. 88a, 91), Kh. P. Pogosyan (refs. 148, 149), L. R. Rakipova (ref. 165), and I. A. Khvostikov (ref. 233).

The book is furnished with an extensive bibliography, culled from material supplied by the Institute for Scientific Information (Institut nauchnoy informatsii) of the Academy of Sciences, USSR. This bibliography should be nearly complete, even though the information is somewhat restricted: older works, as a rule, are omitted if a later work by the same author contains

references to the earlier work. For instance, dozens of articles by I. S. Astapovich on studies of the atmosphere by meteor observations are not included, because there is a recent publication of his general monograph (ref. 7).

The nomenclature of the layers of the atmosphere has changed several times during recent years. The repeated revision of the definitions of individual atmospheric layers is the result of rapid accumulation of new information on the structure of the upper layers and our wider knowledge of the mechanism of these atmospheric processes. The nomenclature used conforms to the latest recommendations of the Meteorology Commission of the World Meteorological Union. According to this, the troposphere and its upper limit (which is also the lower boundary of the stratosphere)--the tropopause--is defined as before. The upper limit of the stratosphere (which is also the lower boundary of the mesosphere) is defined as the level of maximum temperature ordinarily observed at an altitude of 50 to 55 km. The mesosphere, within which temperature decreases with altitude, is bounded above by the mesopause--a layer of minimum atmospheric temperature, usually located at 80 to 85 km. Above the mesosphere is the thermosphere--an extensive region of temperature inversion--and above that is the exosphere.

The author expresses deep gratitude to Dr. L. R. Rakipova and Prof. A. Kh. Khrgian for their valuable criticisms, and to O. V. Yablonskaya for her help in preparing the manuscript.

PART I

STRUCTURE AND COMPOSITION OF THE UPPER LAYERS OF THE ATMOSPHERE

CHAPTER 1. DENSITY AND PRESSURE MEASUREMENT BY THE METEOR METHOD

1. The Meteor Method for Study of the Upper Layers of the Atmosphere

Before 1946 air density above 30-40 km was measured only by an indirect method. Direct determinations have become possible recently by the use of rockets. However, indirect methods have not lost their importance. On the contrary, their systematic use has increased.

Among the indirect methods of density measurement meteor observations are of the greatest importance. By observation of meteors it already was possible in the 1920's to obtain important information on atmospheric density at heights of about 100 km. They also made it possible, for the first time, to detect remarkable peculiarities of the structure of the upper layers of the stratosphere--a temperature maximum at a height of about 60 km and a well-expressed temperature minimum (ref. 205) at the 80 km level. In addition, meteors produce appreciable ionization of air in the lower part of the ionosphere. Now, particularly as a result of radar observations, the meteor method retains its great importance for systematic investigations of the upper layers of the atmosphere.

1.1. General Information. Meteors are bodies of extraterrestrial origin. They have a mass of only a few mg in most cases. Upon penetrating into the Earth's atmosphere at an enormous velocity (10-70 km/sec), meteors are heated instantaneously and as a result become luminescent at a height of 50-130 km (for this reason at one time they were called "shooting stars") and "burn up" (evaporate) before they penetrate into denser layers. But, in rare cases, these bodies are of considerably greater size and weigh tens of tons and, before penetration into the atmosphere, even hundreds and thousands of tons. During deceleration in the atmosphere, larger meteor bodies lose a lesser part of their initial velocity, and therefore can penetrate into deeper layers of the atmosphere, and the largest of them can even reach the Earth's surface, since they have cosmic velocities (ref. 95). Claps and peals similar to thunder, caused by the propagation of sound waves, are audible when a large meteor body penetrates into the layers of the atmosphere below 55 km (ref. 203).

When a swarm of meteor bodies moving in a common orbit in interplanetary space encounters the Earth, the meteors appear to the observer to emanate

approximately from a single point, the radiant; this apparent divergence is caused by perspective. The meteors having a common radiant form a meteor stream, which is assigned the name of the constellation in which its radiant is situated. For example, the name Lyrids is given to the meteor stream with its radiant in the constellation Lyra. As early as 1866 the Italian astronomer G. Schiaparelli discovered a similarity between certain orbits of meteor streams and comets and postulated that meteor streams are formed as a result of the gradual scattering along the orbit of solid particles which make up the nuclei of comets. In the 1870's F. A. Bredikhin pointed out the possibility of an eruption of meteor bodies from the nucleus of a comet. According to this theory, the orbits of individual particles can differ greatly, but they must intersect at the point of eruption, forming one family of orbits.

However, for many meteor streams there are no known nearby cometary orbits, and most comets do not have corresponding meteor streams. In addition to meteors belonging to well-defined meteor streams, there are many individual, sporadic meteors (ref. 110). Their orbits, like the orbits of some meteor streams, have a similarity to the orbits of the minor planets and short-period comets. The origin of these meteors is assumed to be the same as the origin of the minor planets (ref. 203).

Meteor bodies form a cloud around the Sun, with a density decreasing with the distance from the Sun. The density and total mass of the meteor mass in the solar system are insignificant. The total mass of meteor matter does not exceed 1/1,000th of the Earth's mass. The mean distance between meteors in the central part of meteor streams, arising at the time the Earth encounters large meteor showers (Draconids, Leonids), is 30 km. The total mass of the Perseids is estimated at 10^{10} tons (of the order of 10^{-12} of the Earth's mass). The diameter of the swarm of meteor bodies can be as great as several million km. The Earth requires several days to pass through such a swarm, and its radiant is observed several nights in a row (August Perseids), moving in the celestial sphere at an angle up to 1° per day. Table 1.1 gives a list of the principal meteor streams. All the streams can be observed visually. Numerous daytime meteor streams have been discovered and are now investigated regularly by radar. This is possible because of the strong ionization of the atmosphere during the flight of the meteors and the formation of an ion trail which reflects radio waves.

The number of meteors is large. On a clear moonless night it is possible to see an average of 10 meteors an hour with the naked eye, and a far larger number can be seen with a telescope. An especially large number of meteors can be observed using radar sets; this will be discussed in the next section. The luminous intensity of telescopic meteors is less than 100 international candles, and the luminous intensity of visual meteors is less than 1,000. Bolides (large meteors of considerable size, with a brightness exceeding that of Venus) appear from time to time; exceptionally bright bolides, which appear very rarely, exceed the brightness of the Moon. The bolide of the Sikhote-Alin meteorite of Feb. 12, 1947, had the brightness of the Sun, and the Tunguska meteorite of June 30, 1908, was several times brighter than the Sun. The spectra of meteors consist of a number of emission lines; they are caused by the luminescence of the red-hot vapor of meteor matter. The spectrum of luminescence of stony meteor

TABLE 1.1. PRINCIPAL METEOR STREAMS.

Date of maximum	Name of stream	Radiant, degrees		Normal duration, hours
		right ascension	declination	
Jan. 3	Quadrantids	230	+ 52	30-40
Apr. 21	Lyrids	270	+ 33	7-10
Aug. 10-13	Perseids	47	+ 58	40-60
Oct. 22-23	Orionids	96	+ 15	10-20
Nov. 16-17	Leonids	152	+ 22	10-15
Dec. 11-13	Geminids	113	+ 32	60

bodies, which are the most common type (75 percent of cases) is characterized by strong lines of ionized calcium and also contains the lines of iron, chromium, aluminum, nickel, silicon, manganese, magnesium, sodium, titanium and cobalt. Iron meteor bodies for the most part emit the lines of iron. The luminescence of meteors in the visible part of the spectrum is the result of secondary excitation; their principal emission occurs in the region of shorter waves.

1.2. Physical Theory of Meteors. It is possible to draw conclusions on the properties of the air medium, in which motion occurs, on the basis of observations of the motion and luminescence of meteors only on the basis of the physical theory of meteors, which considers the character and laws of interaction of meteor bodies with the air medium.

Meteor bodies of very different mass and size penetrate into the Earth's atmosphere from interplanetary space. The size of the bodies has an important influence on the course of the processes of their deceleration, heating, evaporation and luminescence, and also on the process of atmospheric ionization. For this reason, the physical theory of meteors must consider separately bodies which are large, small and very small (micrometeorites). For example, in a study of the heating of meteor bodies it is convenient to refer to bodies as "large", if they do not become heated through to the center, and in which there is, therefore, an appreciable heat transfer from the heated surface to the colder inner parts. This is the situation, e.g., with stony meteor bodies more than 1 mm in diameter; in the case of iron meteor bodies, as a result of their great heat conductivity, the diameter should not be less than 3 mm. The case of micrometeorites will be discussed separately.

Study of the upper layers of the atmosphere by meteor methods began in 1923, when Lindemann and Dobson, with this purpose in mind, developed the first physical theory of meteors and derived formulas for analysis of physical observations of meteors (ref. 550). Their theory was based on the assumption that a meteor body is heated by a cushion of adiabatically compressed air. On the basis of the heights of appearance and disappearance of meteors, at a level of about 100 km they determined the values of density and temperature. These considerably exceeded those accepted earlier on the basis of the hypothesis of an isothermal stratosphere. This conclusion was confirmed by further investigations, although the physical picture serving as the basis for the Lindemann-Dobson theory is not true. The problem is discussed below.

Compression can be considered approximately adiabatic, if it occurs so rapidly that there can be no appreciable heat loss, but, at the same time, it is slow in comparison with the speed of sound. Meteor bodies move in the atmosphere with a velocity a hundred times greater than the speed of sound. Therefore, here we can speak only of shock compression of air, whose laws differ from the laws of adiabatic compression.

Another important characteristic of these phenomena is that it is only possible to consider the atmosphere a continuous medium subject to shock compression at relatively low heights, where the mean length of the free path of air molecules becomes less than the diameter of the meteor body. It is necessary to consider the collisions of a meteor body with individual air molecules. In 1926 Sparrow, proceeding on the basis of a correct idea that these collisions are inelastic, found that the energy flux at the frontal surface of a meteor body is proportional to the cube of velocity.

The work of Öpik in 1937 (ref. 134) was of great importance (the history of meteor investigations and a detailed bibliography were given in monographs by B. Yu. Levin (ref. 109) and I. S. Astapovich, ref. 7). Öpik, in particular, noted for the first time a relationship between the problem of the energy flux imparted to a meteor body and the accommodation factor--a value characterizing the energy transfer between a meteor body and atmospheric molecules. He analyzed the blocking effect of the "air cushion" and the vapors of the meteor body shielding the frontal surface from the impact of the encountered air molecules. Whipple (1938) gave an interesting (phenomenological) derivation of the principal equations, and estimated the theoretical values of the coefficients of resistance and heat transfer, considering the collisions of individual molecules of a meteor body with air molecules as the collisions of elastic spheres.

In proceeding to an investigation of large meteor bodies evaporating in the lower (and this means denser) layers, it is necessary to take into account the great intensification of the blocking effect of air molecules thrust aside, and the molecules evaporating from the surface of the meteor body; under these conditions a shock wave will be formed. Beginning in 1931 the equations of gas dynamics were used in computation of the pressure and temperature of the shock wave (Epstein). It was found later that due to the enormous temperatures of the shock wave in front of the meteor body (according to first estimates it was more than 10^5 degrees; in actuality it is less), it is necessary to apply the theory of strong shock waves, which takes into account dissociation, ionization and the emission of molecules and atoms. The studies of K. P. Stanyukovich (ref. 181) and O. V. Dobrovol'skiy (ref. 59) were of great importance for the development of this aspect of the physical theory of meteors.

1.3. Motion of a Meteor Body in the Atmosphere. The interaction of meteor bodies from interplanetary space penetrating into the atmosphere begins with the bombardment of the frontal surface by individual air molecules. This is accompanied by deceleration and heating of the body. During the flight of a large meteor body the temperature of the surface increases proportional to the increase of atmospheric density ρ, until the intense evaporation of matter begins to absorb almost all the received energy (ref. 109). This occurs at a height of about 100 km, after the surface temperature reaches 2,000-3,000 $^{\circ}$K.

Heating of small meteor bodies begins sooner than heating of large bodies, but the increase in their temperature occurs considerably slower (proportional to $\rho^{1/4}$).

After onset of intense evaporation, the frontal surface is partially shielded from the impacts of the encountered air molecules by a dispersing cloud of evaporating molecules, and (if the meteor body is sufficiently large) by air molecules thrust aside after collision with the frontal surface.

After the frontal surface is heated sufficiently, strong evaporation begins. As a result, the decrease of mass, which had occurred earlier mostly by erosion, is accelerated many times. Transition to vigorous evaporation occurs in a short segment of the meteor path and is accompanied by rapid intensification of luminescence. The greater the mass and density of the meteor body, the further it penetrates into the atmosphere before it evaporates or loses cosmic velocity. Ordinary and telescopic meteors are, in fact, bodies having a diameter of $2r < 1$ cm, which are decelerated completely or evaporate at heights greater than 80 km, where the length of the free path of molecules is $\lambda > 2r$. Bright meteors and bolides are bodies having $2r > 1$ cm which penetrate below 80 km, i.e., into layers where $\lambda < 2r$. Shock waves develop under such conditions. In this case the investigation of the motion of a meteor body in the atmosphere requires the consideration of the problem of supersonic flow of a continuous air medium around a body. Such problems are solved in gasdynamics and in ballistics. The possibility of the use of ballistic methods is not great, however, since the specific meteor conditions differ appreciably from conditions studied in ballistics (ref. 744). The principal difference between these conditions apparently is the characteristics of the process of heat exchange between the shock wave and the meteor body: under meteor conditions the heat exchange is determined not only by intermolecular collisions, but also is decisively dependent on radiation (ref. 181). In ballistics it is the braking of the body which is primarily considered, and its heating (because of the considerably lower velocities of the bodies studied in ballistics) is studied relatively little; in any case, it usually does not consider a body which reaches the melting or evaporation point. However, the principal role in meteor problems is played by heating and subsequent evaporation, and deceleration most frequently is insignificant. The great complexity of the problem of heat transfer at high Mach numbers makes it difficult to use the methods of gasdynamics in the physical theory of meteors.

A theoretical computation of the deceleration of meteors during their passage through the Earth's atmosphere was published recently by Verniani (ref. 784).

The luminescence of meteor trails is the recombination luminescence of ionized atmospheric gases, as was pointed out for the first time more than half a century ago (Trowbridge). Evaporating molecules undergo intense dissociation, and the forming atoms undergo excitation and ionization. Both rapid and slow meteors create ionized trails along their paths. In the rarefied layers of the atmosphere, where $\lambda \gg 2r$, radiation is created in the entire volume around the meteor body in which there are sufficiently rapid collisions between atoms and ions of metals forming from evaporating molecules and air molecules. The energy of this radiation is proportional to the number of molecules evaporating in a unit time (ref. 109).

However, it must be remembered that the recombination mechanism apparently is inadequate as a source of luminescence of persistent meteor trails. For example, according to the computations of Howkins and Cook (ref. 459), the observed light energy in the region 4,680-5,560 A is 2 orders of magnitude greater than the theoretical value of the energy computed on the assumption that luminescence of the trail is caused by the recombination of meteor and free electrons. Their computations were made using the formula

$$I = \frac{p\alpha_e q^2}{8\pi Dt},$$

where I is the luminous energy emitted by 1 cm of the trail per second, q is the number of pairs of ions per 1 cm of length of the trail, D is the diffusion coefficient, α_e is the recombination coefficient, p is the luminescence yield of the process (the luminous energy emitted during one recombination event)

Howkins and Cook postulated that the persistent luminescence of trails is associated with the formation, along the path of the meteor body, of active nitrogen which then excites the luminescence of neutral meteor atoms.

Chapman (ref. 327) explains the luminescence of stable meteor trails by pointing out that the sodium contained in a meteor body can serve as a catalyst in the process of recombination of atomic oxygen: this process is accompanied by energy release.

1.4. Some Results of the Physical Theory of Meteors. The full physical theory of meteors should take into account all physical processes occurring during the motion of meteor bodies in the Earth's atmosphere. It involves a number of investigations: heating, evaporation and deceleration of a meteor body; processes of dissociation, ionization and luminescence of evaporating molecules and air molecules; condensation of evaporated matter leading to the formation of vapor trails, and also electromagnetic phenomena accompanying the flight of a meteor in the atmosphere. The basic problems of the physical theory of meteors are the problems of heating, evaporation and deceleration of a meteor body, since the processes of luminescence of a meteor and its trail, dissociation and ionization of evaporating molecules and air molecules are caused by the energy carried off by the evaporating molecules of the meteor body.

In 1937-1941 a number of studies by different authors appeared, containing the derivation of the principal equations of the physical theory of meteors--the equations of evaporation and deceleration. A full review of these equations can be found in a book by I. S. Astapovich (ref. 7). As early as 1939-1941 studies by B. Yu. Levin (ref. 107) gave not only the derivation of the principal equations, but also a formula for heating a meteor body, making it possible to find the height of appearance of the meteor (the height at which the "boiling" of the surface layer of the frontal surface begins). The temperature of the frontal surface of a nonrotating stony meteor body is determined by the formula

$$T = \frac{a_m \sqrt{H}}{2\lambda} \frac{v^{5/3}}{\sqrt{\cos z}} \rho, \qquad (1.1)$$

where $a_m = \frac{\lambda}{\delta c}$ is the coefficient of thermal diffusivity, λ is the coefficient of heat conductivity, H is the height of the homogeneous atmosphere, ρ is air density, v is meteor velocity and z is zenith distance of the radiant. Levin showed that for meteor bodies of different velocity the temperatures at the time of appearance are virtually identical, and therefore formula (1.1) makes it possible to find H easily for the height at which meteors appear. The dependence of the height of appearance h on velocity v does not contain any constants characterizing the properties of the meteor body

$$\Delta h = h(v_1) - h(v_2) = \frac{5}{2} H \ln \frac{v_1}{v_2}. \qquad (1.2)$$

Observations show that for meteors with a velocity v = 60-70 km/sec the height of appearance is h ≃ 125 km, and when the velocity is v = 30 km/sec, h ≃ 100 km. It therefore follows that in the 100-120 km layer the height of the homogeneous atmosphere is H = 10-12 km.

By knowing H and stipulating the numerical values of the coefficients of heat conductivity and thermal diffusivity, it is possible to find the density at the height of appearance of meteors of different velocity. The following results were obtained

h km	100	110	125
v km/sec . . .	30	50	70
ρ g/cm^3 . . .	$1 \cdot 10^{-9}$	$3 \cdot 10^{-10}$	$1 \cdot 10^{-10}$

These density values apply to the height of appearance of stony, nonrotating meteor bodies with a flat frontal surface. For another limiting case--for a rotating spherical meteor body--they are greater by a factor of 4 (ref. 108).

The value of the B. Yu. Levin method was that the determination of H and ρ is dependent on the heights of appearance determined from visual observations and, therefore, applies to the maximum heights accessible to meteor methods of investigation.

These numerical results for H and ρ must be considered approximate. The theory of heating of meteor bodies later was improved in studies by V. G. Fesenkov, Whipple, Thomas, B. Yu. Levin, K. P. Stanyukovich, L. A. Katasev and others (these studies are reviewed in a monograph by B. Yu. Levin, ref. 109). We will briefly discuss the theory of heating of micrometeorites, an investigation which, during the last ten years, has assumed great importance.

The heating of very small particles (for which the ratio of surface area to volume is large) occurs considerably more slowly during penetration into the atmosphere than is true for large particles. In the case of particles with $r < 10$ μ, virtually all the resultant energy is expended on thermal radiation. With an increase of ρ, the increase of their temperature later is replaced by a decrease as a result of decrease of v. In the case of sufficiently small particles, this sets in sooner than their temperature attains the melting point

T_{melt}. Whipple has called such particles "micrometeorites." The maximum temperature, equal to T_{melt}, will be reached by such a particle at a point where atmospheric density is

$$\rho_M = \frac{8e\sigma}{a}\frac{T^4}{v_0^3}d. \qquad (1.3)$$

Here a is the accommodation factor, σ is the radius of the micrometeorite, v_o is its initial velocity, and e is the base of natural logarithms.

The maximum temperature of particles of smaller size will be less and is reached in a layer with lesser atmospheric density, i.e., at a great height. The values ρ_M, computed for a case of vertical motion (z = 0) for stone and iron particles (the specific weight of the first is 3 g/cm^3 and of the second is 7.6 g/cm^3) are (ref. 109)

v_o km/sec	11.3	15	30	60
ρ_M g/cm^3 for particles:				
stone	$6\cdot10^{-9}$	$2\cdot10^{-9}$	$3\cdot10^{-10}$	$4\cdot10^{-11}$
iron	$1.3\cdot10^{-8}$	$4\cdot10^{-9}$	$6\cdot10^{-10}$	$9\cdot10^{-11}$

1.5. Photographic Investigations of Meteors. In the development of the physical theory of meteors an important role is played by photographic investigations of meteors (ref. 80). The earlier used visual observations are encumbered by great errors in determination of height. As a result of the inaccuracy of map plotting of the apparent path of a meteor, the heights determined from visual observations can be erroneous by many kilometers. In addition to observational errors, the determination of height is also affected adversely by long-used analytical methods. Much credit belongs to Soviet investigators, especially V. V. Fedynskiy (refs. 202, 203 and 205), for the development of satisfactory analytical methods.

The use of photographic methods of meteor observation simultaneously at two points permits us to determine precise heights and directions of a meteor path. If at least at one of these points an obturator rotates in front of the camera objective, interrupting the exposure 10 to 20 times per sec, the photographs can also be used to determine the velocity and deceleration of a meteor body, which considerably broadens the possibilities of studying the upper layers of the atmosphere by meteor methods. With an obturator the meteor trail on the plate is broken down into individual lines (fig. 1.1), whose measurements make it possible to determine the law of motion.

In the 1920's photographs were obtained with such a method by Lindemann and Dobson. In 1932 photographs were taken using an obturator at Moscow under

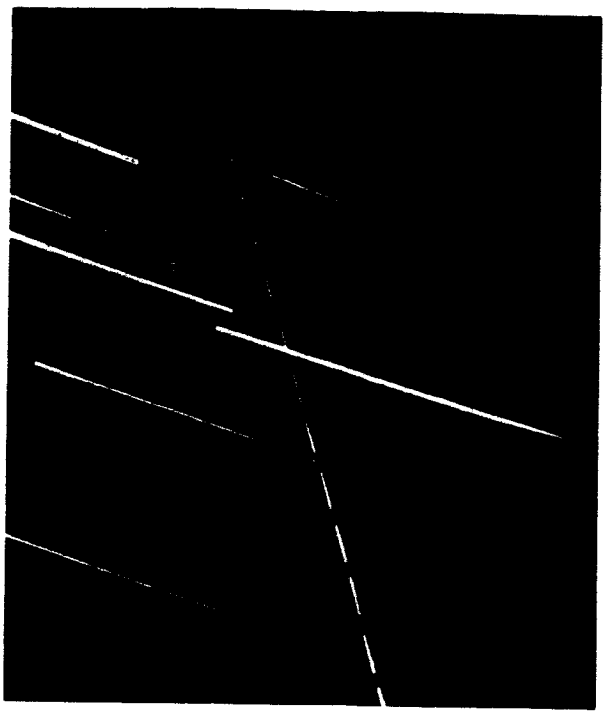

Figure 1.1. Photograph of meteor taken at Dushanbe on Aug. 8, 1951, with a camera whose objective was covered periodically by the blades of an obturator.

the direction of V. V. Fedynskiy. In the first year, on Aug. 14, 1932, successful photographs of a bright meteor were taken and processed by V. V. Fedynskiy and K. P. Stanyukovich by a new method (ref. 205). They obtained extremely important information on the temperature of the upper layers of the stratosphere. Systematic photographing of meteors in the 1930's began at the Astronomical Observatory at Dushanbe, where a meteor patrol is used for this purpose. The meteor patrol consists of two sets of ten cameras (ref. 179). The method of precise photographic processing of photographs was published in 1935 by N. N. Sytinskiy (ref. 184), who applied it to 11 meteors.

Beginning in 1936, the systematic photographing of meteors was begun at Harvard Observatory using two cameras situated at the ends of a base 38 km in length. In the analysis of this material Whipple applied a theory which makes it possible to find atmospheric density at four points along the meteor path: beginning, end, point of maximum brightness and a point near the middle of the path from which deceleration was determined (there are several such points on long paths).

The density determined at the point for which deceleration is known is the most reliable. From the deceleration equation

$$m\frac{dv}{dt} = -C_1 S \rho v^2, \tag{1.4}$$

(S is the area of the cross section of the meteor body, C_1 is the proportionality factor), it is possible to find the mass m of a meteor body. It is postulated that the luminous intensity I of a meteor is proportional to the energy loss in a unit time

$$I = -\frac{1}{2} C_2 \frac{dm}{dt} v^2. \tag{1.5}$$

In the derivation of this equation it is taken into account that the kinetic energy of a meteor body exceeds by hundreds of times the energy necessary for its evaporation, and it is expended mostly during collisions between the evaporating molecules of a meteor body and air molecules. It can be postulated further that a meteor body, decreasing in mass, does not change its form but remains self-similar, that is, $S \sim m^{2/3}$. After substituting into (1.5) the expression for $\frac{dm}{dt}$ from the evaporation equation

$$\frac{dm}{dt} = -C_3 S \rho v^3, \tag{1.6}$$

we obtain as the luminous intensity equation

$$I = C_4 C_2 m^{2/3} \rho v^5, \tag{1.7}$$

showing a sharp dependence of I on velocity--proportional to v^5. For bright meteors the dependence is still stronger, since according to Öpik in this case

$$C_2 = C_{02} v.$$

Taking this into account and substituting into (1.7) the value of the mass from the deceleration equation (1.4), we find the equation for density determination

$$\rho = C v^{-10/3} \left(-\frac{dv}{dt}\right)^{2/3} I^{1/3} \tag{1.8}$$

(in all these equations C, C_2, C_3 and C_4 are proportionality factors).

We now will consider the method for determination of density at the point of maximum brightness. The appropriate formula can be obtained by putting the luminous intensity equation in logarithmic form and subsequent differentiation and substitution from the deceleration equation (1.4) and evaporation equation (1.6) of the expressions for the derivatives $\frac{dm}{dt}$ and $\frac{dv}{dt}$. The term containing the derivative $\frac{d\rho}{dt}$ is transformed as follows

$$\frac{1}{\rho}\frac{d\rho}{dt} = -v\frac{1}{\rho}\frac{d\rho}{dh}\cos z = \frac{v\cos z}{H}. \qquad (1.9)$$

Determination of ρ by this method is characterized by lesser accuracy, and equation (1.9) shows that it is necessary to stipulate value H.

Density at the beginning of the path is determined for the upper point of the path where meteor brightness can be measured. It is assumed that evaporation of the meteor body could not yet appreciably decrease its mass from the initial value, found by using the formula

$$E = \int I\,dt = C_2\frac{m_0 v_0^2}{2},$$

in which meteor deceleration is neglected. After substituting mass from here into the luminous intensity equation we obtain

$$\rho = C_0 I E^{-2/3} v_0^{-4}. \qquad (1.10)$$

Although the use of this formula involves possible systematic errors (ref. 108), it is valuable because it permits determination of density at the maximum heights accessible to the photographic method. Use of the Levin formula (1.1) for temperature at the time of meteor appearance in photographic observations is impossible, because the height at which meteor brightness becomes adequate for producing a trail on a plate differs from the true height.

Finally, an expression can be obtained for density at the end of the path. The initial mass of the meteor body is found on the basis of total luminous energy, using the described method, and (neglecting deceleration) the total mass of the atmosphere along the entire path above the point of disappearance is determined. Stipulating the value of the height H of the homogeneous atmosphere, it is then possible to obtain ρ at the end of the path.

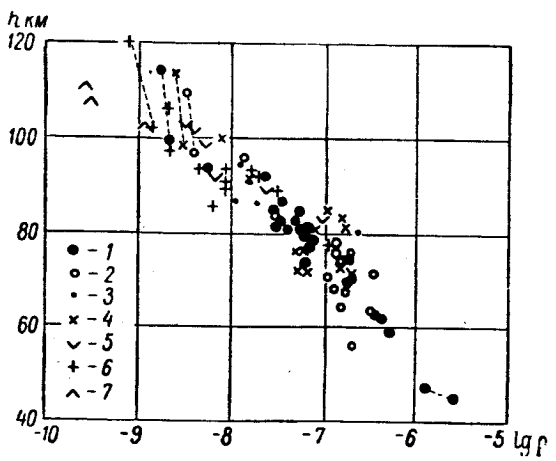

Figure 1.2. Air density in the upper layers of the atmosphere on the basis of meteor determinations. (1) deceleration; (2) end of path (photographic); (3) end of path (visual); (4) maximum brightness (photographic); (5) maximum brightness (visual); (6) "ignition" (photographic); (7) "ignition" (visual).

Whipple's results of determination of ρ, obtained by all four methods, are shown in figure 1.2. On the basis of the results of an analysis of systematic corrections (differences of the density values obtained by different methods), Whipple adopted the following density values as the most probable

Range of heights h in km . . .	58-72	72-80	80-90	90
Mean height h_{mean} in km	67.1	75.9	83.1	94.9
log ρ.	-6.68	-6.95	-7.34	-8.05

It must be remembered that Whipple obtained these results by using simplified formulas. The proportionality factors entering into the deceleration and evaporation equations were considered virtually constant, and he determined their numerical value on the basis of theoretical and experimental data on the motion of bodies at supersonic velocities. However, these data apply to motion in a medium of relatively great density where shock waves are formed. In actuality, however, the particular phenomena occur partly at heights where the length of the free path of air molecules is greater than the dimension of a meteor, or comparable to it. Under these conditions the interaction of a meteor body and the medium involves only individual collisions with molecules. There still are no shock waves; only gradually does the meteor body begin to be progressively surrounded by an envelope of evaporating molecules of increasing density (ref. 108). In the lower layers processes develop which are associated with the flow of air around a meteor body. Air shock waves develop in front of the meteor body and behind it, and these greatly increase the resistance of the medium. At a height of 80 km the shock wave already has a sharply expressed character (ref. 203). More precise development of the theory of these processes has been given in studies by K. P. Stanyukovich (ref. 181) and O. V. Dobrovol'skiy (ref. 59).

Systematic meteor measurements for the purpose of determination of atmospheric density are now being made by Ceplecha in Czechoslovakia (ref. 317). He has refrained from using the lower part of the meteor path because, in this case, there is no assurance of the applicability of the principal initial formulas. Ceplecha believes that the breakdown of these formulas is caused by the excessively great deceleration observed at the very end of the meteor path.

1.6. Difficulties in Application of the Meteor Method. As a result of the systematic use of rockets in recent years for transporting apparatus into the upper layers of the atmosphere for measurement of air pressure and density, it has been possible to obtain independent data on the values ρ at heights of 70-100 km, which in part are contradictory to meteor data. In 1952 Whipple (refs. 431, 801 and 802) and Jacchia (ref. 471) attempted to use rocket data on atmospheric density to obtain the inverse formulation of the problem in analysis of meteor photographs: instead of determining ρ on the basis of data on the deceleration of meteor bodies, whose mass is found by a photometric method, they attempted to determine mass by assuming the value ρ to be known. Whipple found that "dynamic" masses, found by the latter method, are many times less than "photometric" masses. In other words, the values ρ obtained from analysis of meteor photographs were many times less than the values measured using rocket apparatus.

TABLE 1.2. COMPARISON OF VALUES OF AIR DENSITY ρ_M OBTAINED FROM METEOR OBSERVATIONS AND VALUES ρ_R MEASURED WITH ROCKETS (JACCHIA).

h км	$\lg \rho_M$	$\lg \rho_R$	$\frac{\rho_M}{\rho_R}$
45	—5.744	—5.667	1.19
50	—6.006	—5.936	1.17
55	—6.227	—6,199	1.07
60	—6.421	—6.457	0.92
65	—6.607	—6.723	0.77
70	—6.801	—7.012	0.62
75	—7.018	—7.334	0.48
80	—7.287	—7.676	0.41
85	—7.611	—8.034	0.38
90	—7.951	—8.389	0.36
95	—8.273	—8.734	0.34
100	—8.569	—9.063	0.32
105	—8.852	—9.379	0.30
110	—9.131	—9.684	0.28

In order to eliminate this contradiction Whipple postulated (ref. 801) that the density of meteor bodies is not 3-3.5 g/cm^3, as always was assumed before, but only 0.3-1.0 g/cm^3. Jacchia used a different approach. Table 1.2 gives data on air density obtained on the basis of photographic measurements of meteors at Harvard Observatory (ref. 471), and the results of measurements with instruments carried aloft by rockets (ref. 707) (see Section 10). These data indicate the presence of large and systematic discrepancies.

Jacchia believes that such anomalies are the result of fragmentation of meteors (ref. 475). He believes that meteor bodies have a porous and brittle structure, similar to the structure of the particles postulated in the ice model of a cometary nucleus. During the motion of such particles in the Earth's atmosphere there is a fragmentation process--the separation of fine particles from the surface of the meteor body. Beginning in 1949 B. Yu. Levin supported the idea of the multiple fragmentation meteor bodies (ref. 109). From this point of view, the smallness of the dynamic masses of meteor bodies is not the result of the smallness of their densities, but the result of their frequent fragmentation. In the case of fragmentation the determination of mass on the basis of deceleration will give the mean mass of an individual fragment, whereas photometric data will yield the total mass. Studies have appeared recently which continue the discussion of this interesting problem (refs. 159, 160, 415, 472 and 475). In the theory which he developed,Jacchia attempted to compute the masses of the particles separating at the time of a meteor flare. Such computations also have been made by Smith (ref. 732). Discovery of fragmentation by radar observations of meteors will be discussed in Section 2.12.

New possibilities for checking and development of the physical theory of meteors and, therefore, for the further use of the meteor method for the study of the upper layers of the atmosphere have appeared as a result of experiments carried out in the upper layers of the atmosphere, using instruments carried aloft in rockets (investigation of micrometeorites and experiments with

"artificial meteors") and also the use of radar apparatus for study of meteors. These problems are considered below.

1.7. Experiments Using Rockets. Experiments with "artificial meteors" are of great interest. Investigations of supersonic bullets were made first. Allen, Reingart and White (refs. 265 and 702) made laboratory investigations of the flight of metal bullets with a velocity of 2-6 km/sec. At a velocity of 2.5 km/sec, steel bullets lose an insignificant part of their mass and glow faintly, but aluminum bullets at a velocity of 5 km/sec glow brightly. Movement of the bullet is described by the formula

$$v = v_0 e^{-\alpha l},$$

where v_0 is the initial velocity of the bullet, v is velocity after the bullet has traveled the distance l in the air, α is a constant dependent on the composition of the bullet. The emission spectra of the bullets contain lines, bands and a continuous background. The effective vibrational temperature measured from the spectra was 4,100°K.

Over a period of years attempts have been made in the United States to launch artificial meteors by means of rockets. The first experiment was carried out over the test grounds in New Mexico with the ejection (by an explosion) of small shot from the nosecone of an Aerobee rocket. The nosecone, containing the charge, was separated from the rocket after the rocket reached the 56 km level.

The charge was exploded at the 87 km level, and a velocity of about 15 km/sec was imparted to two aluminum shot. There was a bright flare (about -10 stellar magnitude) visible at the Mount Palomar Observatory at a distance of almost 1,000 km as the brightest object in the night sky. One of the shot was photographed after the explosion. Its brightness was about -2 stellar magnitude, which is approximately equal to the brightness of Venus.

Study of micrometeorites is another interesting use of rockets for solution of meteor problems. In recent years investigations of meteor particles were begun in the United States and USSR by direct methods--using apparatus carried into the high layers of the atmosphere by rockets and satellites (refs. 85, 153 and 292). T. N. Nazarova and S. M. Poloskov used apparatus for this purpose which permits recording the number of impacts occurring during collision of the rocket and meteor particles and measuring certain mechanical parameters of meteor particles. The idea behind the measurement apparatus is as follows (ref. 85).

Theoretical computations made by K. P. Stanyukovich showed that in the case of high velocities of meteor particles the momentum recorded during their collision with a rocket is proportional to the energy of a falling particle $\frac{mv^2}{2}$. Measurement of momenta is done with a ballistic sensor which consists of a massive plate suspended on a flat spring; four piezoelectric transducers are connected to this plate. Under the influence of a micrometeorite impact the plate displaces and deforms the piezoelectric transducers and an electric

voltage is produced, which is fed through amplifiers into a radiotelemetric channel. Such a sensor makes it possible to measure the energy of meteor particles with masses from 10^{-9} g or more (at a mean velocity of 40 km/sec).

On the basis of preliminary data, the third Soviet artificial satellite recorded an average of about one impact in 10 min per m^2. There was a brief, sharp increase in the number of impacts to 22 per sec per m^2 (at a height of 1,700-1,800 km). The recorded meteor particles have an energy of about 10^4 erg.

A rocket recorder of micrometeorites was developed at the Naval Research Laboratory in the United States. It consists of photomultipliers, and there is a recording of the light flashes accompanying the impact of a micrometeorite on a special shield mounted on the body of the rocket. This instrument was carried aloft on Nov. 17, 1955, on an Aerobee rocket to a height of 103 km. It was found that at the 85 km level, above which impacts no longer were detected, an average of about 180 impacts per sec per m^2 was recorded. Berg and Meredith (ref. 292), who carried out this experiment, express the opinion that the sensitivity of the instrument made it possible to record extremely small quantities of energy--from $5 \cdot 10^{-3}$ erg or more. It must be remembered that the date of this experiment coincides with the period of the Leonids meteor stream (see Table 1.1).

2. Investigation of Meteors by Radar

In 1931 N. A. Ivanov postulated that meteors play a significant role in the creation of nighttime ionization of the atmosphere. He based his hypothesis on the results of an analysis of conditions for long-range radio communication. V. A. Leushin was the first to record with instruments the numerous fadings during the Draconids meteor stream of Oct. 9, 1933. During the fall of the meteorite "Pervomayskiy Poselok" on Dec. 26, 1933 a team monitoring a radio transmission at the time of the flight of the bolide heard a "sharp whistle" in the loudspeaker (ref. 7). Such a phenomenon occurs during the interaction of two radio waves--direct and reflected from the meteor and its cylindrical ionized trail. Beginning in 1947 these "Doppler whistles" have constantly been used in the determination of meteor velocity (see Section 2.5).

A wave can be reflected from a body (due to diffraction), if the latter is sufficiently great in comparison with the wavelength. Radar, therefore, could acquire practical importance only after due development of the technique of very short waves. This was accomplished in the 1940's, and the beginning of the 1940's marks the beginning of the rapid development of radar observation of meteors. The formation of an ionized column along the path of a meteor in

the atmosphere is accompanied by a scarcely detectable disturbance of the geomagnetic field. This magnetic effect of meteors was discovered by A. G. Kalashnikov (ref. 78) in 1948, using a particularly sensitive fluxmeter.

2.1. General Information. Radar methods for the observation of meteors make it possible to record not only ordinary meteors (visible to the naked eye), but telescopic meteors as well. Radar methods have enormous advantages over other observation methods, such as the possibility of making observations around-the-clock, not only at nighttime, and regardless of weather conditions.

A great many observations have already accumulated, and a number of problems have been worked out on a theoretical basis. These concern the process of meteor ionization of the atmosphere, recombination of the ions in the ion column and their diffusion, etc. This new field now constitutes an independent aspect of the physical theory of meteors.

Study of meteors by radiophysical methods can be carried out in three main directions.

The first is investigation of the astronomical properties of meteors (meteor astronomy). This includes, in particular, the determination of meteor radiants, their velocities, sizes and number.

The second is observation of meteors as a method for study of certain phenomena and processes occurring in the upper layers of the atmosphere, which are of independent interest or which permit conclusions to be drawn concerning the properties of the atmosphere itself: formation of ions, their recombination, composition, diffusion; measurements of drift of meteor trails for determination of wind and turbulent movements in the upper layers of the atmosphere, and determination of density, pressure and height of the homogeneous atmosphere.

The third is study of the influence of meteor ionization on radio wave propagation. This influence is expressed, in particular, by the behavior of the sporadic E_s layer of the ionosphere.

We will mostly discuss problems involved in the second of these directions. Investigations in the first direction are essentially beyond the scope of this book and will be considered only briefly, primarily for familiarization with the measurement methods used in geophysical investigations.

2.2 Radar Equations. The apparatus used in radar observations of meteors is shown schematically in figure 2.1. Transmitter T, feeding antenna A, sends brief (of the order of 10^{-5} - 10^{-6} sec) radio wave pulses CD into space. If the pulses are incident on target P, some part of the wave energy is reflected (scattered); the reflected pulse (radar echo) can be received and amplified by the set. The distance to P can be determined by measuring the time elapsed from the radiation of a pulse by the set to reception of the echo: the velocity of the propagation of radio waves through the atmosphere is known with rather great accuracy.

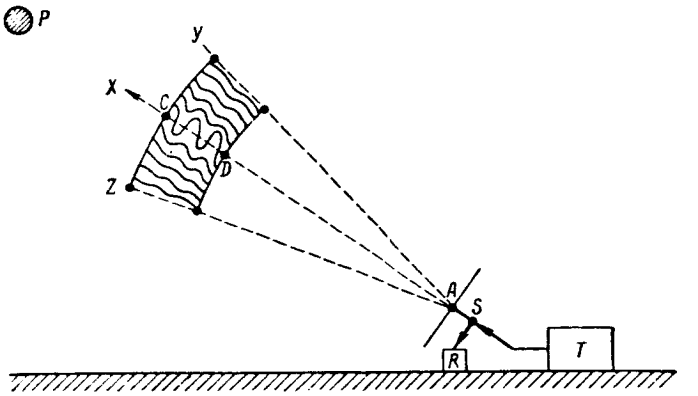

Figure 2.1. Diagram of radar observation of meteor.

In many cases the same antenna is used for transmission and reception. In such cases there is a switch S which connects the antenna to the transmitter at the time of its operation and switches the antenna to the receiver during the time between pulses (ref. 111). The duration of these intervals usually is thousandths of a sec (the pulse frequency is several hundreds per sec). By using a rotating directional antenna we can determine the direction to the target; in this direction the intensity of the reflected signals is maximum.

Intensity of the radar echo is dependent on the parameters of the set (strength, directivity of radiation, etc.), properties of the target and direction to it. We will consider a set (ref. 111) situated at the Earth's surface at the point O (fig. 2.2), which receives an echo from a target. The antenna, used for both reception and transmission, has a directional diagram OZZ'. We will assume that the target is situated on the axis OZ of the antenna beam.

If the transmitter radiated identically in all directions, the flux of radiated energy at the distance R to the target would be $\frac{P}{4\pi R^2}$, where P is the power radiated by the transmitter(in the brief period of its operation). However, the use of a directional antenna increases the energy flux by G times, where G is the absolute directional effect. Its equivalent scattering area (cross section) S_s can be used as a measure of the reflectivity of the target. The target also has always some scattering directional diagram, such as that shown by the dashed line around the point T (fig. 2.2). If, as shown in the figure, the main lobe of this diagram is directed precisely at the set, the flux of reflected (scattered) energy flowing to point O is amplified G times. The product $\sigma = S_s G$ is called the equivalent reflecting area (cross section) of the target. The strength of the reflected signal reaching the point O therefore can be represented by the expression

$$\frac{PG\sigma}{(4\pi R^2)^2}.$$

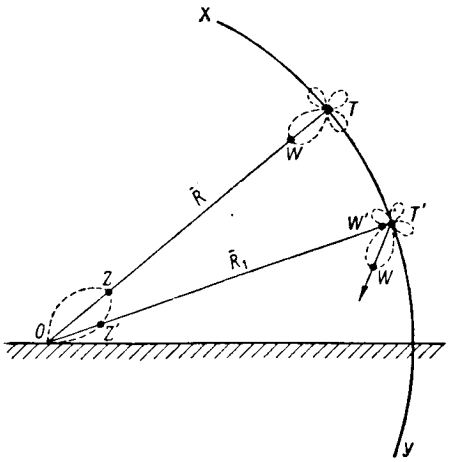

Figure 2.2. Scattering of radio waves from target.

If the antenna, when used for reception, is matched with the receiving part of the set, its equivalent absorbing area is equal (ref. 111) to $\frac{G\lambda^2}{4\pi}$. Therefore, the total quantity of energy ε fed to the first stage of the amplifier of the receiving set is

$$\varepsilon = \frac{PG\lambda^2\sigma}{64\pi^3 R^4}. \qquad (2.1)$$

The scattering factor can easily be determined for simple targets. For example, for a Hertz dipole, which is close to ordinary targets with respect to the values of the scattering factor, the equivalent scattering area S_s is $\frac{3\lambda^2}{2\pi}$ (if the dipole is shortcircuited at the input terminals and its axis is parallel to the electric vector of the incident waves), and the directional effect is G = 1.5. Therefore, for such a dipole

$$\sigma = GS_s = \frac{9\lambda^2}{4\pi}.$$

By substituting this value into equation (2.1) we obtain

$$\varepsilon = \frac{9PG^2\lambda^4}{(4\pi R)^4}.$$

If a plane or mirror antenna is used with an area of 400 m^2 and a transmitter with a pulse power of 100 kw, the pulse power reflected from the mentioned dipole, if the latter is at a distance of 100 km, will be about $\varepsilon = 10^{-11}$ w. This result shows the low strength of the reflected signals used in radar measurements of meteors.

2.3. Theory of Meteor Ionization. The physical theory of meteors discussed in the preceding section (Sections 1.2-1.5) applies primarily to processes influencing the luminescence of meteors. Now we will consider the ionizing effect of meteors, supplementing this theory.

Certain assumptions are made in the theories describing the motion of a meteor through the Earth's atmosphere. One of these is that a meteor particle undergoes individual collisions with air molecules. This is equivalent to the assumption that the meteor body is small in comparison with the length of the free path of molecules. This condition can usually be considered satisfied for not very bright meteors (ref. 500). According to another hypothesis, the energy of a meteor body lost directly to the radiation of the meteor body can be neglected. As pointed out in Section 1, if the diameter of the meteor body is less than 1 μ (micrometeorite), the greater part of its thermal energy is scattered by radiation; such bodies cannot create ionization. Therefore, such small meteor bodies, being too minute for radar observation, are not considered here.

The number of atoms (ref. 500) evaporating in 1 sec from the surface of a meteor body is

$$n = (\mu H)^{-1} mv \cos z \left(\frac{p}{p_{\max}}\right)\left(1 - \frac{1}{3}\frac{p}{p_{\max}}\right)^2. \qquad (2.2)$$

Atmospheric pressure at the level of maximum evaporation is

$$p_{\max} = \left[\frac{(2l/g)}{\lambda v^2 A}\right] m^{1/3} \cos z. \qquad (2.3)$$

In these equations v is the geocentric velocity of the meteor; m is its initial mass; μ is the mass of an individual atom of meteor matter; l is the latent heat of evaporation; z is the zenith angle of the meteor radiant; p is atmospheric pressure; H is the height of the homogeneous atmosphere; g is the acceleration of gravity; λ is the heat transfer coefficient (the ratio of the liberated thermal energy to the air mass through which the meteor passes, multiplied by $1/2\ v^2$); A is the form factor, equal to $A = am^{-2/3}$, where a is the cross section of a meteor at a right angle to its path.

Values from 0.7 to 1.0 are used for λ. The value A is not dependent on m and is only a function of the form of the meteor body and its density ρ. For a spherical particle $A = 1.21\ \rho^{-2.3}$.

Using equations (2.2) and (2.3), Kaiser (ref. 500) obtains the following expressions for the linear density n_1 of electrons (the number of electrons arriving per unit length of the meteor trail), created by the meteor

$$n_1 = \frac{9}{4} n_{\max} \left(\frac{p}{p_{\max}}\right)\left(1 - \frac{1}{3}\frac{p}{p_{\max}}\right)^2, \qquad (2.4)$$

$$n_{max} = \frac{4}{9}\beta(\mu H)^{-1} m \cos z. \tag{2.5}$$

From equation (2.3) we obtain

$$p_{max} = \frac{2gQ}{v^2}\left(\frac{9}{4}Hn_{max}\cos^2 z\right)^{1/3}, \tag{2.6}$$

where

$$Q = \frac{l}{\lambda A}\left(\frac{\mu}{\beta}\right)^{1/3} \tag{2.7}$$

is dependent on the properties of the meteor body and on β, determined as the probability that an individual atom, upon evaporating from the surface of a meteor body, will create a free electron.

Figure 2.3 shows a curve constructed by Kaiser on the basis of equation (2.4). Height h has been plotted along the x-axis and h is read from the level h_{max} at which the ionizing effect of the meteor is maximum: $n_1 = n_{max}$ (height H of the homogeneous atmosphere has been used as the unit of height measurement). The maximum ionization is proportional to the initial mass of the meteor body and is dependent on its velocity (by the ionization probability β).

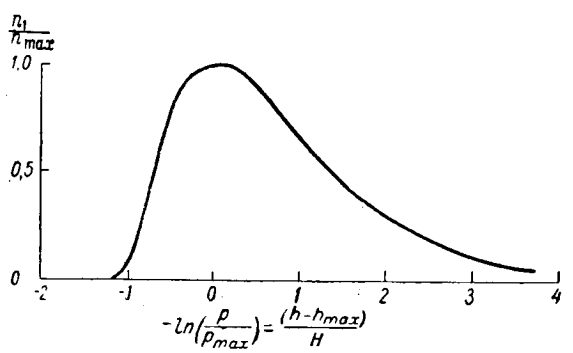

Figure 2.3. Ionization along meteor trail as function of height h.

2.4. Radio Wave Scattering by a Meteor Trail. The ion column developing during the motion of a meteor in the atmosphere contains charged particles of three kinds: positive and negative ions and free electrons. The equivalent scattering area of a particle with the mass m and the charge e (in electrostatic units) is

$$S_s = \frac{8\pi}{3}\left(\frac{e^2}{mc^2}\right)^2, \tag{2.8}$$

where c is the speed of light. The scattering has a directional diagram similar to the diagram of the Hertz dipole, and therefore has the directional effect G = 1.5. We then obtain

$$\sigma = GS_s = 4\pi\left(\frac{e^2}{mc^2}\right)^2. \tag{2.9}$$

Using this formula we obtain for a singly ionized atom of oxygen or nitrogen a value σ of the order of 10^{-34} cm^2. Using the radar equation (2.1) and substituting into it the corresponding numerical values, it can be confirmed that the concentration of positive ions in the ionized column of the meteor trail is too small for the trail to be detected by radar from a distance of about 100 km. Free electrons can play a considerably greater role because of their small mass: their scattering cross section is approximately 10^9 times greater than that of atoms.

The strength of a radar echo from a meteor trail containing n_1 electrons per unit length can be computed by the Lovell-Clegg method, proceeding on the assumption that the trail is narrow in comparison with wavelength (ref. 111). We will consider an element of an ionized column of a meteor trail with the length dx situated at the distance R from the set. The number of electrons which it contains is $N = n_1\,dx$, and the electric charge of this segment is therefore en_1dx and the mass mn_1dx. We then obtain for the scattering cross section

$$\sigma = 4\pi\left(\frac{e^2 n_1\,dx}{mc^2}\right)^2.$$

According to the radar equation (2.1), the strength of the reflected pulse received by the set is

$$\varepsilon_{dx} = \frac{PG^2\lambda^2}{16\pi^2R^4}\left(\frac{e^2 n_1\,dx}{mc^2}\right)^2. \tag{2.10}$$

To obtain the total strength of the radar echo, it is necessary to add the effect of all the elements of the trail, taking into account in this process the phase differences. This diffraction problem is clear from the diagram in figure 2.4, in which the circles represent the surfaces of identical phase of the waves originating from the transmitter 0. Assume these surfaces are $\frac{\lambda}{4}$ apart. The pulses returning to the set 0 after reflection at the point P_0 differ in phase by a half-period from those which arrive after reflection at the point P_1, but coincide in phase with the pulses returning from P_2, P_4, ..., P_{2n}, ... The part of the meteor trail from P_{-1} to P_1 is the first Fresnel zone. Using a vector representation of the pulses sent by individual points of the wave surface P_0, P_1, P_2, ..., in which the vector direction is given by the phase of the oscillations and the length by the amplitude of the oscillations, the problem of the

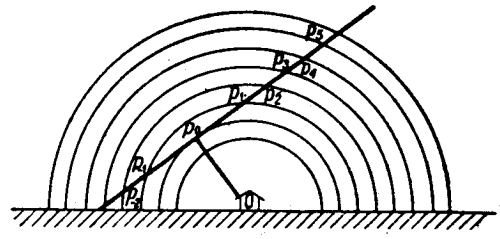

Figure 2.4. Conditions of normal reflection from ionized meteor trail. Circular arcs represent spherical wave surface alternating each one-fourth wavelength (scale is not observed: extent of first Fresnel zone P_{-1} - P_1 should be about 1 percent of length of segment OP_0).

addition of the oscillations, solved rigorously using Fresnel integrals from diffraction theory, can be reduced to a graphic construction (by use of Cornu spirals). In figure 2.5 a, each vector represents a signal returning to the receiver from a unit section of the meteor trail; the vector phase is dependent on the twice-travelled path from an element of the trail to the receiver. If the length of the segment Δx decreases, at the limit when $\Delta x \to 0$ we obtain Cornu spirals (fig. 2.5 b). In such spirals the length of the arc segments corresponds to the length Δx of elements of the trail.

After summing the expressions (2.10) for all elements of the trail, taking into account the phase differences caused by differences in the distances of the individual elements of the trail from the reception point, we obtain the total strength of the signal reflected from the meteor trail in the form (ref. 111)

$$\varepsilon = \frac{PG^2\lambda^3}{16\pi^2 R^3} n_1^2 \left(\frac{e^2}{mc^2}\right). \qquad (2.11)$$

For a typical meteor, ε is of the order of 10^{-11} w. Substituting this value into formula (2.11) we find that there are $n_1 \approx 10^{10}$ electrons per cm of the trail.

2.5. Radiants of Meteor Streams. Discovery of Daytime Streams. The usual method for determination of a radiant is the continuation (extrapolation) of the direction of movement of a group of meteors in the reverse direction: the point of intersection of the extrapolated paths gives the apparent position of the radiant. There are several methods for determination of radiants (ref. 111). The Hay and Stewart method, based on the fact that there will be mirror reflection at wavelengths shorter than 6 m, makes it possible to measure the coordinates of the radiants. The Clegg method uses a moving pencil-beam antenna set up at a single observation station. The McKinley-Millman method, on the other hand, is based on the use of poorly directed antennas at a wavelength of about 8 m set up at three stations approximately at the vertices of an equilateral triangle with 60 km sides.

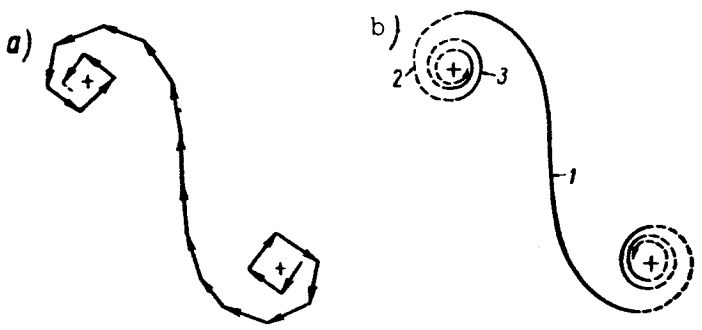

Figure 2.5. Graphic addition of oscillations scattered by individual elements of meteor trail; (a) sum of elements; (b) Cornu spiral: 1-3, zones.

The accuracy of measurement of the coordinates of the radiant is essentially dependent on the directivity of the directional diagram of the radar set. However, the construction of pencil-beam antennas, especially when it is necessary to change the direction of the antenna during measurements, involves technical difficulties. It is,therefore, of great interest to develop methods of determination of a radiant using poorly directed antennas. As previously mentioned, it was this approach which was used by McKinley and Millman. The same method was developed by Ye. I. Fialko (ref. 220) at the Tomsk Polytechnic Institute. In that study he uses the lobing effect of the directional diagram.

The use of radar methods made it possible to observe meteors in cloudy weather and during daytime. This led to the discovery of a large number of meteor streams which encounter Earth in the summer months; the radiants of these streams are situated close to the Sun. Among the principal streams not observed visually or photographically we should mention (ref. 111): the Perseids (June 3), which are characterized by the normal number N = 40 meteors/hour and a velocity of v = 28.8 km/sec in the Earth's atmosphere; the Arietids (June 8, N = 60, v = 37.6) and Taurids (July 2, N = 30, v = 31.5).

Some idea of the character of radar observations of sporadic meteors is given by the measurements of Ye. I. Fialko at Tomsk (refs. 218, 219 and 221a).

Regular radar observations of meteor activity are made in the USSR by many scientific institutions: Academy of Sciences of the Turkmen SSR, at Ashkhabad (ref. 10a), Academy of Sciences of the Tadzhik SSR, at Dushanbe (ref. 174a), the Khar'kov Polytechnic Institute (ref. 81a), the Engel'gardt Astronomical Observatory, at Kazan' (ref. 157a).

2.6. Measurement of Meteor Velocity. Photographic and visual observations of meteors make it possible to determine their velocity by three methods: from direct measurements of the length of the path and time, the oscillating mirror method and from the period of appearance of large streams. The extensive use of radar methods of meteor observations necessitated the creation of methods for measurement of velocity using radio waves. There already are several such methods (refs. 111, 218 and 500).

One of these methods is based on the scattering of radio waves from the ionized anterior part of the meteor. The echo from the meteor is recorded on the screen of a cathode ray tube with an intensity-modulated display. The echo is recorded photographically on tape which moves slowly at a right angle to the time scale. Measurements of this record make it possible to determine the relationship between time and distance, and this can be used in velocity determination. The echo from the anterior part is considerably weaker than the main echo, and the described method is therefore applicable only to a few particularly bright meteors.

A more sensitive method is based on observation of the diffraction of radio waves from an ionized meteor trail (Fresnel diffraction). Imagine a meteor moving along the ray $P_3 P_{-2}$ (see fig. 2.4) in the direction shown by the arrow. As the meteor approaches the point P_0 and comes to the points P_{-1}, P_{-2}, etc., the ionized trail forming behind the meteor will occupy new Fresnel zones. At the point O, where the receiving set is situated, signals will arrive which owe their reflection (scattering) to radio waves in new Fresnel zones, first even and then odd, and the amplitude of the resultant oscillations, as shown by the Cornu spiral (fig. 2.5), will first increase and then decrease. (This phenomenon has a rigorous optical analogy: the diffraction of light from a linear margin of a screen.) In actuality, observations show that the amplitude of reflected signals, following quite frequently one after the other, first increases and then decreases. During the time between successive maxima and minima the meteor moves a distance equal to the half-width of the Fresnel zone, which can be computed if the wavelength of the radio signals and the distance to the meteor R = OP is known. By knowing the distance (half-width of the zone) and the time expended by the meteor in moving this distance (the time between a maximum and the subsequent minimum of echo intensity on the screen of the cathode ray tube), we find the meteor velocity.

The apparatus, developed by the Tomsk Polytechnic Institute (ref. 218) for detection of the diffraction pattern during the flight of a meteor, uses a high pulse repetition rate (600 pulses/sec). In order to eliminate ambiguity in determination of slant range, the apparatus uses "split" sounding pulses at a frequency of 300 pulses/sec (after an ordinary pulse a split pulse is transmitted, followed then by an ordinary pulse, etc.).

Whereas the two preceding methods for the measurement of meteor velocity apply to the use of pulses, there are also methods based on the use of continuous waves. At the beginning of this section we presented facts concerning the occurrence of whistles during radio reception at the time of the flight of bright meteors. The whistle is caused by beats formed by interference of waves of slightly different frequency, propagating in a forward direction along the Earth from the transmitter, and waves reflected from the moving meteor; the frequency of the latter changes as a result of the Doppler effect. However, such a manifestation of the Doppler effect is only observed in very rare cases (meteors causing very strong ionization). The usual whistle is formed as a

result of variations of amplitude and frequency of radio waves during the formation of Fresnel zones (ref. 111). This makes the theory of the "Doppler whistle method" similar to the theory of the previously described diffraction method, but these two methods differ greatly from one another with respect to observation techniques, sensitivity and accuracy. The diffraction method (ref. 569) is more effective.

2.7. Fading of Meteor Echoes and Wind in the Upper Layers of the Atmosphere. Sufficiently prolonged echoes (such as more than 1 sec) sometimes are subject to fading, which is periodic and in most cases complex. Such fluctuations of amplitude have been investigated by Greenhow (ref. 411) and others. The period of fluctuations is proportional to wavelength, and for $\lambda = 8$ m varies from 0.04 to 0.4 sec. Periodic fluctuations can be attributed to the interference of beams reflected from two different points of a trail, which are in movement relative to one another. More complex echoes are associated with the presence of complex movements of the reflecting centers. Greenhow postulated (ref. 411) that these centers are formed as a result of the curvature of meteor trails in a nonuniform wind field in the upper layers of the atmosphere.

Data on these fluctuations and the drift of long trails, obtained by Greenhow from observations made at the meteor experimental station at Manchester University at Jodrell Bank (England), gave important information on winds in the upper layers of the atmosphere (refs. 411 and 412).

Manning, Villard and Peterson (refs. 568 and 569) used continuous waves rather than pulses. They observed fluctuations of echo intensity caused by interference between the Earth wave and a wave reflected from a moving meteor trail. The authors made their observations at Stanford in the United States.

The results of wind measurements made by various authors will be discussed in Chapter 9.

2.8. Scattering of Meteor Trails. Diffusion. The column of ionized gas, forming immediately after the flight of a meteor, gradually scatters under the influence of processes accompanying a decrease of the volumetric concentration of charged particles. The most important of these processes is diffusion, which results in a change of the volumetric density of electrons without a decrease of their linear density n_l. A mathematical investigation of this problem was published by Hexley in 1952. We will now give the principal results, using Kaiser's study (ref. 500) as a point of departure.

The diffusion equations for a cylindrical distribution of electrons and positive ions in the absence of a magnetic field can be written in the following form

$$\frac{\partial n_e}{\partial t} = \frac{D_e}{r}\frac{\partial}{\partial r}\left(r\frac{\partial n_e}{\partial r}\right) + \nabla\left(\frac{eEn_e}{m\nu_e}\right), \tag{2.12}$$

$$\frac{\partial n_i}{\partial t} = \frac{D_i}{r}\frac{\partial}{\partial r}\left(r\frac{\partial n_i}{\partial r}\right) - \nabla\left(\frac{eEn_i}{m_i\nu_i}\right), \tag{2.13}$$

where r is the radius of the cylinder, t is time, n_e and n_i are the electron and ion concentrations, D_e and D_i are the diffusion coefficents as given by the

kinetic theory of gases, m and m_i are electron and ion mass, ν_e and ν_i are the frequencies of collisions, e is electron charge, E is strength of the field created by the space charge; the ratios $\frac{eE}{m\nu_e}$ and $\frac{eE}{m_i\nu_i}$ are the velocities of drift of electrons and ions caused by the field E.

It can be assumed that in the main part of the cylindrical column the concentrations n_e and n_i, also their derivatives, differ little from one another. We can then simplify equations (2.12) and (2.13) and exclude E from them

$$\frac{\partial n_e}{\partial t} = \frac{D}{r}\frac{\partial}{\partial r}\left(r\frac{\partial n_e}{\partial r}\right), \tag{2.14}$$

the diffusion coefficient D is determined approximately from the ratio

$$D \cong \left(D_i + \frac{m\nu_e}{m_i\nu_i}D_e\right) : \left(1 + \frac{m\nu_e}{m_i\nu_i}\right).$$

According to the kinetic theory of gases

$$\frac{m\nu_e}{m_i\nu_i} = \frac{\lambda_i}{\lambda_e}\left(\frac{T_e}{T_i}\frac{m}{m_i}\right)^{1/2} \ll 1,$$

and

$$\frac{D_e}{D_i} = \frac{\lambda_e}{\lambda_i}\left(\frac{T_e}{T_i}\frac{m_i}{m_e}\right)^{1/2},$$

where λ_e and λ_i are the lengths of the free paths and T_e and T_i are electron and ion temperature. We can therefore write

$$D \simeq D_i\left(1 + \frac{T_e}{T_i}\right) = 2D_i, \tag{2.15}$$

if it is assumed that $T_e = T_i$.

Using the gas kinetic expression for D_i, and assuming that ions and neutral molecules have the virtually identical mass μ, we obtain

$$\left.\begin{aligned} D &= \frac{8}{3}\lambda_i\left(\frac{2kT}{\pi\mu}\right)^{1/2} \\ \lambda_i &= \left(\sqrt{2}\pi n_a\sigma_i^2\right)^{-1} \end{aligned}\right\} \tag{2.16}$$

where k is the Boltzmann constant, n_a is the concentration of particles in the atmosphere and σ_i is the mean classical diameter of ions and neutral molecules.

The initial radius of a meteor trail is of the order of the length of the free path λ_a: at heights of about 100 km, where these meteor processes occur,

this is a few cm. Since in our case we are concerned primarily with a meteor trail at a later stage of its development, when its diameter becomes considerably greater, it can be assumed that the initial distribution of ionization is linear, and in this case the solution of equation (2.14) assumes the form (ref. 500).

$$n_e = \frac{n_1}{4\pi Dt} \exp\left[-\frac{r^2}{4Dt}\right]. \qquad (2.17)$$

Taking into account the geomagnetic field, we obtain smaller values D_e and, therefore, smaller values E in the direction across the magnetic field. It can then be assumed that the meteor trail has an elliptical cross section. At some height the coefficient D for transverse diffusion becomes equal to the coefficient D_i and at great heights the field of the space charge changes its sign; therefore, $D < D_i$. This means that the slowly diffusing electrons retard the positive ions. The diffusion coefficient D_e for transverse diffusion decreases by $\frac{\nu_e^2}{(\nu_e^2 + \omega_e^2)}$ times, where ω is the gyroscopic angular velocity of the electrons. An estimate can be made showing that the condition $D_e = D_i$ is satisfied at a height where $\nu_e \approx 3 \cdot 10^5 \text{sec}^{-1}$. In actuality, this condition is satisfied if

$$\left(\frac{\omega_e}{\nu_e}\right)^2 \simeq 4\left(\frac{2m_i}{m}\right)^{1/2},$$

in which we can substitute the values $\omega_e \approx 10^7 \text{ sec}^{-1}$, $\frac{m_i}{m} \approx 6 \cdot 10^4$. Such a collision frequency occurs when there is a concentration of neutral particles of the order of $2 \cdot 10^{13} \text{ cm}^{-3}$, which corresponds to a height of about 100 km. Below this level the influence of the geomagnetic field is small.

L. A. Katasev has derived a formula for determination of the diffusion coefficient from radar observations of meteors by two receivers of different sensitivity (ref. 80).

Under the influence of diffusion an ionized meteor trail should assume a form close to a paraboloid of revolution, extending from the meteor downward. However, for many purposes it can be assumed for simplification that a narrow column of ionized gas is formed instantaneously behind the meteor, and there is subsequent radial diffusion.

In addition to diffusion, the decrease in the ionization space density can be influenced by a loss of electrons by recombination with positive ions and by attachment to neutral molecules with subsequent reciprocal neutralization of the positive and negative ions. These processes will be considered next.

2.9. Recombination and Attachment of Electrons. If, in addition to diffusion, we take into account the recombination of electrons with positive ions, it is necessary to replace equation (2.14) by (ref. 500).

$$\frac{\partial n_e}{\partial t} = \frac{D}{r}\frac{\partial}{\partial r}\left(r\frac{\partial n_e}{\partial r} - \alpha_e n_e^2\right), \tag{2.18}$$

where α_e is the recombination coefficient of electrons. It follows from equation (2.18) that the rate of change of linear electron density n_1 is

$$\frac{dn_1}{dt} = -2\pi\alpha_e \int_0^\infty r n_e^2\, dr.$$

It can be assumed as a first approximation that the change of n_e as a function of r has the same character as (2.17), and, in this case,

$$\frac{1}{n_1} - \frac{1}{n_1^0} \simeq \frac{\alpha_e}{8\pi D}\ln\frac{t}{t_0}, \tag{2.19}$$

$$n_e \simeq \frac{n_1^0}{t\left[4\pi D + \frac{1}{2}n_1^0\alpha_e \ln\frac{t}{t_0}\right]}\exp\left[-\frac{r^2}{4Dt_0}\right], \tag{2.20}$$

where $(4Dt_0)^{1/2}$ and n_1^0 are the initial value of the radius and the linear density of electrons (for $t = t_0$).

If electron attachment is taken into account, the equation must be supplemented by appropriate terms, to wit:

$$\frac{\partial n_e}{\partial t} = \frac{D}{r}\frac{\partial}{\partial r}\left(r\frac{\partial n_e}{\partial r}\right) - \beta_e n_e n_m + \varphi, \tag{2.21}$$

where β_e is the coefficient of electron attachment and φ is a term taking detachment into account. It is possible to obtain an upper estimate of this effect, if it is assumed that each electron which becomes attached to a neutral molecule is entirely lost from the interaction; neglecting detachment and integrating equation (2.21), we obtain

$$\alpha = \alpha_0 \exp\left[-\beta_e n_m t\right], \tag{2.22}$$

and recalling that n_e has a formula similar to (2.17),

$$n_e = \frac{n_1^0}{4\pi Dt}\exp\left[-\frac{r^2}{(4Dt)} - \beta_e n_m t\right], \tag{2.23}$$

where n_m is the concentration of molecules to which electrons can be attached.

According to the estimate made by Kaiser and Greenhow (ref. 505), the recombination rate in meteor trails is such that it corresponds to a value of the recombination coefficient not greater than $5 \cdot 10^{-10}$ cm^3/sec. This value is appreciably less than the value 10^{-8} obtained for the E layer of the ionosphere.

The upper limit of the recombination coefficient can be obtained from a consideration of echo duration. Computations reveal that if the initial linear density of electrons (the number of electrons per unit length of the trail) is appreciably greater than 10^{12} cm^{-1}, the echo will be maintained as long as the space density of electrons near the axis of the trail does not decrease to a critical value. This axial space density of electrons in the course of the time t after the formation of the trail cannot exceed the value

$$2\left[\alpha_e t \ln\left(\frac{t}{t_0}\right)\right]^{-1},$$

where t_0 is found from the condition that $(4Dt_0)^{1/2}$ is the initial value of the radius of the trail, which is approximately equal to the length of the free path λ_a of a molecule. Assuming that this expression is equal to critical density, it is possible to obtain the following relation (ref. 500) for the maximum possible duration of an echo τ_∞

$$\tau_\infty \ln\left(\frac{4D\tau_\infty}{\lambda_a^2}\right) = \frac{2\lambda^2}{\pi\tau_e}\left(\frac{e^2}{mc^2}\right) \qquad (2.24)$$

Greenhow's observations at 4.2 m reveal that τ_∞ can exceed 60 sec; this agrees with the previously stated value τ = 102 sec obtained by Ye. I. Fialko (ref. 218), who used observations at 10 m. Using these values τ_∞, it is possible to employ equation (2.24) to obtain the estimate $\alpha_e \leqslant 3.5 \cdot 10^{-11}$ cm^3/sec. However, according to the measurements made by McKinley and Millman at 9.1 m, the maximum duration of an echo is 30 min, which decreases the upper estimate of the recombination coefficient to the value $\alpha_e \leqslant 4.5 \cdot 10^{-12}$ cm^3/sec.

In order to estimate the maximum possible influence of attachment of electrons, it is possible to use equation (2.23). This equation shows that attachment can be neglected if $\beta_e n_m t \ll 1$. The concentration of oxygen molecules can be used in this case as n_m. According to Kaiser's computations (ref. 500),

$\beta = 10^{-15} - 10^{-16}$ cm^3/sec. The principal observed influence of electron attachment should be a decrease in echo duration and a decrease of the number of persistent echoes.

2.10. Distribution of Characteristic Heights of Meteors. Before proceeding to a consideration of the unusually interesting problem of the measurement of the structural parameters of the upper layers of the atmosphere by radar measurements of meteors, it is necessary to become familiar with the theory of the vertical distribution of meteors. Such a theory was developed by Kaiser (ref. 500). He adopted a distribution function for the masses of meteor bodies in the form

$$\nu_m \, dm = bm^{-s} \, dm, \tag{2.25}$$

where b is a constant dependent on the total flux of meteors (i.e., the total mass of meteor matter falling to Earth in a unit time). Kaiser considered two cases:

(a) meteor streams consisting of groups of uniform velocity with a well-expressed radiant at a point with the zenith distance z;

(b) groups of sporadic meteors of a selected velocity whose reflection points (i.e., imaginary points in the sky from which the radio waves reflected by meteor particles arrive) in their angle of elevation above the horizon are grouped closely around the angle of elevation φ_m.

Assume that the plane of the echo from a meteor stream (i.e., the plane in which lie the radio waves incident on and reflected by meteor particles) forms the angle $\frac{\pi}{2} - \theta$ with the horizontal plane. The normalized vertical distribution observed in an element of the angle $\theta - (\theta + d\theta)$ for meteors with a particular velocity v is represented by Kaiser in the form

$$\nu_1^*(x_1) = \left[\frac{3e^{x_1}}{2e^{3x_1/2} + 1} \right]^{3(S-1)}, \tag{2.26}$$

where $x_1 = \frac{(h - h_1)}{H}$; h_1 is the height where the pressure p_1 and the minimum detected linear density are related to one another by expression (2.6), in which p_{max} and n_{max} should be replaced by p_1 and n_1. The absolute strength of the echo in the element $\theta - (\theta + d\theta)$ is approximately proportional to the expression

$$\left[\frac{\cos^{3/2} \theta S^2}{\theta} \right]^{S-1} \cos^2 \theta,$$

where S (θ) is the polar directional diagram of the antenna (for amplitude) in the echo plane.

The total vertical distribution for a meteor stream is obtained by integration of the elementary distribution (2.26) for the echo plane, taking into account the changes h_1 (or at least n_1) and echo strength. For sporadic meteors the total distribution can be obtained by the successive averaging of the distribution of heights for all echo planes intersected by the antenna beam, taking into account the distribution of sporadic radiants.

The properties of vertical distribution are as follows. For meteors of a single stream, the mean (characteristic) height $\bar{h}$ is close to some height h_m, at which the pressure p_m is determined by the formula

$$p_m = \frac{2GQ}{v^2}\left(\frac{9}{4}Hn_m\cos^2 z\right)^{1/3}, \qquad (2.27)$$

where n_m is the minimum linear density of electrons in the meteor trail detected at the height $\bar{h}$ in the direction of the maximum of the directional diagram of the antenna in the echo plane. Such a relation is also correct for a group of sporadic meteors satisfying this condition (b). The width of the vertical distribution, measured by the deviation δh from the mean height, is dependent only on the height of the homogeneous atmosphere and the exponent in the mass distribution law for meteors.

Ye. I. Fialko (ref. 219) pointed out that the mean characteristic height of the detected meteors is dependent on the parameters of the radar set, but this dependence is poorly expressed. An increase of the sensitivity of the apparatus leading to an increase of the number of recorded meteors by 1-2 orders of magnitude changes the mean characteristic height by only 5-10 km.

A change of the height of atmospheric sounding is achieved for the most part by use of meteors with different velocities.

In order to increase the height of the studied layer, it is necessary to use fast meteors with a radiant having a relatively low position and use apparatus with high directivity, high transmitter power and high receiver sensitivity.

In order to investigate the lower layers of the meteor zone, it is necessary to use reflections from slow meteors whose radiant has a relatively high position, using apparatus of low power and low sensitivity with a half-wave element.

2.11. Determination of Structural Parameters of the Atmosphere. Determination of such parameters, characterizing the structure of the upper layers of the atmosphere, as pressure p and the height H of the homogeneous atmosphere is based on an investigation of meteor heights. Evans (ref. 379), at the meteor experimental station at Jodrell Bank (53°N), measured the distribution of heights for several groups of sporadic meteors with a particular velocity (from 20 to 60 km/sec), and also for several meteor streams. In the period from January through July, 1952, he measured the heights and velocities of 381 sporadic meteors. The

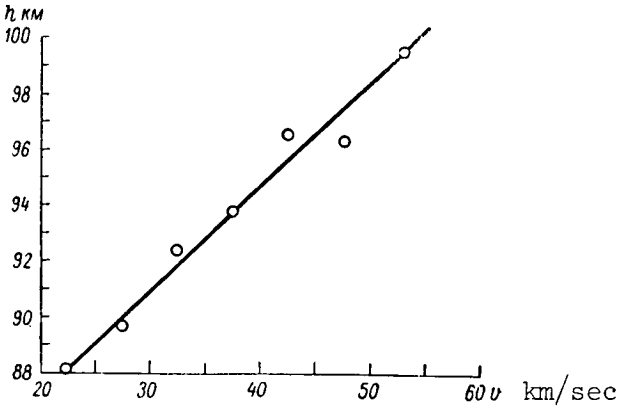

Figure 2.6. Mean height h of meteors as function of their velocity v.

observational results were broken down into seven groups, and for each group he determined the mean height h and the deviation δh (fig. 2.6). As pointed out in Section 2.10, the deviations δh are dependent only on H and the exponent S in the meteor mass distribution law (2.25). The value $S = 2.00$ was adopted for sporadic meteors. By knowing δh for different heights from observations (for these seven groups) Kaiser (ref. 500) computed H for these heights (fig. 2.7). The straight line drawn through these seven points was obtained by the least squares method.

Absolute values of atmospheric pressure at the height h can be computed using formula (2.27). This requires that the function Q be known; Q is dependent on the meteor constants. It is also necessary to know the ionization

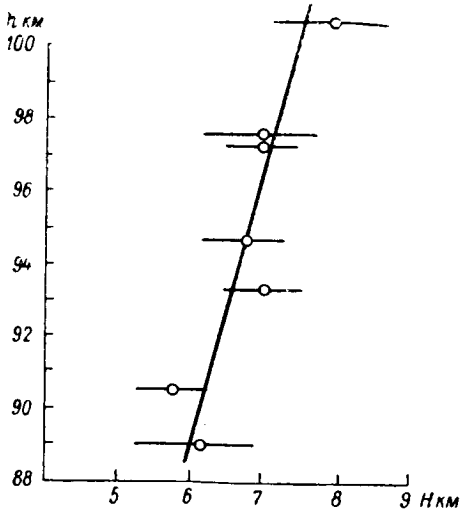

Figure 2.7. Height H of homogeneous atmosphere at different heights h above sea level as indicated by meteor observations at Jodrell Bank.

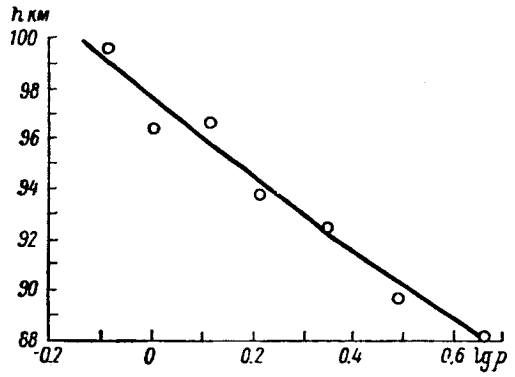

Figure 2.8. Pressure p in dynes/cm^2 at different heights h as indicated by meteor measurements at Jodrell Bank.

probability, which can change with velocity v (2.7). The problem is greatly simplified, because Q need be known only for some single velocity, giving pressure at the same height; this can also be used to compute the pressure change with height by integration of the equation

$$\frac{d \ln p}{dh} = -\frac{1}{H},$$

using the already known values H (fig. 2.7). The results obtained by Kaiser are shown in figure 2.8.

We note that if the molecular weight of air is assumed to be constant, temperature T can be computed from the known values H (fig. 2.7). Having T and p (fig. 2.8) as functions of height, Kaiser computed air density (fig. 2.9).

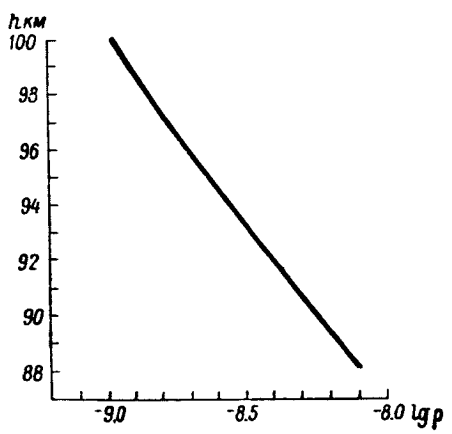

Figure 2.9. Air density ρ in g/cm^3 at different heights as indicated by meteor measurements at Jodrell Bank.

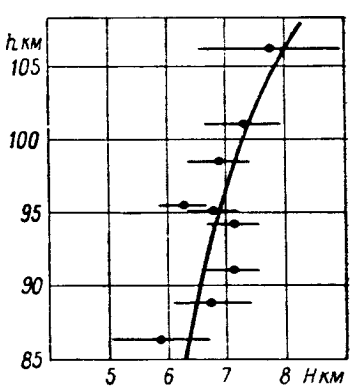

Figure 2.10. Height H of the homogeneous atmosphere on basis of radar measurements.

Evans later made a more detailed investigation of observations of meteor radar echoes (ref. 379). He broke all observations down into nine groups for different meteor velocities, and used the described method to obtain the values of the height H of the homogeneous atmosphere, air pressure and density for heights of 85-105 km. His results (refs. 379 and 501) are shown in figures 2.10 - 2.12.

2.12. Meteor Fragmentation. In Section 1.6 we mentioned Jacchia's meteor fragmentation hypothesis (ref. 475). In 1957 Greenhow and Neufeld (ref. 412) reported that they had obtained proof of the reality of the fragmentation of meteor bodies by the observation of diffraction phenomena.

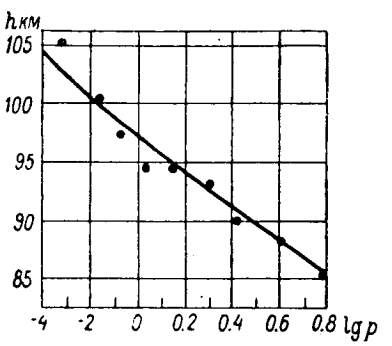

Figure 2.11. Pressure p in dynes/cm^2 at different heights as indicated by measurements at Jodrell Bank.

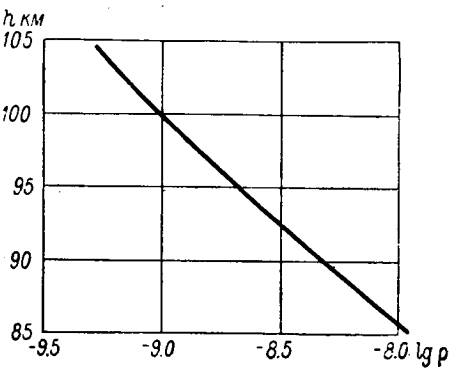

Figure 2.12. Air density ρ in g/cm^3 as indicated by measurements at Jodrell Bank.

Diffraction of radio waves on ionized meteor trails was discussed in Sections 2.4 and 2.6 (figs. 2.4 and 2.5). Greenhow and Neufeld investigated radar echoes from meteors, simultaneously from two points 20 km apart. They noted that the diffraction fluctuations of echo intensity are frequently clear, if the reflection occurs from the upper point of a meteor trail, but the fluctuations become considerably weaker (or disappear entirely) in an echo from a point situated several km farther along the trail. Greenhow and Neufeld attribute this fading of the diffraction pattern to the progressive fragmentation of a meteor body as it moves through the atmosphere. Each meteor fragment should create its own diffraction pattern, and, when the mutual withdrawal of fragments along the trail becomes comparable to the length of the Fresnel zone (fig. 2.4), the diffraction pattern should be "washed out." A velocity difference of 1 km/sec is adequate to wash out the first diffraction maximum on a 1 km path.

CHAPTER 2. STRUCTURE OF THE ATMOSPHERE DETERMINED BY OBSERVATIONS OF THE TWILIGHT SKY

3. Twilight Observations Method

Night does not begin immediately after the Sun sets below the horizon. Day and night are separated by twilight. During the rather prolonged period of twilight the sky brightness rapidly but smoothly and gradually decreases (by thousands of times) before attaining its more or less constant nighttime value. The latter occurs when the Sun is 15-18° below the horizon.

3.1. Photometric Observations of Twilight as a Method for Sounding the Atmosphere. The first steps to the correct explanation of the twilight phenomenon were taken in the Eleventh Century by the outstanding Arab scientist Ibn-Alhazan, the author of a famed study on optics: "And after setting of the Sun its rays continue to illuminate the high layers of the atmosphere." At that time not only was the light scattering phenomenon not known, but not even the law of refraction had as yet been discovered, and information on theoretical optics was limited to the laws of linear propagation and reflection of light. Assuming that twilight illumination occurs as a result of reflection of solar rays from the upper boundary of the atmosphere, Alhazan was able to compute the height of the Earth's atmosphere. Proceeding on the basis that night begins when the angle of depression of the Sun is 19° (end of twilight), he determined by a geometric construction that the height of the atmosphere is 68 km. This was a great discovery, anticipating the broad possibilities of study of structure of the atmosphere by twilight observations discovered in our day.

The light scattering phenomenon was discovered and explained in the second half of the Nineteenth Century. The studies of the famed English physicist Rayleigh in explaining the blue color of the sky were of major significance at that time. Daytime and twilight illumination are created by the scattering of solar rays by air molecules and aerosol particles suspended in the atmosphere (water droplets, dust particles, etc.). The light intensity scattered by a gas is proportional to the density of the latter. After sunset, sky brightness and the illumination of the Earth from the sky decrease rapidly (see the twilight curve in fig. 3.3), because the lower part of the atmosphere gradually plunges into the Earth's shadow and the solar rays illuminate only its upper part. Air density decreases with height, and, as the Earth's shadow continues to rise, scattering of the solar rays occurs in increasingly less dense layers. From sunset to the time of onset of night the shadow BE (fig. 3.1) cast by the Earth successively passes through all the layers of the atmosphere: this begins with the lowest layers and ends in the highest layers where the Earth's air envelope joins interplanetary space (1,000-2,000 km above the Earth's surface). Every day nature itself "carries out" optical sounding of the atmosphere

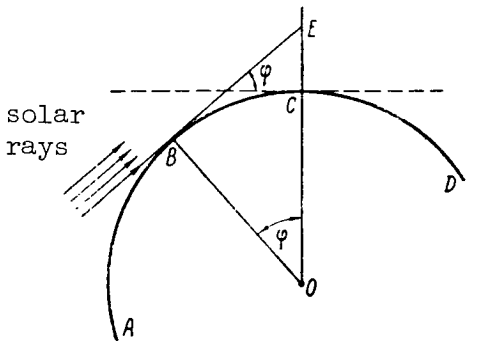

Figure 3.1. Geometric representation of twilight.

throughout its entire thickness. The Earth's shadow at the observer's zenith rises several kilometers each minute, requiring about an hour or more to move the entire path from the troposphere to the upper limits of the atmosphere (the exact time is dependent on the geographic latitude of the place and season of the year: at Leningrad, in June, the Earth's shadow in general does not emerge from the limits of the atmosphere during the entire night, and twilight continues from sunrise to sunset--the "white nights").

We now will consider whether it is possible to use the twilight phenomenon for study of the structure of the atmosphere up to its highest layers. The existence of a proportionality between gas density and the intensity of light which the gas scatters makes it theoretically possible to determine density of the upper layers of the atmosphere from photometric observations of twilight. However, because of the complex character of the phenomenon of atmospheric light scattering, there are great theoretical difficulties involved in the practical implementation of this method. As a result of a number of studies by V. G. Fesenkov, published in 1923-1955, it was possible to develop the general outlines of the theory of the twilight method (refs. 207-211, 215, and 216). After the first careful photometric measurements of the twilight, made in 1916 by Fesenkov and later by N. M. Shtaude (ref. 254) and others, this method came into systematic use for investigation of the structure of the atmosphere, and observations were accompanied by work on improvement of the theory (refs. 31, 55, 56, 103, 147, 167-169, 235, 241, 255-257 and 261). Systematic observations of the twilight sky were formulated at the Abastumani Astrophysical Observatory of the Academy of Sciences of the Georgian SSR. Such observations have been made there by T. G. Megrelishvili continuously since 1942, using highly sensitive electrophotometric apparatus (refs. 116-119). Beginning in the 1920's, work on the study of the atmosphere by the twilight method has been done repeatedly in other countries as well (refs. 298, 310, 360, 461, 462, 513, 525, 545, 705 and 712), especially in Czechoslovakia (refs. 24, 551 and 553) (an additional bibliography of studies of the twilight method can be found in references 24, 119, 229 and 254).

3.2. Theoretical Principles of the Method. We now will discuss the geometric aspects of the twilight phenomenon. Assume ABCD (fig. 3.1) is the surface of the Earth, point O is the center of the Earth, the dashed straight line is the horizon for observer C, BE is the direction of the solar rays, the angle φ is the depression of the Sun below the horizon ($\varphi = z_\bullet - 90^\circ$, where $z_\bullet$ is the zenith distance of the Sun), CE is the desired height h_{shad} of the Earth's shadow (shadow of the solar rays), OC = r, and OB is the normal to the direction of the solar rays tangent to the Earth at point B. We find from the triangle BOE that OB = OE cos φ or r = (r + h) cos φ and hence

$$h_{shad} = \frac{1-\cos\varphi}{\cos\varphi} r = r(\sec\varphi - 1) = r(\operatorname{cosec} z_\odot - 1). \qquad (3.1)$$

At each moment of twilight time only that part of the atmosphere is illuminated by direct solar rays which lies above boundary BE of the shadow. But not all layers of the illuminated part of the atmosphere have an identical role in the scattering of solar rays. Long ago V. G. Fesenkov (ref. 207) pointed out a property of twilight phenomena which is most important for the use of twilight observations for purposes of optical sounding of the atmosphere: at each particular moment the twilight phenomenon is produced by some layer of relatively small thickness. The parts of the atmosphere lying below this layer either are completely excluded because, when the angle of depression of the Sun is sufficiently great, the solar rays pass above these parts (region below shadow BE in fig. 3.1), or because the solar rays are exceedingly attenuated by considerable absorption. However, the parts of the atmosphere lying above such a layer also have a relatively small part in the phenomenon because of their small density, which decreases rapidly with height. There is a relatively thin effective scattering layer, whose height increases as the angle of solar depression increases. This can be illustrated for the visible region of the spectrum by the following data on brightness of the twilight caused by different air layers for $z_\bullet = 97^\circ$, according to V. G. Fesenkov (ref. 207)

Layer, km	25--35	35--45	45--55	85--95
Twilight brightness, %	0.204	6.82	33.4	3.01

If allowance is made for attenuation of the solar rays caused by molecular scattering along their path through the atmosphere (neglecting aerosol scattering and absorption by water vapor, ozone, etc.), the green rays passing over the Earth's surface h_0 (over point B, fig. 3.1) at different minimum heights are attenuated n times; according to reference 207 the values n will be as follows

h_0 km	0	1	2	3	4	6	8	10	12	14	18	26	30
n	575	269	145	73	45	19.2	9.8	5.5	3.5	2.4	1.5	1.11	1.03

The attenuation of the green rays passing through the lower layers of the atmosphere, therefore, is so great that they have very little effect in illumination of the twilight sky.

These circumstances make it possible to simplify the computations in a first-approximation theory considerably. This has been done in the "twilight ray" method proposed by V. G. Fesenkov, later developed in detail by N. M. Shtaude.

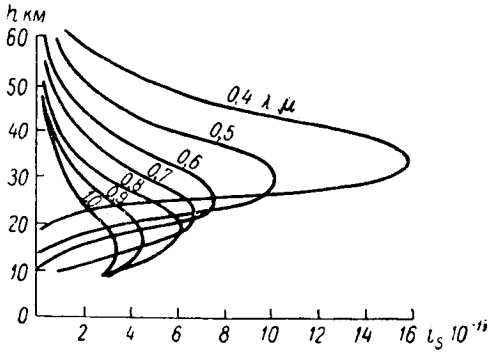

Figure 3.2. Structure of Earth's shadow at different wavelengths λ.

3.3. Structure of the Earth's Shadow in Rays of Different Wavelength. More complete computations show that the shortest distance of the twilight ray to sea level h_0, which in the approximate "twilight ray" theory is considered a constant number, in actuality changes somewhat as a function of $z_\bullet$, most rapidly at the time of the bright part of twilight (ref. 255). With an increase of λ the shortest distance to h_0 decreases, and there is also a gradual change of the form (structure) of the Earth's shadow; at large λ the twilight ray becomes so ill-defined, "washed out," that the use of the twilight ray method is no longer sound.

The cited numerical values n apply to the relatively shortwave region of the spectrum (to the green rays). Figure 3.2 shows the structure of the Earth's shadow in rays of different wavelength, from 0.4 to 1 μ, according to computations made by T. G. Megrelishvili and I. A. Khvostikov (ref. 121). These curves apply when $z_\bullet = 93.4^\circ$; observations are made at a point in the sky situated on the solar vertical at an altitude of 20° above the horizon. Light intensity i_S has been plotted along the x-axis (the extra-atmospheric intensity of solar radiation of a particular wavelength was used as a unit); i_S is the intensity of light scattered by the atmosphere at different heights above sea level h_0 (these heights have been plotted along the y-axis). The Earth's shadow passes at a height of 9 km at this point of the sky, when $z_\bullet = 93.4^\circ$. Directly above the boundary of the shadow i_S is extremely small for $\lambda = 0.4 \cdot 0.6\ \mu$. However, for $\lambda \geqslant 0.7\ \mu$, the value i_S is an appreciable value, even directly at the boundary of the shadow. There is also a decrease of the height h_{twi}, at which i_S has a

maximum value. The curves in figure 3.2 can be used to determine easily the following value h_{twi}:

λ μk	0.4	0.5	0.6	0.7	0.8	0.9	1.0
h_{twi} km	33	29	25	21	18	16	14

It must be remembered that a strong absorption of atmospheric light by water vapor sets in near $\lambda \simeq 0.7\,\mu$. The influence of this absorption is manifested, in particular, by a cutoff of the lower part of the i_S curves (i.e.), the part lying below the maximum). As a result, there is an increase of h_{twi} and the twilight ray becomes narrower (ref. 121). If atmospheric light absorption by water vapor is taken into account in the theory of twilight phenomena, it may be possible to extend the conclusions drawn on the basis of the twilight ray concept to certain parts of the spectrum in the region $\lambda \simeq 0.7\,\mu$. However, such a theory has not yet been developed and, therefore, a sufficiently reliable layer-by-layer sounding of the atmosphere by the twilight ray method can be considered possible only in the relatively narrow region of the spectrum 0.4-0.6 μ. With a decrease of λ there is intensification of the hindering effect of secondary light scattering.

3.4. Atmospheric Structure Determined by Twilight Observations. We now will discuss analysis of the observations made photographically (ref. 256) (Table 3.1). The spectral sensitivity of the photographic plates used was such that the results of the photometric analysis can be applied to the spectral region $\lambda = 0.44\,\mu$.

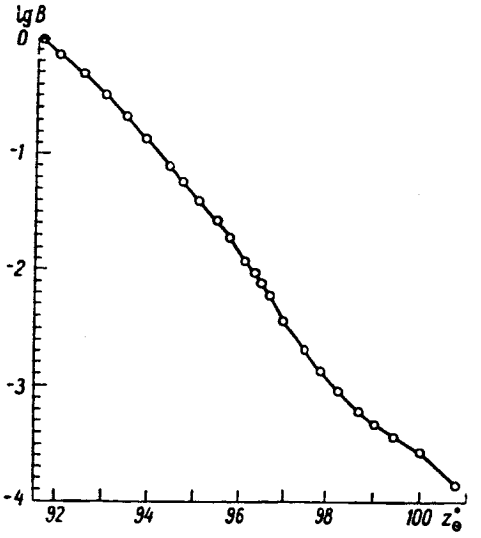

Figure 3.3. Twilight curve.

TABLE 3.1. ANALYSIS OF A TWILIGHT CURVE MEASURED AT PULKOVO IN THE SUMMER OF 1934 (FROM N. M. SHTAUDE).

No. of observations	$z_\odot$	lg B	h_{twi} км	lg p мм	lg ρ g/см³
1	2	3	4	5	6
1	91° 37′	0.000	25.0	1.27	5,60
2	92 02	1.854	26,9	14	46
3	92 32	693	29,8	0.96	27
4	92 59	528	32.6	79	08
5	93 30	333	36.0	59	6.86
6	93 55	147	39.3	41	66
7	94 25	2.928	43.4	19	42
8	94 46	764	46.5	02	24
9	95 06	613	49,7	1.87	07
10	95 25	460	53,0	70	7,88
11	95 43	300	56,2	55	72
12	96 06	106	60,7	36	51
13	96 18	2,020	63.2	1.23	7,37
14	96 28	3.926	65.3	14	27
15	96 38	808	67.4	04	10
16	97 02	590	72.8	2.84	8.94
17	97 27	36	78.7	61	68
18	97 50	17	84.6	42	42
19	98 15	4.99	91.2	24	15
20	98 42	82	98.8	06	9.89
21	99 02	68	104.6	3.96	74
22	99 27	58	112.3	83	56
23	100 02	48	123,7	64	34
24	100 47	18	139,2	42	10

Column 2 of Table 3.1 gives the zenith distance of the Sun at the time of measurement; column 3 gives the logarithm of the measured sky brightness (at the zenith); column 4 gives the height of the twilight ray, i.e., the height to which the computed values of atmospheric pressure (column 5) and density (column 6) should be applied. Figure 3.3 also shows the twilight curve, constructed using the data in Table 3.1 (columns 2 and 3). The sky brightness corresponding to the first measurement arbitrarily has been assigned the value unity (relative measurements). Pressure is indicated in mm Hg and density in g/cm^3. The value p was computed using a formula relating p to the measured brightness of the twilight sky at the zenith

$$B = C_1(1+\cos^2 z_\odot)\frac{e^y-1}{Y}p, \tag{3.2}$$

where C_1 is the proportionality factor, $Y = \tau(z) - \tau(z_\bullet)$, and τ the optical thickness of the atmosphere in directions determined by angle z or $z_\bullet$.

After obtaining p as a function of height h, we can find gradient $\frac{dp}{dh}$, and hence, using the equation of atmospheric statics

$$dp = \rho g\, dh,$$

we can also find the density

$$\rho = \frac{1}{g}\frac{dp}{dh}, \tag{3.3}$$

where g is acceleration of gravity.

The values of the logarithm of density computed using formula (3.3) are given in column 6 of Table 3.1. For comparative purposes figures 3.4 and 3.5 also give the values of pressure and density obtained by direct measurements (ref. 371), using radiosondes and instruments carried aloft in rockets.

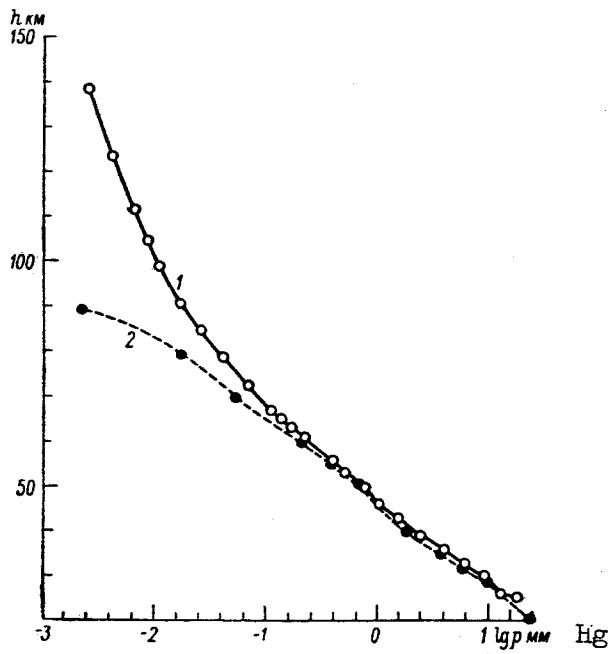

Figure 3.4. Air pressure at different heights determined by twilight (1) and direct (2) methods.

Comparison of the curves reveals that the variation of pressure obtained by twilight observations p_{twi} to a height of 60 km is close to that obtained by direct measurements, but above the 65-70 km level systematically exceeds the pressure value p_{rock}, measured using rockets. The twilight values of density

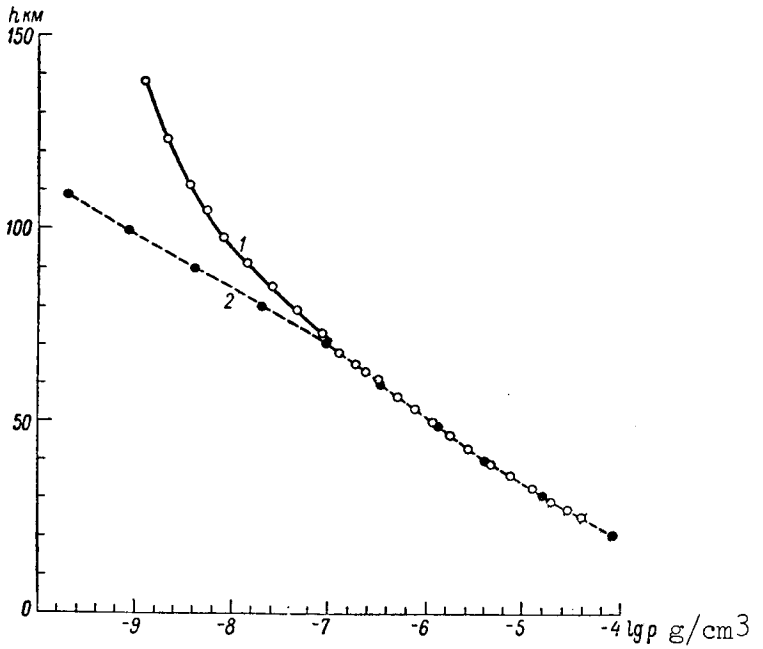

Figure 3.5. Air density at different heights determined by twilight (1) and direct (2) methods.

ρ_{twi} completely coincide with directly measured ρ_{rock} to a height of 70 km, but above this level the curves do not coincide.

3.5 Possible Sources of Excess Brightness. Up to heights of 60-70 km the approximate theory of twilight, based on the concept of the twilight ray, satisfactorily explains the behavior of the phenomena. Brightness measurements of the twilight sky at the zenith, analyzed using the twilight ray formulas, give the correct values of air pressure and density in the stratosphere to heights of 60-70 km. The relative simplicity of the observations and their analysis in such cases make it feasible to use the twilight method systematically for study of atmospheric structure and the changes occurring in it. At great heights the "excess" of pressure $p_{twi} - p_{rock}$ and density $\rho_{twi} - \rho_{rock}$, obtained from the twilight curves, increases systematically with height. The question naturally arises as to what factors are responsible for such large discrepancies, i.e., the reasons for the large "excess" of brightness of the twilight sky at large solar zenith distances ($z_\odot > 97^\circ$), increasing systematically with $z_\odot$. It is clear that there must be additional sources of luminescence of the upper layers of the atmosphere not taken into account in this theory. In general, there can be three such additional sources of luminescence.

The first of these is multiple light scattering. The theory took only first-order scattering into account. It is known from the theory of the brightness of the daytime sky that as a result of multiple scattering of light,

i.e., the effect of self-illumination of the atmosphere, brightness increases by several tens of percent (in dependence on $z_\bullet$, state of the atmosphere, etc.). It is extremely probable that under conditions of twilight illumination the percentage of multiple scattered light is greater than first-order scattering in comparison with daytime, and increases with an increase of $z_\bullet$.

The second source of additional luminescence of the atmosphere can be related to the scattering of light by aerosols. The upper layers of the atmosphere undoubtedly contain some quantity of suspended particles of various kinds (dust particles, water droplets, ice crystals). If it is found that their quantity in the upper layers of the atmosphere is great, the solar rays scattered by them could increase the brightness of the twilight sky considerably.

Finally, in addition to the scattering of light by atmospheric particles there can be luminescence (fluorescence) of air excited by the solar rays. As will be discussed, under certain conditions luminescence of the sky can actually be observed.

The development of a full theory of twilight phenomena which would rigorously take into account all these types of atmospheric luminescence involves great difficulties, some of which cannot be overcome. However, important results were recently obtained in this direction, not only providing a sounder basis and expanding the possibilities of the use of this method for study of structure of the atmosphere, but also coming closer to explanations of certain new phenomena.

These problems will be considered in the following sections.

4. Theory of the Twilight Method, Including Multiple Light Scattering

A rigorous treatment of the problem, including higher-order scattering, leads to an integral equation with three unknown variables of the Fredholm type, which cannot be solved. The result is also dependent on the atmospheric indicatrix of scattering. The latter has been studied inadequately, and possibly changes somewhat from day to day. V. G. Fesenkov considerably improved the twilight method for study of the atmosphere.

4.1. Stratospheric Twilight. In order to facilitate computations of the value of secondary light scattering, V. G. Fesenkov used a considerably simplified approach to the problem. His idea was that twilight in the stratosphere and in the still higher layers of the atmosphere (for brevity, we will use the term stratospheric twilight) produces twilight in the troposphere acting like an external light source, such as the Sun, situated above the observer's horizon, produces luminescence of the sky (ref. 208).

The fact is that light scattering in the lower layers of the atmosphere, which at twilight are in the Earth's shadow, is only higher-order scattering (self-illumination of the atmosphere), since they are not illuminated directly by the Sun. In the higher layers, lying above the Earth's shadow, the higher-order scattering effect, however, is negligibly small, and, as is true from

general considerations, is almost rigorously proportional to first-order scattering. Accordingly, Fesenkov postulates that stratospheric twilight, dependent on the luminescence of rarefied and relatively extremely distant atmospheric layers, is an external source relative to the lower layers of the atmosphere (for brevity we will call them tropospheric layers).

After solving the formulated problem in this way, Fesenkov computed stratospheric twilight in the entire sky for different solar depressions, investigated the illumination of the clear daytime sky for the purpose of determining the indicatrix of scattering, and drew conclusions concerning the influence of the thickness of the atmosphere on sky illumination (ref. 208). The following values were obtained for the indicatrix of scattering $f(\varphi)$; the values show great asymmetry of the indicatrix, especially for small scattering angles φ

φ°	10	20	30	40	50	60	70	80	90
$f(\varphi)$ . .	154	105	82,5	65	49	36.5	28.9	25.2	23.4
φ°	100	110	120	130	140	150	160	170	180
$f(\varphi)$ . .	23,0	23,0	24,8	25,8	26,6	27,3	27,2	27,1	27,0

After deriving a simplified formula for computation of brightness B_1 of stratospheric twilight on the basis of these concepts, Fesenkov computed values B_1 in arbitrary units for 49 different points in the sky (for azimuths A, read from the solar vertical equal to 0, 30, 60, 90, 120, 150 and 180; zenith distances z of points in the sky equal to 80, 70, 60, 50, 40, 30 and 0°) for four values of the zenith distance of the Sun $z_\odot$ equal to 92, 94, 96 and 98°. After deriving an expression (the formulas will be cited at the end of this section with the refinements recently made by Fesenkov) for tropospheric twilight produced by elementary light sources with area sin z dz dA and surface brightness $B_1(z, A)$, Fesenkov carried out graphic integration for the entire sky and computed the brightness of tropospheric twilight B_2 (caused by secondary light scattering) for two points of the sky situated on the solar vertical symmetrically relative to the zenith at an altitude of 20° above the horizon. These values B_2 are cited in Table 4.1, together with the values B_1 for these same two points of the sky, given as comparison. No pretense is made to high accuracy, and V. G. Fesenkov (ref. 208) believes that they only indicate the general character of the phenomenon. Table 4.1 shows that twilight brightness, computed including first-order scattering, is rather closely proportional to the influence of secondary light scattering computed on the basis of this same formula, using as a point of departure the indicatrix of light scattering actually observed in the troposphere.

TABLE 4.1. COMPARISON OF BRIGHTNESSES OF TWILIGHT SKY CAUSED BY PRIMARY B_1 AND SECONDARY B_2 LIGHT SCATTERING, IN ARBITRARY UNITS.

$z_\odot$	B_1		B_2	
	West	East	West	East
92°	1.00	0.64	1.00	0.67
94	0.51	0.132	0.42	0.205
96	0.26	0.014	0.23	0.096
98	0.087	0.000	0.085	0.014

4.2. Secondary Light Scattering at Points in the Sky Symmetrical to the Zenith. In the case of large solar zenith distances V. G. Fesenkov has formulated another method for taking into account the influence of secondary scattering. When $z_\bullet > 98^\circ$, the sky brightness in the eastern part of the solar vertical (evening twilight) at an altutude of 20° is already dependent only on higher-order scattering, because direct solar rays no longer enter this part of the sky. The semi-graphic method, above mentioned, can be used to compute the ratio of secondary scattering at points in the sky symmetrical to the zenith, at which sky brightness is measured. By multiplying the brightness at the eastern point by this ratio we can determine the brightness at the western point, which would prevail if there were only secondary scattering. By subtracting the value from the observed brightness at the western point, we can find the brightness caused only by primary scattering.

After pointing out the extraordinary complexity of the formulated problem, requiring both further development of the problem from a theoretical point of view and further observations, Fesenkov (ref. 208) notes that the most feasible method for twilight measurements, taking into account all these circumstances, is as follows: observations should be made at at least two points of the sky on the solar vertical, both to east and west, until the final end of astronomical twilight; in order to judge the character of the luminescence in the high layers of the atmosphere, it also is desirable to observe the twilight at the zenith (ref. 208). Putting this idea into specific terms (ref. 210), he used such a method for a first preliminary estimate of the value of secondary light scattering in twilight brightness to west and east at solar zenith distances $z_\bullet \leq 97^\circ$.

As we will show, recent measurements have fully confirmed the feasibility of such a formulation of twilight observations. However, at intermediate stages of development of this important method for study of structure of the atmosphere, other points of view developed and from time to time created great difficulties.

A study by Hulburt (ref. 461), which appeared in 1938, was of particular importance in this respect. Whereas numerical data on the behavior of

secondary scattering were obtained by V. G. Fesenkov only for $z_\odot \leq 98^\circ$, Hulburt made computations for greater angles of solar depression, to $z_\odot = 103^\circ$. It was found that when $z_\odot \simeq 97 - 98^\circ$, there is a sort of break in the development of the twilight phenomenon with respect to the influence of secondary light scattering. In the case of zenith observations the role of secondary scattering, which remains quite small at $z_\odot \leq 97^\circ$, begins to increase rapidly when $z_\odot$ becomes greater than 98°. This was the principal result of Hulburt's work, determining its importance, although the method of proof which he used and certain of his conclusions cannot be considered sufficiently sound. We will now discuss the results of this interesting study by Hulburt.

4.3. Sky Brightness at the Zenith. The principal results of Hulburt's computations are given in Table 4.2, where columns 1 and 2 give the values of zenith distance $z_\odot$ of the Sun and corresponding height h_{shad} of the Earth's shadow at the zenith. Column 3 gives the measured brightness B at the zenith and columns 4-6 the computed brightness value caused by primary B_1 and secondary B_2 light scattering at the zenith, also their sum $B_1 + B_2$. It can be concluded from these data that $B_1 > B_2$ for heights of the Earth's shadow $h_{shad} <$ 60 km (i.e., for the height of the twilight ray $h_{twi} < 80$ km, see Section 3). For $z_\odot > 98^\circ$ or $h_{shad} > 60$ km ($h_{twi} > 80$km), B_2 considerably exceeds B_1. This means that the use of the twilight method for determination of air pressure and density in the upper layers of the atmosphere can give correct results only to a height of approximately 60-70 km, because, in the case of large solar zenith distances, the secondary light scattering occurring in the lower layers of the atmosphere, for the most part below 30 km, assumes particular importance. The ratio $\frac{B_2}{B_1}$, according to the data in Table 4.2, remains quite small for zenith distances $z_\odot < 97^\circ$, but for large $z_\odot$ this ratio increases rapidly and becomes extremely large, to wit

$z_\odot$ . .	94°34′	95°36′	96°25′	97°52′	99°36′	100°09′	101°08′	102°02′	102°52′
$\frac{B_2}{B_1}$ . .	0.014	0.055	0.12	1.36	18.5	185	$1.4 \cdot 10^3$	$2.3 \cdot 10^4$	$2.9 \cdot 10^5$

4.4. Air Pressure and Density Determined from Twilight Data. If we now compare the values of pressure p and density p obtained by twilight observations of N. M. Shtaude with the actual values, the discrepancy between them (see Section 3, figs. 3.4 and 3.5) begins exactly at a height of 70 km. The conclusions drawn by Hulburt concerning considerable distortion of the brightness of the twilight sky at the zenith at $z_\odot > 98^\circ$, therefore, in general appear correct. However, his quantitative results should be made more precise.

TABLE 4.2. ROLE OF SECONDARY LIGHT SCATTERING IN BRIGHTNESS OF TWILIGHT SKY AT ZENITH (ACCORDING TO HULBURT).

$z_\odot$	h_T	B	B_1	B_2	$B_1 + B_2$
1	2	3	4	5	6
90°	0	1140	1170	—	1170
94 34′	20	27.5	36.3	0.50	36.8
95 36	30	7.41	7.9	0.43	8.3
96 25	40	2.19	1.8	0.21	2.0
97 52	60	0.339	$8.8 \cdot 10^{-2}$	0.12	0.21
99 36	80	0.0676	$3.4 \cdot 10^{-3}$	0.063	0.066
100 09	100	0.0398	$1.4 \cdot 10^{-4}$	0.026	0.026
101 08	120	0.0158	$5.0 \cdot 10^{-6}$	0.0071	0,0071
102 02	140	0.0076	$2.1 \cdot 10^{-7}$	0.0049	0.0049
102 52	160	0.0040	$8.3 \cdot 10^{-9}$	0.0024	0.0024

Apparently they considerably exaggerate the relative value B_2. Some idea on this point can be obtained directly from a comparison of the results of rocket measurements p_{rock} and ρ_{rock} with the results obtained from twilight observations at the zenith. Figures 4.1 and 4.2 show curves obtained by T. G. Megrelishvili (ref. 119) by electrophotometric measurements of the twilight sky in the near ultraviolet, visible and infrared regions of the spectrum and from rocket data. The figures show rather close agreement between twilight and rocket measurements to the 70-90 km level; above this level there is no agreement, and the ratios $\frac{p_{twi}}{p_{rock}}$ and $\frac{\rho_{twi}}{\rho_{rock}}$ increase rapidly with height, although they do not become as large as indicated by Hulburt's computations, even if the "excess" brightness of the night sky at the zenith is attributed to the effect of multiple light scattering. In actuality, for $h \simeq 140$ km (this is the height of the twilight ray, see Section 3), the ratios $\frac{p_{twi}}{p_{rock}}$ and $\frac{\rho_{twi}}{\rho_{rock}}$ are (figs. 4.1 and 4.2) from 20 to 125, but according to Hulburt's table for this height (i.e., for $h_{shad} = 120$ km, since $h_{twi} = h_{shad} + 20$ km, see Section 3) the ratio $\frac{B_2}{B_1}$ attains 1,400; for $h \simeq 160$ km $\frac{p_{twi}}{p_{rock}}$ and $\frac{\rho_{twi}}{\rho_{rock}}$ are from 40 to 200, whereas $\frac{B_2}{B_1}$ exceeds 2.10^4.

The percentage of secondary light scattering in the twilight sky brightness, for the most part at the zenith, has also been computed by other authors. A number of important studies devoted to investigation of the atmosphere by the twilight method have been published by the well-known Czechoslovakian geophysicist F. Link (refs. 551, 552 and 553). In particular, his computations revealed that at $z_\odot = 100°$ for $\lambda = 5{,}300$ A, secondary scattering

gives 28 percent of the observed total brightness; the percentage of secondary scattering decreases with an increase of wavelength, being several percent of the total brightness in infrared light. Shtaude used a simplified computation method to find the minimum value (lower estimate) of ratio $\frac{B_2}{B_1}$ for the zenith; brightness B_2 of secondarily scattered light was found theoretically from the computed (by the twilight ray method) sky distribution of brightness B_1 of primary scattered light. Using this method, Shtaude made an interesting investigation explaining the dependence of ratio $\frac{B_2}{B_1}$ on the structure (vertical density distribution) of the atmosphere assumed in the computations. Hulburt obtained the following results (variant I) (ref. 257) for an isothermal model of the atmosphere which he used in his computations

$z_\odot^\circ$	92	94	96	98	100
h км	24	35	55	83	115
I. $\frac{B_2}{B_1}$	0.20	0.23	0.52	3.65	97.5
II. $\frac{B_2}{B_1}$	0.20	0.23	0.33	0.62	0.63
III. $\frac{B_2}{B_1}$	0.20	0.23	0.31	0.90	11.4

This variant, corresponding to an obviously understated value of air density at great heights, gives a predominance of secondary scattering for $z \geqslant 98^\circ$.

However, the value of ratio $\frac{B_2}{B_1}$ changes appreciably if the computation is made for a different model of the atmosphere. For example, we will take a vertical distribution of density ρ as obtained from twilight observations at the zenith (figs. 3.4 and 4.2). For heights $h > 80$ km this method gives exaggerated values ρ. In this case (see variant II in the table) ratio $\frac{B_2}{B_1}$ remains less than unity to $z_\odot = 100^\circ$. However, if an intermediate vertical distribution of ρ is taken, which is closer to reality, corresponding to the presence of a temperature maximum at a height of 55-60 km, a minimum at the 80 km level and a sebsequent temperature increase with height for $h > 80$ km, we obtain the intermediate values of ratio $\frac{B_1}{B_2}$, shown in the table as variant III.

The problem of the brightness of the twilight sky in the solar vertical including secondary scattering has also been solved by N. P. Perevertun. He concluded (ref. 147) that secondary scattering at solar zenith distances of

96, 97, and 98° for the parts of the sky situated over the western horizon at an altitude of 50-60°, and also at the zenith and in the entire eastern part of the sky, increases twilight brightness by more than 45 percent (for wavelengths 4,200 and 5,120 Å).

The most rigorous method for the theoretical determination of B_2 from a given structure of the atmosphere was developed by F. F. Yudalevich (ref. 261). If it is applied to a model of the atmosphere obtained from twilight observations at the zenith, we obtain the following values $\frac{B_2}{B_1}$ (for the zenith)

$z_\odot^\circ$	94	96	98	100	102	103	104	105	107
$\frac{B_2}{B_1}$	0.30	0.49	0.76	0.78	0.87	0.97	1.16	1.68	2.40

These data have been used by T. G. Megrelishvili an analysis of twilight curves (see figs. 4.1 and 4.2) for partially freeing measured brightnesses from the influence of secondary scattering.

The problem of the role of multiple scattering in the twilight phenomenon has also been considered in studies by V. L. Ginzburg (ref. 31), V. L. Ginzburg and N. N. Soboleva (ref. 32), G. V. Rosenberg (refs. 167 and 168), and G. V. Rozenberg, I. A. Khvostikov and F. F. Yudalevich (ref. 169). Sato (ref. 712) in Japan received nigh values $\frac{B_2}{B_1}$ for large $z_\bullet$. An unusual method for determination of $\frac{B_2}{B_1}$ was used in France by Robley (ref. 705). The basis of this method is that if the degree of polarization of skylight at the zenith in the bright part of twilight differs little from the theoretical value computed by the Rayleigh formula, at large $z_\bullet$ the observed polarization is much less than the theoretical value. Assuming that the total effect of self-illumination of the atmosphere leads to the polarization of secondarily scattered light, which is close to zero (in actuality, as pointed out by G. V. Rozenberg (ref. 168), there is no justification for this assumption), Robley used the "deficit" of the degree of polarization to compute ratio $\frac{B_2}{B_1}$. He obtained

$z_\odot^\circ$	92	93	94	95	96	97	98	99	100	101	102
$\frac{B_2}{B_1}+B_2$	0.11	0.14	0.14	0.16	0.19	0.28	0.34	0.36	0.38	0.42	0.53
$\frac{B_2}{B_1}$	0.12	0.16	0.17	0.20	0.23	0.38	0.51	0.57	0.62	0.72	1.10

The following conclusion can be drawn from a comparison of these attempts to solve the extremely complex problem of the percentage of secondary scattering

in the brightness of the twilight sky at different solar zenith distances. For $z_\odot \leqslant 97^\circ$ it was possible to obtain a clear result, indicating a relatively small value B_2 in the brightness of the twilight sky at the zenith: ratio $\frac{B_2}{B_1}$ for $z_\odot \leqslant 94^\circ$ does not exceed 0.3, and for $z_\odot \leqslant 97^\circ$ it does not exceed 0.6. On the basis of computed values $\frac{B_2}{B_1}$, it is possible to introduce a reliable correction into the measured brightnesses of the twilight sky, virtually freeing it from the influence of higher-order scattering. An analysis of available determinations of $\frac{B_2}{B_1}$ permits the conclusion that the differences $B - B_2$ (B is the measured sky brightness, B_2 is the computed brightness of secondarily scattered light) can be computed free from the effect of secondary light scattering with an error scarcely exceeding 10 percent of the measured sky brightness when $z_\odot \leqslant 94^\circ$, and scarcely exceeding 20 percent when $z_\odot \leqslant 97^\circ$. Consequently, the effect of secondary scattering under the conditions of twilight illumination of the atmosphere is no hindrance in determination of the vertical distribution of air density and pressure, with an accuracy to 10-20 percent by measurement of twilight curves at the zenith for $z_\odot \leqslant 97^\circ$, i.e., in the region of heights from 25-70 km. For great heights the estimates of ratio $\frac{B_2}{B_1}$ for $z_\odot > 98^\circ$, made by different authors, differ appreciably from one another and are greatly dependent on the assumed structure of the atmosphere. The new method for taking the secondary scattering of light into account, proposed by V. G. Fesenkov and discussed in the next section, is free of this shortcoming.

5. Limits of Applicability of the Twilight Method for Study of the Atmosphere

In order to comprehend the new step recently taken in the theory of the twilight method, we must become familiar with the generalized twilight concept introduced by V. G. Fesenkov and N. M. Shtaude.

5.1. Generalization of the Twilight Concept. Twilight is that part of the day at the beginning and end of night when the Sun is below the horizon, but its angle of depression is not very great and the Earth's shadow therefore is in the limits of the Earth's atmosphere. In contrast to day and night, sky brightness at twilight is very greatly dependent on $z_\odot$.

However, the definition of the concept of twilight can be approached differently by using that interesting peculiarity of the spatial distribution of light scattering under conditions of twilight illumination of the atmosphere (the presence of a well-expressed scattering maximum at great heights), which was discussed in connection with the introduction of the concept of the twilight ray (Section 3, fig. 3.2).

If the presence of a scattering maximum is regarded as a characteristic indicator of twilight phenomena, it is found that twilight begins before sunset and continues after sunrise (ref. 255). It can be shown that even during the daytime, when the Sun is sufficiently low, the lowest layers of the troposphere in actuality add almost nothing to the total brightness of the sky and often even decrease it by absorption. Even before the actual setting of the Sun the Earth's atmosphere reaches the twilight state when the brightness of the daytime sky is determined mostly by the rather high tropospheric and even stratospheric layers. After sunset the effective scattering layer below the observer's horizon continues to rise with an ever-increasing velocity, but the character of the phenomenon does not change essentially (refs. 215, 216). According to computations made by N. M. Shtaude, in the visible part of the spectrum when the coefficient of atmospheric transparency is p = 0.835, "daytime twilight" begins when the Sun is still situated at an altitude of 10° above the horizon (ref. 255). The height of the twilight ray h_{twi} has the following dependence on $z_{\bullet}$

$z_{\odot}^{\circ}$	79.6	80	81	82	83	84	85	86	87	88	89
h_{twi} км	0	0.3	1.1	2.1	3.25	4.45	5.85	7.4	8.8	10.1	11.5

$z_{\odot}^{\circ}$	89.5	89.7	89.8	89.9	90	92
h_{twi} км	12.4	12.75	12,95	13.2	13.5	21.2

The shorter the length of the lightwave and, therefore, the greater the scattering coefficient, the earlier twilight begins. The following table (ref. 256) gives the values of the solar zenith distance $z_{\bullet}$ at which daylight twilight begins for any wavelength λ

λ Å	3000	4000	5000	5550	6000	7000	8000	9000
$z_{\odot}^{\circ}$	43.7	63.2	75.5	79.8	82.3	86.0	88.1	89.5

The existence of daytime twilight serves as a basis for formulating the problem of some kind of unifying theory of the brightness of the daytime and twilight sky. However, until recently all theories of the brightness of the daytime sky applied only to the case of a plane Earth and therefore could not be used in the immediate vicinity of the horizon. The continuous transition of the brightness of the daytime sky into the brightness of the twilight sky cannot be represented by the theory of a plane Earth. In 1955 V. G. Fesenkov published his theory of the brightness of the daytime sky for a spherical Earth (refs. 215 and 216). This theory is more general and it naturally represents a transition to twilight conditions and can be used in computation of the influence of secondary light scattering on the brightness of the twilight sky. This makes it possible to put the twilight method for study of the structure of the atmosphere on a considerably sounder basis, and determines the limits of its applicability more precisely.

5.2. Theory of the Brightness of the Daytime Sky for a Spherical Earth (V. G. Fesenkov). The following premises are at the basis of the theory:

(a) Atmospheric density is determined using the exponential formula

$$\rho = \rho_0 e^{-h/H}, \tag{5.1}$$

and a value of 8 km is used for H.

(b) Light attenuation occurs as a result of simple scattering with an indicatrix of scattering $f(\varphi)$, which can be determined from observations of brightness of the daytime sky. As a result, the attenuation factor b is related to the scattering coefficient s and the indicatrix by the relation

$$b = 2\pi s \int_0^{\pi} f(\varphi) \sin \varphi \, d\varphi.$$

(c) There are no nonhomogeneities in the atmosphere or random turbidity. Light reflection from the Earth's surface is neglected.

The expression for sky brightness can be written in the form

$$B' = S s_0 f(\varphi) \rho_0 p^{m_z} \int_0^{\infty} e^{-\tau(h)\left(m_{z'_\odot} - m_{z'}\right) - h/H} dr. \tag{5.2}$$

This formula is based on the assumption that the coefficient of atmospheric transparency p, determined from observations, is

$$p = e^{-\tau_0},$$

where $\tau_0 = bH\rho_0$ is the optical thickness of the atmosphere at sea level, whereas at the height h

$$\tau = b \int_h^{\infty} \rho \, dh = bH\rho_0 e^{-h/H}, \tag{5.3}$$

and the percentage of light scattered in a unit solid angle of a unit volume

of the atmosphere with density ρ is denoted $s_0 \rho f(\varphi)$. In formula (5.2) $m_{z'_\bullet}$ and $m_{z'}$ denote atmospheric masses (the ratio of the optical thickness at angle $z'_\bullet$ or z' in the considered elementary volume at height h to the optical thickness in the direction to the zenith for this same elementary volume). In order to determine sky brightness B in brightness units of an orthotropic screen at the place of observation, illuminated normally by the solar rays, B' must be divided by the factor

$$s_{\odot} = Se^{-\tau_{0m} z_{\odot}},$$

where $m_{z_\bullet}$ is the atmospheric mass corresponding to the Sun at the place of observation.

After a number of transformations and introducing the new variable x = h/H, V. G. Fesenkov obtains the following expression for B

$$B = \ln pp^{m_z - m_{z_\odot}} \frac{f(\varphi)}{2\pi \int_0^{\pi} f(\varphi) \sin\varphi \, d\varphi} \cdot \int_0^{\infty} \frac{e^{\ln pe^{-x}\left(m_{z_\odot'} - m_{z'}\right) - x}}{\sqrt{1 - \frac{R^2}{(R + H_0 x)^2} \sin^2 z}} \, dx. \qquad (5.4)$$

An important aspect of this theory is the computation of the atmospheric masses $m_{z'_\bullet}$ and $m_{z'}$ corresponding to unfixed heights h above sea level for different values x. We note that z' is the zenith distance determining the slope of the line-of-sight to the direction of the zenith in a scattering volume at height h. After introducing the new variable

$$y = \frac{h - h_1}{H}$$

(h_1 is the height of the considered volume, h is the variable height along the line-of-sight), V. G. Fesenkov derives the expression

$$m_{z'} = \int_0^{\infty} \frac{e^{-x}\left(1 + \frac{h_1}{r} + \frac{Hy}{r}\right) dy}{\sqrt{\cos^2 z + \frac{2h_1}{r} + \frac{2Hy}{r} + \left(\frac{h_1 + Hy}{r}\right)^2}}. \qquad (5.5)$$

Expression (5.5) can be used for computing m_z, as a function of h_1 by numerical integration for any z. For $z < 80^\circ$ this expression can be computed easily by expansion into a series. Neglecting values of the third order of magnitude in ratio H/r, we have

$$m_{z'} = \frac{1+\frac{h_1}{r}}{\sqrt{\left(1+\frac{h_1}{r}\right)^2 - \sin^2 z}}\left(1 + a - \frac{1}{2}\alpha - \beta + \frac{3}{4}\alpha^2 - \alpha a\right), \tag{5.6}$$

where

$$a = \frac{H}{r}\frac{1}{1+\frac{h_1}{r}},$$

$$\alpha = \frac{2H}{r}\left(1+\frac{h_1}{r}\right)\frac{1}{\left(1+\frac{h_1}{r}\right)^2 - \sin^2 z},$$

$$\beta = \frac{H^2}{r^2}\frac{1}{\left(1+\frac{h_1}{r}\right)^2 - \sin^2 z}.$$

When $h_1 = 0$, i.e., for a position of an element at sea level,

$$m_z = \sec z\left[1 + \frac{H}{r} - \frac{H}{r}\sec^2 z\left(1+\frac{3H}{r^2}\right) + 3\frac{H^2}{r^2}\sec^4 z\right] \tag{5.7}$$

or when H = 8 km, H/r = 0.00125, we have

$$m_z = \sec z\,[1.00125 - 0.0012547\sec^2 z + 0.00000469\sec^4 z]. \tag{5.8}$$

Using series (5.6) and (5.8), V. G. Fesenkov obtained the numerical values for m_z, (Table 5.1). Since the computation of m_z, for $z = 85^\circ$ and large values of zenith distance is very inexact when this series is used, formula (5.5), somewhat transformed and simplified for purposes of numerical solution, is used for these values. In particular, for $h_1 = 0$, i.e., at sea level, and when H/r = 1/800, this formula has the form

$$m_z = 40e^{400\cos^2 z}\left(1 - \frac{1}{2}\cos^2 z\right)\int_{20\cos z}^{\infty} e^{-q^2}\,dq + \frac{e^{400\cos^2 z}}{20}Q, \tag{5.9}$$

where

$$q=\sqrt{\alpha+y},$$

$$Q=\frac{\sqrt{\pi}}{4}e^{-\frac{800\cos^2 z}{\pi}}\sqrt{1+\frac{1600\cos^2 z}{\pi}+\frac{1\,280\,000\cos^4 z}{\pi^2}}.$$

For z = 90° this formula gives

$$m_z=40\int_0^\infty e^{-y^2}dy+\frac{1}{20}\frac{\sqrt{\pi}}{4}=40\frac{\sqrt{\pi}}{2}+\frac{1}{20}\frac{\sqrt{\pi}}{4},$$

i.e., m_z = 35.4713.

TABLE 5.1. ATMOSPHERIC MASS $m_{z'}$

COMPUTED BY V. G. FESENKOV.

z°	$\frac{h_1}{r}$								
	0.000	0.001	0.002	0.003	0.004	0.005	0.006	0.007	0.008
0	1.0000	1.0000	1.0000	1.0000	1.0000	1.0000	1.0000	1.0000	1.0000
30	1.1542	1.1538	1.1534	1.1531	1.1527	1.1523	1.1520	1.1516	1.1512
40	1.3043	1.3034	1.3025	1.3015	1.3006	1.2997	1.2989	1.2980	1.2970
50	1.5530	1.5508	1.5486	1.5464	1.5443	1.5422	1.5401	1.5380	1.5359
60	1.9926	1.9867	1.9805	1.9752	1.9695	1.9639	1.9585	1.9529	1.9450
70	2.8971	2.8751	2.8550	2.8345	2.8150	2.7964	2.7780	2.7593	2.740
75	3.8002	3.7489	3.7026	3.6551	3.6149	3.5698	3.5290	3.4894	3.4514
80	5.5561	5.3964	5.2511	5.1165	4.9924	4.8774	4.7704	4.6705	4.5771
85	10.592	9.379	8.629	8.029	7.549	7.151	6.812	6.524	6.266

With respect to the atmospheric mass $mp_{z'}$, corresponding to the direction to the Sun from different elements of a volume situated at different heights h_1, the final expression for it is written in the form

$$m_{\odot}^{z'}=\sqrt{2e^{\alpha_1}}\left[\frac{1+\frac{H}{r}-\frac{H}{r}\alpha_1}{\sqrt{\frac{H}{r}\left(1+\frac{h_1}{r}+\frac{0.35H}{r}\right)}}\left(\frac{\sqrt{\pi}}{2}-\int_0^{\sqrt{\alpha_1}}e^{-q^2}dq\right)+\right.$$

$$\left.+\frac{\sqrt{\frac{H}{r}}Q_1}{\sqrt{1+\frac{h_1}{r}+\frac{0{,}35H}{r}}}\right], \qquad (5.10)$$

where

$$Q_1 = \frac{\sqrt{\pi}}{4} e^{-2\alpha_1/\pi} \sqrt{1 + \frac{4\alpha_1}{\pi} + \frac{8\alpha_1^2}{\pi^2}},$$

$$\alpha_1 = \frac{\cos^2 z'_\odot}{\frac{2H}{r}\left(1 + \frac{h_1}{r} + \frac{0{,}35H}{r}\right)},$$

$$\cos z'_\odot = \cos z_\odot + \cos\varphi\left(\sqrt{\left(1 + \frac{h_1}{r}\right)^2 - \sin^2 z} - \cos z\right).$$

The entire discussion up to this point applies when the observer is at the Earth's surface. The cases when the observer is at a certain height above the Earth's surface is appreciably different (and it is just such a case which is involved when computing secondary scattering of light by atmospheric layers situated at different heights). In this case the real horizon will appear to be lowered to some degree in comparison with the astronomical horizon, and the solar zenith distance can be greater than 90°. Here the solar rays can approach the Earth's surface and again withdraw from it (the variable y can assume negative and positive values). Otherwise the formulas remain essentially unchanged, provided the Earth's radius is assumed to be r + h* (h* is the height of the observer), and all the constants apply to this height. In addition, if $z'_\odot > 90^\circ$, the following term must be added to the expression for $m_{z'_\odot}$

$$K = \frac{4e^{\alpha_1}}{\sqrt{d}}\left(1 + \frac{h_1 - h^*}{r + h^*} - \alpha_1 \frac{H}{r + h^*} \int_{\sqrt{\alpha_1}}^{\sqrt{2\alpha_1}} e^{-q^2}\, dq\right) + \\ + \frac{4e^{\alpha_1}}{\sqrt{d}} \frac{H}{r + h^*} \frac{\sqrt{\pi}}{4}\left(e^{-\frac{2\alpha_1}{\pi}} \sqrt{1 + \frac{4\alpha_1}{\pi} + \frac{8\alpha_1^2}{\pi^2}} - \right. \\ \left. - e^{-\frac{4\alpha_1}{\pi}} \sqrt{1 + \frac{8\alpha_1}{\pi} + \frac{32\alpha_1^2}{\pi^2}}\right), \qquad (5.11)$$

where

$$d = \frac{2H}{r + h^*}\left(1 + \frac{h_1 - h^*}{r + h^*} + \frac{0{,}35H}{r + H}\right),$$

$$\cos\varphi = \cos z_\odot \cos z + \sin z_\odot \sin z \cos A.$$

Table 5.2 gives the values $m_{z'_\odot}$, computed using formula (5.10) for $z_\odot = 90^\circ$, $z = 90^\circ$ on the assumption that in formula (5.1) H = 8 km. It is interesting to note

TABLE 5.2. ATMOSPHERIC MASSES $m_{z'}$ COMPUTED FOR DIFFERENT HEIGHTS h* (IN KM) OF OBSERVER AND FOR DIFFERENT HEIGHTS h_1 (IN KM) OF SCATTERING ELEMENTS ABOVE OBSERVER (V. G. FESENKOV).

$h^* = 0$		$h^* = 4$		$h^* = 8$		$h^* = 12$		$h^* = 16$	
h_1	$m_{z'\odot}$	h_1	$m_{z'\odot}$	h_1	$m_{z'\odot}$	h_1	$m_{z'\odot}$	h_1	$m_{z'\odot}$
0.0	35,46	4.00	35.48	8.00	35.49	12.00	35.50	16.00	35.51
6.4	31.43	10.404	31.44	14.408	31.45	18.412	31.46	22.416	31.47
12.8	28.18	16.808	28.19	20.816	28.19	24.824	28.20	28,832	28.21
19.2	25.51	23,212	25.51	27.224	25.52	31.236	25.52	35,248	29.53
25.6	23.29	29,606	23.29	33.632	23.30	37.648	23.30	41.664	23.31
32.0	21,43	36,010	21.44	40.040	21.44	44.060	21.45	48.080	21.45
38.4	19.84	42,414	19.84	46,448	19.85	50.472	19.85	54.496	19.86
44.8	18.48	49.008	18.48	52,856	18,49	56.884	18.49	60,912	18.49
52.0	17,30	55.412	17.31	59,264	17,31				
57.6	16.27								

that the atmospheric masses $m_{z'}$ remain virtually constant with increasing height above the Earth's surface. This makes it possible to compute them for one mean value h*.

5.3. Determination of Brightness of Secondary Light Scattering. The described theory of sky brightness for a spherical Earth makes it possible to make the computations with the necessary accuracy required for justification and use of the method for determining the brightness of secondary scattering, proposed by V. G. Fesenkov as early as 1934 (Section 4).

Soon after sunset the rapidly growing shadow of the Earth appears in the western part of the sky over the horizon. There is complete absence of primary scattering of light in this shadow. It is sufficient to determine theoretically only the ratio of the brightnesses of the lower layers of the atmosphere, illuminated by the twilight segment at points of the sky symmetrical to the zenith (ref. 215)(e.g., lying to west and east at an altitude of 20° above the horizon on the solar vertical). It is necessary to measure two twilight curves at these two points.

By multiplying the brightness at the eastern point by this ratio, we obtain the brightness which would be present at the western point if there were higher-order scattering only.

By substracting it from the observed brightness at the western point we find the brightness exclusively dependent on first-order scattering (ref. 208).

This method for measurement of twilight curves, mostly freed from the influence of secondary scattering, was used in 1955 by T. G. Megrelishvili (ref. 119). He simultaneously measured sky brightness at two points of the sky

situated on the solar vertical at zenith distances of +70 and -70°. The measurements were made with an electrophotometer consisting of a gas-filled antimony-cesium photocell with a small dark current ($1.3 \cdot 10^{-13}$a) and a single-tube d.c. compensatory amplifier (electrometer tube) with an output resistance of $5 \cdot 10^{10}$ ohms. The electrophotometer was mounted in the Nesmitov focus of a 13" reflector.

Using twilight curves freed from secondary light scattering, Megrelishvili (ref. 119) computed the vertical distribution of pressure to a height of 130 km. Two individual curves, applying to Oct. 13 and 27, 1955, are shown in figure 5.1; rocket data are also shown for comparison. This comparison shows a satisfactory agreement between twilight and rocket measurements to a level of about 100 km.

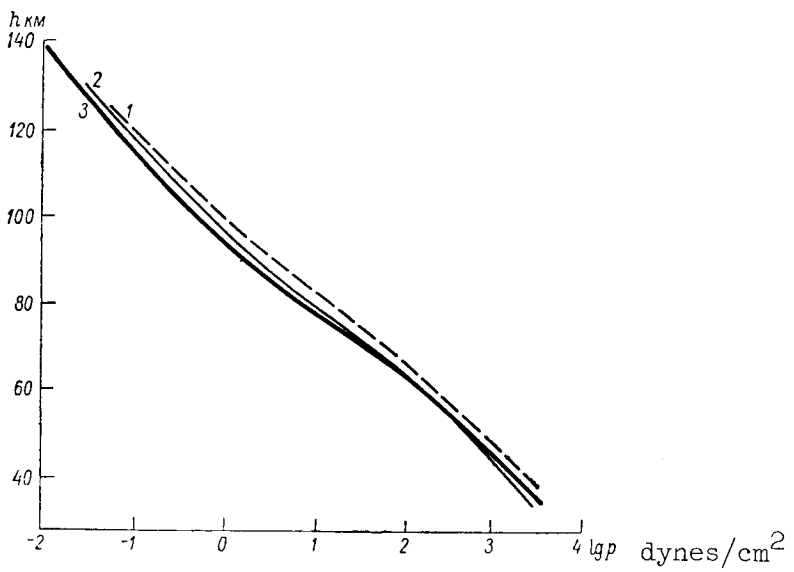

Figure 5.1. Vertical distribution of pressure from twilight curves freed from influence of secondary scattering by V. G. Fesenkov's method. Measurements by T. G. Megrelishvili: 1, Oct. 13; 2, Oct. 27, 1955; 3, measurements by rockets.

5.4. Light Scattering by Aerosols. As already noted, the brightness of the twilight sky can be enhanced by the scattering of light by aerosol particles and sky luminescence. In Chapter 7 (Section 20) we will discuss new data indicating the intensifying role of aerosol scattering of light, beginning at the 90 km level and above. There is a basis for assuming that optical and many physical properties of the thermosphere are dependent on the presence of meteor matter to a far greater degree than was formerly assumed.

We can summarize the present status of the problem of the limits of applicability of the twilight method for study of structure of the atmosphere as follows.

At heights of 20-80 km (stratosphere and mesosphere), twilight observations can be used for a study of the distribution of pressure and density and possible changes of this distribution with time as a function of latitude, etc. In order to increase the accuracy of the results a more detailed investigation of the influence of aerosol scattering must be made.

The role of aerosol scattering greatly increases in the thermosphere. There is a basis for assuming that twilight observations can be used for study of the aerosol composition of the upper layers of the atmosphere, which would be of great importance. In order to make this method effective, it is necessary to improve the method for taking into account light scattering of higher orders, based on V. G. Fesenkov's method. The use of modern high-speed electronic computers may solve the problem of multiple light scattering in a spherical atmosphere under twilight conditions with great completeness and rigor.

In the course of further improvement of the theory of twilight phenomena we must take into account the ozone absorption caused by the Chappuis absorption band. This band extends from 4,500 to 7,500 Å and has two close absorption maxima near 6,000 Å. Under conditions of twilight illumination, solar rays experience an appreciable absorption by ozone; this must be taken into account during measurements in corresponding parts of the spectrum. This problem was considered in 1953-1954 in studies by Hulburt (ref. 462) and Le Grand and Lenoble (ref. 545).

CHAPTER 3. SEARCHLIGHT SOUNDING OF THE ATMOSPHERE

6. Sounding Method

The essence and technique of searchlight sounding of the atmosphere can be explained in a few words. Imagine that at point O (fig. 6.1) there is a searchlight apparatus; the searchlight beam is observed from the side from point A. By sighting an instrument at different points of the beam (M_1, M_2, M_3,...) it is possible to investigate the scattering of light caused by individual air layers at the height of these points. By knowing distance OA at ground level, the angle of elevation of the searchlight beam and angles b_1, b_2, b_3,..., at which light scattering in layers M_1, M_2, M_3,..., is observed in the instrument, it is easy to compute the height of these layers. The intensity, polarization and spectral composition of the scattered light can be investigated. As is known from physical optics, the combination of such data in many cases makes it possible to draw important conclusions concerning the physical properties and the state of the scattering medium.

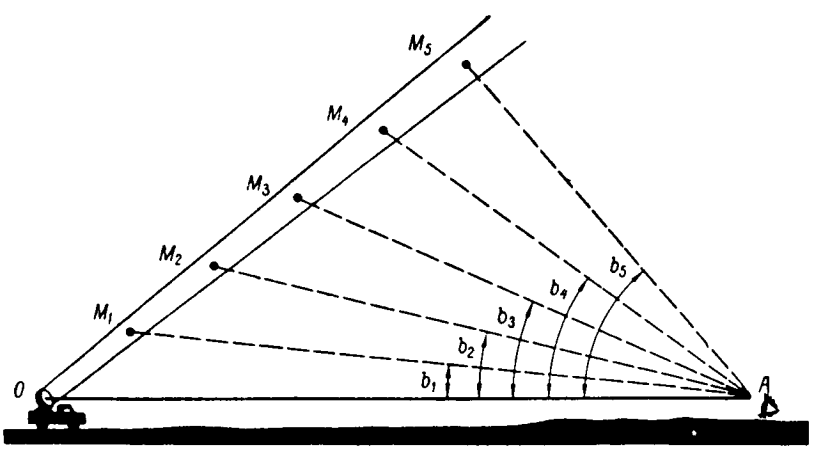

Figure 6.1. Diagram of searchlight sounding of the atmosphere.

6.1. Measurement Methods. The first attempts to use searchlight sounding of the atmosphere were made as early as 1905. In that year V. V. Kuznetsov published a study (ref. 99) on the measurement of cloud height at nighttime, using a searchlight beam. The great luminous intensity of modern searchlight

apparatus permits formulating the problem of sounding the upper layers of the atmosphere. In 1930 Synge (ref. 754) computed that it was conceivably possible to accomplish searchlight sounding to heights exceeding 30 km. He pointed out that the "ceiling" of searchlight sounding of the atmosphere is limited by the brightness of the background of the night sky. In 1936 Tuve, Johnson and Wulf (ref. 773) proposed a modulated searchlight beam and a photoelectric apparatus tuned to the frequency of light modulation for decreasing the effect of the background of the night sky. This method is extremely effective. The method was used for the first time in 1939 by Johnson, Meyer, Hopkins and Mock (ref. 486). These authors observed the scattering of a searchlight beam to a height of 34 km. At present the modulated beam method is used for systematic searchlight sounding of the atmosphere to heights of 60-70 km.

The photographic method for measurement of a searchlight beam, although less effective than the photoelectric method with respect to the accuracy and "ceiling" of measurements, also has certain advantages. These include the documentary and graphic character of the result and the simultaneity of measurements at a large number of points of the beam at different heights. In photoelectric measurements it is necessary to determine the intensity of scattered light at different heights of the beam (such as at points M_1, M_2,..., M_5; fig. 6.1) nonsimultaneously, because during the time which elapses while measuring from point M_1 to point M_5, atmospheric conditions can change.

In 1936 Duclot photographed the vertical beam of a searchlight with a 30 cm mirror and a 5 a voltaic arc. It had a f:1.5 objective. He obtained 30 min and 1 hour exposures, photographing the sweep of the beam to a height of 3.4 km. Duclot planned to investigate the distribution of temperature and density of different layers of the atmosphere by measuring the refraction of the searchlight beam. This proposal could not be implemented because the corresponding refraction effects were too small.

In 1937 the photographic method of observing a searchlight beam was used successfully by Hulburt. In the author's summary of his article (ref. 460), published under the title "Observations of a Searchlight Beam to an Altitude of 28 Kilometers," he stated: "A searchlight beam of great intensity, directed over the observation station from a distance of 18.4 km at angles of 30 and 45° to the horizon, was visible on clear nights to a height of approximately 20 km and photographed to an altitude of 28 km. The photographically measured intensity of the beam was of the same order of magnitude as that computed for molecular scattering on the basis of standard tables of air density in the stratosphere. At a height of 5 km the measured intensity is approximately 7 times greater than the theoretical value, but to a height of 10 km both intensities are approximately equal. This corresponds to the fact that the small quantity of air particles suspended in the air at a height of 5 km becomes disappearingly small at a height of 10 km."

Hulburt used the most powerful searchlight then in the possession of the U.S. Army Corps of Engineers. It had a reflector 152 cm in diameter and a focal length of 62 cm. The intense carbon arc used a 150 a current and 78 w, i.e., 11.7 kw.

The angular discrepancy of the searchlight beam was $1^{\circ}.2$. The photographs were taken on clear moonless nights with a camera with a f:1.8 objective. Exposures were from several minutes to 54 minutes.

Figure 6.2 is one of the photographs of the searchlight beam obtained by Hulburt (exposure 2.2 min). It is easy to detect a highly turbid (containing many aerosol particles) layer of the atmosphere extending from the Earth's surface to a height of 1.8 km. The boundary of the turbid layer and the transition to more transparent air are clearly expressed. Effects of this type were noted still earlier in experiments at the Aerological Observatory at Pavlovsk (near Leningrad), and P. A. Molchanov demonstrated that they are associated with the presence of a temperature inversion.

6.2. Elements of Interpretation Theory (Inverse Problem). Hulburt's data on the relation between the brightness B of the beam and the brightness computed using the Rayleigh formula for pure air B_{Ray} are of great interest.

h km	4.8	5.8	6.7	7.6	8.2	8.7	9.8	10.4	11.0
B/B_{Ray}	7.2	6.7	6.4	6.4	5.6	3.3	2.2	2.3	2.5

Hulburt computed these values without corrections for attenuation along path OM of the searchlight beam (fig. 6.1) and along path MA of the light

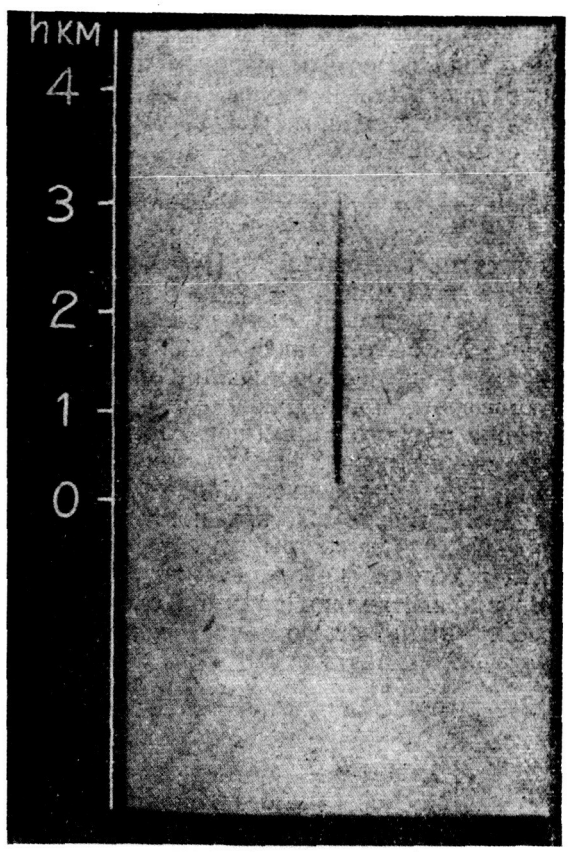

Figure 6.2. Photograph of searchlight beam.

scattered to the observer. Introduction of corrections can change the result appreciably. Computation of the corrections involves great difficulties. In actuality, e.g., in measuring the brightness of the beam at some point M_1 or M_2, M_3,..., it is necessary to compute the attenuation of the beam on paths OM and MA, dependent on the desired value of the scattering power of the different air layers through which the light beam passes on its path.

For practical implementation of searchlight sounding of the atmosphere this problem can be solved approximately by introducing certain simplifying assumptions (ref. 226). We will assume that the atmosphere consists of optically homogeneous layers bounded by horizontal planes M_1P_1, M_2P_2,..... M_5P_5... (fig. 6.3). If at points M_1, M_2, M_3,... on the searchlight beam, at which beam brightness B_1, B_2, B_3 are measured, the values of the attenuation factors caused by light scattering (in measurements in the visible part of the spectrum it is known that absorption can be neglected) are b_1, b_2, b_3,..., we will ascribe an identical scattering power to all points of the air layer (each layer M_i - M_{i-1}, i.e., the layer between the planes M_iP_i and $M_{i-1}P_{i-1}$, where i = 1, 2, 3,...), assuming for the layer the mean value of the attenuation factor

$$\overline{b_i} = \frac{1}{2}(b_i - b_{i-1}).$$

Assuming further that the searchlight beam is a light cone with angle ω at the vertex and that within this angle the luminous intensity of the searchlight has a constant (mean) value I, we can write the following expression for light flux Φ_0, radiated by the searchlight into the atmosphere

$$\Phi_0 = I\omega. \tag{6.1}$$

At distance r from searchlight O (fig. 6.4) the light flux is attenuated, due to light scattering, to the value

$$\Phi_r = I\omega e^{-br}. \tag{6.2}$$

The light flux is scattered in a segment of beam dr

$$d\Phi_r = I\omega e^{-br} b\, dr. \tag{6.3}$$

We will assume initially that light scattering occurs identically in all directions (a spherical indicatrix of scattering). By definition, the luminous intensity of the source is measured by the light flux in a unit solid angle,

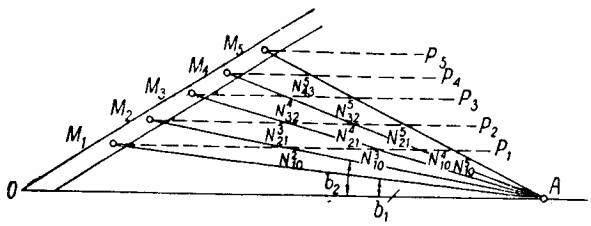

Figure 6.3.

and brightness is measured by the luminous intensity related to a unit surface. Therefore, for brightness B_r of a searchlight beam at point M (fig. 6.4),

viewed from one side from point A, we can write the formula

$$B_r = \frac{I\omega e^{-br} b\, dr}{4\pi\, d\sigma \sin\varphi}, \tag{6.4}$$

where $d\sigma$ is the area of the surface of a sector of the searchlight beam (surface of the cone), corresponding to segment dr

$$d\sigma = 2\sqrt{\pi\omega}\, r\, dr.$$

Thus,

$$B_r = \frac{I\sqrt{\omega}\, e^{-br} b}{8\pi^{3/2} r \sin\varphi}. \tag{6.5}$$

The scattered light in volume M on the path to observer A is attenuated by a factor of e^{bl}, where l = MA. Therefore, the final expression for the brightness of the searchlight beam at point M, measured by the observer from point A, assumes the form

$$B = \frac{bI\sqrt{\omega}\, e^{-b(r+l)}}{8\pi^{3/2} r \sin\varphi}, \tag{6.6}$$

where φ is the angle of scattering.

By rewriting this expression in the form

$$be^{-b(r+l)} = \frac{8\pi^{3/2} rB \sin\varphi}{I\sqrt{\omega}}, \tag{6.7}$$

we obtain the desired equation for determination of the atmospheric attenuation factor b. By measuring brightness B and knowing I, ω, φ, r and l by experimentation, it is possible to determine b.

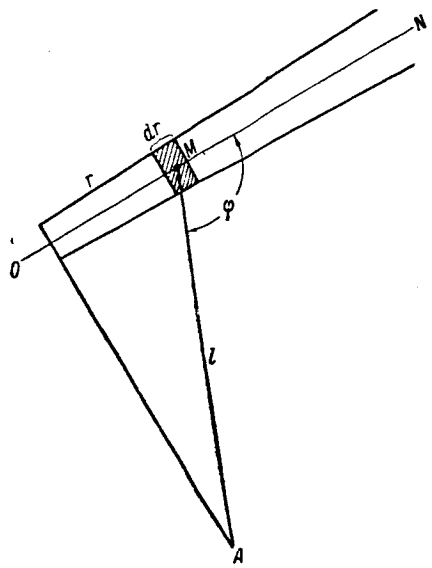

Figure 6.4.

Measurements give the series of values B_1, B_2, B_3,... for the brightness of the searchlight beam at points M_1, M_2, M_3,....

After substituting $B = B_1$ into formula (6.7) we obtain value b for point M_1: $b = b_1$. Proceeding to the analysis of subsequent, higher points, we already can consider the attenuation factor in the lower layer to be known approximately and on the average equal to b_1. Formula (6.7) therefore can be rewritten in the form

$$b_2 e^{-b_1(r+l)} = \frac{8\pi^{3/2} r_2 B_2 \sin\varphi}{I\sqrt{\omega}}, \tag{6.8}$$

hence

$$b_2 = \frac{8\pi^{3/2} r_2 B_2 \sin\varphi}{I\sqrt{\omega}} e^{b_1(r_2+l_2)}. \tag{6.9}$$

At point M_3 attenuation factor b_3 is computed using the similar formula

$$b_3 = \frac{8\pi^{3/2} r_3 B_3 \sin\varphi}{I\sqrt{\omega}} e^{\frac{b_1+b_2}{2}(r_3+l_3)}. \tag{6.10}$$

We can now write a general expression for the attenuation factor at point M_n

$$b_n = \frac{8\pi^{3/2} r_n B_n \sin\varphi}{I\sqrt{\omega}} e^{\frac{b_1 + b_{n-1}}{2}(r_n + l_n)} \tag{6.11}$$

The derived series of values $b_1, b_2, b_3, \ldots, b_n$ corresponds to a first approximation. In order to obtain a second approximation we plot values b_n as a function of the corresponding heights h_n; we obtain an approximate picture of the scattering power of the atmosphere at different heights. After extrapolating the curve at level h = 0, we obtain b_0 at the Earth's surface (if b_0 has not been measured directly by some method). Now it is possible to compute somewhat more precisely value $b = b_1$ at point M_1 by using a formula which follows from (6.7)

$$\bar{b}_1 = \frac{8\pi^{3/2} r_{01} B_1 \sin\varphi}{I\sqrt{\omega}} e^{\frac{b_0 + b_1}{2}(r_{01} + l_{01})} \tag{6.12}$$

In computing b_n from formula (6.11) we used an approximate concept that the attenuation of the beam on path OM_n from the searchlight to point M_n and on path M_nA to the observer occurs as if the entire layer of the atmosphere from the ground to height h_n were homogeneous and at all points had the same attenuation factor

$$b_n = \frac{1}{2}(b_1 + b_{n-1}).$$

However, this part of the computation can now be made more precise, because in making computations by the first approximation formula we already divided this layer into a series of intermediate plane-parallel layers (fig. 6.3) $OA\text{-}M_1P_1$, $M_1P_1\text{-}M_2P_2, \ldots, M_{n-1}P_{n-1} - M_nP_n$, each of which can be considered homogeneous with a scattering coefficient

$$\frac{b_0 + b_1}{2}, \quad \frac{b_1 + b_2}{2}, \ldots, \quad \frac{b_{n-1} + b_n}{2}.$$

Attenuation factor b_2 for point M_2, therefore, will be computed more precisely, if the following formula is used in place of (6.9)

$$\bar{b}_2 = \frac{8\pi^{3/2} r_2 B_2 \sin\varphi}{I\sqrt{\omega}}\, e^{\frac{b_0+b_1}{2}\left(r_{01}+l_{10}^2\right)+\frac{b_1+b_2}{2}\left(r_{12}+l_{21}^2\right)}, \tag{6.13}$$

where (fig. 6.3)

$$r_{01} = OM_1; \quad r_{12} = M_{12}M_2; \quad l_{10}^2 = AN_{10}^2 \quad \text{и} \quad l_{21}^2 = N_{10}^2 M_2.$$

Similarly, for point M_3

$$\bar{b}_3 = \frac{8\pi^{3/2} r_3 B_3 \sin\varphi}{I\sqrt{\omega}}\, e^{\frac{b_0+b_1}{2}\left(r_{01}+l_{10}^3\right)+\frac{b_1+b_2}{2}\left(r_{12}+l_{21}^3\right)+\frac{b_2+b_3}{2}\left(r_{23}+l_{32}^3\right)}, \tag{6.14}$$

where

$$r_{23} = M_2M_3; \quad l_{10}^3 = AN_{10}^3; \quad l_{21}^3 = N_{10}^3N_{21}^3; \quad l_{32}^3 = N_{21}^3M_3.$$

In general, for point M_n

$$\bar{b}_n = \frac{8\pi^{3/2} r_n B_n \sin\varphi}{I\sqrt{\omega}} \times$$

$$\times e^{\frac{b_0+b_1}{2}\left(r_{01}+l_{10}^n\right)+\frac{b_1+b_2}{2_j}\left(r_{12}+l_{21}^n\right)+\cdots+\frac{b_{n-1}+b_n}{2}\left(r_{n-1,\,n}+l_{n,\,n-1}^n\right)},$$

or

$$\bar{b}_n = \frac{8\pi^{3/2} r_n B_n \sin\varphi}{I\sqrt{\omega}}\, e^{\sum_{k=1}^{k=n}\frac{b_{k-1}+b_k}{2}\left(r_{k-1,\,k}+l_{k,\,k-1}^n\right)}, \tag{6.15}$$

where

$$r_{n-1,\,n} = M_{n-1}M_n; \quad l_{10}^n = AN_{10}^n; \quad l_{21}^n = N_{10}^nN_{21}^n, \ldots,$$
$$l_{n,\,n-1}^n = N_{n-1,\,n-2}^n M_n.$$

For infinitely thin layers at the limit, when $(h_n - h_{n-1}) \to 0$, we obtain the precise formula

$$\bar{b}_n = \frac{8\pi^{3/2} r_n B_n \sin\varphi}{I\sqrt{\omega}}\, e^{\int_0^{M_n} b_r\, dr + \int_A^{M_n} b_l\, dl}, \tag{6.16}$$

where b_r is the atmospheric attenuation factor at that point of searchlight beam OM_n which is at distance r from searchlight O, and b_l is the attenuation factor at that point of line of sight AM_n which is at distance l from observer A.

Integral $\int_0^{M_n}$ is taken along searchlight beam OM_n and integral $\int_A^{M_n}$ along line of sight AM_n.

Since at all times we assume that attenuation factor b is not dependent on horizontal coordinates, in place of the two integrations for OM and AM we introduce one integration for height h and use the notations

$$\tau_{M_n} = \int_0^{M_n} b_h \, dh, \tag{6.17}$$

where b_h is the attenuation factor at height h_n, τ_{M_n} is the optical thickness of the air layer from ground level to height h_n, at which point M_n is situated. It is obvious that

$$\int_0^{M_n} b_r \, dr = \tau_{M_n} \sec c, \tag{6.18}$$

where c is the angle of elevation of the searchlight beam and

$$\int_A^{M_n} b_l \, dl = \tau_{M_n} \sec b_n, \tag{6.19}$$

where b_n is the angle of elevation of line of sight AM_n.

The precise expression for the attenuation factor at point M_n at height h_n, therefore, can be written in the form

$$\overline{\overline{b}}_n = \frac{8\pi^{3/2} r_n B_n \sin \varphi}{I \sqrt{\omega}} \, e^{\tau_{M_n} (\sec c + \sec b_n)}. \tag{6.20}$$

It was mentioned earlier that the solution of the inverse problem is complex; this applies to the difficulties involved in solution of integral equation (6.20). But under actual conditions the mathematical aspect of the problem is simplified, because a precise solution cannot be used in searchlight sounding. In actuality, the essence of the problem is that value τ for different heights is not known in advance; in order to determine τ it is necessary to know b as a function of height h, but in order to find b at any height, it is necessary to measure the brightness of the beam at this height and in subsequent computations know τ in advance. Precise formulas are of importance for investigation of the transmission of the beam through a medium with known optical properties (direct problem); they are useless if a study is made of the transmission of a beam through a medium with unknown properties and we wish to determine these properties (inverse problem). In this latter problem we knowingly

are limited to measurement of brightness at a finite number of points of the beam and computation of the attenuation factor for a finite number of heights. Therefore, it makes sense to have only an approximate solution of this problem. The degree of accuracy achieved is dependent on the proximity of the points of the beam at which brightness is measured, i.e., on the thinness of the homogeneous layers into which the atmosphere is approximately divided (ref. 226).

6.3. Sounding in Polarized Light. However, in practical implementation of searchlight sounding of the atmosphere it is necessary to remember that each determination of brightness B_1, B_2,..., B_n involves a certain measurement error. In successive computations of attenuation factors b_1, b_2,..., b_n by use of formulas (6.12) - (6.15) there is a gradual accumulation of errors. For this reason an excessive increase in the number n of layers is undesirable. It is also necessary to consider the indicatrix of scattering, which in our derivation was considered spherical. Therefore, we must introduce a factor dependent on the indicatrix into all equations beginning with (6.4). This complication of the formulas and the corresponding computations is insignificant, but the actual difficulties caused by the need to take the indicatrix of scattering into account are very great, because the indicatrix is essentially dependent on height and can change with time. The searchlight method of sounding the atmosphere is considerably simplified if the absolute values of the scattering coefficient (absolute measurements) are unnecessary, and direct data of the distribution of brightness B_1, B_2,..., B_n along the beam (relative measurements) can be used. In combination with simultaneous measurement of the degree of polarization of scattered light at these same points of the beam and spectral measurements (with light filters), relative measurements can serve as a method for obtaining important information on the optical properties of the atmosphere. Without entering into the details of this problem, which is beyond the scope of our discussion (the method for obtaining data on air density and pressure at different heights by the searchlight method of sounding the atmosphere requires absolute, rather than relative measurements), we will restrict ourselves to a few examples.

Measurement of the degree of polarization along a searchlight beam was accomplished for the first time by I. I. Romantsov (refs. 170, 171 and 172) in 1944. The searchlight beam (11.5 kw) was directed at an angle of 60° to the horizon and was photographed, from a distance of 7.6 km, simultaneously by three identical cameras (ref. 171). A Wollaston prism with a 6° dilution angle was placed in front of the f:2.5 objective of each camera. The cameras were directed to the beam at angles of 20, 40, 60 and 80° to the horizon, with mean exposures of 8, 20, 25 and 45 min. Two photographs with short exposures (8 and 20 min) were taken successively with the same camera. The four photographs taken in this manner, (each had two images of the corresponding part of the beam in two mutually perpendicular polarized components) intercepted the searchlight beam in the atmospheric layer from 1.2 to 13.2 km (fig. 6.5). The ratio of intensities of the two polarized components determines the degree of polarization of the light scattered at different heights. Places where dust or

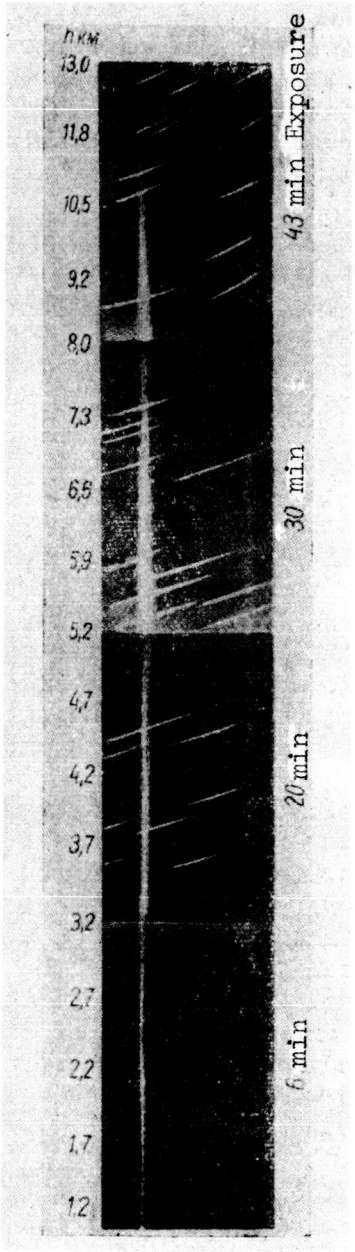

Figure 6.5. Photographs of searchlight beam in polarized light.

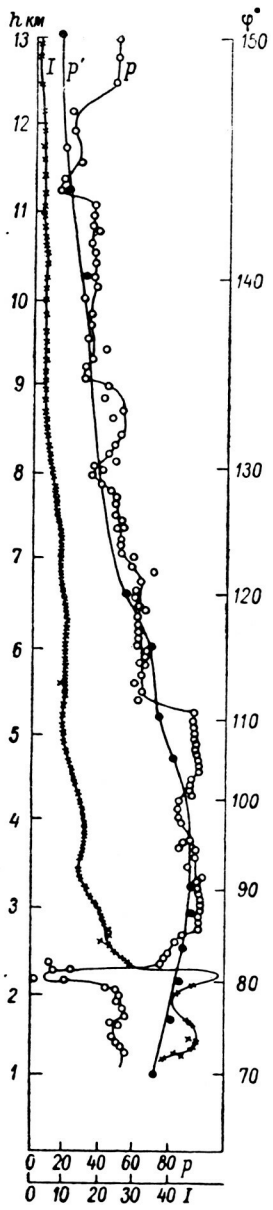

Figure 6.6. Intensity I and degree of polarization p of light scattered by individual air layers as function of height h in km and angle of scattering φ^{o}. Sept. 10-11, 1945.

condensation products have accumulated, but where the cloud stage has not yet developed, and which, therefore, are not visually observable in the sky, can be detected in a searchlight beam of high brightness and low polarization. Atmospheric layers with temperature inversion (such as over clouds) give considerable polarization, indicating great purity of the air (ref. 171). The results of a photometric analysis of the photographs shown in figure 6.5 are given in figure 6.6, where $I = I_1 + I_2$ is the total intensity of scattered light at a particular height (I_1 and I_2 are the intensities of the two polarized components), and p is the degree of polarization of scattered light computed using the formula

$$p = \frac{I_1 - I_2}{I_1 + I_2},$$

where p' is the theoretically computed degree of polarization of light scattered by pure air, dependent on the angle of scattering φ (angle φ is dependent on the direction of the searchlight beam and the angle of observation b, figure 6.1). An attempt at a meteorological interpretation of such optical cross sections of the atmosphere, obtained by the searchlight method of sounding the atmosphere, was made by I. P. Smirnov, who took into account data from aerological sounding and synoptic charts (ref. 178).

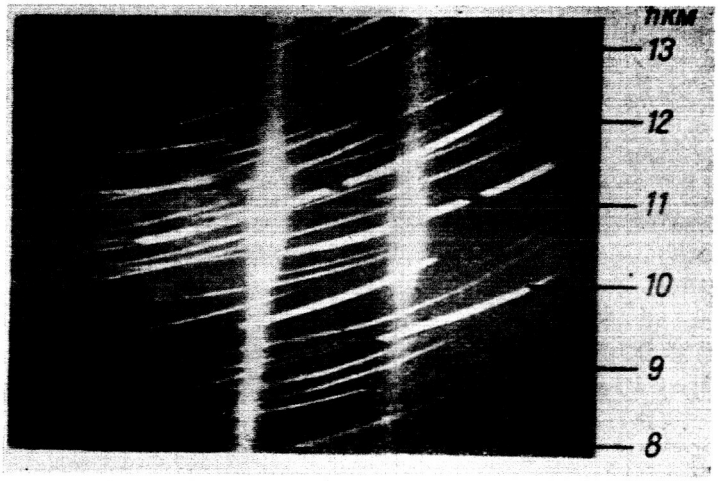

Figure 6.7. Aerosol layer under tropopause photographed in polarized light by searchlight method of sounding the atmosphere.

The photograph in figure 6.7 shows the optical effect of the tropopause detected by the searchlight method of sounding the atmosphere. The tropopause sometimes becomes visible in a searchlight beam because of the aerosol layer underneath (ref. 172). The results of a photometric analysis of the photograph, taken on the night of Aug. 31 - Sept. 1, 1945, are shown in figure 6.8.

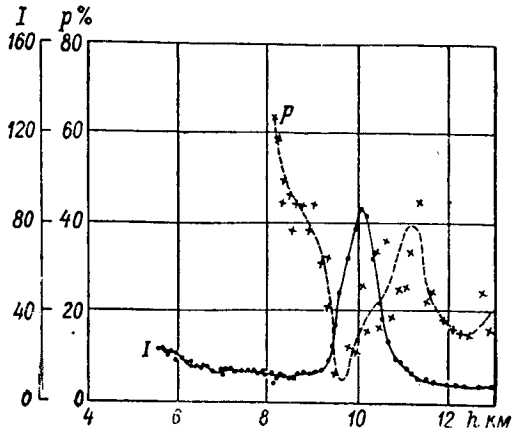

Figure 6.8. Result of photometric analysis of photograph of aerosol layer under tropopause.

Figure 6.9 shows an "optical cross section" of the atmosphere at a height of 26 km, taken Sept. 13, 1953 by A. Ya. Driving and A. I. Smirnova (ref. 65). These photographs of a searchlight beam in polarized light were taken at Bakuriani (Georgian SSR, 41°44'N) at an elevation of 1,800 m above sea level, using three f:1.1 cameras supplied with Wollaston prisms and light filters: the first camera had blue light filters ($\lambda_{eff} = 0.43\,\mu$), the second green ($\lambda_{eff} = 0.50\,\mu$) and the third red ($\lambda_{eff} = 0.62\,\mu$). These photographs are interesting because of the presence of clouds detected at a height of 22.4 km: this height is close to the height of the nacreous clouds usually observed only in winter and mostly over the Scandinavian Peninsula, Finland, Great Britain and Alaska (ref. 236). Driving and Smirnova discovered such a cloud on photographs of a searchlight beam taken at about 0400 hours on Sept. 13, on a windless,dry but cool night with the sky apparently completely clear. Other photographs were taken on that same day in the evening, 18 hours later. Results of the photometric analysis of the two series of photographs are shown in figure 6.10. Three layers of high scattering power can be clearly detected: the first layer at a height of approximately 4 km above sea level, the second at a height of 10-12 km and the third at a height of 21-24 km. The last, the strongest light scatterer, was recorded on the photograph in the form of a stratospheric cloud. The cloud dimensions visible on the photograph correspond to a vertical thickness of about 3 km. The photographs (fig. 6.9) show that the cloud was sufficiently transparent, because despite the great height the searchlight beam,already attenuated, nevertheless penetrated into the atmosphere above the cloud.

On the other set of photographs, taken 18 hours later, there was a decrease of the intensity of scattered light in the region of the stratosphere.

From polarization curves of scattered light A. Ya. Driving and A. I. Smirnova (ref. 65) obtained a radius of cloud droplets of approximately $0.7\,\mu$, on the assumption that at a height of 22.4 km the cloud was relatively monodisperse. This mean radius of droplets of a stratospheric cloud over the

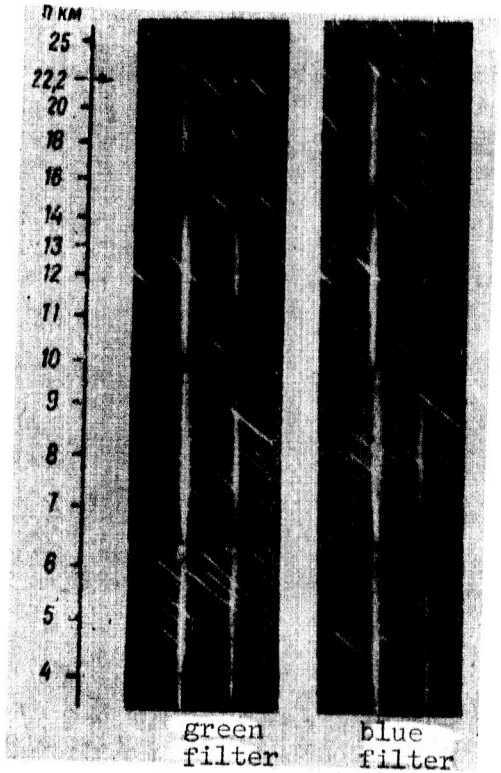

Figure 6.9. "Optical cross section" of the atmosphere (in searchlight beam) in polarized light obtained using green and blue filters. A cloud can be seen in upper part of photographs: its height is 22.4 km.

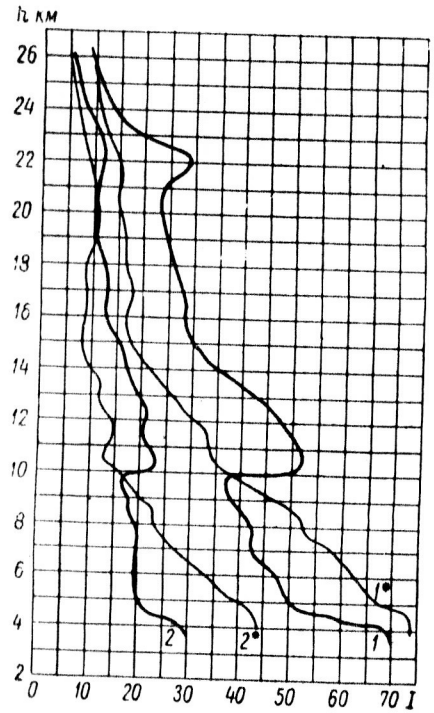

Figure 6.10. Curves of light intensity of searchlight beam scattered by atmosphere at different heights (in relative units). Sept. 13, 1953.
Filters: 1,1*--blue; 2, 2*--green; 1,2--0325 hours--0425 hours; 1*, 2*--2137 hours-2242 hours.

Caucasus is close to the radius of the droplets of a nacreous cloud described by Störmer (ref. 748).

We will present no further details here on the use of the searchlight method of sounding the atmosphere for study of atmospheric stratification and formation of condensation products (ref. 66).

7. Measurement of Air Pressure and Density in the Stratosphere by the Searchlight Method of Sounding the Atmosphere

Systematic measurements of air density in the stratosphere by the searchlight sounding method began in the United States in 1950. These investigations were made by Elterman (refs. 375-378) on a high mountain near the observatory at Albuquerque, New Mexico, in the neighborhood of the White Sands Proving Ground. The searchlight was at an elevation of 2,360 m above sea level and the observation point at a distance of 20.5 km from the searchlight at an elevation of 3,540 m. The same searchlight apparatus was used as in Hulburt's experiments, but with some improvements.

7.1. Elterman's Measurements. During measurements at great elevations the carbon arc operates in a forced regime, and the intensity of the arc discharge increases by 2 kw as a result of an increase of current strength to 180 a (instead of 150 a); this is achieved by decrease of the ballast resistance of the searchlight. The surface of the parabolic reflector is also covered by a layer of rhodium, which improves reflectivity for uv rays. The shutter for covering the searchlight beam consists of a number of blades rotated by an electric motor (fig. 7.1); it changes beam intensity sinusoidally with a frequency of 6 cps.

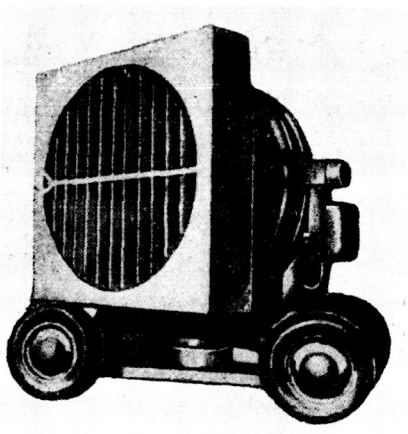

Figure 7.1. Shutter of louvered type for sinusoidal modulation of intensity of searchlight beam (Elterman).

The light receiver consists of a 152 cm parabolic mirror having a photomultiplier with a broad field of view at the focus. The photocurrent is amplified by a narrow-band selective amplifier (band-pass 0.6 cps). The photocurrent created by the measured scattered light of the searchlight beam creates a

potential drop of about 4 v at the input resistance of the amplifier (2.10^8 ohms), if part of the beam at a height of 10 km is recorded, about 1 v at a height of 20 km, about 0.1 v at a height of 40 km and about 0.020 v at a height of 60 km. The amplifier noise level (the noise is created in part by fluctuations of brightness of the night sky) is 0.006-0.011 v (Table 7.1). This makes it possible to sound the atmosphere to a height of about 60 km.

Figure 7.2 is a geometric diagram of Elterman's measurements (ref. 376). Because of the complete identity of searchlight mirror O and receiving mirror A, the angle of aperture of the cone of searchlight rays is $\theta = 1.25^\circ$ and is equal to the angular value of the field of view of the receiver. The scattering volume is determined by the intersection of the cone of rays with the lines of the field of view (sector L along the searchlight beam).

Elterman believes that light scattering in the stratosphere conforms to the Rayleigh law, and that the flux of luminous energy incident on the receiver is

$$I_{p\lambda} = I_{0\lambda} \frac{2\pi^2 (\mu - 1)^2 (1 + \cos^2 \varphi)}{n\lambda^4} L\omega, \tag{7.1}$$

where $I_{0\lambda}$ is the total flux of luminous energy at the wavelength λ incident on a surface perpendicular to the axis of the searchlight beam; μ is the refractive index of the scattering medium; φ is the angle of scattering; n is the number of molecules per cubic centimeter. Since for air $\mu - 1 = \eta_\lambda n$, where η_λ has an almost constant value in the region 3,000-7,000 Å, equal to $1.08 \cdot 10^{-23}$, Elterman replaces equation (7.1) by

$$I_{p\lambda} = I_{0\lambda} \frac{2\pi^2 \eta^2 n (1 + \cos^2 \varphi)}{\lambda^4} L\omega, \tag{7.2}$$

or

$$I_{p\lambda} = K_1 I_{0\lambda} n \frac{(1 + \cos^2 \varphi)}{\lambda^4}, \tag{7.2a}$$

where K_1 is a factor which Elterman assumes to be constant. For this case he has analyzed geometric relations, relating to figure 7.2, which show that the product $L\omega$ remains constant for different angles of view b.

Attenuation of rays on their path in the atmosphere is taken into account by Elterman by the following approximate method (ref. 376). There are three causes of attenuation: molecular scattering of light, light scattering by aerosol particles and light absorption. The attenuation factor association with molecular scattering is known to be

$$b = \frac{32\pi^3 \eta_\lambda^2 n}{3\lambda^4} \tag{7.3}$$

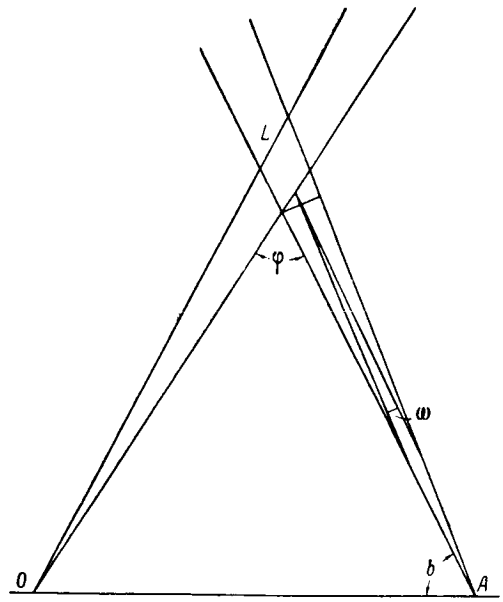

Figure 7.2. Geometric diagram of Elterman's measurements.

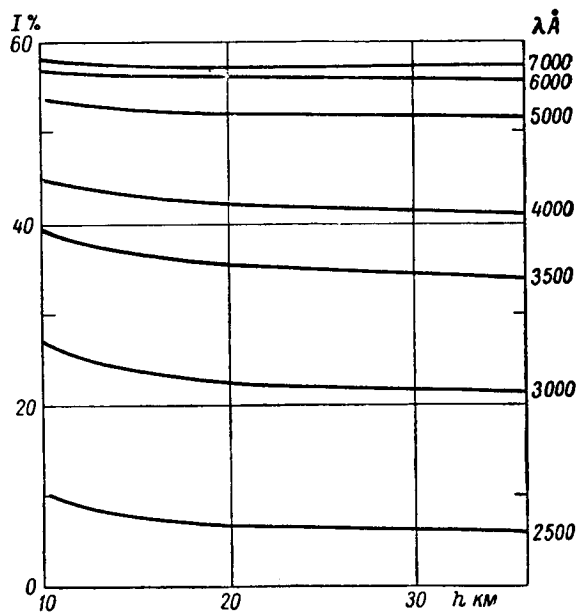

Figure 7.3. Attenuation of energy of searchlight beam by aerosol and molecular scattering of light. I percent--radiant flux in percent of initial value.

Attenuation caused by aerosol scattering and absorption is difficult to compute; it is dependent on such varying factors as industrial haze and mist. Using data from the literature on atmospheric transparency, Elterman assumes that in the case of a vertically directed searchlight beam 10-58 percent of the energy of the radiant flux I reaches a height of 10 km above sea level; this value is dependent on λ as shown in figure 7.3 (see the values applying to a height of 10 km). For heights greater than 10 km Elterman assumes that attenuation occurs only by molecular scattering and computes it using formula (7.3). Results of computations are represented by the curves in figure 7.3, which give the energy of the radiant flux reaching the scattering volume at a particular height. Attenuation is small in the stratosphere, which is the object measured. After analyzing the curves in figure 7.3, Elterman concludes that ratio $\frac{I_{0\lambda}}{\lambda^4}$ in equation (7.2a) for this region of the spectrum, perceived by the photocathode, is almost constant, and consequently he further simplifies equation (7.2a), replacing it by

$$I_p = K_2 n (1 + \cos^2 \varphi), \tag{7.4}$$

where I_p is the integral value of the energy in the effective sector of the spectrum emitted by the scattering volume in the direction φ, and K_2 is a constant (ref. 376). The linearity of the characteristic of the light receiver permits the assumption that voltage E_0, measured at the output of the instrument, is proportional to radiant flux I_p; therefore

$$E_0 = Cn (1 + \cos^2 \varphi). \tag{7.5}$$

This formula is used for computation of air density n (number of molecules per cc). Constant C is determined by comparison with radiosonde readings, from which it is possible to find n using formula

$$n = 7.29 \cdot 10^{18} \frac{p}{T}, \tag{7.6}$$

where p is pressure in millibars and T is absolute temperature, measured by radiosonde at any suitable height h (such as 15 km). The radiosonde readings for each night were used by the Aerological Observatory at Albuquerque to determine

$$C = \frac{E_0}{n (1 + \cos^2 \varphi)},$$

where E_0 is the reading of the receiver used in searchlight sounding for the same height h.

TABLE 7.1. VERTICAL AIR DENSITY DISTRIBUTION (NUMBER n OF MOLECULES PER 1 CM^3) DETERMINED BY SEARCHLIGHT SOUNDING OF ATMOSPHERE (ACCORDING TO ELTERMAN). AUG. 19 - NOV. 16, 1950.

Height, km	Aug. 19-20	Sept. 7-8	Sept. 9-10	Sept. 12-13	Sept. 13-14	Oct. 11-12	Oct. 13-14	Nov. 15-16
9.3	$9.6 \cdot 10^{18}$	$9.2 \cdot 10^{18}$	$9.7 \cdot 10^{18}$	$1.1 \cdot 10^{19}$	$1.1 \cdot 10^{19}$	$9.9 \cdot 10^{18}$	$9.9 \cdot 10^{18}$	$8.3 \cdot 10^{18}$
10.7	7.7	8.2	8.4	$9.5 \cdot 10^{18}$	$9.2 \cdot 10^{18}$	8.1	8.4	7.3
11.9	6.6	7.2	7.2	8.2	7.7	7.0	7.4	6.6
13.3	5.7	6.0	6.2	6.8	6.2	5.9	6.0	5.5
14.6	4.8	5.3	5.5	5.6	5.1	5.0	4.9	4.5
15.9	4.0	4.3	4.3	4.7	4.3	4.2	4.0	3.7
17.4	3.3	3.5	3.3	3.3	3.3	3.3	3.0	2.7
18.8	2.7	2.7	2.6	2.4	2.7	2.4	2.5	2.0
20.5	2.0	2.1	2.0	1.8	2.1	1.9	1.7	1.5
22.3	1.6	1.4	1.4	1.3	1.6	1.4	1.3	1.1
24.4	1.1	$9.8 \cdot 10^{17}$	1.1	$9.4 \cdot 10^{17}$	1.1	$9.3 \cdot 10^{17}$	$8.5 \cdot 10^{17}$	$7.6 \cdot 10^{17}$
27.4	$6.9 \cdot 10^{17}$	6.1	$6.5 \cdot 10^{17}$	5.6	$6.7 \cdot 10^{17}$	5.5	4.9	3.9
29.7	4.6	4.1	4.9	3.7	4.4	3.7	3.3	2.5
31.9	3.4	2.9	3.1	2.8	3.2	2.5	2.3	1.8
34.1	2.4	2.1	2.1	1.8	2.1	1.6	1.6	1.2
37.8	1.2	1.2	1.1	1.1	1.2	$9.7 \cdot 10^{16}$	$8.0 \cdot 10^{16}$	$7.6 \cdot 10^{16}$
41.5	$7.4 \cdot 10^{16}$	$7.8 \cdot 10^{16}$	$7.4 \cdot 10^{16}$	$5.9 \cdot 10^{16}$	$7.7 \cdot 10^{16}$	6.4	5.3	5.1
45.9	4.3	4.2	4.4	3.0	4.2	3.8	3.3	3.1
51.0	2.2	2.2	2.5	1.7	2.0	2.1	2.0	2.0
56.0	1.4	1.4	1.5	$9.1 \cdot 10^{15}$	—	1.2	1.3	1.2
58.6	1.0	1.0	1.1	7.1	$9.5 \cdot 10^{15}$	$9.3 \cdot 10^{15}$	1.0	$7.6 \cdot 10^{15}$
61.8	—	$6.8 \cdot 10^{15}$	$7.5 \cdot 10^{15}$	5.0	6.3	6.2	$6.9 \cdot 10^{15}$	4.7
Noise level	0.011	0.011	0.011	0.011	0.11	0.010	0.010	0.0062
Radiosonde	138	142	140	124	120	142	138	128
data p mb	209.4	207	212	206	204	205	202,2	204.6
T^oK	$4.65 \cdot 10^{-19}$	$4.6 \cdot 10^{-19}$	$4.2 \cdot 10^{-19}$	$5.2 \cdot 10^{-19}$	$5.0 \cdot 10^{-19}$	$5.07 \cdot 10^{-19}$	$5.28 \cdot 10^{-19}$	$6.4 \cdot 10^{-19}$
C	14.6	14.9	15.0	16.65	15.9	14.6	14.6	14.6
h km								

7.2. Vertical Distribution of Density. Regular measurements were begun in the summer of 1950; 8 curves of the vertical distribution of air density (Table 7.1) were obtained in August-November. In most cases these curves coincide well with the standard atmosphere, which was used in those years in the United States for 45°N (fig. 7.4). Elterman notes the presence of a seasonal variation (ref. 376): in August, 1950 the densities were greater than standard, in October somewhat less than standard at heights of 20-25 km, and in November appreciably less than the standard values.

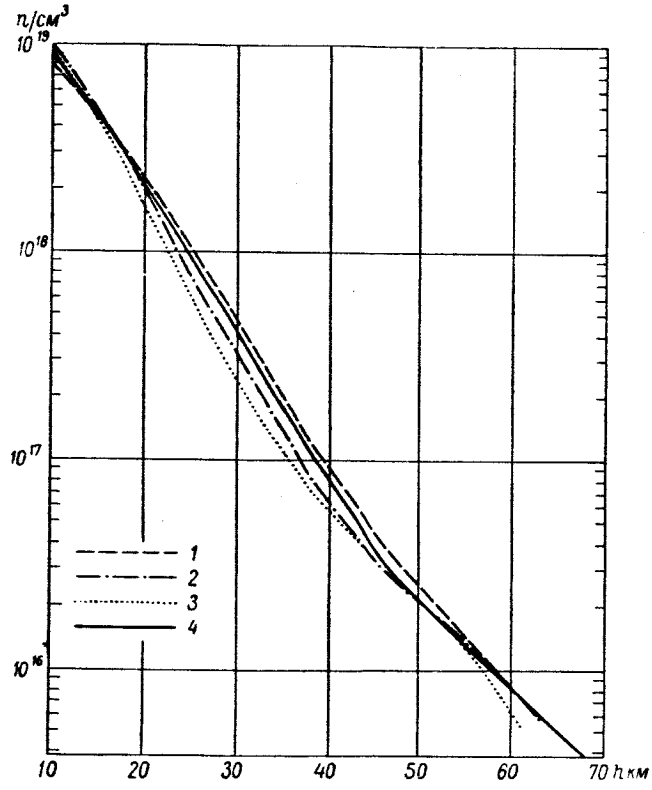

Figure 7.4. Density distribution determined from searchlight sounding data (Elterman), 1950.
1--Aug. 19-20; 2--Oct. 13-14; 3--Nov. 15-16; 4--standard atmosphere.

Elterman cites some data characterizing measurement errors. The distance from the searchlight to the receiver was 21.5 km, measured with an accuracy to 0.3 km; readings of the angles b and the angle of elevation of the searchlight are given with an accuracy of ± 3'; linearity of the amplifier characteristic is determined to an accuracy of 1 percent; accuracy of voltmeter reading is determined to an accuracy of 5 percent, including fluctuations of battery voltage, calibration errors, etc. The measurements are tied into the radiosonde readings for h = 15 km, where the error of pressure measurement is about 6 mb and the error of temperature measurement (at nighttime when the radiosonde is not illuminated by the solar rays) is about 0.5°.

In subsequent years, in the course of regular measurements of air density in the stratosphere, Elterman (ref. 377) introduced improvements in the apparatus and measurement method, resulting in increase of accuracy and increase of the sounding ceiling to 67.6 km. In particular, a light filter was placed in front of the photomultiplier. The light filter absorbed the strong emission lines of oxygen and sodium atoms in the night airglow between 5,500 and 6,500 Å. Allowance for the sky background was improved by measurement of sky brightness when the position of the receiver mirror was at an angle of 120°, i.e., oriented in a direction parallel to the searchlight beam. This control measurement considered, to some degree, the effect of multiple scattering caused by illumination of the atmosphere by the searchlight. As an example we cite the following individual measurements for the typical night of Oct. 22, 1952, when 6 distribution curves (each 30 min) were measured during a 3 hour period (from 2100 to 2400 hours):

Height, km	Instrument readings, microvolt							
	E_1	E_2	E_3	E_4	E_5	E_6	E_m	E_0
9,50	555	550	550	540	540	530	544,3	542,7
20,70	127	120	120	122	125	120	122,3	120,8
37,87	12.0	12,0	12,0	12,0	12,0	12,0	12,0	10,50
60.74	2.04	2,27	2,22	2,45	2,17	2,23	2,230	0,739
67.60	1,78	1,92	2,06	2,03	1,94	1,86	1,931	0,440
E_{120}	1,49	1,69	1,48	1,41	1,48	1,40	1,491	

Here E_1 - E_6 are the readings in the 1st to 6th soundings, E_{mean} is the mean of 6 measurements, E_{120} is the background reading. The corrected reading $E_0 = E_{mean} - E_{120}$ is used in the analysis. Figure 7.5 shows the vertical density distribution obtained from these measurements. Table 7.2 shows the results of 5 series of density measurements over Albuquerque.

Each of the series is the mean of 5-6 soundings made during a period of abou four hours. The constant in formula (7.5) was determined from radiosonde readings at heights of 20-25 km, obtained with an accuracy of ±4 mb and ±1° for pressure and temperature, respectively.

Elterman notes (ref. 377) that to a height of 45 km the night-to-night density distribution remains almost identical. At the 45 km level there is a transition from the region of stable distributions to appreciable variations, attaining 17 percent (fig. 7.6).

The mean density values for October, 1952 agree well with the data for the standard atmosphere to a height of 55 km; above this level they are less than the standard values (about 11 percent at a height of 64 km).

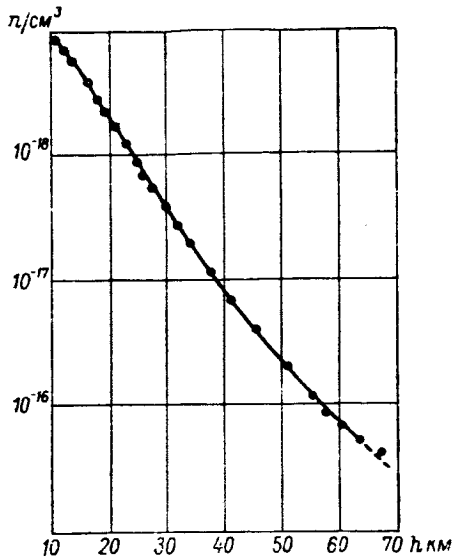

Figure 7.5. Density distribution in stratosphere from measurements with searchlight beam. Oct. 22, 1952 (Elterman).

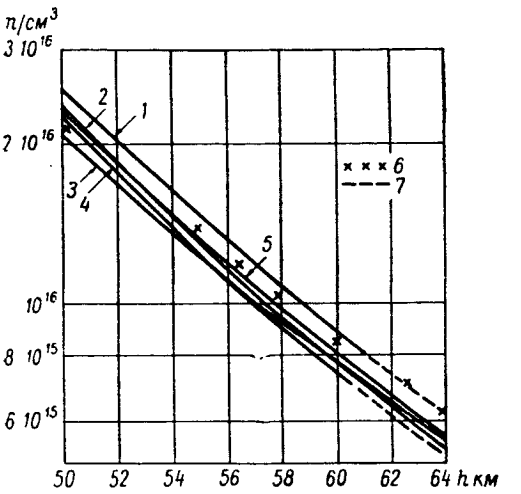

Figure 7.6. Density distribution in 50-64 km region on basis of searchlight sounding data (Elterman).

TABLE 7.2. STRATOSPHERIC AIR DENSITY (NUMBER n OF MOLECULES PER 1 CM^3) DETERMINED BY SEARCHLIGHT SOUNDING. OCTOBER, 1952 (ACCORDING TO ELTERMAN).

Height, km	Oct. 10 1900 hrs 2140 hrs	Oct. 18 1910 hrs 2140 hrs	Oct. 22 0120 hrs 0500 hrs	Oct. 22 2100 hrs 2400 hrs	Oct. 23 2100 hrs 2400 hrs
	1	*2*	*3*	*4*	*5*
9.50	$9.41 \cdot 10^{18}$	$9,88 \cdot 10^{18}$	$9,86 \cdot 10^{18}$	$9,81 \cdot 10^{18}$	$9.92 \cdot 10^{18}$
10,82	7,98	8,54	8,36	8,33	8,44
12,12	6,84	7,22	6,97	7,03	7,07
13,42	5,78	5,94	5,67	5,71	5,86
14,74	4,74	4,74	4,60	4,66	4,73
16,10	3,87	3,79	3,68	3,74	3,82
17,53	3,08	3,00	2,89	2,93	3,03
19,06	2,38	2,31	2,21	2,25	2,31
20,70	1,78	1,74	1,67	1,69	1,76
22,53	1,29	1,27	1,21	1,23	1,28
24,60	$9,05 \cdot 10^{17}$	$8,82 \cdot 10^{17}$	$8,61 \cdot 10^{17}$	$8,75 \cdot 10^{17}$	$9,10 \cdot 10^{17}$
25,98	7,20	7,03	6,83	7,03	7,20
27,53	5,54	5,50	5,32	5,45	5,62
29,83	3,80	3,80	3,66	3,73	3,89
31,85	2,82	2,74	2,68	2,75	2,86
34,16	2,03	1,93	1,88	1,93	1,98
37,87	1,19	1,12	1,08	1,12	1,15
41,29	$7,42 \cdot 10^{16}$	$7,06 \cdot 10^{16}$	$6,63 \cdot 10^{16}$	$6,95 \cdot 10^{16}$	$7,15 \cdot 10^{16}$
45.51	4,23	4,16	3,70	3,97	4,08
50,84	2,30	2,16	1,91	2,04	2,11
55,28	1,42	1,27	1,21	1,21	1,29
57,87	1,09	$9,53 \cdot 10^{15}$	$9,26 \cdot 10^{15}$	$9,26 \cdot 10^{15}$	$9,87 \cdot 10^{15}$
60,74	$8,27 \cdot 10^{15}$	7,25	6,97	7,20	7,62
63,97		5,40		5,33	5,66

7.3. Pressure Determination. In 1952 Elterman made a total of 90 soundings of the atmosphere with a searchlight beam to a height of more than 60 km. The measurements were made on 18 nights (May-October). Elterman took the following important step in analysis of the results of the observations (refs. 377, 378): he used the density distribution curves to compute the air temperature values at heights of 10-67 km (the method and results of temperature determination will be considered in Chapter 5). With the vertical distribution curves for density and temperature Elterman computed air pressure p at these heights.

Table 7.3 gives the mean monthly density and pressure values (1952) and the averaged values for the entire period from May 29 through Oct. 23, 1952.

These data reveal the presence of three layers differing from one another in the character of density change (ref. 378), falling in the limits 9.5-20, 20-45 and 45-67.6 km.

In the 9.5-20 km layer the day-to-day changes of density distribution are small and agree well with radiosonde readings. The density values obtained from searchlight observations usually slightly exceed the radiosonde data, but this difference decreases with height (fig. 7.7). This is due to the influence of non-Rayleigh light scattering.

In the 20-45 km layer there is a small variability of the vertical distribution of density, agreeing with the standard atmosphere.

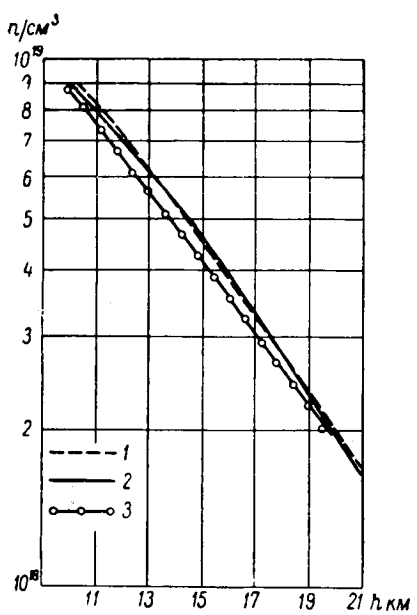

Figure 7.7. Comparison of density distribution obtained by searchlight method of sounding the atmosphere with radiosonde and with standard atmosphere data (Elterman). 1--searchlight sounding (October, 1952; 2--radiosonde; 3--standard atmosphere.

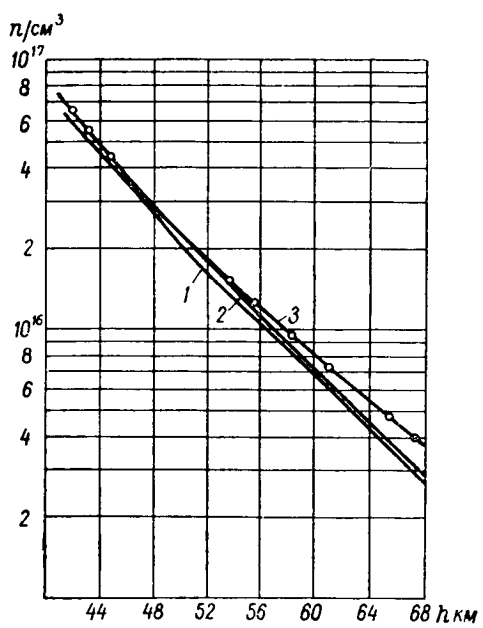

Figure 7.8. Comparison and mean monthly density distribution (searchlight sounding), 1952. 1--June; 2--September; 3--October.

TABLE 7.3. DENSITY (NUMBER n OF MOLECULES PER 1 CM^3) AND PRESSURE p IN mb DETERMINED BY SEARCHLIGHT SOUNDING DATA. 1952. (ACCORDING TO ELTERMAN)

Height, km	June		Sept.		Oct.		May 29 -Oct. 23	
	n	*p*	*n*	*p*	*n*	*p*	*n*	*p*
9.50	$9{,}28 \cdot 10^{18}$	306.8	$9{,}61 \cdot 10^{18}$	305.9	$9{,}82 \cdot 10^{18}$	308,5	$9{,}60 \cdot 10^{18}$	306.9
10.82	8,10	253.4	8,20	250,9	8,38	251,8	8,24	252,1
12.12	6,96	207.2	6,93	205.4	7,09	205.2	6,97	205.6
13,42	5.83	168.0	5.79	166.8	5.82	166.1	5,82	166,9
14,74	4.83	135.2	4,75	134.3	4,68	133.6	4,77	134.2
16,10	3.94	107.0	3.83	106,7	3.77	106.6	3,83	106,7
17.53	3,07	83.82	3,01	83,83	3,00	83,97	3.01	84,25
19.06	2,34	64,53	2,31	64,97	2,31	65,29	2.31	64.97
20.70	1.74	49.18	1.74	49.42	1.72	49.79	1,73	49.60
22,53	1.26	36.30	1.26	36.82	1,25	37.22	1,27	36.94
24,00	$8.76 \cdot 10^{17}$	26.20	$8{,}90 \cdot 10^{17}$	26,50	$8{,}97 \cdot 10^{17}$	26,95	$8{,}93 \cdot 10^{17}$	26.59
25.98	6,92	21.17	7,07	21,34	7.06	21.79	7.08	21,47
27,51	5.40	16,74	5,50	16,83	5,52	17.34	5.48	16.99
29,83	3,72	11.84	3.78	11.88	3,81	12.39	3,78	12,03
31,85	2.73	8.840	2.74	8,834	2.77	9.273	2,75	8.98
34,16	1.90	6,387	1,93	6,355	1,96	6,777	1,93	6.51
37,87	1.09	3,873	1,10	3,803	1,15	4,150	1,11	3,94
41,29	$6.70 \cdot 10^{16}$	2,500	$6.72 \cdot 10^{16}$	2,425	$7{,}14 \cdot 10^{16}$	2,684	$6.76 \cdot 10^{16}$	2.550
45.61	3.80	1,496	3,75	1,430	3,95	1,631	3,84	1,544
50.84	2.00	0,779	1.90	0.753	2,07	0,886	2,00	0,820
55,28	1.20	0,458	1,14	0,446	1,28	0,550	1,23	0,494
57,87	$8.97 \cdot 10^{15}$	0,332	$8.57 \cdot 10^{15}$	0,327	$9{,}94 \cdot 10^{15}$	0,413	$9{,}35 \cdot 10^{15}$	0,366
60.74	6.56	0,230	6,33	0,229	7,53	0,299	6,95	0,257
63,97	4.55	0,149	4,42	0,150	5,53	0,202	4,89	0,170
67.00	2.89	0,887	2,86	0,090	3,86	0,124	3,20	0,104

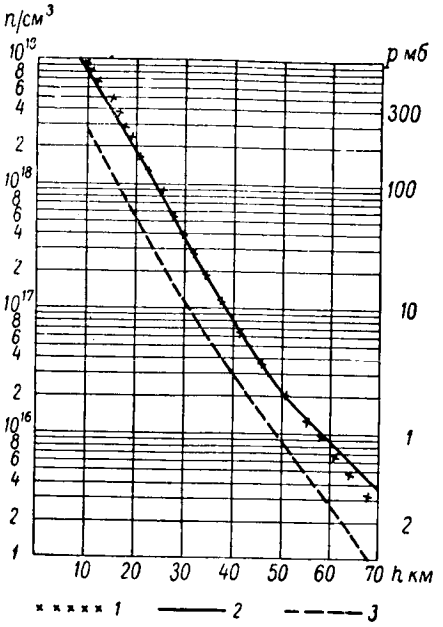

Figure 7.9. Density distribution (1, 2) and pressure distribution (3) over New Mexico, United States, on basis of data from searchlight sounding of the atmosphere (mean for May 29 - Oct. 23, 1952).
1, 3--searchlight sounding; 2--standard atmosphere.

The 45.0-67.6 km layer is characterized by considerable variations. On 1 of the 18 nights there were density values greater than for the standard atmosphere, on 3 nights the density values were the same as for the standard atmosphere, and on 14 nights the density values were smaller (up to 16 percent lower at a height of 60 km). The curves usually converge at a height of ~ 45 km.

Figure 7.8 shows a comparison of the mean curves for heights of 42-67 km for different months in 1952. Figure 7.9 gives a comparison of the mean density distribution curve for May-October 1952, constructed using data obtained by searchlight sounding, and the standard atmosphere; it also shows a pressure distribution curve based on observations of a searchlight beam.

There is every basis to assume that in the coming years the searchlight method of sounding the atmosphere will be used even more extensively for systematic air pressure and density measurements in the stratosphere.

The searchlight method of sounding the atmosphere also is used for study of the temperature regime of the upper layers of the atmosphere (ref. 233).

CHAPTER 4. USE OF ROCKETS AND SATELLITES FOR MEASUREMENT OF ATMOSPHERIC PRESSURE AND DENSITY

8. Measurement of Pressure and Density by Instruments Carried Aloft by Rockets

The first successful attempts to use rockets for atmospheric investigations were made in the United States in 1945, using small Wac Corporal rockets. These rockets, developed by the California Institute of Technology for the artillery forces of the United States Army, carried a payload of about 10 kg to approximately 65 km. However, systematic launchings of rockets into the high layers of the atmosphere did not begin until 1946 in the United States, when that country acquired captured A-4 rockets from Germany.

Study of cosmic radiation by means of rockets was begun in the USSR in 1947 by a group of scientists under the direction of S. N. Vernov. A specially adapted rocket was launched in 1949 to obtain data on the state of the atmosphere at heights up to 100 km (ref. 12). On the basis of the results of this experiment it was possible to formulate clear requirements about the research method and the necessary apparatus. Special geophysical rockets were developed at the request of the Academy of Sciences USSR, and light meteorological rockets intended for extensive and systematic use were constructed at the request of the Main Administration of the Hydrometeorological Service of the Council of Ministers of the USSR. Beginning in 1951 these rockets came into use for regular soundings of the atmosphere.

Rocket apparatus usually is placed in the nosecone of a rocket. Because of the need to avoid distortions introduced by the rocket itself during its flight, including the contamination of air samples by gas trails which accompany the rocket, the apparatus on Soviet geophysical rockets was frequently placed in a special instrument package (ref. 679). The instrument package was placed in a mortar on the side of the rocket and separated from the body on the ascending part of the rocket trajectory after the engine ceased to operate (for further details see figures 8.3 and 8.4).

The use of rockets for investigation of the upper layers of the atmosphere requires preliminary implementation of major theoretical, laboratory and engineering design studies.

The disturbance of the medium by a rapidly moving rocket, or an instrument package separated from it, and the influence of direct solar radiation cause the readings of many instruments to deviate from the true values of the measured parameters of the free atmosphere. It was necessary, therefore, to develop theoretical approaches for computing the true characteristics of the atmosphere from the direct readings of the instruments. It was also necessary

to create measuring instruments and radio equipment for transmitting information to Earth, capable of withstanding strong vibrations and great accelerations. All the rocketborne apparatus had to be of small size and weight.

Research rockets are divided into two classes on the basis of the fuel used: liquid, using a liquid fuel and a liquid oxidizer, and solid fuel, containing an oxidizer in the form of a solid fuel component (of the gunpowder type).

A rocket with a liquid-fuel engine is a more complex system than an engine operating on solid fuel. For a long time liquid-fuel rockets have remained the more perfect of the two, but it can be foreseen that in the future research rockets will employ solid fuel.

A great many requirements are imposed on research rockets. The size of the payload in large-scale rocket sounding usually is 5-10 kg, but it sometimes attains 60-70 kg. Decrease in the weight of research apparatus will make it possible to lower the cost of the rocket.

The height of ascent of the rocket is determined by the experimental problem, and for meteorological purposes it should fall in the range 50-120 km.

The launching of a research rocket should be in a direction close to vertical. Even simple liquid-fuel rockets are complex to handle, and modern telemetric systems require highly skilled servicing personnel. As a result, rocket soundings now are made at specially equipped test grounds or from aboard ships.

In addition to the launching of a rocket directly from the ground, it can be launched from any vehicle aloft: a balloon or aircraft. Due to the fact that in this case the launching of the rocket is in the less dense layers of the atmosphere, it is possible to attain great heights, using an engine of relatively limited power and, accordingly, a rocket of small size. However, the techniques involved in such a launching are quite complex.

Rockets can also be launched from specially equipped vessels. Such work was carried out during the Antarctic voyage of the Soviet expeditionary vessel "Ob'" (ref. 15a), and now is being carried on in the northern and southern hemispheres on the Soviet weather ships "Voyeykov" and "Shokal'skiy" on their voyages through the Pacific Ocean (ref. 69b). American investigators are sounding the atmosphere in the Pacific Ocean, North Atlantic and polar regions (ref. 251).

Tail finning is most important for the stabilization of a rocket in flight; however, this is effective only in flight at a rather great velocity in the dense layers of the atmosphere. Launching towers with guides are therefore used for the launching of uncontrolled rockets.

In addition to the accelerations developing in ascent there are important vibrational accelerations caused by the operation of the engine and aerodynamic effects as the rocket passes through the dense layers of the atmosphere. These rapidly varying accelerations can also be dangerous for the apparatus.

The velocity of the rocket during ascent can attain 1,500 m/sec or more. At such velocities high temperatures develop at the surface of the rocket nosecone, and if there is no thermal insulation or special external protection the measuring instruments can be damaged. A research rocket, therefore, must have a minimum velocity of motion, but this is contradictory to the fact that it must be stable. A compromise solution must be found.

Many measurement results can be transmitted from the rocket by telemetric apparatus, but sometimes it is necessary to recover the records on film or the samples obtained, such as air samples. The problem arises of recovering the instrument package. This can be accomplished by giving the package a form possessing high aerodynamic resistance or by use of parachutes. Systems for the recovery of instruments on parachutes have been used in some American Aerobee rockets, but considerably earlier they were used extensively with Soviet meteorological and geophysical rockets and fully proved their value (ref. 1).

The Soviet meteorological rocket can be cited as an example of a rocket specially adapted for investigation of the stratosphere. It carries instruments for temperature and pressure measurement in the free atmosphere and some other measurements, as will be discussed later.

At a specified time the rocket separates into two parts: the nosecone, which carries measuring instruments and instruments for transmitting information, and the engine. Immediately after separation the parachutes are released and the apparatus descends to Earth supported by them.

The tracking of the ascent of the rocket before separation and the descent of its parts after separation can be accomplished using motion picture base measurements or using a suitable system of radio direction finding.

Arrangement of the instruments is shown schematically in fig. 8.1. A "spire" 25 mm in diameter and 740 mm long is mounted in front of the nosecone of the rocket along its axis. In its foreward part the spire houses thermal manometers of the Pirani type, which measure pressure in the range from $5 \cdot 10^{-3}$ to 5 mm Hg. The outlets of the Pirani gages are situated at a distance of 6.5 calibers from the end of the spire. Pressure in the range 5-760 mm Hg is measured by membrane manometers whose outlets extend to a distance of about 9 calibers from the end of the spire.

It should be noted in particular that the Soviet meteorological rocket is equipped with resistance thermometers which measure air temperature in the range of heights up to 60-80 km (on American and other foreign rockets air temperature at such heights was not determined directly until recently, but from data on the vertical distribution of pressure).

Four resistance thermometers manufactured of tungsten wire 40 μ in diameter are mounted in the central part of the spire. The resistance thermometers are attached at some distance from the surface of the spire and at the time of movement are engulfed by the air flow.

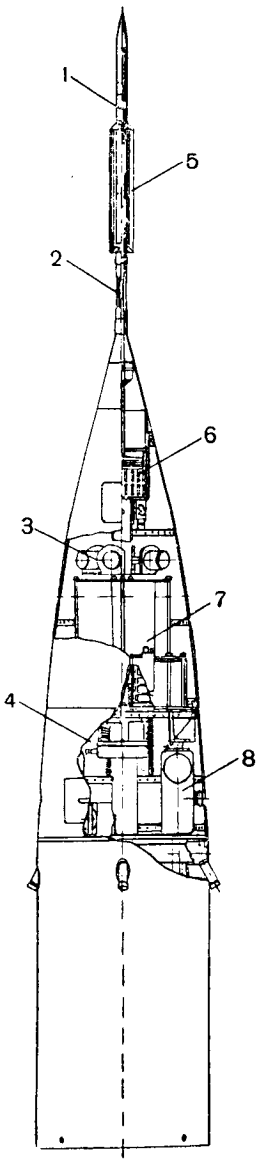

Figure 8.1. Diagram of arrangement of measuring instruments in nosecone of Soviet meteorological rocket. (1) Thermal manometers, (2) bolometers, (3) membrane manometer, (4) transmitter, (5) resistance thermometer, (6) commutator, (7) storage batteries, (8) camera.

A copper resistance thermometer is wound on the central part of the spire for measurement of the temperature of its surface.

On some types of Soviet meteorological rockets there are four bolometers below the thermometers, at the base of the spire. These bolometers are designed for measurement of the flux of solar radiation incident on the corresponding resistance thermometer. In the case of thermal and membrane manometers there

are auxiliary thermometers installed for checking the heat regime within the nosecone. There are four cameras for determining the position of the rocket in space; these are synchronized and are in a single plane with an angle of 90° between the axes of the objectives (ref. 251).

The nosecone of the rocket is divided into three compartments. The first compartment contains the commutator of the telemetric system, the group of membrane manometers and the electric power source. The second compartment contains the radio transmitter of the telemetric system and camera, and the third contains the nosecone parachute.

All the rocketborne measuring instruments are connected to a circuit of unbalanced Wheatstone bridges with a common source of electric current and the diagonals of the bridges are connected to the commutator of the telemetric system. There is time separation of communication channels in the telemetric system. The voltages from the commutator are fed successively to the input of the telemetric transmitter whose frequency changes in accordance with the change of the fed voltage.

The receiving apparatus of the telemetric system consists of a radio receiver with a panoramic attachment. The latter contains a system for automatic changing of the resonance frequency, making it possible, by tuning the receiver at the mean frequency of the transmitter, to watch on a kinescope screen the signals of all the frequencies in the scanning band of the panoramic adapter. The width of the scanning band corresponds exactly to the width of the frequency scanning band of the transmitter.

The signals are recorded by photographing the kinescope screen with a movie camera; the film moves in a direction perpendicular to the scanning trace of the signals.

Each commutation cycle begins with the transmission of reference voltage signals which are fed from a special bridge made up of highly stable resistors. The reference signals ensure calibration of the telemetric system in each commutation cycle during operation of the apparatus.

The telemetric system is freed of interference by recording each signal on movie film several times. Therefore both constant and brief interference can be distinguished from useful signals.

The signal displacement on the telemetric film is proportional to the voltage fed to the transmitter input. Examination of the film on a comparator and the use of the calibration curves of the measuring instruments make it possible to establish the readings of the instruments, recorded as functions of time. Mathematical analysis of the telemetric records together with the results of laboratory experiments for determination of the coefficients entering into the theory makes it possible to find the parameters of the free atmosphere as a function of height (ref. 251).

Some data on the types of rockets used for study of the atmosphere abroad can be found in a book (ref. 678) edited by Boyd and Seaton (in collaboration

with Massey) and later and more complete information in a collection of articles (ref. 626) and in an article by M. G. Kroshkin (ref. 96).

8.1. Measurement Methods. The determination of air pressure and density at great heights by instruments carried aloft in rockets involves many difficulties. Various measurement methods have been developed and used (refs. 263, 538, 563, 625, 706, 707, 726 and 735). The theory of the interpretation of the measurement results should take into account the great velocity of motion of the rocket: in a large part of its trajectory the rocket flies at supersonic velocity. We will now discuss the principal problems involved in the interpretation theory (ref. 251).

We will first consider some physical concepts applied later. The speed of sound is denoted a and is determined by the relation

$$a^2 = \gamma \frac{R}{\mu} T,$$

where $\gamma \frac{c_p}{c_v}$ is the ratio of the heat capacities of the gas at constant pressure c_p and constant volume c_v; R is the universal gas constant; μ is the molecular weight of the gas (for a mixture of gases it is equal to the mean molecular weight) and T is the absolute temperature of the gas.

The Mach number M is the dimensionless ratio

$$M = \frac{V}{a}, \tag{8.1}$$

where V is the velocity of motion of a body relative to the gas medium at a particular point.

The Reynolds number Re is the dimensionless ratio

$$\mathrm{Re} = \frac{LV}{\nu},$$

where L is the characteristic dimension of the body engulfed in the flow; $\nu = \frac{\eta}{\rho}$ is the kinematic viscosity of the engulfing medium (η is its dynamic viscosity; ρ is density).

The Prandtl number Pr is the dimensionless ratio

$$\mathrm{Pr} = \frac{\nu}{\chi},$$

where $\chi = \frac{k}{\rho c_p}$ is the coefficient of temperature conductivity of the gas (k is the coefficient of thermal conductivity).

When computing the effect of free molecular flow on the surface of a solid body, it is necessary to use the concept of the accommodation coefficient α, determined as the dimensionless ratio

$$\alpha = \frac{E - E_r}{E - E_s},$$

where E is the mean energy of the translational, rotational or vibrational degrees of freedom of the molecules colliding with the wall; E_r is the energy of the corresponding degrees of freedom after reflection; E_s is the energy of these degrees of freedom corresponding to the temperature of the wall. The accommodation coefficients show the efficiency of energy transfer of the corresponding degrees of freedom in a single collision of molecules with the wall.

The theory should take into account the existence of different regions of gas flow. We introduce the dimensionless parameter

$$\xi = \frac{M^2}{Re}.$$

If $\xi \ll 1$ the law of engulfment of a body by an onflowing gas is described by the well-known Navier-Stokes equation. This corresponds to the theoretically well-developed field of continuous gasdynamics.

If $\xi \gg 1$ the equations of hydrodynamics are inapplicable. This is flow when the length of the free path of the molecules is so great that the discrete character of the gas medium is the principal factor determining the flow. This less well-studied type of flow is called free molecular.

The least investigated region is where $\xi = 1$. This is shearing flow. An important characteristic of such flow is that in an analysis of streamline flow around a solid body by a gas the relative velocity of flow at the boundary cannot be considered equal to zero. The gas seemingly slides along the surface of the solid body. In addition, if the temperature of the gas is different from the temperature of the engulfed body, there will be a temperature jump at the discontinuity.

According to Tzyan, the discontinuities between the regions of flow are determined by the values ξ: in the region $\xi \leq 0.1$ the laws of continuous gasdynamics apply, in the region $\xi \geq 10$--the laws of free molecular flow, and in the intermediate region--flow with shearing.

These values ξ should be regarded as approximate criteria. In actuality, transition from one region to another is not related to any precise value ξ and occurs continuously.

In rocket soundings the character of the interaction of the instrument changes with height, and as a result of large changes in Mach numbers and Reynolds numbers the process passes through all three regions of flow. For this reason a rigorous allowance for gasdynamic effects of interaction is necessary for the correct interpretation of the instrument readings.

The value ξ is of the order of magnitude of the ratio of the length l of the free path of molecules to the characteristic dimension L of flow multiplied by the Mach number

$$\xi \simeq \frac{l}{L} M.$$

In all problems of atmospheric physics and meteorology dry air can be considered an ideal gas in the molecular-kinetic sense. However, in gasdynamic problems associated with rocket sounding this same dry air can by no means always be considered an ideal medium.

An ideal medium in the gasdynamic sense is a medium for which the properties of heat conductivity and viscosity have vanishing small values.

Adiabatic and isentropic flows are possible only for an ideal gasdynamic medium.

If the velocity V of movement of any body in the air is increased to the speed of sound a, the character of air flow around the body increases substantially, especially in the region of supersonic velocities. The theory accordingly becomes more complicated. The reason for the qualitative change of the phenomenon with transition from subsonic to transonic and supersonic flow is associated primarily with the fact that continuous changes (small perturbations) of pressure, density and velocity are propagated along the gas particles (small volumes of gas) with the speed of sound. If the velocity of flow V is less than the speed of sound a (the Mach number M is small), small perturbations are propagated in all directions, including the direction opposite the velocity of flow. If the flow is supersonic ($M>1$), the perturbations are carried downstream. When the current velocity V is constant (in the case of a small source), the perturbations do not exceed the limits of the cone of perturbations (angle of aperture 2α, where $\sin \alpha = \frac{a}{V}$).

In many cases of supersonic flow (with any deceleration accompanying the transformation of supersonic into subsonic flow), there is formation of a shock wave, a layer with the thickness of the order of magnitude of the free path of molecules, in which there are sharp changes of velocity, density, pressure, temperature and other characteristics of the state of the medium.

When a gas flows around an obstacle at supersonic velocity, a shock wave develops in front of the obstacle; in gasdynamics the shock wave front can usually be considered a geometric surface separating the flow into two regions: in front of and behind the shock wave front.

At the shock wave frontal surface, the parameters of the state of the gas and the velocity of flow experience a discontinuity. The thickness of the shock wave front is of the order of magnitude of the free path of the molecules in the gas. Therefore, with increasing distance into the upper layers of the atmosphere the thickness of the shock wave front in front of the rocket expands, and in the long run the concept of a shock wave loses it meaning.

Depending on the configuration of the engulfed body, the wave front can touch the fore point of the obstacle or be at some distance from it in the direction of the oncoming flow.

In the case of axial flow around a cone, the picture is determined by the angle of aperture: with increase of the latter to some critical value (and at a constant Mach number) the shock wave front withdraws from the point in the direction of flow.

Gasdynamics makes it possible to compute the state of the gas and the velocity of flow behind the shock wave front, if the state and velocity of the gas in front of the shock wave front are known. The simplest formulas are derived for a plane front orthogonal to the flow.

Pressure p_1 directly behind the shock wave front will be equal to the pressure on the fore part of the cone, because in the space from the front to the nose of the cone the flow experiences total deceleration. Therefore, after denoting the Mach number in this region of space by M_1, we obtain the following formula for deceleration pressure

$$p_a = p\left(1 + \frac{\gamma-1}{2} M_1^2\right)^{\frac{\gamma}{\gamma-1}},$$

in which the value p_a is the pressure directly on the point of the cone (p is pressure to the front).

The relationship between the Mach number M of free flow and M_1 is established in gasdynamics in the following form

$$M_1^2 = \frac{1 + \frac{1}{2}(\gamma-1)M^2}{\gamma M^2 - \frac{1}{2}(\gamma-1)}$$

These two equations relate the gas pressure in free flow and total pressure through the Mach number of free flow. This relationship was established by Rayleigh.

Figure 8.2 shows photographs of a uniformly moving flow engulfing a body whose configuration is similar to the configuration of the forward part of the body of a rocket. The pattern of streamline flow around the body is shown in these photographs as it appears to an observer related to the body (ref. 175). If the velocity of relative flow (velocity of a steady-state flow at an infinite distance from the body) is subsonic, the surrounding flow is smooth (fig. 8.2a), the trail behind the projectile is filled by eddies and the body experiences resistance, caused by the formation of the eddies and friction on the surface of the body. As velocity V approaches the speed of sound, supersonic zones form

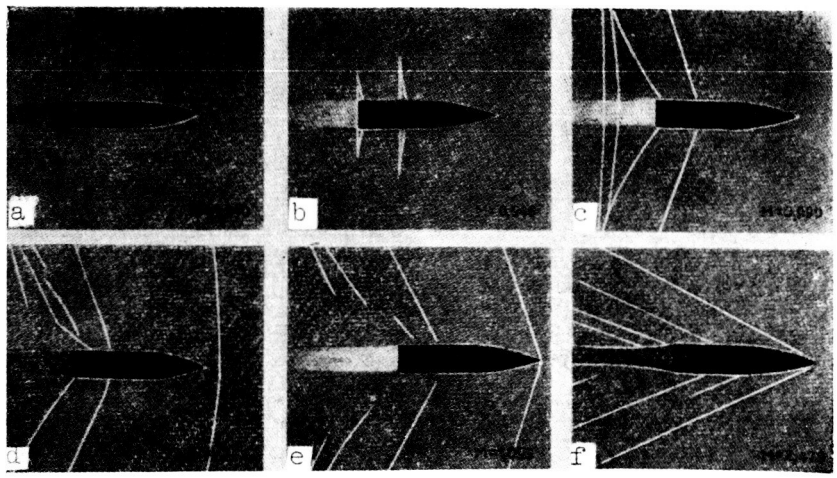

Figure 8.2. Shadow photographs of a shell during free flight at subsonic ($M < 1$) and supersonic ($M > 1$) velocities.

near the body. Figures 8.2b and 8.2c show shadow photographs of the shock wave appearing at the end of the supersonic zones near the body at the time of transonic flow. When supersonic velocities are reached, the shock waves become stronger, assume a conical configuration and begin at the tip and tail of the engulfed body (fig. 8.2f).

During the flight of a rocket at supersonic velocity the air pressure, density and temperature at its surface can differ considerably from these values distant from the rocket, i.e., in the undisturbed flow (for brevity we will refer to them as undistorted values). On a theoretical basis it is possible to determine the relationship between the measured values and the conditions in the undisturbed medium around the rocket; this is necessary in an analysis of the data obtained during rocket investigations of the upper layers of the atmosphere. However, for practical purposes such measurements involve serious difficulties and can usually be made only approximately for individual cases. The problem is simplified if we are concerned with a fully slowed-down flow. In the case of an adiabatic slowing of the flow, there is a transformation of the kinetic energy of the flow into thermal energy, and therefore deceleration pressure (velocity head), deceleration density and deceleration temperature exceed the pressure, density and temperature of the oncoming flow by a certain number of times, which can be computed precisely. For example, the deceleration temperature is 800°K when the rocket velocity is 1 km/sec. Deceleration pressure can be measured reliably at the tip of the rocket nosecone. When there is total deceleration of the flow of an ideal medium in the region of continuous gasdynamics, an equilibrium temperature T_a will be established, determined by the relation

$$T_a = T\left(1 + \frac{\gamma - 1}{2} M^2\right), \tag{8.2}$$

where T and M are the temperature and the Mach number of free flow, respectively, T_a is the temperature of adiabatic slowing which is established in an ideal medium posssessing velocity V = Ma, if all its kinetic energy of ordered motion $1/2\ \rho\ V^2$ is transformed without losses into the energy of disordered thermal motion.

The pressure setting in when there is total adiabatic slowing (p_a) can be determined from (8.2), if the temperature is expressed through pressure in accordance with the adiabatic equation

$$p_a = p\left(1 + \frac{\gamma - 1}{2} M^2\right)^{\frac{\gamma}{\gamma - 1}}.$$

During flow around bodies the viscosity and heat conductivity of the medium are manifested in some layer adjacent to the engulfed surface; this is called the boundary layer.

As a result of viscosity there will be slowing of the gas in the layer, but in an analysis of this process it is no longer possible to regard the gas as an ideal medium.

We will visualize a thermometer, placed in a high-velocity gas flow, and will attempt to determine what steady-state temperature will be recorded by it (ref. 251).

This important problem has been solved only for the special case of a flat thermometer engulfed by a gas, when the velocity vector of the flow is parallel to the plane of the thermometer.

We will first consider the pattern obtained during the flow of an ideal medium. Due to the absence of viscosity, the gas will slide freely along the surface of the thermometer and will everywhere possess velocity $\vec{V}$ and temperature T. However, if the velocity vector $\vec{V}$ is turned 90° counterclockwise, the temperature of adiabatic slowing determined by equation (8.2) is established at the surface.

Since in the course of real measurement the thermometer everywhere will be exposed to the flow, and therefore viscosity appears in the boundary layer, the approximation expressed by the concept of an ideal medium is not suitable. The problem should be solved taking viscosity and heat conductivity into account.

Solution of this problem for gasdynamic flows leads to the following result. If the solution was obtained with a boundary condition for T expressing absence of heat exchange between the thermometer and the gas, and for $\vec{V}$ expressing absence of sliding along the discontinuity, an equilibrium temperature T_e should be established at the surface of the thermometer; T_e is expressed as follows

$$T_e = T\left(1 + r(\mathrm{Pr})\frac{\gamma-1}{2}M^2\right). \tag{8.3}$$

where r(Pr) is some function of the Prandtl number, called the temperature restitution coefficient.

When $\mathrm{Pr} \leq 1$, the value $r(\mathrm{Pr}) = \sqrt{\mathrm{Pr}}$. For this reason formula (8.3) in the region of continuous gasdynamics can be replaced by the following

$$T_e = T\left(1 + \sqrt{\mathrm{Pr}}\frac{\gamma-1}{2}M^2\right). \tag{8.4}$$

For air Pr = 0.72, $\gamma = 1.4$. and we can write

$$T_e = T(1 + 0.17M^2).$$

This formula can be used for an approximate estimate of the temperature setting in at the surface of a body engulfed by a high-velocity air flow.

We note that when Pr = 1, formulas (8.4) and (8.2) coincide and $T_e = T_a$. This means that in the case of plane-parallel flow along a wall such a gas behaves as an ideal medium.

In an experimental investigation r is considered a function of the following variables

$$r = r(\mathrm{Pr}, \varphi', l, \xi, M, p), \tag{8.5}$$

where φ' is the angle of attack, l is the form factor taking into account the difference between the form of the thermometer and a plate.

In accordance with (8.1) and (8.3), r can be represented in the form

$$r = \frac{T_e - T}{\frac{1}{2}\frac{V^2}{c_p}}, \tag{8.6}$$

which is convenient in experimental investigations.

With such an approach it becomes possible to go outside the limits of the region of gasdynamic flow by making an experimental study of the form of the function (8.5) on the basis of tests in wind tunnels.

It can be shown for free molecular flow (on a theoretical basis) that at large M for a plane thermometer and $\varphi' = 0$

$$r = \frac{2\gamma}{\gamma+1},$$

which for air leads to a value r = 1.18; with a decrease of M the value r increases somewhat further.

The results of exposure of fine long wires in wind tunnels have shown that r in actuality is dependent on ξ, M, φ' and p.

For convenience in the experimental study of the influence of viscosity and heat conductivity on the value of deceleration pressure, as a result of its nonlinearity relative to M^2 we can introduce the coefficient s of pressure restitution, much like (8.6), determined by the relation

$$s = \frac{p_e - p}{\frac{1}{2}\rho V^2},$$

making it easy to obtain

$$p_e = p\left(1 + \frac{\gamma}{2} sM^2\right) = p\left(1 + \frac{s}{2}\frac{\mu}{R}\frac{V^2}{T}\right).$$

We note that r = 1 corresponds to adiabatic slowing.

Significant errors can arise as a result of the release of gases from the body of the rocket. It is possible to decrease the influence of the release of gases and other disturbances introduced by the rocket into the investigated medium by employing the instrument packages used in the investigations. The instrument packages are used for making measurements distant from the rocket. The instrument package is carried aloft to a specified height in the rocket mortar. At a programmed height it is ejected from the mortar and continues its motion by inertia. After the instrument package is separated from the rocket, the measuring apparatus is switched on, and measurements in the atmosphere are begun. As it falls downward the parachute opens and the instrument package, with all instruments intact, reaches the surface (ref. 128).

A completely different principle is the basis for the method of measuring air density from precise observations of the trajectory of a falling sphere. Careful determinations of the trajectory of a sphere make it possible to estimate the deceleration it experiences. Density of the medium can be computed from the deceleration value. This method will be discussed in greater detail in Section 8.4.

Finally, a completely independent group of methods for determining air pressure at the height of the ionospheric E layer and above it is based on measurement of the absorption of solar X-radiation as a function of height and density measurement from the absorption of radiation and air luminescence (ref. 336).

Atmospheric pressure p, density ρ and absolute temperature T are related to one another by the equation of state

$$p = \rho RT \qquad (8.7)$$

and the barometric formula

$$dp = - \rho g \, dh, \tag{8.8}$$

where g is the local value of acceleration of gravity at height h. If two parameters are measured, the equation of state gives the value of the third, expressed by molecular weight m. Then, by using the equation of state, the barometric formula can be transformed in such a way that it contains two of the three values p, ρ and T. Consequently, if one of the values is obtained as a function of height from the measurements, the second can be computed by corresponding differentiation or integration, with the error customary in such operations. The relation between p and ρ does not include the mean value of the molecular weight m, but it is essential that m be in the formulas relating T to ρ or p.

8.2. Manometers. A rocket flying in the upper layers of the atmosphere passes through air layers in which the pressure changes from hundreds of millimeters to thousandths and millionths of a millimeter Hg. There is no instrument to measure such differing pressures, and therefore manometers of several types are usually carried on the same rocket.

Two types of manometers have been selected for pressure measurement in the USSR (ref. 128): a magnetic electrical discharge manometer and a thermal manometer. The first type is used for pressure measurements in the range $5 \cdot 10^{-2}$ - $1 \cdot 10^{-5}$, and the second type in the range 0.8-0.05 mm Hg.

The operation of thermal manometers is based on the fact that the heat conductivity of gases is dependent on pressure, if the latter becomes less than some limit at which the length of the free path of molecules becomes commensurable with the size of the container. If a metal filament heated by an electrical current is placed in a container filled with gas at sufficiently low pressure, the decrease of the pressure of the gas surrounding the filament will result in a decrease of the quantity of heat emanating from the filament, which in turn causes an increase of the temperature of the filament, if the heat flux to it remains constant. A temperature increase occurs until the heat loss through heat conductivity of the gas no longer increases, due to the increase of the temperature of the filament to such an extent that equilibrium between the quantity of the received and released heat again sets in.

The principal instrument is a Pirani gage. The sensing elements--a mechanical resistor for high pressures and a thermistor for low pressures--are connected to the opposite arms of a Kelvin bridge. Since the thermistor possesses a negative temperature coefficient of resistance, both resistors change the balance of the bridge in the same direction.

Influence of the temperature of the manometer walls on its readings is excluded by compensation due to the change of the supply current of the bridge and indirect heating of the thermistor.

The manometer is attached to the inner surface of the wall of the rocket The inertia of the instrument is about 0.5 sec at a pressure of 0.2. Change in resistance of the filament indicates the change of the temperature of the filament and therefore the change of gas pressure. The transfer of heat from the filament through the gas is dependent on the degree with which the gas molecules upon collision with the filament assume a mean velocity corresponding to the temperature of the filament, i.e., the heat transfer depends on the mechanism of reflection of the molecule from the filament (on the accommodation coefficient), which is different for different gases. Manometers based on heat conductivity, therefore, must be calibrated by comparing their readings with other manometers.

In order to broaden the limits of measurements with a thermal monometer, French investigators have developed an instrument which uses a thermistor as a second sensing element (ref. 470).

At very small pressures (less than 10^{-3} - 10^{-4} mm Hg), the heat conductivity of gases becomes so insignificant that its further change with still greater pressure decrease can no longer exert an appreciable influence on the heat regime of the filament, this determines the lower limit of sensitivity of this manometer.

The operation of a magnetic electrical discharge manometer is based on the principle that the strength of a gas discharge current depends on the gas pressure within the manometer.

As already mentioned, in the investigations the apparatus was enclosed in an instrument package separating from the rocket in the upper layers of the atmosphere. The manometer sensors were mounted in the upper, open compartment of the instrument package (fig. 8.3). The intake openings of the manometers are in places where wind tunnel experiments have shown that the deviation of local pressure from statistical pressure is not more than ±30 percent for angles of attack not exceeding 20° and for Mach numbers not greater than 2.7.

The lower compartment of the instrument package contains measuring instruments, photorecorder, clock and power source. The compartment is tightly sealed. Normal atmospheric pressure is maintained in this compartment and in the airtight conduit through which pass the high-voltage leads in the upper compartment; this pressure is maintained during the entire measurement process. The electrical leads emerge from the lower compartment and enter the upper compartment through special vacuum connections.

The manometers are carried aloft in a sealed condition with specified internal pressure. At the required height a special bulge at the end of the manometer tube (fig. 8.4) is broken, the manometer is then open to the atmosphere, and pressure measurement in the surrounding atmosphere begins (ref. 128).

In some experiments for the measurement of pressures in the range from 1 atm to 20 mm Hg, a manometer with an aneroid capsule is used (ref. 625). Pressures of less than 10^{-3} mm Hg are measured with ionization manometers. The

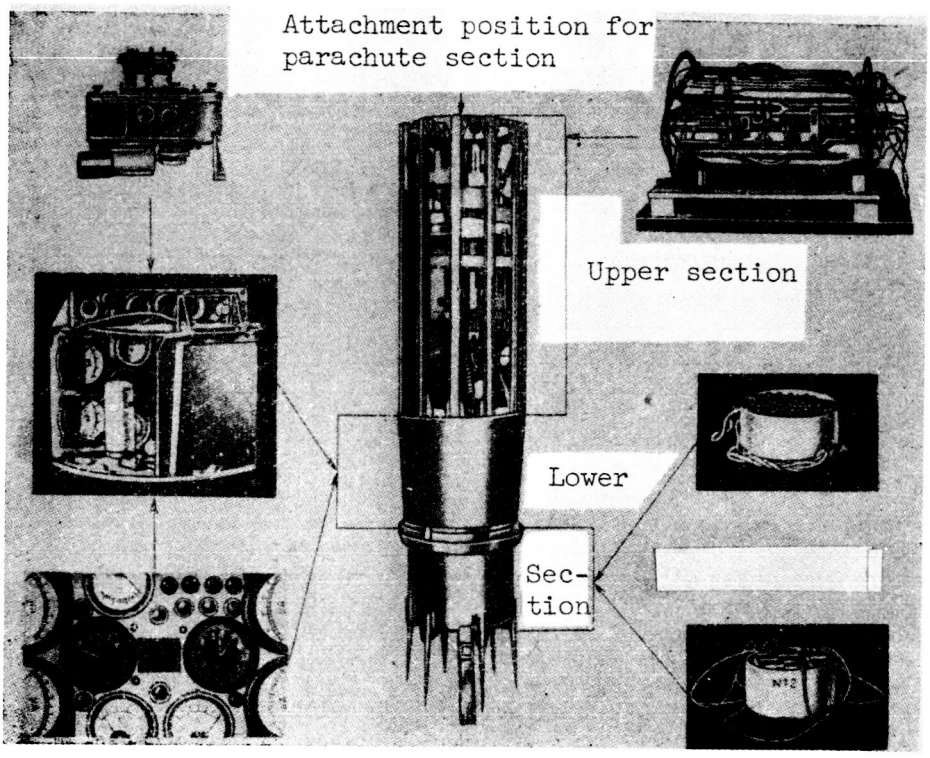

Figure 8.3. Instrument package used in investigations.

operation of ionization manometers, which can be designed using any standard three-electrode system such as used in radio tubes, is based on the phenomenon of impact ionization of molecules by electrons.

The kinetic energy which an electron acquires with the passage of a potential difference of V volts is equal to eV, where e is the electron charge. When this energy exceeds a certain critical value, there will be some definite probability that the collision between an electron and a molecule of the gas leads to the formation of a positive ion. This probability changes in dependence on the value V and on the nature of the gas.

An electron possessing a relatively great velocity ionizes a molecule when colliding with it. If a constant accelerating potential is maintained at a level exceeding the ionization potential V_i, at low pressures the mean number of positive ions formed by one electron changes linearly with a change of gas pressure.

Under these conditions the rate of formation of positive ions at a specified constant electron current can serve as a measure of pressure. An ionization manometer is a discharge tube in which there is not only a cathode and

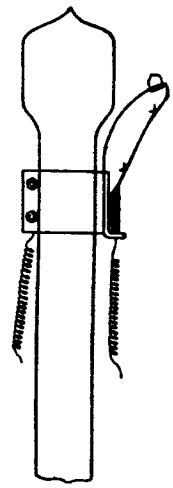

Figure 8.4. Appearance of bulge at end of manometer with hammer for breaking bulge.

anode, but also a third electrode--a collector with a negative potential relative to the cathode. The ion current in the collector circuit, whose intensity is a measure of gas pressure in the tube, is fed to the telemetric circuit. Specialists at the United States Naval Research Laboratory use Phillips ionization manometers with a cold cathode for pressure measurements in the range 10^{-3} - 10^{-6} mm Hg. In certain cases a Havens "cyclic manometer" (ref. 427) is

is used for pressure measurements from 1 to 10^{-3} mm Hg. In investigations made on Aerobee rockets by a group of electrical engineers at the University of Michigan, extensive use was made of a manometer called "alphatron." This instrument (refs. 726, 735) is an ionization manometer in which the ionization energy source is a small quantity of radium (usually about 1 mg). The α-particles emitted by the radium source possess sufficient energy to produce many ionization events at the time of collisions with the gas particles filling the manometer. Accordingly, the arranged electrodes create an electrical field which traps the ionization products. The current developing in the external circuit is proportional to the number of particles ionized in 1 sec, and, therefore, to the gas density in the chamber.

Measurements established that the temperature of the manometer walls and, therefore, of the gas do not change appreciably during the short time of the rocket flight. Therefore, for this range of densities the ratio of gas pressure to its density is constant, and consequently the alphatron can be calibrated for pressure measurements.

Figure 8.5 shows the standard design of the alphatron.

The main external characteristic curve of one such manometer used for rocket measurements is shown in figure 8.6. This is a typical curve of the dependence of current intensity I on pressure p in the chamber (at constant temperature). The minimum measured pressure is essentially dependent on the

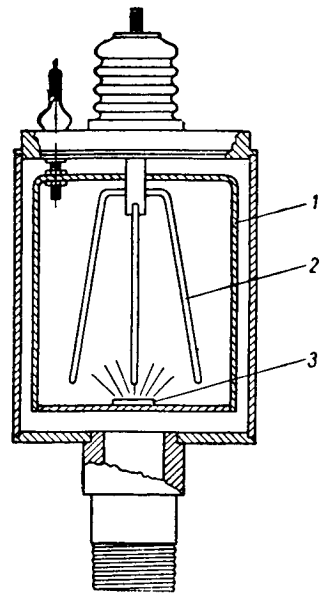

Figure 8.5. Diagram of alphatron manometer. (1) Electrode, (2) collector electrode, (3) radium source.

strength of the "dark current"--the value which the lower part of the curve approaches asymptotically. The upper measurement limit is determined by the recombination of ionized particles until the ionization products are trapped and measured; this corresponds to the knee at the upper part of the curve. The current intensity at the manometer output is only 10^{-8} - 10^{-10} a, and a multistage current amplifier therefore must be used. The wide range of pressures which can be measured by this instrument (about four orders of magnitude) makes it necessary to use several scales of different sensitivity.

In order to increase the accuracy of the alphatron readings the entire range of pressures measured by it has been divided into eight subranges, each of which corresponds to an interval of voltages fed to the telemetric circuit, from 0-5 v. For example, the sixth subrange is designed for pressures of 0.06-0.005 mb, the fifth--for 0.3-0.06 mb, the fourth for 1.23-0.3 mb, etc. In each subrange the voltage at the output is 0-5 v.

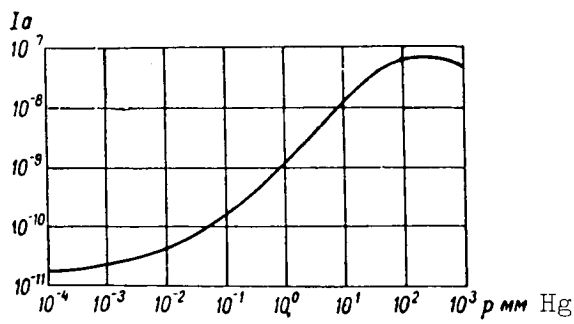

Figure 8.6. Characteristic curve of alphatron manometer.

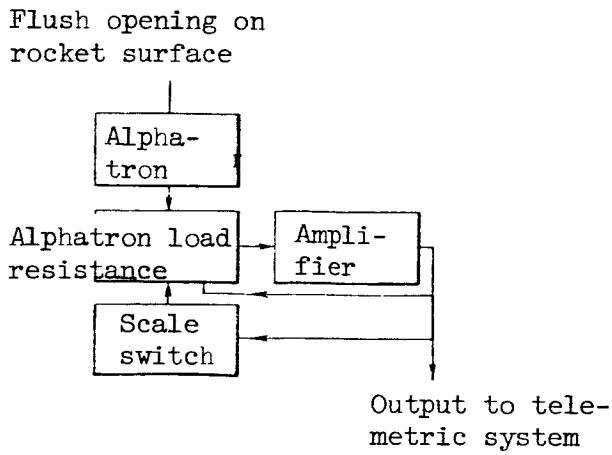

Figure 8.7. Block diagram of pressure measurement by alphatron.

A rough block diagram of this instrument is shown in figure 8.7. The alphatron current passes through a load resistance (up to $2.5 \cdot 10^{11}$ ohms), which is connected in series to the circuit of the control grid of an electrometer tube serving as input resistance for the first amplification stage. The following sections of the amplifier contain, in particular, two voltage amplification stages. For a step change of sensitivity there is a replacement of the load resistance of the alphatron. This is accomplished by an automatic sensitivity switch which is triggered in dependence on the signal strength at the amplifier output. The switch contains two thyratrons which control a solenoid rotating in two directions. If the voltage of the output signal exceeds a previously set value or becomes less than some other specified value there will be switching--replacement of the load resistance of the alphatron by an adjacent resistance (smaller or greater, respectively).

In addition to these manometers there is one which has been proposed (but is not in extensive use), which is based on use of isotopes (ref. 776). A foil to which a thin layer of material with adsorbed tritium is applied (up to 400 Mc) is attached to the inner side of the cylindrical chamber of this instrument. The strong β-radiation emitted by the tritium ionizes the gas in the chamber. A positive potential is fed to the foil and the insulated filament situated along the axis of the chamber is fed a negative potential. The developing current decreases the potential difference ΔV, and when it attains a specific value a pulse is fed and the initial potential difference is restored. The process is repeated at intervals of time

$$T = \frac{C \Delta V}{\alpha p_0},$$

where C is the capacitance of the chamber, p_0 is pressure in the chamber and α is a constant. The instrument withstands an overload up to 100 g and weighs 85 g.

We also will discuss the ion altimeter described by Zito (ref. 815). This instrument has a radioactive ionization manometer with a cold cathode as a sensing element. The instrument operates to a height of 45-75 km. It is enclosed in a thermostat which ensures a constancy of temperature in the range $\pm 0.1^{\circ}$. The instrument also includes an electromechanical amplifier with a converter to a frequency of 400 cps, a two-channel servoamplifier, motors and potentiometers. The output is a rotating rod occupying 21,600 positions for a range of heights up to 45 km. The altimeter weighs 2.5 kg. The accuracy of height measurement (on the basis of pressure) is 0.2 percent.

8.3. Some Problems in the Analysis of Observations. At the surface of a "true"-flying rocket, i.e., a rocket whose longitudinal axis at all times is parallel to the flight trajectory, there is a zone some distance from the nose of the rocket at which pressure has the same value as in the surrounding undisturbed medium (for brevity, we will refer to it as the "zone of undistorted pressure"). In the first experiments in investigation of the upper layers of the atmosphere with rockets an effort was made to place the manometers in this zone. The presence and position of the zone of undistorted pressure was established both experimentally in wind tunnels and theoretically (refs. 128 and 625). In addition, this was checked by comparison of rocket measurements with the readings of radiosondes obtained during this same period of time near the rocket launching point. A detailed checking reveals that pressure coincides with an accuracy of 1-2 percent. Since such good agreement of control comparisons applies to parts of the trajectory in which the rocket flies with a transonic velocity, there is great assurance that in the entire extent of the flight the measurements give the true values of atmospheric pressure. This assurance is further supported by the fact that comparison of the vertical pressure distribution curves obtained using rockets with greatly differing ascent ceilings, and therefore flying at a particular height with an extremely dissimilar velocity, will not have serious systematic errors in the sectors where the curves are superposed on one another (ref. 625).

However, the situation changes if the rocket moves at a certain angle of attack, i.e., in such a way that the direction of flight does not coincide with the direction of the axis of the rocket. In this case there will be an error whose value depends on the angle of attack. This systematic error always must be taken into account since any rocket in flight experiences yawing. The effective angle of attack is caused either by the character of motion of the rocket alone or by the joint effect of the motion of the rocket and the atmospheric wind. By a comparison of simultaneous readings of manometers carried on different sides of the body of the rocket, it is possible to detect the influence of the angle of attack on the result of determination of true pressure and take this influence into account when estimating the total probable error. According to data of the United States Naval Research Laboratory (ref. 625), the probable error in pressure measurement at heights less than 75 km, including the effect of yawing of the rocket and the effect of the atmospheric wind, does not exceed 10 percent. Due to the influence of yawing and outgassing of the rocket, the pressure measured at a height much greater than 75 km can differ greatly, such as by a factor of 2, from the true value (ref. 625).

Atmospheric pressure can be determined also from measurements along the nosecone of the rocket. As previously mentioned, these measurements do not give

true pressure values directly, even if the rocket experiences no yawing in flight. In this case the conversion from measured to desired values requires a special theory whose principles have been presented in a review by Ye. G. Shvidkovskiy (ref. 251) and reproduced briefly in Sections 8.1 and 8.3. We recall that for simplification of the theory it is customary to take advantage of the fact that the nosecone of the rocket has a form close to a cone. In the analysis of measurements this makes it possible to apply the theory of streamline flow around a cone by an air current having any velocity. When rocket measurements are made in the upper layers of the atmosphere, it is most common to deal with supersonic velocities.

We will now also consider the kinetic effects in free molecular flow. The peculiarities of free molecular flow lead to the development of effects characteristic only of highly rarefied gases.

Visualize an instrument which is in essence a cavity which communicates to the atmosphere through an opening in the wall (without conduits). Such an instrument can be a manometer, a gas analyzer or a simple flask for sampling the air.

Interaction of the instrument will occur in conformity to the laws of free molecular flow, if the size of the opening is considerably smaller than the length of the free path of molecules.

We will assume that the instrument moves in the atmosphere with a velocity V and an angle of slope of the velocity vector to the plane of the opening of ϑ. We also will assume that within the instrument the gas molecules immediately assume the temperature T_i of the walls, i.e., a = 1. Then, when there is stationary pressure in the instrument and with certain simplifying assumptions there will be the following relation for the partial values of the gas components

$$N = N_i \frac{v_i}{v\chi}, \tag{8.9}$$

where N and v are the numerical density and the most probable thermal velocity of gas molecules of a particular type in the atmosphere; the i denotes these same values within the instrument; χ is a complex function of the argument

$$\beta = \frac{V \sin \vartheta}{v}.$$

We can draw important conclusions from equation (8.9) concerning the differences of the state of the rarefied gas and the continuous medium within the instrument.

By using the equation of state of an ideal gas, an expression for pressure can be derived from (8.9)

$$p = p_i \frac{T}{T_i} \frac{N}{N_i}. \tag{8.10}$$

According to the kinetic theory of gases

$$v = \sqrt{\frac{2RT}{\mu}}.$$

By comparing v with the expression for the speed of sound a, we find

$$a = \sqrt{\frac{\gamma}{2}}\, v,$$

i.e., the speed of sound differs from v by a coefficient approximately equal to 0.85.

If some value $\frac{V}{v}$ is recorded, which for practical purposes means the recording of the Mach number, χ will be a function only of ϑ. Assuming $M > 1$, χ will possess the values: $\chi(0) = 1$ (in actuality this property applies for any $M \geq 0$) and $\chi(90^\circ) = 2\ \pi\beta$.

We will assume for simplicity that the atmosphere was formed by two gases with different molecular weights. Further conclusions remain valid for an arbitrary number of components.

After assigning one prime to the first component and a double prime to the second, we note that $\mu' \neq \mu''$, $T' = T'' = T$, $T_i' = T_i'' = T_i$.

We will now consider the case $\vartheta = 0$ (shearing flow). From (8.9) we have

$$\frac{N'}{N''} = \frac{N_i'}{N_i''},$$

consequently, the composition of the gas in the instrument remains the same as outside the instrument (in the atmosphere).

The total pressure in the atmosphere will be p' + p" and according to (8.10)

$$p' + p'' = (p_i' + p_i'') \sqrt{\frac{T}{T_i}}.$$

consequently, the total pressure in the instrument differs from the total pressure in the atmosphere as a result of the difference of the temperatures of the instrument and atmosphere. This phenomenon is characteristic only of a rarefied gas. It is absent if the discrete structure of the gas can be neglected and the gas is considered a continuum.

We will now discuss the case $\vartheta = 90^\circ$.

Now $\chi = 2\beta\sqrt{\pi}$, and by using an approach similar to the above we obtain

$$\frac{N'}{N''} = \frac{N_i'}{N_i''} \sqrt{\frac{\mu''}{\mu'}},$$

consequently, with the movement of the instrument in the direction of the external normal to the opening, the composition of the gas in the instrument will differ from that of the atmosphere. Within the instrument the gas is enriched by heavier molecules. Assuming, for example, that $\mu'' = \mu'$ and $\frac{N'}{N''} = 1$, within the instrument we obtain $N_i'' = 2N_i'$.

A similar computation of total pressure gives

$$(p' + p'') = \sqrt{\frac{R}{2\pi V^2} \frac{\mu'}{\mu''} \frac{T^2}{T_i}} \left(\frac{p_i'}{\sqrt{\mu'}} + \frac{p''}{\sqrt{\mu''}} \right),$$

consequently, the total pressure in the atmosphere is related complexly to the partial pressures within the instrument.

As a result it is found that the gas composition coincides with the composition of the atmosphere only in exceptional cases, and the total pressure never will be equal to it.

When a vacuum line is used, the picture of the phenomenon becomes still more complex. When the vacuum line connects the instrument and the atmosphere, Knudsen flow can develop, which is considered from the combined point of view of hydrodynamic and molecular concepts. In such cases, on the contrary, enrichment of the composition of the gas in the instrument by lighter molecules must be expected. Computations of the phenomenon of mass selection under different conditions have been published by A. I. Repnev (ref. 166a). A. I. Ivanovskiy and A. I. Repnev made a detailed study of the problem of the density gradient in the cavity of the instrument during free molecular flow (ref. 69a).

V. G. Belekhova (ref. 10) considered the relative motion of an instrument package in a free molecular flow of a rarefied gas. She demonstrated, in particular, that in the case of free molecular flow within the cavity of the container of the design which she considered (fig. 8.4) an equilibrium state is established in less than 0.05 sec (equilibrium between the quantity of entering and escaping molecules).

8.4. Rocket Density Measurements. If the methods of aerodynamics of continuous media are used we can establish, theoretically, the approximate relation between deceleration pressure p_0', measured on the nosecone of the rocket, and the density ρ of the surrounding medium. If a rocket engulfed in a supersonic flow does not experience yawing, the deceleration pressure is determined by the Rayleigh formula, which for a diatomic gas can be represented in the form (refs. 623 and 429).

$$p_0' = 0.92\rho V^2 + 0.46p + \ldots, \qquad (8.11)$$

where p is the true pressure of the surrounding medium and V is rocket velocity. If the Mach number exceeds 3, all the terms on the right-hand side of equation (8.11) can be neglected except the first, with which we determine density directly. In the case of smaller Mach numbers, it is possible to correct the density value computed by the indicated method, taking into account terms of a higher degree of smallness. For angles of attack up to 10° and somewhat larger, this formula gives an error not exceeding several percent.

This method has been repeatedly used in rocket investigations of the upper layers of the atmosphere by the United States Naval Research Laboratory (ref. 625). Since the actual yawing of the rocket usually greatly exceeded 10°, the derived density values contain a systematic error up to 20 percent.

At heights greater than 120 km density measurements were made by the United States Naval Research Laboratory by another method, which ingeniously makes use of the great yawing of the rocket. In the upper part of its trajectory the rocket ceases to be governed by its control mechanisms (ensuring the stability of its longitudinal axis), begins to move sideways and therefore to rotate. Each of the manometers alternately installed on the rocket is turned forward (in the direction of motion of the rocket) and backward; the pressures which they indicate therefore, are modulated with a period equal to the period of rotation of the rocket. By using the kinetic theory of gases it can be shown that in this case the true air density ρ (expressed in g/m^3) is related to the amplitude Δp of these pressure modulations (expressed in mm Hg) by the relation (for derivation see ref. 623, Section 28).

$$\rho = \frac{0.182\,\Delta p}{V \sin\theta}, \tag{8.12}$$

where rocket velocity V is expressed in km/sec and θ is the angle between the axis of the rocket and the normal to the entrance of the manometer.

The error in such measurements, made in the upper rarefied layers of the atmosphere, is mostly determined by the presence of atmospheric winds and the influence of gases released from the manometer and rocket. The error can be estimated only with difficulty and only approximately. The probable error in density measurement (ref. 625) is from 20 percent to a factor of 2.

A completely different method for measurement of air density in the upper layers of the atmosphere was developed and used by specialists at the University of Michigan, Bartman, Chaney, Jones and Liu (United States) (ref. 281). A sphere is ejected from an Aerobee rocket at a great height and its falling is tracked from the Earth with great accuracy. Data on the trajectory are used to compute the deceleration of the sphere and thereby the density of the medium through which the sphere is moving.

The forces acting on a freely falling body, whose density is great in comparison with the density of the surrounding medium, consist of gravitational attraction and aerodynamic resistance. Lateral forces caused by rotation of the sphere can be neglected in comparison with resistance, since in these experiments the peripheral rotational velocity is negligibly small in comparison with

the velocity of rotational motion (ref. 281). In a general case resistance is expressed as

$$D=\frac{1}{2}\rho V^2 AC_D, \tag{8.13}$$

where ρ is density of the medium, V is velocity of the body relative to the atmosphere, A is the maximum area of the cross section of the body (midsection), C_D is the resistance coefficient (a dimensionless parameter). The equation of motion of a freely falling body can be written in the form

$$\vec{g}-\frac{d\vec{V}}{dt}=\frac{\rho AC_D}{2m}|V|\vec{V}, \tag{8.14}$$

where $\vec{g}$ is gravitational acceleration, t is time and m is the mass of the body.

The vector equation (8.13) can be transformed into an equation for components. The relative velocity $\vec{V}$ can be expanded

$$\vec{V}=\vec{v}-\vec{w}, \tag{8.15}$$

where $\vec{v}$ is the velocity of the body relative to the Earth and $\vec{w}$ is wind velocity, determined as the local velocity of the atmosphere relative to the Earth and assumed to be invariable.

Experiments with the sphere are used for determination of undistorted density ρ through other parameters of equation (8.14). The values A and m are measured before flight, g is a known function of height

$$g(h) = g_0 - 0.0003086h,$$

where g_0 is gravitational acceleration at sea level in cm/sec^2 and h is height above sea level in meters.

In theory wind velocity can be determined from experiments with a falling sphere. The horizontal component can be determined from the readings of instruments measuring the trajectory of the sphere. The influence of the vertical wind component cannot be distinguished from the influence of the density gradient, if the experiment is made with a single sphere, but it can be determined by simultaneous observation of the falling of two spheres with a different ratio $\frac{A}{m}$. However, due to the low accuracy of this method and technical difficulties, this method for determination of the vertical wind component has not been fully developed.

Equation (8.14) can be used to derive an equation for the vertical component. Under the condition that the horizontal component of velocity of the body can be neglected in comparison with the vertical component, this equation can be written in the form

$$\frac{2m}{AC_D v^2 \cos^2\beta}\left|g - \frac{dv}{dt}\cos\beta\right| = \rho\left(1 - \frac{2w\cos\alpha}{v\cos\beta} + \frac{w^2\cos^2\alpha}{v^2\cos^2\beta}\right), \tag{8.16}$$

where α and β are angles formed with the vertical by the velocity vectors of the wind and sphere, respectively.

It can be assumed that the vertical wind velocity component w is small in comparison with velocity v cos β of the sphere, i.e.,

$$\frac{w\cos\alpha}{v\cos\beta} \ll 1,$$

the influence of the wind on density determination, therefore, is an effect of the second order of smallness

$$\frac{2\rho w\cos\alpha}{v\cos\beta}.$$

Computation of density was done by using the approximate formula (ref. 281)

$$\rho = \frac{2m}{V^2 AC_D\cos^2\beta}\left(g - \frac{dV}{dt}\cos\beta\right). \tag{8.17}$$

The resistance coefficient C_D is dependent on velocity (Mach number) and Reynolds number. The values C_D were determined from ballistic data and also from experiments in a wind tunnel and other similar measurements; they were used in experiments with a large sphere at the same Mach and Reynolds numbers.

The sphere for these experiments was an inflated thin-walled envelope made of 16 glued nylon sections, 0.5 mm thick. After ejection of the sphere from the rocket, it was filled with nitrogen, whereas prior to this moment it had been maintained under pressure in a glass flask within the sphere. Within the envelope there is a miniature DOVAP (Doppler Velocity and Position) radio transmitter with antenna, which receives signals from the DOVAP ground system and returns them. Several simultaneously operating DOVAP ground stations, spaced in a particular pattern on the surface, obtain the necessary data on the trajectory of the falling sphere.

We will now cite computations in which a right-hand system of rectangular coordinates with an origin at the rocket launching site is used: the x_1 axis is directed to the east, x_2 to the north and x_3 normal to the plane x_1x_2. After

addition of 1,200 m (the elevation of the launching site above sea level) the x_3 coordinate indicates height above sea level. The DOVAP system gives information on the position of x_1, x_2 and x_3, the velocity components $\dot{x}_1$, $\dot{x}_2$, $\dot{x}_3$ and the acceleration $\ddot{x}_1$, $\ddot{x}_2$, $\ddot{x}_3$ as functions of time (twice each second).

The vector equation of motion of the sphere (8.14) can be replaced by equations for the components

$$g + \ddot{x}_3 = -\frac{\rho A C_D}{2m}(\dot{x}_3 - w_3)\left[(\dot{x}_1 - w_1)^2 + (\dot{x}_2 - w_2)^2 + (\dot{x}_3 - w_3)^2\right]^{\frac{1}{2}}, \tag{8.18}$$

$$\ddot{x}_2 = -\frac{\rho A C_D}{2m}(\dot{x}_2 - w_2)\left[(\dot{x}_1 - w_1)^2 + (\dot{x}_2 - w_2)^2 + (\dot{x}_3 - w_3)^2\right]^{\frac{1}{2}}, \tag{8.19}$$

$$\ddot{x}_1 = -\frac{\rho A C_D}{2m}(\dot{x}_1 - w_1)\left[(\dot{x}_1 - w_1)^2 + (\dot{x}_2 - w_2)^2 + (\dot{x}_3 - w_3)^2\right]^{\frac{1}{2}}, \tag{8.20}$$

where w_1, w_2 and w_3 are the easterly, northerly and vertical wind components, respectively, relative to the launching site.

If the wind is neglected, assuming in equation (8.18) that $w_1 = w_2 = w_3 = 0$, we obtain

$$\rho = -\frac{2m(g + \ddot{x}_3)}{AC_D \dot{x}_3 v}, \tag{8.21}$$

where

$$v = (\dot{x}_1^2 + \dot{x}_2^2 + \dot{x}_3^2)^{\frac{1}{2}} \tag{8.22}$$

is the resultant velocity of the sphere relative to the launching site. Equation (8.21) is used for computation of density. For a given height h it can be written in the form

$$\rho(h) = -\frac{2m\left[g + \ddot{x}_3(h)\right]}{AC_D(h)\,\dot{x}_3(h)\,v(h)}. \tag{8.23}$$

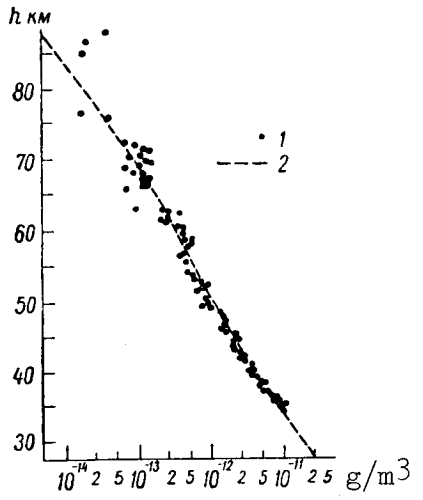

Figure 8.8. Results of air density measurements by falling sphere method (1) and standard curve adopted by United States Rocket Committee (2).

The error of the result caused by neglecting the wind can be evaluated using equation (8.18). The greatest effect is introduced by neglecting the vertical velocity component. If this wind component attained 30 m/sec, the maximum error would be about 10 percent, whereas neglecting a horizontal wind of the same velocity would lead to an error of only 1 percent. It is impossible to introduce a correction for the vertical wind component due to the lack of necessary information on the wind (ref. 281). The probable error of measurement of accelerations, as shown by an analysis of the readings of the DOVAP system, is from 0.2 to 0.9 m/sec^2 in different launchings of the sphere (of four launched on May 14 and Dec. 11, 1952, and Apr. 23 and Nov. 29, 1953). The resistance coefficient is determined with an error of 5 percent.

Thus, the random errors of density measurement can attain a large value, and this explains the considerable scatter of points in the measurement results. This is shown in figure 8.8, where vertical density distribution is shown on the basis of data for the second flight (Dec. 11, 1952) and for comparison--the standard distribution accepted in that year (1952) in the United States (ref. 707). The great value of the method is that it is based on completely different principles than other rocket methods. This is very important for intercomparison. The average density data obtained from measurements of the deceleration of a falling sphere make it possible to obtain rather reliable data. Figure 10.7 (Section 10) shows a curve of vertical density distribution obtained as a result of averaging data for all four flights; for the first and fourth flights the measurements were averaged for layers 2 km thick and for the second and third for layers 4 km thick.

8.5. Use of the Accelerometer. Attempts to improve the accelerometer method undertaken some time ago warrant considerable attention. Jones (ref. 496) reported the development of an accelerometer which directly measures the acceleration caused by resistance of the medium. The high sensitivity of the

accelerometer made it possible for Jones to dispense with a light envelope and use a relatively heavy metal sphere for observations; the latter is less sensitive to wind effects (vertical wind component).

The acceleration of a falling sphere can be determined relative to various points (bodies) of reference. In measurements with the DOVAP system the Earth serves as such a body. However, a different approach can be used. Let us imagine that two spheres are ejected simultaneously from a rocket: one is heavy and experiences virtually no deceleration from friction with the air, whereas the other is light. By determining acceleration of the relative motion of the two spheres, i.e., by using the heavy sphere as a reference point (body), we actually would determine the "acceleration of deceleration."

Jones applied this type of principle. Among the various designs and aerodynamic concepts he selected those suitable for a variant in which the reference system was an internal (rather than external) falling body.

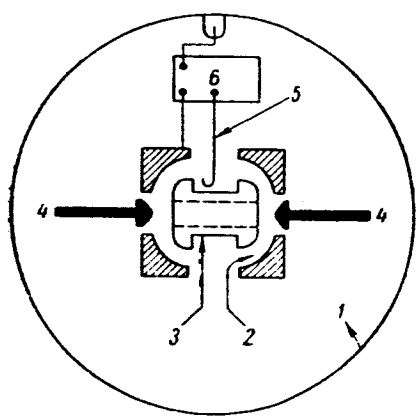

Figure 8.9. Diagram of Jones accelerometer.

Figure 8.9 schematically represents the general idea and design of the instrument. A rigid spherical housing 1, 177 mm in diameter, is ejected from a rocket at the required height. Within this housing there is attached an enclosure 2 with a coil inside. This coil can be set properly, centered precisely at the center of the enclosure by the adjusting screws 4. After ejection of the instrument from the rocket the screws 4, controlled by electromagnets, are relaxed, leaving the coil 3 freely suspended within the enclosure 2. The housing 1 experiences braking by friction on the air, but the coil 3 remains a freely falling body. The coil therefore will experience greater acceleration than the walls of the housing and, after being displaced a given value (0.47), closes the electrical current circuit, coming into contact with the contact wire 5 (a spring of silver wire 0.05 mm in diameter). With the closing of the current circuit, current supplied by a 6 v battery, a signal is excited in the transmitter 6 and is transmitted; under the influence of the electromagnets the screws 4 converge, moving into the zero position, and the coil 3 thereby is returned to the center of the enclosure. The configuration and design of coil and cavity are

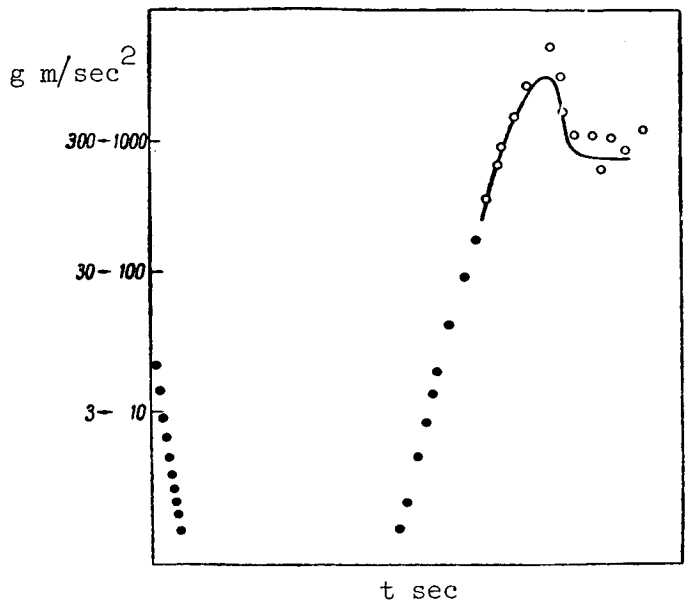

Figure 8.10. "Accelerations of deceleration" of metal sphere, measured on June 24, 1955 by Jones accelerometer ejected from a Deacon rocket attaining a height of 105 km.

such that the system operates identically in any direction, and the orientation of the axis of the instrument relative to the vertical is, therefore, without importance.

In order to obtain the necessary accuracy and the desired intervals of measurement of acceleration the accelerometer must be manufactured very carefully. In particular, the size of the most important components cannot depart from the specified values by more than ± 0.03 mm, and the free motion of the coil (4.7 mm) should be identical in all directions to an accuracy of ±0.05 mm.

Laboratory tests have shown that the instrument measures accelerations in the range from 0.01 - 5 g with an accuracy to about 1 percent. The travel time (the time expended by the coil in movement from the center of the cavity to its wall) at an acceleration of 5.1 and 0.01 g and a travel distance of 4.7 mm is 0.014, 0.031 and 0.312 sec, respectively. The travel time is transmitted telemetrically to Earth through the transmitter 6 and the sphere 1 itself is used as a dipole antenna; for this reason an insulation spacer extends along the equator of the sphere.

The telemetric signals are recorded on Earth by a special electronic circuit, which records the duration of the travel time to an accuracy of 10^{-5} sec.

In 1955 the new accelerometer was used for determination of air density at heights of 30-80 km. It was carried into the upper layers of the atmosphere by a Deacon rocket. On the ascending branch of the trajectory the sphere was ejected at a height of 61 km and by inertia was carried aloft to a height of 105 km in the 155th second. Results of measurements of deceleration pressure are shown in figure 8.10. The minimum acceleration measured at the peak of the

trajectory was 0.005 g. After 284 seconds the instrument readings obviously were exaggerated (apparently the battery had discharged and the tip of the contact wire 5 had burned up). If measured acceleration values are used to compute air density, the results agree well with the rocket data obtained by other methods (ref. 496). The solid curve in figure 8.10 represents the value of accelerations computed on the basis of a standard vertical density distribution.

8.6. Measurement of Solar X-Radiation. A method for determining atmospheric density based on measurement of the density of the flux of solar X-radiation reaching the ionosphere has been used successfully by Byram, Chubb and Friedman (ref. 314). By using photon counters carried aloft in rockets, they measured the flux density at different heights for the spectral regions 8-20, 44-60 and 44-100 Å. They determined the extra-atmospheric values of the density of the fluxes for these three regions by extrapolation to a zero air mass. Then they computed the absorption of X-radiation between 110 and 128 km. Byram, Chubb and Friedman computed atmospheric density on the basis of the known absorption coefficient for air. Similar measurements were continued by Chubb, Byram, Friedman and Kupperian (ref. 336). These experiments gave extremely important results which will be discussed in Section 10.1.

8.7. Measurement of Solar Ultraviolet Radiation. Air density in the upper layers of the atmosphere can be measured from the absorption of solar ultraviolet radiation. For example, the radiation in the region 1425-1500 Å experiences absorption only by molecular oxygen, and the intensity of this radiation can therefore be used for a study of the vertical distribution of O_2. Such measurements (ref. 336) gave valuable information concerning the structure of the "O_2 - O" region (for further details see ref. 233).

Extremely interesting data can be obtained from the measurement of radiation absorption in the Ly-α line. Dry air absorbs this radiation poorly; the absorption coefficient is equal to approximately 0.044 $cm^{-1}atm^{-1}$. However, the absorption of these wavelengths is very great in water vapor, and the absorption coefficient attains 390 $cm^{-1}atm^{-1}$. The presence of water vapor in the air in a quantity of 10^{-4} (one mol of water per 10^4 air mols) should almost double the absorption coefficient of air. Measurements of the quantity of water vapor in the upper layers of the atmosphere will be discussed in Section 19.

8.8. Diffusion of Sodium Vapor. I. S. Shklovskiy and V. G. Kurt have measured atmospheric density at extremely great heights (430 km) by a method differing substantially from all those described above: they used the results of a study of diffusion of a cloud of sodium vapor formed by a rocket. The rocket carried special apparatus for vaporizing metallic sodium mixed with thermite (vaporizers of this type are used for creating clouds of sodium vapor for wind measurement, see Section 29). Such an experiment was carried out on Sept. 19, 1958 (ref. 253). About 4 kg of sodium was evaporated at the peak of the trajectory of a geophysical rocket at a height of 430 km; this led to the

formation of a sodium vapor cloud. At the time the experiment was made, the Earth's shadow at the observation point was situated at the 250-300 km level, and the cloud illuminated by the Sun was therefore observed on the background of a dark twilight sky. The Sun's rays excited a bright fluorescence of sodium vapor and the cloud emitted the strong resonance lines D_1 and D_2 of sodium.

The rate of diffusion determining the rate of expansion ("swelling") of the cloud depends on the density of the medium in which there is diffusion of the sodium vapor. Shklovskiy and Kurt solved the corresponding diffusion differential equation for the spherically symmetrical problem.

The bright sodium vapor cloud was repeatedly photographed. In order to obtain the absolute values of cloud intensity the photographs were standardized by a tie-in to the extrafocal images of stars. The photographic observations were accompanied by photoelectric measurements of the center of the cloud. These data were used in drawing isophotes, and the dependence of brightness at the center of the cloud on time was determined. The size of the cloud increases with time t approximately proportional to $t^{1/2}$.

The results of measurements by Shklovskiy and Kurt will be cited in Section 10.3.

Pressman and Marmo have proposed a refinement of the theory of the method used by Shklovskiy and Kurt (ref. 681).

8.9. Use of a Mass Spectrometer. The mass spectrometers widely employed at present for study of air composition in the upper layers of the atmosphere were used by Townsend and Meadows (ref. 769) for determining density. The relationship between pressure and the total ion flux in the instrument was determined for this purpose during the calibration of the mass spectrometer in the laboratory. The mass spectrometer was installed in the nosecone of an Aerobee-Hi rocket: under these conditions total pressure p_g can be measured. By applying the formulas used in manometer measurements the value of total pressure can be used to compute atmospheric density ρ.

The computation formula has the form

$$\rho = \frac{p_g}{V \cos\sigma \sqrt{2\pi R' T_g}},$$

where $R' = \frac{k}{m}$, T_g is the temperature of the spectrometer tube, V is rocket velocity, computed from data obtained by radar tracking of the rocket and σ is the angle of attack determined from the readings of two magnetometers and a phototube.

According to the estimate made by Townsend and Meadows, the total error in measuring pressure is about 20 percent, including the error in calibration of the instrument and interpretation of the data. The error in height determination does not exceed 2 km.

The atmospheric density distribution at heights of 110-170 km determined over Fort Churchill will be discussed in Section 10.2.

8.10. Technique of Rocket Measurements. In order to obtain a full idea concerning the different stages in rocket experiments from an investigation of the upper layers of the atmosphere, requiring both special apparatus and the extensive use of various auxiliary technical means, we will discuss two studies in this field in greater detail.

We will first discuss the apparatus used by the research team at the University of Michigan in the United States for transmitting to Earth the pressure readings measured by an alphatron on Aerobee rockets. Figure 8.11 shows a simplified block diagram of the instrument system for pressure measurement on Aerobee rockets (ref. 360). The diagram shows only one alphatron with the associated amplifier and scale switch circuits, although usually not less than five such independently operating alphatrons are used simultaneously. One of these alphatrons is used for pressure measurements at the tip of the nosecone and the other four for pressure measurements at different points on the surface of the nosecone. The other elements of the system shown in figure 8.11 are not duplicated.

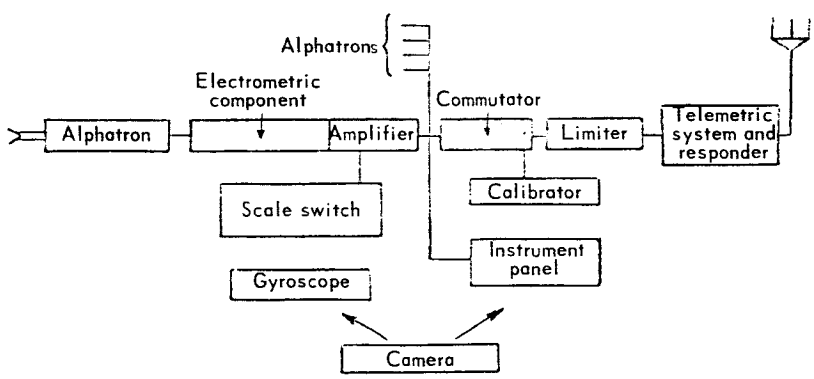

Figure 8.11. Block diagram of apparatus used on Aerobee rocket.

The general sequence of measurements is as follows. The manometer, amplifier and scale switch (sensitivity regulator), acting jointly, transform the measured pressure into an electrical signal, which is fed through a commutator and limiter to the radiotelemetric system. The telemetric system, used simultaneously as a "responder" for radiotriangulation intersections of the rocket from the Earth, transmits the necessary information to three ground stations at which the interpretation and recording of data is accomplished.

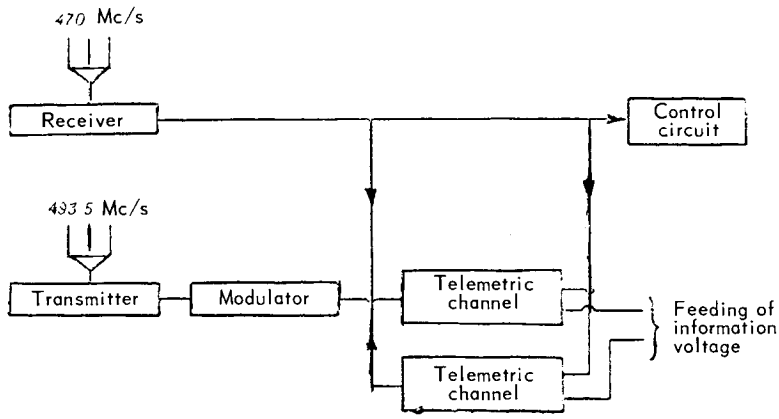

Figure 8.12. Block diagram of "telemetric system + responder" system used by the University of Michigan on Aerobee rockets.

All the voltages fed into the telemetric system are controlled by the limiter. The limiter uses a thermionic or semiconductor diode, giving the voltage a bias. It is designed to protect the telemetric system from receiving voltages beyond the range 0 - +5 v. In the event of overvoltages or the feeding of a signal of negative voltage the operation of the telemetric system can be disrupted.

The "telemetric system-responder" arrangement solves three problems:

1. transmission of experimental data to surface stations for recording;
2. transmission of signals to Earth, determining the position of the rocket in space;
3. reception of signals from Earth, controlling the operation of the rocket and the measuring apparatus.

The block diagram (fig. 8.12) illustrates the interaction of different parts of the system. The pulses of a surface interrogation station at a frequency of 470 Mc/s are received by the rocket, where they trigger the operation of the modulator-transmitter circuit. The transmitter begins to respond (transmit) at a frequency of 493.5 Mc/s. The response signals (remote-control pulses) are received at Earth by three stations at a sufficient distance apart (35-65 km), and are reproduced on an oscilloscope. By photographing the oscilloscope scale on which the pulses of the interrogation station and the response pulses of the "responser" are visible, separately, it is possible to obtain data for determination of distance to the rocket.

The pulses of the interrogating station also are used for triggering the telemetric part of the system, which in turn (with a certain specified lag) creates a pulse for triggering the modulator. The lag of this "telemetric" pulse is controlled by the voltage of the information signal fed from the manometer. For example, with the feeding of a zero voltage the pulse of telemetric channel 1 lags 50 μ sec behind the remote-control pulse. If the voltage

is 5 v, the lag attains 200 μ sec. Channel 2 operates in the same way, but the lag is greater.

Thus, the single pulse of the interrogation station causes a remote-control pulse, whose lag relative to the interrogation time can be used to determine the distance from the rocket to the ground station and also causes the pulse for each telemetric channel, whose lag relative to the remote-control pulse determines the value of the applied information voltage. These three pulses, upon being received by a ground station, are used for modulation of the intensity on the oscilloscope. Time scanning by the oscilloscope begins under the influence of the remote-control pulse. By photographing the oscilloscope it is possible to record the voltages in volts for the entire period of rocket flight.

In a study by LaGow and Ainsworth (ref. 541) entitled "Arctic Upper Atmosphere Pressure and Density Measurements with Rockets," the authors used small Deacon rockets launched from shipboard (including icebreakers) for experiments in northern latitudes, where for a long time there were no launching pads for heavy rockets.

Deacon rockets were carried aloft into the stratosphere from shipboard by a stratospheric balloon (with an envelope 20.7 m in diameter). When the stratostat attains the specified height of 25 km, a pressure relay switches on the powder-propelled rocket engine suspended from the stratospheric balloon on a cable 30 m long. When the engine is started, the rocket is freed of a housing designed to safeguard it against cooling at the time of its prolonged ascent on the stratospheric balloon. At the same time the launching basket for the rocket is separated. When launched from sea level the rocket ascends to a height of 25 km. If the launching is at a height of 25 km, there is a considerable decrease of velocity loss due to air resistance, and the ceiling reached increases to 80 km.

Deceleration pressure and true air pressure were measured in flight. In the analysis of these data it was possible to obtain information on air pressure, density and temperature. The deceleration pressure p'_0 on the nosecone of the rocket was determined, using a differential aneroid manometer (fig. 8.13), whose readings are proportional to the difference between the deceleration pressure and the true pressure p_{true}. The latter was measured through an opening in the ring zone at a distance of seven rocket calibers (or the nosetube of the rocket) from the tip of the rocket (or the end of the nosetube), where the pressure on the walls of the rocket differs little from the true pressure (i.e., the pressure in the undisturbed surrounding medium). Tests in a wind tunnel have revealed that deceleration pressure does not depend on the yaw, if the angle of attack does not exceed 30°. However, pressure p_a measured in the zone of undistorted pressure depends on the angle of attack σ and the Mach number M (fig. 8.14). Pressure p_a was measured by the same aneroid manometer as was deceleration pressure, but after eightfold compression. The compression chamber 4 was used for the latter purpose (fig. 8.13); itspiston made 1 cycle of motion

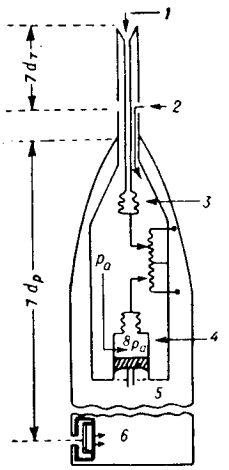

Figure 8.13. Instruments for pressure measurement (Deacon rocket). (1) To deceleration pressure chamber, (2) ditto, for true pressure, (3) manometer for measuring difference, (4) chamber, eightfold compression, (5) piston, (6) Pirani gage; d_T, tube diameter, d_p, rocket diameter.

per sec. At great heights, where the true pressure became less than 0.1 mm Hg, it was measured by a Pirani gage, in which the tungsten filament was 4 μ thick. Additional apparatus included a resistance thermometer for measurement of the temperature of the walls of the Pirani gage, an accelerometer for measurement of the period of rotation of the rocket, a pressure switch (25 mm Hg) for triggering the compressor of the true pressure manometer and a pressure unit commutator.

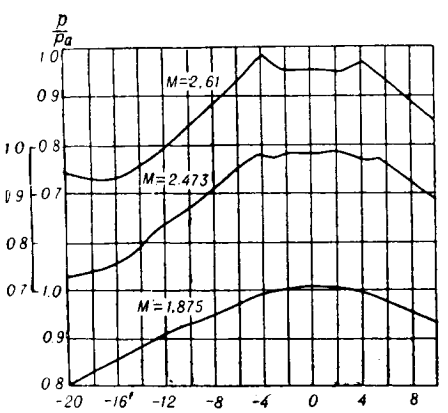

Figure 8.14. Dependence of pressure p_a measured in the "true pressure" zone p_{true} on the angle of attack σ and the Mach number M.

The instrument readings were transmitted to Earth by a two-channel radiotelemetric system. The antenna for the 300 mw transmitter consisted of the rear and nose sections of the rocket, which served as two dipole elements. The first channel was used for recording the time of rotation of the rocket. The readings of all manometers and all data on the calibration voltages were fed to the contacts of the commutator connected to the second channel of the telemetric system. Switching by the commutator occurred 1.5 times per sec. The ground station consisted of a receiver, two demodulators and a two-channel recorder. Figure 8.15 shows a deceleration pressure (p_{dec}) curve and a true pressure (p_{true}) curve, based on rocket measurements at 74°N.

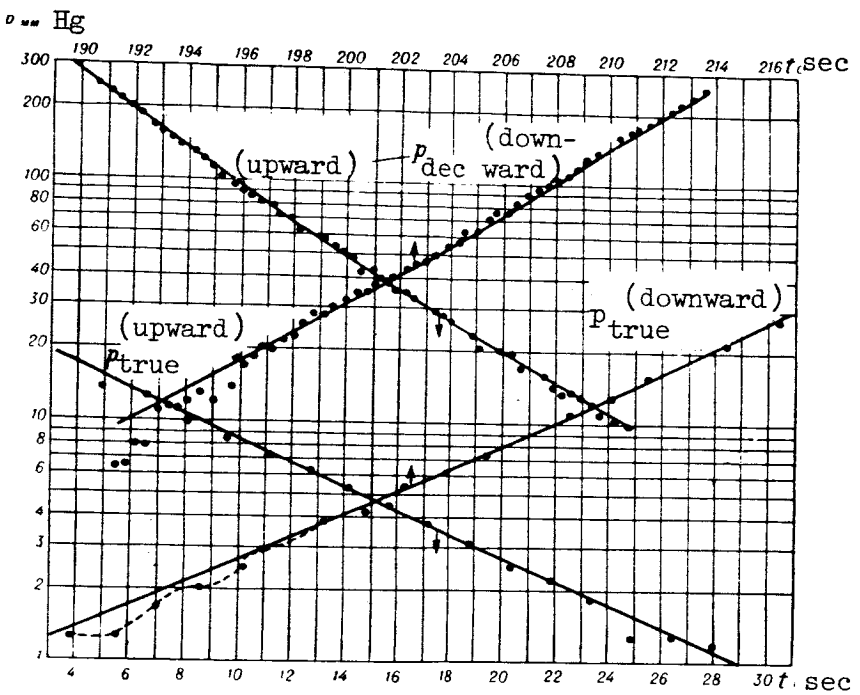

Figure 8.15. Deceleration pressure p_{dec} and true pressure p_{true}, measured during rocket sounding of the atmosphere at 74°N.

It should be noted that due to technical difficulties associated with the implementation of rocket sounding of the atmosphere by no means every rocket launching produces results. For example, of six launchings of Deacon rockets undertaken in 1953 only two were successful. The reasons for the failures in the other cases were as follows: failure of the telemetric apparatus to operate (one case); at a height of 9 km the stratospheric balloon burst; the rocket separated from the balloon at a height of 25 km, but the rocket engine failed to operate (one case); the large yaw of the rocket made it impossible to measure true pressure satisfactorily (one case).

9. Measurement of Pressure and Density of the Upper Layers of the Atmosphere Using Artificial Earth Satellites

Launchings of artificial Earth satellites were accomplished in accordance with the program of scientific investigations of the International Geophysical Year (1957-1959). The world's first artificial Earth satellite was created in the USSR and launched successfully on Oct. 4, 1957. The orbital parameters of the first and subsequent Soviet artificial Earth satellites made it possible to observe them on all continents in a large range of latitudes. This opened up great possibilities for the solution of various scientific problems. In particular, the Soviet satellites opened up a new era in investigations of the structure of the upper layers of the atmosphere. The use of rockets for investigation of the upper layers of the atmosphere gave to science completely new and remarkable possibilities. However, rocket methods characteristically have shortcomings, in particular, they yield only limited quantities of data. The launching of a rocket permits study of the state of the stratosphere and ionosphere only over a single point and only for a few minutes. An artificial Earth satellite is a long-lived automatic laboratory, sounding the atmosphere at different heights, latitudes and longitudes.

Artificial Earth satellites can be used in two ways for measurement of air density in the upper layers of the atmosphere: as a transport vehicle (like a rocket) for carrying measuring apparatus into the upper layers of the atmosphere and as a body moving rapidly through the upper layers of the atmosphere, experiencing deceleration in dependence on the density of the atmospheric layers through which it passes. This second method, based on careful observations of the evolution of satellite orbits from the Earth's surface, is basically new and makes it possible to obtain independent data on atmospheric density with relatively high accuracy.

9.1. Satellite Deceleration. During the motion of a body in a liquid or gaseous medium it is acted upon by the retarding force of friction, whose magnitude is dependent on density ρ of the medium and velocity V of motion of the body and its form and orientation. Computation of the force of resistance is simplified in the case of a spherical body.

In sufficiently high layers of the atmosphere the mean length l of the free path of molecules considerably exceeds the dimensions L of the satellite. In this case each molecule collides with and rebounds from the walls of the satellite without interacting with other molecules. In other words, the condition $l \gg L$ makes it possible to neglect collisions between the molecules of the oncoming flow and molecules escaping the moving surface. This appreciably simplifies the computation of air resistance, which in this case consists of single collisions of molecules. Another simplification arises when the velocity of motion of a body is great in comparison with the thermal gas kinetic velocity of air molecules.

Under such conditions the force of resistance acting on a plane surface for given V and ρ is dependent on the angle at which the collision occurs and the accommodation coefficient α which is equal to the percentage of kinetic

energy lost during reflection. More exactly α is determined in the following way

$$\alpha = \frac{E - E_r}{E - E_w}, \tag{9.1}$$

where E is the energy (translational or vibrational or rotational degrees of freedom) carried by the colliding molecules, E_r is the actual energy after reflection and E_w is the energy after reflection, if it corresponded to the temperature of the surface (ref. 51). If $\alpha = 1$ (inelastic collision), a molecule adheres to the surface, losing all its kinetic energy; it then escapes at a velocity corresponding to the thermal energy at the temperature of the wall. In the cases with which we are concerned, this velocity is relatively small. In the case of an elastic reflection $\alpha = 0$, a molecule rebounds from the surface without loss of energy. In the second case the resistance experienced by the body at the time of its motion in the atmosphere exceeds by a factor of two the resistance in the first case. At intermediate values $0 < \alpha < 1$ (semielastic collisions), the force of resistance also has an intermediate value.

The value of the accommodation coefficient depends on the velocity and the material of which the satellite is made (on the ratio of the molecular weights of the air and the material of the walls), and cannot be predicted precisely. If the walls of the satellite are made of magnesium, $\alpha \simeq 0.6$, or of steel--$\alpha \simeq 0.4$. In the case of normal incidence this means that the force of resistance will be 1.63, or 1.78 times greater than for completely inelastic collisions (ref. 644). The difference is not very great, but nevertheless is significant.

At different points of the frontal surface of a moving medium there are all possible angles of incidence from 0 - 90°. At an angle of incidence of 45° the resistance for elastic and inelastic collisions is identical; at lesser angles of incidence resistance increases for elastic collisions and at greater angles of incidence increases for inelastic collisions. This means that in the case of a spherical body the force of resistance F will have the same value for elastic and inelastic collisions, and therefore F is not dependent on the accommodation coefficient and is determined precisely by the formula

$$F = \pi r^2 \rho V^2. \tag{9.2}$$

This formula makes it possible to compute ρ from observations of motion (deceleration) of a satellite if the satellite is a sphere of the radius r. If deceleration was determined from observations of a satellite during the period of one revolution around the Earth, the derived density value gives the averaged value $\bar{\rho}$ for the region of the atmosphere through which the satellite passed. For a circular orbit $\bar{\rho}$ is equal to the true density of the atmosphere at satellite height. In the case of an elliptical orbit, the average value $\bar{\rho}$ can be used to compute density ρ_p at perigee, if the law of decrease of

density with height at this level is known. If the barometric formula is used

$$\rho = \rho_p e^{-h/H},$$

where H is the height of the homogeneous atmosphere, H must be known for computation of ρ_p from $\bar{\rho}$. The observed deceleration can be used to determine the value of the product $\rho_p \sqrt{H}$.

In the case of an elliptical orbit, differing little from a circle of the radius R, it is easy to obtain the following approximate formula for the relative decrease of radius of the satellite orbit

$$\frac{\Delta R}{R} = -\frac{4\pi^2 R \rho r^2}{m}, \qquad (9.3)$$

where m is satellite mass and ΔR is the change of radius in one revolution.

We will cite numerical estimates in order to present more graphically the procedure for computation of ρ from the results of observations of the evolution of satellite orbits (ref. 644). We will assume the following parameters of a spherical satellite: r = 25 cm, m = 9,200 g, $R = 7 \cdot 10^8$ cm. Then, using formula (9.3), we obtain

$$\Delta R = -1.32 \cdot 10^{18} \rho. \qquad (9.4)$$

Decrease of orbital radius ΔR can be derived from the observed decrease of the period of revolution, using Kepler's third law (the square of the period is proportional to the cube of the orbital radius, formula (9.5). For example, if in one day (14 satellite revolutions) the radius decreases by 1.1 km, i.e., $\Delta R = -7 \cdot 10^3$ cm per revolution, it follows from formula (9.4) that $\rho = 5.3 \cdot 10^{-15}$ g/cm^3. A decrease of radius by 1.1 km in one day can be determined reliably even from not very precise visual observations (photographic measurements are approximately a thousand times more precise).

This numerical example shows how sensitive the method is for determination of extremely small air density values in the upper layers of the atmosphere from observations of satellite motion. Table 9.1 gives the values ΔR computed using formula (9.4) for different ρ; the table also gives the heights to which these densities can be applied hypothetically(ref. 644).

When the decrease of the radius ΔR of the satellite orbit becomes greater than 10 km in one revolution, the approximate formulas (9.3) - (9.4) are no longer applicable. In this case the satellite can no longer complete one orbit and ends its existence like a meteor, rapidly losing height and melting at a height of about 110 km. According to Table 9.1, the "height of destruction" is approximately 180 km.

TABLE 9.1. EVOLUTION OF SATELLITE ORBIT.

	h км						
	120	160	200	250	300	400	500
ρ g/см^3	$7\cdot10^{-11}$	$2\cdot10^{-12}$	$3\cdot10^{-13}$	$4\cdot10^{-14}$	$5\cdot10^{-15}$	$1.4\cdot10^{-15}$	$7\cdot10^{-16}$
ΔR км	(900)[1]	(26)[1]	4.0	0.53	0.066	0.019	0.009

[1] Destruction of satellite.

In conclusion we cite data on the velocity of change of the period of revolution ΔT of three American satellites (ref. 344) with perigees of different height h_p

Name of satellite	h_p km	ΔT min/day
Explorer IV (1958 ϵ)	260	-0.030
Explorer I (1958 α)	365	-0.0076
Vanguard I (1958 β_2)	656	-0.00031

9.2. Evolution of the Orbit of the First Soviet Artificial Earth Satellite and its Carrier Rocket. The approximate computations applied to a satellite of the simplest form for computations--spherical. We will now become familiar with the computation of a more complex variant when the form of the body is arbitrary.

The rigorous solution of the problem of determination of atmospheric density from the observed deceleration of a satellite was given by Soviet authors as early as 1957-1958 (refs. 109a, 141, 142 and 258). It was shown that in order to study the evolution of the orbit of an artificial Earth satellite close to the Earth under the influence of atmospheric resistance, with certain admissible assumptions concerning the slow change of orbital elements, the following equations describing the process must be considered

$$\frac{dp}{dN} = -cp^2 \int_{-\pi}^{\pi} \frac{\rho \sqrt{1 + 2e\cos\vartheta + e^2}}{(1 + e\cos\vartheta)^2}\, du,$$

$$\frac{de}{dN} = -cp \int_{-\pi}^{\pi} \frac{\rho \sqrt{1 + 2e\cos\vartheta + e^2}}{(1 + e\cos\vartheta)^2}(e + \cos\vartheta)\, du,$$

where p is the orbital parameter, e is eccentricity, ϑ is the true anomaly, u is an argument of latitude, N is the sequence number of the revolution, ρ is

density at a particular point in the orbit, $c = \frac{C_x F}{m}$ is the ballistic coefficient, F is the characteristic area of the satellite surface, m is its mass and C_x is the coefficient of aerodynamic resistance. Near the perigee the dependence of density on height h is approximated by a formula of the type

$$\rho = \rho_p e^{-\frac{h-h_\pi}{H}},$$

where ρ_p is density at the perigee height h_p and H is the height of the homogeneous atmosphere.

The estimates made revealed (ref. 109a) that the eccentricity of the first Soviet artificial Earth satellite was sufficiently great that even when there are atmospheric inhomogeneities, it is possible, following substitution of an expression for ρ into this equation, to remove value ρ_p from the integral sign with a small error in computations. The following approximate formula for density determination follows from these transformations

$$c\rho_p\sqrt{H} = -\frac{2}{3}\frac{(1+e)\sqrt{e}\,\frac{d\ln T}{dN}}{(1+e)\sqrt{2\pi r_\pi (1+e)}}.$$

M. L. Lidov (ref. 109a) derived a formula for computation of the coefficients of aerodynamic resistance, using a model of an ideally unoriented body. In the case of the carrier rocket of the first satellite, the motion near the center of mass was regular precession. After comparing data on the evolution of the orbits of the first satellite and its carrier rocket, which differed greatly in size, M. L. Lidov concluded that the additional resistance associated with the motion of a charged satellite in the plasma of the ionosphere is insignificant. He also obtained estimates of the diurnal and latitudinal changes of density, and established that at a height of 228 km on the daytime side the pressure should be greater than on the nighttime side: this apparently indicates the ascent of the column of air occurring on the daytime side.

Data on the evolution of the orbit of the first Soviet artificial Earth satellite were used for a study of structure of the atmosphere by many foreign authors as well. For example, Horn obtained a very simplified solution of the problem, but his numerical computations, while without pretense to accuracy, are graphic.

As a simplification, Horn (ref. 453) assumed the orbit to be close to circular and used the following approximate and rounded-off values: he assigned the date Oct. 5, 1957 to the satellite launching (in actuality it was Oct. 4), assumed the apogee and perigee to be 900 and 250 km (the actual height of the apogee of the first satellite was 950 km), the corresponding distances from the center of the Earth to be 7,270 and 6,620 km, the satellite velocity to be 8,000 m/sec and the period of revolution to be 1.6 hours. He

then suggested the applicability of Kepler's laws (this is rigorously correct only for airless space). Kepler's third law can be written in the form

$$\frac{R^3}{T^2} = \text{const}, \tag{9.5}$$

or, substituting $V = 2\pi R$, in the form

$$V^2 R = \text{const}. \tag{9.5a}$$

The numerical values of the constants can be obtained by substituting into Kepler's law the parameters of lunar motion: R = 384,400 km, T = 27.822 days, V = 1.023 km/sec. We then obtain $\frac{R^3}{T^2}$ = 10,190 and V^2R = 402,400. For the satellite T = 1.6 hours = 5,760 sec and from formula (9.5) we obtain the mean values

$$R = 6968 \text{ km},$$

or

$$h = 598 \text{ km}.$$

From formula (9.5a) we obtain

$$V = 7{,}600 \text{ m/sec}.$$

Horn also assumed that the separation of the satellite and carrier rocket occurred on Oct. 5 without an appreciable reciprocal acceleration, i.e., their velocity relative to the Earth at the time of separation was virtually identical. Later the carrier rocket decelerated more rapidly than the satellite, and by Oct. 30 the carrier rocket had outpaced the satellite by one revolution. In 25 days the satellite had completed 25·15 = 375 revolutions, whereas the carrier rocket had completed 376. We will use the subscripts "1" to denote the values applying to Oct. 5, "2" for those applying to Oct. 30 and "12" for those applying to the mean values for the period from Oct. 5 through 30. We then have: V_1 = 7,600 m/sec, R_1 = 6,968 km, h_1 = 598 km, V_{12} = 7,607 m/sec, R_{12} = 6,955 km, h_{12} = 585 km, V_2 = 7,614 m/sec, R_2 = 6,942 km, h_2 = 572 km.

By the use of equation (9.5a) it is possible to make transformations which we will use for consideration of the changes of the total energy E of the carrier rocket. By representing E in the form of the sum of kinetic and potential energy (the latter is negative), after corresponding transformations we obtain the following expression for the loss of total energy

$$E_1 - E_2 = \frac{1}{2} m (V_2^2 - V_1^2).$$

Horn assumed further that the reason for this energy decrease is associated with the collision of the carrier rocket with the gas molecules of the atmosphere,

and he considered these collisions to be inelastic (ref. 453). Assuming that initially the motion of these molecules was disordered (nondirectional), it can be concluded that velocity in the direction of motion of the carrier rocket is equal to zero. After collisions with the carrier rocket, the molecules acquire the mean velocity V_{12}. If their total mass is equal to M, after collision their kinetic energy is equal to $\frac{1}{2} MV_{12}^2$. By denoting the path travelled by the carrier rocket in 25 days by s_{12}, the area of the cross section of the carrier rocket by q, and mean air density on the path s_{12} by ρ_{12}, we find that

$$M = s_{12} q \rho_{12},$$

where $s_{12} = 376 \cdot 2\pi \cdot R_{12}$.

Assuming that the loss of kinetic energy of the carrier rocket is equal to the increment of the kinetic energy of the air molecules, we obtain:

$$\frac{1}{2} q s_{12} \rho_{12} V_{12} = \frac{1}{2} m (V_2^2 - V_1^2),$$

or

$$\rho_{12} = \frac{m}{q} \frac{V_2^2 - V_1^2}{s_{12} V_{12}^2} = \frac{m}{q} \cdot 2.24 \cdot 10^{-13}.$$

These expressions, which are rough approximations, nevertheless show that there is regular dependence of the evolution of the orbit and accordingly the result of determination of density of the medium on the transverse load, i.e., the ratio $\frac{m}{q}$.

In his further computations Horn used as a point of departure the fact that by Nov. 22 the carrier rocket had already passed the satellite 6 times. In the second interval of time, the 23 days from Oct. 30 to Nov. 22, the satellite made 345 revolutions around the Earth and the carrier rocket 350. By denoting the values applying to Nov. 22 by the subscript "3" and the mean values for the period from Oct. 30 to Nov. 22 by the subscript "23", we can write the following values for the carrier rocket, much as was done before: $V_{23} = 7{,}637$ m/sec, $R_{23} = 6{,}901$ km, $h_{23} = 531$ km, $V_3 = 7{,}660$ m/sec, $R_3 = 6{,}860$ km, $h_3 = 490$ km.

Air density for the second period of time is

$$\rho_{23} = \frac{m}{q} \frac{V_3^2 - V_2^2}{s_{23} V_{23}^2} = \frac{m}{q} \cdot 7.94 \cdot 10^{-13}.$$

Horn concluded, therefore, that air density in the layer of the atmosphere whose mean height is 531 km is 3.5 times greater than in the next layer with a mean height of 585 km.

These computations by Horn are rough approximations. In particular, they are in need of substantial refinement with respect to the heights at which the observed deceleration occurs. Horn related the observed satellite deceleration to a mean height. However, according to Section 9.1, this characterizes atmospheric density at perigee.

9.3. Computation of the Lifetime of Satellites. In a study by Casci and Giavotto (ref. 316) it is assumed that air density is known from rocket measurements to a height of 220 km. Above this level the distribution of density ρ with height h can be represented by an exponential formula of the following form:

$$\rho = k \exp\left[-\frac{h}{H}\right], \tag{9.6}$$

where k and H are two constants. By assuming such a simple dependence between density ρ and height h, we reduce the problem to computation of the two constants k and H.

Computation of the lifetime of a satellite is a problem which usually is solved approximately; in some cases it does not require a high accuracy of solution. For example, Casci and Giavotto assume an accuracy to 1 percent to be adequate. This makes it possible to introduce a number of simplifications, both in the formulation of the problem and in numerical computations. Simplification of the conditions of the problem centers primarily on the following three problems:

(a) The dependence of ρ on h is given in a form convenient for computations. Whereas Casci and Giavotto used an exponential law (9.6), Groves (ref. 416) used as the basis of his computations a quadratic dependence in the form

$$\frac{\ln \rho}{\rho_0} = -\frac{(h-h_0)}{H_1} + \frac{(h-h_0)}{H_2^2}. \tag{9.7}$$

The use of the two constants H_1 and H_2 makes it possible to take into account temperature change with height:

(b) The expression for atmospheric resistance is used in approximate form.

(c) Motion of the satellite is considered perturbed Keplerian motion and the perturbation is assumed to be small.

Casci and Giavotto (ref. 316) derived an equation for the lifetime τ of a satellite

$$\tau = \frac{\pi \sqrt{K}}{2p} \int_{a_f}^{a_0} \frac{da}{\sqrt{a} \int_{a(1-e)}^{a(1+e)} \frac{\exp\left[-\frac{r-R}{H}\right]\left[K\left(\left(\frac{2}{r}\right)-\left(\frac{1}{a}\right)\right)-2\Omega \cos i \sqrt{K a (1-e)^2}\right]}{\sqrt{\frac{|(ae)^2-(a-r)^2|}{[r(2a-r)]}}} dr}. \tag{9.8}$$

Here the constant $K = k_g M$ (k_g is the gravitational constant, M is the Earth's mass, the constant $\frac{1}{2} C_r \frac{m}{S}$ (C_r is the resistance coefficient, m and S are the mass and cross section area of the satellite), a and e are the semi-major axis and the eccentricity of the osculating ellipse, a_0 is the initial value a, a_f is the final value a, r is height relative to the Earth, R is the mean radius of the Earth, Ω is the angular velocity of the Earth's rotation and i is the inclination of the orbit relative to the Earth's equator.

The solution of the equation for τ was programmed and implemented using a high-speed computer (ref. 316).

It should be noted that the use of such approximate solutions does not yield a full solution of the problem in a general case. In addition, as shown by an analysis (ref. 142), the use of approximate methods for determination of τ can lead to appreciable errors in some cases. For this reason D. Ye. Okhotsimskiy, T. M. Eneyev and G. P. Taratynova undertook the development of a method to determine the lifetime of a satellite for the general case of its motion quite rapidly and reliably. Their investigation revealed the existence of universal relationships between the principal parameters of the osculating ellipse (height of perigee and apogee or the parameter and eccentricity), correct for any satellites and dependent only on the law of distribution of air density with height. The equations were integrated on a BESM high-speed electronic computer of the Academy of Sciences of the USSR. In addition to an investigation of the problem of the lifetime of the satellite, based on a study of the secular changes of the orbital elements due to air resistance, it was possible to estimate the perturbations caused by the influence of other perturbing factors (Earth's flattening, rotation of the atmosphere together with the Earth). The methods for using an electronic computer for computation of the orbit of an artificial satellite with a simultaneous allowance for all perturbing forces acting on the satellite are discussed in studies by G. P. Taratynova (ref. 186) and I. M. Yatsunskiy (ref. 263).

9.4. Computation of Atmospheric Density. By knowing the lifetime τ of a satellite, the transverse load $\frac{m}{S}$ and the initial parameters of the orbit, we can use equation (9.8) to derive the relation between constants K and H, and therefore determine ρ. Casci and Giavotto used this method to analyze data on the motion of the first Soviet satellite. They consider these data to be most reliable and precise, since the initial characteristics of the orbit and the value of the transverse load $\frac{m}{S}$ are known for it with good accuracy and its spherical form makes the corresponding computations very reliable (ref. 316). The data on density obtained by Casci and Giavotto will be cited in Section 10.4.

The problem is solved somewhat differently by Groves (ref. 416). He expressed the rate of change of a and e (the notations are the same as in equation (9.8) through ρ and the true anomaly f, and integrated them for one revolution. The quadratic law was used for ρ (9.7). The orbits were assumed to be quite elongated, making it possible to reduce orbital integration to integration for f for the immediate neighborhood of the perigee (the corresponding error does not exceed several percent). The problem of determination of ρ is reduced to determination of the coefficients H_1 and H_2 in (9.7).

Groves derived an equation to determine H_1 from the change of perigee height.

The coefficient H_2 cannot be determined from data for a single satellite. Groves

found H_2 from data on six satellites, including the first and second Soviet

satellites. The contribution of this term to the height of the homogeneous atmosphere is about 8 percent.

Groves used this method to compute ρ from data on the second Soviet satellite (at a height of about 220 km), the American satellite Explorer III (at a height of about 180 km) and the third Soviet satellite. His results will be cited in Section 10.4.

The publication of studies devoted to the refinement of methods for computing atmospheric density from observations of the evolution of the orbits of artificial Earth satellites is continuing (refs. 417, 527 and 806).

9.5. Manometer Measurements. Until now we have considered methods for determination of atmospheric density based on measurements of the evolution of a satellite orbit. Is it possible to measure air pressure and density, at a great height using manometers carried aloft by satellites, the same as by rockets? Such measurements at great heights involve great difficulties, which have partly been considered in Section 8. Due to the experimental complexity of such measurements the apparatus used in their implementation must be small in size and weight. Such measurements still have not been made on American satellites because of their small size and weight. They were made for the first time on the third Soviet satellite launched May 15, 1958. This satellite carried two thermal ionization and one magnetic manometers, designed for measurement of pressure in the range 10^{-6}-10^{-9} mm Hg.

A number of difficult problems arise in measuring such low pressures (ref. 129):

(1) what photoemission of the manometer electrodes is caused by solar short wave radiation;
(2) whether the abundant release of gas by surface of the satellite hinders pressure measurement;
(3) where the manometers should be placed;
(4) whether pressure can be measured in an ionized medium by ionization manometers;

(5) what dynamic effect is involved, etc.

These problems were considered in studies by B. S. Danilin, V. V. Mikhnevich, A. I. Repnev and Ye. G. Shvidkovskiy (refs. 51 and 129) and B. A. Mirtov. We will now discuss some conclusions from these interesting investigations.

When the velocity of motion of the satellite is about 8 km/sec, the deceleration temperature is tens of thousands of degrees. In the case of thermal equilibrium, atomic oxygen would be ionized at this temperature to the third ionization potential. However, thermal equilibrium in actuality does not set in. Computations reveal that such "impact" ionization, as well as "impact" dissociation, for all practical purposes can be neglected.

The satellite will acquire a positive charge as result of a photoeffect under the influence of solar ultraviolet radiation and collisions with positive ions; collisions with electrons will impart a negative charge. Changes of satellite potential should be expected with transit through the F layer, because this will influence fluxes of ions and electrons in the manometer.

The presence of natural atmospheric ionization can cause an ion current up to 10^{-7} a in the manometer. The entry of these ions into the working cavity of the manometer can be eliminated by ion traps installed at the entrance (ref. 51).

B. A. Mirtov has shown that with proper pressurization of a satellite (the leakage of gas should not exceed 1 cm^3/sec at atmospheric pressure) and the use of materials with low vapor elasticity, the release of gas by the satellite exerts virtually no influence on pressure or density measurements in the atmosphere, if the direct entry of the released gas into the manometer is prevented.

During the creation of the Soviet satellite much work was done on determination of the vapor elasticity of different construction materials at a temperature of 20-300° C and the time required for outgassing of different materials after their prolonged presence at atmospheric pressure. The satellite was constructed from materials satisfying the formulated requirements (ref. 129).

According to an estimate made by V. V. Mikhnevich, the error in measurement of pressure and density caused by a possible change of air composition is about 20 percent at a height of 200 km and about 60 percent at a height of 500 km. A preliminary analysis of all errors, including errors in determination of height, velocity, calibration, telemetry and also in the principal assumptions made in interpretation, reveals that the error in measurement of density above 200 km at individual points can attain 200 percent. Further analysis of the measurement results, taking into account data obtained on rockets and satellites, including data on air composition at these heights, can decrease this error (ref. 129).

Figures 9.1 and 9.2 schematically show thermal ionization and magnetic magnetometers used for density and pressure measurements on the third Soviet

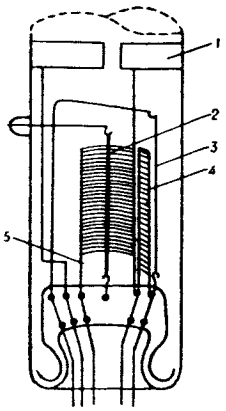

Figure 9.1. Thermal ionization manometer used on third Soviet satellite. (1) trap; (2) collector, (3) filament--cathode, (4) grid for stabilization of emission, (5) accelerating grid--anode.

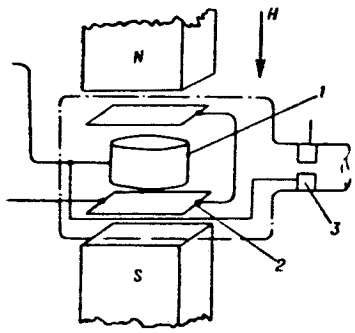

Figure 9.2. Magnetic manometer used on third Soviet satellite. (1) frame--anode, (2) plate--cathode, (3) trap.

satellite (ref. 129). The use of ordinary ionization manometers for pressure measurement in the range 10^{-5}-10^{-9} mm Hg in an ionized medium (ionospheric F layer) is difficult since the currents formed in the manometer by atmospheric ions and electrons are comparable with the manometer currents, which are a measure of pressure. In the thermal ionization manometers, used on the third Soviet satellite, special screens and traps were used to accomplish the separation of these currents, and only currents being a measure of pressure were recorded.

In order to decrease the photocurrents from the collector in the thermal ionization manometer, the collector was made in the form of a thin wire 2 (fig. 9.1). Due to the additional grid 4 between the cathode and anode there is an autostabilization of the emission current.

The manometer current is amplified by a dc amplifier and is fed to the input of the telemetric system. The block diagram of the instrument is shown in figure 9.3. The manometer is carried into the upper layers of the atmosphere in

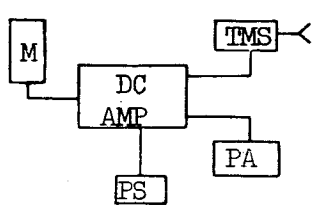

Figure 9.3. Block diagram of instrument (third Soviet satellite). (M) manometer, (dc Amp) dc amplifier, (TMS) telemetric system, (PA) programming apparatus, (PS) power source.

an evacuated state and is opened at a certain height (fig. 8.3). During the entire flight the ion current of the manometer is recorded continuously, the amplifiers are calibrated periodically, as well as the emission current of the manometers, and the temperature of the manometer wall is also measured.

10. Results of Pressure and Density Measurement with Rockets and Satellites

The preceding sections (Sections 1-5.7) gave the results of measurement of air pressure and density at different heights, obtained by a number of indirect methods--from meteor and twilight observations and the searchlight method of sounding the atmosphere. Now we will discuss the results of rocket soundings and measurements made using artificial Earth satellites.

10.1. Rocket Measurements to Heights of 100-130 Km. Table 10.1 presents the mean values of pressure from measurements with thermal manometers, made regularly using meteorological rockets in the middle latitudes of the Soviet Union. The mean density values were obtained using the equation of state of a gas. The mean square error of one pressure measurement with thermal manometers was 4 percent. In this same region pressure measurements to great heights were

TABLE 10.1. MEAN WEIGHTED VALUES OF PRESSURE p AND DENSITY ρ FROM MEASUREMENTS BY MANOMETERS CARRIED ABOARD METEOROLOGICAL ROCKETS (MIDDLE LATITUDES OF THE SOVIET UNION).

h км	*p* мм Hg	ρg/м³	*h* км	*p* мм Hg	ρg/м³
55	0.638	1.09	66	0.0734	0.144
52	0.488	0.842	68	0.0516	0.102
54	0.360	0.627	70	0.0374	0.0769
56	0.310	0.550	72	0.0305	0.0594
58	0.222	0.402	74	0.0210	0.0449
60	0.171	0.316	76	0.0150	0.0327
62	0.131	0.245	78	0.0110	0.0239
64	0.0939	0.181	80	0.00750	0.0163

made using geophysical rockets; in addition to the manometers carried directly aboard the rocket, the investigations were made with instrument packages which separated from the rocket (see Section 8). The mean atmospheric pressure obtained on the basis of instrument package measurements (ref. 128) is given in Table 10.2. The mean square measurement error was about 10 percent. The mean pressure determined from measurements in the instrument containers and by geophysical rockets (ref. 128) is given in Table 10.3.

In the United States a large part of the rocket measurements was made over the White Sands Proving Ground, New Mexico (32°24'N, 106°22'W). Table 10.4

TABLE 10.2. ATMOSPHERIC PRESSURE OBTAINED FROM INSTRUMENT PACKAGE MEASUREMENTS (USSR).

h км	p мм Hg	h км	p мм Hg	h км	p мм Hg
55	$4.0 \cdot 10^{-1}$	72.5	$4.0 \cdot 10^{-2}$	90	$1.2 \cdot 10^{-3}$
57.5	3.1	75	2.7	92.5	$6.9 \cdot 10^{-4}$
60	2.3	77.5	1.7	95	4.3
62.5	1.6	80	1.0	97.5	2.8
65	1.2	82.5	$5.9 \cdot 10^{-3}$	100	1.8
67.5	$8.8 \cdot 10^{-2}$	85	3.9	102.5	1.2
70	5.8	87.5	1.9	105	$8.6 \cdot 10^{-5}$
				107.5	6.8

TABLE 10.3. ATMOSPHERIC PRESSURE FROM INSTRUMENT PACKAGE AND GEOPHYSICAL ROCKET DATA (USSR).

h км	p мм Hg	h км	p мм Hg	h км	p мм Hg
57.5	$3.15 \cdot 10^{-1}$	72.5	$4.14 \cdot 10^{-2}$	87.5	$1.93 \cdot 10^{-3}$
60	2.39	75	2.69	90	1.15
62.5	1.71	77.5	1.69	92.5	$6.90 \cdot 10^{-4}$
65	1.23	80	1.01	95	4.30
67.5	$8.75 \cdot 10^{-2}$	82.5	$5.90 \cdot 10^{-3}$	97.5	2.77
70	6.05	85	3.35	100	1.81

gives the results of winter measurements, and Table 10.5--summer measurements (ref. 625) of pressure made at this point in different years.

Figure 10.1. shows a curve published in 1955 by the Naval Research Laboratory in the United States as the "standard" vertical distribution of pressure (common logarithms are plotted along the y-axis) (ref. 625). The curve was constructed from the data in Tables 10.4 and 10.5 and also from individual measurements made at different latitudes, and then made more precise together with the curve for density ρ (fig. 10.2, ref. 625) in such a way that the temperature value computed from the derivative $\frac{dp}{dh}$ (i.e., from the slope of the curve in figure 10.1) coincided with the temperature computed from the equation of state of the gas (8.1) by joint use of the curves for p and ρ. Below 160 km (with the exception of data for May 3, 1949) it was possible to make the curves more precise without exceeding the limits permitted by measurement error; the temperature values computed by these two methods did not differ from one another by more than a few percent. Above 160 km the reciprocal agreement of the finally

TABLE 10.4. RESULTS OF ROCKET PRESSURE MEASUREMENTS OVER WHITE SANDS PROVING GROUND.

	Winter					
	p mm Hg					
h km	Oct. 10 1946 11^h02^m	Mar. 7 1947 11^h23^m	Jan. 22 1948 13^h13^m	Jan. 28 1949 10^h20^m	Apr. 6 1949 09^h57^m	Dec. 12 1950 00^h15^m
1.2	—	—	655	662	—	—
10	—	—	205	200	—	—
42	—	2.2	1.6	1.8	—	—
43	—	1.7	—	1.57	—	—
44	—	—	1.30	1.37	—	—
45	—	1.5	1.21	1.19	—	—
46	—	—	—	1.08	—	—
47	—	1.00	1.00	0.93	—	—
48	—	0.86	0.87	0.85	—	—
49	—	—	—	0.74	—	—
50	—	0.66	0.76	0.66	—	—
51	—	—	0.65	0.57	—	—
52	—	—	0.60	0.51	0.57 ± 0.04	—
54	—	0.49	0.49	—	—	—
55	—	—	0.43	—	—	—
61.3	—	—	—	0.17 ± 0.03	—	—
63	0.140	—	—	—	—	—
64	—	0.144	—	—	—	—
64.7	—	—	0.107	—	—	0.109 ± 0.004
65	0.112	0.124	—	—	—	—
66	0.098	—	—	—	—	—
67	0.092	0.100	0.086	—	—	—
68	—	0.086	0.074	—	—	—
69	0.067	0.074	0.060	—	—	—
70	0.061	—	0.047	—	—	—
71	0.052	0.050	—	—	—	—
72	0.045	0.042	0.033	—	—	—
73	—	0.033	0.030	—	—	—
94	—	—	$1.2\cdot10^{-3}$	—	—	—
112	—	$1\cdot10^{-4}$	$1.4\cdot10^{-4}$	—	—	—
120	—	—	$1.4\cdot10^{-5}$	—	—	—
122	—	$3.5\cdot10^{-5}$	3.5	—	—	—

selected curves was not so good (the data for great heights experienced considerable changes as a result of satellite measurements). This corrected curve is used for comparisons with other series of experimental data.

Table 10.6 gives the results of measurement of atmospheric density in the upper layers of the atmosphere over White Sands Proving Ground (ref. 625) (Naval Research Laboratory of the United States). The measurement error does not exceed 20 percent, except for the data for a height of 160 km. The table does not give the result of an individual density measurement at a height of 219 km made on a Viking rocket on Aug. 7, 1951 at 1100 hours. Density was 10^{-7} g/m^3 (probable error of 20 percent). An average curve (fig. 10.2) was constructed by this method on the basis of these data and also the results of measurements

TABLE 10.5. RESULTS OF ROCKET PRESSURE MEASUREMENTS OVER WHITE SANDS PROVING GROUND.

	Summer	p mm Hg		
h km	Aug. 5 1948 18^h37^m	May 3 1949 09^h14^m	Aug. 7 1951 11^h00^m	May 7 1954 10^h00^m
1.2	662	656	—	—
10	218	213	—	—
41	—	2.1	—	—
42	2.0	1.70	—	—
43	1.7	1.50	—	—
45	1.38	1.21	—	—
46	—	1.06	—	—
47	1.10	0.97	—	—
48	—	0.83	—	—
49	0.85	0.72	—	—
50	0.74	0.64	—	—
51	0.65	0.52	—	—
52	—	0.48	—	—
53	0.52	0.43	—	—
54	0.45	0.40	—	—
55	0.41	0.35	—	—
56	—	0.30	—	—
57	0.33	0.26	—	—
59	—	0.20	—	—
62	—	0.114	—	—
63	—	0.106	—	—
64	—	0.086	—	—
65	—	0.079	—	—
66	—	0.072	—	—
67	—	0.066	—	—
68	—	0.062	—	—
69	—	0.058	—	—
70	—	0.052	—	—
71	—	0.042	—	—
72	—	0.038	—	—
73	—	0.033	—	—
76.3	—	—	—	$1.95 \cdot 10^{-2}$
79.5	—	—	—	1,7
82.4	—	$(7 \pm 2) \cdot 10^{-3}$	—	—
82.6	—	—	—	$5.1 \cdot 10^{-3}$
84.3	—	—	—	3.3
85.7	—	—	—	2.7
89.2	—	—	—	1.7
92.4	—	—	—	$5.4 \cdot 10^{-4}$
94.3	—	—	$6.2 \cdot 10^{-4}$	—
97.0	—	—	4.8	—
100.4	—	—	3.3	—
102	—	—	*$3.2 \cdot 10^{-4}$	**$3.6 \cdot 10^{-4}$
102.9	—	$2.7 \cdot 10^{-4}$	—	—
106.5	—	$1.8 \cdot 10^{-4}$	—	—
108	—	—	$2.1 \cdot 10^{-4}$	$1.5 \cdot 10^{-4}$
113	—	—	$9.0 \cdot 10^{-5}$	$8.8 \cdot 10^{-5}$
119	—	—	$4.5 \cdot 10^{-5}$	$4.7 \cdot 10^{-5}$
124	—	—	$1.6 \cdot 10^{-5}$	$2.0 \cdot 10^{-5}$
128	—	—	***$0.85 \cdot 10^{-5}$	***$1.7 \cdot 10^{-5}$

* Using manometer mounted in northwestern quadrant.
** Using manometer mounted in southeastern quadrant.
*** ± 40 percent.

TABLE 10.6. RESULTS OF ROCKET DENSITY MEASUREMENTS OVER WHITE SANDS PROVING GROUND.

h km	ρ g/m³ Mar. 7 1947 11^h23^m	ρ g/m³ Aug. 5 1948 11^h37^m	h km	ρ g/m³ Mar. 7 1947 11^h23^m	ρ g/m³ Aug. 5 1948 18^h37^m
61	—	0.39	70	0.129	—
62	—	0.35	71	0.114	—
64	—	0.26	73	0.090	—
65	—	0.24	75	0.063	—
66	—	0.21	76	0.057	—
67	—	0.19	78	0.042	—
68	—	0.17	79	0.035	—
69	0.151	0.14	156	$(2.0\pm0.5)\cdot10^{-6}$	

over the equator and in northern regions. Figure 10.3 shows the results of individual measurements by the United States Naval Research Laboratory over White Sands Proving Ground in comparison with the average curve.

A research team at University of Michigan in the United States used a somewhat different method for measuring pressure (using deceleration pressure and pressure on the surface of the nosecone). Figure 10.4 shows the results of measurements made on June 20, 1950 on an Aerobee rocket, obtained on the basis of this theory (ref. 726). They make it possible to form a clearer idea concerning the character of the initial data(deceleration pressures at the tip

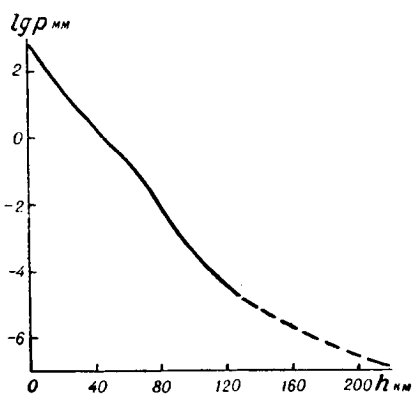

Figure 10.1. "Standard" (average) vertical pressure distribution. Values above 130 km (dashed curve) are extrapolated.

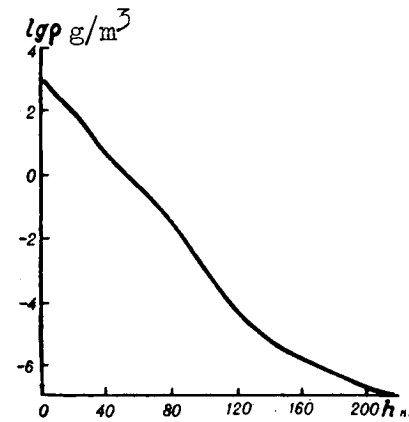

Figure 10.2. "Standard" (average) vertical density distribution.

of the rocket nosecone and pressures at the surface of the nosecone) and the final results (undistorted pressure, i.e., pressure in the surrounding undisturbed medium). In this case the accuracy of determination of true pressure was estimated at 3 percent.

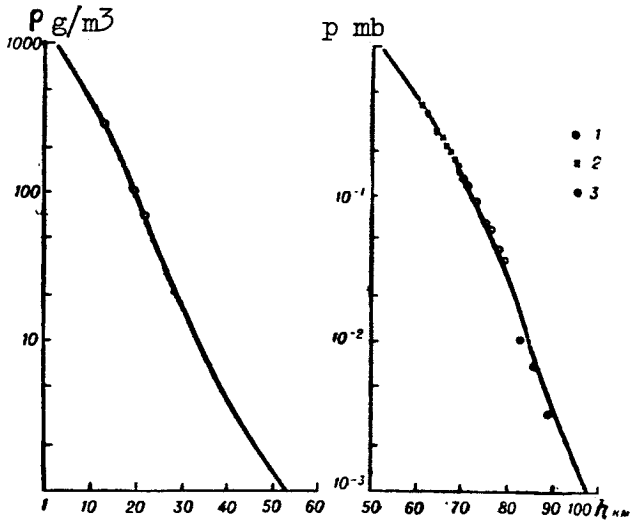

Figure 10.3. Vertical density distribution over White Sands Proving Ground. (1) Mar. 7, 1947, 1123 hours; (2) Aug. 5, 1948, 1837 hours; (3) Sept. 29, 1949, 0958 hours.

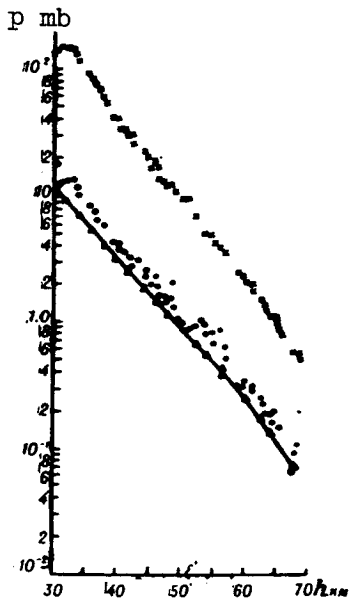

Figure 10.4. Vertical pressure distribution.

The relatively large scatter of pressure values at the surface of the nosecone was caused by rotation of the rocket, whose angle of yaw increases with height. Deceleration pressure in general does not reveal such cyclic variations, because it remains independent of the angle of yaw as long as this angle remains in the limits of 30°. Near the 35 km level it can be noted, although not very clearly, that there is a maximum of the ratio of pressure at the nosecone surface and deceleration pressure to undistorted pressure. This maximum does not reflect the properties of the atmosphere; apparently this is so because, at the indicated height, the Mach number and rocket velocity attain their maximum values (ref. 726) (the end of the active part of the trajectory, when all fuel was expended and the rocket engine ceased its operation).

In the second experiment, carried out on Sept. 13, 1951, the error in determination of undistorted pressure, in the opinion of the authors (ref. 726), was decreased to 1.5 percent (the results are shown in figure 10.5).

The specialists of the United States Naval Research Laboratory, using formula (8.3), computed the vertical density distribution, proceeding on the basis of comparison of the pressure distribution curve (fig. 10.4) and the density distribution curve (fig. 10.3). This comparison (fig. 10.6) revealed satisfactory agreement. Figure 10.7 shows the results of density measurements obtained by the team at University of Michigan from observations of the deceleration of a falling sphere (ref. 281). Comparison of these data and data obtained by the United States Naval Research Laboratory, using a completely different method (fig. 10.8), shows that they coincide rather closely; however, at the upper part of the curves the density values differ by a factor greater than 1.5 (ref. 625).

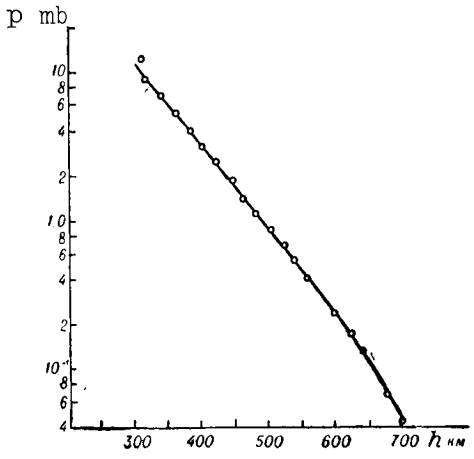

Figure 10.5. Vertical pressure distribution.

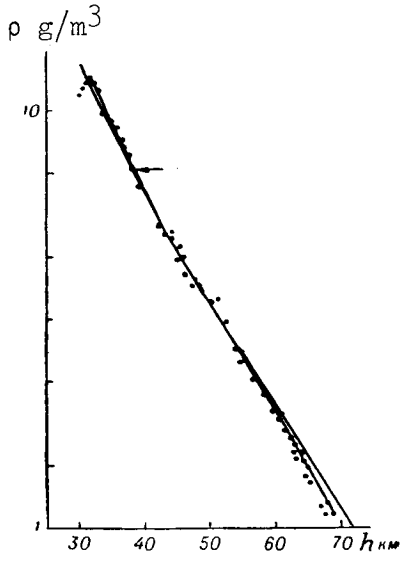

Figure 10.6. Air density distribution computed by United States Naval Research Laboratory (1) from data on deceleration pressure on Aerobee rocket obtained on June 20, 1950 by team at University of Michigan.

However, later measurement considerably impaired the agreement between the results obtained in the United States by different methods. In particular, this applies to measurements made by Byram, Chubb and Friedman (ref. 314). They determined air density ρ from absorption of solar x-radiation (Section 8.6). The values ρ, which they obtained at heights of 110-128 km, were smaller by a factor of approximately 3 than the mean values accepted by the United States Rocket Committee.

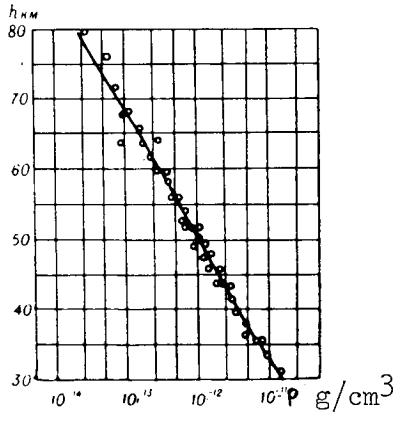

Figure 10.7. Average data on density obtained by group at University of Michigan from observations of deceleration of freely falling sphere.

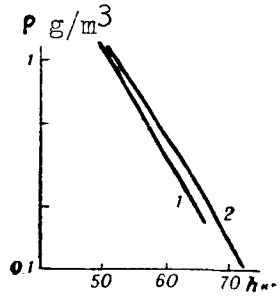

Figure 10.8. Comparison of data on density obtained from manometer measurments (1) and data on deceleration of falling sphere (2).

The opinion of Byram, Chubb and Friedman that former rocket measurements gave exaggerated values p and ρ at heights somewhat exceeding 100 km was confirmed by a study by Horowitz and LaGow (ref. 454). These authors measured p and ρ, using an ionization magnetic cold cathode. An important characteristic of this work was the introduction of a correction for emanation of gas by the rocket. The pressure and density, which they measured to a height of 140 km, were approximately four times smaller than the values adopted by the United States Rocket Committee. The results obtained by Horowitz and LaGow are shown in Table 10.7, and schematically in figure 10.13. These authors believe that their data are more precise, and they note a number of improvements in the method and good agreement with the measurements made by Byram, Chubb and Friedman.

TABLE 10.7. PRESSURE AND DENSITY MEASURED WITH ALLOWANCE FOR CORRECTION FOR RELEASE OF GAS BY ROCKET.

h км	p мм Hg	ρ g/cm^3	h км	p мм Hg	ρ g/cm^3
100	$1.1\cdot10^{-4}$	$2.5\cdot10^{-4}$	180	$6.9\cdot10^{-7}$	$2.3\cdot10^{-7}$
120	$8.0\cdot10^{-6}$	$1.2\cdot10^{-5}$	200	4.2	1.4
140	2.1	$1.2\cdot10^{-6}$	220	2.7	$9.0\cdot10^{-8}$
160	1.1	$4.3\cdot10^{-7}$			

10.2. Measurements in the Arctic. The program for rocket investigations of the high layers of the atmosphere carried out in the Soviet Union provides for measurements in the Arctic and in Antarctica, as well as in the middle latitudes (Section 10.1). Arctic investigations are made at Kheys Island (Franz Josef Land, $\varphi = 80.5^\circ$N, $\lambda = 58.0^\circ$E). Rocket soundings of the atmosphere in Antarctica were made on the diesel-electric "Ob'" in accordance with the International Geophysical Year program.

American investigators originally did not have rocket launch sites in the northern latitudes and they therefore used small Deacon rockets launched from

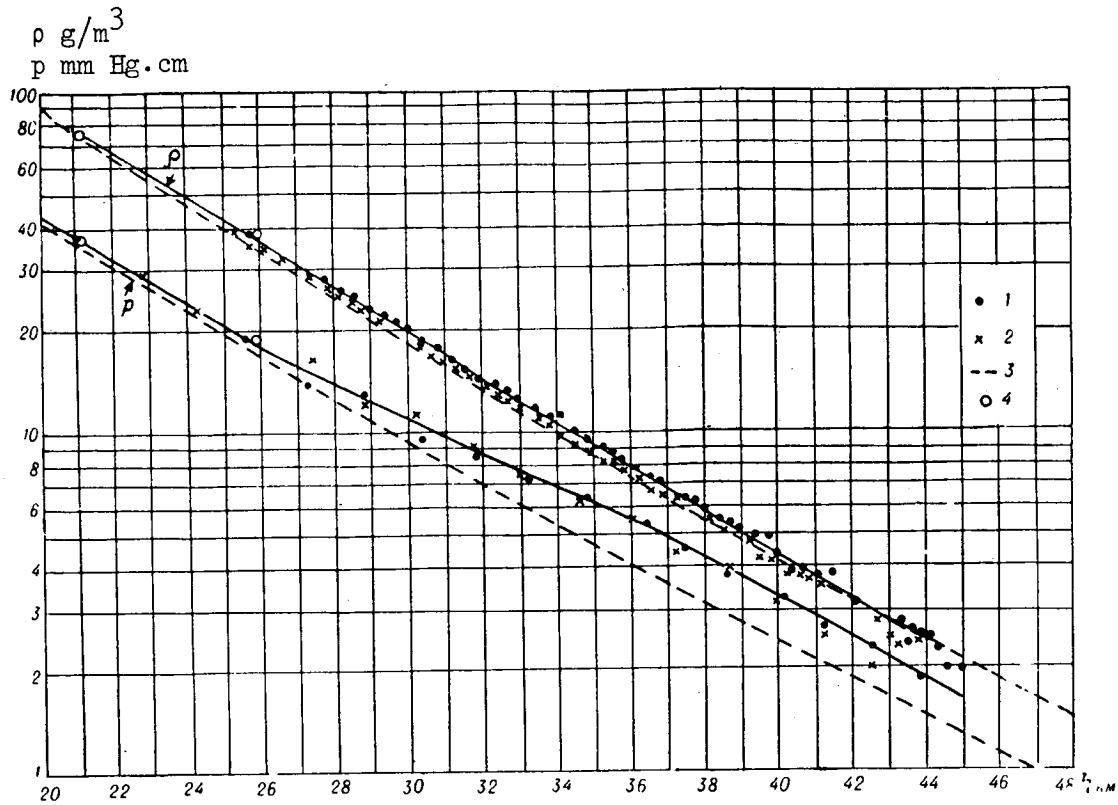

Figure 10.9. Vertical pressure and density distribution in atmosphere from measurements in the Arctic (74°34'N, 94°29'W). (1) ascent (August), (2) descent (1953, (3) White Sands Proving Ground (33°N), (4) mean for July-August for 4 years (1949-1951).

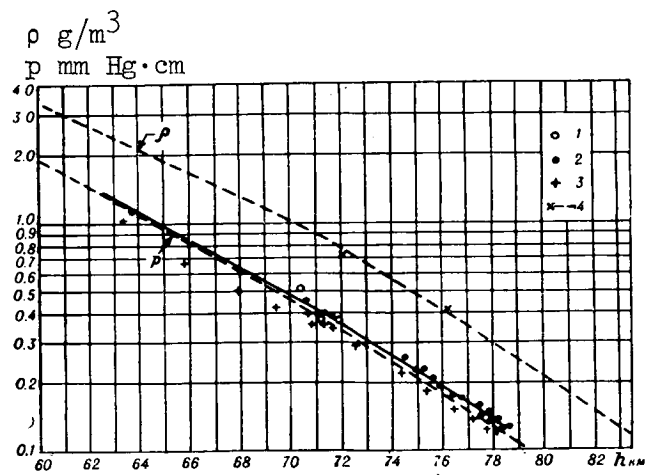

Figure 10.10. Vertical pressure and density distribution from measurements at 62 and 74°N. (1, 2) ascent, (3) descent, (4) White Sands Proving Ground (33°N).

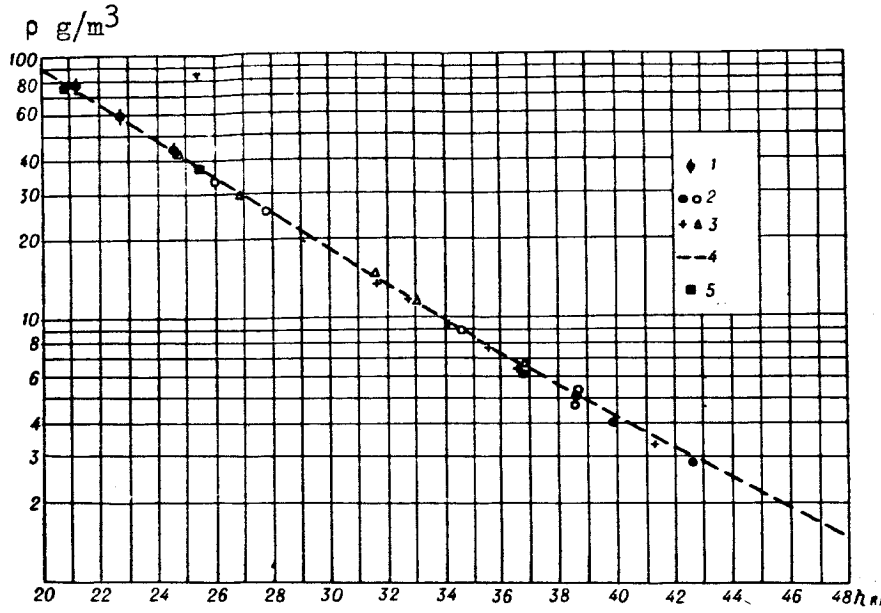

Figure 10.11. Vertical density distribution over Fort Churchill. (1) radiosonde, (2) ascent of NRL-7 and NRL-10, (3) descent, (4) White Sands Proving Ground (33°N), (5) mean for July-August for 4 years (1949-1951).

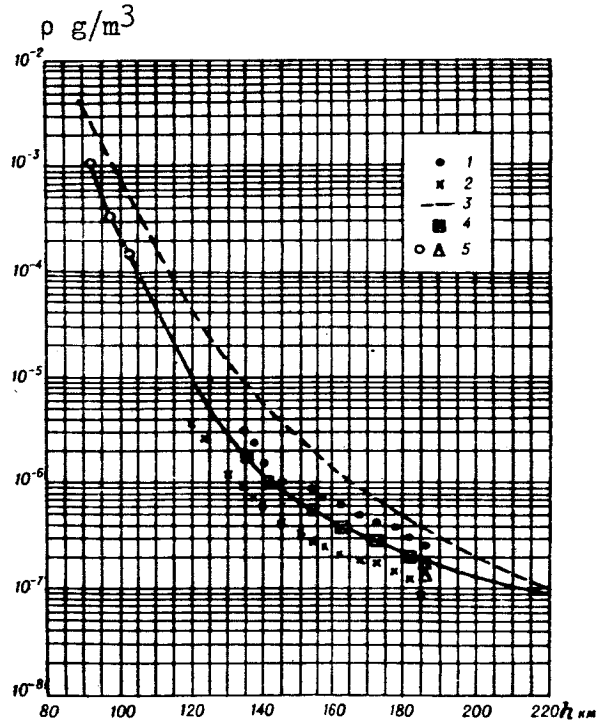

Figure 10.12. Vertical density distribution in 1956-1961. (1) ascent, (2) descent, (3) White Sands Proving Ground (33°N), (4) mean "ascent-descent", (5) from slope of pressure curve.

vessels, including icebreakers (ref. 541, Section 8.8). A rocket launch site was set up in later years in Canada (Fort Churchill, 58°46'N, 94°10'W). The results obtained in references 541 and 542 at latitudes 59-75°N using small Deacon rockets are shown in figures 10.9 - 10.11. For comparative purposes the graphs also indicate (dashed curves) the variation of pressure p and density ρ with height on the basis of measurements at White Sands Proving Ground situated 26-42° to the south.

Figure 10.12 shows density values obtained by manometer measurements at the test grounds at Fort Churchill, made in 1956-1957 using Aerobee-Hi rockets at relatively great heights.

Figure 10.13 gives a comparison of mass spectrometer measurements of density at Fort Churchill (ref. 769) with the measurements of Horowitz and LaGow (ref. 454). The curve accepted by the United States Rocket Committee is shown for comparison.

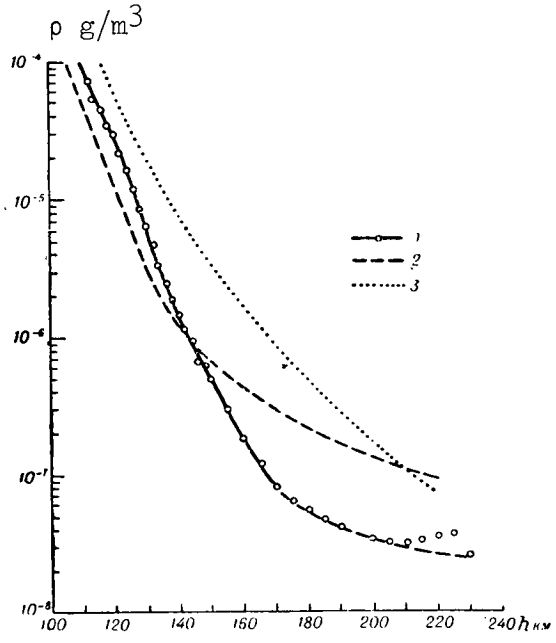

Figure 10.13. Vertical density distribution over Fort Chruchill 59°N. (1) and White Sands Proving Ground (2, 3) 33°N on Nov. 20, 1956 (1) NRL-48, (2) ref. 454, (3) United States Rocket Committee.

10.3. Rocket Measurements at Great Heights. The maximum height at which density has been measured was attained during rocket investigations in the USSR. In February 1958, a daytime-launched geophysical rocket carried manometers aloft to measure atmospheric density to a height of 260 km.

Table 10.8 gives a summary of data on atomospheric density on the basis of measurements by instrument packages and rockets (ref. 129) in the middle latitudes of the European part of the USSR.

TABLE 10.8. ATMOSPHERIC DENSITY FROM INSTRUMENT PACKAGE AND ROCKET MEASUREMENTS IN MIDDLE LATITUDES OF SOVIET UNION.

h км	ρ g/cm^3	h км	ρ g/cm^3	h км	ρ g/cm^3
60	$3.9\cdot10^{-7}$	130	$7.4\cdot10^{-12}$	200	$2.7\cdot10^{-13}$
70	1.36	140	3.2	210	2
80	$2.9\cdot10^{-8}$	150	1.7	220	1.6
90	$3.3\cdot10^{-9}$	160	$9.5\cdot10^{-13}$	230	1.25
100	$4\cdot10^{-10}$	170	6.4	240	1.1
110	$9.8\cdot10^{-11}$	180	4.4	250	$9\cdot10^{-14}$
120	2.2	190	3.3	260	6.9

Table 10.9 shows a comparison of the results of rocket determinations of density from measurements by instrument packages and geophysical rockets in the USSR (ref. 129) and by a Viking 7 rocket in the United States (ref. 454).

We already described a method for atmospheric measurements at a height of 430 km by observation of the diffusion of sodium vapor (Section 8.8). I. S. Shklovskiy and V. G. Kurt, on the basis of observations made on Sept. 19, 1958 (ref. 253), obtained atmospheric density values $\rho = 6.7\cdot10^{-15}$ g/cm^3, and a particle concentration $n = 2.5\cdot10^{8}$ cm^{-3}, which agrees well with the values obtained from the deceleration of Soviet and American satellites (Table 10.11).

TABLE 10.9. COMPARISON OF RESULTS OF MEASUREMENT OF ATMOSPHERIC DENSITY MADE IN THE USSR AND THE UNITED STATES.

	ρ g/cm^3 on basis of data in	
	ref. 129	ref. 454
100	$4\cdot10^{-10}$	$2.5\cdot10^{-10}$
150	$1.7\cdot10^{-12}$	$6.6\cdot10^{-13}$
200	$2.7\cdot10^{-13}$	1.4
220	1.6	$9.0\cdot10^{-14}$
228	1.3	
260	6.9	

The vapor diffusion method is of the greatest importance because it is completely independent.

10.4. Measurements by Satellites. The most important result of study of the structure of the Earth's atmosphere from observations by artificial Earth satellites is establishment of the fact that atmospheric density (and temperature) at heights of 200 km and more considerably exceeds the earlier accepted

values. This was discovered by observations of the first artificial satellite, launched on Oct. 4, 1957 in the Soviet Union, and was confirmed fully by subsequent measurements.

P. Ye. El'yasberg (ref. 258), after analyzing data on secular changes of the orbital elements of the first satellite and its carrier rocket (he used a method based on an idea by I. M. Yatsunskiy), obtained a mean density value

$\rho = 2.9 \cdot 10^{-13}$ g/cm^3 at a height of 225 km.

Specialists at the Smithsonian Astrophysical Observatory, who observed the motion of the first satellite, concluded (refs. 350 and 738) that at a height of about 220 km ρ is greater than the values accepted in the United States by almost 9 times. According to old data, the satellite should have had a lifetime of 27 months, but it was found that it survived only 4 months.

According to the observations of the first Soviet satellite, published by Harris and Jastrow (ref. 422), at the 400 km level density exceeds by approximately 40 times the value adopted in the ARDC model (United States). King-Hele and Leslie (ref. 526), on the basis of analysis of about 400 observations of this Soviet satellite, obtained the unexpectedly high values $H = 70 \pm 24$ km and $H = 65 \pm 7$ km for the height of the homogeneous atmosphere at a level somewhat above 200 km; they believe that these values must be decreased by 25 percent, if the Earth's asphericity is taken into account.

The large density values ρ at great heights h indicate a slow decrease of ρ with height h, i.e., at greater values of height H of the homogeneous atmosphere. For a given value of the mean molecular weight of the atmosphere, large values H must be interpreted as an indication of high temperatures. Paetzold (ref. 651) reported that observations of the first Soviet satellite and its carrier rocket indicate a temperature in the 200 km region of about 1,000°K, and near 500 km the temperature attains 2,500°K.

Figure 10.14 shows the results of measurement of density on rockets and some preliminary data on atmospheric density obtained by use of the satellite (V. V. Mikhnevich, ref. 129). As a comparison the graph shows the United States Standard Atmosphere of 1956 (model ARDC-1956). These same data are given in Tables 10.9 and 10.10. The curve constructed on the basis of measurements by an instrument package is plotted approximately in the sector 10^{-13}-10^{-14}.

Casci and Giavotto (ref. 316), whose method is discussed in Section 9.3, after solving equation (9.8) using high-speed computers, analyzed data on the motion of the first Soviet satellite. They consider these data (ref. 316) to be the most reliable and precise because the initial characteristics of the orbit and the value of the transverse load $\frac{m}{S}$ were known with a high degree of accuracy and its spherical form makes the corresponding computations

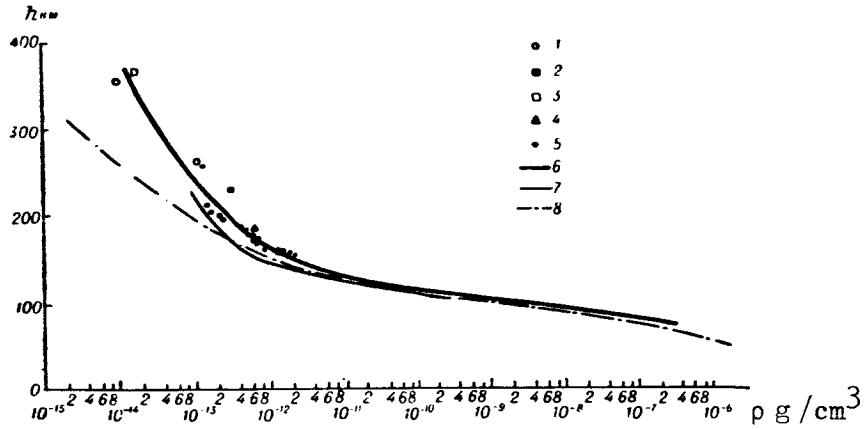

Figure 10.14. Atmospheric density from measurements on rockets and satellites. Satellites: (1) third Soviet satellite, manometers; (2) first, second and third Soviet satellites, deceleration, (3) 1958 α, deceleration, (4) 1958 γ, deceleration. Rockets: (5) USSR, February 1958, (6) USSR, rockets, instrument packages, (7) US, Viking 7, (8) United States Standard Atmosphere, 1956.

most reliable. Casci and Giavotto determined constants k and H of equation (9.6) from observations; knowing them, they computed density as a function of height. Their results are as follows: H = 17-38 km; $k = 1.906 \cdot 10^{-8}$ g/cm^3.

On the basis of observations (ref. 421) of the satellites Explorer (Feb. 5 - May 17, 1958) and Vanguard (May 1 - June 25, 1958) Harris and Jastrow determined the mean height of the homogeneous atmosphere as 73 ± 10 km and a temperature of 1,250 ± 200°K for the region between 400 and 700 km. Later these same authors (ref. 423), after analyzing data from the Minitrack radio-tracking system for the first Soviet satellite and the satellites Vanguard I and Explorer I, gave a value 95 ± 10 km for H and 1,600 ± 200°K for the temperature above 300 km.

TABLE 10.10. ATMOSPHERIC DENSITY FROM MEASUREMENTS ON SOVIET SATELLITES (V. V. MIKHNEVICH).

h km	ρ g/cm^3	Measurement method
208	$(2{,}4 \cdot 3{,}2) \cdot 10^{-13}$	From satellite deceleration
260	$1 \cdot 10^{-13}$	From reading of manometer mounted on satellite (preliminary values)
355	$8.8 \cdot 10^{-15}$	

In Section 9.4 we discussed the method for analyzing observations of satellites proposed by Groves (ref. 416). The dependence of ρ on h was represented

by this author as a quadratic function (9.7). After analyzing observational data on the deceleration of six satellites whose perigees were at heights from 174 to 656 km, including the first and second Soviet satellites (fig. 10.15), he used the least squares method to determine the coefficients of formula (9.7) and derived the following expression for the dependence of ρ on h

$$\ln \rho = -28.59\,(\pm 0.15) - \frac{h-200}{46\,(\pm 5)} + \qquad (10.1)$$

$$+ 0.028\,(\pm 0.013)\,\frac{(h-200)^2}{(46)^2},$$

where h is in kilometers and ρ in g/cm^3. The density values computed with this formula are shown in Table 10.11. It must be remembered that formula (10.1) was derived using data applying to different latitudes, seasons and time of day, and the values given in Table 10.11 must therefore be regarded as means.

TABLE 10.11. DEPENDENCE OF AIR DENSITY ON HEIGHT FROM OBSERVATIONS OF SATELLITE DECELERATION.

h км	ρ g/cm^3	h км	ρ g/cm^3	h км	ρ g/cm^3
150	$1.2\cdot10^{-12}$	350	$2.0\cdot10^{-14}$	550	$9.6\cdot10^{-16}$
200	$3.8\cdot10^{-13}$	400	$8.4\cdot10^{-15}$	600	5.3
250	1.4	450	3.8	650	3.2
300	$5.0\cdot10^{-14}$	500	1.9	700	2.0

On the basis of observations of the satellite Explorer III, Groves (ref. 416) found value H = 39 ± 9 km at heights of about 180 km, and from observations of the second Soviet satellite (which he analyzed by a somewhat different method) H = 36 ± 15 km at a height of about 220 km. In another of his studies (ref. 416), presenting an analysis of density values determined from observations of six satellites at heights from 150 to 700 km, Groves found H = 46 ± 5 km at a height of 200 km and 39±9 km and 36 km at a height of 180 km.

The density value cited in Table 10.11 for a height of 200 km is 3.5 times greater than the value adopted earlier by the United States Rocket Committee; at a height of 500 km it exceeds by a factor of 18 the density according to the United States Standard Atmosphere of 1956 (model ARDC-1956).

10.5. Models of the Atmosphere Including Satellite Observation Data. These data show the presence of considerable discrepancies in the results obtained by different authors and evaluations of some of these results. There are three principal reasons for this: (1) the rigorous theory of the problem is extremely complex and therefore approximate methods are used, and the computation methods used by different authors sometimes differ considerably from one another; (2) sometimes the authors used inadequately precise factual data on satellite parameters. Uncertainty of the value of the cross section of satellite resistance is of particular importance, if its form is aspherical.

TABLE 10.12. ATMOSPHERIC DENSITY COMPUTED BY VARIOUS AUTHORS FROM SATELLITE DECELERATION DATA (FROM SUMMARY OF SCHILLING AND STERNE).

h км	ρ g/cm^3	Satellite	h км	ρ g/cm^3	Satellite
656	$3.5\cdot10^{-16}$	1958 β2	215	$4.7\cdot10^{-13}$	1957 α2
368	$1.5\cdot10^{-14}$	1958 α	212	4.8	1957 β1
368	1.4	1958 α	212	4.4	1957 β1
275	8.5	1957 α2	211±4	4.6	1957 β
241	$2.5\cdot10^{-13}$	1957 α2	206±7	5.4	1957 α2
233	2.2	1957 β1	202±4	7.3	1957 α1
232±5	1.5	1957 α2	201±4	6.7	1957 α2
220	5.7	1957 α1	200	4.0	1957 α2
220	4.5	1957 α2	197	7.0	1957 β1
220	4.0	1957 α2	186	6.7	1958 γ

For example, for the cylindrical satellite Explorer the maximum and minimum areas differ by a factor of 20. Harris and Jastrow (ref. 421), analyzing the observations of this satellite, used a constant value, averaged for all possible orientations, for the computations; others usually do the same. (3) Seasonal, latitudinal and other variations of atmospheric structure (Section 11). Different satellites move in their orbits at different seasons of the year and in different latitude zones, and initially it is not possible therefore to take the corresponding corrections into account.

For this reason there is great interest in studies in which attempts are made to combine observations of different satellites and obtain a more general picture of the structure of the upper layers of the atmosphere. Such preliminary models of the atmosphere, based on satellite observations of 1957-1958, first appeared in 1959. We will discuss them as fully as possible, together with the principal results published in the literature in 1959-1961.

Table 10.12 gives a summary of density determinations made by different authors on the basis of deceleration of the satellites 1957 α 1 (carrier rocket of the first Soviet satellite), 1957 α 2 (first Soviet satellite), 1957 β 1 (second Soviet satellite), 1958 α, 1958 β 1, 1958 β 2, 1958 γ, 1958 δ 1 (carrier rocket of the third Soviet satellite) and 1958 δ 2 (third Soviet satellite).

Kallmann (ref. 508) considers three models of the atmosphere proposed recently (models A, B, C). She believes that model A, reproduced in Table 10.13, agrees best with the results of measurements made by satellites and rockets. The equations relating ρ, p, T and acceleration of gravity g, which Kallmann used in computing this table, will be considered in Section 10.5 (Table 10.19).

Grimminger (ref. 413) cites the results in three variants (three models of the atmosphere), based on publications during the IGY period. His data are given in Table 10.14, which for comparison gives the results of Sterne and also Harris and Jastrow.

TABLE 10.13. MEAN VALUES OF DENSITY ρ, PRESSURE p AND HEIGHT H OF HOMOGENEOUS ATMOSPHERE FROM MEASUREMENTS ON ROCKETS AND SATELLITES (KALLMANN, MODEL A).

h km	ρ g/cm^3	p dynes/cm^2	H km	g cm/sec^2
90	$3.994 \cdot 10^{-9}$	$2.262 \cdot 10^{0}$	5.9	953.5
100	$6.933 \cdot 10^{-10}$	$5.339 \cdot 10^{-1}$	8.1	950.5
110	1.818	1.811	10.5	947.6
120	$6.339 \cdot 10^{-11}$	$7.667 \cdot 10^{-2}$	12.8	944.7
130	2.655	3.719	14.9	941.8
140	1.237	1.984	17.1	938.9
150	$6.108 \cdot 10^{-12}$	1.155	20.2	936.0
160	3.240	$7.355 \cdot 10^{-3}$	24.3	933.1
170	1.888	5.041	28.7	930.2
180	1.208	3.636	32.4	927.4
190	$8.295 \cdot 10^{-13}$	2.707	35.3	924.6
200	5.906	2.059	37.8	921.8
210	4.314	1.594	40.2	918.9
220	3.220	1.215	42.4	916.2
230	2.447	$9.939 \cdot 10^{-4}$	44.5	931.4
240	1.886	7.977	46.4	910.6
250	1.472	6.459	48.3	907.9
260	1.160	5.273	50.2	905.1
270	$9.218 \cdot 10^{-14}$	4.338	52.1	902.4
280	7.383	3.593	54.1	899.7
290	5.957	2.996	56.1	897.0
300	4.841	2.515	58.1	894.3
310	3.963	2.123	60.1	891.6
320	3.266	1.802	62.1	888.9
330	2.710	1.538	64.0	886.3
340	2.263	1.319	66.0	883.6
350	1.902	1.136	67.8	881.0
360	1.609	$9.816 \cdot 10^{-5}$	69.4	878.4
370	1.370	8.513	71.0	875.8
380	1.173	7.404	72.3	873.2
390	1.012	6.454	73.3	870.6
400	$8.745 \cdot 10^{-15}$	5.635	74.2	868.0
420	6.553	4.321	76.4	862.9
440	4.970	3.337	78.3	857.8
460	3.823	2.590	79.5	852.8
480	2.961	2.016	80.3	847.8
500	2.281	1.576	81.9	842.9
520	1.761	1.238	83.9	838.0
540	1.367	$9.780 \cdot 10^{-6}$	85.9	833.1
560	1.068	7.769	87.8	828.3
580	$8.418 \cdot 10^{-16}$	6.200	89.4	823.5
600	6.683	4.966	90.8	818.8
620	5.284	3.993	92.8	814.1
640	4.174	3.228	95.6	809.5
660	$3.297 \cdot 10^{-16}$	$2.628 \cdot 10^{-6}$	99.0	804.9
680	2.599	2.157	104	800.3
700	2.039	1.789	110	795.8
720	1.613	1.500	118	791.3
740	1.286	1.273	126	786.8
760	1.029	1.092	136	782.4
780	$8.253 \cdot 10^{-17}$	$9.477 \cdot 10^{-7}$	148	778.0
800	6.632	8.327	162	773.7

By having a series of density values ρ for different heights h, it is possible to use the barometric formula in the form

$$\rho = \rho_0 e^{-h/H}$$

for computations of H (thereby assuming that a barometric formula in this form is applicable under conditions characteristic of the atmosphere at great heights).

The computations by Sterne (refs. 739 and 742) indicate a density at a height of 220 km of $4.5 \cdot 10^{-13}$ g/cm^3 on the basis of observations of the evolution of the orbit of the satellite 1957 α 2 and $5.7 \cdot 10^{-13}$ g/cm^3 on the basis of observations of the satellite 1957 α 1. Data for the satellite 1957β at a height of 233 km give $\rho = 2.2 \cdot 10^{-13}$ g/cm^3.

P. Ye. El'yasberg and V. D. Yastrebov, after analyzing observations of the first, second and third Soviet artificial Earth satellites, computed (ref. 259) density using the formula

$$\rho_p = \frac{\Delta T}{S\sqrt{H}} f(a, e, H), \qquad (10.2)$$

where ρ_p is air density at the minimum flight height of the satellite above the Earth's surface, ΔT is the decrease of the period of revolution of the satellite in one orbiting of the Earth, S is a factor determining the influence of air resistance, f (a, e, H) is a function dependent on H, the semimajor axis a and eccentricity e of the orbit and changing slowly with a change of these values. In this case it is assumed that air density at height h can be found using the formula

$$\rho(h) = \rho_p \exp\left(-\frac{h - h_{\min}}{H}\right) \qquad (10.3)$$

(This formula is inapplicable in the exosphere, see ref. 233.)

The derived density values, computed for a height of 246 km, are given in Table 10.15.

Siry (ref. 729) analyzed observations of the Soviet satellite 1957 α 2 and the satellites Explorer I (1958 α) and Vanguard I (1958 β 2), and obtained the vertical density distribution shown in figure 10.15; as a comparison the model of the atmosphere proposed by Nicolet (ref. 635) is also shown.

The "preliminary" model of the atmosphere proposed by Kallmann in 1959 (ref. 508) is given in Table 10.16, where height H of the homogeneous atmosphere is given using model A (in this same study the author discusses two other models of the atmosphere, but she considers these to be less sound).

TABLE 10.14. VALUES OF DENSITY (G/CM^3) OBTAINED BY VARIOUS AUTHORS FROM OBSERVATIONS OF SATELLITE DECELERATION.

h km	Sterne	Harris and Jastrow	Grimminger (models I-III at latitudes 45 and 0°)					
			model I		model II		model III	
			45	0	45	0	45	0
220	$4.0 \cdot 10^{-13}$	—	$8.6 \cdot 10^{-13}$	$25.9 \cdot 10^{-13}$	$18.6 \cdot 10^{-13}$	$25.9 \cdot 10^{-13}$	$18,6 \cdot 10^{-13}$	$25.9 \cdot 10^{-13}$
368	$1.4 \cdot 10^{-14}$	—	$2.6 \cdot 10^{-14}$	$5.9 \cdot 10^{-14}$	$1.6 \cdot 10^{-14}$	$5.9 \cdot 10^{-14}$	$2.3 \cdot 10^{-14}$	$5.9 \cdot 10^{-14}$
405	—	$9.0 \cdot 10^{-15}$	$11.6 \cdot 10^{-15}$	$31.4 \cdot 10^{-15}$	$11.6 \cdot 10^{-15}$	$31.9 \cdot 10^{-15}$	$10.6 \cdot 10^{-15}$	$30.7 \cdot 10^{-15}$
720	—	$1.2 \cdot 10^{-16}$	$0.9 \cdot 10^{-16}$	$6.5 \cdot 10^{-16}$	$0.9 \cdot 10^{-16}$	$6.6 \cdot 10^{-16}$	7.2	$13.1 \cdot 10^{-16}$
1000	—	—	$5.6 \cdot 10^{-18}$	$5.5 \cdot 10^{-17}$	$4.6 \cdot 10^{-18}$	$6.1 \cdot 10^{-17}$	1.6	2.9

TABLE 10.15. AIR DENSITY OF HEIGHT OF 246 KM FROM OBSERVATIONS OF ORBITS OF SOVIET ARTIFICIAL EARTH SATELLITES.

Satellite	1	2	3
Density, g/cm^3	$1.40 \cdot 10^{-13}$	$1.73 \cdot 10^{-13}$	$1.72 \cdot 10^{-13}$

In 1960 Kallmann (ref. 509) published an extensive analysis and generalization of observations of the evolution of the orbits of a number of satellites (Table 10.17). Kallmann also gave particular attention to density data obtained by Soviet investigators (the report of V. V. Mikhnevich at the Fifth General Assembly of the Special IGY Committee, Moscow, August 1958), comparing them with her earlier (1950) computations (Table 10.18). On the basis of all these data Kallmann (ref. 509) in 1960 constructed a model of the atmosphere from 90 - 800 km (density, pressure, height of the homogeneous atmosphere), given in Table 10.19. Kallmann determined the vertical pressure distribution using the barometric formula and the equation of state of an ideal gas by numerical integration. It should be noted that Kallmann made the computations without making any assumptions concerning the temperature gradient or the height of the homogeneous atmosphere.

An interesting study of this problem was published in 1960 by Mathur and Mitra (ref. 579). After generalizing the results of measurements of atmospheric

density from the deceleration of satellites made in the USSR and the United States, they devised a "self-consistent" model of the atmosphere for heights of 130-1,000 km. They obtained a value of 462°K for atmospheric temperature at the 130 km level with a rapid increase to 2,000°K at a height of 600 km; according to their computations there are isothermal conditions above this level. Mean molecular weight decreases from 22.6 at a height of 130 km to 16.0 at the 450 km level. The model of the atmosphere computed by Mathur and Mitra is given in Table 10.20.

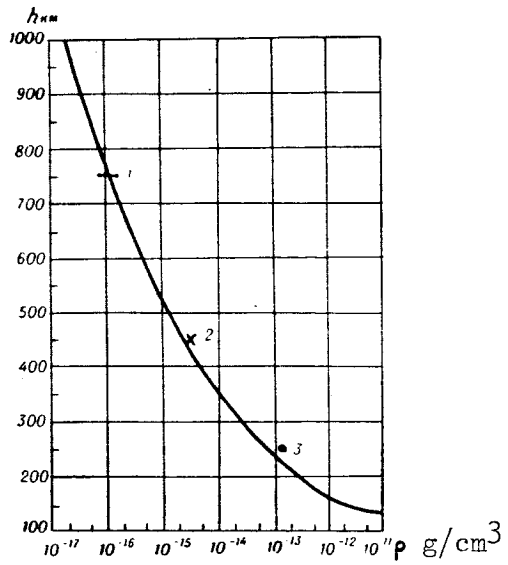

Figure 10.15. Atmospheric density indicated by satellite observations. (1) 1958 β_2, (2) 1958 α, (3) 1957 α_2.

TABLE 10.16. HEIGHT H OF HOMOGENEOUS ATMOSPHERE FROM ROCKET MEASUREMENTS AND OBSERVATIONS OF SATELLITES AT DIFFERENT HEIGHTS.

h км	*H* км	*h* км	*H* км	*h* км	*H* км	*h* км	*H* км
90	5.9	220	42.4	350	67.8	560	87.8
100	8.1	230	44.5	360	69.4	580	89.4
110	10.5	240	46.4	370	71.0	600	90.8
120	12.8	250	48.3	380	72.3	620	92.8
130	14.9	260	50.2	390	73.3	640	95.6
140	17.1	270	52.1	400	74.2	660	99.0
150	20.2	280	54.1	420	76.4	680	104
160	24.3	290	56.1	440	78.3	700	110
170	28.7	300	58.1	460	79.5	720	118
180	32.4	310	60.1	480	80.3	740	126
190	35.3	320	62.1	500	81.9	760	136
200	37.8	330	64.0	520	83.9	780	148
210	40.2	340	66.0	540	85.9	800	162

TABLE 10.17. AIR DENSITY DETERMINED FROM OBSERVATIONS OF SATELLITES AT DIFFERENT LATITUDES.

h km	ρ g/cm^3	Satellite	Latitude, °
186	$6.7 \cdot 10^{-13}$	1958 γ, Explorer III	34 N
190	7.0	1958 δ1, Sputnik III	40
190	3.6	1958 δ1, " III	40
197±1	7.0	1957 β, " III	
201±4	6.7	1957 α2, " I	39 N
202±4	7.3	1957 α1, " I	
206±7	5.4	1957 α2, " I	
211±4	4.6	1957 β, " II	
212	4.8	1957 β, " II	
215	4.7	1957 α2, " I	39 N
220	4.0	1957 α2, " I	39
232±5	1.5	1957 α2, " I	
233	2.2	1957 β1, " II	
241	2.5	1957 α2, " I	
262,5	1.35	1958 ε, Explorer IV	51 N—51 S
275	$8.5 \cdot 10^{-14}$	1957 α2, Sputnik I	
368	1.4	1958 α, Explorer I	
405	$9.4 \cdot 10^{-15}$	1958 α, " I	
656	$3.5 \cdot 10^{-16}$	1958 β2, Vanguard I	
720	$1.2 \pm 0.3 \cdot 10^{-16}$	1958 β2, " I	

TABLE 10.18. AIR DENSITY (G/CM^3) FROM MEASUREMENTS ON GEOPHYSICAL ROCKETS AND SATELLITES.

	USSR		Computations by Kallmann (1958)		
h km	Geophysical rockets	Satellites	Model A	Model B	Model C
100	$4 \cdot 10^{-10}$		$5.0 \cdot 10^{-10}$	$7.1 \cdot 10^{-10}$	$5.0 \cdot 10^{-10}$
150	$4.7 \cdot 10^{-12}$		$6.1 \cdot 10^{-12}$	$8.1 \cdot 10^{-12}$	$1.7 \cdot 10^{-12}$
200	$2.7 \cdot 10^{-13}$		$5.0 \cdot 10^{-13}$	$8.6 \cdot 10^{-13}$	$5.0 \cdot 10^{-13}$
220	1.6		3.0	4.5	3.8
228	1.3	$(2.4—3.2) \cdot 10^{-13}$	2.7	—	—
260	$6.9 \cdot 10^{-14}$	$1 \cdot 10^{-13}$	1.1	$1.5 \cdot 10^{-13}$	$1.2 \cdot 10^{-13}$
355		$8 \cdot 10^{-15}$	$1.2 \cdot 10^{-14}$	$2.5 \cdot 10^{-14}$	$1.9 \cdot 10^{-14}$

Systematic investigations for development of a model of the structure of the atmosphere on the basis of the results of observations of the motion of satellites are being made, in particular, at the Smithsonian Astrophysical Observatory. Thorough studies in this field have been published by Whitney (refs. 804 and 805). We particularly note his work on the development of "linear" models (in these computations there is assumed to be a linear dependence of temperature on height). Whitney (ref. 805) computed the vertical

TABLE 10.19. ATMOSPHERIC MODEL (KALLMANN, 1960).

h км	ρ g/cm^3	p dynes/cm^2	*H* км	g cm/sec^2
90	$3.994 \cdot 10^{-9}$	$2.262 \cdot 10^{0}$	5.9	953.5
100	6.993	$5.339 \cdot 10^{-1}$	8.1	950.5
110	$1.818 \cdot 10^{-10}$	1.811	10.5	947.6
120	6.339	$7.667 \cdot 10^{-2}$	12.8	944.7
130	$2.655 \cdot 10^{-11}$	3.719	14.9	941.8
140	1.237	1.984	17.1	938.9
150	$6.108 \cdot 10^{-12}$	1.155	20.2	936.0
160	3.240	$7.355 \cdot 10^{-3}$	24.3	933.1
170	1.888	5.041	28.7	930.2
180	1.208	3.636	32.4	927.4
190	$8.295 \cdot 10^{-13}$	2.707	35.3	924.6
200	5.906	2.059	37.8	921.8
220	3.220	1.251	42.4	916.2
240	1.886	$7.977 \cdot 10^{-4}$	46.4	910.6
260	1.160	5.273	50.2	905.1
280	$7.383 \cdot 10^{-14}$	3.593	54.1	899.7
300	4.841	2.515	58.1	894.3
320	3.266	1.802	62.1	888.9
340	2.263	1.319	66.0	883.6
360	1.609	$9.816 \cdot 10^{-5}$	69.4	878.4
380	1.173	7.404	72.3	873.2
400	$8.745 \cdot 10^{-15}$	$5.635 \cdot 10$	74.2	868.0
420	6.553	4.321	76.4	862.9
440	4.970	3.337	78.3	857.8
460	3.823	2.590	79.5	852.8
480	2.961	2.016	80.3	847.8
500	2.281	1.576	81.9	842.9
550	1.207	$8.711 \cdot 10^{-6}$	86.9	830.7
600	$6.683 \cdot 10^{-16}$	4.966	90.8	818.8
650	3.710	2.910	97.2	807.2
700	2.039	1.789	110	795.8
750	1.150	1.177	130	784.6
800	$6.632 \cdot 10^{-17}$	$8.327 \cdot 10^{-7}$	162	773.7

TABLE 10.20. ATMOSPHERIC MODEL (MATUURA AND MITRA, 1960).

h км	ρ g/cm^3	Mean molecular weight	*H* км	*T*°K
130	$2.74 \cdot 10^{-11}$	22.6	17.4	462
140	1.41	22.6	19.7	515
150	$7.88 \cdot 10^{-12}$	21.8	21.9	561
160	4.63	21.3	24.2	604
170	2.85	20.5	26.4	630
180	1.83	19.9	28.7	670
190	1.21	19.5	30.9	709
200	$8.33 \cdot 10^{-13}$	19.2	33.2	749
210	5.85	18.9	35.4	787
220	4.20	18.7	37.7	828
230	3.18	18.2	39.5	845
260	1.31	17.5	44.8	922
300	$4.97 \cdot 10^{-14}$	16.9	51.5	1023
340	2.14	16.5	58.1	1128
400	$7.10 \cdot 10^{-15}$	16.2	68.0	1297
450	3.17	16.0	76.4	1435
500	1.54	16.0	84.7	1591
600	$4.43 \cdot 10^{-16}$	16.0	101.2	1903
700	1.60	16.0	110.0	2068
800	$6.00 \cdot 10^{-17}$	16.0	110.0	2068
900	2.40	16.0	110.0	2068
1000	1.00	16.0	110.0	2068

distribution of atmospheric density at heights of 150-800 km, agreeing with data obtained from observation of the change of the period of revolution of Soviet and American Earth satellites as a result of their deceleration in the atmosphere. Whitney used five points obtained in 1957-1958 at heights from 185 to 656 km, using five different satellites. Each of the points is the result of averaging over a long period of time (several months) in order to exclude density variations, which apparently are related to variations of the intensity of solar radiation in the short wave part of the spectrum. Latitudinal averaging also was carried out. We know that data on the change of satellite period can be

used to find the product $\rho\sqrt{H}$, where ρ is density and H is the height of the homogeneous atmosphere. Therefore, in order to obtain ρ, Whitney used different models of vertical temperature distribution. Then the values ρ are determined more precisely by the successive approximations method; the process usually converges after the first step. The author tested several models of vertical temperature distribution in which it is assumed that there is a linear temperature variation in a certain range of heights. The following density distribution was closest to the experimental data:

h km	200	300	400	500	600
log ρ	-12.30	-13.40	-14.02	-14.63	-15.22

In conclusion we will cite an article by Champion and Minzner (ref. 320) containing a concise, but rather complete review of the results of study of the structure of the atmosphere obtained up to 1959, using rockets and satellites. Figure 10.16, taken from this study gives a comparison of the two official models of the atmosphere adopted recently in the United States (models ARDC 1956 and 1959) and two models developed by the Smithsonian Astrophysical Observatory.

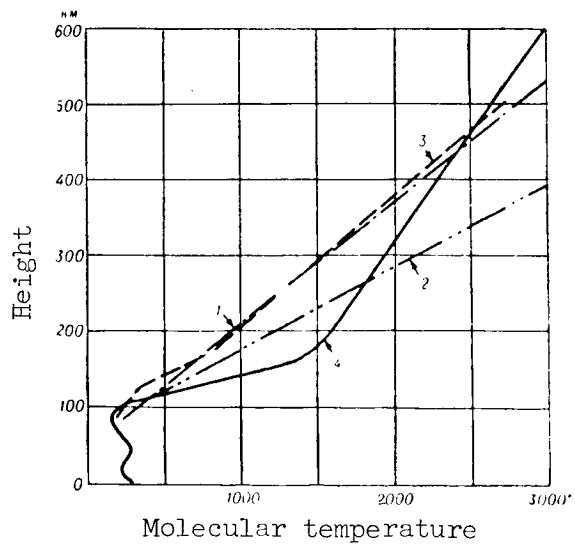

Figure 10.16. Comparison of temperature profiles corresponding to certain models of the atmosphere. (1 and 2) Models 1 and 2 of the Smithsonian Astrophysical Observatory; (3) ARDC-1956 model; (4) ARDC-1959 model.

The problem of a model of the atmosphere for great heights continues to be vigorously discussed in the geophysical and astrophysical literature (ref. 655). A. D. Bolyunov (ref. 14) has critically compared different measurements of the structural parameters of the upper layers of the atmosphere. In his opinion the fact that as a result of heat conductivity the heat flux can either be constant or increase with height above 250 km can serve as a criterion for evaluating the reality of the temperature distribution.

Previously we were repeatedly forced to discuss to some degree the problem of the mean molecular weight. This problem will be considered in greater detail in the chapter on air composition (Section 18).

These are the principal results of investigation of the upper layers of the atmosphere obtained from observations of the deceleration of artificial Earth satellites. We have seen that many of these models of the atmosphere differ considerably from one another. One of the reasons for this is the limited quantity of data used in individual investigations and the resulting low accuracy of temperature determination. However, there undoubtedly is another reason: the occurrence of considerable variations of pressure, density and temperature with time (diurnal and seasonal variation, etc.) and in space (latitude dependence, etc.). Since the observations of different authors usually apply to different periods of time and to different latitude zones, they obtain different results from analysis of data on deceleration of satellites. Strictly speaking, in order to compare the different results, an allowance should be made for these differences in observational conditions.

However, an analysis of the discrepancies in the results of determination of structure of the atmosphere obtained from satellite observations made in different periods of time and at different latitudes has made it possible to establish the existence of considerable variations of temperature, pressure and density of the upper layers of the atmosphere as a function of a number of factors.

11. Pressure and Density Variations

An analysis of available data on air pressure and density in the upper layers of the atmosphere shows that the values applying to the same height, but obtained by different authors sometimes differ considerably from one another. In addition to the measurement errors, sometimes extremely large, such discrepancies to a certain degree depend on the fact that the measurements were made at different times and at different latitudes. Analysis of available data indicates the presence of changes in structure of the atmosphere in its upper layers as a function of latitude, solar activity, season of the year and day. We will discuss these variations, but it must be stated at once that many of the noted relationships should be considered only preliminary, and further detailed observations are necessary for their confirmation and refinement.

11.1. Seasonal and Diurnal Variations. The occurrence of small seasonal density changes in the upper layers of the atmosphere was noted as early as 1937 by Öpik. He discovered that during the year the height of meteor trails

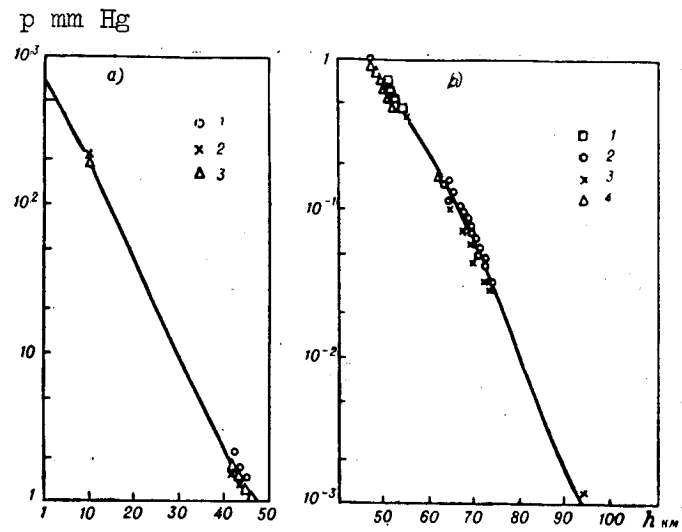

Figure 11.1. Pressure over White Sands Proving Grounds in winter (United States Naval Research Laboratory). (a) 1--Mar. 7, 1947, 1123 hours; 2--Jan. 22, 1948, 1313 hours; (3) Jan. 28, 1949, 1010 hours; (b) 1--Oct. 10, 1946, 1102 hours; 2--Mar. 7, 1947, 1123 hours; 3--Jan. 22, 1948, 1313 hours; 4-- Jan. 28, 1949, 1020 hours.

first increases and then decreases; the amplitude of these variations is approximately 4 km with a minimum in March and a maximum in August-September. These variations (fluctuations) were confirmed in part directly by determination of air density from meteor observations. Determinations made by Jacchia (ref. 471) indicate that the annual variation of density ρ is $\Delta \log \rho \sim 0.1$-0.6, with a minimum in spring. In a later study (ref. 472) Jacchia reexamined the problem, taking meteor fragmentation into account, and reached the following conclusion. At a height of 92 km (mean height of the meteors which he investigated) there are seasonal variations with an amplitude of 15 percent of the mean density value.

In the lower layers (below 68 km) no seasonal variations of density were discovered by Elterman in his measurements by the searchlight method of sounding the atmosphere (ref. 378). In particular, he established the presence of three layers which differ from one another in the character of change of density. These layers occur at the 9.5-20, 20-45 and 45-67.6 km levels. The greatest variations occur in the 45-67.6 km layer, and the curves of vertical distribution of density measured at different times usually converge at about $\sim$ 45 km.

The diurnal variation of air density in the upper layers of the atmosphere can be detected by meteor observations and twilight observations. Öpik's data indicate that during the course of the night the height of meteors decreases by an average of 3 km. This corresponds to an evening-to-morning decrease of density by 60 percent ($\Delta \log \rho = -0.2$). A comparison of the morning and evening twilight curves gives a value close to this. According to Link's data (ref. 555),

twilight observations indicate that the decrease of log ρ from evening to morning is 0.1-0.2 (at a height of about 90 km).

The results of rocket measurements of pressure for winter are shown in figure 11.1a and b and for summer in figure 11.2a and b at latitude 33°N. An average curve has been plotted on all curves for comparative purposes. Although the position of individual groups of points relative to the mean winter curve differs little from the position in summer (e.g., in the 60-70 km layer),

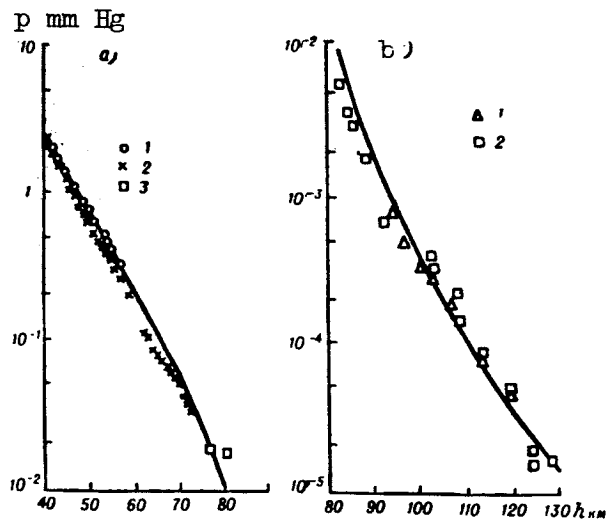

Figure 11.2. Pressure over White Sands Proving Grounds in summer (United States Naval Research Laboratory). (a) 1-- Aug. 5, 1958, 1837 hours; 2-- May 3, 1949, 0914 hours; 3-- May 7, 1954, 1000 hours. (b) 1-- Aug. 8, 1951, 1100 hours; 2--May 7, 1954, 1000 hours.

nevertheless, the measurements are insufficiently numerous to permit drawing of any conclusions. We should bear in mind the possibility of the existence of irregular changes of pressure and density (depending on weather conditions, particularly on changes of circulatory processes) against whose background regular (diurnal and seasonal) variations can be detected only when sufficiently long series of observations are available.

According to measurements at latitude 59° (Fort Churchill, Canada), the seasonal density variations at heights of 30-45 km are in general small, less than 10 percent.

A preliminary communication by Stroud (ref. 750) on measurements made at different latitudes in the North Atlantic, and in part at lower latitudes (33 and 38°N), indicates that air density at a height of about 200 km over Fort Churchill (59°N) on a summer day is 20 times greater than on a winter night and on a winter day 10 times greater than on a winter night.

As a result of the launching of four Aerobee-Hi rockets at Fort Churchill in accordance with the IGY program, LaGow, Horowitz and Ainsworth (ref. 543)

obtained data on the diurnal, annual and latitudinal changes of density of the upper layers of the atmosphere, which will be considered in Section 11.2.

In proceeding now to observations of the deceleration of satellites it must be remembered, as pointed out by L. I. Sedov, that the diurnal variations of atmospheric density at heights of 200 km or more should appear in the form of fluctuations of the rate of change of the period of revolution of a satellite around the Earth with time. We can also cite a paper by P. Ye. El'yasberg (ref. 258), who computed density at a height of 225 km and received a mean density value $\rho = 2.9 \cdot 10^{-13} g/cm^3$ from observations of the secular changes of the orbital elements of the first Soviet satellite and its carrier rocket, and $\rho = 4.1 \cdot 10^{-13}$ g/cm^3 from observations of the second Soviet satellite. The discrepancy between the cited values can be attributed to diurnal variations of density of the upper layers of the atmosphere. Groves (ref. 416) also reported on noted irregularities in the deceleration of the second Soviet satellite and also the third Soviet satellite and its carrier rocket. He feels that these changes should be attributed to the movement of satellite perigee from the daytime to the nighttime side as a result of precession of the orbital plane of the satellite. Groves attributes the increase of atmospheric density at a height of 220 km during the daytime in comparison with nighttime to an ascent of the entire atmosphere as a result of expansion of the lower layers (at a height of about 100 km) caused by heating by solar radiation.

Similar conclusions were drawn by Jacchia (ref. 473) after investigating fluctuations of the deceleration of the second and third Soviet satellites and the American satellite Vanguard. Jacchia summarizes his investigations as follows: there is a large diurnal effect at great heights (greater than 350 km), decreasing almost to zero at the 200 km level (ref. 474).

The rapid increase of diurnal variation with height also was confirmed by an analysis of observations of the deceleration of satellites made by King-Hele and Walker (ref. 530). They used observations of 21 satellites and carrier rockets, including observations of three Soviet rockets and two of their carrier rockets. Table 11.1 gives the results obtained by King-Hele and Walker. A diurnal variation can also be traced at heights of less than 350 km, but it is not very great there and is masked by large errors in the result and by variations of a different nature. Day-to-night changes in the structure of the atmosphere become very great beginning at a height of about 350 km.

11.2. Latitude Dependence. Data on air density in the upper layers of the atmosphere in different geographic regions from observations of meteors and the twilight sky suggest the presence of a latitude dependence of the vertical distribution of density. Both methods indicate that at about 90 km density increases with latitude. According to Link's summary (ref. 555), air density in this layer at $50^\circ N$ is greater than at $30^\circ N$ by a factor of approximately 4, if meteor data are used in this determination, or by 60 percent, if twilight observations are used.

TABLE 11.1. DIURNAL CHANGES OF DENSITY AND HEIGHT OF HOMOGENEOUS ATMOSPHERE IN UPPER LAYERS OF ATMOSPHERE FROM OBSERVATIONS OF FLUCTUATIONS OF DECELERATION OF 21 ARTIFICIAL EARTH SATELLITES.

h км	$\rho g/см^3$		H км	
	Day	Night	Day	Night
180	$7.0 \cdot 10^{-13}$		30	
190	5.1		36	
200	3.9		43	
210	3.2		47	
220	2,5		44	
230	2.0		42	
240	1.5		41	
250	1.2		40	
260	$9.4 \cdot 10^{-14}$		41	
270	7.2		42	
280	5.7		44	
290	4.6		47	
300	3.7		50	
350	$1.7 \cdot 10^{-14}$	$1.4 \cdot 10^{-14}$	74	53
400	$9.1 \cdot 10^{-15}$	$5.5 \cdot 10^{-15}$	83	56
450	5.1	2.3	90	59
500	3.1	1.0	99	62
550	1.9	$4.4 \cdot 10^{-16}$	109	65
600	1.2	2.0	118	69
650	$8.1 \cdot 10^{-16}$	1.1	126	73
700	5.5	$5.0 \cdot 10^{-17}$	133	77

TABLE 11.2. AIR PRESSURE AND DENSITY OVER EQUATOR.

h км	p мм Hg	h км	p мм Hg	h км	$\rho g/см^3$
0	760	59	0,23	39	$5.9 \cdot 10^{-6}$
10	222	62	0.15	43	2.5
13.7	130	65	0,100	46	2.0
48	0.90	68	0.070	66	$2.0 \cdot 10^{-7}$
56	0.31				

Rocket data obtained at different latitudes are of great interest for judging the reality of the latitude effect. Table 11.2 gives density and pressure values obtained on May 11, 1950 over the equator (the longitude of the point of rocket sounding was 160°W). Comparison with the average curve of the United States Navy Research Laboratory for White Sands Proving Ground (33°N) reveals that the density distribution over the equator has no appreciable differences from the distribution over White Sands Proving Ground; the pressure values are somewhat less than over White Sands.

Somewhat more numerous measurements have now been made in the high-latitude regions of North America. Comparison of these measurements with the standard

curve of the United States Rocket Committee, derived on the basis of sounding over the White Sands Proving Ground (ref. 707), led LaGow and Ainsworth (ref. 541) to the conclusion that the vertical distribution of density at 53, 55, 62 and 75°N is approximately the same as over White Sands Proving Ground, but the pressure values are appreciably greater, especially at about the 40 km level. The number of soundings was not sufficiently great to permit drawing final conclusions concerning the value of the latitude dependence of the vertical distribution of pressure.

Two years later these same authors, in collaboration with Horowitz (ref. 542), reported additional results of measurements made in the summer of 1953 and 1954, using small rockets called Rockoons (stratospheric rockets). These observations revealed that at 62 and 74°N the pressure at a height of 30-45 km exceeds the pressure over White Sands Proving Ground (the increment can attain 30 percent), but at the 70 km level pressure is approximately the same.

This meridional pressure gradient at heights of 30-45 km should give rise to an easterly geostrophic wind. LaGow, Horowitz and Ainsworth (ref. 542) feel that in general this agrees with the results of wind determination from the anomalous propagation of sound and using high-level pilot balloons in summer (see Chapter 9).

LaGow, Horowitz and Ainsworth (ref. 543), after comparing measurements made on four Aerobee-Hi rockets at Fort Churchill (59°N) in accordance with the IGY program and former measurements at the White Sands Proving Ground (33°N), concluded that density at heights of 30-70 km in summer is 5-10 percent greater than at these same heights at latitude 33°; in winter the density values at heights of 25-40 km are 10-20 percent less than the corresponding summer values, and therefore they are 5-10 percent less than the values for 33°. At a height of 200 km, the density in summer and autumn in the daytime is greater than the summer value by $1.4 \cdot 10^{-7}$ g/cm^3, measured in August 1951 at 33°N; at a height of 188 km in autumn in the daytime the density is $5.2 \cdot 10^{-7}$ g/cm^3, which is approximately 40 percent less than the value for a summer day. At a height of 110 km the atmospheric pressure over Fort Churchill in autumn and summer is approximately identical, but is approximately 2.5 times greater than the corresponding pressure over White Sands Proving Ground.

Interesting results have been presented in a preliminary communication by Stroud (ref. 750), concerning measurements made at various latitudes in the North Atlantic and partly at lower latitudes (33 and 38°N). Investigators of the vertical density distribution by the falling spheres method have discovered, as Stroud writes, an "unexpectedly great" dependence of air density on latitude at the 50 km level: about 2 percent degree of latitude.

Some idea concerning the latitude effects of temperature in the thermosphere can apparently be obtained by a comparison of the values of the height of the homogeneous atmosphere derived from rocket measurements in the Arctic (Table 11.3) with a model of the atmosphere proposed by Kallmann. The values

TABLE 11.3. STRUCTURE OF UPPER LAYERS OF THE ATMOSPHERE FROM ROCKET MEASUREMENTS IN THE ARCTIC (FORT CHURCHILL, 59°N).

h км	p мм Hg	ρ g/cm^3	$H = \frac{RT}{mg}$ км
100	$3.0 \cdot 10^{-4}$	$7.2 \cdot 10^{-10}$	6,0
110	$6.5 \cdot 10^{-5}$	1.3	7,0
120	2.1	$2.6 \cdot 10^{-11}$	12
130	1,3	$6.4 \cdot 10^{-12}$	29
140	$9.9 \cdot 10^{-6}$	3.0	47
150	8.2	1.9	63
160	7.1	1.4	76
170	6.3	1.1	85
180	5,7	$8.9 \cdot 10^{-13}$	91
190	5,1	7.9	93
200	4.6	7.0	94
210	4.1	6.2	95

derived by Kallmann are based on observations of satellites and rocket measurements applying for the most part to the middle and low latitudes, whereas Horowitz and LaGow (ref. 455) obtained their data from rocket measurements in the Arctic at a latitude of 59°N in daytime in the summer (July 29, 1957). It can be seen from a comparison of the data in these two tables that at heights of 100-120 km the height H of the homogeneous atmosphere in the Arctic is less and at heights of 130-210 km is greater. If the mean molecular weight m is assumed to be identical in both cases, it follows from this comparison that above 130 km the Arctic atmosphere in summer is considerably warmer than in the temperate latitudes. This conclusion requires confirmation.

Manometer measurements made during three rocket launchings at Fort Churchill indicate that atmospheric density at heights of 150-180 km is less than over White Sands Proving Ground (ref. 750). A similar conclusion was drawn by Townsend and Meadows (ref. 769), who measured density distribution over Fort Churchill (59°N) with a mass spectrometer. They compared their results with a curve constructed by Horowitz and LaGow for latitude 33°N (White Sands Proving Ground). Townsend and Meadows concluded that density over Fort Churchill at heights of 110-145 is greater than over White Sands Proving Ground, and at heights of 150-170 km the relation is the reverse.

The cited results of rocket sounding reveal that whereas the presence of latitudinal changes of pressure in the upper layers of the atmosphere is indisputable, data on density variation are in part contradictory. However, even here a comparison of the data of Stroud (ref. 750) and Townsend and Meadows (ref. 769) with the results of twilight determinations (ref. 555) of density at a height of 90 km gives basis for assuming the reality of latitude variations of density. Approximately the same meridional density gradient is obtained, according to Link's summary (ref. 555), at a height of 90 km, i.e., 3 percent per degree of latitude.

We also note that the irregularities in the deceleration of the second and third Soviet satellites, which Groves (ref. 416) attributed to diurnal

density variations, can also be related to latitudinal density variations. For example, King-Hele and Walker (ref. 528) believe that these irregularities possibly indicate that atmospheric density at a height of 220 km increases considerably somewhere between 35 and 28°N (a later study by these authors (ref. 529) reports the possibility of a 50 percent density increase between latitude 40° and the equator).

11.3. Density Variations Caused by Solar Activity. L. I. Sedov pointed out the possibility of deceleration of the rotation of a satellite around its center of mass during interaction with the geomagnetic field (ref. 176). The theoretical computations of Yu. V. Zonov confirmed that the development of eddy currents in the metal "skin" of a rotating satellite leads to an appreciable secular decrease of its angular velocity of rotation. V. I. Grigorovskiy (ref. 41) established the presence of rapid variations of the period of rotation of the second Soviet satellite, duplicating (with some lag) the variations of sunspot number (Wolf numbers); in his opinion this indicates there is an influence of variations of solar activity on the state of the Earth's magnetic field.

As pointed out by P. Ye. El'yasberg and V. D. Yastrebov, certain peculiarities in the change of motion of satellites indicate a change in the state of the Earth's atmosphere occurring under the influence of solar activity (ref. 259). By observing the carrier rocket of the third Soviet Satellite, King-Hele and Walker (ref. 529) were able to investigate the rate of change of the period of revolution of the rocket around the Earth $\frac{dT}{dt}$ and noted that this value has unstable behavior, although the rocket brightness changed regularly with a period of from 8.5 sec in July to 9.5 sec in November, 1958. The latter fact indicates that the rotation of the rocket could not exert an appreciable influence on the irregularity of its deceleration, and the mean area of the rocket cross section could be used in the law of resistance: the irregularity of the change of the value $\frac{dT}{dt}$ must be attributed to changes of atmospheric density. Similar circumstances also were established with respect to the motion of the second Soviet satellite. Both satellites had an initial perigee of 226 km; 10 days before the destruction of the second satellite, the height of its perigee was about 180 km.

Figure 11.3 shows data on the rate of change of the period of revolution of the carrier rocket of the third Soviet satellite. The error in determination of $\frac{dT}{dt}$ from observations, according to the estimate made by King-Hele and Walker, was 0.1 sec/day. As a comparison the figure shows the theoretical curve computed on the assumption that atmospheric density does not change with time. The computations were made by King-Hele and Walker (ref. 529), using formula

$$\frac{dT}{dt} = -\frac{3e_0 T_0}{4\tau\sqrt{1-\frac{t}{\tau}}},$$

where t is the time elapsing from the moment of launching; τ is lifetime of the satellite; e_0 is the initial value of eccentricity and T_0 is the initial value of the period.

King-Hele and Walker feel that the distinguishing characteristic of these curves is variations with a period of 28 days, which is close to the period of the Sun's rotation on its axis relative to Earth (27.3) days. On this basis it was postulated that changes of air density can be caused by corpuscular streams propagating radially from the Sun: these streams encounter Earth every 27-28 days and create the well-known periodicity of geomagnetic activity, auroras and cosmic rays.

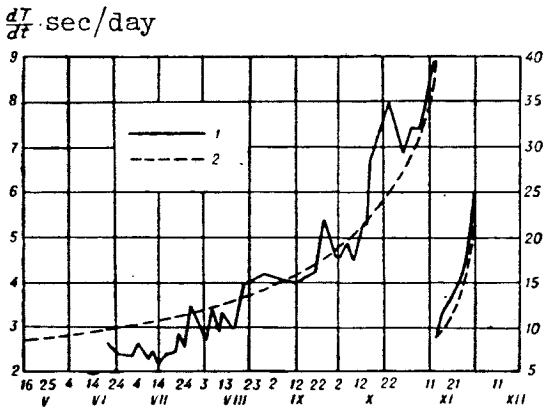

Figure 11.3. Rate of change of period of revolution of carrier rocket of third Soviet satellite. (1) observed, (2) theoretical.

After analyzing observations of other satellites, King-Hele and Walker note the presence of a similar periodicity and point out that the influence of solar activity should be reflected more strongly than the diurnal and latitudinal changes of atmospheric density and the influence of lunar tides.

Jacchia (ref. 473) also discovered variations of the deceleration of satellites with a period of 27-29 days. He established that the variations of the deceleration of the carrier rocket of the third Soviet satellite (fig. 11.4) and the American satellite Vanguard I coincide in phase. The results obtained by Jacchia apparently indicate rhythmic pulsations of the atmosphere as a whole, whose amplitude increases with height. Jacchia is inclined to attribute these pulsations to solar effects. He has reported a similarity of the deceleration curve and the curve of solar radio emission at wavelengths of 20 and 10.7 cm in November, 1957 - February, 1958. This has been discussed by Whitney (ref. 804), who compares the deceleration curves of the satellite 1958 β 2 (satellite Vanguard I) with the intensity of solar radio emission (fig. 11.5). Whitney undoubtedly is correct when he writes with respect to these curves that "correlation with solar activity is remarkably good." These variations, correlating with solar activity, increase with height from 15 percent at the 200 km

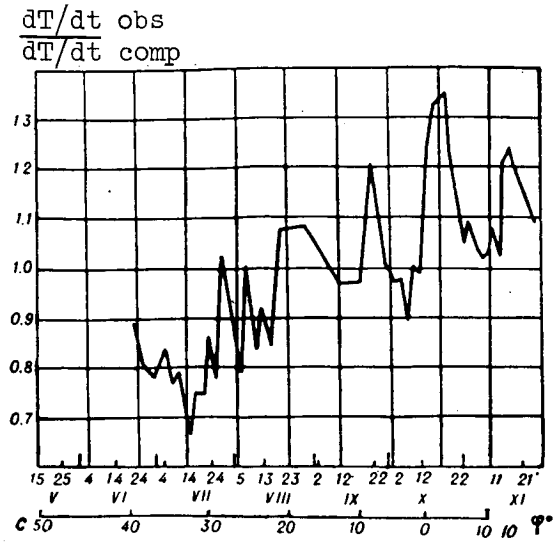

Figure 11.4. Rate of change of period of revolution of carrier rocket of third Soviet satellite.

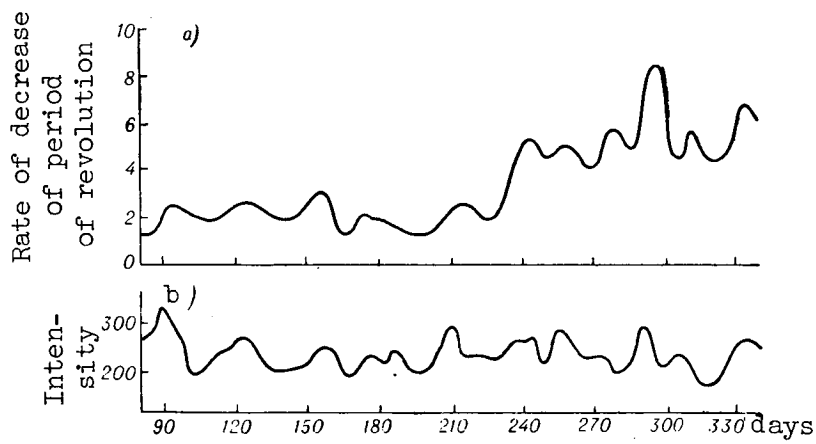

Figure 11.5. Comparison of variations of rate of deceleration of satellite Vanguard I (a) with intensity variations of solar radio emission at the wavelength $\lambda = 10.7$ cm (b), 1958.

level to 50-70 percent at the 600 km level. Apparently it is solar corpuscular radiation which is most important, rather than solar wave radiation, since the deceleration fluctuation usually lags by two days behind a burst of solar radio emission (ref. 804).

Other authors also have postulated such solar activity effects. Bartels cites stereophotogrammetric investigations of auroras, which make it possible to postulate the existence of strong variations of the upper boundary of the

atmosphere in connection with a change of geomagnetic activity and also the intensity of solar corpuscular streams. At the time of a storm, auroras are observed at heights up to 1,000 km, whereas ordinarily they are observed below 400 km. Such variations in the height of the atmosphere can be the cause of variations of air resistance to a satellite in orbit. Bartels notes in this connection that in February, 1958 the diurnal change of the period of revolution of the second Soviet satellite increased from 3.9 to 5 sec/day and then again decreased to 4.5 sec/day.

We should also mention several other studies in which the authors have investigated the effect of solar activity. Paetzold (ref. 653) notes that considerable changes of satellite acceleration occur on an average of every 10-15 days. It can be postulated that there are interplanetary clouds of protons with a diameter of 10^7-10^8 km. Jastrow (ref. 477) established that, on the basis of observations of satellite motion, density changes of the upper layers of the atmosphere correlate well with the intensity of solar radio emission at wavelengths of 10 and 21 cm and reveal a tendency to a 27 day frequency. In some cases, especially after large chromospheric flares, there was slowing of the satellite 1-2 days after the flare, simultaneous with the commencement of a magnetic storm. This fact indicates considerable heating of the upper layers of the atmosphere as a result of interaction with solar corpuscular streams arriving from active regions on the Sun. Heating of the atmosphere and development of auroras in the high latitudes, in Jastrow's opinion, can be attributed to the interaction between particles of the outer radiation belt and atmospheric atoms and molecules. Heating of the upper layers of the atmosphere in the auroral zones and the subsequent convective transport of heat to other latitudes should lead to a correlation between atmospheric circulation and solar activity.

Jacchia (ref. 474) also notes a sudden increase of density in the entire atmosphere above 200 km at the time of magnetic storms. King-Hele and Walker (ref. 530) discovered a slow density decrease at a height of 180-250 km, beginning in mid-1958 and lasting to the end of 1959, possibly correlating with the 11-year cycle of solar activity; this conclusion was confirmed in references 817 and 820. Johnson (ref. 488) estimates that at a height of about 200 km the pressure and temperature are approximately identical over the Earth's entire surface as a result of large-scale air movements which equalize the gradients. At these heights the centrifugal and Coriolis forces, which in the lower layers are an obstacle to the equalization of pressures, are balanced by viscosity. For this reason the author assumes that the considerable differences in the structure of the upper layers of the atmosphere found in rocket investigations at different latitudes can be attributed to the fact that the measurements were made at different times in relation to the solar cycle.[1] The problem of density variations of the upper layers of the atmosphere continues to be discussed in the literature (refs 507, 531, 532, 656, 657 and 659).

---

[1] On the basis of observations of 13 artificial Earth satellites from January, 1961 to January, 1963 with a decrease of solar activity from 1958 through 1963. The value ρ_{400} (density at a height of 400 km) decreased by a factor of 5 and

11.4. Tidal Variations. After a study of the conclusions expressed by Groves (ref. 416) Parkyn postulated that the observed irregularities of satellite deceleration are of a tidal nature (ref. 669). Tidal variations of density have been discovered by other authors as well from satellite observations. However, tidal movements in the upper layers of the atmosphere are manifested most clearly in ionospheric data and in wind measurements (see Chapter 12).

Footnote continued

ρ_{600} by a factor of 30 (ref. 820). According to the summary listed as reference 817, ρ_{700} during the daytime is 10 times greater than at nighttime and is an order of magnitude greater at the time of high solar activity: in general, ρ can change by a factor of 100. Similarly, the temperature T_{700} can vary by 1,000°.--Author Note.

CHAPTER 5. HEAT REGIME OF THE UPPER LAYERS OF THE ATMOSPHERE

12. Indirect Methods for Temperature Measurement in the Upper Layers of the Atmosphere

Modern data and concepts on the heat regime of the upper layers of the atmosphere have been presented in detail in an extensive monograph by K. Ya. Kondrat'yev and O. P. Filipovich (ref. 91) and also by the author (ref. 233). In this book we therefore limit ourselves only to a concise description of the measurement methods with which we can form concepts of the temperature field in the upper layers of the atmosphere and the factors determining it; also included is a more detailed review of several studies appearing after publication of the two books mentioned.

All existing methods for temperature measurement in the atmosphere at great heights can be arbitrarily divided into two principal groups: indirect and direct. Indirect methods include those for determination of the temperature of air layers situated at a great height by the use of surface apparatus. In order to make direct measurements it is necessary in most cases to carry all the measurement apparatus aloft or at least to send a considerable part of it directly into the particular layers of the stratosphere, mesosphere or thermosphere.

12.1. Acoustic Methods of Temperature Measurement. In discussing the indirect methods we will first review the acoustic methods, followed by optical and ionospheric methods.

The first reliable information on temperature at heights up to 50 km was obtained in the 1920's as a result of study of anomalous sound propagation. Strictly speaking, the basic structural part of the upper stratosphere, specifically, a well-developed temperature inversion at heights of 25-35 to 45-50 km, was discovered as a result of these acoustic investigations.

The use of acoustic methods for temperature measurement was based on the use of the dependence of the speed of sound a in the air medium on the temperature T of the medium. In thermodynamic form this relationship is expressed as

$$a = \sqrt{\gamma RT} = \sqrt{\frac{\gamma p}{\rho}}, \tag{12.1}$$

where γ is the ratio of the specific heat capacities, R is the gas constant, p is the static pressure at a point and ρ is density of the medium.

If the parameters (a_1, T_1, ρ_1, p_1) of a gas at a certain point are known in an isoentropic flow, their values at any other point are determined from the relation

$$\frac{a}{a_1} = \left(\frac{T}{T_1}\right)^{1/2} = \left(\frac{\rho}{\rho_1}\right)^{\frac{\gamma-1}{2}} = \left(\frac{p}{p_1}\right)^{\frac{\gamma-1}{2\gamma}}. \qquad (12.2)$$

If the air temperature at a height of about 25 km in the middle latitudes is approximately 215°K and then rapidly increases with height and attains values of approximately 275°K at about the 45 km level, the corresponding values of the speed of sound at these two levels are 295 and 332 m/sec. Such a considerable vertical gradient of the speed of sound causes a curvature of the sound rays (refraction of sound waves) propagating from a ground source (shot point) in an upward direction with subsequent return ("bending") of the sound waves to the ground. This gives rise to zones of silence and zones of anomalous audibility surrounding the sound source (shot point); acoustic measurements of the waves arriving from the atmosphere to a zone of anomalous audibility make it possible to determine the speed of sound at the level of return of the sound waves, and temperature can be determined using formula (12.2).

Another variant of the acoustic method, also based on investigations of the characteristics of a sound wave passing through a considerable thickness of the atmosphere, is based on the observation of explosions of bombs dropped from aircraft. This method has been used in the United States (ref. 233). Bombs weighing 1,640 kg were dropped from a B-29 heavy bomber onto a bombing range in the Rocky Mountains (ref. 346). Three bombs were dropped in each experiment, each 35 km apart along some meridian or latitude. The recording of the explosion waves was at four points, two on each side of the bombing range, 225 and 250 km from the points of impact.

Relationship (12.2) also is used for local acoustic measurements of air temperature. This method was developed by M. I. Mordukhovich (refs. 133 and 134). The apparatus, carried aloft by a stratospheric balloon, consists of a sound source and a receiver. These measure the time spent by a sound wave in travelling the distance (about 1 m) between the source and the receiver, i.e., the speed of sound. Using this method, Mordukhovich obtained the air temperature values in the stratosphere; they apparently were very precise and reliable. However, the apparatus needed for carrying out such local temperature measurements is complex, which complicates the extensive use of this promising method in aerology.

The acoustic method has been used for temperature measurements in the mesosphere using rockets. Several grenades are ejected from a vertically ascending rocket at specified times; the sounds of the grenade explosions are recorded at sound-gaging stations on the ground (fig. 12.1). In comparison with the method based on observations of zones of anomalous sound audibility of explosions, the rocket-grenade method gives an increase of the ceiling of the acoustic method. Information based on data on anomalous audibility of explosions always is limited by the height of that layer of the inversion (mesopeak) at which there is complete internal reflection of the sound ray. This level is situated at a height of about 50 km. However, if the sound source is raised above the reflecting layer, acoustic sounding of the atmosphere can be carried to a height of 80 km and even somewhat higher. In this case the sounding ceiling is determined by the absorption of sound, which becomes extremely great if the mean length of the free path of molecules becomes comparable to the length of the sound wave.

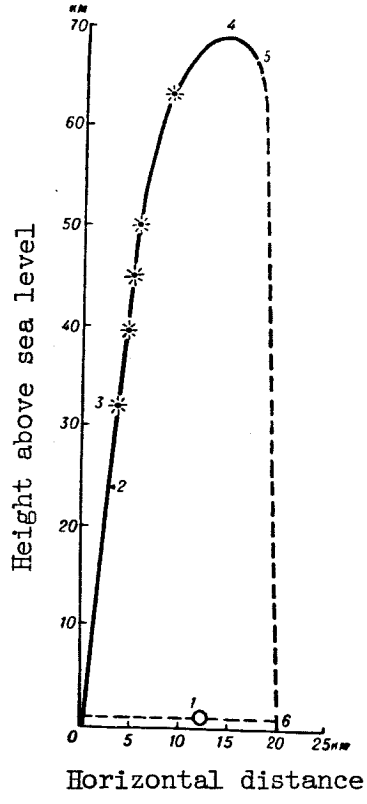

Figure 12.1. Typical trajectory of Aerobee rocket showing site of explosions of grenades (asterisks) relative to acoustic monitoring stations. 1, sound ranging station; 2, stop engine, 43 sec (1000 m/sec); 3, first shell explosion; 4, summit, 140 sec; 5, separation of rocket tail section 167 sec; 6, fall to Earth, 285 sec.

In addition to temperature measurement, the rocket-grenade method makes it possible (refs. 639 and 760) to measure wind direction and velocity simultaneously (Section 23).

12.2. Optical Methods. There is a great variety of methods for determining air temperature in the upper layers of the atmosphere, based on analysis of various optical phenomena. These can be divided into three principal groups. The first includes all those methods which give information on the vertical distribution of air density or pressure. The second group includes methods based on a study of the absorption spectra of the atmosphere, and the third--its radiation spectra. We now will discuss the first group of methods.

By use of the equation of state

$$p = \frac{\rho RT}{m} \qquad (12.3)$$

(m is mean molecular weight) it is possible to transform the barometric formula as follows

$$dp = -\rho g\, dh \tag{12.4}$$

(g is the local value of acceleration of gravity at height h), so that it will contain two of the three values p, ρ and T. If measurements give one of the values as a function of height, the second of these values can be computed by appropriate differentiation or integration. We now will consider cases where the vertical distribution of pressure p = p(h) or density ρ = ρ(h) is known. For example, ρ can be excluded from the equation of state (5.1) and the barometric formula (5.2), and an equation derived relating p and T

$$\frac{dp}{p} = -mg\frac{dh}{RT}.$$

Introducing an expression for the height of the homogeneous atmosphere

$$H = \frac{RT}{mg},$$

we can rewrite the preceding equation in the form

$$\frac{dp}{p} = -\frac{dh}{H},$$

hence

$$\frac{1}{H} = -\frac{1}{p}\frac{dp}{dh}. \tag{12.5}$$

Thus, by differentiating for height the function p = p(h), derived experimentally, we find the value $\frac{1}{H}$. If the mean molecular weight m of air is considered known (and to a height of about 100 km it can be considered virtually constant and equal to m = 28.9), value H can be used to compute the temperature

$$T = \frac{mgH}{R},$$

$$T = -\frac{pmg}{R\frac{dp}{dh}}. \tag{12.6}$$

If p is excluded from the equation of state and the barometric formula, we obtain the relation between ρ and T. After differentiating for this purpose the equation of state

$$dp = d(\rho T)\frac{R}{m}$$

and substituting the value dp into the barometric formula, we obtain

$$d(\rho T) = -m\rho g\frac{dh}{R}.$$

This equation is integrated

$$\rho_2 T_2 - \rho_1 T_1 = -\frac{mg}{R}\int_{h_1}^{h_2}\rho\, dh,$$

hence

$$T_2 = \frac{1}{\rho_2}\left(\rho_1 T_1 - \frac{mg}{R}\bar{\rho}\Delta h\right). \tag{12.7}$$

In this equation m, R and g are known constants; if the vertical density distribution $\rho = \rho(h)$ is established experimentally, densities ρ_1 and ρ_2 are known for heights h_1 and h_2, and it is possible to compute the mean density value $\bar{\rho}$ in a layer with thickness $\Delta h = h_2 - h_1$. Equation (12.7) therefore makes it possible to find temperature T_2 at height h_2, if temperature T_1 at height h_1 and the vertical density distribution between h_2 and h_1 are known.

If optical sounding of the atmosphere is conducted in detail, i.e., density values ρ_1, ρ_2,... are measured at sufficiently small intervals of height $\Delta h = h_2 - h_1$, function $\rho = \rho(h)$ within the limits of interval Δh can be approximated with sufficient accuracy by the exponential function

$$\rho = \rho_1 e^{-bh}, \tag{12.8}$$

where b is a constant. In this case

$$\rho_2 = \rho_1 e^{-b\Delta h}$$

and the mean density can be computed

$$\bar{\rho} = \frac{1}{\Delta h}\int_0^{\Delta h} \rho\, dh = \frac{\rho_1}{\Delta h}\int_0^{\Delta h} e^{-bh}\, dh,$$

which after integration gives

$$\bar{\rho} = \frac{\rho_1}{b\,\Delta h}\left(1 - e^{-b\,\Delta h}\right) = \frac{\rho_1 - \rho_2}{b\,\Delta h},$$

or

$$\bar{\rho} = \frac{\rho_1 - \rho_2}{\ln \frac{\rho_1}{\rho_2}},$$

since $\ln \frac{\rho_2}{\rho_1} = -b\Delta h$. By substituting the derived value $\bar{\rho}$ into equation (12.7), we obtain finally

$$T_2 = \frac{\rho_1 T_1}{\rho_2} - \frac{mg\left(\frac{\rho_1}{\rho_2} - 1\right)\Delta h}{R \ln \frac{\rho_1}{\rho_2}}. \qquad (12.9)$$

Optical investigation of the vertical distirbution of pressure $p = p(h)$ and density $\rho = \rho(h)$ can be accomplished by several methods, the most important of which are: (a) the meteor method (refs. 80, 109 and 127); (b) the twilight observation method (refs. 226, 377 and 378), and (c) the searchlight sounding method (refs. 226, 377 and 378) (Chapters 1-3).

Each of these three methods can be used for a study of the temperature regime of the upper layers of the atmosphere using equations (12.6) and (12.9), taking into account the limitations (particularly, the influence of aerosol scattering). A large number of investigations have been made for this purpose, primarily in Czechoslovakia, USSR and United States, and important results were obtained. The first information on the principal characteristics of the temperature regime of the atmosphere to a height of 85 km--the structure of the warm layer at a height of 45-55 km (stratopause) and the existence of a cold layer at the 80 km level (mesopause)-- was obtained by meteor observations. Lindemann and Dobson (ref. 550) reported that in 1923 they analyzed the distribution curve of the heights of disappearance of meteors and concluded that at a height of 60 km there is a layer of higher temperature, which they identified with the ozone layer. The presence of a temperature minimum at a height of 80-85 km was detected for the first time in 1935 by V. V. Fedynskiy and K. P. Stanyukovich (ref. 205) as a result of a photographic study of a bright meteor.

Systematic determinations of air temperature to a height of 67 km were made by Elterman (refs. 377 and 378) by the searchlight sounding method. After obtaining the density distribution $\rho = \rho(h)$ directly from observations of a searchlight beam, he computed temperature using a formula similar to equation (12.9). The initial temperature value T_1 used in the computations is based on the readings of a radiosonde at any height h_1 of about 10-20 km, and the computations were made at height intervals Δh between 1.3 and 5.3 km. In 1952 Elterman made 90 soundings on 18 nights from May through October.

However, the use of methods based on formulas (12.5) and (12.9) involves an additional error in the results, because these formulas were derived by differentiation or integration of the empirically found functions $p(h)$ or $\rho(h)$. In the first case the temperature is computed from the difference of two close values (pressure), which always leads to a large increase of the relative error. In the second case, when temperature is computed "interval by interval," by gradual transition to higher layers, there is a gradual accumulation of errors. A correct evaluation of the error in the results, therefore, assumes particular importance in such cases. In a number of studies the authors express doubt as to the reliability of the temperature values obtained by the searchlight sounding method, and the problem as a whole still has not been subjected to a final theoretical analysis. The control investigations made by Elterman (ref. 378) are, therefore, of great interest. He compared air temperature measurements at heights of 10-70 km, made simultaneously by four independent methods: radiosondes, searchlight sounding method, instruments carried aloft by an Aerobee rocket and observations of the anomalous audibility of sound. These data indicate satisfactory agreement of the results.

We will now discuss the method of determining air temperature in the upper layers based on an analysis of atmospheric absorption spectra. The absorption spectrum of ozone can be used for this purpose. Theoretically it is possible to determine the ozone temperature in the stratosphere by optical observations from Earth. The dependence of the ultraviolet absorption spectra of oxone on temperature is used for this purpose.

The absorption spectrum of ozone in the ultraviolet region is characterized by the fact that regularly alternating, poorly expressed maxima and minima are superposed on a smooth absorption curve. It was discovered as early as 1931 that the absorption coefficients at the minima decrease with a decrease of temperature, and at the maxima have almost no dependence on temperature. As a result a change of the temperature of ozone leads to a change of the contrast between the absorption maxima and minima. The influence of temperature in the region of the Huggins band is particularly significant.

However, subsequent laboratory investigations of this effect revealed contradictions between the data of different authors. According to E. Vassy (ref. 779), absorption at the minima changes with temperature approximately linearly. However, the measurements of Barbé and Chalonge, made with great care, differ from the data of Wolf and Melvin and also those of E. Vassy (ref. 780) at low temperatures. According to Barbé and Chalonge, the dependence of absorption on temperature is different for different wavelengths, but there is a common feature for all of the curves: their shape is close to a parabolic curve. In

contrast to the results of Wolf and Melvin, the absorption coefficients α at the maxima do not remain constant, but are rather sensitive to temperature; the general character of the temperature dependence at the maxima and minima is similar. However, the measurements of Barbé and Chalonge also indicate that the contrast of the bands has a strong and rather regular dependence on temperature.

This temperature dependence of the contrast of absorption has been repeatedly used for approximate determinations of the temperature of the ozonosphere, but it is necessary to bear in mind the difficulties involved in the practical application of this method, because information on the temperature dependence of the absorption spectra of ozone obtained by different authors does not always agree. Among the relatively recent investigations by this method we mention the work of Paetzold and Zschörner (ref. 650). The accuracy of temperature determinations is low. It is not absolute temperature values but the relative values, i.e., temperature changes from one observation to the next, which have the greater reliability. Finally, it is not entirely clear to what height the derived temperature should be assigned. The method gives some mean temperature for the entire ozonosphere, with individual layers having different temperatures. In a study of the heat balance of the atmosphere it is, therefore, extremely important to measure atmospheric absorption in the infrared region of the spectrum. An airborne spectrometer for measurement of infrared radiation is described by Houghton, Moss and Chamberlain (ref. 458). A conference devoted to spectroscopic methods of study of the stratosphere and mesosphere was held in New York in September, 1960. In particular, data were presented on the absorption and radiation of water vapor, carbon dioxide gas, ozone and hydroxyl molecules and oxygen and sodium atoms. The conference devoted great attention to the methods for such measurements made from the ground, stratospheric balloons and aircraft (ref. 397).

We will now discuss methods for estimating temperature from the emission spectra of the atmosphere. There are three possibilities in this direction: (a) analysis of the distribution of intensities in the molecular bands of the spectra of auroras and the night airglow (spectrographic method), (b) measurement of the width of the spectral lines in these same spectra (interference method), and (c) study of the vertical distribution of auroral intensity (photometric method).

The spectrographic method can be used to determine the "rotational" and "vibrational" temperatures. The basis for the concept of these temperatures and their determination is that under conditions of thermodynamic equilibrium the distribution of gas molecules by excited states (vibrational and rotational levels) depends on temperature (corresponding to the Boltzmann law). The higher the temperature, the greater is the number of the molecules at the more excited levels. Therefore, at higher temperatures there is an increase of the relative intensity of those spectral lines in the spectra of gas emission which are emitted at the time of transitions of molecules from higher energy levels. By experimentally establishing the distribution of intensities in the gas emission spectrum, we can compute that temperature which corresponds to this distribution (ref. 252).

The following equation is used for determination of rotational temperature

$$I(J) = \text{const}\, \nu^4 i(J) \exp\left\{-F(J)\frac{hc}{k}\frac{1}{T_{\text{rot}}}\right\}, \tag{12.10}$$

where F(J) is the rotational energy of the J-th state, i(J) is the intensity factor, ν is frequency, I(J) is the intensity of the rotational line, k is the Boltzmann constant, h is the Planck constant, c is the speed of light. The following approximate expression (first term of the expansion) usually is used for F(J)

$$F(J) \simeq B_\nu J(J+1), \tag{12.11}$$

where B_ν is the rotational constant of the upper state (ref. 790).

However, it must be remembered that in the upper layers of the atmosphere, where the gas density is small, the distribution of molecules by excited levels can differ appreciably from that which would prevail under conditions of thermodynamic equilibrium at the same kinetic temperature.

The rotational temperature T_{rot} is determined from the distribution of intensities in the rotational bands of the gas emission spectrum. The value of the rotational temperature can be approximately identified with kinetic temperature only in a medium in which the molecules remain in an excited state sufficiently long to undergo several collisions. However, if the majority of molecules leave excited levels earlier than several collisions occur with surrounding gas particles, an equilibrium distribution will not be attained, and the rotational temperature measured from the distribution of intensities can differ considerably from the kinetic temperature. In the rarefied air of the upper layers of the atmosphere collisions of gas particles occur relatively rarely and it is more reliable, therefore, to determine temperature from forbidden systems for which the initial (upper) level is metastable with a long lifetime.

It is necessary to bear in mind that in the case of auroral glow it is not temperature excitation which is involved, but excitation by collisions with fast particles. For this reason for determination of temperature from the distribution of the intensities of rotational lines, it is necessary to know the mechanism of excitation. For example, Jones and Harrison (ref. 490), in considering the excitation of the first negative system of nitrogen bands from the ground state of a neutral N_2 molecule, or from the ground state of a N_2^+ ion (this is without particular importance here because the constants B_ν'' in both cases are virtually identical), postulated that in the case of excitation by electron collision the total moment of momentum of a molecule remains constant. In this case the distribution of excited molecules by rotational levels should be the same as for unexcited molecules. Therefore, the distribution of intensities should give the kinetic temperature in the auroral region.

In general, in the case of excitation by collision with a fast particle, there can be a transport of the angular momentum which will lead to an increase of the observed rotational temperature (ref. 708).

For observations of auroras illuminated by the sun it also must be remembered that there can be an optical excitation of auroral glow, in which the distribution of molecules by excited states can correspond to radiant equilibrium in the field of solar radiation, rather than to the kinetic temperature of the surrounding medium (this problem was considered in a study by Bates (ref. 283) in relation to vibrational levels).

The absence of significant self-absorption is necessary to obtain correct data on temperature; this condition usually is observed.

The value of the"vibrational temperature" for the upper electron state can be judged from the relative intensity of bands within the system of bands. The vibrational temperature T_{vib} in no case can be interpreted directly as the kinetic temperature. The fact is that an equilibrium distribution of vibrational levels is established with greater difficulty than for rotational levels; when there is low density of the medium of the upper layers of the atmosphere, the redistribution of molecules in the upper electron states cannot occur sooner than spontaneous radiation. In the first investigations of this kind a vibrational temperature of 7,700°K was obtained as a result of the unfounded application of the Franck-Condon principle and concepts on thermodynamic equilibrium. However, even the more rigorous analytical methods lead to high values of vibrational temperature.

More complete information on the rotational and vibrational temperatures were obtained from an analysis of the spectra of luminosity of the night sky. Meinel$_0$(ref. 592) investigated the rotational structure of the 0-1 band at λ = 8,645 A of the forbidden atmospheric system of the O_2 molecule. He found that in most cases the rotational temperature is 150°K and varies in the range $\pm 20^\circ$, but in individual cases, when the band is particularly strong, the temperature increases to $200 \pm 10^\circ$. J. and M. Dufay found T_{rot} = 130°K. An interesting laboratory investigation of the atmospheric O_2 system was made by Branscomb (ref. 305). This investigation concluded that collisions in the upper layers of the atmosphere occur sufficiently frequently, so that thermal equilibrium between the surrounding particles and the rotational levels of an excited molecule sets in prior to a radiation event.

This important problem has also been discussed in a number of studies of other authors.

The most reliable data on rotational temperature were obtained from the spectra of the vibrational-rotational bands of OH hydroxyl molecules (Meinel bands). These bands develop in transitions from levels possessing a particularly great lifetime. There is a basis for assuming that these bands are

emitted by a layer situated at a relatively low height (about 70-90 km in the middle latitudes), where collisions occur rather frequently. Rotational temperature therefore scarcely differs much from the kinetic temperature. Meinel (ref. 593) used several OH bands in the infrared region of the spectrum to obtain $T_{rot} = 260 \pm 5^{\circ}K$. J. and M. Dufay found $T_{rot} = 255\text{-}270^{\circ}K$ from the maximum of the P branch in the infrared region, and Cabannes discovered large variations of T_{rot} in the range 150-250°K from several bands in the yellow and red parts of the spectrum.

In northern Greenland Chamberlain and Oliver obtained a number of spectra with OH bands in the visible and infrared regions, from which they determined $T_{rot} = 300\text{-}350^{\circ}K$, i.e., appreciably greater than in the middle latitudes. The height of the emitting layer over the Arctic was not determined, but Chamberlain and Meinel believe that it should not differ greatly from the height at lower latitudes. They believe that the increase of rotational temperature indicates that the kinetic temperature over the polar regions is higher. This result agrees with the concept that convection is the most important mechanism of energy exchange in the upper layers of the atmosphere below the 80 km level. They postulated that variations of convective currents are one of the causes of the observed temperature values; these currents are found in the region below the temperature minimum at a height of 80 km and lead to the formation of noctilucent clouds.

The increase of rotational temperature of hydroxyl with latitude was confirmed by V. S. Prokudina (ref. 157). At latitude 55°43' she obtained 12 spectra which she used for determing a mean temperature of $240 \pm 20^{\circ}K$, and at latitude 68°15' a mean value of $300 \pm 30^{\circ}K$. However, at lower latitudes this behavior apparently does not apply. At latitude 40°21' (Byurakan Observatory, Armenian SSR) N. I. Fedorova (ref. 198) found a mean value of $233 \pm 16^{\circ}K$. At 44°N (Haut-Provence Observatory, France) Dufay determined the hydroxyl rotational temperature as 250°K. This regularity apparently is not manifested so clearly in the high latitudes. For example, in January-April, 1958 Kvifte in Norway obtained a rotational temperature of the emitting layer of 215°K from the (6.1) and (9.3) hydroxyl bands.

On the whole, the problem of interpretation of rotational temperature, determined from the hydroxyl bands, still is not entirely clear. We will cite two recent studies (1960) as examples.

Conn and Gasch, using harmonic analysis methods, studied the structure of the hydroxyl rotational-vibrational bands in the night airglow spectrum in Canada in the region 1.0-1.6 μ and determined the rotational temperature. In three observations they obtained values 277, 242 and 245°K. They found that the intensity of the Q branch is less than the intensity of the P branch, which disagrees with theoretical computations.

An article by Wallace (ref. 790) was devoted to analysis of formula (12.10) for determination of rotational temperature. He demonstrated that the approximate expression (12.11) usually used for rotational energy F(J) can lead to

considerable error. Wallace proposes that this error be decreased by the introduction of an empirical constant into the computation formula. He recalculated a series of values T_{rot}, obtained earlier from the hydroxyl bands; he found that the temperature decreased by approximately 8 percent. Wallace believes that the corrected values of the rotational temperature (185-242°K for latitudes less than 60°N) agree better with rocket data (160-250°K) if the height of the hydroxyl emission is assumed to be in the range 60-80 km.

In conclusion we will consider other molecules. Cabannes and Dufay found T_{rot} = 230°K from several Vegard-Kaplan bands of the N_2 molecule in the region 4,050-4,550 Å on the basis of band width and the distance between the maxima of the strong R branch and the very weak P branch. Swings and Barbé used the Herzberg bands of O_2 molecules in the ultraviolet region of the spectrum to obtain very low values T_{rot} = 150-220°K, which was confirmed by Chamberlain, who found $T_{rot} \leq 200°K$.

An additional uncertainty in the possibility of using data on temperature obtained from the night airglow spectrum is introduced by the fact that the true height of the emitting layers, to which the measured temperature should be assigned, is not always known (ref. 233).

We will further discuss interference measurements of the width of the lines in the spectra of auroras, the night airglow and the twilight sky. Theoretically, the kinetic temperature of the upper layers of the atmosphere can be determined by measuring the Doppler broadening of the atomic lines of atmospheric emission. The forbidden lines, such as the green line λ = 5,577 Å, have a small natural width, and the broadening caused by collisions is small due to the rarefaction of the medium in the upper layers. The line broadening, therefore, can be accounted for almost entirely as a Doppler effect, making it possible to use line width to judge kinetic temperature at the emission level.

However, in the practical implementation of the interference method, the determination of Doppler temperature involves two difficulties. The accuracy of determination of line width or profile is not easily accomplished. Another difficulty involved is associated with the strong turbulent movements of the upper layers, which complicate the interpretation of the measured line width.

The Doppler width Δ of a line is determined using the formula

$$\Delta = 0.82 \cdot 10^{-6} \lambda \sqrt{\frac{T}{m}}, \qquad (12.12)$$

where λ is wavelength, T is the absolute temperature of the emitting gas, m is its atomic weight. The accuracy of interference measurements of the width of atmospheric emission lines has increased considerably in recent years. This was achieved by several methods. The use of special multilayer dielectric coatings of the plates of a Fabry-Perot etalon (e.g., 5-layer coating, refs. 674

and 794) increased the transparency (transmission) of these etalons with a simultaneous increase in the definition of the interference bands. High-speed interferometers were developed with photoelectric recording of interference bands (ref. 514) to replace the photographic recording always used earlier. This made it possible to investigate rapidly changing auroral forms and also avoid long exposures (5-10 hours or more) when studying the emission lines of the night airglow. During long exposures the interference bands become slightly fuzzy due to inevitable variations of air temperature and pressure. The apparatus is usually placed in a thermostat and pressure chamber to decrease this poor definition. Finally, we must mention the use of interference light filters with a narrow transmission band, which attenuate the effect of the continuous spectrum to a considerable degree. The fact is that quite recently a night airglow emission (of atmospheric origin) was discovered, which is characterized by a continuous spectrum; previously only lines and bands emitted by atoms and molecules in the upper layers had been known. This continuous background (as well as the background created by starlight) decreases the contrast of the interference bands and leads to their apparent broadening.

Armstrong investigated the width of the green line of oxygen in the spectra of quiescent arcs of auroras. He used a Fabry-Perot photoelectric interferometer and obtained a temperature of approximately 330-410°K. Further investigations led Armstrong to the conclusion (ref. 269) that the temperature of those regions of the atmosphere where the emission of the green auroral line occurs (different auroral forms are involved) can range from 255 to 540°K.

T. M. Mulyarchik (ref. 135) measured the width of the green line of oxygen in the winter of 1958-1959 at the Northern Station of the Institute of Physics of the Atmosphere of the Academy of Sciences USSR. He investigated individual auroral forms. He employed a Fabry-Perot interferometer with glass plates having a multilayer dielectric coating. In the lower parts of bright rayed forms and homogeneous arcs Mulyarchik obtained a mean temperature of 195±25°K in poorly defined fibrous forms and 250±30°K in a diffuse glow. The highest temperature, 325±40°, was obtained during well-developed pulsating forms.

The temperature measured from a photograph of the undisturbed night sky is 260±35°K. This possibly indicates an increase of the temperature of the emitting layer with an increase of geographic latitude (see above, concerning the rotational temperature determined from the hydroxyl bands).

Armstrong (refs. 269 and 270) received a temperature from 180 to 220°K for the green line of the night airglow; he considers a value of 190°K to be most probable. Measurements made by Phillips (ref. 674) in California in the United States indicate that the width of this line corresponds to a temperature of 155-230°K.

On the basis of measurements of the width of the green line in the Sahara, Perren obtained a temperature of 175-235°K.

The temperature regime of the upper layers of the atmosphere was also investigated by interference measurements of the width of other spectral lines. T. M. Mulyarchik obtained a temperature in the range from 1,200-3400°K from

the width of the red line of oxygen 6,300 Å in auroras near Murmansk (there is a basis for assuming that the observed luminescence develops in layers above 200 km). A temperature of 1,210±50° was obtained in an almost undisturbed night sky; there is a basis for assuming that the emitting layer was situated at a height of 250-300 km.

T. M. Mulyarchik obtained 1,850-2,000°K with an error of ±300° from the width of the nitrogen line 5,200 Å in auroral spectra.

Cabannes and Dufay, at the Haut-Provence Observatory, determined the width of the red line 6,300 Å in night airglow spectra ranging from 0.024-0.026 Å; this corresponds to a temperature $T \leq 440$-$550°K$.

The described interference methods were also used for determination of the width of the red line of oxygen emitted by the Earth's atmosphere at twilight. These measurements were made by Wark at the Geophysical Institute in Alaska. According to papers by Phillips (ref. 674) and Wark (ref. 794), this line profile corresponds to a temperature of 750±200°K. Wark attributes such a high temperature to the fact that the twilight emission of this line develops at a considerably greater height than does the green (night sky) line--at about 100 km, whereas the red (twilight) line develops above 150 or 200 km.

An evaluation of the temperature regime of the upper layers of the atmosphere on the basis of measurements of the vertical distribution of auroral brightness was given by the author in his book (ref. 233).

12.3. Investigation of the Temperature Regime of the Atmosphere by Observations of Ionospheric Processes. The rate of processes directly or indirectly influencing the propagation of radio waves in the ionosphere is dependent on the temperature of the medium. This creates the prerequisites for judging the temperature of the ionospheric layers on the basis of observations of radio wave propagation. Several methods have now been developed for estimating the temperature of the upper layers from the results of ionospheric measurements.

One of the methods is based on a calculation of the number of collisions. This can be obtained from measurements of radio wave absorption in the ionosphere or from measurements of the reflection coefficient as a function of radio wave frequency.

On the basis of an analysis of different variants of computations (for different gradients $\frac{\Delta T}{\Delta h}$), N. S. Gerzon (ref. 29) obtained the following dependence of temperature on height as the most probable values:

h км	100	150	200	250	300	350	400
T°K	300	825	1350	1875	2400	2950	3450

Comparing these data with the results obtained by other methods, we note that they agree for heights of 150-200 km. At the 100 km level the actual temperatures are appreciably lower (see following Sections).

V. M. Polyakov (ref. 151) proposed a method for determining air temperature and density in the ionosphere from the measured values of the effective number of collisions of electrons with heavy particles, electron density and the effective coefficient of recombination, and from the increments of these values in a finite interval of time. The author derived formulas which are correct if the measured effective coefficient of recombination can be identified with the coefficient of volume recombination of a gas. The Polyakov method is theoretically more perfect, but it also requires more precise measurements. In particular, it is necessary to measure as precisely as possible the radio wave absorption in the reflection region.

V. M. Polyakov (ref. 152) proposed that the difference in the temperature dependence of the number of collisions between electrons and neutral particles and ions be used for determination of the temperature and density of the gas in the region of the ionosphere. This difference can occur in the F region of the ionosphere, because at that level there can be a relatively high degree of the ionoization of gas.

Another method for estimating the temperature in the upper layers of the atmosphere is based on the measurement of the half-thickness of the ionized layer. As shown by observations by the pulse method of sounding of the ionosphere (ref. 233), the vertical distribution of ionization near the maximum of the electron concentration can be approximated rather well by the parabolic distribution obtained from the theory of formation of a simple ionized layer, developed by S. I. Kryuchkov (refs. 97 and 98) and S. Chapman. Assume h_m is the height of the maximum of the electron concentration; h' is the height at which the electron concentration is equal to zero; h_0 is the height at which an increase of the electron concentration from zero begins. The theory of a parabolic layer shows that the "half-thickness" of a layer y_m is approximately equal to 2H (H is the height of the homogeneous atmosphere). The pulse method for sounding of the ionosphere (ref. 233) determines heights h_m and h_0; by knowing these heights it is possible to compute H using formula

$$2H = Y_m = h_m - h_0.$$

Measurements made by this method by different authors apply to different times, but the temperature of the ionosphere can vary greatly as a function of season and time of day. By taking this into account and averaging some of the results, it is possible to represent the available values of the height H of the homogeneous atmosphere as a function of the height h approximately in the following form (ref. 127):

			w.m.	s.m.	w.m.	s.m.
h km	70	100	200	200	250	300
H km	6	10	35	50	50	70

where w.m. is winter midday and s.m. is summer midday.

Another method for estimating the temperature of the ionosphere is based on data on the recombination coefficient. The recombination of ions is a process of combining of positive and negative (including an electron) ions into a neutral system. The recombination coefficient α characterizing the rate of formation of neutral systems is essentially dependent on temperature. This relationship can be expressed approximately by the equation $\alpha = cT^r$, where c and r are constants.

It is known from observations that α changes with height. If the value of the exponent r is known, the change of α can be used to judge the character of the change of temperature with height. However, recombination phenomena in the ionosphere are highly varied; this variance is dependent on the great variety in the nature of the charge carriers and the states in which they exist after ionization. For example, the mechanism of combination of a free electron with a positive ion differs radically from a case when there is a transfer of a charge from an ordinary negative ion to a positive ion or when two ions having charges of opposite sign are neutralized as a result of contact. Determination of the exponent r, therefore, involves great difficulties and is not sufficiently reliable. However, all investigations indicate the existence of a region of high temperature above the 100 km level.

There have been interesting observations of the thermal radio emission of the ionosphere. It was established 10 years ago that during favorable periods of "stillness in the ether," when there are no industrial radio interferences or atmospheric discharges, it is possible to record reliably the natural (thermal) emission of the ionosphere on intermediate waves. It was demonstrated as early as 1951 that the temperature of the D region of the ionosphere can be determined by measuring ionospheric radio emission at a frequency of 2 Mc/s. The principal difficulty of the method involves determination of the height of the layer to which these temperatures should be ascribed (ref. 394). Dowden (ref. 361) recently attempted to overcome this difficulty.

The effective temperature T_a of the receiving antenna of a set for measuring the "radio voice" of the ionosphere (half-wave dipole) can be identified approximately with the mean weighted value of the ionospheric temperature T_i and the Earth's temperature T_e

$$T_a = \beta T_i + (1 - \beta) T_e \qquad (12.13)$$

where β is antenna efficiency. By computing β from the parameters of the apparatus and knowing T_a and T_e from observations, it is possible (ref. 144) to compute the ionospheric temperature T_i by using formula (12.13). Extensive data on the diurnal and seasonal variation of the atmosphere at a height of 70-75 km were published in 1960; these data were obtained by the method described in reference 137. Some of these data, applying to a point in the auroral zone of the southern hemisphere (55°S, 159°E, geomagnetic latitude -62°), are represented in figure 12.2.

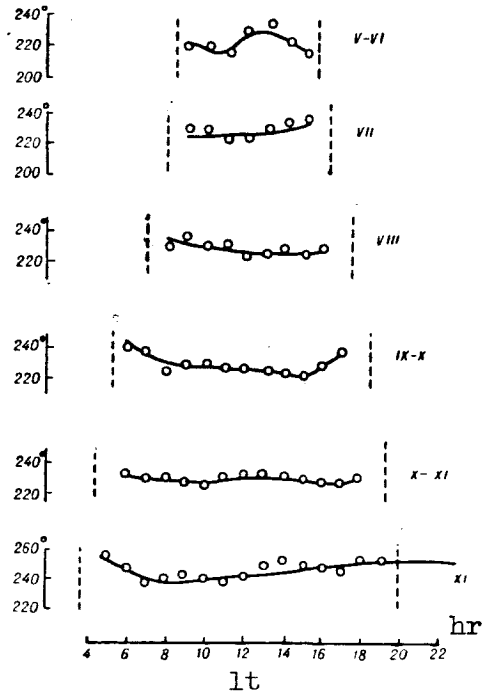

Figure 12.2. Diurnal temperature variation of D region of the ionosphere in different months in southern hemisphere in different months in southern hemisphere from observations of thermal radio emission of the ionosphere. E) sunrise, W) sunset.

Determination of the electron temperature is of basic importance. During ionization of molecules and atoms in the upper layers of the atmosphere the absorbed photon usually has more energy than is needed for ionization. Since the electron mass m_e is thousands of times less than the mass m of the ions,

the energy excess appears mostly in the form of kinetic energy of the freed electron. As pointed out by G. Drukarev, the relationship between the gas temperature T and the electron temperature T_e at the time of ionization in the

F2 layer can be represented by the relation

$$T_e = T + 3.88 \cdot 10^5 (h\nu - W), \tag{12.14}$$

where $h\nu$ is the energy of the ionizing photon of the frequency ν, W is the ionization potential. However, this energy excess of the electrons is gradually lost as a result of collisions. The mean part of the energy lost at the time of each collision of an electron, expressed in fractions of the mean energy of an electron, is

$$\frac{\Delta E}{E} = \frac{8mm_e\left(1 - \frac{T}{T_e}\right)}{3(m_e - m)^2}. \tag{12.15}$$

Since $m \gg m_e$, then

$$\frac{\Delta E}{E} = \frac{8 m_e A}{3m(T + A)}, \qquad (12.16)$$

where $A = 3.88 \cdot 10^5 (h\nu - W)$.

We will now estimate the time in which the temperature T_e acquired by an electron decreases to T. Assume $h\nu = 25$ ev, which corresponds to a wavelength of ionizing radiation $\lambda = 493$ Å. If $W = 15$ ev, $T = 3{,}000^\circ$ and the mean molecular weight of air in the ionosphere can be assumed to be 20; then $\frac{\Delta E}{E} = 7.3 \cdot 10^{-5}$ per collision. As the number of collisions we can use the experimental value $2 \cdot 10^3$ sec^{-1}. In this case T_e becomes equal to T in 25 sec in the F2 layer and in a lesser time in the E layer. Thus, the excess energy of the electrons is distributed quite rapidly among the heavy particles, and it can be concluded that the electron temperature in the ionsophere in actuality is equal to the gas temperature (ref. 29).

13. Study of the Heat Regime of the Atmosphere by Rockets and Satellites

It is very difficult to measure air temperature on a moving rocket because any body (thermometer) exposed to the flow detects not only the thermal, but also the kinetic energy of the ordered motion of the encountered air molecules. The influence of this factor can be very great. Furthermore, the use of ordinary methods of temperature measurement is prevented by factors associated with flights at sonic and supersonic velocities. For example, the measurement conditions are disrupted due to the formation of a boundary layer near the instrument.

Because of these difficulties the temperature of the atmosphere in many cases is not determined directly from rocket data, but instead is computed from the vertical pressure and density distribution.

The principal results in the study of the thermal state of the stratosphere and mesosphere were obtained in the USSR by use of resistance thermometers and meteorological rockets.

13.1. Use of Resistance Thermometers. M. N. Izakov developed a resistance thermometer method for measurement of air temperature in the stratosphere and mesosphere. The thermometers are carried aloft by meteorological rockets to a height of 70-80 km. It was found possible, on the basis of a study of the physical picture of the phenomena occurring during movement of the thermometer in the gas, to decrease the unwanted influences of the instrument design and to develop a method for computing atmospheric temperature from the thermometer

temperature. We will now discuss the principal results of this theory. This first requires a discussion of the process of heat exchange between a plate and a high-velocity gas flow. In order not to complicate the computations excessively, we will take into account only part of the total heat exchange caused by forced convection (ref. 251).

The density S_c of the heat flux received by the plate during forced convection with a high velocity of surrounding flow usually is represented in the form

$$S_c = -h(T_s - T_e), \tag{13.1}$$

where h is the heat exchange coefficient. At small velocities of flow, when $T_e \simeq T$, formula (13.1) becomes the ordinary formula of convective heat exchange.

The introduction of T_e into (13.1) in place of T, when the plate has a homogeneous temperature T_s, ensures that h is not dependent on the Mach number in the gas dynamic region of flow. The formula for h in this case has the form

$$h = 0.5915 k T F \sqrt{\mathrm{Re}}, \tag{13.2}$$

where k is the coefficient of heat conductivity of the gas; the Reynolds number Re is related to the length L of the plate and

$$F^2 = \sqrt{\frac{T}{T_s}} \frac{T_s + B}{T + B},$$

where B is a constant in the well-known Sutherland formula, expressing the dependence of gas viscosity on temperature.

The factor F in (13.2) is caused by high gas temperature near the surface around which the flow passes. In precise computations it is necessary to consider the dependence of viscosity on temperature. In the case of approximate computations or small velocity values M, this effect can be neglected, and then F = 1.

It follows from the theory of heat exchange of a plate in a free molecular flow, as applied to the simplest case of shearing flow, that energy E of the translational motion of molecules transferred to 1 cm^2 of the plate in 1 sec is expressed by the relation

$$E = \frac{\rho a^3}{\sqrt{2\pi\gamma}} \left[\frac{1}{2} M^2 + \frac{2}{\gamma} \right] \tag{13.3}$$

when the accommodation coefficient is equal to unity.

It can be assumed that at a height of 80 km there are favorable conditions for free molecular flow around the thermomenter. At a velocity M = 1 the energy computed with formula (13.3) will be only 20 percent of the value of the solar constant. There is a basis for assuming that near the 80 km level there is a boundary of possible use of the thermometer as a temperature gage of the free atmosphere. At great heights, due to the low density of the medium, the thermometer more likely is in radiation equilibrium with bodies external in relation to the atmosphere than with the air of the atmosphere. We will now turn directly to the theory of measurement of temperature by a rocketborne thermometer (ref. 1).

According to the conservation principle, the increment of thermal energy of a thermometer is equal to the sum of the flux from the external medium and the heat release by internal sources.

Assume O and A are the volume and external surface of the thermometer, respectively. The increment of the thermal energy of the thermometer is $cOdT_w$, where c is the heat capacity of a unit volume and T_w is the temperature of the thermometer, which we will assume to be uniform, measured directly by the instrument during rocket sounding.

The heat flux through the outer surface of the thermometer can be divided into three components. The first is the result of forced convective heat exchange with the atmosphere. The heat flux during time dt, corresponding to a temperature increment by dT_w, is written in the form (ref. 251)

$$- h(T_w - T_e)A\, dt.$$

The second is the heat flux caused by radiation exchange between the thermometer and bodies external in relation to the atmosphere. This flux is denoted by

$$AS\, dt,$$

where S is the density of the radiation flux. Finally, the third is caused by the heat conductivity of the material of the thermometer and can be represented in the form

$$\xi(T_s - T_w),$$

where T_s is the known temperature of the part of the instrument container to which the thermometer is attached, and ξ is a coefficient characterizing the heat conductivity from this part to the thermometer. The value ξ depends on the properties of the material and the method for attachment of the thermometer to the container.

The heat source in the thermometer is the current from an electrical circuit. The heat released is

$$0.24\sigma i^2 dt,$$

where σ is the total electrical resistance of the thermometer and is current intensity.

On the basis of the principle of conservation of energy we have

$$cO\,dT_w = -h(T_w - T_e)A\,dt + AS\,dt + \xi(T_s - T_w)\,dt + 0.24\sigma i^2\,dt.$$

On the basis of formula (8.3) we obtain

$$T_e = T + \frac{r\mu(\gamma-1)}{2\gamma R}V^2,$$

and after substitution into the latter equation

$$T = T_w - \frac{r\mu(\gamma-1)}{2\gamma R}V^2 + \frac{c\theta}{hA}\frac{dT_w}{dt} - \frac{S}{h} - \\ - \frac{\xi}{hA}(T_s - T_w) - \frac{0.24\sigma i^2}{hA}.$$

The terms of the equation are expressed through parameters measured during the time of the flight or known from preliminary laboratory experiments. In solving the equation relative to the desired temperature T of the medium, the equation can be given the following form (ref. 1):

$$T = T_f - r\frac{\gamma-1}{2\gamma R}\mu V^2 + \frac{\rho_f s_f W}{hS}\frac{dT_f}{dt} - \frac{1}{h}\left[\frac{\varepsilon_1(1+a_1)}{\pi}\Phi_s + \right. \\ \left. + \frac{\varepsilon_2(1+a_2)}{2}\Phi_e - \varepsilon_e\sigma T_f^4 + 0.15\varepsilon_e\sigma_0 T_p\right] - \frac{Q}{hS} + \xi(T_f - T_p). \quad (13.4)$$

Here T_{fil} is temperature of the filament, r is the thermal coefficient of restitution, μ is the molecular weight of air, V is the velocity of the rocket, T_{pin} is the temperature of the pin to which the thermometer is attached, ρ_{fil} and c_{fil} are the density and heat capacity of the material of the thermometer, W and S are the volume and area of the surface of the thermometer, γ and R are the ratio of the heat capacities and the gas constant, h is the heat exchange coefficient, t is time, ε_1 and ε_2 are the coefficients of absorption of short and longwave radiation by the thermometer, ε_3 is the coefficient of radiation of longwave radiation, a_1 and a_2 are the coefficients of reflection of short and

longwave radiation by the pin, Φ_S and Φ_E are the fluxes of solar radiation and the longwave radiation of the Earth and atmosphere, Q is the Joule heat released in the thermometer by the current of the measuring circuit, and ξ is the parameter of heat transfer through the supporting system of the thermometer.

The second term on the right-hand side of equation (13.4) expresses the influence of deceleration of flow, i.e., the fact that during the movement of the rocket the thermometer detects not only the thermal energy of air molecules, but also the kinetic energy of their ordered motion. At great heights the laws of heat exchange between the thermometer and a high-velocity flow of rarefied gas are complicated by the fact that the gas can no longer be considered a continuous medium. This is reflected in a change of the dependence of coefficients r and h on the parameters of the flow. In the case of free molecular flow there is a theory whose conclusions have been used in these computations: experimental data obtained during the exposure of tungsten wires in a wind tunnel were used for flow with shearing (ref. 1).

The third term (13.4) takes into account the thermal inertia of the thermometer, and the fourth expresses the influence of solar radiation and longwave terrestrial radiation (direct and reflected from the pin) as well as the radiation of the thermometer and pin itself. The fifth term takes into account the influence of heating of the thermometer by the current of the measuring circuit and the sixth, heat transfer through the supporting system of the thermometer.

All the terms accept the second in equation (13.4) are negligibly small to a height of about 50 km, and small at heights of 50-70 km. However, at great heights their value increases rapidly. The small value of these terms in a considerable part of the trajectory can be attributed to the fact that the sensing element of the thermometer is an extremely thin and long wire (40 μ in diameter and 30 cm in length).

TABLE 13.1. MEAN TEMPERATURE VALUES DERIVED USING RESISTANCE THERMOMETERS.

h км	*T*°K	*h* км	*T*°K	*h* км	*T*°K	*h* км	*T*°K
0	294	22	218	42	265	62	247
2	278	24	219	44	269	64	241
4	261	26	224	46	274	66	236
6	247	28	227	48	274	68	231
8	233	30	231	50	272	70	226
10	220	32	235	52	269	72	221
12	217	34	240	54	266	74	217
14	215	36	246	56	261	76	213
16	215	38	251	58	256	78	213
18	216	40	258	60	252	80	214
20	216						

It was assumed in the derivation of equation (13.4) that the thermometer is engulfed in a transverse flow and does not fall in the boundary layer of the pin. Computations have shown that the mean square error of an individual temperature measurement to heights of 40 km does not exceed $\pm 5^{\circ}$, at a height of 50 km is $\pm 10^{\circ}$ and at a height of 70-75 km attains $\pm 20^{\circ}$.

Table 13.1 gives the mean temperature values measured over the middle latitudes of the territory of the Soviet Union using meteorological rockets. Figures 13.1 and 13.2 show the results of measurements of temperature in the stratosphere for individual months of 1957 and 1958 in the middle latitudes and in the Arctic (refs. 12, 249-251).

The resistance thermometer method described is extremely promising and apparently will be used still more extensively for study of the temperature regime of the stratosphere and mesosphere. In particular, by the use of such thermometers it is possible to make precise measurements (with an error of $0.6\text{-}1.1^{\circ}$ at

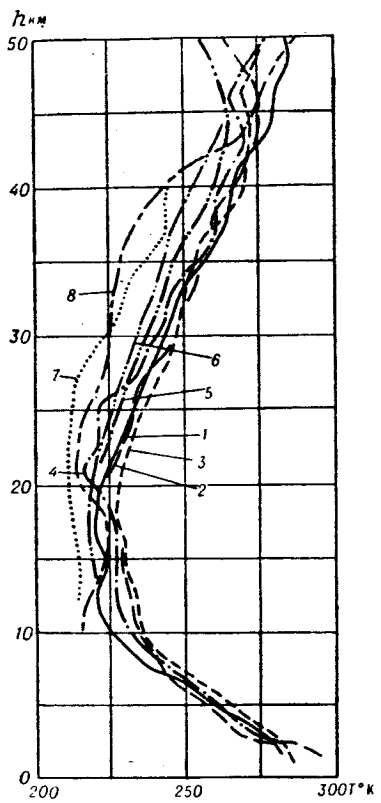

Figure 13.1. Vertical temperature distribution in middle latitudes of USSR (meteorological rockets). (1) May, (2) June, (3) July, (4) August, (5) September, (6) October, (7) December 1957 (8) February 1958.

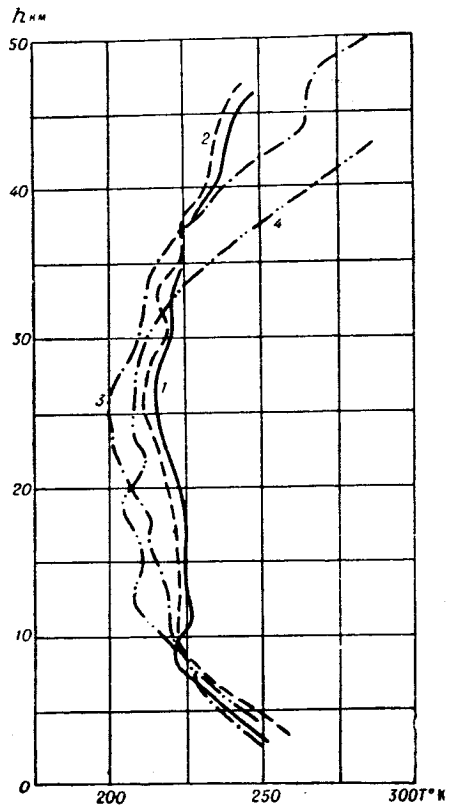

Figure 13.2. Vertical temperature distribution in Arctic (Kheys Island, 80°N). (1) October, (2) November, (3) December 1957, (4) January 1958.

a height of 30 km) of the temperature of the free atmosphere on balloons to heights of 30-35 km (ref. 32).

An interesting thermometer with a vibrating filament has been proposed recently by Petit (ref. 673a). The principal component of the instrument is a fine steel filament which is attached to a frame by a special method, so that the length of the filament does not change with change of temperature. The influence of temperature changes is reflected in a change in the tension of the filament, and as a result there is a change of frequency of its natural vibrations. The author has calculated that the "radiation-convection" error in temperature measurement to a height of 40 km should not exceed 1°. The suitability of the thermometer for measurements in the upper layers is not clear, since the diameter of the thermometer filament (0.05-1 mm) becomes comparable to the length of the free path of air molecules, and as a result there is an appreciable change of the laws of surrounding flow.

At Cape Mugu, California, in the United States (34°07'N, 119°07'W), and at other stations there is regular sounding of the atmosphere by meteorological rockets. At a height of 60 km a parachute with an instrument package is ejected from the rocket. This instrument package contains a thermistor for temperature measurement and a radiotelemetric transmitter (ref. 578).

13.2. Artificial Sodium Vapor Clouds. Blamont, Donahue and Lory (ref. 299) have measured atmospheric temperature by a completely new method in Algeria, using a French Veronique rocket. They investigated the sunlight scattered at the time of evening twilight by a sodium vapor cloud at heights of 100-150 km. They made a study of the structure (width) of the resonance lines of the yellow doublet of atomic sodium, dependent on the temperature of the cloud, which for all practical purposes was considered to equal the temperature of the surrounding medium. In studying line structure, they employed a method developed as early as 1944 by Bricard and Kastler (ref. 309) for measurement of the twilight glow of the atmosphere. The apparatus used consists of a high-power spectrograph; in front of the spectrograph slit there is a vessel containing sufficient sodium vapor for partial absorption of the D line of the sky. The following ratio is measured

$$R=\frac{I}{I_0}, \tag{13.5}$$

where I_0 is the intensity of the rays entering the vessel and I is the intensity of the emerging rays. Without discussing here the methods for measuring factor R (a detailed description of this method can be found in the author's book, ref. 229), we will limit ourselves to a concise explanation of the theory of the method.

Temperature T_a and optical thickness τ of the sodium vapor in the vessel are known from experimentation. The intensity of the arriving ray, if the width of the line is due solely to Doppler broadening, is proportional to the value

$$I_0 = \int \exp(-x^2)\,dx, \tag{13.6}$$

where

$$x^2 = mc^2 \frac{(\nu - \nu_0)^2}{\nu_0^2 RT}. \tag{13.7}$$

Here m is the atomic weight of sodium, T is the temperature of the sodium cloud, assumed equal to the temperature of the surrounding medium (atmosphere), R is the gas constant and ν_0 is the frequency of the center of the line. The intensity of the ray emerging from the vessel, corresponding to the same point of the cloud, is proportional to the value

$$I = \int \exp(-x^2) \exp[-\tau \exp(-ax^2)]\,dx, \tag{13.8}$$

where

$$a = \frac{T}{T_a}. \tag{13.9}$$

Ratio R is dependent only on T, if T_a and τ are known, which makes it possible to compute T from measured R.

Blamont, Donahue and Lory carried out an experiment on Mar. 2, 1960. A Veronique rocket, which rose 188 km into the atmosphere, was used for ejection of 280 g of sodium into the ionosphere. The forming vapor cloud, illuminated by the Sun's rays, reached the upper layers of the atmosphere. The height of individual points was determined by triangulation. The temperature values computed with these formulas are shown in Table 13.2. As we will see later, these values for heights of about 150 km are appreciably lower than the values accepted by many authors (for example, used in the United States Standard Atmosphere of 1959 ARDC-1959).

TABLE 13.2. IONOSPHERIC TEMPERATURE MEASURED FROM THE LINE WIDTH OF THE GLOW OF ARTIFICIAL SODIUM CLOUDS.

h км	T°K	h км	T°K
100	215±25	130	325±65
110	240±30	140	400±80
120	275±45	150	515±150

13.3. Computation of Temperature from Vertical Distribution of Pressure and Density. Using the equation of state (12.3) relating atmospheric pressure

p, density ρ and absolute temperature T, it is possible to transform the barometric formula (12.4) so that it contains two of the three values p, ρ and T. If one of these values is determined as a function of height from measurements, the second can be computed by differentiation or integration. If the vertical distribution of p is known, it is possible to compute T by using formula (12.6). However, if the distribution of density ρ has been measured, on the basis of the equation of state we can write

$$\rho = \frac{mp}{RT}, \tag{13.10}$$

therefore, by virtue of (12.4), we obtain after integration

$$T = \frac{m}{R\rho}\int_h^\infty \rho g\, dh. \tag{13.11}$$

Determination of temperature by differentiation of the function p = p(h) by use of formula (12.6), or integration of the function ρ = ρ(h) by use of formula (13.11), requires a knowledge of the mean molecular weight m of the air. However, the problem of the values m at great heights still remains inadequately studied. The computation of kinetic temperature using formulas (12.6) and (13.11) therefore is usually done in several variants: assuming m to be constant at all heights and equal to the mean molecular weight of dry air in the lower layers of the atmosphere, m = 28.966, or rounded off to m = 29 (the temperature computed in this way sometimes is called "molecular" and denoted T_{29}) or assuming that above 90 or 100 km m decreases with height in conformity to some law.

Table 13.3 gives temperature values on the basis of measurement data for the middle latitudes of the territory of the Soviet Union (instrument packages and geophysical rockets). These data (ref. 128) were obtained by analysis of a smoothed mean pressure curve, using formula (12.6). The computations were made on the assumption that the composition of the air is constant to a height of 100 km, air is dry and m = 29.

Regular measurements of air density in the upper layers of the atmosphere are made in the United States by the falling spheres method (see article by Bartman in the collection of articles in ref. 13). The determined density distribution also was used for temperature computations by the authors of reference 281. This computation differs somewhat from that used in other studies. Integrating the barometric formula

$$dp = -g\rho\, dh$$

and using the equation of state in the form

$$p = \rho\frac{RT}{m},$$

they obtained a formula for pressure p_h at height h in the form

$$p_h = \int_h^{h_0} g\rho\, dh + p_0, \tag{13.12}$$

where $p_0 = \rho_0 R T_0$ is pressure at height h_0, and ρ_0 and T_0 are density and temperature at this same height. However, according to the equation of state,

$$p_h = \rho_h \frac{RT_h}{m},$$

where ρ_h and T_h are air density and temperature at height h. From these equations the following expression is derived for T_h

$$T_h = I_h + \rho_0 \frac{T_0}{\rho_h}, \tag{13.13}$$

where

$$I_h = \frac{\int_h^{h_0} g\rho\, dh}{\rho_h \frac{R}{m}}. \tag{13.14}$$

TABLE 13.3. ATMOSPHERIC TEMPERATURE OVER THE MIDDLE LATITUDES OF THE USSR (FROM MEASUREMENTS BY INSTRUMENT PACKAGES AND GEOPHYSICAL ROCKETS).

h km	T°K	h km	T°K	h km	T°K	h km	T°K
57.5	303	70	221	82.5	154	95	181
60	282	72.5	204	85	154	97.5	192
62.5	263	75	187	87.5	156	100	208
65	245	77,5	172	90	163		
67.5	237	80	161	92.5	173		

Equation (13.10) can be used for computation of temperature at height h from the ratio of densities $\frac{\rho_0}{\rho_h}$, known from measurements by assuming that temperature T_0 at height h_0 is known. If T_0 is unknown, an appropriate value can

be accepted for it. This computation method has one important characteristic: the inaccuracy in determination of T_h, caused by the inaccuracy of the initial value T_0 used, decreases with continuation of the computations to the next layers, because in this case, with an increase of the height difference $h - h_0$, the first term on the right-hand side of equation (13.3) for T_h increases more rapidly than the second, and rather rapidly becomes dominant. For example, if h_0 at 15 km is less than h, I_h is approximately 10 times greater than the ratio $\frac{\rho_0 T_0}{\rho_h}$, and the error in I_h caused by the error in T_0 becomes negligibly small (ref. 281).

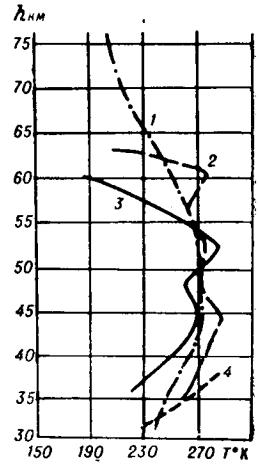

Figure 13.3. Vertical temperature distribution over White Sands Proving Ground, computed from air density values (falling spheres method). (1) May 14, 1952, (2) Apr. 23, 1953, (3) Dec. 11, 1952, (4) Sept. 29, 1953.

The temperature cross sections of the atmosphere obtained by this method are shown in figure 13.3. Computations were made every 2 km (launchings 1 and 4) and every 4 km (launching 2 and 3).

13.4. Other Rocket Methods. A method for measuring air temperature directly in individual layers of the atmosphere, which does not require vertical averaging, was developed at the University of Michigan in the United States (ref. 726). This method uses the ratio of the pressures measured near different points on the rocket (for further details see the book, ref. 233). Another method used at this same university is based on measurement of the angle formed by a shock wave relative to the axis of the rocket. Analysis of

the properties of shock waves accompanying a rocket flying at supersonic velocity reveals that with increase of the M number the angle of the shock wave decreases. By measuring the angle of the shock wave during flight of the rocket and knowing the velocity of the rocket, it is possible to compute the local speed of sound, which is equal to

$$\sqrt{\gamma \frac{R}{m} T},$$

where γ is the ratio of the heat capacities $\frac{c_p}{c_v}$. Thus it is possible to determine T. This method for measurement of air temperature in the upper layers of the atmosphere was used in a number of experiments by the specialists at the University of Michigan in the United States.

The shock wave was observed in the experiment as a pressure jump. The investigators concluded that it was present from the readings of a thermal manometer which moved forward and backward near the surface of the nosecone of the rocket. By knowing the direction of movement it was possible to establish the position of the shock wave relative to the rocket, and to determine the angle formed by the shock wave. The principal experimental difficulty (and measurement error) involved in the practical implementation of the method is caused by the poor definition of the shock wave. This method was used for temperature measurements (ref. 625) at heights of 30-45 km.

Further details on the theory of rocket methods of temperature measurement in the upper layers of the atmosphere and the instruments used can be found in a collection of articles (ref. 13) and in reference 251.

13.5. Measurements by Satellites. In Section 9 we described a method for computing atmospheric density using the results of measurements of satellite deceleration and a method for using manometers on satellites. By using such measurements and computations to obtain density or pressure values as a function of height above sea level, it is possible to compute temperature by using formulas of the type (12.6) and (13.11).

A. Ya. Pressman and S. P. Yatsenko (ref. 156) have proposed one of the possible principles for direct measurement of temperature of the ionosphere at heights of 250-300 km. They computed the ion flux through the bottom of a narrow tube mounted on an artificial satellite, considering the ionosphere as a rarefied plasma. The derived formulas and numerical characteristics, generally speaking, can be used for determination of the temperature of the upper layers of the atmosphere (by measurement of the thermal velocities of ions), but this requires overcoming great experimental difficulties and considerable generalization of theory (checking for the presence of a Maxwellian distribution of ion velocities in the atmosphere, allowance for the potential of the satellite surface, etc.).

14. Principle Patterns of the Heat Regime of the Upper Layers of the Atmosphere

It is not the purpose of this book to give special consideration to the results of temperature measurements using radiosondes. These measurements, which have revealed the heat regime of the atmosphere in detail under different conditions,are extremely extensive. They give information on the atmosphere to a height of 25-30 km, in some cases to 35-40 km. The principal problems considered in this book apply to higher layers. The results of radiosonde measurements will be cited as the need arises for the purpose of comparison and more complete analysis.

In Sections 12 and 13 we presented individual results of measurements of temperature made at great heights by acoustic, optical and radio methods and by rockets and satellites. This section contains a concise summary of the principal results obtained in this field.

14.1. Temperature Profile of the Atmosphere. Many important characteristics of the structure of the atmosphere are shown by its temperature profile. Figure 14.1 presents a curve of the vertical temperature distribution in the atmosphere characteristic of the middle and subpolar latitudes at a time of high solar activity.

The temperature stratification of the atmosphere is the basis for one of the principal systems of designation (nomenclature) of atmospheric regions (layers). The stratosphere is situated above the troposphere, which is characterized by a rapid decrease of air temperature with height, averaging approximately 6°/km. The distinguishing characteristic of the stratosphere is a temperature increase with height (inversion). In the lower part of the stratosphere (to 25-30 km) the temperature gradient usually is small, and sometimes the regime is close to isothermal. The upper boundary of the stratosphere (stratopause) is situated at a height of about 50 km, but depending on latitude, season of the year and character of atmospheric processes can descend by 5-7 km below this level or rise above it.

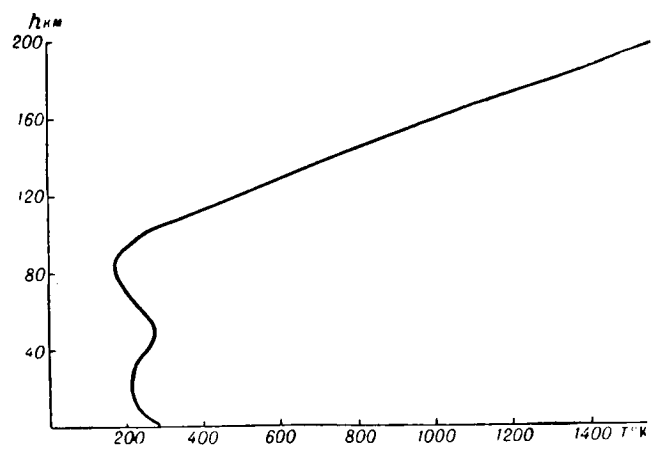

Figure 14.1. Mean temperature profile of atmosphere.

The "middle" region of the atmosphere, the mesosphere, includes the layers beginning at the stratopause, characterized by an opposite (in comparison with the stratosphere) sign of the temperature gradient: a temperature decrease with height. At a height of about 85 km the temperature attains its minimum value: the air in this region at times is cooled to 150-160°, sometimes even to 130°K. This level of minimum temperature is called the mesopause (for further details about the heat regime of the mesopause see Section 21.4) and is the upper boundary of the mesosphere and at the same time the beginning of a new region. Above the mesopause there is a "hot region," the thermosphere, in which there is a well-developed temperature inversion. At a level of about 150 km or above, the atmospheric temperature becomes very high (fig. 14.1).

14.2. Heat Regime of the Stratosphere and Mesosphere. Figures 13.1 and 13.2 show curves of the vertical distribution of temperature, constructed using data from sounding of the atmosphere by meteorological rockets in the middle and high latitudes of the USSR (refs. 1, 464, 521 and 598). These curves give extensive data for judging the seasonal temperature changes at these latitudes. The stratosphere can be characterized by adding mean seasonal curves for 40°N in the United States (fig. 14.2). These curves were constructed by Conover and Wentzien (ref. 339) on the basis of a 4 year series of measurements (1948-1952) using radiosondes. An interesting characteristic of the curves is the identical character of increase or decrease of air temperature from season to season at all heights in the troposphere and stratosphere, except for the 16 km level. At that level the temperature changes little during the course of the year.

Arnold and Lowenthal, on the basis of radiosonde measurements in the United States (New Jersey, 40°N), established an extremely interesting shift of the date of the summer temperature maximum, and an increase of the amplitude of annual temperature with an increase of height. Whereas at the 50 mb level the date of

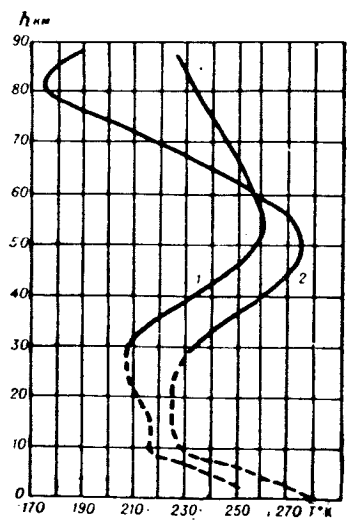

Figure 14.2. Mean seasonal curves of vertical temperature distribution over Belmar (United States, 40°N, 74°W) from measurements with radiosondes. (1) winter, (2) summer.

the maximum on the average falls on July 13 and the amplitude of the annual variation is A = 3.4°, at the 10 mb level on June 18, A = 6.2°, at the 5 mb level on June 8, A = 7.1°, at the 3 mb level on May 28, A = 7.1° and at the 2 mb level on May 25 amplitude A attains 14.7°.

Data on the intraseasonal temperature changes are of great interest. In this connection we should mention the sudden warmings of the stratosphere, repeatedly observed in the winter (January-February).

According to Kh. P. Pogosyan (ref. 149), aperiodic changes of temperature and wind in the stratosphere are an ordinary phenomenon. In the course of several days the temperature in that region often can increase or decrease by 10-20°, and sometimes more.

Data on temperature and wind sounding on Jan. 8-14, 1960 at Belmar, New Jersey, clearly reveal a sudden warming at a height of about 30 km, accompanied by a disruption of the wind regime. At a height of 30.5 km, the temperature on Jan. 8, was -50°, by Jan. 11, it had increased to -25°, then it decreased to -40° and remained at this level for several days. The temperature at heights of 35 and 26 km during this period remained constant (-30° and -50°, respectively). These temperature variations were associated with sharp changes of the wind direction and velocity. At a height of 35 km the zonal wind component on Jan. 8 was westerly at 370 km/hour, and then the wind velocity decreased rapidly. By Jan. 12, the zonal flow at this level was weak and easterly. On Jan. 15, the wind again became westerly at 185 km/hour. The center of the zone of the weak easterly wind was displaced relative to the center of the zone of high pressure by one day and by 4 km in height. These temporal vertical cross sections, in Conover's opinion (ref. 338), reflect the diurnal variations of the position and intensity of the circumpolar center of low pressure and associated centers of high pressure, which can be traced on charts of the 10 mb surface.

According to Kh. P. Pogosyan (ref. 149), the intraseasonal changes of the temperature and wind fields in the lower stratosphere are associated with intense processes of interlatitudinal air exchange. In the northern hemisphere these processes occur more intensely in winter than in the warm season of the year, and, therefore, large temperature anomalies in the stratosphere are noted in the winter months. Cyclonic and anticyclonic activity play a major role in this process. Such processes developed most intensely in January, 1958, and, as pointed out by G. D. Zubyan (ref. 69), were the result of advection of air masses

According to temperature measurements made by the rocket-grenade method by Nordberg and Stroud (ref. 639) at Guam Island (13.5°N, 145°E) in the IGY period, nine soundings at nighttime from Nov. 3-25, 1958 established the presence of discrepancies between the data of individual launchings of 10° at a height of 57 km and of 35° at a height of 75 km. According to their estimate, the temperature measurement error was not more than ±5°. It can be assumed, therefore, that there are considerable day-to-day temperature changes.

The data of Brasefield (ref. 308) apply to heights of 30-80 km and are based on measurements at White Sands, New Mexico (33°N). Analysis of these

data revealed the presence of seasonal changes of temperature: at heights of 20-53 km the summer temperatures are considerably above the winter temperatures, whereas at 53-73 km winter temperatures are higher than those of summer.

Analysis of data from two rocket launchings at Fort Churchill, Canada, in winter and summer revealed (ref. 750) that at heights of 40-50 km the winter temperature is approximately 20° lower than in summer; summer data have a smoother vertical temperature variation. According to the data presented by LaGow, Horowitz and Ainsworth (ref. 542), the temperature in the Arctic at heights of 20-45 km is subject to considerable seasonal variations: temperature (and pressure) are higher on long summer days. Ten soundings with Aerobee rockets at Fort Churchill to a height of 95 km revealed that at 50 km the temperature in summer is 275°K and in winter is 265°K, and at 80 km in summer is 270°K and in winter is 230°K. Cases of an unusual atmospheric temperature stratification between 50 and 80 km were recorded during winter measurements.

Murgatroyd constructed mean meridional cross sections of the temperature field for summer and winter in the northern hemisphere, generalizing many data on temperature obtained prior to 1956 by direct and indirect methods (refs. 91 and 233). These cross sections permit us to form some idea concerning the amplitude of the annual temperature variation at different heights. A remarkable characteristic of the heat regime of the upper layers of the atmosphere was discovered. The sign of the annual variation changes with transition through the level of approximately 70 km; at lesser heights it is warmer in summer and at greater heights it is warmer in winter. In this connection we should mention a characteristic of the seasonal temperature variation in the region of the mesopause, where winter temperatures are higher than summer temperatures: the absolute value of the summer - winter difference increases with geographic latitude. The lowest temperatures are observed in summer at latitudes 60-70°N. This result, having great general importance for many problems involved in the physics of the upper layers of the atmosphere, and in particular for understanding the seasonality of the appearance of noctilucent clouds, is confirmed by rocket measurements of temperature (acoustic grenade method) at a latitude of 59°N (Fort Churchill). If we compare the approximate variation of summer and winter temperatures to heights of 85-87 km, published in 1959 by Stroud, Nordberg, Bandeen, Bartman and Titus (ref. 753), it is found that the summer - winter difference attains -60°. These authors report that the winter temperatures of the mesopause on individual days considerably exceed the mean temperature indicated on the curve: in two cases a temperature greater than 250°K was measured at a height of 80 km; this exceeds the summer temperature by 75°.

14.3. Thermosphere. The general character of the temperature distribution in the thermosphere to a height of 200 km in a period of maximum solar activity is illustrated in figure 14.1. The higher layers have been studied mostly by satellites; their temperature is subject to especially significant changes.

Satellite observations obtained data on the height H of the homogeneous atmosphere, rather than direct information on temperature. In Section 10 (Tables 10.13, 10.16, 10.19 and 10.20) we presented data on the values H at heights of 90-1,000 km, which can be used for direct computation of the ratio

of temperature T to molecular weight m. For example, the computations of Tuomikoski (ref. 772) gave

H km	200	300	400	500	600	700	800	900	1000
$\frac{T}{m}$	47	83	120	132	135	160	180	170	150

Increase of the ratio $\frac{T}{m}$ with height was caused both by an increase of T and a decrease of m. The methods and results of computation of m at great heights are presented in Section 18. Table 10.20 gives the values m and T for heights of 130-1,000 km, according to Mathur and Mitra (ref. 579). The temperature values at heights of 130-200 km, according to data in reference 579, are appreciably less than those cited in figure 14.1. This discrepancy characterizes the status of the problem of the thermal regime of the thermosphere, since large errors of temperature determination are detected (especially due to the absence of complete data on the change of m with height) and particularly significant variations of temperature as a function of latitude, season and solar activity are noted (see Section 11). However, undoubtedly there is a rapid increase of temperature with height, up to layers directly adjacent to the upper boundary of the Earth's atmosphere: the atmospheric temperature at the 200 km level is close to a value of about 1,000°K or more, at the 500 km level--to a value 1,500°K or more, and at the 1,000 km level--to a value 2,000°K or more.

After analyzing the joint results of observations of the third Soviet satellite and the American satellites Explorer I, Explorer IV and Vanguard II, which had perigees of 216, 359, 263 and 567 km, respectively, Phillips (ref. 675) found that in the region 216-359 km the temperature of the atmosphere changes little with height (isothermal state), but above this region there is a rapid increase of temperature with height. The mean temperature gradient is approximately 4.9°/km in the region 216-567 km, but in the region 263-567 km it increases to 5.9° km. If it is assumed that the molecular weight at all heights has a constant value m_0, as a result of an analysis we can obtain the most probable values of the "molecular" temperature T_M cited in Table 14.1. However, if it is assumed that the molecular weight m decreases with height, as indicated in the last column of Table 14.1, we obtain considerably smaller values of the true temperature T_{true}.

Sharp changes of the structure of the upper layers of the atmosphere (Section 11) are apparently caused predominantly by temperature changes. Groves (ref. 416), after investigating variations of the rate of change of the period of revolution of the second and third Soviet satellites and their carrier rockets, concluded that the observed irregularities of deceleration of satellites can be related to a change of perigee from the daytime to the nighttime side as a result of precession of the orbital planes of the satellites. The increase of atmospheric density at a height of 220 km during the daytime in comparison with

TABLE 14.1. AIR TEMPERATURE FROM OBSERVATIONS OF SATELLITE MOTION.

Height km	T_{mol}	T_{true}	$\frac{m}{m_0}$
216	1162—1368	713—838	0.613
263	1248—1378	734—810	0.588
300	1368—1544	781—882	0.571
359	1368—1809	767—991	0.561
400	1761—1985	1039—1108	0.558
500	2412—2710	1336—1500	0.554
567	2695—3341	1493—1852	0.554

nighttime is attributed by Groves to an ascent of the atmosphere beginning with the 100 km level, caused by heating of air by solar radiation.

An indirect demonstration of the strong heating of the thermosphere, illuminated by the Sun's rays, is the high rotational temperature of 2,100°K obtained by Hunten, Koenig and Jones (ref. 465) for a sunlit aurora observed on Sept. 3-4, 1958 at heights of 300-600 km (first negative system of N_2^+ bands). However, this temperature may not correspond to the kinetic temperature of the atmosphere, but to the radial equilibrium of N_2^+ ions in the field of solar radiation.

The conclusion, drawn by Groves (ref. 416), that diurnal variations of density are the cause of the observed irregularity of the deceleration of the satellite has been questioned by Parkyn (ref. 669), who attributed these irregularities to the effect of atmospheric tides.

14.4. Thermal Processes in the Stratosphere. The heat balance of any region of the atmosphere is determined by many factors: absorption of shortwave and corpuscular solar radiation and longwave backward scatter, radiant heat exchange and heat exchange through heat conductivity, convection, turbulent heat exchange, heat transport accompanying circulatory processes, etc.

The importance of the different factors determining the heat balance of the atmosphere changes appreciably with height. For example, the role of molecular heat conductivity is negligibly small in the troposphere and stratosphere, but it becomes large in the thermosphere. The heating caused by the absorption of solar uv radiation changes greatly with height: it is small in the mesosphere and acquires decisive importance in the thermosphere. A graphic idea of this situation can be obtained from the curves of the dependence of the absorption of solar rays of different wavelength on height above the Earth's surface. Hinteregger's data (fig. 14.3) are the latest and most complete for the shortwave part of the spectrum (ref. 443). He obtained these data for conditions of a normal Sun (absence of high solar activity) at midday ($\cos z \simeq 0.8$, where z is solar zenith distance) in the middle latitudes (White Sands Proving Ground).

The activity of certain processes depends on the position of this region of the atmosphere relative to the Earth's magnetic poles and primarily on its

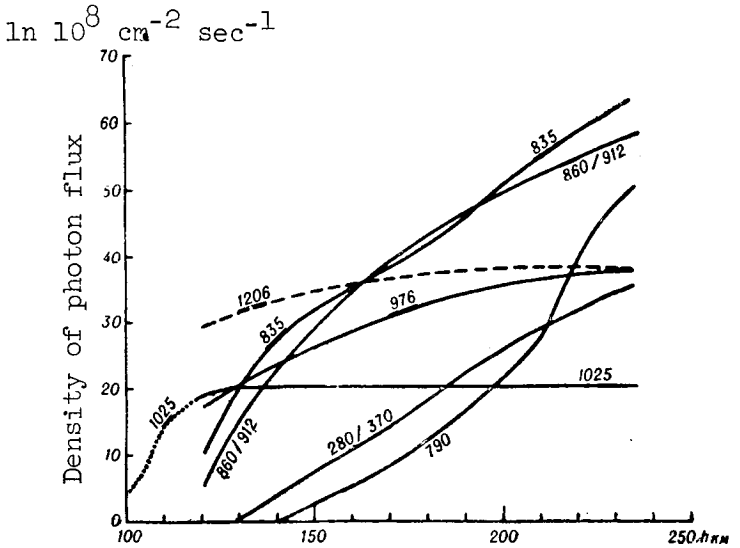

Figure 14.3. Attenuation of fluxes of solar photons during passage through the upper layers of the atmosphere from measurements made with a rocketborne automatic monochromator on Aug. 23, 1960. The figures along the curves indicate wavelength in Ångstroms.

heating due to the absorption of solar corpuscular radiation. In the auroral zone this heating is a considerable value not only in the thermosphere, but also in the mesosphere and possible even in the upper part of the stratosphere.

The heat balance of the stratosphere is to a large degree determined by radiant heat exchange, but this factor is by no means the only one. The major study of Ohring (ref. 641) contains a computation of shortwave, longwave and total radiation balances for all components of the atmosphere absorbing radiation (ozone, water vapor, carbon dioxide gas) for 10° latitude zones of the northern hemisphere by seasons (January, April, July, October). The entire stratosphere has been studied as a whole. The principal contribution to the longwave balance of the stratosphere is from water vapor and carbon dioxide gas. The radiation cooling of the stratosphere caused by the radiation of these molecules is compensated only to a small degree by the positive component of the radiation balance caused by ozone (9.6-μ band). The total radiation balance of this region of the atmosphere (10-55 km) always is negative. Its absolute value increases with the latitude of the place, and in the annual variation in the low and high latitudes there is a maximum in summer and a minimum in winter (in the temperate latitudes the maximum falls in spring and the minimum in autumn).

This longwave cooling is to a large degree compensated by the absorption of solar ultraviolet radiation by ozone and of solar infrared radiation by water vapor. The total shortwave radiation balance has a maximum in summer and increases with latitude in the warm part of the year. The total radiation balance is negative to the north of the narrow transitional zone $35\text{-}45^\circ$, but

TABLE 14.2. AVERAGED RADIATION BALANCE OF STRATOSPHERE OF NORTHERN HEMISPHERE AS A WHOLE (10^{-3} CAL/CM^{2}MIN).

Radiation balance	January	April	July	October	Entire year
Entire stratosphere. . .	-1	-2	+5	-2	0
Upper part of stratosphere.	-1	-1	+3	-4	-0.8

to the south of it is positive. This zone is distinguished by the presence of a thermal state of the stratosphere close to radiation equilibrium. In this zone there should be an intense interlatitudinal advection of heat from a source situated in the southern latitudes of the stratosphere into the stratosphere in the high latitudes. The radiation balance as an average for the entire stratosphere of the northern hemisphere, if Ohring's results are used as a point of reference, should be close to zero (Table 14.2). The second line of this table gives the results of Ohring's computations for the 21-55 km layer. In this case the distribution of the radiation balance is different. The radiation balance here is positive in summer at all latitudes. There should be heat transport toward the pole in winter and toward the equator in summer.

14.5. Radiation Heating of the Mesosphere. Computations of the radiant flux of heat into the higher layers of the atmosphere were made by Murgatroyd and Goody (ref. 617). They constructed mean monthly meridional cross sections of radiation heating due to absorption of solar radiation by ozone and oxygen in the region 30-90 km for the northern hemisphere. A study of the cross sections reveals that the vertical distribution of the shortwave radiant heat flux is similar to the vertical temperature profile: there is a maximum of heating at the 45-55 km level and a minimum at the 80-85 km level where the values of radiation heating are close to zero; the heat flux increases rapidly with height above this minimum.

In order to take into account the influence of the longwave radiant heat flux Murgatroyd and Goody (ref. 617) made appropriate computations taking two absorption bands into consideration: the ozone band 9.6 μ and the carbon dioxide band 15 μ. The results applying to carbon dioxide gas are cited in Table 14.3. Close values were obtained by Plass (ref. 678). The 9.6 μ ozone band causes somewhat less cooling, up to 3°/day (refs. 618 and 677).

In summarizing the values applying to the long and shortwave components of the radiant heat flux, Murgatroyd and Goody (ref. 618) discovered that to a large degree these two components compensate for one another. As a result, the state of the mesosphere (from 30° in the winter hemisphere to 60° in the summer hemisphere) is close to radiant equilibrium. However, on the basis of

TABLE 14.3. RADIATION CHANGES OF TEMPERATURE CAUSED BY 15 μ CARBON DIOXIDE BAND HEIGHT, KM.

Height, km	25	30	35	40	45	50	55	60
Temperature changes, °/day	-1.7	-2.8	-4.1	-5.2	-6.6	-6.8	-5.0	-3.8

this meridional cross section it is difficult to form a correct idea concerning the vertical temperature profile and its seasonal variations. For example, the air temperature at a height of about 80-85 km according to these computations should be higher than in winter, but we know that in actuality this is not the case. The same can be said of the seasonal changes of temperature of the mesosphere.

It is apparent that some important characteristics of the vertical temperature profile within the stratosphere and mesosphere, its seasonal and latitudinal relationships, are not determined by factors associated with absorption and radiation of radiant energy, but primarily by other processes: interlatitudinal advective heat transport, vertical movements and (especially in the high latitudes) the effects of corpuscular streams. However, these complex processes apparently transpire differently in different geographic regions. For example, Nordberg and Stroud (ref. 639), after analyzing data from rocket sounding of the stratosphere and mesosphere at Guam (13.5°N, 145°E), concluded that the thermal regime of these layers in the equatorial zone is determined mostly by the absorption of solar radiation, and considerable day-to-day variations are superposed du to dynamic processes. However, the heat regime in the high latitudes in winter in these layers is determined by large-scale dynamic processes which cannot be attributed to absorption of direct solar radiation. Some of these problems will be considered in the following sections. It should be emphasized at once, however, that for the time being there is no theory which would explain even approximately the entire temperature profile of the mesosphere (and stratosphere) and its changes with latitude during the course of the year.

The applicability of Kirchhoff's law in the rarefied medium of the upper layers of the atmosphere is an interesting problem. Analysis of this problem (refs. 91 and 233) leads to the following results.

When a medium has a low density (upper layers of the atmosphere) the conditions of thermodynamic equilibrium are not satisfied,but there is monochromatic radiant equilibrium, i.e., a state of the medium in which at each specific frequency as much radiation is radiated as is absorbed.

Transition from one type of equilibrium to another occurs at heights of about 60 km, according to Goody (ref. 409) or 75 km (according to Curtis and Goody, ref. 347). The inaccuracy of the initial data can change the estimate of the latter value by ±10 km (ref. 347).

14.6. Processes Determining the Heat Regime of the Thermosphere. Air heating as a result of ionization and dissociation is of importance in this region of the atmosphere.

Usually during ionization more energy is absorbed than is necessary for ionization; the energy excess is released mostly in the form of the kinetic energy of a freed electron (since the electron mass is thousands of times less than the mass of the ions). The energy excess of the ions is lost rather rapidly as a result of collisions, being distributed among the heavy particles. The absorption of ionizing radiation, therefore, is accompanied by an increase in the temperature of the absorbing layer. Similar phenomena accompany dissociation.

The special process of cooling by radiation is of great importance in the upper layers of the atmosphere; this process can be well developed only above the 60-100 km level. We have in mind the radiation of atomic oxygen, whose ground state (lower energy level) ^3P has three levels (sublevels): $^3P_0$, $^3P_1$ and $^3P_2$, situated very close together. The two lower levels differ in energy by only 0.020 ev, but the $^3P_0$ and $^3P_2$ levels differ by 0.028 ev; the level $^3P_1$, therefore, can be excited easily by ordinary thermal collisions with other atoms or molecules or collisions with electrons. The transition from the level $^3P_1$ to $^3P_2$ corresponds to magnetic dipole radiation and possesses a high probability (according to Pasternak's computations, it is equal to $8.9 \cdot 10^{-5}$ sec^{-1}). There are also rather favorable conditions for the excitation of the $^3P_0$ level, with subsequent transition to the $^3P_1$ level. These transitions are accompanied by radiation in the far infrared region of the spectrum. Thus, oxygen atoms at all times expend heat reserves in the atmosphere, taking thermal energy from the surrounding medium by the collision process and expending it in radiation processes of two types (ref. 284)

$$\left.\begin{aligned} O(^3P_1) &\rightarrow O(^3P_2) + h\nu \\ O(^3P_0) &\rightarrow O(^3P_1) + h\nu \end{aligned}\right\} \qquad (14.1)$$

Such an expenditure of thermal energy on radiation should occur most intensively at a height of about 100 km, since in the lower layers there is almost no atomic oxygen (the degree of dissociation of oxygen approaches zero) and in the higher layers the number of collisions is small.

The high efficiency of the processes of excitation of the states $^3P_1$ and $^3P_2$ of oxygen atoms and processes (14.1) makes these processes an important element of the heat balance in the ionosphere as a "coparticipant" of heat conductivity. Heat conductivity becomes an important mechanism regulating the thermal state of the atmosphere in its upper layers. Like Bates (ref. 284) we

can conceive that the heat exchange in the higher layers of the ionosphere occurs almost entirely by heat conductivity; as a result, there is always a downward transfer of a great quantity of heat expended by the atmosphere at a level of about 100 km by radiation through processes (14.1).

The influence of molecular heat conductivity on the vertical temperature distribution in the thermosphere can be seen in the results obtained by Johnson. Johnson concluded that the principal contribution to the energy balance at heights of 100-130 km is from light absorption in the region 1,300-1,800 Å, and at greater heights--220-900 Å. According to Johnson's estimates, applying to the middle latitudes, the heat loss by radiation is an order of magnitude less than the loss due to heat conductivity; therefore, the energy received by the atmosphere as a result of absorption of solar radiation can be equated to the heat flux lost as a result of heat conductivity. Assuming that the heat conductivity coefficient is known, Johnson finds the vertical temperature gradient, and uses this in turn to find the vertical temperature distribution. In the integration of the heat conductivity equation the boundary condition used is temperature at a height of 130 km, known from rocket measurements.

Johnson's computations indicate that the rapid temperature change at heights of 100-200 km is slowed at great heights: at a height of about 300 km the distribution becomes virtually isothermal. The temperature values are approximately 400°K at a height of 130 km and increase to 1,000°K at the 300-km level.

The study of the structure of the upper layers of the atmosphere using artificial Earth satellites (Sections 13.5 and 14.1) led to somewhat different results from the conclusions drawn in Johnson's study. In the first place, this remark applies to the absence of isothermal conditions at heights of about 300 km or more. These discrepancies can be attributed to the fact that in addition to the absorption of solar shortwave radiation taken into account by Johnson there are also other powerful sources of energy determining the additional heating of the upper layers of the atmosphere. Among such sources we particularly mention the solar corna, corpuscular streams, magnetohydrodynamic waves, etc. These sources of energy and the heating mechanisms will be considered below.

Whitney, on the basis of the concepts of Bates on the role of heat conductivity and radiation of atomic oxygen through mechanism (14.1) and the physical model of the upper layers of the atmosphere developed by Nicolet (ref. 635), also computed the temperature distribution, solving the corresponding heat conductivity equation (ref. 805). Whitney numerically integrated an equation also taking into account the radiation of atomic oxygen. This result was used in order to establish at what heights radiation effects are negligible and, therefore, whether a simplified model taking into account only the heat conductivity of the air is suitable. According to his computations, this model is applicable at heights of 300 km or more, and he obtained the following temperature and density values

h km	140	200	300	400	500	600
T° K	560	754	1026	1258	1465	1653
lg ρ g/cm^3	-11.07	-12.15	-13.25	-14.03	-14.65	-15.18

14.7. Thermal Effect of the Solar Corona and Meteor Streams. We have seen that some computations of the heat balance of the thermosphere led to the conclusion that the solar heat carried by radiation is insufficient for explaining the high temperatures of the upper layers of the thermosphere. The problem of the existence of "excess heating" of the thermosphere was most clearly formulated in 1951 by Bates (ref. 347). Search for the mechanisms which could ensure the necessary additional heating of the thermosphere led Chapman to the hypothesis of a hot solar corona extending to the limits of the solar system (1956-1958). According to this model, the solar corona consists of neutral or ionized hydrogen and has high heat conductivity. As a result, there is a constant outward heat loss (ref. 330). It can be assumed that the corona consists of protons and electrons with identical concentration n. The temperature T and n are dependent only on distance R, read from the center of the sun. Chapman assumes that T has maximum $T = T_0$ at distance $R_0 = 7.36 \cdot 10^{10}$ cm, which is $0.4 \cdot 10^{10}$ cm greater than the "solar radius" $R_\odot = 6.96 \cdot 10^{10}$ cm. The heat conductivity K of the gas, consisting of protons and electrons, can be computed. According to Chapman's computations,

$$K = AT^{5/2} \quad \text{ergs/deg} \cdot \text{cm} \cdot \text{sec}, \tag{14.2}$$

where $A = 5.2 \cdot 10^{-7}$. Equation (14.2) can be rewritten in the form

$$K = K_0 \left(\frac{T}{T_0}\right)^s, \tag{14.3}$$

where $s = \frac{5}{2}$, K_0 is the heat conductivity coefficient when $T = T_0$. The heat flux F through a sphere of radius R is not dependent on R and is determined by the expression

$$F = -4\pi R^2 K \frac{dT}{dR}. \tag{14.4}$$

Assuming the value $T_0 = 10^6$ °K, Chapman computed the temperature of the coronal gas at the distance at which the particular planet is situated from the Sun; he obtained:

Mercury	280 000°K	Mars	190 000°K
Venus	240 000	Jupiter. . .	135 000
Earth	219 000	Saturn . . .	115 000

For flux F he obtained the result $F = 1.38 \cdot 10^{26}$ ergs/sec. If a value differing from 10^6 is used for T_0, the flux changes by y times.

T_0	$5 \cdot 10^5$	$1.5 \cdot 10^6$	$2 \cdot 10^6$	$3 \cdot 10^6$
y	0.088	4.13	11.3	46.8

According to certain estimates, in outer space the heat loss of the corona by radiation is $2.7 \cdot 10^{26}$ ergs/sec, or two times greater than the loss through heat conductivity.

If it is assumed that $n_0 = 2 \cdot 10^8$ particles/cm^3 for the hottest part of the corona, at the Earth's orbit $n \simeq 10^3$; the result of computation of n depends substantially on the assumed value T_0. If $T_0 = 10^6$ or $1.1 \cdot 10^6$, or $1.2 \cdot 10^6$, then n = 340, or 1,300, or 4,200 particles/cm^3.

In actuality, the solar corona does not possess spherical symmetry, as assumed by Chapman as a simplification. Photographs taken at the time of eclipses indicate that the corona has a great extent in some directions and a lesser extent in others, and that the configuration of the corona changes during the sunspot cycle. The influence of this variability on the heat regime of the outer part of the Earth's atmosphere is dependent on the rate of change in comparison with the time necessary for establishing an equilibrium thermal state of the atmosphere. The problem is further complicated if we take into account the influence of the Sun's magnetic field, the corona and the Earth on the heat conductivity of the interplanetary (coronal) gas (refs. 328 and 330).

According to Chapman's estimate, the temperature of the outer part of the Earth's atmosphere at a distance of 5 Earth radii from the Earth can attain 10^5 degrees under the influence of hot coronal gas. In this case the mean temperature gradient between this level and the F2 region would be about 4°/km; the Earth's atmosphere would receive a quantity of $2.4 \cdot 10^{19}$ ergs of coronal heat per sec. The entire problem of the transfer of such a great quantity of energy from the corona to the Earth and the mechanism of this transfer should be the subject of further study (ref. 328).

The opinion has been expressed repeatedly that streams of meteor particles exert a possible influence on certain physical processes in the upper layers of the atmosphere: nighttime and daytime luminosity of the sky, ionospheric phenomena, including nighttime ionization, and heating.

Proceeding on the basis of certain assumptions on the quantity of meteor particles entering the Earth's atmosphere each second, and the character of the particle-size distribution (reference is to the L distribution), Kaiser and Seaton derived the following expression for estimating the value of energy E entering the atmosphere due to meteor particles, whose radius r does not exceed some stated value $r_0 (r \leq r_0)$:

$$E = 1.6 \cdot 10^{13} r_0^2 \quad \text{ev/cm} \cdot \text{sec},$$

where r is in cm.

Kaiser and Seaton assume that the contribution of meteor particles to the heat balance of the ionsophere can be considerable, but this problem requires further study.

Chapman's study (ref. 328) cites an estimate indicating that "zodiacal" dust particles (i.e., particles apparently forming part of the medium wherein the zodiacal light is formed by the scattering of the Sun's rays) can contribute an energy of the order of $3 \cdot 10^{17}$ ergs/sec to the Earth's atmosphere. Part of this energy is absorbed by the atmosphere below 100 km, but a large part of the energy associated with the effect of the finest particles would be concentrated in the upper layers of the atmosphere.

14.8. Magnetohydrodynamic Waves. The methods of a new scientific discipline--magnetohydrodynamics, which studies the interaction of an electromagnetic field with a fluid or gaseous electrical conductor, considered as a continuous medium, have come into use in geophysics. The theoretical basis for magnetohydrodynamics is the classical equations of an electromagnetic field and the equations of hydrodynamics (the equations of motion of a continuous medium). The phenomena characteristic of magnetohydrodynamics are manifested in electrically conductive media of great extent; magnetohydrodynamics is, therefore, applicable to the problems of geophysics and especially astrophysics.

Magnetohydrodynamics studies the motion of an electrically conductive fluid in a magnetic field. The electrical currents developing in this process change the external field and lead to a mechanical effect of the magnetic field on the fluid. This interrelationship between motion and the field is a specific characteristic of magnetohydrodynamics (ref. 342).

In many problems cosmic gas masses and air masses in the upper layers of the Earth's atmosphere, despite extremely low density, can be considered a continuous medium if the linear dimensions of the considered phenomena exceed the mean length of the free path of the gas particles, which gives a sound basis to the hydrodynamic approach to the study of these phenomena (ref. 183).

As a result of the interaction between electromagnetic and hydrodynamic phenomena, small disturbances in the conducting medium when a magnetic field is present are propagated in the form of waves with properties different than those of ordinary sound or electromagnetic waves. The conducting medium in the magnetic field also acquires a singular anisotropy, because the velocity of wave propagation is dependent on the direction of propagation in relation to the magnetic field.

It can be shown (ref. 342) that the mechanical effect of the magnetic field is equivalent to the sum of hydrostatic pressure $\frac{\mu H^2}{8\pi}$ and stress $\frac{\mu H^2}{4\pi}$ along the lines of force (here H is magnetic field strength and μ is magnetic permeability). In an incompressible fluid hydrostatic pressure can be balanced by the pressure of the fluid, so that only the stress $\frac{\mu H^2}{4\pi}$ is effective. By analogy with the

theory of oscillations of tense strings it can be assumed that with such stress there can be transverse waves along the lines of force, propagating with the velocity a, where

$$a^2 = \frac{\mu H^2}{4\pi\rho}$$

(ρ is the density of the medium). The existence of such waves, called magnetohydrodynamic waves, was predicted in 1942 by Alfvén.

Compressibility does not exert an appreciable influence on the dynamics of a gas, if the velocities of motion are small in comparison with the speed c of sound propagation. It can, therefore, be assumed that magnetohydrodynamic waves in a gas are propagated approximately the same as in a fluid, if their velocity is substantially less than c. This conclusion also was confirmed by a more detailed study (ref. 342).

Magnetohydrodynamic waves do not have an analogue in ordinary hydrodynamics. In a certain sense it can be assumed that they are transverse waves and the oscillations occur perpendicular to the undisturbed magnetic field H. The transverse character of these waves means that the conducting medium in a magnetic field acquires a singular elasticity in relation to the shear of its adjacent layers. Magnetohydrodynamic waves are not accompanied by density change and therefore are possible both in a compressible and in an incompressible medium. From the point of view of the microscopic theory of an ionized gas, magnetohydrodynamic waves represent a limiting case of ordinary electromagnetic waves in an ionized gas corresponding to frequencies considerably less than the gyrofrequency of ions (ref. 183).

In 1958 Dessler demonstrated that magnetohydrodynamic waves of great amplitude can develop in the upper layers of the ionosphere at the time of injections of corpuscular clouds (solar corpuscular streams) (ref. 354). These waves apparently can be the cause of brief fluctuations of the geomagnetic field observed at the Earth's surface (this problem has been considered in the author's book, ref. 233). In this case we are concerned with the possibility of a thermal effect of these waves, specifically, their heating of the ionosphere. Such a possibility was considered by Dessler in 1959 (ref. 355).

At great heights the electrical conductivity of the surrounding medium is quite great and in that region therefore the scattering of magnetohydrodynamic waves caused by collisions between electrons and ions and between ions and atoms can be neglected. However, at lower levels the collisions between ions and neutral atoms give rise to a new scattering mechanism which can be the cause of appreciable heating of the atmosphere. Reference is to a special mechanism of dissipation of the energy of electrical currents in partially ionized gases, absent in a fully ionized gas. Additional dissipation of the energy of electrical currents occurs as a result of the loss of velocity of electrons and ions, relative to neutral atoms, due to collisions of charged and uncharged particles (ref. 342).

It was demonstrated in Dessler's study (ref. 355) that when a magnetic field is present, and if the density of neutral particles is a quite large percentage

of the entire gas density, "reduced conductivity" can be used for computation of scattering. In the absence of neutral atoms we assume "zero conductivity," since the frequency of collisions of charged particles does not change due to the appearance of a magnetic field.

When a magnetohydrodynamic wave is propagated in a partially ionized gas, the ions and electrons follow the movements of the wave, whereas the neutral particles are not affected by the electrical forces of the wave. However, the electromagnetic energy can be transferred to neutral atoms by collisions of ions with atoms. These collisions, depending on their character, can play an important role, because there can be large relative velocities of motion of ions relative to neutral atoms. A similar dissipation mechanism occurs in a partially ionized gas, but it is absent in a fully ionized gas.

Dessler (ref. 355) computed the heating of the ionosphere caused by scattering of the energy of magnetohydrodynamic waves moving downward through the ionosphere. He had to make certain assumptions concerning the amplitude and frequency spectrum of magnetohydrodynamic waves. He demonstrated, in general form, that maximum heating occurs at a height of approximately 175 km. The absolute value of the heating could not be computed because the result essentially depends on the values of the amplitudes and frequency spectrum of the magnetohydrodynamic waves used, but under "quiet" conditions magnetohydrodynamic heating apparently cannot exert an appreciable influence on the temperature of the ionosphere in the F region; it is 10^{-9} w/m^3 at heights between 150 and 200 km. But during a magnetic storm magnetohydrodynamic heating can become extremely significant and can even be the cause of the observed rise of the F region; the zodiacal dust can make its contribution and warrants attention. Although dust particles can be subject to photoionization, the geomagnetic field nevertheless does not act on them to the same degree as on particles of coronal gas.

14.9. Heating of the Atmosphere by Solar Corpuscular Streams and Electrical Currents. At all times the Earth's atmosphere is bombarded by corpuscular streams emanating from the Sun (for a detailed description see the author's book, ref. 233). In estimating the maximum quantity Q of heat which the atmosphere can receive from a corpuscular stream (energy passing through 1 cm^2 in 1 sec) it can be assumed that

$$Q = nV\frac{mV^2}{2}, \tag{14.5}$$

where m is particle mass. If it is assumed as a minimum estimate, e.g., that $V = 10^8$ cm/sec and $n = 1$ cm^{-3}, and if it is assumed that the fluxes consist of protons, by using formula (14.5) we obtain $Q \simeq 0.8$ erg/cm^2 sec; in turn assuming a maximum estimate $V = 3\cdot10^8$ cm/sec and $n = 10^4$, we obtain $Q \simeq 2.2\cdot10^5$ ergs/cm^2 sec. The solar constant of 2 cal/cm^{2}min corresponds to $1.4\cdot10^6$ ergs/cm^{4}sec. If

it is assumed that the percentage of energy of corpuscular streams expended on ionization and other elementary processes is not a very large value, (e.g., does not exceed half the total energy), it follows from the computation that in periods and in regions of the injection of powerful streams of corpuscles (auroral zone) the heat received by the upper layers of the atmosphere from corpuscular streams can attain 5-10 percent of the solar constant. It must be taken into account that corpuscular streams are almost entirely held back at great heights (more than 80-100 km); the heat capacity of the rarefied upper layers of the atmosphere is small, and because of these energies the air temperature at great heights can increase by tens and hundreds of degrees.

Measurements on satellites are of exceptional importance for obtaining more reliable and systematic data on the energy of corpuscular streams. The third Soviet satellite carried special apparatus for recording strong fluxes of electrons with an energy of the order of 10^4 ev at heights up to 1,900 km. Data presented by V. I. Krasovskiy indicate that the energy density in these corpuscular streams exceeds 100 ergs/cm^2. The energy of the fluxes reaching the heights of the F region of the ionosphere is up to 1 erg/cm^2sec, which can be a source of strong heating of the corresponding atmospheric layers; this effect would be enhanced with increase of height and latitude.

We will now consider to what extent the percentage of the energy of corpuscular streams transformed into heat, assumed above as a rough estimate, corresponds to reality. This percentage is dependent on the mechanism of dissipation of the energy of the streams in the atmosphere. The energy of the streams can be transformed directly into heat as a result of collisions with molecules, atoms and ions in the atmosphere. Another possible mechanism, mentioned by V. I. Krasovskiy, is related to "frozen-in" magnetic fields transported by corpuscular streams (ref. 233). Acting on the geomagnetic field, the fields of the condensations and fluxes of corpuscles can excite induced currents in the conducting layers of the Earth's atmosphere; the Joule heat of the latter can cause the heating of the atmosphere.

Another possible mechanism is associated with shockwaves (Section 14.8).

The problem of the conditions and degree of heating of the atmosphere from the energy of corpuscular streams requires further systematic study, but this latter heat source undoubtedly plays an important role in the heat regime of the upper layers of the atmosphere. Attempts are being made to establish empirical relationships between corpuscular streams and heating of the atmosphere even at relatively low heights, such as 20 km (ref. 793). This heat source plays an important role in the heat balance of the upper layers of the atmosphere.

We now will proceed to a consideration of electrical currents. According to an estimate made by B. M. Rubashev (ref. 174), about 40 percent of the initial energy of a stream is expended on heating in the collision process. The energy released at the level of the E region of the ionosphere, on the basis of different estimates, is from 10^{-7} to 10^{-2} erg/cm^3sec. With respect to Joule heat,

Rubashev's estimate for heights of the E region gives an energy release in the auroral zone at the time of a magnetic storm of $2 \cdot 10^{-4}$ erg/cm^{3}sec. In order to estimate the temperature increase, Rubashev numerically solved the non-stationary heat balance equation in the form

$$\frac{dQ}{dt} = 0.4 \frac{mV^3 n}{2} - c_p A \frac{\partial^2 T}{\partial y^2} - \varkappa \frac{\partial^2 T}{\partial z^2}, \qquad (14.6)$$

where Q, m, V and n have the same value as in formula (14.5), c_p is heat capacity at constant pressure, A is the coefficient of macroturbulent exchange, $\frac{\partial T}{\partial y}$ is the meridional temperature gradient, $\varkappa$ is the heat conductivity coefficient and z is a horizontal coordinate. In the derivation of equation (14.6) B. M. Rubashev had in mind the following mechanisms of heat loss: radiation, molecular heat conductivity, horizontal macroturbulent advection and convection. Analysis led him to conclude that only two mechanisms need be taken into account at these heights: molecular heat conductivity, the third term on the right-hand side of equation (14.6) and macroturbulent horizontal advection, second term on the right. It is found that there is a heating of 0.2-300°K in a time of 80-190 sec, depending on conditions.

Thus, at the time of strong magnetic storms there should be an intense heating of the upper layers of the atmosphere by this mechanism.

14.10. Radiation Belts and Other Sources. The radiation belts, discovered as a result of measurements made on satellites by S. N. Vernov and others in the USSR and Van Allen in the United States, undoubtedly are great reservoirs of energy acting in many ways on the upper layers of the atmosphere, including its heat regime. For the time being it is difficult to judge the quantitative characteristics of these effects; as a sample orientation we can use an energy value of the order of 1 erg/cm^{2}sec, transported by electron fluxes at the level of the F region at a latitude of about 50°N: this estimate was previously stated, based on measurements on the third Soviet artificial Earth sattellite. We note in conclusion that there can also be other mechanisms and sources of the energy of heating of the upper layers of the atmosphere: infrasonic oscillations generated in the atmosphere by ocean waves, etc. However, it is improbable that these sources could exert an appreciable influence on the thermal state of the upper layers of the atmosphere.

CHAPTER 6. GAS COMPOSITION OF THE ATMOSPHERE

15. Model of a "Mixed" Atmosphere

Air composition in the lower layers of the atmosphere has been determined with great accuracy and with the exception of water vapor content is characterized by great constancy.

15.1. Composition of Surface Air. Several different characteristics of the composition of dry air are given in Table 15.1. In the column "Pressure" the abbreviation "cm^2" is read (ref. 469) as "square centimeter of the Earth's surface."

TABLE 15.1. COMPOSITION OF DRY ATMOSPHERE.

Gas	Volume, %	Mass, %	Reduced thickness of gas layer above sea level, cm	Pressure, g/cm^2	Total mass, g
N_2	78.09	75.51	624 600	757.4	$3865 \cdot 10^{18}$
O_2	20.98	23.15	167 600	232.2	1184
A	0.93	1.28	7 440	12.8	65
CO_2	0.03	0.046	220	0.46	$235 \cdot 10^{16}$
Ne	0.0018	0.00125	14	0.0125	$64 \cdot 10^{15}$
He	0.00052	0.000072	4.2	0.00072	$37 \cdot 10^{14}$
CH_4	0.00015	0.000094	1.2	0.00094	43
Kr	0.0001	0.00029	0.8	0.0029	150
N_2O	0.00005	0.00008	0.4	0.0008	$4 \cdot 10^{15}$
H_2	0.00005	0.0000035	0.4	0.000035	$18 \cdot 10^{13}$
O_3	0.00004	0.000007	0.3	0.00007	35
Xe	0.000008	0.000036	0.06	0.00036	$18 \cdot 10^{14}$
NO_2	0.0000001	0.0000002	0.0008	0.000002	$1 \cdot 10^{13}$
I_2	$2 \cdot 10^{-11}$	$1 \cdot 10^{-10}$	$2 \cdot 10^{-7}$	$1 \cdot 10^{-9}$	$5 \cdot 10^{9}$
Rn	$6 \cdot 10^{-18}$	$5 \cdot 10^{-17}$	$4 \cdot 10^{-14}$	$5 \cdot 10^{-16}$	$2 \cdot 10^{2}$

These data were obtained mostly by chemical analysis of air in the lower layers and partly from data on the telluric spectrum; the latter are of independent interest and will be considered separately.

For a long time the percentage content of carbon dioxide in air was assumed to be constant, but an increase of its concentration was recently observed and was attributed to increase in the use of fossil fuels. There is an annual discharge of $6 \cdot 10^9$ tons of carbon dioxide into the atmosphere; the additional absorption of infrared radiation resulting from this discharge can cause a temperature increase of 0.6-1.2° per century. Observations made during the IGY period permitted determination of the seasonal changes of the concentration of carbon dioxide gas (a maximum in the spring in the growing season and a minimum in the autumn at its end). It is assumed that the reason for these changes is the life function of vegetation; this is confirmed by the amount of C^{12} and C^{13} isotopes near vegetated areas. In the southern hemisphere seasonal variations of the carbon dioxide concentration are of the same character, but their amplitude is considerably less; this can be attributed to the lesser area occupied by vegetation, animals and man. Air exchange between the hemispheres should decrease the amplitude of the variations in both hemispheres, because the phases of the variations are opposite. Theoretical computations show that about one-fifth of the air from one hemisphere flows into the other in each half-year period (ref. 809).

15.2. Absorption Spectrum of the Atmosphere. The absorption spectrum of the Earth's atmosphere in the form in which it can be obtained by observations of extraterrestrial radiation sources from ground level (telluric spectrum) is formed as a result of the absorption of radiation by molecules occurring mostly in the lower layers of the atmosphere. The telluric spectrum, therefore, will be discussed only briefly, with reference to the data shown in figure 15.1, curve 2.

TABLE 15.2. MOLECULES DETECTED IN THE EARTH'S ATMOSPHERE.

Molecule	Molecular weight	Content, reduced cm	Remark	Molecule	Molecular weight	Content, reduced cm	Remark
N_2	28.1	624 600	1	$C^{12}O^{16}O^{18}$	46.0	0.67	3
O_2	32.0	167 600	1	N_2O	44.0	0.4	3
$O^{16}O^{18}$	34.0	659	2	O_3	48.0	0.3	
$C^{12}O_2^{16}$	44.0	320	3	CO	28.0	0.06-0.15	3
				H_2O	18.0	10^3-10^4	
$O^{16}O^{17}$	33.0	134	2	HDO	19.0	0.4-4	
$C^{13}O_2^{16}$	45.0	1.5	3				
CH_4	16.0	1.2	3				

Remarks: 1, chemical determinations; 2, mass spectrograph; 3, spectroscopic determinations. Reduced centimeters, thickness of layer formed by a particular gas at pressure of 1 atm and temperature of 0°.

Table 15.2 gives a list of gases detected in the Earth's atmosphere, with an indication of their isotopic composition and quantity. Much important information given in the table was obtained from a study of the spectra of absorption in the atmosphere.

15.3. Telluric Spectrum. The Sun emits radiation at all wavelengths from x-rays to radio waves, but the solar spectrum observed from the Earth's surface contains many gaps caused by absorption of the corresponding wavelengths in the Earth's atmosphere. There is complete absence of the region from 0 to 0.3 μ (absorption by O_3, O_2, N_2 molecules, and N and O atoms). The atmospheric absorption spectrum in the region between 0.3 and 24 μ (Table 15.3) will be discussed briefly. In the column headed "Intensity" there is a rough estimate of the intensity of absorption lines and bands using a 5 unit scale.

Figure 15.1 schematically shows the change in the spectrum of solar radiation after its passage through the Earth's atmosphere (the Sun is assumed to

TABLE 15.3. MOLECULAR BANDS IN TELLURIC SPECTRUM BETWEEN 0.3 and 24 μ.

$\lambda\,\mu$	Molecule	Intensity	$\lambda\,\mu$	Molecule	Intensity	$\lambda\,\mu$	Molecule	Intensity
0.3400	O_3	Very weak	0.7710	O_2	Weak	1.91	H_2O	Strong
0.4664	O_4	Very weak	0.7955	H_2O	Average	1.96	CO_2	Strong
0.5436	H_2O	Weak	0.8059	H_2O	Weak	2.01	CO_2	Strong
0.5714	H_2O	Very weak	0.8226	H_2O	Average	2.05	$C^{13}O_2^{16}$	Average
0.5750	O_3	Very weak	0.8237	H_2O	Weak	2.06	CO_2	Strong
0.5770	O_4	Very weak	0.8465	H_2O	Weak	2.09	$C^{12}O^{16}O^{18}$	Very weak
0.5796	O_2	Average	0.9061	H_2O	Average	2.11	N_2O	Very weak
0.5872	O_3	Very weak	0.9200	H_2O	Average	2.14	H_2O	Average
0.5915	H_2O	Average	0.9419	H_2O	Strong	2.16	N_2O	Very weak
0.5918	H_2O	Weak	0.9434	H_2O	Average	2.20	CH_4	Average
0.5942	H_2O	Weak	0.9681	H_2O	Average	2.26	N_2O	Weak
0.6020	O_3	Very weak	0.9724	H_2O	Weak	2.32	CH_4	Average
0.6288	O_2	Average	1.017	H_2O	Weak	2.35	CO	Very weak
0.6290	O_4	Very weak	1.067	O_2	Weak	2.66	H_2O	Very strong
0.6314	H_2O	Weak	1.111	H_2O	Average	2.69	CO_2	Very strong
0.6379	O_2	Average	1.135	H_2O	Strong	2.77	CO_2	Very strong
0.6513	H_2O	Very weak	1.141	H_2O	Average	3.57	N_2O	Average
0.6884	O_2	Strong	1.209	H_2O	Average	3.67	HDO	Average
0.6897	$O^{16}O^{17}$	Very weak	1.268	O_2	Average	4.26	CO_2	Very strong
0.6901	$O^{16}O^{18}$	Weak	1.343	H_2O	Strong	4.38	$C^{13}O_2^{16}$	Average
0.6970	O_2	Weak	1.379	H_2O	Very strong	4.51	N_2O	Strong
0.6981	H_2O	Average	1.388	H_2O	Strong	4.63	H_2O	Strong
0.7032	H_2O	Weak	1.434	CO_2	Strong	4.75	O_3	Average
0.7227	H_2O	Average	1.455	H_2O	Strong	4.81	CO_2	Strong
0.7232	H_2O	Weak	1.475	H_2O	Average	6.27	H_2O	Very strong
0.7324	H_2O	Average	1.61	CO_2	Average	7.14	HDO	Strong
0.7620	$O^{16}O^{18}$	Average	1.67	CH_4	Average	9.6	O_3	Strong
0.7621	O_2	Strong	1.87	H_2O	Very strong	15.0	CO_2	Very strong
						16.2	CO_2	Average
						17.0	N_2O	Average

be in the zenith). By comparison of curves 4 and 5 it is possible to obtain information on the principal water vapor absorption bands in the 0.65-1.5 μ region; a computation (ref. 389) was made for a case when the quantity of water vapor in the atmosphere corresponds to a layer of liquid water 2 cm thick. Figure 15.2 shows in greater detail the structure of the absorption bands of O_2 molecules (band A), H_2O (bands ρ, σ, τ, Φ, Ψ, Ω, X, Y), CO_2, CH_4 and N_2O.

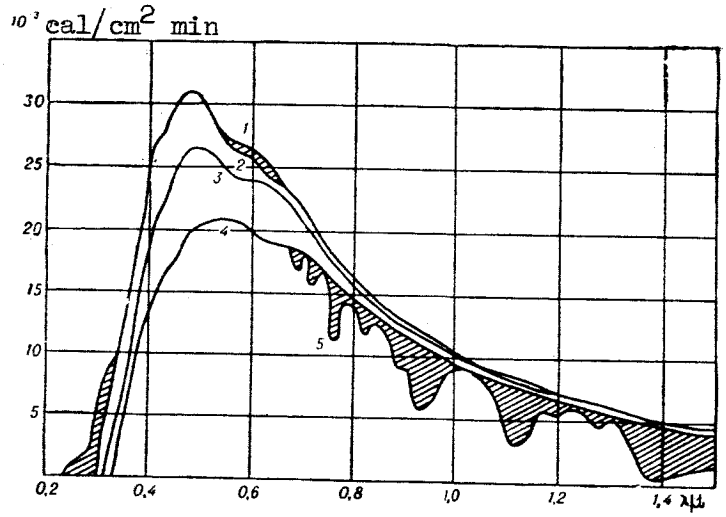

Figure 15.1. Change of spectrum of solar rays during their passage through the Earth's atmosphere. 1, solar extraterrestrial spectrum; 2, spectrum of solar rays after passage through ozonosphere; 3, same, taking into account attenuation due to molecular scattering; 4, same, taking into account attenuation by atmospheric dust; 5, same, taking into account absorption by water vapor.

For some years the solar spectrum in the 2.8 to 23.7μ region has been recorded at the high-mountain scientific station at the Jungfrau (Switzerland) with an instrument of high resolution. A total of 3,624 telluric lines have been discovered, of which Migeotte and Neven (ref. 596) have interpreted 3,244. Most of the lines belong to the following molecules (the number of lines belonging to a particular molecule is shown in parentheses)

H_2O	(1187)	CO_2 (558)	CO (60)	CH_4 (663)
H_2O^{17}	(12)	$C^{13}O_2^{16}$ (79)	$C^{13}O^{16}$ (29)	N_2O (800)
H_2O^{18}	(53)	$C^{12}O^{16}O^{18}$ (2)	$C^{12}O^{18}$ (17)	$N^{11}N^{14}O^{16}$ (6)
HDO	(180)			O_3 (527)

In these tables there are no sodium lines, but from the luminosity spectra of the twilight sky it is known that at a height of 70-90 km there always

is a certain quantity of Na atoms (ref. 233). Scrimger and Hunten (ref. 724) report the discovery of faint telluric D lines of sodium. However, complex apparatus is needed for this purpose.

15.4. Isotopic Composition. Study of the absorption spectrum of the atmosphere using instruments of sufficiently high resolution gives important information on isotopic composition. Table 15.2 shows that spectral methods can establish the presence of three types of CO_2 molecules in the atmosphere, differing in the isotopic composition of the atoms which they include, specifically: $C^{12}O_2^{16}$, $C^{13}O_2^{16}$ and $C^{12}O^{16}O^{18}$.

Benedict (ref. 291) identified some telluric lines of the infrared solar spectrum and established that they belong to water vapor molecules with an isotopic composition of H_2O^{16}, H_2O^{17} and H_2O^{18}. The relative intensity of the lines agrees with the normal isotopic composition of natural water.

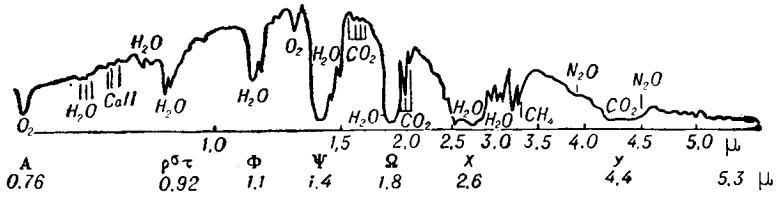

Figure 15.2. Infrared solar spectrum in region 0.76-5.3 μ (according to Langley, 1900).

It must be remembered that mass spectrometer investigations have shown that the water from melting snow is lighter than rainwater. During prolonged precipitation the density of rainwater decreases gradually (there is disruption of the normal relation of isotopes O^{16}, O^{17} and O^{18} equal to 99.76, 0.04 and 0.20 percent). Dansgaard established (ref. 348) that the percentage of isotope O^{18} in precipitation changes somewhat with the passage of fronts.

According to Table 15.2, the atmosphere also contains HDO molecules; this is also confirmed by new measurements on the Jungfrau (ref. 596).

The isotopic composition of atmospheric oxygen is of great interest. In addition to O_2 molecules (molecular weight m = 32), Earth's atmosphere contains molecules $O^{16}O^{17}$ (m = 33) and $O^{16}O^{18}$ (m = 34)(Table 15.2).

In addition, measurements of the solar spectrum at the high-mountain station on the Jungfrau in the 2.8-23.7 μ region permitted Migeotte and Neven (ref. 596) to identify 6 lines of the molecule $N^{11}N^{14}O^{16}$ (in addition to 800 lines of the N_2O molecule), 29 lines of the $C^{13}O^{16}$ molecule and 17 lines of the $C^{12}O^{18}$ molecule (in addition to 60 lines of the CO molecule).

Measurements made by Goldberg (ref. 405) at Mount Wilson Observatory indicate the following content of isotopes of carbon dioxide gas (in cm of a reduced layer for sea level): CO_2--320 cm, $C^{13}O_2^{16}$--1.54 cm, $C^{12}O^{16}O^{18}$--0.67 cm.

15.5. Elementary Theory of the Gravitational Diffusion Separation of Gases. Until relatively recently (at least to 1933), the opinion was common that air composition in the high layers of the atmosphere is characterized by a predominance of light gases. Such a conviction was based on corollaries from the hydrostatic equation (barometric formula)

$$dp = \rho g\, dh, \tag{15.1}$$

which, with the assistance of the equation of state

$$p = \rho \frac{RT}{m} \tag{15.2}$$

can be transformed to

$$p = p_0 e^{-\frac{mg}{RT} h} \tag{15.3}$$

or

$$p = p_0 e^{-\frac{h}{H}}, \tag{15.4}$$

where $H = \frac{RT}{mg}$, i.e., the height of the homogeneous atmosphere. By virtue of (15.2), the barometric formula (15.4) for pressure can be rewritten for density in the form

$$\rho = \rho_0 \frac{T_0}{T} e^{-\frac{h}{H}}. \tag{15.5}$$

In equations (15.3)-(15.5) p_0, ρ_0 and T_0 apply to the level h = 0, and p, ρ and T apply to the level at the height h.

Since the atmosphere is a mixture of gases, equation (15.3) should apply to the partial pressure p_i of the i-th air component

$$p_i = p_{0i} e^{-\frac{m_i g}{RT} h} = p_{0i} e^{-\frac{h}{H_i}}, \qquad (15.6)$$

where $H_i = \frac{RT}{m_i g}$. This equation shows that the greater the molecular weight m_i of a particular gas, the greater is the vertical decrease of its partial pressure p_i. Pressure decreases by e times with an increase of height by H km. If in model computations we consider an isothermal atmosphere with a temperature $T = 300^\circ K$, for nitrogen ($m_1 = 28$), oxygen ($m_2 = 32$), helium ($m_3 = 4$) and hydrogen ($m_4 = 1$), the height of the homogeneous atmosphere will be $H_1 = 9$ km, $H_2 = 8$ km, $H_3 = 63$ km and $H_4 = 250$ km, respectively. These figures make it possible to represent graphically how rapidly the relative content of light gases should increase with height. At the height h = 125 km the partial pressure p_1 of nitrogen should decrease by almost $e^{\frac{125}{9}}$ times, i.e., by a factor of 10^6 in comparison with the surface pressure p_{01}; oxygen p_2 by $e^{\frac{125}{8}}$ times, i.e., approximately by $6 \cdot 10^6$ times; helium p_3 by $e^{\frac{125}{63}}$ times, i.e., by a factor of 7, and hydrogen p_4 by $e^{\frac{125}{250}}$ times, i.e., only by a factor of 1.6. In other words, the nitrogen content relative to the content of oxygen should increase at a height of 125 km in comparison with the percentage composition of surface air by a factor of 6, helium by a factor of almost 10^6, and hydrogen by a factor of almost $4 \cdot 10^6$. Accordingly, in the textbooks on meteorology published in the 1920's or 1930's, the postulated composition of the air in the high layers of the atmosphere was presented, as an example, as indicated below (ref. 796) (in percent of volume):

h km	(Geocoronium)	Hydrogen	Helium	Nitrogen	Oxygen
80	19	55	4	21	1
100	28	67	4	1	--

If geocoronium is disregarded (it is cited as a curious example of still relatively recent (1928) speculations on air composition in the high layers of the atmosphere), the computations show that hydrogen, present at the Earth's surface in only minimum quantities, is already 14 percent by volume at a height of 50 km and more than 90 percent at a height of 100 km. A. Wegener wrote in 1928: "Thus, above 100 km the atmosphere should consist almost entirely of pure hydrogen" (ref. 796).

One of the principal results of the work in physics of the high layers of the atmosphere in the last 25 years is that Wegener's conclusion is completely disproved.

15.6. Investigations on the Stratospheric Balloon "SSSR-1." Initial data on the increase of the percentage of light gases with height were obtained in 1933 from analysis of air samples from the stratosphere, collected aboard the stratospheric balloon "SSSR-1." During the flight time of this stratospheric balloon on Sept. 30, 1933, to a height of 19 km (a record at that time), a crew consisting of G. A. Prokof'yev (commander), K. D. Godunov and E. K. Birnbaum carried out scientific investigations of cosmic rays and the distribution of meteorological elements. Included in these investigations was the collection of air in special cylinders, each with a capacity of 1 liter, manufactured of carefully processed glass. It was possible to return and precisely measure air samples taken at a height of 18.5 km. It was found that the volumetric content of nitrogen at this height is 78.13 percent and oxygen 20.95 percent. By comparing these results with the data in Table 15.1, we can see that the air composition at a height of 18.5 km coincides with the composition at groundlevel with an accuracy to 0.04 percent. Since nitrogen is 8/7 times lighter than oxygen, if there is a separation of heavy and light gases in the Earth's gravitational field, the ratio of the volumetric content of N_2 and O_2 at a height of 18.5 km should change by 28 percent, as derived from formula (15.6). At the Earth's surface this ratio is 3.72:1 (Table 15.1) and at the 18.5 km level it should increase to 4.77:1. However, at that level the ratio of the volumetric content N_2/O_2 is actually equal to virtually the same value: 78.13:20.95 = 3.73:1. The percentage content of O_2 should decrease to 17.7 percent, but actually is 20.95 percent.

15.7. Mixed Atmosphere. These results of analysis of air samples from the stratospheric balloon "SSSR-1" definitely demonstrated that at least to a height of 18.5 km there is no separation of light and heavy gases in the stratosphere, and, therefore, there is a constant vertical mixing of the atmosphere.

At approximately this same time certain indirect evidence was obtained indicating that the atmosphere is apparently "mixed" to great heights of the order of 100 km. The most important evidence was interpretation of the spectra of auroras and night airglow, especially interpretation of the well-known green line with wavelength 5,577 Å. The origin of this line remained a mystery prior to 1925, although various hypotheses were offered to explain it. The experiments of McLennan and Shrum in 1925 (ref. 586) demonstrated that the green line is emitted by atomic oxygen. It was also established that the numerous bands in the spectra of auroras and the night sky are emitted by N_2 molecules. It was found that even the high layers of the atmosphere, the site of auroral glow and night airglow (height of about 100 km), apparently have the same nitrogen-oxygen composition as the lower layers. In addition, despite most careful study of the spectra, it was impossible to detect indications of hydrogen in the glow of the high layers of the atmosphere.

16. Air Samples. Use of Mass Spectrometer

Soon after analysis of air samples collected aboard the stratospheric balloon "SSSR-1" (Section 15) revealed that air composition remains as homogeneously mixed to a height of 18.5 km as in the troposphere, attempts were made to obtain air samples from higher layers.

16.1. Air Samples. Until 1946 air samples were collected by stratospheric and pilot balloons. Great successes were attained by E. and W. Regener. They were able to obtain and investigate air samples from heights of 25-29 km. Extensive investigations were also made by Paneth (ref. 665). These experiments confirmed the results obtained on the stratospheric balloon "SSSR-1," but at heights greater than 20 km they noted a tendency to an insignificant separation of light and heavy gases. E. and W. Regener focused their attention on helium. It was possible to measure the content of this gas precisely and, because of its low atomic weight, especially significant vertical variations could be expected. It was found that the percentage content of helium increases from 0.00052 percent in the troposphere to 0.00054-0.00057 percent at a height of 20-25 km. Such an insignificant increase only slightly exceeds the limits of errors in analysis. If the atmosphere were in an equilibrium state of total diffuse separation of heavy and light gases in the Earth's gravitational field, the helium content at a height of 20 km should increase to 0.0045 percent, i.e., by a factor of almost 9.

The quantities of ions in the stratosphere have also been measured (ref. 539).

After 1946, when rockets were used for sending instruments into far higher layers of the atmosphere, one of the principal problems of rocket investigations was the study of air composition. Was there a more significant separation of light and heavy gases above 30 km ? To what heights was the mechanism of vertical mixing effective?

The chief difficulty in the method of air sampling in the high layers is the considerable decrease of the quantity of gas collected in the cylinders. Samples obtained from a height of 18 km contained only 50 cm^3 of air, samples from a height of 30 km--9 cm^3, from a height of 60 km--0.2 cm^3, and from a height of about 100 km--only 2-3 mm^3 of air (these volumes have been reduced to normal conditions). Under these conditions there is an increase of requirements on attenuation of "outgassing" of the used apparatus, sorption and desorption of gas by the walls of the cylinder and gas release from the body of the rocket itself. The methods of laboratory analysis of samples become very complicated.

The great velocity of the rocket, which can exceed several times the speed of sound, also causes serious difficulties.

In the Soviet Union, in contrast to similar foreign investigations, samples are not taken by the rocket itself but by a special automatic container which

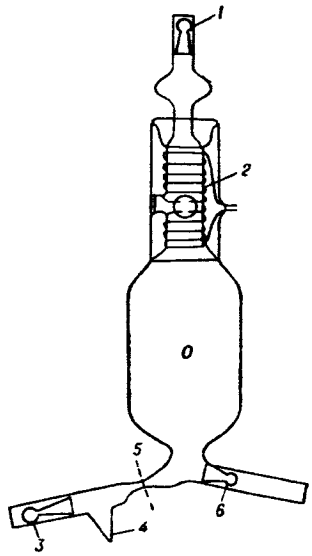

Figure 16.1. Cylinder for air sampling (B. A. Mirtov). 1, 3 and 6, extensions for sealing cylinder to laboratory apparatus for analysis; 2, electric heater for stopcock; 4, branch for initial evacuation; 5, sealing-off point.

separates from the rocket at a great height (Section 8). Glass cylinders with volumes of 0.4 and 3.0 liters are used in air sampling (fig. 16.1).

Glass cylinders have advantages over the metal cylinders used in foreign investigations. They possess the greatest vacuum efficiency with respect to outgassing, and the gases, including oxygen, nitrogen and argon are well retained in them. The most important part of the cylinder is a stopper, which should open the cylinder automatically at a particular time and then reliably seal it (airtight) after a specified time. Of the various stoppers tested, those which have proven effective are a mercury seal and vacuum stopcocks using ceresin wax (ref. 123) (ceresin is a mineral wax, a mixture of solid high-polymeric hydrocarbons of the paraffin series C_nH_{2n+2}).

In studies of air composition in the high layers of the atmosphere carried out in the USSR, an average of 2-5 days passes from the time of taking the air sample to its analysis (in American scientific work the time lapse is 1.5-18 months). During this time, sorption and desorption can change the gas composition of the sample appreciably, and it is desirable, therefore, to create good conditions for storing the sample. This is accomplished by transferring the sample from the cylinder to a narrow capillary immediately after it is taken. The air sample is compressed to a great pressure (such as atmospheric). In this case the surface of the glass, on which the sorption phenomena are dependent, can be decreased by a factor of 10^4 or more.

A somewhat different method for sampling air has been used in the United States, where the principal investigations were made during rocket sounding of the atmosphere over the test grounds at White Sands, New Mexico. The method of air sampling was developed by the Aerodynamics Department, University of Michigan, under the direction of Jones (ref. 493). Analysis of the samples was carried out with the participation of the Radio Chemistry Laboratory, Great Britain, under the direction of Paneth (refs. 318, 319, 402 and 662).

The experimental difficulties already mentioned, which must be dealt with in rocket investigations of air composition, were the reason why the results obtained in the United States in the first experiments were partially erroneous. Certain later results must also be corrected.

The air samples were collected in steel cylinders carefully evacuated by vacuum pumps before placement on the rocket. Metal cylinders were used because only inert gases--argon, neon and helium--were used, for which storage in glass containers is unsatisfactory. In addition, the recovery (descent by parachute) of glass cylinders involves great difficulties. The cylinders were connected by a thin-walled tinplated copper tube to the "flow chamber" of the rocket, and then sealed. During the rocket flight atmospheric air penetrated through a narrow opening into the body of the rocket and passed through the flow chamber to a vent at the tail of the rocket. At a time established by the flight program the cylinder closed automatically; the cylinder was filled with air from the flow chamber. After several seconds the cylinder was again sealed automatically. The cylinders falling to the Earth are removed to a laboratory where the air from them is pumped into glass containers and shipped to agencies for chemical analysis.

16.2. Analysis of Air Samples. There are many methods for chemical analysis of gas mixtures, but they are unsuitable for analysis of the small quantities of gas in the samples collected from great heights (70-80 km or more). Therefore, for investigations of the air composition at great heights in the atmosphere, it was necessary to develop a new technique of microanalysis, suitable for analysis of fractions of 1 mm^3 of the gas mixture.

In the 1930's, when air samples were obtained from the stratosphere using stratospheric and other balloons, the analysis of air samples was carried out on the basis of a limited program, and specifically for the content of only two gases: helium and oxygen. But by the late 1940's samples taken from the high layers of the atmosphere by rockets using a broader program could be investigated by this method. The quantity of oxygen, nitrogen, argon, neon and helium was determined (refs. 123 and 661). In foreign countries a physicochemical method of analysis is used for these purposes. This method consists of fractional separation by alternate absorption of different components by special absorbents; the remaining components (nitrogen, inert gases) are separated by fractional sorption on charcoal cooled by liquid air. The quantity of any gas is judged from the residual pressure in the apparatus, measured with great accuracy at all stages of the process. This method of analysis was proposed by Langmuir as early as 1912 and developed for use in these atmospheric investigations by Paneth and Glückauf (refs. 402 and 663) in 1946. The method permits highly accurate analysis of the composition of a gaseous mixture, if its quantity is not less than several mm^3.

The method of quantitative spectral analysis of gaseous mixtures developed by S. E. Frish was used in the Soviet Union for analysis of small quantities of gas. With this method 2-3 mm^3 of air (under normal conditions) can be analyzed. Further improvement of the method (ref. 123) made it possible to analyze tenths and even hundredths of a mm^3 of air. On the average the spectral analysis method has a relative error in determination of the quantity of any gas in a mixture of about 5-6 percent.

The first experiments in the United States gave an unexpected result--total absence of oxygen in the samples. Later it was found that the reason for this serious defect of the method was the "combustion" of oxygen during heating at the time of sealing the cylinder: the oxygen oxidized the copper from which the tube connecting the cylinder and flow chamber was made, when this tube was heated during sealing (see Riesbeck and Vyborg, Martin, ref. 13).

In the second stage of these investigations in the United States it was established that, beginning at a height of 60 km, there is an appreciable separation of light and heavy gases. The ratio $He:N_2$ in the air samples was twice as great as at the Earth's surface. There was also a small increase of the $Ne:N_2$ ratio and a small decrease of the $Ar:N_2$ ratio, shown in Table 16.1 (ref. 412).

TABLE 16.1. RESULTS OF ANALYSIS OF AIR SAMPLES OBTAINED BY ROCKETS FROM HIGH LAYERS OF ATMOSPHERE.

h км	*V* см³	Separation factor		
		He	Ne	Ar
1	2	3	4	5
50.4—53.3	8,6	0.981	1,003	0.008
54.7—58,3	2.04	1.01	—	1.009
55.6—58.2	6.78	0.998	1.005	1.001
58.2—60.3	5,15	1.035	1.008	0,996
57.0—64.3	0,398	1.133	1.040	0.962
64.3—67.0	0.415	1,44	1.08	0,929
64.3—71.0	0,204	1.57	1.23	0.90
67.0—69.6	0,218	2.02	1.18	0.89
69.6—71.8	0,232	2,41	1.20	0,85
84.4—89.0	0,015	2,95	1.39	0.82
89.0—93.2	0.0032	—	—	0.82

Column 1 of Table 16.1 gives the intervals of height h during the rocket flight within which air samples were taken; column 2 gives the total air quantity V (reduced to normal conditions) recovered from the high layers of the atmosphere in 81 steel cylinders. Column 3 shows the separation factor of

helium, i.e., the ratio He:N_2 in a sample divided by the He:N_2 ratio in surface air; columns 4 and 5 give the same values for neon and argon. If the separation factor is equal to unity, this means an absence of separation of atmospheric components; values greater than unity indicate enrichment of air by a particular gas, and values less than unity indicate impoverishment.

However, these results, obtained with great difficulty by numerous scientists, now are becoming somewhat doubtful due to possible imperfection of the method.

16.3. Occurrence of Diffusion Separation of Gases in the Mesosphere. The following is the basis for doubts as to the reality of changes of the separation factor for helium, neon and argon with height, indicated in Table 16.1. It was established that the apparatus used for sampling of air can itself create an apparent diffuse separation of heavy and light gases and, therefore, the results obtained in the atmosphere cannot be considered final; further investigations are required (ref. 493). The problem is the character of the flow of gases through the tube connecting cylinder and flow chamber. The most rigorous theory of this process was developed by A. I. Repnev (ref. 166a). The atmospheric air from this chamber fills the cylinder through this tube in only a few seconds (due to the great velocity of the rocket, its height changes so rapidly that all the measurements must be made in a short time, because otherwise the height to which the result must be related becomes too ambiguous). But under conditions of great rarefaction of the atmosphere at great heights, where the length of the free path of molecules ceases to be a small value in comparison with the dimension of the tube, the rate of filling of the cylinder with gas from the flow chamber, proportional to the pressure difference $p_2 - p_1$, is dependent on the molecular weight m of the gas. Under such conditions there is free molecular flow in which the flow b rate per second is dependent on the nature of the gas using the Knudsen formula

$$b = \left(\varepsilon p + \frac{1}{Z}\right)(p_2 - p_1), \tag{16.1}$$

where $\varepsilon = \frac{\pi r^4}{8\eta l}$ is the Poiseuille factor (r and l are radius and length of the tube, η is viscosity), Z is a function of the molecular weight m and the diameter of the tube; the numerical value of this function is proportional to $m^{1/2}$. The smaller the value m, the greater is b. If the time during which the tube is open and the cylinder is filled with air is not long, the content of the cylinder can differ somewhat from the outside air in the direction of a predominance of light gases.

Taking these circumstances into account, in a report presented at a session of the Royal Society of Great Britain on Mar. 26, 1954, Paneth set forth his opinion of the results (presented in Table 16.1) as follows: "It is still an unsolved problem as to what air composition in cylinders coincides with the composition of the air medium from which samples are taken; it must be remembered

TABLE 16.2. SUMMARY DATA ON AIR COMPOSITION AT GREAT HEIGHTS.

h km	Pressure in cylinder, mm	Gas in % of volume		
		O_2	N_2	Ar
65	0.17	19.0	80	0.91
75—80	0.020	21.0	78	0.93
	0.025	21.0	78	0.93
80	0.011	21.5	78	Weakly
	0.010	19.0	80	0.86
	0.015	22.0	77	0.87
	0.008	23.0	76	0.90
82—85	0.004	24.5	74	0.77
	0.0037	20.5	78	0.79
	0.0044	19.0	80	0.91
85	0.0037	21.0	78	0.86
	0.0032	21.0	78	0.90
	0.0034	21.0	78	0.88
95	0.0012	21.5	77	0.76

that the conditions under which the samples are taken are extremely unusual, because the rocket is moving at supersonic velocity through an extremely rarefied gas, and it is not impossible that the separation of light and heavy gases occurs only at the time of collection of the samples... At this time it is impossible, on the basis of theoretical investigation of the problem, to say anything definite concerning our results (Table 16.1--Author's note) for heights exceeding 60 km... The only way to solve this problem is to continue rocket experiments under the most varied conditions for taking air samples" (ref. 664).

We will now turn to the results of investigations made in the USSR. Table 16.2 gives summarized data for measurements made in 1951-1956 (ref. 123).

The following conclusions can be drawn from this table.

1. There is no appreciable change in the $\frac{O_2}{N_2}$ composition to a height of 95 km, i.e., the air composition remains nitrogen-oxygen.

2. At heights of 85-95 km the quantity of the heaviest gas, argon, is somewhat less than on the surface of the Earth.

The first of the conclusions is of basic significance and can be regarded as reliably established.

However, final solution of the problem of whether the small decrease of the percentage of argon indicates the existence of diffusion separation at heights of about 100 km is possible only by accumulation of measurements at the greatest possible heights and by an increase of accuracy of measurements. We will return to the existence of diffusion separation of heavy and light gases after familiarization with mass spectrometer measurements.

16.4. Mass Spectrometer Measurements. The air sampling method discussed above has certain shortcomings and involves certain difficulties. As we have seen, the very process of sampling air by use of rocketborne cylinders sometimes can change the air composition. The cylinders must be returned to Earth intact, but this cannot always be done in the case of glass cylinders. Further changes of the composition of the air in the cylinder can occur during storage. The ceiling for its use is also limited. It might be possible to overcome these shortcomings if analysis of air composition could be made directly in the free atmosphere, i.e., in flight, and if the readings could be transmitted telemetrically to Earth. However, development of such a method involves difficulties, because the measurements are made in the rarefied layers of the atmosphere with a rapidly flying rocket. The method, obviously, should be particularly sensitive and extremely fast-acting (low-inertia instruments should be used). These requirements could be satisfied by a method based on the use of a mass spectrometer. However, this method requires complex apparatus, and it is very difficult to adjust its operation on a rocket. It is not surprising, therefore, that the first attempts of this kind, begun as early as 1949, were unsuccessful. A number of rocket launchings with mass spectrometers in 1949-1951 were unsuccessful. In 1953, however, the difficulties finally were overcome, and the first data were obtained (ref. 770). Several successful investigations of this type have already been made.

The measurements are made with a Bennett radio-frequency mass spectrometer. In contrast to an ordinary mass spectrometer, it does not require a magnetic field. In the first section of the instrument the air entering from the atmosphere is subjected, first, to ionization by bombardment by electrons; the air is then sucked into the main section. The latter is a tube with a system of grids. A negative potential is applied to the first grid, creating a field drawing ions into the tube. An accelerating voltage is applied to the second grid. The acceleration imparted to the ions is dependent on their masses, and maximum velocity is acquired by those ions whose movement occurs at a certain velocity and in a certain phase relative to the times of change of field sign. The third grid is for deceleration; it creates a reverse field and traps all ions except those with maximum velocity. Ions which overcome the decelerating field reach the anode; a large resistance is applied to the external circuit. The anode current creates a relatively large potential drop at the ends of the resistance, and this is fed to the input of a dc amplifier and then to the telemetric transmitter.

Gases released from the surface of the rocket are a major source of errors.

The accuracy of laboratory calibration of the mass spectrometer is approximately 20 percent; an additional scatter of readings of about 15 percent is caused by the noise of the dc amplifier. Special telemetric apparatus has been devised for transmission of mass spectrometer readings to the Earth (ref. 788).

Various kinds of methodological difficulties are encountered in making a direct analysis of the gas composition of the high layers of the atmosphere with mass spectrometers. For example, one of the difficulties in measurement of the neutral composition of the atmosphere, using a radio-frequency mass spectrometer, is that the instrument reacts identically both to a direct flux

of particles of undisturbed composition and to a reverse flux of particles which have experienced multiple collisions with the walls of the instrument and are essentially deprived of atomic components (recombination and reaction on the walls). Much attention must therefore be given to further improvement of the mass spectrometer measurements method (refs. 75 and 154).

The first successful measurements (ref. 770) were made at nighttime on Feb. 12, 1953, when a mass spectrometer was carried aloft by an Aerobee NRL-13 rocket at White Sands Proving Ground to a height of 137.3 km. The second successful experiment was carried out by Meadows and Townsend, also under nighttime conditions (at 2200 hours), on Dec. 12, 1955, when a mass spectrometer was carried aloft by an Aerobee NRL-28 rocket. A Bennett mass spectrometer was used, but a somewhat improved model (ref. 587). In order to increase the resolution, the three grids were supplemented by a fourth, and the strength of the electron emission in the preliminary ionization chamber was increased. The instrument made mass measurements in the spectral range between the values of atomic weights 56 and 6.

It must be remembered that the ratio of the anode currents and the height of the peaks on the trace measured in these experiments are dependent not only on the relative quantity of the corresponding gases in the air, but also on their capacity for ionization in the preliminary ionization chamber. Furthermore, if the pressure in the spectrometer is high (about 10^{-4} mm Hg), the instrument readings also are dependent on the ion cross section in comparison with the cross section of neutral molecules (ref. 587).

The mass spectrometer measurements of Feb. 12, 1953, revealed that the ratio of the quantities of argon and nitrogen remains approximately constant to a height of 137 km. From an estimate of the accuracy of the measurements we can conclude that if the diffusion separation of nitrogen N_2 (molecular weight 28) and heavier argon (atomic weight 40) began at a height of 60 km, as was determined initially from an analysis of air samples (see Table 16.1), the change of the ratio $\frac{Ar}{N_2}$ at a height of 130 km would be quite large and would be detected by the mass spectrometer (ref. 770). On this basis it was concluded that diffusion separation does not occur to a height of 137 km.

One of the mass spectrograms obtained Dec. 12, 1955, was recorded telemetrically in a period of approximately 1 sec during the descent of an Aerobee rocket, when the axis of the rocket formed an angle of 11° to the vertical and the rocket was moving tail first at a velocity of 1.06 km/sec. According to these data (ref. 587), under such conditions the pressure in the mass spectrometer could be an entire order of magnitude less than the true pressure in the atmosphere. The spectrogram has peaks corresponding to the usual air components: CO_2 (and N_2O)--mass 44 atomic units, Ar--mass 40, O_2--mass 32 and 16, N_2--mass 28 and 14 and water vapor--mass 18. There also were peaks for masses 46 and 23.

Atomic ions O and N can be formed in the preliminary ionization chamber of the spectrometer, and therefore the presence of masses 16 and 14 on the spectrogram does not necessarily indicate the presence of atomic oxygen and nitrogen in the free atmosphere (ref. 587). It can be assumed that particles with mass 46 and NO_2 molecules and those with mass 23 are Na atoms. The first of these were observed at heights of 80-88 km and the second at heights of 75-90 km; in both cases the maximum value of the peak on the spectrogram was at a height of 85 km.

Whereas these two mass spectrometer experiments made at latitude 33°N (White Sands Proving Ground) gave no indications of the existence of an appreciable diffusion separation of light and heavy atmospheric components, somewhat different results were obtained from atmospheric sounding over Fort Churchill (59°N). Meadows and Townsend (ref. 588) sent a radio-frequency mass spectrometer aloft to a height of 241 km on Nov. 20, 1956, in an Aerobee-Hi rocket. A total of 96 spectrograms in the interval from 6 to 52 atomic mass units was obtained on the ascending branch of the trajectory at heights of 105-241 km, and 7 additional spectrograms were obtained during rocket descent. The ratio $\frac{Ar}{N_2}$ was determined; at the surface of the Earth this was assigned the value unity (separation factor). It was 0.5 at a height of 115 km and gradually decreased with height to about 0.2 at the 140-150-km level. Having analyzed these data, Meadows and Townsend concluded that, during the period of measurements over Fort Churchill, there was diffusion separation of argon and nitrogen beginning at a height of approximately 105 km; above the 112 km level there was diffusion equilibrium of these gases. After comparing these conclusions with the preceding results of measurements over White Sands, where no such diffusion separation was observed, Meadows and Townsend concluded that the reason for this difference could be related either to the great difference of geographic latitude between these two points (59 and 33°N) or to the fact that the experiments were made at different times.

New soundings during the IGY period led Meadows and Townsend to the conclusion that diffusion separation in the Arctic atmosphere begins at a height of about 110 km (ref. 589). Johnson, after generalizing the results of mass spectrometer investigations of the high layers of the atmosphere made by the United States Naval Research Laboratory over a 10 year period, concluded that the diffusion separation of gases in the gravity field in the northern hemisphere begins between 100 and 120 km (ref. 480).

Important mass spectrometer investigations of the structural parameters of the Earth's atmosphere at heights from 100 to 210 km have been made in the USSR by A. A. Pokhunkov (ref. 155). He used a five-stage radio-frequency mass spectrometer for study of the neutral composition of the upper layers of the atmosphere. He demonstrated that the concentration of atomic oxygen at a height of 200 km is not less than 10 percent of the concentration of molecular oxygen. Measurement of the relative concentration of the inert gas argon in comparison with molecular nitrogen shows the presence of diffusion separation at heights greater than 100 km.

16.5. Determination of Ion Composition of the Ionosphere. The radio-frequency mass spectrometer method has been used repeatedly for determination of the ion composition of the ionosphere. Extremely important investigations have been made using Soviet artificial Earth satellites, and also geophysical and space rockets. A radio-frequency mass spectrometer of the type described was used, but without a preliminary ionization chamber. When making ionospheric investigations, the ions were collected from the free atmosphere directly into that section of the spectrometer where the analysis is made.

The first measurement was made in the United States on May 7, 1954, on a Viking No. 10 rocket, at 1000 hours. The mass spectrometer recorded the presence of positive ions with an atomic weight from 8.2 to 49.2. The measurements were made at heights of 93-219 km; the most clearly expressed peaks on the mass spectrogram were in the 93-124 km layer. The results (ref. 482) were regarded as preliminary, requiring confirmation in later experiments, because part of the record was difficult to explain. The measurements were also distorted by the charge of the body of the rocket, appearing and changing during the course of the flight, and by the release of gases from the rocket. At heights of 93-124 km there was a predominance of ions with weights 16, 26, 30 and 32; the presence of positively charged particles with atomic weights 12, 18, 19, 21, 23, 38 and 45 was less clearly expressed. Above 124 km there was a predominance of ions with mass of 16 and 32 atomic units.

On the basis of these measurements it can be assumed that the air in the high layers of the atmosphere (above 93 km) consists of atoms and molecules having the following atomic weight (the tentative identification of these ions is given in parentheses)

12* (C)	16* (O)	18* (H_2O)
19* (F or H_3O)	21	23 (Na)
26* (CN or C_2H_2)	30* (NO)	32* (O_2)
38*	45	48 (?)

The asterisks denote values obtained earlier by Townsend, Meadows and Pressly (ref. 770) during an investigation of air composition by a spectrometer with a preliminary ionization chamber.

The next experiment was carried out at nighttime on 8 June 1955. A similar mass spectrometer was carried aloft on an Aerobee rocket to a height of 120 km. Additional steps were taken for prevention of a distorting influence of the rocket and its gases. Analysis of the telemetric data revealed that these steps apparently were successful (ref. 481). Positive ions, with mass number 28, probably N_2^+, were found to exist in the 98-120 km layer. Negative ions and ions with other atomic weights were not discovered, although the sensitivity of the spectrometer was adequate to detect them, if their concentration was not less than 1 percent of the N_2^+ concentration. The experiment was repeated half a year later in the daytime. Two mass spectrometers were carried aloft to a height of 131 km on Nov. 29, 1955, at 1016 hours on an

Aerobee rocket. The data obtained differed appreciably from the results of the nighttime measurements (ref. 483). No positive ions at all were discovered, but the presence of negative ions with atomic weights 46, 32, 29, 22 and 16 was established. Ions with a mass 46 predominated, and their quantity was approximately 96.5 percent. It can be assumed that these are NO_2^- ions. Ions with mass 32 (O_2^-) and 16 (O^-) were present in quantities of about 1.6 and 0.7 percent. Masses 29 and 22 are not encountered among the known components of the atmosphere; their identification is difficult.

Extremely important information on the composition of the highest layers of the ionosphere has been obtained in the USSR. A single-stage geophysical rocket, which reached a record height of 473 km, was launched in the middle latitudes of the European part of the USSR Feb. 21, 1958, at 1142 hours Moscow time, in accordance with the IGY program. The numerous instruments for complex investigation of the upper layers of the atmosphere, with a total weight of 1,520 kg, included a mass spectrometer, mounted in a container carried aloft to a height of more than 200 km. The instrument sensor was a mass spectrometer tube directly open to the atmosphere.

Study of the telemetric records gave data on the ion composition at heights from 105 to 206 km. It was found that at these heights there is a predominance of ions with mass number 30; these can be interpreted as nitrogen oxide molecules NO.

Ions with mass number 16 also were recorded in the upper part of the trajectory; these were ions of atomic oxygen.

Interesting considerations of the processes influencing the ion composition of the high layers of the atmosphere (molecular ions) have been published by A. D. Danilov (ref. 50).

16.6. Measurements by the Third Soviet Artificial Earth Satellite. The third Soviet artificial Earth satellite, weighing 1,327 kg, was launched on May 15, 1958. The total weight of the scientific and measurement apparatus and power sources carried in the satellite was 968 kg. The satellite trajectory was at an altitude up to 1,880 km above all the points on Earth between the Arctic and Antarctic Circles. The satellite also carried apparatus for study of the spectrum of the masses of positive ions (ref. 71). The mass spectrometer tube entrance was directly exposed to surrounding space. The tube contained a number of fine wire grid electrodes situated at definite, precisely specified distances apart. The grids were followed by a collector, a metal plate for collecting the ions entering the mass spectrometer tube and passing through all grids.

Different direct and alternating voltages from the electronic unit of the mass spectrometer were fed to the electrodes in the tube. These voltages were selected in such a way that only those ions could reach the collector which had passed through the tube with some optimal velocity. The ions passing through with velocities greater or less than the optimal velocity did not reach the collector. The velocity at which the ions pass through the mass spectrometer

tube is determined, on the one hand, by their mass and, on the other hand, by the voltage applied across certain of the tube grids, resulting in acceleration of the ions.

The accelerating voltage periodically changes from zero to its maximum value. As a result, optimal velocity is imparted alternately to ions with different mass numbers. When ions reach the collector, a current pulse develops in its circuits which is amplified and transmitted to Earth by the telemetric system. The accelerating voltage across the grids in the mass spectrometer tube at that particular time is transmitted simultaneously.

If there are only ions of a single mass in the ionosphere, the receiving station records one pulse of the ion current per cycle. The mass number of ions corresponding to each pulse can be determined by comparison of the record of the spectrum of the masses with the record of the accelerating voltage of the mass spectrometer. The principal difficulty involved in the interpretation of the mass spectra of the ions is separation of the principal (true) mass peaks from the harmonic (spurious) peaks. Figure 16.2 gives some idea of the character of the record of the spectra; it shows copies of four traces received from the third Soviet artificial Earth satellite (ref. 72).

In all spectra the most clearly expressed peak was one whose mass number was close to 16, after introduction of a correction taking satellite velocity into account. On this basis the peak was identified with the peak of atomic oxygen O^+.

The mass spectrometer measurements made by V. G. Istomin show that there is a predominance of ions of atomic oxygen in daytime at heights from 225 to 1,000 km in the ionosphere. Molecular ions of nitrogen, nitrogen oxide, oxygen and ions of atomic nitrogen were also detected. The content of molecular ions decreases rapidly with an increase of height. Beginning at 500 km the atmosphere becomes atomic. A dependence of ionospheric composition on latitude was also established. These results, which are of basic importance, are illustrated in figures 16.3-16.5.

According to data presented by V. G. Istomin (ref. 72) the altitudinal dependences of the relative concentrations of molecular ions of oxygen, nitrogen and nitrogen oxide have an approximately identical character. Maximum intensity is characteristic of the ion of nitrogen oxide; its intensity at a height of about 230 km is 25-35 percent of the intensity of an ion of atomic oxygen. The molecular ion of second greatest intensity is oxygen ion O_2^+. Its intensity at perigee was approximately 7-12 percent in relation to atomic nitrogen. The intensity of the peak of molecular nitrogen at perigee was 1.5-3 percent.

An unusual characteristic of figures 16.3-16.5 is that all derived curves break down clearly into two branches: southern and northern. The points in the figures are numbered in the sequence of increase of geographic latitude: points 1 and 2 apply to southern latitudes (before perigee) and points 3-7 to northern latitudes (after perigee). On all curves the southern branch passes

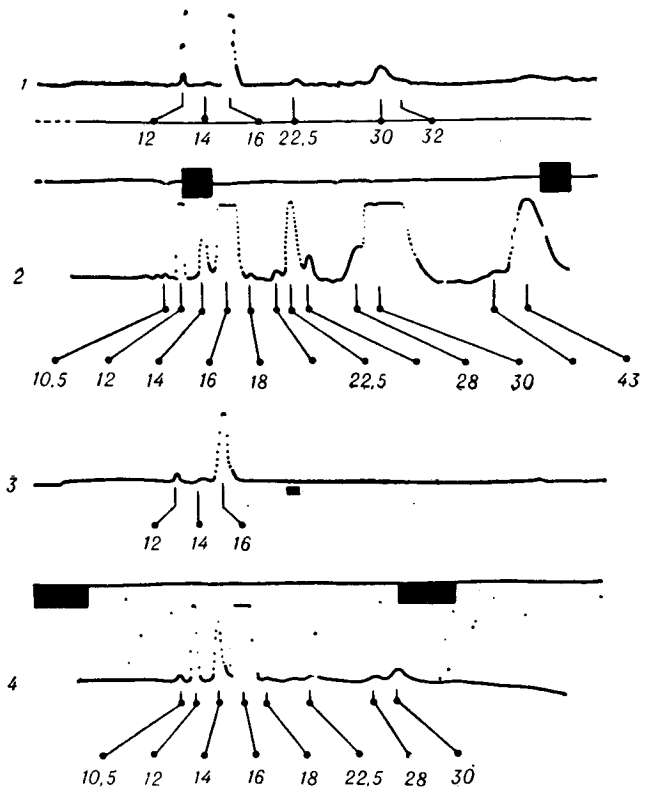

Figure 16.2. Records of mass spectra of ions obtained by third Soviet artificial Earth satellite, May 23, 1958, at about 0900 hours, Moscow time.
1, 2, records from low- and high-sensitivity channels of mass spectrometer amplifier, height 230 km, 55°N;
3, 4, same, height 350 km, 64°N.

below the northern branch, indicating an increase of concentration of ions of nitrogen oxide, molecular oxygen and molecular nitrogen, relative to the concentration of ions of atomic oxygen with an increase of geographic latitude.

The peak of the ion of molecular oxygen is traced to a maximum height of 400 km, where the relative intensity of O_2^+/O^+ peak is about 0.1 percent; the peaks of ions of nitrogen oxide and molecular nitrogen are traced to a height of 500 km. At heights of 400-500 km the intensity of NO^+ and N_2^+ peaks in relation to O^+ becomes approximately identical, and equal to 0.2-0.1 percent. Thus, only above 500 km is there an absence of molecular ions: with an accuracy to 0.1 percent the ionosphere becomes purely atomic oxygen and atomic nitrogen (ref. 72).

Another basic result obtained by V. G. Istomin from mass spectrometer measurements on the third Soviet artificial satellite applies to atomic nitrogen.

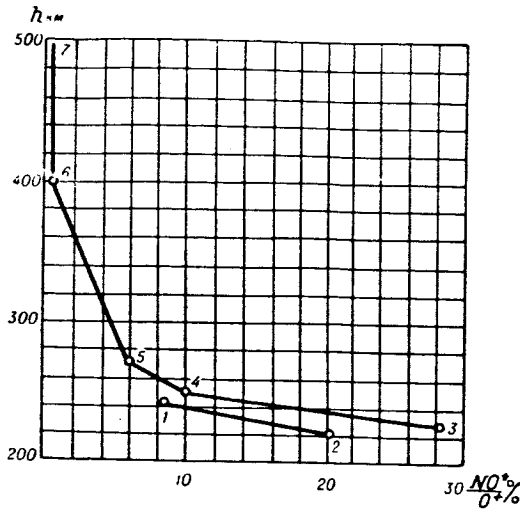

Figure 16.3. Change of relative intensity of ion peak of nitrogen oxide as function of height and geographic latitude (on basis of data for one revolution of the third Soviet artificial Earth satellite, May 22, 1958).

The ion current (peak intensity) of atomic nitrogen changes in relation to atomic oxygen as a function of height and geographic latitude in the range from 1.3 to 8-10 percent. There is a definite tendency to an increase of the (relative) content of ions of atomic nitrogen. This dependence is represented graphically in figure 16.6. The ratio of intensities plotted along the X-axis is close to the ratio of concentration of ions of atomic nitrogen and oxygen (ref. 72). Each point on the graph was determined as a result of averaging of measurements

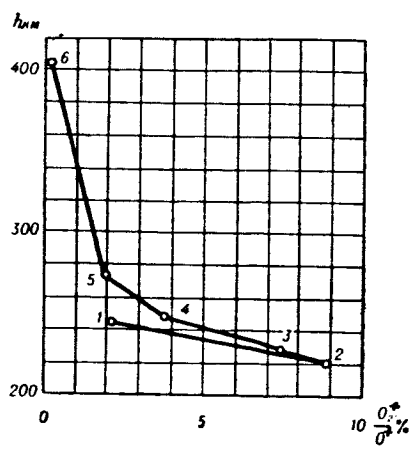

Figure 16.4. Change of relative intensity of ion peak of molecular oxygen as function of height and geographic latitude (on basis of data for one revolution of the third Soviet artificial Earth satellite, May 22, 1958).

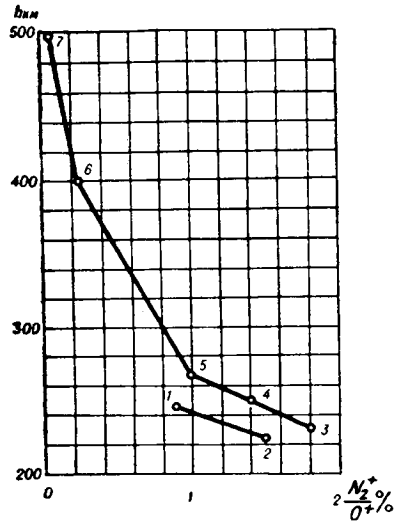

Figure 16.5. Change of relative intensity of an ion peak of molecular nitrogen as function of height and geographic latitude (on basis of data for one revolution of the third Soviet artificial Earth satellite, May 22, 1958).

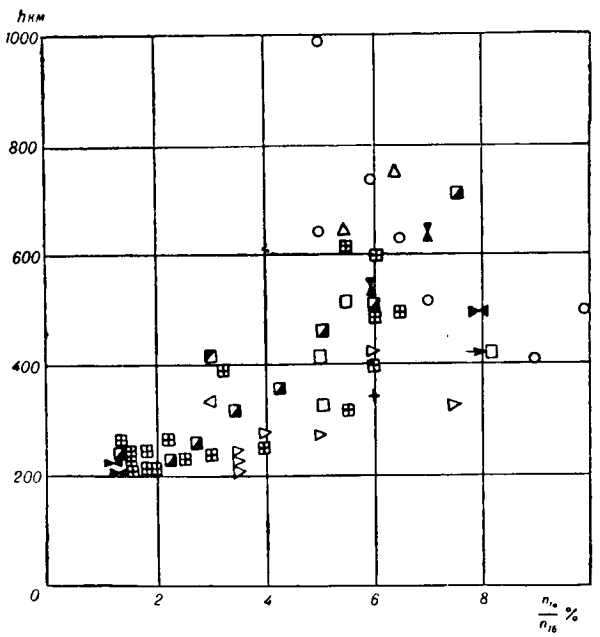

Figure 16.6. Change of ion concentration of atomic nitrogen in relation to ions of atomic oxygen as a function of height (on basis of data from 12 revolutions of third Soviet artificial Earth satellite, May 18-24, 1958).

of several spectra (from 5 to 20 spectra). The different points relate to different revolutions around the Earth. There is a rather great scattering of points, at certain heights attaining ±3 percent, in part not caused by random measurement errors, but reflecting real changes in the composition of the ionosphere from day to day and from one revolution around the Earth to the next. Mass spectrometer measurements on the third satellite also established that ionospheric composition is dependent on geographic latitude. The relative content of ions of atomic nitrogen at heights of 225-350 km increases considerably with transition from the region 30-50°N to the region 55-65°N. The relative content of ions of molecular nitrogen, molecular oxygen and nitrogen oxide also is considerably greater in the region 55-65°N than at more southerly latitudes (ref. 72). Mass spectrometer investigations of the ion composition of the upper layers of the atmosphere are continuing vigorously (refs. 73, 74, 76, 77 and 758).

16.7. Quantity of Nitrogen Molecules. Ghosh and Sharma made interesting counts of the quantity of nitrogen molecules situated above the levels 95, 100, 105, 110 and 120 km (ref. 401). They used rocket measurement data on the intensity of solar x-radiation of different wavelengths (column 2, Table 16.3).

TABLE 16.3. QUANTITY OF NITROGEN MOLECULES ABOVE DIFFERENT LEVELS AS DETERMINED BY DIFFERENT AUTHORS.

h km	Ghosh and Sharma	Kallmann, Waite and Newell	Miller
95	$1.1 \cdot 10^{19}$	$4.0 \cdot 10^{19}$	$3.8 \cdot 10^{19}$
100	$7.7 \cdot 10^{18}$	1.4	1.2
105	4.3	$8.3 \cdot 10^{18}$	$7.0 \cdot 10^{18}$
110	3.4	3.2	2.6
120	1.9	$9.0 \cdot 10^{17}$	$7.0 \cdot 10^{17}$

16.8. Artificial Luminescence of the Atmosphere. Interesting data on the composition of the high layers of the atmosphere can be obtained with rockets by filling them with various chemical reagents. Upon reacting with various atmospheric components, certain reagents can cause chemiluminescence. The behavior of the luminescent cloud forming as a result of this reaction can be studied in certain respects by observations from the Earth's surface. Since discussion of these problems does not fall within the scope of this book (they are discussed in reference 233), only a brief listing of the principal reactions will be given here.

The ejection of 8.3 kg of nitrogen oxide at a height of 105 km at nighttime was accompanied by the formation of a luminescent cloud with a diameter of several km. The luminescence was formed by reaction between NO and atmospheric atomic oxygen. It can be used to estimate the concentration of the latter. In order to make a similar estimate of the concentration of atomic nitrogen, an attempt could be made to use reactions with hydrocarbons and their chlorine derivatives. The ejection of ethylene (1957) indicated the presence of N atoms in the atmosphere. More intense luminescence could be produced

by a reaction with CH_2Cl_2. Daytime ejection of NO at a height of 95 km caused the formation of an ionized cloud. Various alkali metals (sodium, calcium, cesium) have been used for similar purposes. The ejection of ozone can facilitate the checking of an important reaction in the atmosphere, accompanied by the emission of a hydroxyl (ozone-hydrogen reaction). The introduction of reagents possessing a high electron affinity, such as SF_6, into the atmosphere could decrease the natural local electron concentration (ref. 715).

17. Theory of Diffuse Separation of Gases in the Atmosphere

If the air were initially completely mixed and farther aloft convective, and all other movements leading to mixing ceased at a certain level, after a certain time the individual components would be redistributed vertically under the influence of molecular diffusion. The equilibrium state in the region above this level would correspond to Dalton's law--each gas would be distributed as if other gases were absent. The density of the q component of the atmosphere (q = 1, 2, 3,...) would change with height h proportional to $\exp\left(-\frac{h}{H_q}\right)$, where H_q is the height of the homogeneous atmosphere for a particular component. Strictly speaking, the time required for establishment of the Dalton state is infinitely great, but it is possible to compute the time in which a state is established differing from an equilibrium state by a stipulated small value. Such computations were made by Morris, Epstein, Mitra and Raksheet (ref. 127), Nicolet (refs. 628 and 629) and Mange (ref. 638). It was found that years are required for the establishment of any perceptible diffuse separation in the stratosphere. The diffuse separation of heavy and light gases in the Earth's gravitational field is, therefore, an extremely slow process, which explains the homogeneous composition of the air to great heights: very weak convection is adequate for bringing the effect of molecular diffusion to a complete standstill.

However, the diffusion coefficient D increases rapidly with height; it is inversely proportional to air density. The effect of diffuse separation in the upper layers of the atmosphere can be appreciable. According to computations made by Mitra and Raksheet (ref. 127), there is no appreciable diffuse separation at a height of 100 km after 1,000 hours, but at a height of 125 km the degree of diffuse separation attained after this time is 3 percent, at a height of 150 km it is 10 percent, and at an altitude of 200 km it is 45 percent.

We will now consider, in greater detail, the method for computing the rate of diffuse separation as given by Chapman (ref. 326), taking into account the influence of the vertical distribution of air temperature.

17.1. Computation of the Rate of Diffuse Separation. We will consider the simplest case when the gas consists only of two components whose molecules have the masses m_1 and m_2, and for unambiguity it will be assumed that $m_1 > m_2$. It will be assumed that only the external gravitational forces

$m_1 g$ and $m_2 g$ act on the molecules. The properties of the medium will be considered dependent only on height (horizontally stratified atmosphere). Finally, it will be assumed that an atmosphere of this kind is first mixed completely at all levels, and the way in which the separation of the heavy and light components occurs will be considered.

There should be equal but oppositely directed fluxes of molecules $n_1 w_1$ and $n_2 w_2$, caused by diffusion, relative to some plane through which there is no pure transport of molecules; here n_1 and n_2 are the concentrations and w_1 and w_2 are the mean velocities (directed vertically upward). Thus, $n_1 w_1 = -n_2 w_2$. It can be shown (refs. 322 and 334) that in this case the diffusion equation has the form

$$n_1 w_1 = -n_2 w_2 = \\ = -nD\left[\frac{d}{dh}\left(\frac{n_1}{n}\right) + \frac{n_1 n_2 (m_2 - m_1)}{np\rho}\ \frac{dp}{dh} + \frac{k_T}{T}\frac{dT}{dh}\right]. \tag{17.1}$$

Here $p = knT$ is pressure, $n = n_1 + n_2$, ρ is density, T is temperature, k_T is the thermal diffusion ratio.

We will consider the physical sense of each of three terms in the right-hand side of the equation. The first of these--the concentration gradient--exists when there is nonhomogeneity of composition. The part of the diffusion flux associated with it acts in such a way as to annihilate the gradient and make the composition homogeneous. Since it was assumed arbitrarily that the atmosphere is a homogeneously mixed medium, the first term must be considered equal to zero. The second term corresponds to the pressure gradient, which causes a flux of heavier molecules into the region of higher pressures. This process can be compared with the action of a separator which separates cream from milk: the heavier part of the milk is directed outward and the lighter part is directed toward the inner part of the separator. Similarly, in the atmosphere the heavier molecules tend to settle in comparison with the others. The third term is dependent on the temperature gradient: it determines the thermal diffusion flux whose direction is dependent on the sign of k_T. In general, this sign is such that the flux of heavier molecules is directed into the region of cold.

In this case there will be diffusion caused by the pressure and temperature gradients. The expression for the flux, dependent on diffusion in the pressure field, can be transformed by using the relations

$$\frac{p^{-1}\,dp}{dh} = \frac{d(\ln p)}{dh} = -\frac{1}{H}, \tag{17.2}$$

$$H = \frac{kT}{\bar{m}g} = \frac{RT}{\bar{M}g}, \tag{17.3}$$

where $\bar{m}$ and $\bar{M}$ are the mean molecular mass and the weight $n\bar{m} = n_1 m_1 + n_2 m_2$, respectively. The diffusion flux in the pressure field can be represented in the form of the product $\frac{nDA}{H}$, where

$$A = \frac{n_1 n_2 (m_2 - m_1)}{n^2 \bar{m}}. \tag{17.4}$$

Then we compute the coefficients D and k_T. The diffusion coefficient D is inversely proportional to n and therefore nD is dependent only on T. For many gaseous mixtures nD is proportional to T^S

$$nD \sim T^s, \tag{17.5}$$

where S is a constant (ref. 334). It is known that for O_2 and N_2, S = 0.79; since for T = 293°K and at atmospheric pressure D = 0.22, the following equation applies

$$nD = 0.22 \left(\frac{T}{293}\right)^{0.79} n_0, \tag{17.5a}$$

where $n_0 = 2.69 \cdot 10^{19}$.

The thermal diffusion ratio k_T also can be expressed in the form $\frac{n_1 n_2 \alpha}{n^2}$, where α is called the thermal diffusion factor (ref. 334). It is known that for O_2 and N_2 $\alpha = 1.018$, and the dependence on T and the ratio $\frac{n_1}{n_2}$ is so weak that it can be neglected.

17.2. Computation of Diffusion Fluxes. Chapman (ref. 326) computed the diffusion flux to a height of 80 km on the assumption that air consists of 79 percent N_2 molecules and of 21 percent O_2 molecules. In this case $k_T = 3 \cdot 10^{-3}$ and $A = -2.3 \cdot 10^{-2}$; a value 28.9 must be assumed for $\bar{M}$. In all his computations he used as a point of departure the vertical temperature distribution accepted in 1952 by the United States Rocket Committee (ref. 707).

This distribution has been represented by curve A in figure 17.1. After breaking the atmosphere down into layers 2-3 km thick (their boundaries have been indicated by the dots on the curves in figure 17.1) and using the formulas, Chapman computed the thermal diffusion flux $(n_1 w_1)_T$ and the diffusion flux in the pressure field $(n_1 w_1)_p$ (curves B and C, figure 17.1). The flux caused by the pressure gradient is everywhere negative (directed downward) and has a value of the order of $1.6 \cdot 10^{11}$ mol/cm^2 sec, varying little from level to level. The thermal diffusion flux B is far less (by two orders of magnitude), but its vertical variations are relatively great and in absolute value differ little from the $(n_1 w_1)_p$ variations. In addition, its sign changes from level to level; e.g., in the troposphere it is directed upward and in the stratosphere, in the 17-45 km layer, downward. On the whole, the diffusion flux everywhere is directed downward, since

$$(n_1 w_1)_p \gg (n_1 w_1)_T.$$

We will now determine at what rate molecular diffusion can change the concentration n_1 of molecules of any kind. Since

$$\frac{dn_1}{dt} = -\frac{d}{dt}(n_1 w_1),$$

it is possible to determine $\frac{dn_1}{dt}$ numerically for each level, finding the difference of fluxes $n_1 w_1$ from level to level from figure 17.1. However, this difference method, in which the values differ so little from one another, cannot give precise results. For this reason Chapman finds an expression for $\frac{dn_1}{dt}$ with values obtained by direct experimentation. Expression (17.1) can be used for $n_1 w_1$ for this purpose; here the diffusion flux in the pressure field is replaced by its value $\frac{nDA}{H}$. The following equation is then obtained for the desired velocity

$$\frac{dn_1}{dt} = -\frac{d}{dh}(n_1 w_1) = \frac{d}{dh}\left[-\frac{nDA}{H} + \frac{nD}{T} k_T \frac{dT}{dh}\right], \qquad (17.6)$$

in which A is a constant. After differentiating equations (17.3) and (17.5) we obtain

$$\frac{d(nD)}{dh} = \left(\frac{S}{T}\right) nD \frac{dT}{dh}, \qquad (17.7)$$

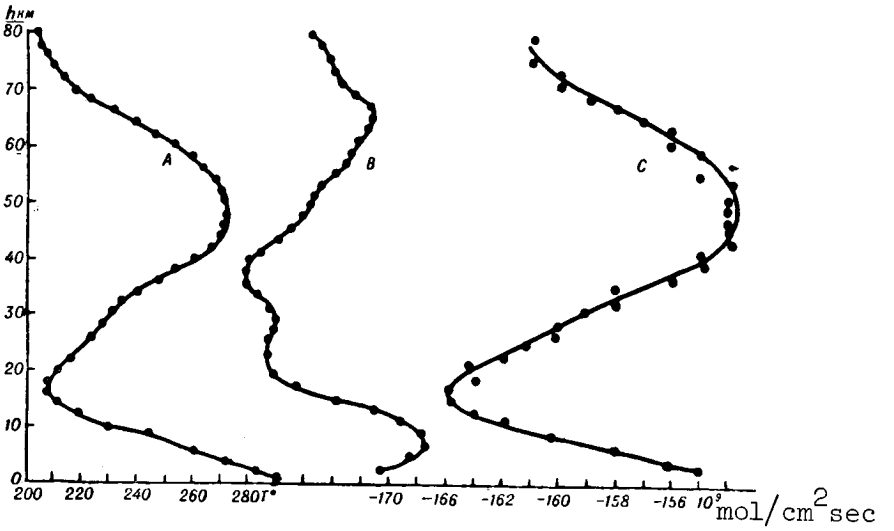

Figure 17.1. Computation of thermal diffusion and diffusion fluxes caused by pressure gradient.

$$H^{-1}\frac{dH}{dh}=T^{-1}\frac{dT}{dh}-g^{-1}\frac{dg}{dh}. \tag{17.8}$$

If a is the Earth's radius, then

$$\frac{g}{g_0}=\frac{a^2}{(a+h)^2},$$

therefore

$$g^{-1}\frac{dg}{dh}=-\frac{2}{a+h},$$

hence

$$H^{-1}\frac{dH}{dh}=T^{-1}\frac{dT}{dh}+\frac{2}{a+h}. \tag{17.9}$$

The value $\dot{n}_1=\frac{dn_1}{dt}$ consists of two terms determined by diffusion in the pressure field $\dot{n}_{1p}$ and by thermal diffusion $\dot{n}_{1T}$

$$\dot{n}_{1p}=\frac{d}{dh}\left(-\frac{nDA}{H}\right),$$

$$\dot{n}_{1T}=\frac{d}{dh}\left(\frac{nD}{T}k_T\frac{dT}{dh}\right).$$

Using (17.7) and (17.9), we obtain

$$\dot{n}_{1p} = (1 - S)\frac{nDA}{H}\frac{d(\ln T)}{dh} + \frac{2nDA}{H(a+h)}. \tag{17.10}$$

Differentiating the second term and substituting from (17.7) we obtain

$$\dot{n}_{1T} = k_T nD\left\{S\left[\frac{d(\ln T)}{dh}\right]^2 + \frac{d^2(\ln T)}{dh^2}\right\}. \tag{17.11}$$

The four terms of which $\dot{n}_1 = \dot{n}_{1p} + \dot{n}_{1T}$ consists, according to (17.10) and (17.11), can be computed directly because they contain values known from measurements. According to Chapman's computations, the term in the expression for $\dot{n}_{1p}$ caused by change of g with height is of the order of 500 mol/cm^{3}sec. It changes somewhat with height since $\frac{nD}{H}$ is dependent on T; its value is negative. The first term in $\dot{n}_{1p}$ is the most important; its sign is variable and its value is from 10^4 to -3,600. Curves of functions $\dot{n}_{1p}$ and $\dot{n}_{1T}$, computed by Chapman, are shown in figure 17.2, and a curve of function $\dot{n}_1$ (for O_2 molecules) in figure 17.3 (curve A).

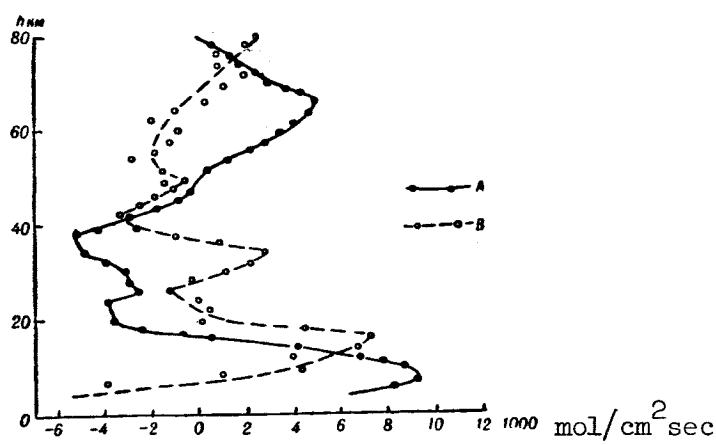

Figure 17.2. Rate of change of concentration of O_2 molecules caused by diffusion in the pressure field ($\dot{n}_{1p}$, curve A) and thermal diffusion ($\dot{n}_{1T}$, curve B).

In computing $\dot{n}_{1T}$ it is necessary to use the vertical second derivatives of ln T; their numerical value is determined with a large error. For this reason the $\dot{n}_{1T}$ curve in figure 17.2 (curve B) is shown as a smoothed dashed line drawn between the computed values. Similarly, $\dot{n}_{1p}$, the derivative of $\dot{n}_{1T}$, changes sign vertically; its numerical value varies in the range of $\pm 4{,}000$ $mol/cm^3 sec$.

Curve A in figure 17.3 shows that over the White Sands Proving Ground in the United States, the region to which Chapman's initial computational data on temperature apply, diffusion creates a tendency to increase O_2 concentration in the troposphere and stratosphere to a height of about 20 km, especially at the level of the tropopause where the increase of concentration exceeds 10^4 $mol/cm^3 sec$. This same tendency is observed above 55 km, but in the ozonosphere (20-55 km) the process has the reverse direction.

The rate of diffusion separation can change appreciably depending on local peculiarities of temperature stratification, e.g., at a level of about 70 km $\dot{n}_{1T}$, under certain conditions, can increase to 10^4.

The value $\dot{n}_1$ is such that the change of n_1 in 10^7 sec (4 months) does not exceed 10^{11}. Even at a height of 80 km, this is a small part of the mean concentration n_1 (about $4 \cdot 10^{14}$). A disruption of the temperature distribution, except for particularly large disruptions, scarcely changes the percentage of N_2 and O_2 at the indicated height.

17.3. Helium Diffusion. In Section 16 we discussed data from an analysis of air samples taken by rockets from the high layers of the atmosphere. We have seen that in these investigations it is of great importance to determine the quantity (percentage) of helium. Data on the rate of helium diffusion can also be of interest in computations of the dissipation of helium from the atmosphere. We will therefore discuss computations of helium diffusion. Whereas , for oxygen the ratio of the masses of molecules was $m_1 > \bar{m}$, the inverse relation $m_1 < \bar{m}$ applies for helium; for this reason the sign of A also becomes opposite, and this in turn changes the sign of flux $\dot{n}_{1p}$,i.e., the diffusion flux of He atoms in the pressure field is directed upward. Since the relative difference of masses $\frac{\bar{m} - m_1}{\bar{m}}$ for He is far greater than the difference $\frac{m_1 - \bar{m}}{\bar{m}}$

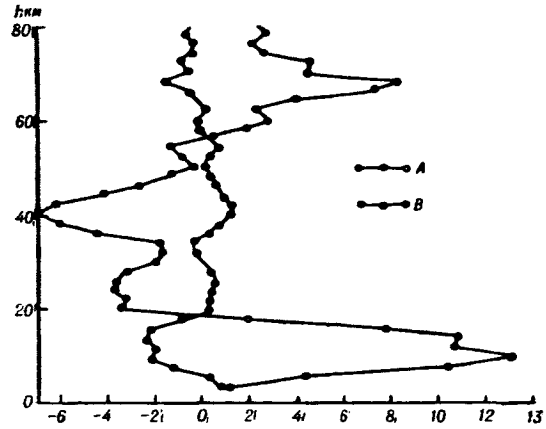

Figure 17.3. Rate of change of concentration of O_2 molecules (curve A, 10^3 mol/cm^3 sec) and He atoms (curve B, atoms/cm^3 sec).

for O_2, the relative value of the He diffusion flux in the pressure field is considerably greater (according to Chapman's computations (ref. 481), by a factor of 20) than the O_2 flux in the air; the absolute value of the He flux is small because of lack of concentrations of these atoms in the atmosphere. Thus, the relative rate of change of n_1 for He is greater than for O_2 and is more dependent on thermal diffusion and the gradient T: at a height of 80 km for four months the percentage of He in the air can change by 0.1 percent. Chapman emphasizes that this change can be a decrease of concentration, not necessarily an increase, as implicitly assumed in a number of earlier studies.

Curve B in figure 17.3 was constructed using Chapman's computations (ref. 326) for helium in the atmosphere ($\overline{M} = 28.9$); a unit on the scale is equal to 1 He atom·1 cm^3.sec. For He value $\dot{n}_1$ is over three orders of magnitude less than for atmospheric O_2; in general the sign is opposite, although the curves are not entirely similar, because ratio $\dot{n}_{1p}$ in these two cases is somewhat different than ratio $\dot{n}_{1T}$.

17.4. Diffusion Redistribution of Gases in Absence of Convective Mixing. In all these computations it was assumed that to a height of 80 km the atmosphere has a constant composition as a result of convective mixing; in addition, it was assumed implicitly that the temperature distribution is constant. This

means that velocities w_1 and w_2 in fact are equal to zero at each level, and that the values computed from the diffusion equations are balanced and cancelled by fluxes with opposite directions created by mixing. If this is not actually the case, the downward directed O_2 flux leads to an accumulation of these molecules at lower levels and to a corresponding deficit at upper levels; the process for helium would have an opposite direction. In the absence of convective mixing, this redistribution is characterized by the gradients

$$\frac{d\left(\frac{n_1}{n}\right)}{dh} \quad \text{and} \quad \frac{d\left(\frac{n_2}{n}\right)}{dh},$$

which will increase until their values become adequate, in accordance with the diffusion equation, to reduce w_1 and w_2 to zero. If the temperature is the same at all heights, the final state will be as described by Dalton's law, but in the actually observed temperature distribution the state should differ, at least slightly, from the state described by Dalton's law. It is of interest to discuss this process in somewhat greater detail (ref. 326).

We will consider an isothermal atmosphere consisting of two gases (1 and 2) with individual height of the homogeneous atmosphere H_1 and H_2; in the case of complete mixing this height is equal to H. Assume that n_{10} and n_{20} denote the concentrations of molecules at the Earth's surface for a homogeneous composition. Then, if change of g with height is neglected, the total quantity of molecules 1 and 2 will be equal to $n_{10}H$ and $n_{20}H$. If the state of the atmosphere changes and becomes such that it is described by Dalton's law at this same temperature, the surface concentrations will assume such values n_{10}' and n_{20}' that the total quantity of molecules of a particular kind remains as before. Consequently,

$$n_{10}H = n_{10}'H_1 \quad \text{and} \quad n_{20}H = n_{20}'H_2,$$

which is equivalent to the equations

$$n_{10}m_1 = n_{10}'\overline{m} \quad \text{and} \quad n_{20}m_2 = n_{20}'\overline{m},$$

where

$$n_{10}m_1 + n_{20}m_2 = (n_{10} + n_{20})\overline{m},$$

so that

$$n'_{10}+n'_{20}=n_{10}+n_{20}.$$

The following relations are satisfied at height h

$$n_1=n_{10}\exp\left(-\frac{h}{H}\right) \qquad \text{and} \qquad n_2=n_{20}\exp\left(-\frac{h}{H}\right),$$

if the air is mixed and

$$n_1=n'_{10}\exp\left(-\frac{h}{H_1}\right) \qquad \text{and} \qquad n_2=n'_{20}\exp\left(-\frac{h}{H_2}\right),$$

if the state is described by Dalton's law.

If $m_1 > m_2$, then $n_{10}' > n_{10}$ and $n_{20}' < n_{20}$ and redistribution will be accompanied by an increase of n_1 from the Earth's surface to the height h_1, determined from the equation

$$n_{10}\exp\left(-\frac{h_1}{H}\right)=n'_{10}\exp\left(-\frac{h_1}{H_1}\right)$$

or

$$\bar{m}\exp\left(-\frac{h_1}{H}\right)=m_1\exp\left(-\frac{h_1}{H_1}\right).$$

Above this level n_1 should decrease. Using the last equation, after putting it into logarithmic form, we find

$$h_1=\frac{H\bar{m}}{m_1-\bar{m}}\ln\frac{m_1}{\bar{m}}.$$

By expanding the logarithm into a series, this equation can be rewritten in the form

$$h_1=H\left(1-\frac{1}{2}x+\frac{1}{3}x^2-\ldots\right),$$

where

$$x = \frac{m_1 - \bar{m}}{\bar{m}} = \frac{n_{20}(m_1 - m_2)}{n_{10}m_1 + n_{20}m_2},$$

if $x^2 < 1$, as applies for the O_2 - N_2 and He - air systems. For O_2 - N_2 the ratio $\frac{h_1}{H} = 0.95$; for He - air the ratio is equal to 2.3 (assuming $\frac{n_{He}}{n_{air}} = 5 \cdot 10^{-6}$).

If the composition of the atmosphere is mixed homogeneously to some level h_0, and farther aloft there is diffusion redistribution, the critical height will be $h_0 + h_1$, provided there is no exchange through the h_0 level.

17.5. Stratospheric Mixing of Radioactive Settling. The constancy of air composition to great heights indicates that the gravitational-diffusion separation of gases cannot occur in the lower layers of the atmosphere because of intense vertical mixing of the air. Vertical movements will be discussed in greater detail in Chapter 10, where we will point out only one of the new approaches for determination of the rate of vertical mixing of air. This approach is based on measurements of the rate of settling of radioactive products of atomic and nuclear explosions. Interesting estimates have been published by Libby and Palmer (ref. 548).

Observations of the rate of settling of radioactive products made in 1959 revealed that the products of high-latitude nuclear explosions are retained in the atmosphere about 8 months, and the products of explosions in equatorial regions fall out considerably more slowly, in approximately 5 years. In this connection Libby and Palmer cite the Gold model of meridional circulation, in

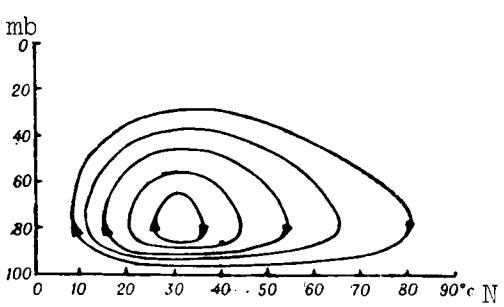

Figure 17.4. Model of meridional circulation, based on measurements of rate of radioactive fallout.

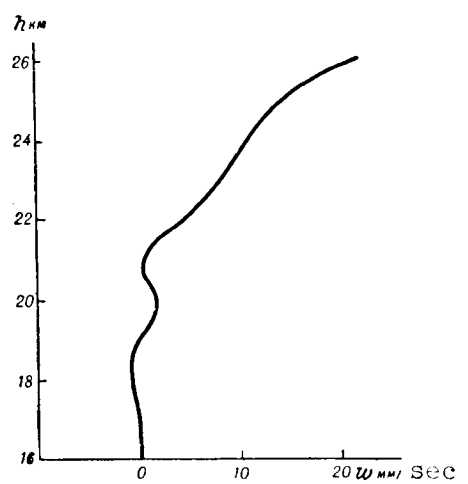

Figure 17.5. Mean monthly value of vertical wind component w over Marshall Islands (5°N, 170°E) for Feb., 1954.

which an ascending current penetrates into the stratosphere in the equatorial region and a descending current returns to the troposphere in the high latitudes. This model is confirmed by numerous observations of radioactive fallout throughout the world, and on the basis of computations by Libby and Palmer can be represented as shown in figure 17.4. The meridional component of velocity of these currents, according to their estimate, is 2-5 km/hour for the current propagating toward the equator in the lower layers of the stratosphere; the current toward the pole, attaining great heights, has a velocity approximately 10 times greater. Figure 17.5, constructed by Libby and Palmer on the basis of the continuity equation, using a horizontal wind as a point of departure, gives some idea of the vertical wind velocity. The mean value of velocity at the tropopause level is assumed equal to zero.

18. Change of Molecular Weight with Height

These data show that to heights of 100 km there are no appreciable changes of atmospheric composition, and therefore the mean molecular weight m of air can be considered constant. However, for a study of the structure of the higher layers of the atmosphere by satellites it is necessary to know the numerical value m at heights of 200-300 km or more. In particular, by determining the heights of the homogeneous atmosphere from observations of the deceleration of satellites

$$H = \frac{RT}{mg},$$

we can compute temperature T if value m is known (Section 13).

18.1. Existence of Diffusion Separation and Its Level. Above the 100 km level, molecular weight can decrease appreciably as a result of dissociation of oxygen molecules and possibly nitrogen as well. The large values H determined from observations can indicate not only a high temperature of the atmosphere but also a low molecular weight. Nicolet was one of the first to analyze new data on the high values of atmospheric density in its upper layers from this point of view.

According to Nicolet (ref. 635) it is impossible to devise a satisfactory model of the atmosphere without taking into account the diffusion process. In computations of the possible values of mean molecular weight there is no basis for assuming the presence of an appreciable dissociation of nitrogen molecules. The ratio

$$\frac{\text{oxygen}}{\text{nitrogen}} = \frac{n(O) + 2n(O_2)}{n(N) + 2n(N_2)}$$

cannot be regarded as invariable with height (here n is the concentration of the corresponding particles).

Information on the existence and level of diffusion separation of gases can be obtained by studying the change of the relative content of gases with height. Such measurements indicate that above 100 km, but apparently below 150 km, the percentage content of the light gases begins to increase appreciably. A detailed exposition of these interesting investigations can be found in

a monograph by B. A. Mirtov (ref. 125). Here we will limit ourselves to a reference to measurements made by A. A. Pokhunkov (ref. 154), using a rocket-borne mass spectrometer. He investigated the level of separation of argon and molecular nitrogen, and established that the ratio of the ion currents of argon and nitrogen has a tendency to a monotonic decrease at heights of 100-175 km, evidence of the presence of diffusion separation at a height somewhat greater than 100 km.

By taking into account certain results of a study of the dynamics of the high layers of the atmosphere, it can be postulated that the level of diffusion separation of the heavy and light gases in the Earth's atmosphere can vary appreciably at different times of the year and day, at different latitudes and during different states of solar activity. This complicates the problem of the dependence of the mean molecular weight of the atmosphere on height.

18.2. Changes of Mean Molecular Weight. Miller (ref. 597) attempted to estimate, on a theoretical basis, the possible changes of composition with height and to determine the mean molecular weight m. He found that at heights of 0-90 km m is constant and equal to 29 (to be more exact, m = 28.966), but above this level m decreases as follows

h km . . .	100	200	300	400	500	600
m	26.0	22.6	18.5	16.8	16.2	15.7

Miller did his work before the launching of Earth satellites (1957). More recent data were available to Ionetsava. Proceeding on the basis of density values obtained from observations of the deceleration of satellites, and taking into account the theoretical analysis of Nicolet (ref. 635) and other authors working on the problem of vertical distribution of atomic and molecular oxygen and nitrogen, Ionetsava computed the structure of the atmosphere at heights of 100-400 km for the middle latitudes. His "standard atmosphere" is given in Table 18.1. An increase of the percentage content of light gases with height can be traced not only from the figures in the last column of this table, showing a decrease of the mean molecular weight, but also from the data in the four preceding columns. By definition of height H of the homogeneous atmosphere, the greater the value H, the slower is the decrease of the concentration n (quantity of particles per cm^3) of particles of a particular kind with height h

$$n = n_0 \exp\left(-\frac{h}{H}\right).$$

In the case of atomic oxygen the height of the homogeneous atmosphere H(O) at all levels is greater than the values $H(O_2)$ and $H(N_2)$, which indicates that the increase of percentage content of atomic oxygen continues to the 400 km level. Comparison of values for the quantity of particles of different kinds per cm^3 reveals that, whereas at the 100 km level n(O) is less than

TABLE 18.1. STRUCTURE AND COMPOSITION OF UPPER LAYERS OF THE ATMOSPHERE IN MIDDLE LATITUDES (IONETSAVA, 1960).

h км	$T°$ K	p mm Hg	ρ g/см³	Quantity of particles/cm³				Height H*				Mean mol w
				n (O)	n (O_2)	n (N_2)	Total n	H (O)	H (O_2)	H (N_2)	Mean	
100	210	$3.25 \cdot 10^{-4}$	$6.76 \cdot 10^{-10}$	$2.10 \cdot 10^{12}$	$2.53 \cdot 10^{12}$	$1.03 \cdot 10^{13}$	$1.50 \cdot 10^{13}$	11.4	5.7	6.5	6.7	26.87
110	290	$8.78 \cdot 10^{-5}$	1.22	$8.55 \cdot 10^{11}$	$3.60 \cdot 10^{11}$	$1.71 \cdot 10^{12}$	$2.93 \cdot 10^{12}$	15.8	7.9	9.0	10.1	24.99
120	380	3.78	$3.82 \cdot 10^{-11}$	3.75	$9.10 \cdot 10^{10}$	$4.96 \cdot 10^{11}$	$9.62 \cdot 10^{11}$	20.7	10.4	11.8	14.0	23.71
130	453	1.99	1.61	2.02	3.15	1.92	4.25	24.8	12.4	14.2	17.6	22.61
140	513	1.18	$8.04 \cdot 10^{-12}$	1.22	1.30	$8.71 \cdot 10^{10}$	2.22	28.2	14.1	16.1	20.8	21.66
150	567	$7.51 \cdot 10^{-6}$	4.46	$7.84 \cdot 10^{10}$	$5.99 \cdot 10^{9}$	4.35	1.28	31.2	15.6	17.8	24.0	20.84
160	616	5.06	2.67	5.30	2.98	2.34	$7.93 \cdot 10^{10}$	34.0	17.0	19.4	27.0	20.14
170	661	3.55	1.70	3.71	1.57	1.32	5.19	36.6	18.3	20.9	30.0	19.55
180	702	2.57	1.13	2.67	$8.69 \cdot 10^{8}$	$7.81 \cdot 10^{9}$	3.54	39.0	19.5	22.3	32.8	19.04
190	740	1.91	$7.78 \cdot 10^{-13}$	1.97	4.99	4.77	2.50	41.3	20.6	23.6	35.5	18.62
200	775	1.45	5.53	1.48	2.96	3.00	1.81	43.3	21.7	24.8	38.0	18.26
210	807	1.12	4.03	1.13	1.81	1.94	1.34	45.3	22.6	25.9	40.4	17.95
220	837	$8.79 \cdot 10^{-7}$	3.00	$8.75 \cdot 10^{9}$	1.13	1.27	1.01	47.1	23.6	26.9	42.6	17.69
240	893	5.58	1.75	5.41	$4.62 \cdot 10^{7}$	$5.70 \cdot 10^{8}$	$6.04 \cdot 10^{9}$	50.6	25.3	28.9	46.8	17.28
260	945	3.68	1.07	3.47	2.02	2.78	3.76	53.8	26.9	30.7	50.7	16.97
280	993	2.50	$6.82 \cdot 10^{-14}$	2.28	$9.26 \cdot 10^{6}$	1.40	2.43	56.9	28.5	32.5	54.4	16.75
300	1038	1.74	4.49	1.54	4.44	$7.29 \cdot 10^{7}$	1.62	59.8	29.9	34.2	57.7	16.59
320	1080	1.23	3.04	1.06	2.21	3.93	1.10	62.6	31.3	35.8	60.9	16.46
340	1119	$8.90 \cdot 10^{-8}$	2.10	$7.45 \cdot 10^{8}$	1.13	2.18	$7.68 \cdot 10^{8}$	65.3	32.6	37.3	63.8	16.36
360	1155	6.51	1.48	5.31	$5.98 \cdot 10^{5}$	1.24	5.44	67.8	33.9	38.7	66.6	16.29
380	1188	4.82	1.06	3.84	3.23	$7.22 \cdot 10^{6}$	3.92	70.1	35.1	40.1	69.1	16.23
400	1218	3.61	$7.75 \cdot 10^{-15}$	2.81	1.79	4.28	2.86	72.3	36.2	41.3	71.5	16.19

*Of homogeneous atmosphere km.

15 percent of the total quantity n of particles per cm^3 ($\frac{n(0)}{n} = 0.14$), at the 200 km level the quantity of oxygen atoms is 82 percent of the total quantity of particles, and at a height of 400 km it exceeds 98 percent.

19. Water Vapor in the Stratosphere

Until relatively recently most meteorologists were of the opinion that stratospheric air is characterized by an extremely low relative humidity. This opinion was not based on the results of measurements, but on indirect considerations. Among the latter the most important was the long-established conviction that there were no clouds beyond the limits of the troposphere. It was not possible to measure relative or absolute humidity reliably in the high layers of the troposphere, much less in the stratosphere. A major difficulty in such measurements is that in these layers the air temperature is always very low and the moisture content is extremely small (as we will see later, the elasticity of water vapor in the stratosphere sometimes can drop to 10^{-5} mm Hg). Air humidity measurements at low negative temperatures (of the order of -50°) involve great experimental difficulties even in the surface layers, where in case of necessity it is possible to use complex apparatus (e.g., measurements of absorption by the absolute weight method). The need for carrying an instrument aloft for measurements in the free atmosphere involves additional limitations. Instruments for radiosondes should have little weight and operate automatically. In the case of aircraft sounding the great speed of movement requires instruments with low inertia.

19.1. Gol'tsman Hygrometer. For a long time the only instrument used in all forms of sounding of the free atmosphere was the hair hygrometer. The increase of inertia of the hair with temperature decrease makes this method unreliable for the vertical sounding of the atmosphere to great heights. The humidity value measured by a hair hygrometer and transmitted by a radiosonde is subject to great suspicion and can differ from true humidity by tens of percent (ref. 33).

The first reliable and systematic measurements of stratospheric humidity were made using the dew point (frost point) method, in which that temperature is determined at which water vapor present in the atmosphere at some partial pressure begins to condense (sublimate) on some cooled surface. This method for low temperatures was developed in the USSR by M. I. Gol'tsman (ref. 33). The instrument which he designed to be carried in the basket of a stratosphere balloon was constructed in 1937. The instrument can be described briefly as follows.

A metal mirror with a thermojunction is attached to one end of a curved brass tube and small quantities of liquid oxygen are poured into the other open end. The brass tube is covered on the outside by ebonite heat insulation. This method results in gradual cooling of the mirror (its temperature can be reduced easily to -150°). When observing the mirror, it is necessary to determine the precise time of onset of water vapor condensation. This can be

done by the dark-field method proposed for such purposes by M. I. Gol'tsman (ref. 452) as early as 1926 (the mirror is observed visually in a microscope). A method using a photocell is convenient for automatic recording of the onset of condensation. This objective method was used for the first time by M. I. Gol'tsman (ref. 33) in 1932. The directed beam of light falls on the mirror at an angle of 30°, and after being reflected from it, is incident on the photocell; the photocurrent is measured by a galvanometer. Since the reflectivity of the mirror is decreased at the time of appearance of dew, the deflection of the galvanometer, previously stable, begins to decrease from the time of appearance of traces of condensation. Simultaneous determination of mirror temperature gives the dew point. A detailed description of these methods can be found in the book listed as reference 33.

Systematic measurements of air humidity at the height of the tropopause and in the stratosphere were begun in Great Britain in 1943-1945 by Dobson, Brewer and Quaylong (ref. 60). Their apparatus was constructed entirely on the principles proposed by M. I. Gol'tsman. The instrument consisted of an aluminum cap containing benzine, cooled by solid carbon dioxide or liquid air. This cap could be cooled to very low temperatures by spraying its lower surface with cooled benzine or liquid air. The temperature of the mirror was determined thermoelectrically or using a resistance thermometer. The appearance of a precipitate from water vapor sublimation elements on the mirror is recorded either by the dark-field method or using a photocell.[1]

19.2. Measurements over Southern England. Figure 19.1 shows the results of observations made by Dobson, Brewer and Quaylong at the time of the first ascent, accompanied by measurements in the stratosphere. The ascent was made on Dec. 22, 1943, in a flow of polar air which rapidly subsided. On this day the stratosphere began at a height somewhat more than 9 km. The curves show that the frost point falls very rapidly immediately upon entry into the stratosphere. The frost point could not be measured in the upper part of the ascent, because it was not possible to cool the cap sufficiently to obtain a visible precipitate (ref. 60).

A similar result was obtained in the ascents of May 5, 1944, (fig. 19.2) when the stratosphere began below 9 km, and on May 30, 1945, when the beginning of the stratosphere was situated at a height of 10 km (fig. 19.3), although the ascents were made under different meteorological conditions.

These data apparently confirmed the traditional point of view that the stratosphere is a region of dry air. Although the authors (ref. 60) pointed out that for many ascents it is necessary to determine whether there always is a decrease of the frost point above the tropopause, they nevertheless thought that an extremely rapid decrease of the frost point directly upon entry into the stratosphere is typical. They also noted that the sudden decrease of

---

[1] The British authors call this instrument the "Dobson-Brewer hygrometer." Considering its development, it should be called the "Gol'tsman hygrometer," or at least the "Gol'tsman-Dobson-Brewer hygrometer."

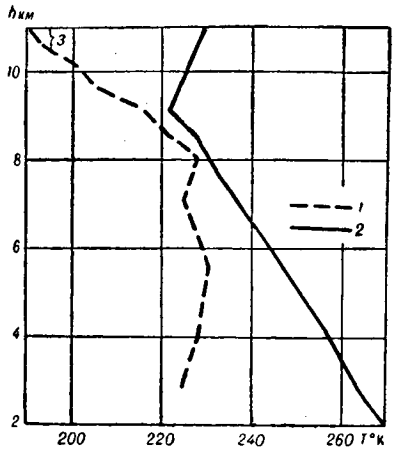

Figure 19.1. Frost point (1) and air temperature (2) on the basis of the first measurements in stratosphere over England, Dec. 22, 1943. 3, doubtful, no precipitation.

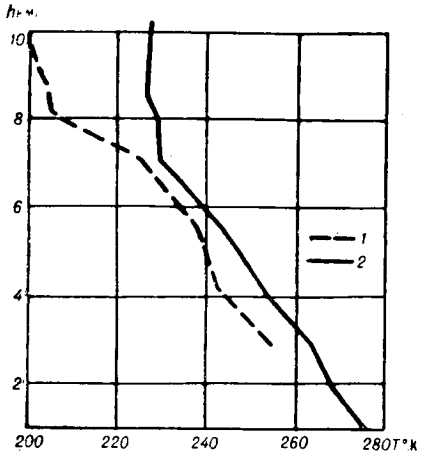

Figure 19.2. Frost point (1) and air temperature (2) on basis of observations over England, May 5, 1944.

the frost point above the tropopause agrees with the known phenomenon that the vapor trail left by an aircraft at great heights is shortened upon ascent into the stratosphere, which can be attributed to the rapid evaporation of the trail in very dry air.

As an explanation of the extreme dryness of stratospheric air, Dobson, Brewer and Quaylong believe that the only effective process of disappearance of water vapor from stratospheric air is the cooling of ascending air, leading to the sublimation of water vapor. The forming ice particles, upon settling, leave this air layer. These authors believe that this process occurs near the equator, where the stratosphere is coldest and where the ascending currents in the troposphere are extremely strong.

In recent years British investigators have succeeded in raising the "ceiling" of humidity measurements to a height of 15 km by use of this condensation hygrometer. This required preliminary compression of the air. The fact is that there is a temperature limit below which the frost point method is virtually inapplicable, since the ice layer on the mirror becomes invisible. This critical temperature is at about -85°. Below this temperature the ice apparently forms on the mirror in a glassy state, and it is difficult to detect the film. In actuality, Burton and Oliver, using the x-ray structural analysis method for study of the process of water vapor sublimation on a metal surface at low temperatures, discovered that at a temperature below -110° glassy ice is formed, which at higher temperatures undergoes transition into a crystalline precipitate (ref. 60). This explanation has been disputed by Mason (ref. 711).

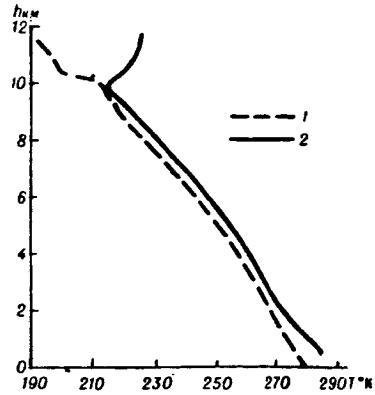

Figure 19.3. Frost point (1) and air temperature (2) on basis of observations over England, May 30, 1945.

In order to expand the region of applicability of the condensation hygrometer in the direction of lower frost points, Dobson proposed the use of preliminary air compression (ref. 710). Computations show that if the air is compressed from an initial pressure of 115 mb (which corresponds to a height in the atmosphere of 12-13 km) to a pressure of 1,000 mb, the frost point increases by more than 20°. For a long time it was impossible to use this method in actual practice, because the liberation of moisture from the surface of an ordinary compressor greatly distorted the results (ref. 267). In 1955, when the Meteorological Service of Great Britain began to use jet aircraft for sounding of the atmosphere, Goldsmith proposed that a jet aircraft compressor be used for these purposes (ref. 407). Compressed outside air, fed from the aircraft compressor, rather than ordinary air, enters the hygrometer chamber. The compressor receives air in such a large quantity that the influence of water vapor released from the surface of the apparatus is negligibly small (ref. 359).

Using this method Murgatroyd, Goldsmith and Hollings made several dozens of measurements of air humidity in the upper layers of the troposphere and lower layers of the stratosphere in a jet aircraft (refs. 616 and 617). They established that the frost point gradually decreases with height above the tropopause, approaching a constant value between -81.7 and -84.4°. At a height of about 15 km there was no significant difference between summer and winter data. The frost point gradients also decrease with height. In some cases there are jumps of the frost point gradient at the "humidity tropopause," situated at a height of 600-3,000 m above the ordinary tropopause. In the case of a "high tropopause" (10.8 km and above, average 11.4 km), the air temperature and the frost point are less than the corresponding values at these same levels in the case of a "low tropopause" (10.5 km and lower, average 9.6 km).

Dobson cites the mean results of humidity measurement (ref. 359) for 21 ascents over southern England (fig. 19.4). This figure shows not only the frost point, but also the water vapor content of the air (in g per m^3): it

decreases with height above the tropopause. Dobson notes two circumstances as being particularly important: the unusual dryness of the air at a height of about 15 km, where the water vapor quantity is less than 1 mg/m^3 and the fact that the frost point at the 15 km level is equal to the minimum air temperature measured in the upper layers of the troposphere over the equator (ref. 359). Figure 19.5 shows the vertical distribution h (relative to the tropopause level) of the mean values of air temperature and frost point (based on these data). Later measurements by Helliwell, Mackenzie and Kerley (ref. 435) to a height of 15 km gave similar results.

19.3. Mechanism of Formation of Dry Air in Lower Layers of the Stratosphere (According to Dobson). Dobson believes that the reason for the dryness of stratospheric air is that this air at some time passes through a very cold region (upper layers of the troposphere and lower layers of the stratosphere) near the equator and that a large part of the water vapor there condenses and falls. At present the lowest frost point measured in the stratosphere in the middle latitudes (fig. 19.4) is approximately equal to the minimum air temperature measured in the lower layers of the stratosphere.

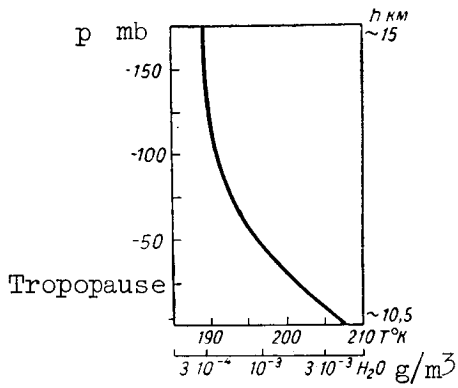

Figure 19.4. Frost point and quantity of water in stratosphere over England.

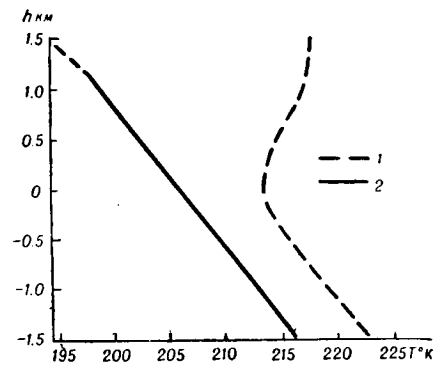

Figure 19.5. Mean air temperature (1) and frost point (2) in upper layers of troposphere and lower layers of stratosphere over southern England.

In Section 36 we will discuss a model proposed by Dobson, which clarifies his hypothesis concerning the mechanism of formation of dry stratospheric air.

There are also other points of view on the reasons for dryness of the air in the stratosphere. Some investigators believe it is more probable that water vapor molecules are decomposed photochemically in the high layers of the atmosphere (above 90 km) under the influence of solar uv radiation (ref. 711).

It should be noted that at present it is not established that the stratosphere is everywhere as dry as it was found to be over southern England. The fact is that measurements made in other geographic regions by other methods give very different results, as we will see later.

19.4. Detection of Moist Air above 15-20 Km. Data on air humidity obtained by Barrett, Herndon and Carter, and also by Brasefield, to heights of 30-35 km, are of particularly great interest. We now will discuss these studies in greater detail.

Figure 19.6a shows the dependence of frost point and air temperature on height, as determined from measurements by Barrett, Herndon and Carter (ref. 279) on July 1, 1949, when the stratosphere began at a height of 13.5 km. The presence of high humidity was established not only under the tropopause (at a height of 12.6 km the frost point was equal to air temperature, i.e., the relative humidity was 100 percent), but in the lower layers of the stratosphere as well (100 percent humidity at the 15.8 km level). According to these measurements on Aug. 26, 1949, when the stratosphere began at a height of 12 km (fig. 19.6b), the lower layers of the stratosphere again were characterized by high humidity, and in the 14-15 km layer the relative humidity again was 100 percent. On Jan. 7, 1951, (fig. 19.6c) high humidity close to saturation was found in an extensive region (12-16 km) in the lower part of the stratosphere.

The conclusion drawn by Barrett, Herndon and Carter that there is high humidity in the stratosphere is fully confirmed by measurements made by Brasefield (ref. 307). Brasefield used a hygrometer of a new type, designed for use in a radiosonde. Humidity is measured using a saturated solution of lithium chloride in the form of a thin electrolytic film between two metal electrodes in combination with an attachment for measuring the temperature of the film. A current of about 25 v is fed to the electrodes for heating the film. The elasticity of water vapor of the unheated film is usually less than its elasticity in the surrounding space and the moisture content of the film therefore gradually increases. This leads to decrease of its resistance and to strengthening of the current, together with increase of the temperature of the film, until the elasticity of the water vapor is comparable to its elasticity in the surrounding space. If the temperature of the film rises above an equilibrium value, there will be decrease of the moisture content of the film and its

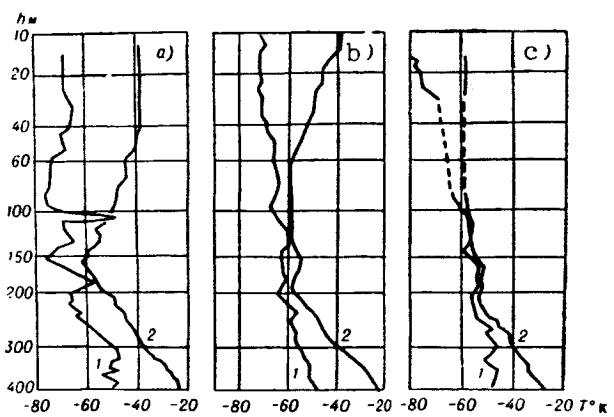

Figure 19.6. Frost point (1) and air temperature (2) in stratosphere.
a, July 1, 1949; b, Aug. 26, 1949; c, Jan. 7, 1950.

resistance increases. This causes decrease of the energy released in the film in a unit time and accordingly a temperature decrease to an equilibrium value. Humidity measurement, therefore, essentially involves determination of the equilibrium temperature of the film of lithium chloride and finding (from tables) the elasticity of the vapor of a saturated solution of lithium chloride at this temperature.

A cylindrical ceramic thermistor 3 mm in diameter and 4.5 cm long was used for measuring the temperature of the film of lithium chloride. Only its 6 mm central part was sensitive to temperature. The resistivity of the thermistor was from $2 \cdot 10^4$ ohms at 45° to 10^6 ohms at -65°. If the humidity of the surrounding air is less than the humidity over a saturated solution of lithium chloride (about 15 percent), the equilibrium temperature of the hygrometer is the temperature of the medium, regardless of the dew point. Under these conditions the instrument readings remain undetermined; they indicate only the upper limits of the possible dew point value. However, in the investigated region of the atmosphere a humidity less than 15 percent is encountered much

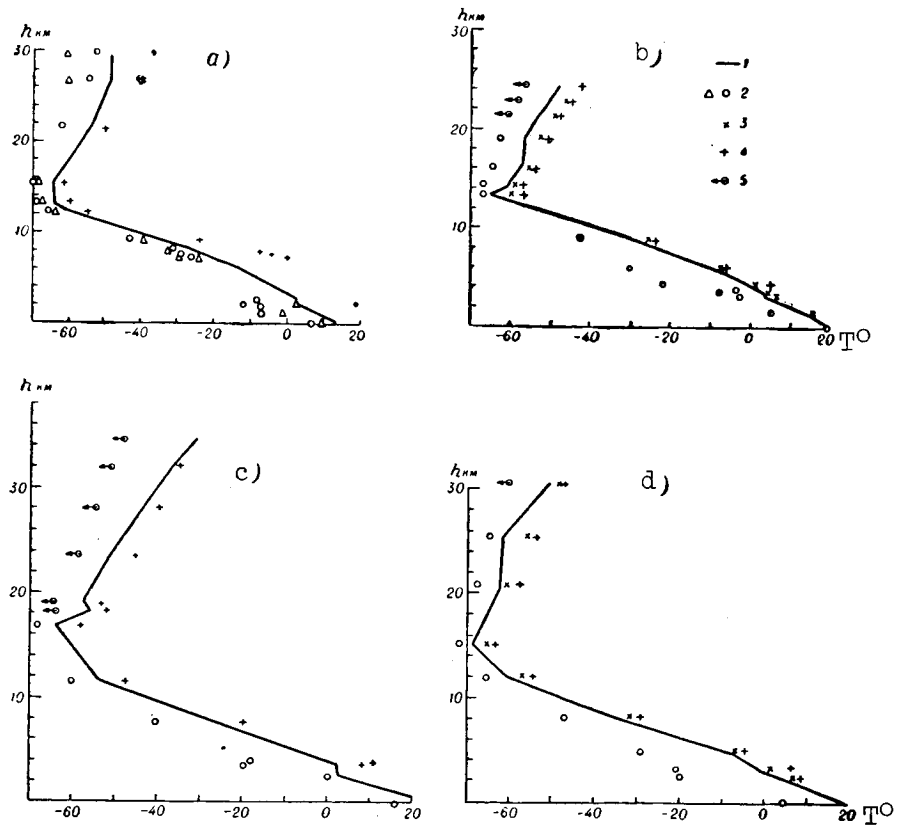

Figure 19.7. Humidity measurements over Belmar, New Jersey. a, May 19, 1952; b, Aug. 17, 1953; c, Sept. 16, 1953; d, Nov. 18, 1953. 1, air temperature; 2, dew (frost) point; 3, temperature of control thermistor; 4, hygrometer temperature; 5, upper limit of dew (frost) point.

more frequently than a humidity greater than 15 percent. The instrument inertia is such that its readings can be considered correct if the dew point changes no more rapidly than 0.5°/min.

A balloon with a neoprene envelope with a nominal weight of 7,500 g, designed especially for nighttime flights, was used for carrying aloft the radiosonde-hygrometer. Initial attempts at daytime launchings revealed the presence of anomalously high temperatures, detected by the hygrometer and control thermistor.

The results of sounding (at Belmar, New Jersey) are shown by Brasefield in four standard curves (ref. 307). One of these (fig. 19.7a) illustrates data from the first launchings, in which a hygrometer of a different type (charcoal element) was used simultaneously for checking the results; the results were close. The second figure (fig. 19.7b) is an example of measurements with a "control" thermistor, and the third (fig. 19.7c) is an example of measurements without it (which decreases accuracy). The fourth (fig. 19.7d) is typical of winter measurements. Brasefield states that the most interesting of his results is an increase of dew point established in many cases above the tropopause, and the presence of a higher dew point than the temperature of the tropopause at a height of about 20 km. He believes that at present it is impossible to explain this anomalously high humidity with certainty; the most probable cause may be the penetration of ice crystals into the stratosphere under the influence of strong vertical currents (ref. 307).

19.5. Optical (Spectral) Measurements. The absorption spectrum of water in liquid and gaseous states contains a large number of absorption bands in the near and far parts of the infrared spectrum (fig. 19.8). As early as 1912, Fowle developed a spectroscopic method for measuring the water vapor content in the atmosphere on the basis of absorption of infrared solar radiation (refs. 390-392). This method was used for a classical series of observations of atmospheric humidity in accordance with the program of the Astrophysical Observatory of the Smithsonian Institution for determination of the solar constant. This method is also used widely at the present (refs. 193, 395).

Further measurements are given in reference 194. In recent years attempts have been made to use the reradiation of the Earth and atmosphere for this purpose (in the far infrared region) by means of spectrometric measurements from aircraft and artificial Earth satellites (ref. 88). In addition, studies now are appearing on the investigation of the absorption of solar radiation by instruments carried aloft into the stratosphere. Interesting experiments of this type have been made by Gates (ref. 395), M. S. Kiseleva, B. S. Neporent and V. A. Fersenkov (ref. 82) and B. S. Neporent, V. F. Belov, and others (ref. 137). It must be remembered that measurement of the water vapor concentration on the basis of absorption in the infrared region is made difficult by the presence of a fine structure of the absorption spectra, not resolved by ordinary spectral instruments. The absorption laws become extremely complicated under these circumstances. A second complication of a general character is associated with the possibility of the existence of water in the stratosphere not only as vapor, but also in condensed form (liquid water, ice).

Instruments with diffraction gratings constructed by B. S. Neporent and others (ref. 137) are designed for determination of air humidity at different heights on the basis of the attenuation of solar radiation in the 1.4, 1.9 and 2.6 μ absorption bands of water. The absorption of water vapor in some region of concentrations and pressure of foreign gases was investigated first under laboratory conditions; it was found that the square root law in the following simple form could be used

$$A = 1 - \frac{I}{I_0} = kp^a \sqrt{l},$$

where A is the absorption factor; I_0, I are the intensities of incident and transmitted radiation; l is the quantity of precipitated water; p is the total pressure of the mixture (water vapor plus the foreign gas), and k, a are constants.

The apparatus was carried aloft into the stratosphere in the neighborhood of Khar'kov and Moscow by automatic stratospheric balloons. After drifting briefly at maximum height, the instrument was released from the balloon and descended by parachute (ref. 82). The air humidity measurements at 1.4 μ were made to a height of about 11 km; the stronger bands 1.9 and 2.6 μ were used at greater heights. However, even with these bands adequately precise measurements could only be made to a height of 15-20 km.

B. S. Neporent, V. F. Belov and L. A. Kudryavtseva (ref. 138) found that the total vertical distribution of water content above 12 km amounts to approximately 50 μ of precipitable water.

In 1956 spectrometric measurements of humidity from an aircraft were made over England by Jones and Roberts (ref. 491). They investigated the H_2O absorption bands, beginning at a height of 9 km.

A series of interesting studies on this problem was published in 1960 (refs. 395, 457, 573 and 608). Gates carried out an investigation which was important in methodological respects. He carefully measured the solar spectrum in the region 0.85-2.7 μ with an instrument with high resolution (refs. 395 and 398). He used a recording spectrometer in which the rays pass twice through a NaCl prism. Figure 19.8 shows the results of the measurements by Gates (ref. 398); the deflections (readings) of the spectrometer recording instrument were plotted along the Y-axis, and the absorption bands were identified beneath the spectrum.

The Ballistics Research Laboratory in the United States launched rockets with nose cones containing infrared hygrometers with a tracking device. The latter oriented the optical system on the Sun (ref. 573). A reflection grating and a pair of slits separated the 1.38 and 1.26 μ absorption bands for comparison. Light from the slits fell alternately on a lead sulfide photoresistor. The difference in resistance in these alternating cases was a measure of water vapor quantity. Due to a defect of the surface apparatus, data were received for only 28 seconds of the flight. This same laboratory carried out several

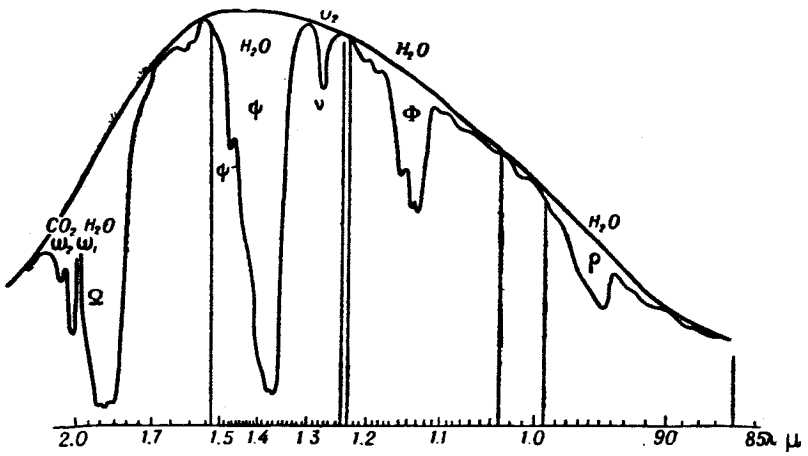

Figure 19.8. Solar spectrum in near infrared region.

launchingsof automatic stratospheric balloons for humidity measurement, using a modified frost point hygrometer. It was established by measurements over White Sands (33°N in the United States) (one flight) that there are four layers of enhanced humidity in the lower layers of the stratosphere, between 9.5 and 18.5 km.

A report published by Marks indicates that in the high latitudes different results were obtained in different geographic regions. Whereas at Thule, Greenland, it was noted that the stratospheric air is extremely dry, in Canada (one flight at Fort Churchill and one at Fort Monmouth) considerable quantities of water vapor were measured in the lower and middle layers of the stratosphere. In a report on these humidity measurements (ref. 573) Marks writes: "In order to evaluate correctly the significance of the latter results, it is necessary to recall the opinion of certain investigators that there is a virtual absence of water vapor in the stratosphere."

We already discussed in detail the results of measurements over England, which indicate a low air humidity in the lower layers of the stratosphere. These measurements were made with a Gol'tsman frost point hygrometer (Section 19.2). In order to check the readings of this hygrometer, Houghton and Seeley carried out spectroscopic measurements. They studied absorption in the 2.7 μ band to a height of 14.5 km (ref. 457); the apparatus was carried aloft in an aircraft. It was found that the stratosphere over England contains little water vapor: the layer of precipitable water in a vertical atmospheric column above the 14.5 km level is only 4.5μ . This value corresponds to a mean content of water molecules of $3 \cdot 10^{-6}$ (3 water molecules per million air molecules).

A study by D. and F. Murcray, Williams and Leslie (ref. 608) is very interesting. They measured the quantity of water vapor in the stratosphere from absorption in the 6.3 μ band.

A spectrometer with a rock salt prism (Litthrow system) and a semiconductor bolometer as a radiation detector was used during the ascent of an automatic infrared spectrophotometer into the stratosphere on June 19, 1959, to a height of 27.6 km in New Mexico in the United States. The spectrometer was oriented on the Sun by a biaxial tracking system. The spectrum in the region 1-10 μ was recorded by an automatic instrument; spectrum scanning required 18 sec. The stratospheric balloon was launched at about 0600 hours, and the ascent continued to 0730 hours, after which the balloon drifted for approximately one hour. The apparatus returned to Earth by parachute. At the 27.6 km level there were extremely significant fluctuations of the quantity of water vapor, indicating the presence of a horizontal nonhomogeneity of its distribution. The quantity of precipitable water in the vertical column of the atmosphere above 27.6 km was not less than 20 μ, and the specific humidity above this level varied from $1.5 \cdot 10^{-4}$ to $3.4 \cdot 10^{-4}$ g/g. Measurements of specific humidity in the 12-27 km layer are particularly interesting; they give a value 30-60 times smaller, i.e., $5.6 \cdot 10^{-6}$ g/g. We see from the summary in reference 608 that rather numerous measurements of other authors give a specific humidity value of about $2 \cdot 10^{-6}$ g/g for the lower layers of the stratosphere for all cases. Thus, in the upper layers of the atmosphere there is a considerable increase of specific humidity with height.

In accordance with this, we can note that the water vapor content in the stratosphere apparently is subject to extremely large changes in time and space (depending on height and geographic coordinates). In addition to the great dryness of the air constantly observed in the lower layers of the stratosphere (to 15 km) over England, there are cases of extremely high humidity. There is a basis for assuming that changes of humidity of stratospheric air are caused by large-scale circulation processes, accompanied by vertical exchange between the troposphere and stratosphere or stratosphere and ionosphere.

19.6. Computed Measurements. In Section 16 we became acquainted with rocket measurements of air composition using a mass spectrometer. These data indicated the presence of appreciable quantities H_2O molecules in the air to heights of about 100 km. The first indications of this type were obtained by Townsend, Meadows and Pressly (ref. 770) on the basis of data from a mass spectrometer carried aloft in a rocket to a height of 137 km on Feb. 12, 1953. A maximum of particles with a molecular weight of 18 was also recorded on a trace obtained by Meadows and Townsend (ref. 587) on Dec. 12, 1955, at a height of 83.9-84.4 km. This result was confirmed when determining the ion composition of the ionosphere by rocketborne mass spectrometers. The record from a mass spectrometer carried aloft by a "Viking No. 10" rocket on May 7, 1954 (ref. 482) revealed the presence of H_2O molecules at heights of 93-124 km.

Unfortunately, for the time being, mass spectrometer measurements give only qualitative results which make quantitative determinations of the water vapor content in the upper layers of the atmosphere impossible.

CHAPTER 7. AEROSOL COMPOSITION OF THE ATMOSPHERE

20. Dust Particles in the High Layers of the Atmosphere

In recent years investigators have devoted ever increasing attention to the detection of solid (dust) particles in the high layers of the atmosphere. Strictly speaking, this problem is separate from the problem of the composition of air, which is determined by the presence of atoms and molecules in a gaseous state or as vapor. However, in reality the study of solid particles present in a suspended state in the atmosphere is closely related to the problem of air composition. For this reason the chapter on air composition will be followed by available data on dust particles in the high layers of the atmosphere. At all times solid particles enter the high layers of the atmosphere "from above" and "from below", i.e., from interplanetary space and from the lower layers of the atmosphere. Some particles apparently are formed directly in the stratosphere (fig. 20.3). We will first consider the data on aerosol particles in the stratosphere (up to 30 km).

20.1. Aerosol Particles in the Stratosphere. Junge, Chagnon and Manson published an extensive investigation of aerosol particles in the stratosphere (up to 30 km) in 1961 (ref. 498). They studied the vertical distribution of particles, particle-size distribution, and their origin and physical and chemical structure. They first considered the vertical distribution of the concentration of an aerosol from the theoretical point of view on the assumption of the existence of equilibrium between eddy diffusion, sedimentation, settling and coagulation. The results then were compared with experimental data, specifically with vertical distributions as indicated by Aitken nuclei counters, which measure particles with a radius r from 0.01 to 0.1 μ, and with vertical distributions determined by special traps (impactors) which measure particles with a radius from 0.1 to 1.0 μ. In the first case they discovered a decrease of the concentration almost to zero with an ascent to a height of 20 km (fig. 20.1, curve 1). In comparison the figure shows temperature sounding curves 2 and 3 for two close times of observation--before and after measurements with an Aitken counter. Measurements on other days sometimes indicated a still sharper decrease of the concentration with height.

Particles with a radius of 0.1 - 1.0 μ have a completely different distribution when the maximum of the concentration C is observed at the 20 km level (fig. 20.2). The particle-size distribution is constant with time. A maximum was discovered between 0.01 and 0.1 μ, and the concentration changes inversely proportional to the square of radius in the region 0.1 - 1.0 μ. Figure 20.3 is a composite diagram of the average particle-size distribution with an indication of their probable origin. Few data were obtained on particles with a radius greater than 1.0 μ because of their low concentration. In the region of these dimensions there apparently are considerable fluctuations. Particles

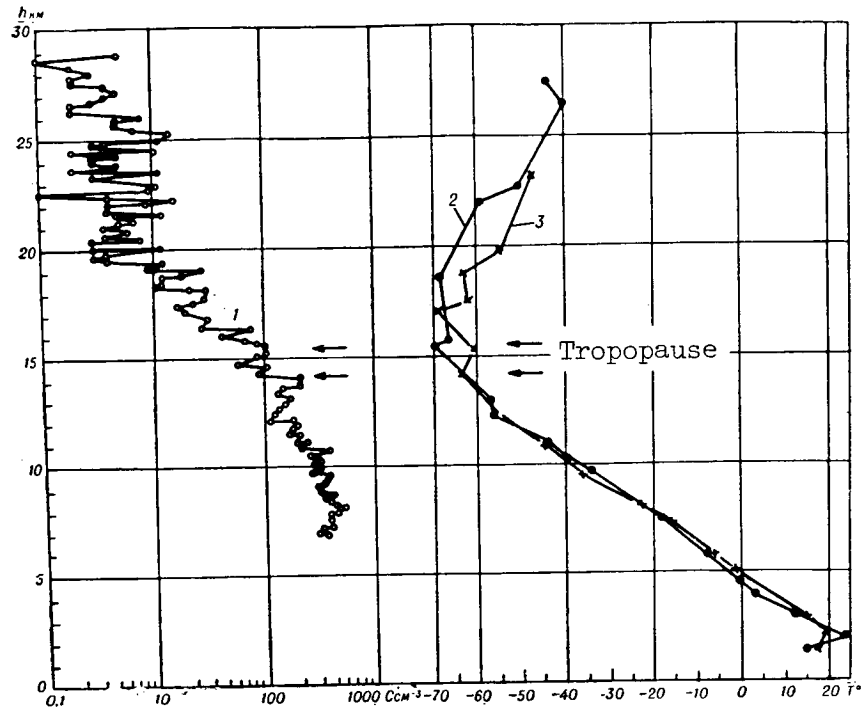

Figure 20.1. Vertical distribution of nuclei measured with Aitken counter at 0900 hours, June 25, 1959 (1) and vertical temperature profile at 1900 hours, July 24 (2) and 0700 hours, July 25 (3). Measurements at Denver, Col., USA.

with a radius of 0.1-1.0 μ were collected in concentrations adequate for detailed investigations. They were hygroscopic, and during analysis with an electron microscope it was found that sulfur and traces of iron and silicon were the predominant components of the aerosol particles. Figure 20.4 is a photograph of particles taken with an electron microscope. According to the description in ref. 498, most of the particles are similar to remnants of droplets of salt solutions which have evaporated without crystallization.

On the basis of all observations Junge, Chagnon and Manson concluded that there are three large groups of aerosol particles in the stratosphere: with a radius less than 0.1 μ, 0.1-1.0 μ and more than 1.0 μ. The first group is of tropospheric origin and the third is of extraterrestrial origin; the particles of the second group are formed in the stratosphere itself, possibly with the oxidation of H_2S and SO_2.

Samples of dust particles taken with aircraft apparatus have been analyzed by Fireman and Kistner (ref. 388). As early as the Nineteenth Century it was established that magnetic spheres on the ocean floor are of cosmic origin. In recent years these conclusions have been confirmed and considerably expanded. Fireman and Kistner attempted to discover similar (but smaller) particles in the stratosphere. The concentration of dust particles larger than 3μ at a height of 12 km varies from one particle (or less) per 5 m^3 to 12 particles

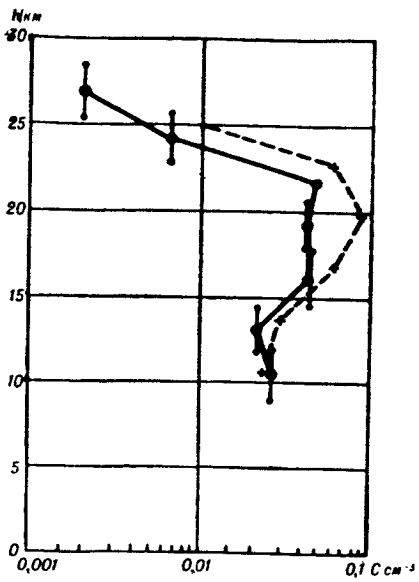

Figure 20.2. Vertical distribution of particles measured by counter (impactor) by Mills at Denver, Col. USA. Vertical lines represent the interval of heights for taking samples.

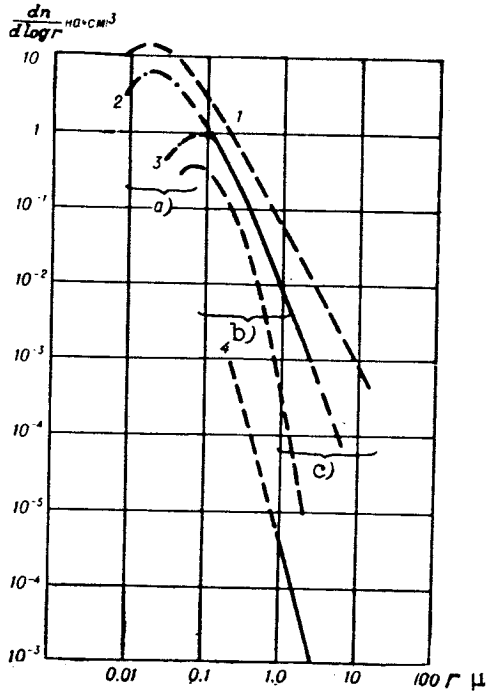

Figure 20.3. Average particle-size distribution. a, tropospheric; b, stratospheric; c, extraterrestrial origin. 1, all particles; 2, particles less than 0.1 μ for lower layers of the stratosphere; 3, same for heights greater than 20 km; 4, micrometeors (estimate for 20 km level).

per 1 m^3. The particles often are present in the form of dust clouds. Analysis of the particles by electron diffraction and neutral activation methods indicate the presence in particles of iron, nickel, cobalt, manganese, chromium, copper, zinc and aluminum. An estimate of the upper limit of 30,000 tons per year is obtained as the arrival on the Earth of particles from interplanetary space, if particles with a radius of 3-30 μ are considered. In these particles the ratio of the concentrations of iron, nickel and cobalt is the same as in meteorites.

Among similar investigations we mention a study by Crozier and Seeley. They collected meteor dust in the lower layer of the stratosphere and also used apparatus carried aloft in a high-level aircraft (ref. 802). According to their measurements, there is one particle larger than 10 μ, each 10^5 cm^3. Hodge and Wildt (ref. 444), in observations lasting one year, established that 1.1 particles of meteoric origin with a radius of 3-10 μ settle on 1 cm^2 of the Earth's surface in one day. This corresponds to the settling of $5 \cdot 10^5$ tons of

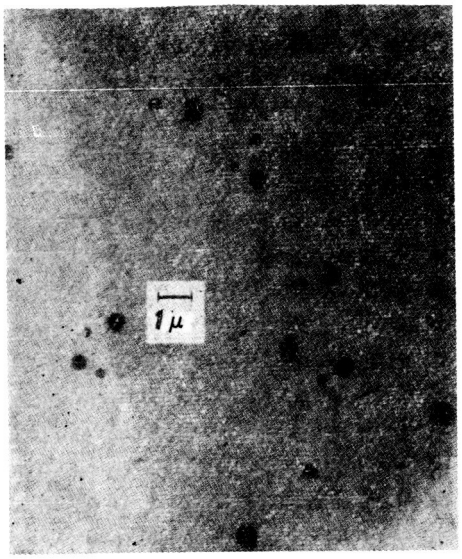

Figure 20.4. Electron micrography of particles collected by trap (impactor) by Kassell, Apr. 18, 1958 at Denver, Col., USA, at height of 18.8 km.

particles of this type on the entire surface of Earth in one year. Aircraft samples of cosmic dust also have been studied by Parkin and Hunten (ref. 668).

A similar discussion of the properties of an atmospheric aerosol is found in a review (ref. 696) by Reeger.

20.2. Meteor Dust. Much as it is possible to measure the vertical distribution of ozone in the stratosphere by studying the shadow of Earth's atmosphere on the lunar disk at the time of lunar eclipses (for further details see the author's book, ref. 233), similar observations can be used to investigate the dust content of the high layers of the atmosphere. It has been shown that there is an additional attenuation of light in the high layers of the atmosphere which many authors attribute to the existence of a dust layer. Earth's shadow, observed in projection on the lunar disk, has a definite structure dependent primarily on the Earth's atmosphere. The central parts of the shadow are subject to the influence of the entire atmosphere, primarily its lower layers (in the central part there is a very appreciable attentuation of brightness by tropospheric dust, as shown in ref. 647), but at the margins of the shadow the influence of the high layers of the atmosphere becomes operative. Photometric investigations of the margin of the Earth's shadow were begun as early as 1933 by Link (for a bibliography of studies made in the initial period see the reviews listed as refs. 24 and 755). These studies led to the hypothesis that at a height of about 100 km there is a dust layer (the shadow is 1.7-3.0 percent broader than it could be in the case of a pure atmosphere, ref. 84). It should be noted that ordinary optical measurements of atmospheric transparency of the vertical sounding type fail to give clear data on the attenuating layer in the high layers of the atmosphere because of the smallness of light absorption in it. The zenith ray is attenuated by only 2-3 percent in

the layer (ref. 648), whereas the tangent rays, projected on the lunar disk at the time of an eclipse, are attenuated by a factor of almost 2 (by 0.5-0.75 stellar magnitude, ref. 467). By interpreting twilight curves (see Chapter 2), Link concluded that the absorbing dust layer fills the entire atmosphere more or less uniformly from its lower layers to a height of the order of 100 km.

Undoubtedly the greater part of the dust in the high layers of the atmosphere is of cosmic origin. Space is filled with rarefied matter in gaseous and dust states. Clouds of cosmic dust are concentrated for the most part in the galactic plane. Light scattering by galactic dust matter emanates in the galactic glow whose brightness is 30-60 percent of the total brightness of the stars, where as in the direction of the galaxy it is almost 80 percent.

Such dustlike matter also fills Earth's planetary system, concentrated primarily in the plane of the ecliptic (ref. 212). The light absorption of this medium is so small that for all practical purposes it cannot be detected, but the glow caused by the scattering of sunlight by this medium can be observed on the dark background of the night sky, in any case in regions close to the Sun. This glow is known as the zodiacal light. The energy distribution in the spectrum of this glow is almost the same as the spectrum of the Sun itself, as should be the case if the scattering particles are large in comparison with the length of the light wave. The origin of the dust matter apparently is related to the gradual disintegration of the asteroids due to their collision with meteors. The dust matter arising from such disintegration, as a result of braking by light pressure (radiation braking) fills interplanetary space (ref. 212).

The dust in interplanetary space consists of tiny particles of different sizes. Individual particles of the dust medium meet with Earth, and upon entering into the Earth's atmosphere can be observed in the form of "shooting stars." According to data given by Whipple (ref. 799), the particles whose diameter exceed 4 μ form the phenomenon of luminescent meteors, whereas smaller particles are braked in the high layers of the atmosphere before they are heated to luminescence, and slowly descend into the lower layers of the atmosphere and to the Earth's surface.

The optical thickness Δ of the absorbing dust layer in the atmosphere has been represented by Link (ref. 556) in the form of the product

$$\Delta = m_0 kT,$$

where m_0 is the mass of meteor matter entering the atmosphere each sec per 1 cm^2; k is the attenuation factor, computed per unit mass; T is the time required for settling of dust particles to the Earth's surface. Measurements give a value Δ in the range 0.004-0.04. Link has made an attempt to determine k and T, which are dependent on particle size.

Careful astrophysical measurements make it possible to detect a decrease of atmospheric transparency following large meteor showers. The atmosphere is cleared of the dust excess, and normal transparency is restored in a time of the order of T = 100 days. Computations of the time required for the free falling of a particle from a height of 100 km to the Earth's surface give a value of the same order of magnitude, approximately 30-50 days (refs. 304 and 311).

The time T of falling of particles of the radius r in a fixed atmosphere whose density decreases exponentially with height from the 100 km level, where they experienced sudden braking and lost their cosmic velocities, to the lower boundary of the stratosphere, is expressed by Link by the approximate formula

$$\log T = -1.5 \log r + C,$$

where C is equal to 1.4 for metal particles and 1.6 for stone particles. According to this formula the time for falling of particles measuring $4\ \mu < 2r < 14\ \mu$ is 30-100 days. With a decrease of radius the value T increases rapidly; for particles $2r = 1\ \mu$ it approaches 1 year.

Taking into account the neutral character of absorption, Link assumes that the particles have a diameter of the order of 10^{-3} - 10^{-4} cm; the most effective diameter is 2-6 μ. By applying the theory of non-Rayleigh light scattering for particles of this size, it is possible to estimate the absorption coefficient k. Having the values Δ, k and T and using the equation $\Delta = m_0 kT$, Link computed m_0 and found that $m_0 = 10^{-14}$ g/cm^2 sec. It follows that about 5,000 tons of meteor dust falls to Earth in 1 day (ref. 557). Data from meteor statistics permit estimation of the total mass of visible meteors penetrating into the atmosphere each day. A value of the order of 1 ton was obtained. Invisible meteor dust is considerably greater in magnitude. Computations taking into account the concentration of dust matter in interplanetary space, as can be estimated from the brightness of the zodiacal light (a value of the order of 1 particle per 10^6 m^3 is obtained), give an influx of meteor dust of about 10^3 tons per sec, which is close to the result obtained by Link.

The size of particles of meteor dust in the atmosphere still cannot be considered finally established. Whereas Link believes that the effective diameter of particles is 2-6 μ, computations made by Swestka (ref. 755) indicate a diameter of less than 0.4 μ. He feels that particles with a diameter of the order of 4 μ can exist in the atmosphere only in very limited quantity. Only about 7 percent of the particles of this size entering into the Earth's atmosphere retain their magnitude at the time of arrival at the Earth's surface; 93 percent break down into smaller particles. The time required for the falling of particles with a diameter of 0.4 μ from a height of 100 km in a fixed atmosphere is very great, but Swestka believes that the settling of meteor dust can be accelerated considerably by turbulent mixing.

These computations by Sweskta have been criticized by Link (ref. 558). He believes that an analysis of the known optical properties of the atmosphere gives a value of the order of 10^{-4} cm as diameter of the particles.

On the basis of observations of radio wave reflections from ionized meteor trails it was found (ref. 500) that the diameters of the meteor particles responsible for ionization fall in the 40 - 200 μ range. However, it must be

remembered that small particles (less than 5 μ according to Whipple, refs. 799 and 800) do not produce ionization.

Determination of the quantity of dust constantly present in the high layers of the atmosphere, its vertical distribution, the sizes of the dust particles and their optical properties has great importance for determination of the limits of applicability and improvement of such important optical methods for the study of the atmosphere as searchlight sounding and the twilight method (see Chapters 2 and 3). In addition, dust particles can exert an influence on physical processes in the atmosphere. As demonstrated by L. R. Rakipova, the heating of dust particles by solar rays can be a source of heat and vertical mixing in the stratosphere (refs. 161 and 162). They can form a part of noctilucent clouds (Section 21). Bowen, who investigated the influence of meteor dust on the fall of precipitation (ref. 304), concluded that dust particles can be condensation nuclei. After settling gradually from the high layers of the atmosphere, they enter into tropospheric clouds and stimulate the falling of precipitation. Discussion of Bowen's conclusions still continues, with both supporters (ref. 356 and 642) and opponents (ref. 621) of his position. In particular, Bhalotra (ref. 295), who investigated statistics for precipitation in India over a period of several decades, failed to confirm Bowen's conclusions. The maxima in the intensity of precipitation which can be related to meteor streams are as numerous as those without this relationship.

Swinbank (ref. 756) pointed out that the quantity of water falling at the time of a heavy shower can be the result solely of tenfold exchange in the troposphere due to vertical movements. Even if meteor dust disrupts the colloidal stability of a cloud, it cannot be assumed that it can exert an influence on dynamic processes of such magnitude.

Interesting computations of the downward propagation of small particles of cosmic origin by turbulent mixing were published by A. A. Dmitriyev (ref. 57).

In 1956-1957 it was noted that there are appreciable quantities of dust particles in the ionosphere at heights greater than 100 km. N. B. Divari, (ref. 54), interpreting data on the change of the spectral composition of the twilight sky, obtained in 1946 by T. G. Megrelishvili and recently confirmed by him, postulated that with increasing height, beginning at about the 100 km level, particles appear which scatter light neutrally or even proportional to wavelength λ^{+1} (molecular scattering proportional to λ^{-4}). The law $\sim \lambda^{+1}$ is valid for particles, the ratio of whose radius r to λ is a value of the order of

$$\frac{r}{\lambda} = \frac{5}{\pi} .$$

In this case r is approximately 1 μ.

According to Hoffmeister's data (ref. 449), meteor dust is present in the atmosphere at heights of 90-180 km.

The presence of meteor particles in the high layers of the atmosphere can be detected by apparatus carried aloft in rockets. The rocket carried plates of soft metal on which scratches and pits could be observed with a microscope after the flight (ref. 802). After several minutes of exposure of a plate with an area of about 1,000 cm^2, it was possible to observe pits whose diameter was 10-100 μ. On the basis of the number of pits and the exposure time of the plate, it was possible to compute that the concentration of meteor particles was such that there is an average of 1 particle in a volume of 10^6 cm^3. Micrometeorites are meteor bodies with a diameter less than 100 μ (according to the terminology introduced by Whipple, a micrometeorite is a particle of cosmic matter which, because of its insignificant mass, is capable of penetrating into the Earth's atmosphere, heating throughout its entire volume, and releasing heat by radiation, remains unmelted; in such cases the particle mass remains constant and in the final analysis they settle on the Earth's surface, ref. 808). They also have been recorded using a metal microphone carried on the surface of the rocket skin. Signals from the microphone are fed through an amplifier along a telemetric line to Earth. At first an "ultrasonic boom" was noted during the flight of the rocket. Most investigators interpreted this phenomenon to be the result of "bombardment" of the rocket by micrometeorites. The study of instrument parameters revealed that the bombarding particles should possess energies of the order of 10^{-2} erg. It follows that the mass of particles is approximately 10^{-12} g (particle diameter of about 2 μ), and that there is one particle in a volume of 10^8 cm^3.

According to Whipple's computations (ref. 802), the probable number of collisions with particles possessing energies greater than 10^{-2} erg is 10 collisions per sec per m^2. During the 144 sec flight of a V-2 rocket (between the 70th and 214th sec of flight) a total of 66 collisions was recorded, i.e., an average of 1 collision each 2.2 sec, which does not differ greatly from Whipple's theoretical computations.

The study of micrometeorites has assumed particular importance since the launching of artificial earth satellites. This is true because micrometeorites with their great kinetic energy can inflict damage on satellites by penetrating their skins.

On the basis of measurements on an "Aerobee" rocket it was computed that in one day 40,000 - 80,000 tons of meteor dust fall to the Earth's surface. This dus consists of particles of micrometeorite size whose apparent (stellar) magnitude ranges from 10-30. According to measurements on the satellite 1958 α, the daily influx of meteor dust in February was 10,000-13,000 tons (refs. 362 and 363).

The method for investigating micrometeorites on rockets and satellites has been considerabley improved by Soviet investigators. T. N. Nazarova, S. M. Poloskov and their colleagues measured impacts by use of a ballistic sensor.

Their measurements considerably improved the data obtained by foreign investigators. Measurements on the third Soviet artificial earth satellite recorded an average frequency of impacts of micrometeorites of about 6 per 1 m^2 per hour or $4.4 \cdot 10^{-12} g/m^2 sec$ (for 2 stellar magnitudes). In addition, there were brief sharp increases of the number of impacts. At heights of 1,700-1,800 km at the time of sharp increase in the frequency of impacts, their number reached 22 per m^2 per sec; at heights of 1,300-1,500 and 500-600 km, an average of 10 and 9 impacts per sec, respectively, was recorded per m^2 of surface.

Proceeding on the assumption that the impact registered by the sensor upon contact with a particle is proportional to its energy, it is concluded that the recorded meteor particles possess energies of about 10^4 erg.

Important information on the properties and quantity of meteor dust is obtained from observations of the radio echoes of meteors (ref. 506).

The settling meteor dust finally falls on the Earth's surface and on the surface of the oceans. Many investigators collected such dust by use of special containers, a sticky microscope object glass, glycerin-smeared plates, etc. In some cases dust is obtained from rain or sea water, hail (ref. 311) and snow (ref. 93). There have been rare cases of the fall of considerable quantities of meteor dust. The most recent of these cases was recorded at Omsk on Sept. 3, 1956, where up to 1 g of dust fell per 1 m^2. Falling of meteor dust at the time of a heavy rain on July 2, 1941 also was recorded at Omsk. The rain was reddish and analyses revealed that it contained meteor dust. It is also possible to compute the balance of meteor dust on the Earth from the quantity of dust settling over a long period. Analysis of sea water made by Petersen in Sweden and Rotshey indicates that the arrival of meteor dust into the atmosphere is 0.1 ton (8,500 tons per day) per sec. If it is assumed in the computations that the mean diameter of a dust particle is 10 μ, the mentioned influx of dust matter is 10^3 particles per day per m^2. This corresponds to a concentration of 1 particle per 10^7 cm^3 (or 1 particle in a vertical atmospheric column with a cross section of 1 cm^2).

20.3 Volcanic Dust. An enormous quantity of dust was ejected into the stratosphere at the time of the famed eruption of the volcano Krakatao in 1883. Although strong volcanic eruptions occur relatively rarely, the dust particles ejected into the high layers of the atmosphere are especially fine and can remain suspended there for a long time. The presence of dust of volcanic origin in the high layers of the atmosphere, therefore, is not a very rare phenomenon and in appropriate cases should be taken into account.

At the time of particularly powerful eruptions, such as Krakatao volcano in 1883 and Katmai volcano in 1912, such great quantities of dust were ejected

into the stratosphere that its presence was manifested in the form of anomalous twilights, a large decrease of atmospheric transparency (by 10 percent), a sharp increase of the solar aureole (ref. 278), etc. The quantity of ejected dustlike matter and ash is much less at the times of more frequent eruptions of lesser intensity. It is far more difficult to detect the presence of dust in the stratosphere in these cases. However, a new means has been discovered recently for detecting such dust. As a result of the increase of the ceiling of modern aircraft, regular flights in the stratosphere at heights of 12-15 km (scheduled passenger flights and aircraft sounding of the atmosphere for meteorological purposes) have become increasingly common. During flights at great heights, fliers sometimes discover dust clouds in the stratosphere. These clouds usually are difficult to observe from the Earth because they are very transparent in a vertical direction. However, due to their great horizontal extent they are easily visible from the side, if the observer is approximately at the same height as the clouds. An example are the dust clouds observed over western Europe from July 24 to Aug. 4, 1953. Thus, Jacobs (ref. 476) expresses the opinion that rarefied and very high (12-15 km) clouds consisting of ice crystals and dust particles appear more frequently than was formerly assumed.

Jacobs describes in greater detail a thin cloud layer observed from an aircraft over England at a height of 15 km during July 27-30, 1953. The thickness of the layer was 100-150 m. Judging from the external appearance, the clouds contained a large quantity of dust particles. After analyzing atmospheric conditions he concluded that the clouds consisted of dust particles and small ice crystals. The tropopause in the region of appearance of the clouds was at a height of 8.5 km.

These same clouds were observed in a number of places in western Europe, and in places their height was as great as 22 km. The appearance of the clouds apparently was related to the eruption of an Alaskan volcano on July 9, 1953. It is interesting to note that atmospheric turbidity also was noted during observations of a lunar eclipse (ref. 783) occurring during this period (July 26). The density of the Earth's shadow had an anomalously high value, about 6.0 (at the center of the shadow for green light), rather than the nearly normal value 4.8 during the eclipse of Jan. 29, 1953.

The appearance of dust clouds over the western part of England after eruption of an Alaskan volcano in 1955 also can be mentioned (ref. 312).

In this same reference Bull and James give interesting data on stratospheric dust over western England. Between 1000 and 1045 hours on Apr. 3, 1956, the pilots of an aircraft at a height of 15 km observed a layer of "clouds" of dust at a height of about 1.5 km above the aircraft, that is, 16.5 km above the Earth's surface. Insofar as the pilots could judge, the clouds extended over the entire southwestern part of England. When viewed from directly below, the clouds had a whitish color, were transparent and the sky above them was blue. On a flight on Apr. 4, these same pilots passed through a layer of haze 15 m thick at a height of 12 km; this layer was more undulating than the day before. On these days the tropopause was at a height of 10.8 km and the dust clouds, therefore, obviously were in the stratosphere.

These authors (ref. 312) conclude that the appearance of dust clouds over England in April 1956 can be attributed to the transport of volcanic dust after the eruptions of Bezymyannyy volcano on Kamchatka on Mar. 30 and Apr. 1, 1956. At that time the dust clouds attained heights of 20 km. The dust fell around the volcano in a radius of 80 km. A layer of dense haze was observed over Alaska at 1000 hours on Apr. 3 at a height of 3 km, but no dust was observed over the United States. An analysis of the high-level pressure field made it possible to determine the paths of air masses at heights of 12-16 km. The authors (ref. 312) used high-level pressure pattern charts for the 100 mb level for 0300 and 1500 hours for each day from Mar. 30 through Apr. 3; two of these have been reproduced in figures 20.5 and 20.6. Figure 20.7 shows the plotted paths followed by air masses at the 100 mb level (curves 1 and 2) and the 200 mb level (curve 3), computed "backwards" from Apr. 3-2, beginning from Aldergrove in northern Ireland (curve 1) and from a point 5° to the east of Aldergrove (curve 2) (dust clouds were observed in this area on Apr. 3, 1956) and "forward" from Mar. 30 to Apr. 1, beginning from Kamchatka (curve 3). In order for an airborne particle to arrive at Aldergrove at 1800 hours on Apr. 3 on Apr. 2 at 0900 hours, it would have had to be at the point 77°N, 40°W, as shown by curve 1. Bull and James do not believe that the determination of this point is very reliable. They believe a more reliable point is 80°N, 20°W, where an airborne particle would have to be at 0900 hours on Apr. 2 in order to arrive 5° east of Aldergrove at 1800 hours on Apr. 3 (curve 2).

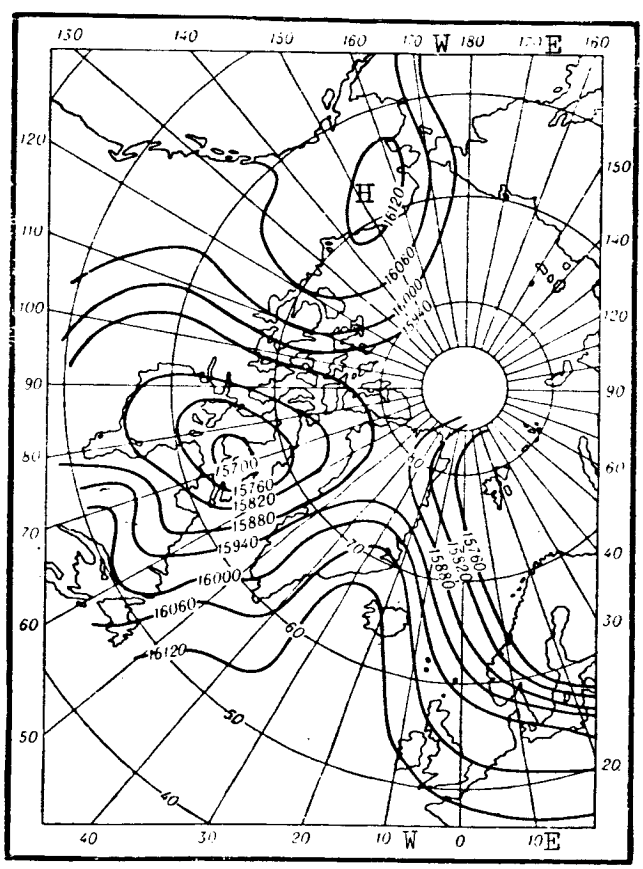

Figure 20.5. Pressure pattern chart of 100 mb surface to north of 50°N at 1500 hours on Mar. 31, 1956.

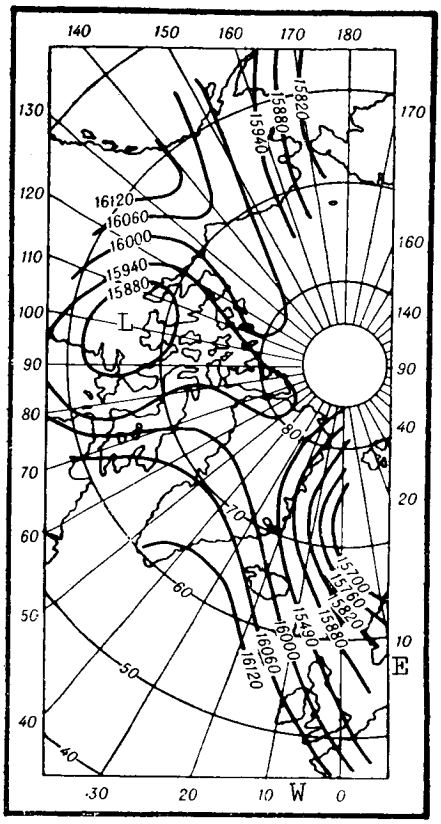

Figure 20.6. Pressure pattern chart of 100 mb surface to north of 50°N on Apr. 2, 1956.

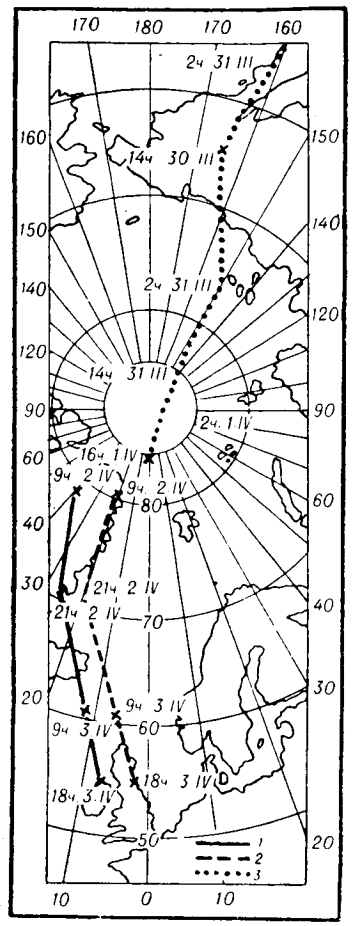

Figure 20.7. Paths of air masses. ч = hour.

The distance from Bezymyannyy volcano on Kamchatka to the point 80°N, 40°W, calculated along a great circle, is about 5,000 km. The airborne particle required about 75 hours to cover this distance, giving a mean velocity of movement of the dust cloud from the point of its ejection across the polar basin of about 70 km/hour. Bull and James believe that it has been established quite reliably that the dust clouds observed in the stratosphere over western England on Apr. 3-4, 1956 were formed from dust ejected into the atmosphere by a volcano on Kamchatka on Mar. 30 and Apr. 1 of that year. During this period the air masses moved at a height of about 16 km from Kamchatka to western England across the polar basin and Greenland.

20.4 Ascent of Dust from the Earth's Surface in Ascending Air Currents. Two sources of the dust content of the stratosphere have been considered: meteor dust and volcanic eruptions. In addition, the dust carried upward from the Earth's surface by ascending air currents can penetrate to relatively great heights in the troposphere. We now will consider whether air currents can entrain dust even to greater heights, even into the stratosphere. Data on the

variations of the vertical distribution of O_3 molecules make it possible to postulate the existence of more or less intense vertical exchange in the atmosphere to heights as great as 30-50 km. A confirmation of this possibility is the high air humidity sometimes detected at heights of 30-35 km (see Section 19). Of course, such ascending air currents can entrain only fine dust particles and carry them from the troposphere into the stratosphere, since too great a vertical velocity would be required for carrying large particles upward.

Data from aircraft measurements made by Crozier and Seeley (ref. 802) indicate that in the lower layers of the stratosphere there is one particle with a diameter greater than 10 μ per each 10^5 cm^3, that is, 100-1,000 times more than can be attributed to meteor dust. This excess can be caused by dust particles carried aloft from Earth's surface by ascending air currents.

Hoffmeister (ref. 448), on the basis of interpretation of some twilight curves, concluded that at a height of about 16 km there is an aerosol layer which changes in thickness from time to time. He believes that this layer is related to manifestations of atmospheric turbulence. Bigg (ref. 297) confirmed the existence of such peculiarities on twilight curves. However, this problem cannot be regarded as solved at this time because T. G. Megrelishvili (ref. 594) and I. A. Khvostikov (ref. 523) objected to Bigg's method of interpretation of twilight phenomena. In particular (Chapter 2), twilight phenomena can be used for atmospheric sounding only at great heights (more than 20 km).

20.5. Influence of Aerosol Particles on Optical Properties of the Atmosphere. V. I. Myukhkyurya (ref. 136) investigated the vertical distribution of the aerosol component of the sunlight extinction coefficient (measurements from an aircraft). He did not discover an exponential decrease of the extinction coefficient. Similar investigations were made by G. P. Faraponova (ref. 197) and others. G. P. Gushchin showed that above 6 km the optical thickness of aerosols still is a considerable value, on the average equal to 24 percent of the entire optical thickness of aerosols (ref. 48). A. A. Dmitriyev and A. Ye. Mikirov investigated the influence of cosmic dust and the disintegration products of meteors on the actinometric characteristics of the atmosphere (ref. 58).

The relationship between some properties of the high layers of the atmosphere and meteor matter was analyzed theoretically by B. A. Mirtov. He concluded that at the 92-96 km level in the atmosphere there is a transition with non-Rayleigh scattering being replaced by Rayleigh scattering. At a still greater height there is a transition from Rayleigh to non-Rayleigh scattering. In addition, Mirtov postulates that the luminosity of the night sky in the green line of oxygen can be of meteoric (micrometeoric) origin.

An attempt can be made to estimate the quantity of dust matter by analyzing the results of searchlight sounding. This requires comparison of the measured intensities of the light scattered by individual atmospheric layers and the intensities computed for a purely molecular atmosphere. Elterman (ref. 378) reports the discovery at heights of 9.5-20 km of a small excess of the brightness of scattered light over that which should be caused by the molecular scattering of light by pure air. He believes that this light excess is caused by the presence

of aerosol particles at the mentioned heights. V. M. Morozov (ref. 606) has published 3 curves obtained by searchlight sounding of the atmosphere. They indicate that the actual intensity of scattered light at almost all heights from 5 to 30 km exceeds the intensity of molecular scattering by a factor of 1.5-2. According to the data presented by Elterman (ref. 378), based on an analysis of 90 searchlight sounding curves, there is no excess of the brightness of scattered light at heights of 20-45 km.

At the beginning of this section we discussed data obtained from observations of lunar eclipses which permit detection of additional turbidity of the Earth's atmosphere, apparently caused by meteor dust. A further study of these phenomena indicates the possibility of detecting dust of terrestrial origin in the relatively high layers of the atmosphere. In the brightness distribution of the eclipsed Moon it was found that in Earth's shadow there is a predominance of brightness in the eastern part of the shadow in comparison with the western part for identical distances from the center of the shadow (according to data presented by V. P. Dzhapiashvili, ref. 52, it is more conspicuous in blue light than in yellow). V. M. Chernov and V. F. Chistyakov postulated that this effect is caused by a large quantity of dust and vapor in the evening (western) part of the Earth's shadow in comparison with the morning (eastern) part. If this hypothesis is correct, it would be possible to use observations of lunar eclipses for a quantitative estimate of the difference in the dust content in the evening and morning parts of the Earth's atmosphere (ref. 52). The diurnal variation of the transparency of the high layers of the atmosphere cannot be related to variations of the quantity of meteor dust entering the high layers; apparently it should be interpreted as the result of the vertical redistribution of turbidity-causing particles caused by vertical exchange in the stratosphere.

A phenomenon of great interest was first discovered by Danjon by analysis of observations of 70 lunar eclipses over a period of nearly a hundred years (1823-1920). He discovered periodic changes of the brightness and color of lunar eclipses in rigorous dependence on the 11 year sunspot cycle. For 2 years after a minimum of solar activity the lunar eclipses are very dark, but as the maximum of activity approaches, the Moon becomes increasingly brighter at the time of eclipses. This pattern was confirmed by Vaucouleurs for the eclipses occurring from 1920 through 1943. A similar dependence was found by Dyubua for the brightness of earthlight on the Moon. As is well known, earthlight is created by the Sun's rays, reflected and scattered by the Earth and its atmosphere. Dyubua found that earthlight gradually becomes brighter with approach to the epoch of the minimum of solar activity, but darkens appreciably immediately after the minimum of activity (ref. 781).

The Danjon law and the observations by Dyubua show an increase of the turbidity of the Earth's atmosphere and, therefore, of its scattering capacity, as soon as a new cycle of solar activity begins. In 1956 E. Vassy postulated that the cause of this turbidity is the deep penetration of solar corpuscular radiation into the atmosphere (a little below the level of the auroras), resulting there in the formation of clouds (solar corpuscles stimulate the formation of condensation nuclei, ref. 781).

It should be remembered that in recent years it has become increasingly possible to relate a number of meteorological phenomena in the troposphere and

stratosphere to solar activity, but a consideration of this problem is beyond the scope of this book. It must be assumed, however, that further investigations of periodic changes of the brightness of lunar eclipses and earthlight on the Moon will be a source of new information on the vertical redistribution of atmospheric aerosols in the stratosphere, caused by exchange between the troposphere and stratosphere.

In this section we have considered data on "dry" aerosol particles in the high layers of the atmosphere--dust particles. Other aspects of the problem of aerosol particles in the high layers of the atmosphere are the products of condensation and crystallization. This requires mention of the two special types of clouds in the high layers of the atmosphere--nacreous and noctilucent clouds. These problems will be discussed in Section 21.

21. Nacreous and Noctilucent Clouds

The problem of stratospheric (nacreous) clouds is closely related to the problem of the aerosol composition of the air in the high layers of the atmosphere discussed in Section 20. These clouds appear very rarely at great heights, and were observed in winter at a height of 20-30 km. In addition, there are clouds above the stratosphere (noctilucent clouds), observed in summer at heights of 70-90 km. The problem of the origin and constitution of these clouds is related directly to the study of water vapor and dust particle content in the high layers of the atmosphere (Sections 19 and 20). Since nacreous and noctilucent clouds possess some unusual properties (discrete time, geographic area of occurrence and height of formation), their origin is of great interest for the meteorology of the stratosphere and a number of aspects of the physics of the high layers of the atmosphere.

21.1. Nacreous Clouds. Clouds in the stratosphere at a height of 20-30 km, called nacreous clouds (termed iridescent clouds in England), are the rarest form of clouds. They have been observed only about 200 times (ref. 438).

The beginning of systematic observations of nacreous clouds was the work of Mon in Oslo in 1871. In a period of 21 years he succeeded in observing them 42 times. Beginning in 1890 Störmer organized regular observations of clouds at Norwegian observatories established for the study of auroras. Störmer obtained excellent photographs of nacreous clouds, including color photographs, and repeatedly measured their height from a base up to 160 km long.

Nacreous clouds are observed almost exclusively in the winter months. Table 21.1 gives data obtained by Mon (1871-1892), Störmer (1926-1957) and Hesstvedt. Hesstvedt (who prepared this summary) expresses the opinion that some of the cases of observation of nacreous clouds cannot be considered reliable because an inadequately experienced observer can mistake altocirrus clouds for nacreous clouds (ref. 438). Hesstvedt, therefore, separates those observations based on reliable data from the total number and groups them as "real" observations; he regards those as "real" which were made by experienced meteorologists or independently by two observers.

TABLE 21.1. APPEARANCE OF NACREOUS CLOUDS IN DIFFERENT MONTHS.

Place of observation	Jan.	Feb.	Mar.	Apr.	May	June	July	Aug.	Sep.	Oct.	Nov.	Dec.	Total
Southern Norway, 1871-1892 (Mon)	16	6	3	--	1	1	2	--	--	--	2	11	42
Southern Norway, 1926-1957, all observations (mostly Störmer)	30	29	1	3	--	--	1	1	--	--	4	15	84
Northern Scandinavia, all observations (Störmer)	16	15	3	--	--	--	--	--	--	--	1	7	42
Southern Norway, 1926-1957, real observations	20	20	1	1	--	--	--	--	--	--	1	9	52
Northern Norway, 1926-1957, real observations	9	3	--	--	--	--	--	--	--	--	1	4	17
Southern Norway, 1946-1950, all observations	4	6	1	--	--	--	1	1	--	--	--	2	15
Southern Norway, 1946-1950, real observations	4	6	1	--	--	--	--	--	--	--	--	2	13

The initial observations by Mon were not accompanied by height measurements and, therefore, part of the clouds which he recorded may or may not be nacreous clouds. If all observations are considered, 86 percent fall in the winter months (December, January and February) (Table 21.1). According to Stormer's data, all the appearances of nacreous clouds (except 2), recorded after 1926, fall in a period of about 4.5 months--between Nov. 13 and Apr. 2. In the case of "real" observations the percentage of occurrences in winter is still greater, 94 percent.

Nacreous clouds appear in very limited regions (ref. 237): they have been seen in the Scandinavian countries, Finland, Great Britain, Scotland and Alaska. However, there are indications that under suitable meteorological conditions high clouds also are observed at other latitudes, and not only in winter (ref. 64). Ross observed a nacreous cloud in India (11°N) in April. A. Ya. Driving, N. V. Zolotavina, M. N. Polozova and A. I. Smirnova (refs. 64-66) in the Caucasus (42°N) used polarized light for photographing a cloud at a height of 22.4 km, illuminated at night by a searchlight. One case of observation of a nacreous cloud in the southern hemisphere is reported (ref. 605) from the Australian base Mawson in Antarctica.

Störmer's determinations show that the height of nacreous clouds on the average is close to 25 km (Tables 21.2 and 21.3).

Nacreous clouds usually are brightly colored: red, orange, green, blue and violet colors are arranged either in irregular patches or in bands in the same sequence as in the rainbow. The colors apparently are caused by diffraction in ice crystals or more likely, in small water droplets (ref. 64). The angular radius of the aureole, according to Störmer's data of Feb. 19, 20, 1932, is 15-18°; this indicates diffraction on droplets with a diameter of about 2 μ. A cloud observed in a searchlight beam at a height of 22.4 km over Bakuriani (in the

TABLE 21.2. MEAN HEIGHT OF NACREOUS CLOUDS DETERMINED BY PHOTOGRAMMETRIC MEASUREMENTS (STÖRMER).

Measurements	Dec. 30, 1926	Jan. 18, 1929	Feb. 2, 1930	Jan. 29, 1932	Feb. 19, 1932	Feb. 20, 1932	Feb. 6, 1934
Number of points	15	235	28	238	253	138	215
Mean height, km	24	24.1	24.1	27.4	24.8	23.2	24.7

Caucasus) apparently consisted of drops with a mean radius of about 1.5 μ. This conclusion is based on the results of measurement of the degree of polarization of scattered light at different angles of scattering (ref. 65). Ordinary clouds consist of larger drops.

Hesstvedt, (ref. 438) on the basis of measurements of the angular dimensions of aureoles, obtained values from 0.95 to 1.5 μ for the radius of droplets of nacreous clouds. According to his computations, the quantity of particles per unit volume of a nacreous cloud is 10-500 times less than in ordinary tropospheric clouds, and the liquid water content is 10^3 - 10^4 times less.

Data on air temperature and humidity in the stratosphere in a period of formation of nacreous clouds are very limited. It can be postulated that the clouds are formed at exceptionally low temperatures at a height of about 25 km, at about 195-200° K and lower.

The form of nacreous clouds makes it possible to postulate that they are formed in airwaves on the leeward side of a mountain range. This is confirmed by an unquestionable relationship between the appearance of the clouds and the presence of mountain ranges and currents directed at right angle to these ranges. Observations show that such airwaves are formed on the leeward side of ranges to a height exceeding the height of ranges by a factor not less than 4-5. If the amplitude of airwaves is 1 km, at an initial temperature of -40° and a relative humidity of 39 percent condensation of water vapor begins at the peak of the wave, whereas at a temperature of -60° an initial humidity of 24 percent is adequate (ref. 237).

In investigating the problem of the undulating character of the clouds, it is necessary to note an interesting communication by Hesstvedt (ref. 437). When there was a certain synoptic condition in the periods of occurrence of nacreous clouds, he simultaneously observed undulating altocirrus clouds in the region of the tropopause. The length of the wave for these clouds, according to Störmer's measurements and those of other investigators, is approximately 40 km; the doubled amplitude is about 1.5 km. The opinion has been expressed that airwaves, at whose crests nacreous clouds are formed, are characterized by the same length of wave. Hesstvedt postulated that the length of the wave can be considered the distance between two nacreous clouds lying on a straight line in the direction of the wind (this supposition corresponds to conditions under which nacreous clouds are formed only near the crest of a wave). Measurements made in different years from 1926 to 1956 indicate a surprising constancy of the wavelength of airwaves under the conditions when nacreous clouds are observed. This is clear from

TABLE 21.3. WAVELENGTH OF AIRWAVES FROM OBSERVATIONS OF NACREOUS CLOUDS AND THEIR HEIGHTS (HESSTVEDT).

No. of measurements	Date	Nacreous clouds		Height of cirrus clouds, km
		wavelength, km	height, km	
1	30 Dec. 1926	35	27.7 ± 1.6	
2	13 Jan. 1929	42	24.1 ± 1.6	
3	12 Feb. 1930	37	24.0 ± 1.6	12.6 ± 1.5
4	29 Jan. 1932	45	27.4 ± 1.8	
5	19 Feb. 1932	42	24.8 ± 2.6	
6	20 Feb. 1932	30	23.2 ± 1.7	
7a	6 Feb. 1934	45	24.7 ± 2.4	12.1 ± 1.2
7b	6 Feb. 1934	40	24.7 ± 2.4	
8	16 Feb. 1946	40	21.0 ± 3.8	
9	29 Feb. 1956	39	21.5 ± 2.1	
Mean		39.5	24.3	12.4

Table 21.3, which gives the results of 10 such measurements. In 2 cases, undulating altocirrus clouds were observed simultaneously; their heights are given in the table.

The problem of the character of the synoptic conditions under which nacreous clouds are observed is very interesting. This problem has been investigated systematically only by Mon and Dietricht (ref. 237) and recently by A. Ya. Driving (ref. 64). In particular, Driving pointed out the possible role of the winter stratospheric jet stream in the northern part of Europe. Such a systematic study was also made by Hesstvedt (ref. 438). The gradual increase of the ceiling of radiosondes now permits construction of synoptic charts for the 25 mb level (about 24 km) and above. Analysis of such high-level charts apparently will lead to a more thorough understanding of the conditions for the formation of nacreous clouds.

The relationship between the formation of nacreous clouds and the presence of well-developed cyclones noted in the early investigations was not confirmed by Hesstvedt's data. A detailed analysis of synoptic conditions under which nacreous clouds are observed has shown (ref. 438) that only a few winter cyclones are accompanied by the formation of clouds.

Hesstvedt attributes great importance to the polar front: he postulates that nacreous clouds are formed for the most part near a line situated midway between the warm and cold fronts of the wave of the polar front. Nacreous clouds are formed equally well in tropical and polar air masses with a high (cold) and low (warm) tropopause. The formation of nacreous clouds is not dependent on the temperature profile of the atmosphere below 15 km. The air temperature at the level of occurrence of nacreous clouds apparently is considerably lower than the mean seasonal values. The cooling of air to a temperature necessary for formation of a nacreous cloud is the result of cooling of arctic air

during its movement through the tropospheric frontal cyclone (a temperature decrease by 10-15°) and additional cooling during local ascent caused by lee waves.

A. Ya. Driving, who also investigated the synoptic conditions favorable for the formation of nacreous clouds, pointed out the possible role of the winter stratospheric jet stream in the northern part of Europe (ref. 64).

Hesstvedt noted close correlation between the theoretical determination of the critical temperature of homogeneous formation of nuclei in supercooled water and the experimental data on the freezing of water droplets reported by some investigators (ref. 438). Such correlation exists if a value of 31.7 erg cm^{-2} is accepted for the specific surface free energy of "ice-water" discontinuity. It was demonstrated theoretically that pure water cooled to -117° would remain in a supercooled (or glassy) state for a long time. The temperatures measured at the time of appearance of nacreous clouds vary in the range from -85 to -100°, and the concentration of condensation nuclei is about $0.5/cm^3$. Hesstvedt has computed the rate of growth of droplets for these conditions and obtained a theoretical value of 1.2 μ or less for the radius of particles with a narrow particle-size range.

21.2. Noctilucent Clouds. The first observations of the unusual clouds called "noctilucent clouds" were made in 1885. Ernst Hartwig, a specialist at the Astronomical Observatory of Tartu University, observed them 11 times from June 23 through Aug. 1, (ref. 195). They were observed simultaneously by Jesse near Berlin. However, even before this, on the evening of June 13, 1885, the famed Russian astronomer V. K. Tseraskiy had noted strange clouds. Tseraskiy wrote: "They are different in appearance from the others, particularly striking due to their color. These clouds shone brightly in the night sky with pure white, silvery rays, sometimes with a faint bluish hue, in the immediate vicinity of the horizon assuming a yellowish, golden shade. There were cases when they gave off considerable brightness, so that the walls of the buildings glowed conspicuously and indistinct objects stood out sharply" (ref. 239).

It appeared that these clouds were situated at great height. Their bright illumination and the luminosity in the night sky suggests that they are situated above the Earth's shadow and therefore are illuminated directly by the Sun's rays. It is possible to determine the true altitude of noctilucent clouds from the angle of solar depression and the apparent altitude of the clouds above the horizon. The first such determinations revealed that this height certainly exceeds 50 km, i.e., much higher than all known cloud forms.

On June 26, 1885 Tseraskiy made a direct determination of the height of noctilucent clouds by simultaneous observations from two points. A. Belopol'skiy, later one of the most outstanding Russian astronomers and astrophysicists, participated in these base measurements. Belopol'skiy made his observations in the village Listvyanakh, near Pushkin, along the Yaroslav railroad, and Tseraskiy made his observations at Moscow. The distance between these points was 32 km. From the observations of June 26 both observers obtained a height of noctilucent clouds of 73.5 km.

The measurements made by Tseraskiy and Belopol'skiy were visual, and therefore there was no pretense to great accuracy. Later photography came into use for

base measurements of the height of noctilucent clouds, and this resulted in a greater accuracy. It was established that the average height of noctilucent clouds is 82 km. Jesse, in Germany, who discovered noctilucent clouds almost simultaneously with Tseraskiy (a few days later), obtained an average height of 82.9 km in 1889 and 82.1 km in 1891; measurements by K. D. Pokrovskiy in Russia in 1897 gave a value of 82 km; and Störmer in Norway in 1932 determined a height of 81.4 km, and later 82.2 km in 1934. Individual (unaveraged) determinations rarely give heights which do not fall in the range 75-90 km (a bibliography of investigations of noctilucent clouds published up to 1939 is included in a study by I. S. Astapovich (ref. 6).

The great height of noctilucent clouds and the constancy of this height is an important property which is manifested clearly when clouds of different forms are observed simultaneously. In this case clouds of ordinary types stand out on the background of the sky as a dark mass, whereas noctilucent clouds shine brightly. In 1951 N. I. Grishin was able to take a photograph of such clouds near Moscow (fig. 21.1). Figure 21.2 is a photograph of noctilucent clouds in a clear sky.

Noctilucent clouds constantly move rapidly. This makes it possible to obtain important information on air currents in the high layers of the atmosphere. The selection of the place and time of their appearance is illustrated in figures 21.3 and 21.4. In the northern hemisphere they usually are observed in a narrow geographic zone between 45 and 70° latitude; in the southern hemisphere they appear randomly and rarely. It follows from individual observations that the climatic characteristics of the southern hemisphere establish the zone of noctilucent clouds in latitudes lower than in the northern hemisphere. The problem of the frequency of occurrence of noctilucent clouds has been repeatedly discussed in the literature. There are reports of the total absence of noctilucent clouds in individual years and even in the course of several successive years (ref. 38). In a summary prepared by Shpangenberg, who collected 42 reports on observations of noctilucent clouds in western Europe in 1932-1941 from different sources, their occurrence is distributed by years as follows:

Figure 21.1. Tropospheric clouds on background of noctilucent clouds on night of June 10-11, 1951.

Year	1932	1933	1934	1935	1936	1937	1938	1939	1940	1941	Total
Number of Observations	4	11	10	5	4	2	1	0	1	4	42

The highest percent of recorded occurrences of noctilucent clouds falls in the period of observations of the Second International Polar Year (1932-1933) and can be attributed to the increased attention of observers to all clouds, in conformity with a special program (noctilucent clouds did not constitute a separate field of research during the Second International Polar Year). The cited summary cannot be regarded as sufficiently complete (ref. 38). A summary of observations in the USSR prepared by G. O. Zateyshchikov and V. A. Bronshten lists 25 dates of appearance of noctilucent clouds in 1936. In recent years the interest in noctilucent clouds has increased considerably, and the greater attention of observers has led to a great increase in the number of recorded appearances of noctilucent clouds. According to patrol observations of the members of the Moscow and Gor'kiy Divisions of the All-Union Astronomical and Geodetic Society, in a 6 year period (1950-1955), 97 occurrences of noctilucent clouds were observed in the European part of the USSR (ref. 38); there were 10 in 1950, 21 in 1951, 8 in 1952, 19 in 1953, 17 in 1954 and 22 in 1955. A summary prepared by Paton (ref. 709) for Scotland indicates that noctilucent clouds were observed 22 times in the years 1939-1953. In the northern hemisphere noctilucent clouds are observed only in the warm part of the year, for the most part in July; they are observed less frequently in June and August. But when they do appear, the noctilucent clouds usually cover large areas, 10^4 to 10^5 km^2.

L. F. Gromova (ref. 42) has analyzed 369 cases of observations of noctilucent clouds in the northern hemisphere from 1885 through 1956 and determined (in arbitrary relative numbers) the distribution by months and latitude zones (see Table 21.4). In this table corrections were introduced to take into account climatological data on the number of clear nights and change in the duration of the twilight hours favorable for observations of noctilucent clouds. Their earliest appearance is in the second 10 day period of April and the latest is in the first 1 day period of October.

Figure 21.2. Noctilucent clouds.

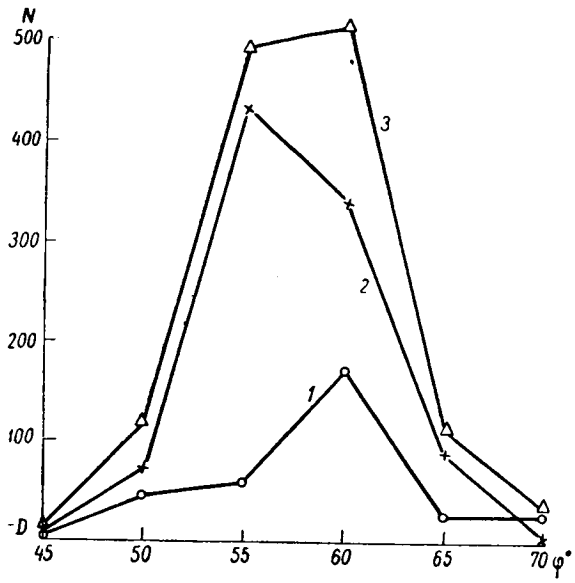

Figure 21.3. Distribution of number N of cases of visibility of noctilucent clouds by latitude. 1, 1957; 2, 1958; 3, 1957 and 1958.

A thorough investigation of the climatology of noctilucent clouds was made under the direction of V. V. Sharonov (ref. 246) and by T. D. Pavlova (ref.143). These investigations were based on the observations of the network of stations of the Hydrometeorological Service of the USSR during the IGY period. Some of the results are shown in figures 21.3 and 21.4.

The structure of noctilucent clouds as viewed from Earth sometimes is characterized by great complexity and variety (ref. 92). There can be sharply defined or blurred bands, "jets," ridges and crests, undulating curves, eddy-like formations with a diameter as great as 2-3° and large vortices with a diameter greater than 3°. The simplest form of noctilucent clouds is a so-called "veil", apparently situated below the other forms of noctilucent clouds and visible against their background as a nebular formation with a delicate white or bluish glow; it frequently precedes the appearance of other forms (by 0.5-1 hour). A morphological classification of noctilucent clouds has been developed by N. I. Grishin (ref. 36). This classification was adopted in the USSR for observations under the International Geophysical Year Program.

TABLE 21.4. FREQUENCY OF APPEARANCE OF NOCTILUCENT CLOUDS (L. F. GROMOVA AND V. V. SHARONOV).

Latitude	Apr.	May	June	July	Aug.	Sep.	Oct.	Total
45°	0	0	0	1	0	0	0	1
50	0	0	4	6	0	1	0	11
55	0	4	47	78	3	2	1	135
60	1	1	29	69	16	1	0	117

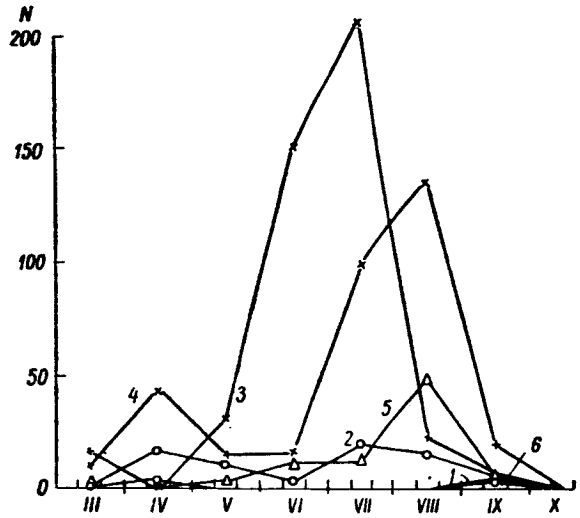

Figure 21.4. Distribution of number N of cases of visibility of noctilucent clouds by months and latitudes in 1958. 1, 45°; 2, 50°; 3, 55°; 4, 60°; 5, 65°; 6, 70°.

On the basis of morphological criteria noctilucent clouds are divided into four types of formations: I, veil; II, bands; III, crests (waves); IV, eddies.

The veil (type I) has some external similarity to cirrus clouds of amorphous outlines--Cirrus nothus. There are many varieties of the veil type with respect to configuration, extent and relative brightness. In most cases this type is an irregular, occasionally flickering glow of some part of the twilight sky, sometimes with a scarcely noticeable fibrous structure. The outer boundaries of a veil are determined with difficulty and only approximately. With a more attentive study of these clouds the boundary of a veil can be traced several degrees further. The boundaries of a veil, therefore, are determined with extremely low accuracy. In many cases a veil appears independently of other forms of noctilucent clouds on a completely clear horizon. In other cases a veil accompanies more complex forms of these clouds. A veil frequently precedes the appearance of other more complex forms of noctilucent clouds. In such cases the brightness of the veil gradually increases. High-power binoculars with a large view field can detect thin jets, bands and "crests", characteristic of these clouds, sooner than the naked eye. However, each specific appearance of noctilucent clouds differs in all its external genetic and morphological properties (ref. 40a).

Available data, and especially films of slow-motion movies, have led N. I. Grishin to the conclusion that a veil is the initial and simplest form of the existence of noctilucent clouds. In the initial stage there is an accumulation of elementary cloud particles causing turbidity of a specific volume of the atmosphere. Then, if atmospheric processes are favorable, the initial cloud particles become larger, simultaneous with the formation of new particles, creating a clearly visible veil. The process of growth of cloud particles is

confirmed by its color changes and spectrophotometric data. Noctilucent clouds in the early stages of their formation, when they are of low brightness, have a bluish color. With increase of brightness their color changes to bright blue with a greenish or sometimes yellowish hue.

In addition to the nebular veil, in many noctilucent clouds there are formations of a more regular configuration in the form of narrow (IIb) and broad (IIa) bands. The movement of these details indicates the speed and direction of airflow. Narrow bands in combination with a veil sometimes form the entire field of noctilucent clouds; then these clouds are similar to fibrous cirrus clouds (Cirrus filosus). Movie surveys indicate that the form IIb is formed from a veil mass by the entrainment of some of its parts by the airflow of the surrounding medium of the atmosphere. The direction of the IIb bands then indicates the direction of flow. This direction changes with time; at the same time, there is a change in the arrangement of the IIb bands. In rare cases a veil is formed in a broad and uniform airflow. The entire mass of the veil is entrained by this flow and is drawn out into an extremely long (up to 1,000 km), poorly outlined band. In the latter case the morphological structure is determined by one or more intersecting, branching, poorly defined IIa bands.

In noctilucent clouds it is far more common to observe mobile and constantly changing wavelike formations. They are almost always visible and therefore serve as distinguishing characteristic for identification of noctilucent clouds by new observers. The transparency of noctilucent clouds and their great distance from the observer permit use of optical means for recording and studying the great variety of undulating formations (ref. 40a).

At this time the nature of noctilucent clouds cannot be considered finally solved. There are different opinions concerning their origin. It was postulated initially that noctilucent clouds consist of volcanic dust. At the time of the remarkable eruption of the Krakatao volcano in 1883, about 19 km^3 of volcanic products (tens of millions of tons (ref. 761)) were ejected. After penetrating into the stratosphere, the volcanic ash was carried in the atmosphere for several years, everywhere giving rise to unusually beautiful twilights. It is no accident that noctilucent clouds as a phenomenon of the high layers of the atmosphere were discovered in these years, almost simultaneously in Russia and Germany. There is also another instructive case which confirms the influence of the intrusion of large quantities of dustlike matter into the high layers of the atmosphere on noctilucent clouds. This was the fall of the Tunguska meteorite on June 30, 1908. A blindingly bright fireball was observed for several seconds before the meteorite fell. A dense dust trail, which remained intact for several hours, was left along the path of this bolide. There was a deafening explosion, heard over a 1,000 km away, at the time of the fall of the meteorite into the basin of the Podkamennaya Tunguska River (Krasnoyarskiy Kray) at 0700 hours. At the time of the explosion there was an energy release of approximately 10^{21} erg. The explosion induced a seismic wave and also an air shock wave which was recorded on the barograms of many Siberian meteorological stations, at Leningrad and in England. It was possible to measure the velocity of propagation of the pressure wave. After the fall of the meteorite, bright noctilucent clouds were visible in Europe and western Siberia. During

the motion of the meteor through the atmosphere at a cosmic velocity, an enormous quantity of meteor matter was scattered into the atmosphere and held there a long time. Bright nights were observed until August (ref. 94).

L. A. Kulik, the famed investigator of the Tunguska meteorite, postulated in 1925 that the noctilucent clouds owe their origin to meteors, from the finest and lightest parts of the products of sublimation of meteor matter associated with penetration of meteors into Earth's atmosphere. The formation of the lightest clouds from cooled products of sublimation occurs continuously, and in Kulik's opinion this fine dust is distributed in a layer at a height of 80-100 km. This layer usually is invisible, but the situation changes when Earth intersects an "active" part of the orbit of some comet, particularly when there is favorable illumination of the zone of the twilight segment, at the time when morning and evening twilight converge in the polar latitudes. Kulik pointed out that late in June the Pons-Winnecke comet makes its closest approach to Earth. He believed that the cause of the strong development of noctilucent clouds could be found in the fall of meteors in relationship to some comet.

Many investigators have advanced the point of view that noctilucent clouds consist of meteor dust. In actuality, meteoric dust particles should constantly be present in the high layers of the atmosphere (this problem was discussed in Section 20). Hoffmeister (ref. 445) believes that noctilucent clouds consist of meteor particles with a diameter of 1-100 μ. The latitudinal distribution of visibility of noctilucent clouds is attributed by Hoffmeister to the presence of stratospheric antitrades which carry meteor dust from the low into the high latitudes (ref. 447). The meteor hypothesis has also been supported by Vestine, who found a correlation between the appearance of noctilucent clouds and meteor streams. Other authors also postulate the existence of such a correlation, but there is contradictory evidence as well. As early as 1935 Ye. I. Tikhomirov correctly pointed out (ref. 191): "In any case, it is clear from Vestine's diagram that it is absolutely impossible to ascribe the origin of noctilucent clouds to volcanic eruptions, as is done by inertia by the authors of various meteorology textbooks, but that the joint effect of both factors (volcanic and meteoric--Author) facilitates the more frequent appearance of noctilucent clouds."

A different point of view was expressed by Wegener in 1926. In his opinion, noctilucent clouds in their composition are similar to ordinary clouds, and, being the product of condensation of water vapor, they consist of ice crystals. The appearance of noctilucent clouds is reminiscent of altocirrus clouds, and it is possible that they are a sort of "superhigh" cirrus clouds--"ultracirrus." The development of noctilucent clouds as a result of the condensation of water vapor seemed to Wegener to be "somewhat more probable" than a volcanic origin. The work of Humphreys (ref. 463) was of great importance for the development of this hypothesis. In that study he made an approximate computation for 60°N. He assumed that the temperature of the stratosphere is constant to a height of 18 km and is 228° K; it then decreases smoothly to 210° K at a height of 25 km and remains constant to a height of 35 km. Farther aloft there is a temperature inversion, increasing rapidly to 315° K at a height of 40 km. Still higher, between 40 and 60 km, there is an isothermal layer (warm layer, T = 315° K). Then, at the base of the stratosphere, the relative humidity is 50 percent, i.e., water vapor is present in the air in the proportion 1/4,000.

Above 10 km the relative (percent) content of water vapor in the air is identical at all heights and everywhere equal to 1/4,000. In this case the vapor becomes saturated at a temperature of 160° K. If it is assumed that a rapid temperature decrease begins above 60 km, 7° per km, and continues to indefinitely great heights, at the 82-83 km level the temperature should decrease to 160° K, i.e., condensation of water vapor can occur at that level. Thus, the condensation hypothesis of the origin of noctilucent clouds leads to the conclusion that at a height of 80-85 km the air temperature, at least in periods of the appearance of clouds, should be low, of the order of 160° K.

Before continuing consideration of the problem of the origin of noctilucent clouds, certain of their optical properties will be discussed.

21.3. Spectra and Other Optical Properties of Noctilucent Clouds. Interesting observations of changes of the color of noctilucent clouds in Scotland have been reported by Paton (ref. 670). In one case he noted that the color of noctilucent clouds changed from bright blue to white. In his opinion this "suggests that there was an enlargement of cloud droplets by condensation" (ref. 762). Paton feels that it is necessary to investigate the spectra of these clouds for solution of the problem of the nature of noctilucent clouds.

In actuality, investigation of spectra can yield valuable information on the nature of noctilucent clouds. As early as 1924 I. I. Putilin (ref. 158) expressed the idea that noctilucent clouds can be photoluminescent. Particles of noctilucent clouds not only can scatter sunlight, but also be fluorescent. If the photoluminescence of noctilucent clouds could appreciably influence their brightness, the spectrum of their luminescence should differ from the spectrum of solar rays which experience scattering on particles of noctilucent clouds. It is improbable that dust particles can be fluorescent, but the photoluminescence (fluorescence and even phosphorescence) of ice crystals at low temperatures is entirely possible (e.g., as a result of absorption of solar ultraviolet radiation).

The spectrum of noctilucent clouds was obtained for the first time by Störmer in Norway in 1932 (ref. 747). He reported that there were no emission lines noticeable on the photograph and the spectrum in no way differed from the spectrum of the night sky. But Störmer's photograph apparently was not analyzed photometrically. It must be remembered that the photoluminescence of bodies at low temperatures usually does not contain lines in its spectrum, but more or less "washed-out" bands. Next, it is necessary to take into account the low optical density of noctilucent clouds. Stars are visible with undiminished brightness through the clouds. I. S. Astapovich has estimated that the absorption of light caused by noctilucent clouds is less than 0.001 stellar magnitude (ref. 6). Under such conditions it is impossible to obtain a spectrum of noctilucent clouds without a great admixture of light of the twilight sky. The detection of the "washed-out" bands of photoluminescence of particles of noctilucent clouds against the background of the continuous spectrum of the sky, if they do exist, is possible only by a careful photometric analysis of the spectra.

Such a spectrophotometric study of noctilucent cloud was begun by N. I. Grishin (ref. 37) in 1951. He used a State Optical Institute high-power (f:1) spectrograph near Moscow to obtain 80 spectra of noctilucent clouds and 30

spectra of the twilight sky near clouds in the region 4,000-6,800 Å. The spectrograms were calibrated and the best 15 were investigated. The intensity of the spectrum of the twilight sky was subtracted from the intensity of the spectrum of noctilucent clouds. Six maxima were found on the curve of distribution of spectral energy: three very clearly expressed peaks in the blue part (λ_1 = 4,230 Å, λ_2 = 4,480 Å, λ_3 = 4,630 Å); two poorly expressed maxima in the yellow-green part (λ_4 = 5,000 Å, λ_5 = 5,300 Å), and a broad strong maximum in the red part (λ_6 = 6,500 Å). It was found that the relative intensity of the maxima changes from night to night. By a comparison of the curves for bright and faint clouds, Grishin discovered that the increase of brightness of noctilucent clouds is accompanied by an intensification of the λ_2 and λ_6 maxima. It is to be hoped that the study of the spectra of noctilucent clouds will be continued. Such work was recently begun in Scotland by Paton (ref. 762). An important investigation of the true color of noctilucent clouds has been made by V. V. Sharonov (ref. 248).

The investigations of Störmer have a direct relation to the considered problem. In the 1930's he noted that the visibility of noctilucent clouds decreases rapidly when the solar rays illuminating them pass below 30 km above the horizon. If such an observation is correct, it suggests that the brightness of noctilucent clouds is influenced appreciably by their illumination by solar ultraviolet rays. This was pointed out by I. S. Astapovich and V. V. Fedynskiy in 1940 (ref. 206). However, Hoffmeister (ref. 447), observing noctilucent clouds at Sonneberg in the summer of 1951, arrived at a negative conclusion. As early as 1896 Jesse (ref. 6) calculated that if the constant value 82 km is used for the height of noctilucent clouds the angular height h_T of the upper boundary of the clouds in the solar azimuth should change as a function of solar depression $h_\odot$ as follows (ref. 6)

$h^\circ_\odot$	11.4	11.7	12.0	12.5	13.0	13.5	14.0
h°_T	12	11	10	8	6	4	3

Late in the Nineteenth Century K. D. Pokrovskiy used a similar relation for an indirect determination of the height of noctilucent clouds (the method of "a ray tangent to the earth's surface"). This method also is used sometimes at the present time (ref. 113). Hoffmeister, assuming the height of noctilucent clouds to be 82 km, determined from the position of their upper margins on photographs the minimum distance from Earth's surface at which the solar rays illuminating the clouds pass. In the case of the clouds observed on June 18, 1951 this distance changed from 0 to 20 km, increasing toward morning, and on the average was 7 km.

The discussed problem has been studied most fully by V. F. Chistyakov and V. G. Teyfel' (refs. 241-243). Assuming the height of the layer of noctilucent clouds to be constant (82 km), they computed the angular height h_T of the apparent boundary of noctilucent clouds as a function of the angle of solar

depression $h_{\odot}$ on two assumptions: the ray is tangent to Earth's surface and luminescence occurs under the influence of solar ultraviolet radiation whose flux is cut off by the absorbing ozone layer at a height of approximately 30 km. Comparison of results of computations with the actually observed height of the boundary of noctilucent clouds for 62 cases of an individual evaluation has revealed that the observed boundary almost always lies lower than initially assumed. The authors believe that this indicates the untenability of the "ray tangent to the earth's surface" hypothesis and confirms the correctness of the second hypothesis (photoluminescence) (refs. 241 and 243). Later they drew more precise conclusions, indicating that in an epoch of minimum solar activity the angular heights of the upper boundary of noctilucent clouds sometimes satisfy the "ray tangent to the earth's surface" hypothesis better (ref. 242).

A shortcoming in the method used in a number of these investigations is the need for postulating constancy of the height of noctilucent clouds. It is known that this height can change in certain limits; therefore, more rigorous conclusions can be drawn if there is a simultaneous independent determination of the height of the layer of noctilucent clouds over the Earth's surface (triangulation measurements).

During the IGY period observations of noctilucent clouds were made in several countries in accordance with a broadened program (refs. 25, 41, 112, 140 and 180). There was a considerable improvement of the method for reducing cloud coordinates (ref. 22) and making photogrammetric determinations of their heights (ref. 19). There were photometric measurements of great importance for understanding noctilucent clouds (refs. 21, 247, 540 and 599), especially measurements of the polarization of the luminescence of clouds (refs. 810 and 811).

21.4. The Nature of Noctilucent Clouds. This brief review of different points of view on the nature of noctilucent clouds shows that the problem of the origin of these clouds still remains unsolved (pages 314-316). The hypothesis of a dust composition of noctilucent clouds apparently encounters difficulties associated with explaining the heights of the clouds. The coincidence of the mean level of noctilucent clouds with the height of the temperature minimum (80-85 km) is an important indication of the correctness of the condensation hypothesis. However, some authors note the possibility of an accumulation of dust at this temperature minimum. Ludlam (ref. 563) regards the formation of a dust layer at a height of 80 km to be a possible result of the ascent of dust clouds entrained from the lower region of the atmosphere by convective currents. Under the inversion at the 80 km level, where the dust-laden air loses its buoyancy and spreads out horizontally, the dust concentration will increase. Convective movements can attain great intensity over the principal part of the ozonosphere, greatly heating as a result of absorption of ultraviolet radiation. According to Wexler, very great, even superadiabatic temperature gradients can develop for this reason in the range of heights 55-80 km.

It must be taken into account, however, that the possibility of the ascent of dust particles together with ascending air currents is dependent not only on the velocity of the ascending currents, but also on the size of the particles. The rate of descent of small particles at the considered heights

was computed by Link (ref. 554), using the Stokes' formula with Millikan's corrections. It was found that the velocity v is proportional to the radius of the particle r and its density δ and inversely proportional to air density ρ. At the 80 km level the rate of descent is several cm/sec, if $r = 10^{-5}$ cm.

The mean free path λ of air molecules at a height of 80-85 km is about 1 cm, i.e., it greatly exceeds the postulated diameter of the particles. Ludlam (ref. 563) therefore thinks it is preferable in computations of the velocities of descent to use the empirical data presented by Knudsen. After measuring the resistance K exerted by rarefied air to the movement of a tiny sphere (measurements were made to a pressure of 0.14 dynes/cm^2), Knudsen obtained the formula

$$K = 6\pi\eta r v \left(1 + 0.683\varkappa + 0.354\varkappa e^{-1.845\varkappa}\right)^{-1}, \tag{21.1}$$

where η is the viscosity coefficient, $\varkappa = \frac{\lambda}{r}$. If $\varkappa \gg 1$, as occurs in this case, the following approximate expression can be used for K

$$K = 6\pi\eta r v \varkappa, \tag{21.2}$$

hence $v = \varkappa v_S$, where v_S is the rate of descent, determined from Stokes' law.

By using formula (21.2), Ludlam (ref. 563) obtained for particles with density $\rho = 2.5$ g/cm^3

$$v = 4.2 \cdot 10^{-6} r^2 \varkappa. \tag{21.3}$$

If $r = 10^{-5}$ cm, $\varkappa = 3.7 \cdot 10^4$, then v = 16 cm/sec; if $r = 10^{-4}$ cm, then $\varkappa = 3.7 \cdot 10^3$ and v = 160 cm/sec.

There is a basis for assuming that the radius of the particles making up noctilucent clouds falls in this range $0.1 < r < 1\,\mu$. An estimate made by Deirmendjian and Vestine (ref. 353), based on an analysis of the spectra of luminescence of noctilucent clouds (reference is to the spectra published by N. I. Grishin in ref. 37; see Section 21.3), gives $r = 0.4\,\mu$. With such a radius the velocity of the ascending air currents should be a large value, specifically about 1 m/sec.

Such an explanation of the formation of dust clouds at a height of 80-85 km raises the following serious objections. Noctilucent clouds occupy enormous areas in most cases, about 10^5 km^2, and sometimes more. If the mechanism of accumulation of dust particles is as indicated in Ludlam's review (ref. 563), it would apparently be necessary to postulate the existence of ascending currents over large areas, such as 100 · 1,000 km^2. In a region of horizontal spreading of air currents, the dust particles will descend under the influence of gravity at a rate of about 1 m/sec, or 3-4 km/hour. Such "convective dust clouds" should be mushroom-shaped with bulging at the center; however, at the present time there are no observations in the literature confirming the existence of noctilucent clouds of this shape.

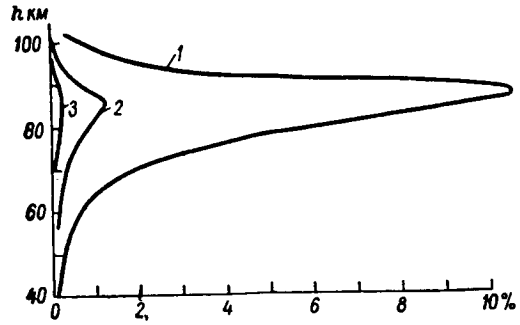

Figure 21.5. Dependence on height of ratio of intensity of light scattered on meteor particles to intensity of light scattered on molecules. 1, angle of scattering 10°; 2, same, 90°; 3, same, 170°.

There are two types of ascending movements of the greatest importance in the troposphere: convection, caused by thermal and dynamic factors, and air movement along a frontal surface (upside motion). Air ascent at the maximum scales, encompassing thousands of km^2, is related to ascending movements along the surface of a warm front. However, such ascent is characterized by low velocities of vertical movements (of the order of a few cm/sec); the ascent occurs smoothly along a slightly sloping discontinuity. However, as was mentioned, the uplifting of dust clouds requires velocities of ascending movements tens of times greater (about 1 m/sec). In addition, at present there are no direct data to confirm the existence of atmospheric fronts at such great heights as 80 km.

Ludlam (ref. 563) considered the formation of a dust layer (cloud) at a height of 80 km to be the result of ascent of dust clouds entrained from the lower region of the atmosphere by convective currents. However, A. A. Dmitriyev and A. Ye. Mikirov (refs. 57 and 58) attribute the formation of such layers to the peculiarities of downward propagation by the turbulent mixing of fine particles of cosmic origin. Figure 21.5 shows curves which they computed, with certain assumptions, for the scattering of light by meteor particles; the maximum is situated at a height of about 87 km, which is close to the level of noctilucent clouds (82 km). On these curves the maximum of aerosol scattering is a value of the order of 1-10 percent of the molecular scattering of light.

The coincidence of the mean height of noctilucent clouds and the height of the temperature minimum (mesopause) can be explained simply and naturally on the basis of the condensation hypothesis. This can be shown graphically, if the value of atmospheric pressure p at different heights is compared with elasticity E of saturated water vapor at the temperature of a particular height. The elasticity e of water vapor in the atmosphere is always less than p, regardless of whether the vapor is saturated or unsaturated. In actuality, if the atmosphere consisted only of water vapor, e would everywhere be equal to p. But total atmospheric pressure p consists of the partial pressures of nitrogen p_n, oxygen p_o, other gases and water vapor e

$$p = p_n + p_o + \ldots + e,$$

and therefore e < p. But since e ≤ E (by definition), if at any height p < E, then at this height, of necessity, e < E and therefore, no matter how great the concentration of water vapor at this height, there cannot be (at a particular temperature) a state of saturation. Comparison of the curves of vertical distribution of p and E therefore make it possible to detect regions where cloud formation is impossible. This is illustrated in figure 21.6, where curve 1 is the pressure distribution over the middle latitudes of the USSR; curve 2 is the value E for mean air temperature values at each particular height over the same latitudes, according to data presented by V. V. Mikhnevich (refs. 128 and 132), and curve 3 is the value E for temperatures measured over Fort Churchill (59°N) in summer (ref. 750).

Curves 2 and 3 were constructed in the following way. They are based on the temperature values indicated, and the value of the elasticity of saturated vapor was determined for each temperature. The elasticity of saturated vapor was determined for all temperatures to -20° relative to water, because the cloud droplets often remain liquid at this temperature, and sometimes even to -30° (supercooling phenomenon); the elasticity of water vapor over ice was determined for lower temperatures.

The points of intersection of the curves in figure 21.6 have been denoted by the letters, B, C and D. The regions situated between the points B and C and above D are "forbidden" because the condition E ≤ p is not satisfied. In actuality, clouds never are observed at these heights (ref. 230). Near the upper boundary of the "permitted" region AB in which E ≤ p and condensation therefore can occur, nacreous clouds are formed from time to time. Noctilucent clouds are observed in the second permitted zone CD.

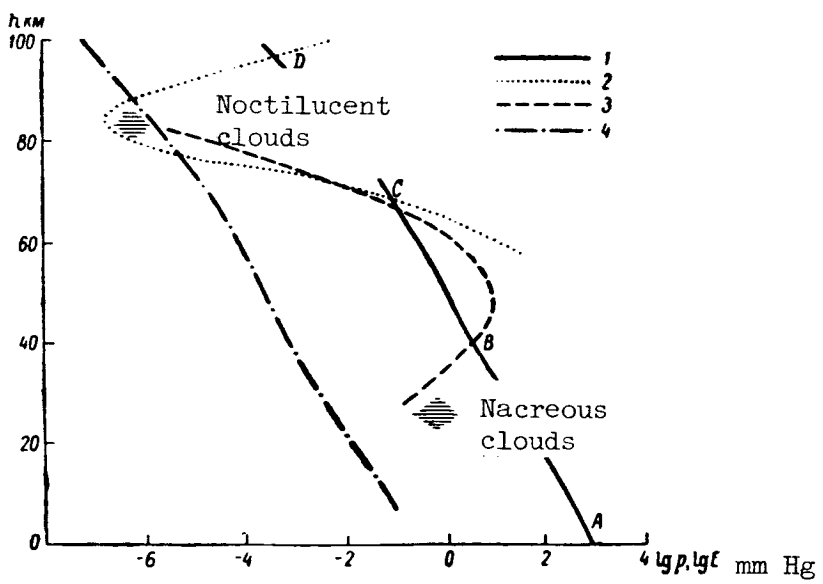

Figure 21.6. Position of "permitted" and "forbidden" zones in Earth's atmosphere. Clouds can be formed in the "permitted" zones AB and CD.

The condition $E \leq p$ is necessary for the process of water vapor condensation (precipitation); the following inequality can be considered as a sufficient condition

$$E \leq ap, \tag{21.4}$$

where a is the water vapor content in the air (the ratio of concentration of H_2O molecules to total concentration of all molecules); in the atmosphere $a \ll 1$.

We now will consider whether condition (21.4) is satisfied in the rarefied zone CD. Earlier it was considered indisputable that water vapor cannot be present in any appreciable quantities at heights of about 80 km. Many investigators still adhere to this point of view.

For example, Ludlam (ref. 563) points out that water vapor density at the 80 km level is approximately $3 \cdot 10^{-14}$ g/cm^3 (air density there is close to $3 \cdot 10^{-8}$ g/cm^3; it therefore follows that $a = 10^{-6}$). Ludlam bases this conclusion on the results of soundings made by the British Meteorological Service (ref. 617), which have shown that the frost point beginning at a level of 3-5 km above the tropopause tends to a constant value of about 193°K; this corresponds to a relative humidity of less than 1 percent. Ludlam assumes the air temperature at a height of 80 km to be 220-230° K. He concludes that it is improbable that noctilucent clouds are formed as a result of water vapor condensation, and "therefore it is natural to give serious consideration to the theory of formation of noctilucent clouds, which regards the latter as accumulations of dust carried to corresponding heights above the earth's surface or from interplanetary space." Deirmendjian and Vestine, in their paper (ref. 353), also decided against the possibility of the formation of noctilucent clouds as a result of condensation, citing this review by Ludlam.

In our opinion, new data on air humidity in the stratosphere and air temperature at the mesopause do not give a basis for such assertions.

In 1933 Humphreys (ref. 463) calculated that if a value $a = 1/4{,}000$ is assumed for a height of 82 km, vapor can be saturated at this level at a temperature $T_{con} = 160°$ K. Computations based on modern data of atmospheric structure make it possible to refine the result obtained by Humphreys and lead to a value $T_{con} = 165°$ K. According to Brasefield's (ref. 307) measurements (Section 19.4), the water vapor content in the stratosphere (above 18-20 km) sometimes increases with height. If ratio a is computed from his data, the following values are obtained for certain dates:

	May 19, 1952			Sept. 16, 1953			
h km . . .	22	27	30	23	28	32	35
a. . . .	1:5000	1:700	1:360	1:2000	1:550	1:200	1:120

If it is assumed that at a height of 80 km the value a "sometimes" is 1:1,000 (it should be recalled that noctilucent clouds are a rare phenomenon), the formation of noctilucent clouds as a result of condensation requires a temperature $T_{con} = 174^{\circ}K$; for $a = 10^{-4}$ the temperature $T_{con} = 162^{\circ}K$; for $a = 10^{-5}$ the temperature $T_{con} = 153^{\circ}K$. Section 19.5 also gave the measurements of Murcray, Williams and Leslie (ref. 608), who discovered a high air humidity in the high layers of the atmosphere: for the entire atmosphere above the 27.6 km level they obtained a = 1:2,500. This value a corresponds to a saturation temperature of about 170°K.

An air temperature at the mesopause of about 150-170°K cannot be considered impossible, at least at certain latitudes and during individual short periods of time. As data are accumulated on the structure of Earth's atmosphere at a height of 50-100 km and the accuracy of determination of air temperature increases, there is a sort of "cooling" of the mesopause: it was found that the temperature of the mesopause T_m is lower than was assumed earlier. In actuality, from the "standard atmosphere" adopted by the National Advisory Committee (NASA) in the United States in use until 1952, it appeared that $T_m = 235^{\circ}K$. In 1952 the United States Rocket Committee revised the standard atmosphere, taking into account the results from rocket sounding: in particular, for the mesopause it was necessary (ref. 707) to adopt the lower value $T_m = 205^{\circ}K$. A new model of the atmosphere was published in the United States in 1956 (it was proposed by the Air Research and Development Command, abbreviated "ARDC-1956 model"). In this model $T_m = 195^{\circ}K$. A still lower temperature was adopted in the ARDC-1959 model. A temperature of 165°K was measured (ref. 750) over Fort Churchill in summer at a height of 80 km. Measurements by the Institute of Applied Geophysics (IPG) of the Academy of Sciences USSR with rockets over the middle latitudes of the USSR give (ref. 128) a value $T_m = 154 \pm 30^{\circ}K$. It should be mentioned that the results of the IPG agree well with the temperature determinations made spectroscopically. On the basis of this, Armstrong (ref. 270) makes the following deduction. Spectroscopic investigations show that the temperatures at the minimum at a height of 80-85 km are considerably lower than 200°K and possibly as low as 130°K. However, a considerably more probable temperature value at the minimum is 150°K, if preference is given to the measurements made by V. V. Mikhnevich.

Byram, Chubb and Friedman (ref. 314), who used photon counters carried aloft in rockets for measurement of solar x-rays reaching the layers between 128 and 110 km, computed atmospheric density using the known mass absorption coefficient for air. They obtained density values which were approximately three times less than the mean value indicated in reference 707. This result was confirmed by Haurwitz and LaGow who measured air pressure and density at heights of 90-220 km, using magnetic ionization manometers with a cold cathode carried aloft on a "Viking 7" rocket. This work is interesting, because in the analysis

of the measurements the authors attempted to take into account the influence of the gas release of the rocket, which had not been done previously in the United States. Haurwitz and LaGow (ref. 454) obtained density values at heights up to 140 km of only one-fourth of the density reported (ref. 707). As confirmation that their results, which coincide with measurements of the absorption of the x-radiation of the solar corona, are more precise than the data in reference 707, Haurwitz and LaGow cite a number of improvements in their method.

Since air density is 3 to 4 times less than had been assumed for heights greater than 100 km, the general picture of the structure of the high layers of the atmosphere requires change. In particular, it must be assumed that the air temperature at heights of about 100 km is appreciably less than the earlier accepted values. Corresponding computations can be made with the barometric formula.

In actuality, after analyzing the theoretical results obtained by Byram, Chubb and Friedman and those of Haurwitz and LaGow, Nicolet showed that to explain the earlier low density values a value $T_m = 150^\circ K$, or even less must be used as the temperature minimum. In his papers of 1958 and 1959 (refs. 633 and 636) Nicolet assumes a temperature of $150 \pm 10^\circ K$ for a height of 85 km. Dalgarno (ref. 349) also assumes that the air temperature at the mesopause is about $150^\circ K$.

It is known(Section 14.2) that the air temperature T_m at the mesopause is subject to many variations (seasonal, as a function of latitude, etc.). In a number of other investigations (refs. 1 and 752) much higher temperatures were recorded at these heights than indicated above. However, we are concerned with the minimum possible values T_m in Earth's atmosphere. These data show that if a value $T_m = 154^\circ K$ is assumed, as determined by V. V. Mikhnevich (refs. 128 and 132), the estimate is not too low.

We note that at $T_m = 150^\circ K$ water vapor becomes supersaturated even when $a = 10^{-5}$. However, if it is assumed that a = 1:4,000 (this condition corresponds to curve 4 in fig. 21.6), the formation of noctilucent clouds as a result of condensation (precipitation) of water vapor is possible at those temperatures measured by rockets over the middle latitudes in the USSR and in summer over Canada; this is shown by the intersection of curves 2 and 3 with curve 4 (fig. 21.6).

On the basis of the condensation hypothesis we can also present an easy and natural explanation of other important characteristics of noctilucent clouds: the special character of their distribution in time and space (annual variation and latitudinal distribution). In short, noctilucent clouds are only formed where it is "sufficiently cold." These computations, based on an estimate of air humidity in the high layers of the atmosphere, show that a temperature of 160-170°K can be considered "sufficiently low." Modern data on the heat regime of the high layers of the atmosphere (Section 14.2) show that such

a temperature is observed in the northern hemisphere only to the north of the 45th-50th parallel and only in summer. A detailed analysis of the problem (made by us in May 1961 (ref. 234) and later by Hesstvedt, ref. 439)) reveals that the seasonal and latitudinal characteristics of the distribution of noctilucent clouds can be explained from this point of view.

In conclusion, we will analyze the problem of condensation nuclei and precipitation. The formation of droplets or ice crystals from saturated vapor does not occur if there are no condensation nuclei and precipitation. Dust particles of volcanic or meteoric origin can serve as such nuclei. The three "competing" hypotheses of the origin of noctilucent clouds (volcanic, meteor and condensation hypotheses) could be combined to a certain extent by pursuing this line of thought. V. A. Bronshten has suggested that there is stimulation of water vapor condensation by condensation nuclei entering the high layers of the atmosphere as meteor dust. The presence of a correlation between the appearance of noctilucent clouds and meteor streams, if one exists, does not contradict the condensation theory. However, the problem of the nature of the condensation nuclei for noctilucent clouds remains completely uninvestigated. With very low temperature (about -100°) the formation of noctilucent clouds apparently should occur by the process of precipitation; this requires particles in the form of crystals or even ice crystals themselves (ref. 243).

With respect to the volcanic hypothesis, we must consider the possibility of ejection of a large quantity of water vapor into the high layers of the atmosphere at the time of eruption, in addition to ejection of dustlike matter (ref. 463). The water vapor present in the ozonosphere does not condense due to the relatively high air temperature; instead, as a result of convection, it gradually penetrates to the condensation level (80 km). A great quantity of vapor is ejected during eruptions. Humphreys has estimated that so much water vapor is ejected into the atmosphere in 18 hours of successive eruptions of Vesuvius that its condensation would form 1 km^3 of liquid water (ref. 463). However, I. S. Astapovich has estimated that a noctilucent cloud of moderate dimensions, covering several tens of thousands of km^2, only contains a few kilograms of matter. This quantity of water of volcanic origin, therefore, would suffice for 10^{10} appearances of noctilucent clouds of moderate dimensions, i.e., for 10^7-10^8 years, if the water vapor ejected into the high layers of the atmosphere during volcanic eruptions can be retained there for an indefinitely long period and expended only on the formation of noctilucent clouds.[1] Volcanic eruptions, therefore, could be of great importance for the formation of noctilucent clouds, but it is by no means mandatory to assume that noctilucent clouds consist of volcanic dust.

[1]In August 1962 two rockets were launched to a height of 100 km in northern Sweden for the collection of noctilucent cloud particles. One rocket was launched into the noctilucent cloud and the other into the same region of the atmosphere, but into a clear sky. In both cases dust particles were discovered in the 75-95 km layer, but in the first case they were larger and the largest of them were covered by a coating of ice (ref. 821).--Author's Note.

Part II

DYNAMICS OF THE UPPER LAYERS OF THE ATMOSPHERE

CHAPTER 8. METHODS OF WIND MEASUREMENT IN THE UPPER LAYERS OF THE ATMOSPHERE

Observations of air movements in the upper layers of the atmosphere and their interpretation and generalization constitute one of the most complex branches of the physics of the upper layers of the atmosphere. Movements of masses in the atmosphere are characterized by great variability; they are dependent on geographic region, height above sea level, time of day and season and are subject to many aperiodic influences. In order to detect any patterns and to obtain an overall picture of circulatory processes, it is therefore necessary to have an enormous amount of observational data, accumulated over a long period of time at many stations and at different heights. Furthermore, measurements of the velocity and direction of movement of air currents involve serious difficulties, particularly at great heights. The quantity of observational data on wind is enormous, e.g., it considerably exceeds the number of determinations of temperature or air composition in the upper layers of the atmosphere, but for the time being it is completely inadequate for determination of the principal patterns. Available concepts of circulatory processes are in many respects more unclear and unreliable than the previously presented data on the structure and composition of the upper layers of the atmosphere.

However, the problem of air currents in the upper layers of the atmosphere is particularly important, both in theoretical respects and for practical purposes. Discussion of this problem will begin with consideration of the principal methods for wind measurement in the upper layers of the atmosphere.

All available methods can be divided into three groups. One of these is based on the tracking of the movements of artificial or natural bodies freely floating in the atmosphere. Tracking is done visually, photographically or by radio techniques. Another group involves measurement of the movements of ion clouds. These methods involve exclusively the use of radio techniques (for the most part radioastronomical methods). They are applicable only for heights greater than 100 km (wind in the ionosphere). The methods for interpretation of observations in some respects are of dubious reliability, but on the whole this group of methods makes it possible to obtain important data. The third group includes acoustic measurements, using the influence of movements of the medium on the velocity of sound waves propagating in this medium. The region of heights at which these methods can be used is in most cases limited, and the theory of interpretation of observations is sometimes complex. On the whole, this area of investigations of the upper layers of the atmosphere is now in a state of rapid development.

22. Drift of Bodies Freely Floating in the Atmosphere

Some of the methods for measurement of wind velocity and direction in the free atmosphere are based on observations of the movement of some body freely floating in the atmosphere and moving together with the air medium surrounding it. Such bodies can be artificial, such as a light envelope filled with hydrogen, i.e., a pilot balloon, a radio pilot balloon or a smoke cloud formed by special artillery smoke shells or by smoke charges ejected from rockets. In addition, a parachute used for lowering rocket equipment from the upper layers of the atmosphere can be used. Finally, every possibility is used for observing the drift of natural atmospheric formations such as clouds and meteor trails. Visible light (visual and photographic observations) and radio waves are used in the observations.

22.1. Use of Radiosondes and Radio Pilot Balloons. The pilot balloon method, long used in aerology for the study of tropospheric winds, has a limited "ceiling," especially in cloudy weather and at nighttime, and on days when fogs and precipitation occur at the Earth's surface it cannot be used at all (ref. 79). Development of methods for the radio direction finding of radiosondes for the purpose of measuring the wind in clouds or above them was begun in 1936-1937 at the Pavlovskaya Aerological Observatory (near Leningrad) under the direction of the outstanding Soviet aerologist P. A. Molchanov, inventor of the radiosonde. Radiometric methods can be used in any weather and at any time of day.

Radio direction finding involves determination of the direction (line) of propagation of the radio waves emanating from an observed object carrying a radio transmitter. In this method radio receivers of a special design are used; they have pencil-beam antennas (direction finders). Modern methods of radio direction finding can track a radiosonde to great heights, even when the tracked radio source has withdrawn a considerable distance from the launching point (ref. 79).

New possibilities in the field under discussion have appeared with the development of radar. Radar can determine the distance and angular coordinates of the object by means of a transmitting and receiving apparatus (radar set). The set transmits radio waves to the object and receives them after reflection from the object. Measurement of distance by a radar set is based on the time required for propagation of the radio waves and is accomplished by the phasometric or pulse method.

The method for determination of the position of a pilot balloon in space using a pulse radar set was developed and used for aerological purposes for the first time at the Central Aerological Observatory in Moscow. This method involves use of a radio pilot balloon, i.e., a target for the reflection of radio waves suspended by a rubber balloon filled with hydrogen. The target of the radio pilot balloon reflects part of the electromagnetic energy incident on it as a narrow beam of radio waves from the radar set transmitter back in the direction of the radar set receiver. The receiving component of the radar apparatus is supplied with means for determination of the slant range, position angle and azimuth of the radio pilot balloon.

With these data it is easy to compute the height of the radio pilot balloon and the horizontal projection of its flight path and, therefore, the wind velocity and direction. At a height of 15-20 km the determination of mean wind velocity for 4 min periods of time (i.e., for atmospheric layers about 1,500 m thick) can be done with an error of ±2 m/sec. Details on radar apparatus and radio pilot balloons and the method of wind determination using these techniques can be found in a book by A. B. Kalinovskiy and N. Z. Pinus (ref. 78). The ceiling of modern apparatus of this type (ref. 722) is as much as 30-35 km.

22.2. Rockoons. The use of radar for wind measurement at greater heights is possible only when other objects are used as targets. Several such approaches or at least attempts to solve this problem at the present time can be mentioned.

According to reference 510, the United States Communications Corps Laboratory in 1955 began experiments with the use of a small Loki rocket for wind measurements at heights of 25-40 km. This rocket can carry 400-800 g of chaff aloft. The idea of the wind measurement method is that the chaff is ejected from the rocket at a previously designated height, and its further movement is tracked by radar for wind determination. Similar analyses have also been made by the United States Naval Research Laboratory (ref. 510).

In the first experiments the Communications Corps Laboratory checked the effectiveness of using chaff. In this investigation about 400 g of chaff was first placed in several light envelopes (balloons) filled with hydrogen. Each balloon also carried aloft a radar target for reflection of radio waves (passive target). The flight of such a radio pilot balloon was tracked by radar operating at a wavelength of 10 cm, with an effective range of 90 km. When the radio pilot balloon had withdrawn a great distance, its response signals became very weak, but at this time one of the envelopes burst and the chaff was scattered in all directions. A very strong response signal appeared at once, but then began to become less well defined and to weaken. After 14 min the signal was already so poorly defined and weak that the radar could no longer record it. In another case radar sets operating at 10 and 3 cm tracked a cluster of chaff for 12 min. Eventually it was possible to track chaff ejected from a radio pilot balloon at a height of 27 km for 40 min.

Later the experiments were carried out at White Sands Proving Ground with a cluster of chaff weighing 200-400 g, carried in a Loki rocket. In the 35th second of the flight the chaff was ejected from the rocket. After a number of failures it was possible to track a cluster of metallized nylon dipoles (weighing about 0.5 kg) by radar for a period of 20 min. This made it possible to determine wind direction and velocity. These data were confirmed by wind determinations made for control purposes using an ordinary pilot balloon. The velocity of falling of the dipoles from a height of 27-24 km averaged 3 m/sec.

According to a preliminary report by Kampe (ref. 510), a complex method is being developed at the Evans Communication Laboratory, involving use of a light parachute made of a metallized fabric. It is planned that this parachute be ejected from a rocket at a great height, and that its descent be tracked by radar. Since the parachute can drift a great distance when there is a strong wind and thus be removed from radar range, it is planned that a powerful radio

apparatus weighing less than 1 kg (with batteries), capable of transmitting about 40 min, be attached to the parachute.

Methods of this type are now being considerably improved, and widely used for systematic wind measurements at heights of 40-90 km (mostly 40-60 km). Some idea concerning the character of such measurements made by American investigators can be obtained using Smith's data (ref. 733).

A total of 750,000 plastic pieces of chaff with a length of 5 cm, with a metal coating and with a total weight of 400 g, was used. Radar (10 cm) was used for tracking the resulting target cloud.

In July-August, 1958, 20 two-stage rockets were launched at Johnston Island in the equatorial part of the Pacific Ocean; the nose compartment of these rockets contained clusters of these dipoles. The dipoles were accompanied by a mechanical timing device and an explosive device for ejecting them. Three such launchings occurred in May, 1958 in Nevada in the United States. In 23 launchings it was possible to make 742 wind measurements at heights of 40-90 km; the mean wind was measured at intervals of 60 sec. The mean square error of velocity was 12 m/sec.

Many hundreds of rockets now have been launched by the scientists of the United States for making wind measurements by this method.

22.3. Drift of Clouds of Smoke and Sodium Vapor. Observations of the drift of smoke clouds appearing at a height of up to 30 km during the explosion of artillery shells were made at Dover (England). Data were obtained on wind direction and velocity in winter and summer.

In connection with the development of tracers for rockets and high-altitude aircraft, compounds have been produced which yield chemical smoke visible from great distances. Wind can be determined by observing the drift of such smoke trails.

Smoke clouds rarely are used for wind measurements in the stratosphere.

Interesting possibilities for the study of certain phenomena in the upper layers of the atmosphere are afforded by the use of sodium clouds (Section 8.8). We will now discuss the use of such clouds for study of air currents in the lower layers of the ionosphere.

As a result of strong heating and subsequent evaporation of metallic sodium carried in small quantities (about 1 kg) to a height of about 100 km or more by a rocket, a cloud of sodium vapor is formed in the upper layers of the atmosphere. If such a cloud is generated at twilight, when the lower layers of the atmosphere (up to 50-70 km) already are plunged into the Earth's shadow, but the cloud itself still is illuminated by the Sun's rays, we can observe a relatively strong luminescence of the cloud (for several minutes). If the evaporation of the sodium continues during the upward flight of the rocket, a luminescent trail is left behind the latter. The configuration of the trail gradually changes under the influence of the wind, whose velocity and direction change with height. If

the expansion of the trail is radial (in a coordinate system moving with the wind), the direction and velocity of movement of the center of the trail immediately give the direction and velocity of the wind prevailing at a particular height.

In determining the drift of the luminous trail, it is usually photographed from three points somewhat distant from each other. This measurement methodology is explained in the article by Manring, Bedinger, Petit and Moore (ref. 571).

22.4. Observations of the Movement of Nacreous and Noctilucent Clouds. Observations of nacreous clouds (Section 21) have shown that they are in constant and relatively rapid motion, but the direction of their movement usually does not coincide with the direction of the prevailing winds in the upper layers of the troposphere and lower layers of the stratosphere. We can, therefore, assume the presence of a level at which there is a change in the direction of the prevailing winds, and that this level must be situated beneath the region in which nacreous clouds are observed.

There have been interesting observations of the drift of noctilucent clouds, situated at considerably greater heights (averaging 82 km). These heights are less accessible for study by other methods. The wind data obtained from observations of the drift of these clouds, therefore, are very valuable. Such observations revealed the presence of extremely great velocities of air movement at heights of about 80 km. The wind direction and its change conform to rather clearly expressed patterns.

The character of movement of noctilucent clouds is complex. An analysis made by N. I. Grishin (refs. 39 and 40) reveals that the authors of a number of published studies, in measuring the "drift" of noctilucent clouds, in actuality often measured the phase velocity of individual details or the velocity of movement of the entire wave field and interpreted this as actual movement, indicating the wind velocity value at the level of noctilucent clouds. As a result, they obtained values of from 10 to 300 m/sec for the drift velocity of noctilucent clouds. Grishin (ref. 40) believes that these results must be subjected to a critical reevaluation.

N. I. Grishin has successfully used slow-motion cinematography for the study of the movement of noctilucent clouds. He has drawn the following conclusions.

(a) Noctilucent clouds are a relatively thin layer at the level of the mesosphere, at whose surface it is easy to observe wave and vortical motions, but for methodological reasons the region of direct study of laminar flow and drift of noctilucent clouds is limited.

(b) The movement of structural formations of type II (bands) can be reliably measured only in a direction perpendicular to their generating lines. Measurements of optical condensations in the bands of noctilucent clouds, like in other formations, are unreliable due to the close relationship between these condensations and wave oscillations of great amplitude.

(c) The results of a general analysis of the data obtained from a movie survey confirm the need for continuing this work, and making measurements of the heights of individual morphological formations in noctilucent clouds.

(d) Meteor trails and noctilucent clouds advantageously supplement one another in information on the dynamic state of the stratosphere and should be used jointly in appropriate investigations (ref. 40).

We also can refer to Witt (ref. 809a), who observed noctilucent clouds which moved, as a whole, in a southwesterly direction with a velocity of 100 m/sec, whereas a system of well-expressed waves propagated considerably more slowly in the opposite direction.

22.5. Drift of Meteor Trails. Dust and gaseous (nighttime luminescent) meteor trails can be distinguished. Dust trails are rarely observed at heights of 30-80 km after the flight of bolides. These trails are visible only when the corresponding part of the atmosphere is illuminated by the Sun's rays. Gaseous trails appear at a height of 80-100 km, and quite frequently are visible in a telescope after the flight of bright meteors.

The duration of luminescence of gaseous trails usually is several minutes. During this time the trail can move appreciably in the telescopic field of view, indicating a drift of the trails in the air currents of the upper layers of the atmosphere. It has been found that observations can be used to determine the linear velocity and direction of drift. The movement of the trails undoubtedly is a passive drift of ionized luminescent masses of gas entrained by horizontal air currents. Thus, observations of the drift of meteor trails can determine wind velocity and direction at a height of 80-100 km. Meteor observations have established the fact of nonuniformity of air currents in the upper layers of the atmosphere, forcing rejection of the older points of view that the stratosphere is a zone of uniform laminar flow, in contrast to the troposphere with its turbulent movement.

As early as 1934-1938, N. I. Gur'yev and A. M. Bakharev at the Astronomical Observatory of the Academy of Sciences of the Tadzhik SSR (Dushanbe) made observations of 41 meteor trails and analyzed them for wind determination. They found that many trails (more than half) gradually become broken or curved (ref. 200). In this investigation they obtained direct indications of the turbulent character of air movements in the upper layers of the atmosphere.

In recent years the possibilities of wind measurement in the upper layers of the atmosphere from observations of the drift of meteor trails have broadened considerably as a result of the use of radar. As already mentioned, a meteor leaves behind it an ionized trail as it passes through the atmosphere. Radar signals are reflected from these ionized air masses. It was found possible to record radar echoes from very weak meteor trails as well as strong ones. The number of meteors recorded by radar, therefore, considerably exceeds that which can be observed by optical (visual and photographic) observations. In addition, in contrast to optical observations, radar observations can be made not only at night, but also during the day, and in any kind of weather. As a result, in a short time extensive radar measurement data on meteors accumulated, considerably supplementing the data on winds in the upper layers of the atmosphere.

Several types of special radars have been developed in order to measure the extremely rapid drift of ionized meteor trails (up to 100 m/sec or more) with the necessary accuracy and ensure a large "field of view" of the recording apparatus. Considerable work along these lines has been done in England, where a well-equipped meteor experimental station, Jodrell Bank Observatory of Manchester University, was established near Manchester. We will now discuss one of the radars at this station, developed by Greenhow (ref. 411).

The principle of a coherent pulse radar was used in the measurements; the method is based on the measurement of the distance travelled by a reflection from the ionized meteor trail as a function of drift of the trail. The direction of movement of the meteor trail was determined by measurement of the phase of the reflected signal in relation to the pedestal (coherent) frequency of the transmitter. The coherent pulse measurement principle combines the advantages of simple radars with those of continuous radiation radars. As a result, Greenhow recorded about 8,500 meteor radar echoes per day on his set; of these 40 percent were suitable for determination of wind velocity and direction at a height of 80-100 km. It is significant that the measurements could be made day and night, since the hourly observed number of meteors only rarely becomes less than 50 (usually several hundred reflections are observed in 1 hour, and only in the evening, when meteor activity is minimal, does the number of recorded echoes decrease appreciably). The transmitter in Greenhow's set operates at a wavelength of about 8.3 m. Pulse duration is 20 μsec, pulse power is 100 kw, pulse frequency is 150 per sec. The height of the meteor trail is computed from echo duration, which depends on the diffusion coefficient of ionized particles, determined by atmospheric pressure. With transition from the 80-100 km level the duration of the echo decreases from 0.5-0.02 sec.

Groves has published a theory of statistical analysis of wind measurements from radar echoes based on the least squares method (ref. 416). He demonstrated the possibility of detecting vertical movements and temporal wind variations from an analysis of observations which at first glance apparently simply indicate the presence of a constant horizontal wind.

22.6. Night Airglow and Auroras. The use of photoelectric recording photometers of high sensitivity with interference light filters permits (several times a night) rapid measurement of the celestial spectral brightness of the night sky for a narrow sector near a strong spectral line of the night airglow (such as the green line, λ = 5,577 Å). It was found that the sky usually contains large luminescent "clouds" (hundreds of kilometers in diameter) which seemingly stand out against the background, i.e., there are regions of increased intensity of a line emitted by the upper layers of the atmosphere. A comparison of the distribution of isophotes at different hours of the night reveals that the isophotes gradually move during the night, which apparently indicates a drift of those high air masses (100 km or more) in which luminescence develops (ref. 703). The character of this drift is usually rather regular. For example, the observations of Huruhata, Tanabe and Nakamura (ref. 468) in Japan indicate that regions of infrared luminescence move during the night predominantly from southwest to northeast through the western part of the sky. Drift velocity and the height of the luminescent region can be estimated. Thus, such

photometric observations provide data on air currents in the upper layers of the atmosphere.

Some data of this type can also be obtained from the movements of auroras. It was noted long ago that sometimes individual parts of an aurora drift in a certain direction. Meinel and Schulte photographed auroras with an automatically recording wide-angle f:2 movie camera with a spherical convex mirror and discovered the drift of individual parts of auroras in a westerly direction in the evening hours and in an easterly direction in the morning hours (ref. 595). Velocities are determined with an accuracy to 10 percent. The height of the auroras was computed from photographs taken at two stations situated 450 km apart.

McLaughlin, in observing a bright aurora, discovered that before midnight the drift in the northwestern sector of the sky occurs from north to west, whereas in the northeastern sector there was no drift (ref. 585). After midnight drift was noted to the east in the northeast sector, but it was absent in the northwest sector. Meek (ref. 590) photographed auroras at Saskatoon, Canada, and established that in 19 of 58 cases there was an easterly direction of movement and in 14 cases a westerly direction; in the remaining cases it was possible to note only movement in a north-south direction. Hartlein and Kimball analyzed 40,000 movie frames with images of auroras and established that 57 of the 120 auroras recorded definitely showed movement to the west or east. In 39 cases the movements had a complex character. In 8 cases there was a reversal of direction during the night (between 2200 hours in the evening and 0200 hours in the morning). Bless, Hartlein and Kimball assume that when there is a stable movement of auroras it occurs to the west at the beginning of the night and to the east at the end of the night, while in the middle of the night the movement can occur both to the west and to the east.

Kaiser, studying auroras in 1950-1955 by the pulse sounding method using meter radio waves (auroral radar echoes), discovered considerable velocities of movement of regions of ionization of auroras (ref. 504). Almost all the morning and evening echoes indicate approach of the reflecting region to the observation point (Jodrell Bank) or its withdrawal. The time of change of direction coincides with the time of the nighttime minimum of frequency of appearance of echoes (about 2100 lt). The radial velocity of movement of the regions of ionization attains 500 m/sec. It is improbable that these velocities corresponded to the real movement of air masses; more likely they represent the apparent effect of a redistribution of ionization (ref. 504).

Systematic observations of the movements of auroras were made under the IGY program. The "all-sky" camera proposed by A. I. Lebedinskiy (refs. 296, 380, 381, 523 and 744) was widely used for these purposes. The results of the observations will be considered in the next chapter.

Methods for measurement of the movements of inhomogeneities must be included among the methods for wind measurement in the upper layers of the atmosphere based on the study of the drift of bodies freely floating in the atmosphere. However, these methods also have certain peculiarities, and they will, therefore, be considered separately in Section 25.

23. Acoustic Methods

In Chapter 5 (Section 12.1) we described acoustic methods for the measurement of air temperature in the upper layers of the atmosphere. The essence of these methods is that the speed of sound a in the atmosphere depends on air temperature T. Reliably measured values a therefore can be used to determine T. But in a study of these methods we repeatedly found that the accuracy of temperature measurement decreases when there is a wind in those layers of the atmosphere through which a sound wave passes, since the speed of sound propagation between two specific points changes if the medium separating these two points itself comes into motion (the velocity vector a of sound waves and the velocity vector w of the medium are combined). This fact is a deficiency of the acoustic method of temperature measurement, but it nevertheless opens up new possibilities for determination of wind velocity and direction by acoustic measurements.

It was shown in Chapter 5 that the acoustic method is used in three ways for measurement of atmospheric temperature: from the anomalous propagation of sound and by observations of the explosions of grenades ejected from rockets or the explosion of bombs dropped from an aircraft. The same three methods can be used for measurement of wind velocity. We will begin the consideration of these methods with observations of anomalous sound propagation.

23.1. Anomalous Sound Propagation. The first observations of this kind were made during the First World War in 1914-1918. Tremendous artillery barrages at the time of battles in the northern part of France and Flanders were heard in winter in the western part of Germany, but they could not be heard in summer. However, the opposite was observed in London: the thundering of the barrages was heard in summer, but not in winter. On the basis of these and certain similar data, Whipple as early as 1918 postulated that these phenomena are associated with the existence of strong and moderate winds, predominantly westerly in winter and easterly in summer, in the stratosphere at heights greater than 20 km. This hypothesis was confirmed by subsequent observations. In the investigation of the audibility of the sound of strong explosions it was found that the zones of silence and anonymous audibility often have an elongated asymmetrical configuration relative to the point of the explosion, rather than a circular configuration.

The computation of the path of a sound ray is considerably complicated when the wind is taken into account. Groves (ref. 414) derived a ray equation for the general case of a nonhomogeneous medium, taking into account the motion of the medium, proceeding on the basis of the concepts of D. I. Blokhintsev (ref. 13) on the possibility of the solution of the problem by the methods of geometrical acoustics (for further details see the author's book, ref. 233). He derived a general equation in vector form and considered its solution with certain simplifying assumptions (plane problem, speed of sound and wind are dependent only on height z). An analytical expression of the integrals in the wave front equations can be obtained only for special cases of the dependence of the speed of sound and wind on height. Therefore, in practical application of the acoustic sounding method, observations are usually analyzed using approximate formulas derived with a number of simplifying assumptions. We now will discuss the investigations of Murgatroyd (refs. 610-612) made in 1944-1945 in England.

He made acoustic measurements of wind and air temperature to a height of 50 km. The analyzed data from these measurements were published in 1955.

Figure 23.1 shows a map of the location of explosion and detection points in England. Microphone apparatus for the recording of sound was installed at each receiving point at the corners of a square or a triangle with 5 or 10 km sides. They were connected with a recording device in which the readings of string galvanometers were photographed by a projection mechanism onto a moving film. Synchronizing marks were automatically applied to the film from a chronometer, which at definite times closed the current circuit, causing triggering of one of the string galvanometers. The arrival times for sound at each of the microphones can be read on the film with an accuracy of several sonic meters (hundredths of a second).

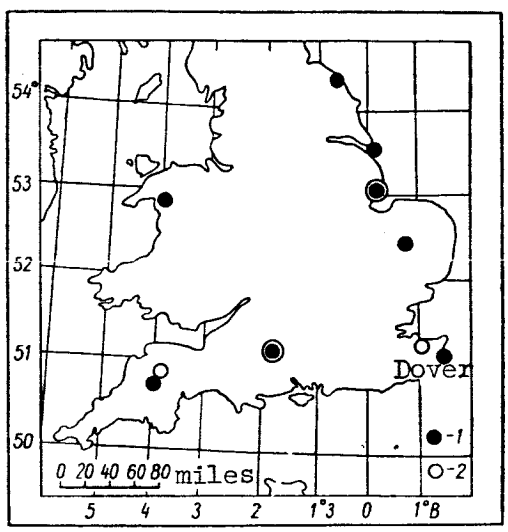

Figure 23.1. Location of shot points (1) and detection stations (2)--microphone apparatus) in England during acoustic determination of the wind to a height of 50 km (according to Murgatroyd).

In processing the observations Murgatroyd (ref. 613) made three assumptions:

(a) the propagation of sound through the atmosphere from the point of the explosion to the microphones can be analyzed taking only refraction into account;

(b) the general (Laplace) law for the speed of sound in a gas is correct for the entire path of the sonic ray;

(c) the atmosphere can be considered as consisting of homogeneous horizontal layers (at a given level the wind and temperature are constant over the entire area of sound propagation).

We will assume that the sound source S and the microphone M are at the same level. Assume X_a denotes the distance SM, t_a is the total propagation time and

Z is the maximum height of the path of the sound ray, x, y, z are rectangular coordinates of the selected point P on the path relative to the point S (x is parallel to the SM axis, z is vertical to the SM axis), t is time expended by sound on propagation from S to P. The normals to the wave front (Murgatroyd considers the wave surface to be plane) on the entire path of the ray are parallel to some vertical plane Ω forming the angle φ to the xz plane. The distance from the microphone M to the plane Ω is denoted Y_a.

The horizontal wind components at the height z, parallel and perpendicular to the plane Ω are denoted w and w'. The speed of sound is represented in the form

$$a = \text{const}\sqrt{T}. \tag{23.1}$$

The slope of the normal to the wave is denoted ψ. Then the general refraction law is written by Murgatroyd in the form

$$a\sec\psi + w = k, \tag{23.2}$$

where k is the characteristic velocity of the ray, equal to the horizontal speed of sound at the peak of the path.

From the equations of kinematics

$$\frac{dx}{dt} = (a\cos\psi + w)\cos\varphi - w'\sin\varphi, \tag{23.3}$$

$$\frac{dz}{dt} = a\sin\psi, \tag{23.4}$$

$$\frac{dy}{dt} = (a\cos\psi + w)\sin\varphi + w'\cos\varphi \tag{23.5}$$

and it follows (we take into account that φ is constant)

$$X_a\cos\varphi = 2\int_0^z \frac{a\cos\psi + w}{a\sin\varphi}\,dz, \tag{23.6}$$

$$Y_a = X_a\sin\varphi = -2\int_0^z \frac{w'}{a\sin\psi}\,dz, \tag{23.7}$$

$$t_a = 2\int_0^z \frac{dz}{a \sin \psi}. \tag{23.8}$$

In analysis of the data Murgatroyd used radiosonde data on air temperature and wind at heights of 0-18 km. The values X_a, t_a, φ and k can be obtained directly from acoustic measurements. Using the cited equations it is possible to compute the path of the sound wave to a height of 18 km. Due to the difficulties associated with the computation of temperature and wind above the 18 km level from acoustic data, Murgatroyd derived approximate equations, correct with an accuracy to terms of the first order $\frac{n}{a_o}$, where $n = k - (a + w)$, $a_o = 337.6$ m/sec is the standard speed of sound in air at 10° and 50 percent humidity. Due to the smallness of the angle φ it can be assumed that $\cos \varphi = 1$. Then the equations (23.6)-(23.8) can be represented in the form

$$X_a = \sqrt{2a_0}\int_0^z \frac{1}{\sqrt{n}}\left(\frac{k}{a_0} - \frac{5n}{4a_0} - \frac{a - a_0}{2a_0}\right)dz; \tag{23.9}$$

$$t_a = \sqrt{2a_0}\int_0^z \frac{1}{\sqrt{n}}\left(1 + \frac{3n}{4a_0} - \frac{a - a_0}{2a_0}\right)dz, \tag{23.10}$$

where t_a is measured in sonic meters;

$$Y_a = \sqrt{2a_0}\int_0^z \frac{1}{\sqrt{n}}\left(\frac{w'}{a_0}\right)dz, \tag{23.11}$$

where the ratio $\frac{n}{a_o}$ in the lower layers of the stratosphere can attain a value 0.25, but is usually much less.

Murgatroyd replaces these equations by the approximate relations

$$X_a \simeq t_a \simeq \sqrt{2a_0}\int_0^H \frac{dh}{\sqrt{n}}, \tag{23.12}$$

$$t_a - X_a \simeq \sqrt{2a_0}\int_0^H \frac{1}{\sqrt{n}}\left[\left(1 - \frac{k}{a_0}\right) + \frac{2n}{a_0}\right]dh. \tag{23.13}$$

These and the following equations apply only to the layer above the 18 km level; h denotes the height above this level and H is the maximum height of the sound path above it.

The total time t_a, the total distance X_a and the total lateral distance Y_a can be measured, and the time t_b, distance X_b and lateral distance Y_b can be computed for those sectors of the sound path which lie between the 0 and 18 km levels. It is therefore possible to find the "residual" values of time $t_a - t_b$, distance $X_a - X_b$ and lateral distance $Y_a - Y_b$ for the upper part of the path above the 18 km level. The following approximate equations are correct for this "residual layer"

$$\frac{X_a - X_b}{\sqrt{2a_0}} \cong \frac{t_a - t_b}{\sqrt{2a_0}} \cong \int_0^H \frac{dh}{\sqrt{n}} = g, \tag{23.14}$$

$$\frac{(t_a - t_b) - (X_a - X_b) + \left(\frac{k}{a_0} - 1\right)(X_a - X_b)}{\sqrt{2a_0}} \frac{a_0}{2} = \int_0^H \sqrt{n}\, dh = f, \tag{23.15}$$

$$\frac{Y_a - Y_b}{\sqrt{2a_0}} = \int_0^H \frac{1}{\sqrt{n}} \left(\frac{w'}{a_0}\right) dh = m. \tag{23.16}$$

The values g, f and m can be determined from measurements. If a definite law of dependence on height is assumed for n, the equations (23.14)-(23.16) can be integrated directly. Murgatroyd considers three variants of the dependence of n on z above the 18 km level: a linear dependence and also a parabolic and exponential change of n.

23.2. Case of Linear Dependence of Wind and Temperature on Height. The actual change of n with height can differ considerably from the linear law; however, if the atmosphere is divided into sufficiently thin plane-parallel horizontal layers, within the limits of each layer the linear dependence can correspond rather closely to the true change of n with height. In a number of investigations it has been shown (refs. 345 and 701) that a two-layer model of the atmosphere can be used. Accordingly, Murgatroyd considers two layers, the first of which is bounded by the heights 18-35 km, while the second extends from the 35 km level to the maximum height of the path of the sound ray (this usually is about 50 km above the Earth's surface).

The subscripts "0" and "1" will be used to denote values applying to the 18 and 35 km levels. Between h = 0 and h = h_1 (h is height relative to the 18 km level) the postulated linear variation of the wind components and speed of sound with height can be described by an expression of the type

$$w' = w'_0 + \frac{h\,(w'_1 - w'_0)}{h_1}, \tag{23.17}$$

it therefore follows that

$$n = n_0 + \frac{h\,(n_1 - n_0)}{h_1}. \tag{23.18}$$

Similarly, the linear dependence between h_1 and H (H--the maximum height of the path of the sound ray--changes in dependence on azimuth) and between h_1 and the selected fixed height h_2 can be represented by the expressions

$$w' = w'_1 + \frac{h - h_1}{H - h_1}(w'_H - w'_1),$$
$$w' = w'_1 + \frac{h - h_1}{h_2 - h_1}(w'_2 - w'_1).$$

We introduce the wind components u and v, directed to the east and north, respectively, so that

$$\left.\begin{aligned} w &= u\sin\beta + v\cos\beta \\ w' &= u\cos\beta - v\sin\beta \\ n &= k - (a - w) = k - a - u\sin\beta - v\cos\beta \end{aligned}\right\} \tag{23.19}$$

Then the preceding two equations can be rewritten in the form

$$\left.\begin{aligned} w' &= w'_1 + \frac{h - h_1}{H - h_1}[(u_H - u_1)\cos\beta - (v_H - v_1)\sin\beta] \\ w' &= w'_1 + \frac{h - h_1}{h_2 - h_1}[(u_2 - u_1)\cos\beta - (v_2 - v_1)\sin\beta] \end{aligned}\right\} \tag{23.20}$$

Therefore, the following equations are correct for n

$$n = n_1 - \frac{h - h_1}{H - h_1}[a_H - a_1 + (v_H - v_1)\cos\beta + (u_H - u_1)\sin\beta],$$
$$n = n_1 - \frac{h - h_1}{h_2 - h_1}[a_2 - a_1 + (v_2 - v_1)\cos\beta + (u_2 - u_1)\sin\beta].$$

Since n = 0, at height h = H, then

$$n = n_1\left(1 - \frac{h - h_1}{H - h_1}\right), \tag{23.21}$$

$$n_1 = (a_H - a_1) + (v_H - v_1)\cos\beta + (u_H - u_1)\sin\beta, \tag{23.22}$$

$$n_1 = \frac{H - h_1}{h_2 - h_1}\left[(a_2 - a_1) + (v_2 - v_1)\cos\beta + (u_2 - u_1)\sin\beta\right]. \tag{23.23}$$

By using equations (23.18) and (23.21) for n and (23.17) and (23.20) for w' in two layers: from 18-35 km and from 35 km to H, it is possible to integrate equations (23.14)-(23.16). The results of integration are

$$n_1 = \frac{a_0}{2(X_a - X_b)}\left[3(t_a - t_b) - 3(X_a - X_b) + \right.$$
$$\left. + 3(X_a - X_b)\left(\frac{k}{a_0} - 1\right) - h_1\sqrt{32\frac{n_0}{a_0}}\right], \tag{23.24}$$

$$H - h_1 = \sqrt{\frac{n_1}{a_0}}\left(\frac{X_a - X_b}{2\sqrt{2}} - \frac{h_1}{\sqrt{\frac{n_1}{a_0}} + \sqrt{\frac{n_0}{a_0}}}\right), \tag{23.25}$$

$$(Y_a - Y_b)\sqrt{\frac{a_0}{2}} = \frac{2}{3}\frac{h_1}{n_1 - n_0}\left[(w_1'\sqrt{n_1} - w_0'\sqrt{n_0} + \right.$$
$$\left. + \frac{2(w_0' n_1 - w_1' n_0)}{\sqrt{n_1} + \sqrt{n_0}}\right] + \frac{2}{3}\frac{H - h_1}{\sqrt{n_1}}(2w_H' + w_1'). \tag{23.26}$$

Equation (23.24) can be used to find n_1, and then formula (23.25) can be used to compute H.

If equations (23.24) and (23.25) are used for three different azimuths, and n_1 and H are found for three different values β, equation (23.19) can be used to compute values a_1, u_1 and v_1, and equation (23.23) can be used to compute values a_2, u_2 and v_2.

If equation (23.26) is used, it is sufficient to have data for only two azimuths. The unknown values in equation (23.26) are w_H' and w_1', assuming H and n_1 are known. It can be seen from (23.20) that w'_H can be replaced by a linear function of w_2' and w_1' or of u_1, v_1, u_2 and v_2. Equations of the type (23.26) for each azimuth, therefore, can be transformed into equations containing linear combinations of u_1, v_1, u_2 and v_2. In addition, the two linear equations for a_1, u_1 and v_1 can be obtained from (23.19) for two azimuths. Finally, the two linear equations for a_2, u_2 and v_2 can be derived from (23.23) for two azimuths (ref. 613).

Thus, when measurements are made along two azimuths, it is possible to determine six unknown values: a_1, u_1, v_1, a_2, u_2 and v_2; the subscripts "1" applies to a height of 35 km, and "2" to a height such as 50 km. Values a can be recalculated directly into temperature by using formula (23.1).

This theoretical possibility of analyzing experimental data, when measurements have been made in only two directions, is complicated in practice by the fact that the equations used are extremely sensitive to observational errors. It is most difficult to determine precisely the initial times of arrival of sound waves at the recording microphones. Murgatroyd therefore recommends the use of this method of analysis only in experiments in which the sound waves arrive from three or more different azimuths (ref. 613). When there are measurements in three azimuths, it is necessary to write 9 equations with six unknowns, in four azimuths--12 equations, etc. Then the least squares method can be used for determination of the most probable values of the desired parameters and the influence of observational errors is thus decreased.

23.3. Parabolic and Exponential Change of Wind and Temperature with Height. The parabolic equation of change of n with height above the 18 km level is written by Murgatroyd (ref. 613) in the form

$$n = \frac{n_0}{1-\mu}\left(1-\frac{h}{H}\right)\left[1-\mu\left(1-\frac{h}{H}\right)\right],$$

where $n = n_0$ when $h = 0$, and $n = 0$ when $h = H$. It is necessary to determine the constant μ and the maximum height H of the path of the sound ray. If it is assumed that $0 < \mu < 1$ (where $\mu = \sin^2 \gamma$), integration of equations (23.14) and (23.15) gives

$$g = \frac{2\gamma H}{\operatorname{tg}\gamma \sqrt{n_0}},$$

$$\frac{2f}{gn_0} = \operatorname{cosec}^2 2\gamma - \frac{\operatorname{ctg} 2\gamma}{2\gamma}.$$

These equations can be used to determine H and μ and therefore for a particular azimuth find the parameters of the parabolic dependence of n on h, satisfying the conditions of sound propagation over a given distance in a given time. If the results of measurements in three azimuths are obtained, equations (23.19) make it possible to compute a, u and v for some selected heights, such as 20, 30 and 40 km above the Earth's surface (ref. 613). Unfortunately, in this method the extremely useful equation (23.16) cannot be used and it is not possible, therefore, to find results from measurements in two azimuths, as was possible in the preceding case of a two-layer linear model.

The exponential dependence of n on height can be represented by the expression

$$\frac{n}{n_0} = \frac{1 - \exp[\lambda(h - H)]}{1 - \exp(-\lambda H)},$$

in which the constant λ and the maximum height H are the desired values. In this case the solution method is similar to that used for a parabolic dependence.

Other such relationships, approximating the true vertical wind and temperature, are, of course, possible, but Murgatroyd (ref. 613) and other investigators (refs. 345 and 358) have concluded that the two-layer model, in which each layer is approximated by a linear dependence of wind and temperature on height, is the most desirable for analysis of acoustic observations for determination of wind and temperature in the upper layers of the atmosphere.

23.4. Observations of Explosions of Bombs Dropped from an Aircraft. The method of determining wind from observations of the explosions of heavy bombs dropped from an aircraft is a variety of the method based on the study of the anomalous propagation of the sound of large explosions. This method has been developed in the United States since 1950. Bombs weighing 1,640 kg were dropped from a B-29 heavy bomber onto a bombing range in the Rocky Mountains. Three bombs, each at distances of 35 km apart, were dropped along the meridian or latitude in the experiments carried out by Crary and Bushnell (ref. 346) in 1951. The explosion waves were recorded at four stations, two on each side of the bombing range, at a distance of 250 and 450 km from the point of the explosion.

A two-layer model was used in analyzing the data for wind determination. The results of the wind determination will be given in the next chapter. In these investigations it was by no means always possible to obtain reliable results, due to the difficulties in separating the influence of the wind and temperature along the path of the sound waves.

23.5. Observations of Explosions of Grenades Ejected from Rockets. This acoustic method has been considered in application to the problem of study of the temperature regime of the upper layers of the atmosphere. One of its principal advantages over observations of the anomalous audibility of the sounds of explosions set off at the Earth's surface is an increase of the sounding ceiling to 80 km or more. Another equally important advantage is that in these experiments the investigated sound is propagated almost vertically in the atmosphere, making it possible to separate the wind and temperature effects more clearly than in other acoustic methods, and while retaining the high accuracy of approximate computations, separately determine the layer-by-layer wind and temperature values (ref. 385).

In deriving analytical formulas it is assumed that the horizontal variations of wind velocity and temperature are small in a horizontal distance up to 15 km, and that the wind is horizontal (the vertical component of wind velocity in the investigated region is extremely small in comparison with the speed of sound). Computations were made by the successive approximations method. The

first step is to find temperature values not corrected for wind influence; these temperature values are then used to compute wind velocity. The temperature values are determined more accurately by taking into account wind data for each layer (the limits of the layer are determined by the heights of two successive explosions of grenades, see fig. 12.1). The temperature and wind data converge rapidly to their final value, and it is therefore sufficient to repeat the computation by the successive approximations method only once (ref. 385).

The described "rocket-grenade" method of wind (and temperature) measurement is being used systematically at the present time (ref. 511), and improvement of the analytical method is continuing (refs. 414 and 415).

24. Wind Measurements Using Guided Missiles

In 1956 Reisig published a study on the application of a method for wind measurement at heights up to 60 km, using guided missiles (ref. 699). The measurements are made partially with surface apparatus which tracks the flight of the missile and partially with instruments carried on the missile itself; the readings of these instruments are transmitted along a telemetric line. The idea of such measurements was expressed as early as 1953 by Newell (ref. 623). The idea of the method is based on a study of "velocity triangles," formed by three velocity vectors, namely, vector of velocity of the missile relative to the Earth v_g, vector of velocity of airflow relative to the missile v_a and vector of wind velocity w. "Velocity triangles" are constructed in two mutually perpendicular planes: pitch plane and yaw plane of the missile.

The velocity vector of the missile relative to the Earth v_g is determined from data obtained by precise tracking of missile flight. This can be done using optical motion picture theodolites or a DOVAR radio-frequency system. The three velocity components in Cartesian coordinates v_x, v_y, v_z are obtained by differentiation of the corresponding coordinates along the X-, Y- and Z-axes, determining the successive positions of the missile (Y-axis--vertical, X-axis--in the direction of the shot). Thus

$$v_g = (v_x^2 + v_y^2 + v_z^2)^{1/2}.$$

The direction of the vector v_g is given by the angle θ_p, formed by the tangent to the missile path and the vertical (Y-axis). The angle θ_p is computed from the corresponding velocity components

$$\theta_p = \arccos\left(\frac{v_y}{v_g}\right).$$

For the angle in the yaw plane the formula is written

$$\theta_y = \arcsin\left(\frac{v_z}{v_g}\right).$$

Gyroscopes within the missile are used to measure the angles φ_p in the pitch plane which determine the position angle φ_y (it indicates the direction of the longitudinal axis of the missile relative to a system of Cartesian coordinates). In addition, an instrument carried in the nose cone of the missile measures the angle of attack α. Reisig notes that with a change of the angle α the maximum error arises in wind determination because the velocity of the missile is extremely large and even a strong wind gives rise to only a small angle of attack (ref. 699). The accuracy of wind measurement is the greater the stronger the wind or the slower is the speed of the missile.

The measured values v_g, α_p, α_y, φ_p, φ_y, θ_p and θ_y can be used to compute the wind components w_p (projection on the pitch plane), w_y (projection on the yaw plane) and total wind vector w. Reisig uses for this purpose the following formulas, which he derived on the assumption of horizontality of the wind (ref. 699).

$$w_p = v_g\left[\operatorname{tg}(\alpha_p + \varphi_p)\cos\theta_p - \sin\theta_p\right],$$
$$w_y = v_g\left[\operatorname{tg}(\alpha_y + \varphi_y - \theta_y)\right],$$
$$w = v_g\left[\frac{1-\cos^2(\alpha_p+\varphi_p-\theta_p)}{1+\cos 2(\alpha_p+\varphi_p)} + \frac{1-\cos 2(\alpha_y+\varphi_y-\theta_y)}{1+\cos 2(\alpha_y+\varphi_y-\theta_y)}\right]^{1/2},$$

and the corresponding formulas for angles determining the direction of the total wind vector w.

Reisig believes that this method for wind measurement has advantages over all others, because with it we can determine the wind profile to a height of 60 km, it requires less than 2.5 min, and it gives instantaneous values of the local wind. Other methods require averaging for a layer of great thickness.

Unfortunately, this study does not give an evaluation of the accuracy of the results.

The method was used with guided missiles in 1954-1955 for measurement of three curves of the vertical distribution of wind velocity and its direction. These results will be considered in Chapter 9.

Tolefson and Henry (ref. 766) used observations of a condensation trail left by a rocket during its vertical launching for wind measurement. The trail

was photographed by two cameras with a 15 m base between them. Tolefson and Henry made a number of wind measurements in the troposphere (up to 10-13 km) by this method.

25. Falling Spheres Method

In Section 8.4 we described a method for measuring atmospheric density, using a falling sphere. The theory of the method, as stated in equations (8.5)-(8.15), shows that observations of this kind can be used for wind determination as well.

McCrosky believes that the use of an aluminized elastic envelope (for increasing albedo), such as now manufactured in the United States by order of NASA, will make it possible to increase the ceiling of this method considerably above 100 km. He carried out a numerical integration of the equation of motion of a freely falling sphere equation (8.6), proceeding on the following assumptions (ref. 584):

(1) the vertical density distribution corresponds to the American model ARDC-1956;

(2) C_D everywhere is equal to unity;

(3) initial velocity is equal to zero;

(4) diameter of the balloon is 30 m and weight is 27 kg.

McCrosky's computed values of relative velocity V and acceleration $g - \frac{dV}{dt}$ are shown in figure 25.1.

Observations from the ground can be used to determine the coordinates of a falling sphere as a function of time. The horizontal movements of the sphere are a measure of the horizontal wind components, and the slowing of the free fall of the envelope depends on atmospheric density and the vertical wind component.

There are several methods for tracking a falling sphere for determination of its path.

The balloon can be photographed from the ground. If this is done at a suitable time at twilight, when the sky is dark and the envelope is illuminated by the Sun, the envelope will be visible from a distance of 170 km as a star of magnitude -5.5. The balloon also can be photographed on a moonlit night. When there is a full Moon, the brightness of the balloon will be equivalent to the brightness of a star of magnitude +7.5 (powerful cameras used in tracking satellites are needed for photographing the balloon).

The falling envelope can be illuminated by a searchlight.

If an accelerometer is placed within the sphere, its readings can be transmitted by telemetric apparatus (Sections 8.4 and 8.5). It is best to place the

accelerometer at the center of the envelope; in this case the influence of rotation is eliminated.

Finally, a radar set can be used to track the path of a falling sphere.

When photographic tracking is used, it is possible to measure acceleration of 0.3 m/sec^2 with an error of 0.05 m/sec^2 (ref. 584).

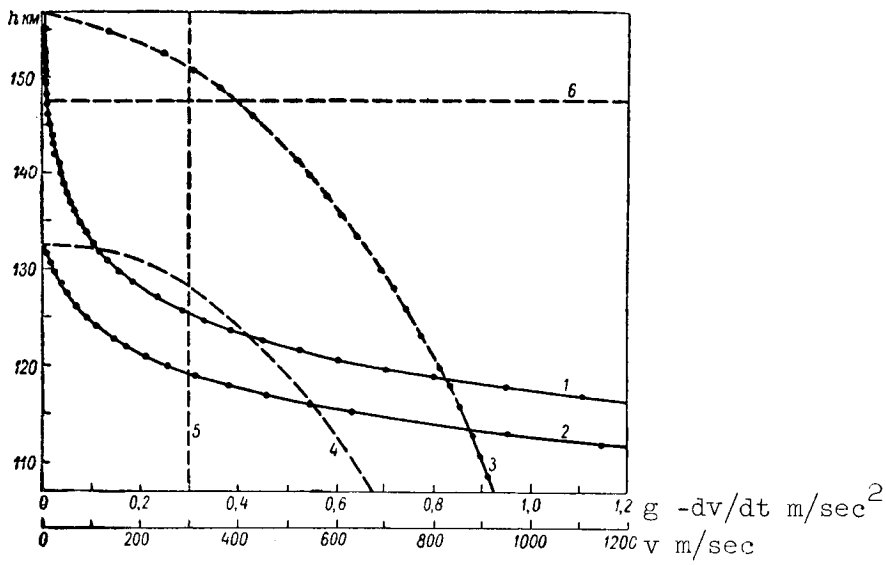

Figure 25.1. Relative velocity of falling sphere and acceleration. 1, velocity when falling from a height of 157.5 km; 2, same, from height of 132 km; 3 and 4, corresponding accelerations; 5, Mach number equal to unity; 6, Knudsen number equal to unity.

We will now discuss measurements with accelerometers. The methods described in Sections 8.4 and 8.5 were based on the use of one accelerometer. The accuracy of measurements increases if acceleration is measured by three accelerometers on an inertial platform placed in the inflated spherical envelope. According to computations made by Otterman, Sattinger and Smith (ref. 646), density measurements in this case are possible to a height of 150 km with an error of 20 percent, and wind measurements to a height of 120 km with an error of 10 m/sec.

26. Wind Measurements in the Ionosphere

Some of the methods for wind measurement in the upper layers of the atmosphere discussed in Sections 22, 23 and 25 can be used to make measurements in the ionosphere, whose beginning is situated approximately at a height of 60-70 km. These include observations of the drift of noctilucent clouds, meteor trails and luminescent regions of the night sky, and also acoustic investigations of explosions of grenades ejected from rockets. Interpretation of the

measurements made by certain of the indicated methods requires a certain caution. We will not discuss here the differences between the wind and turbulence--these concepts are considered in sufficient detail in general meteorology and in monographs on the physics of the upper layers of the atmosphere, and there is no need to discuss this problem further. However, the differences between a wind and the drift of an air particle is a different matter. To what extent can the degree of velocity and drift direction of ionospheric inhomogeneities or an ionized meteor trail be identified with the wind, i.e., with the movement of the entire neutral medium? B. L. Kashcheyev and V. N. Lebedinets believe (ref. 81a) that if the ionized meteor trails did not move with the entire air mass, this deviation would be due to the effect of the geomagnetic field. In the middle latitudes the Earth's magnetic field is tilted at a great angle. For this reason there inevitably would develop a considerable vertical component of velocity, and not only a horizontal component. However, drift measurements indicate the presence of a horizontal velocity of several tens of meters per second, but the vertical component does not exceed 1.5 m/sec.

The movement of ionized trails and also of ionization inhomogeneities, taking into account the influence of the Earth's magnetic field, has been considered rather rigorously by Martyn (ref. 575a) and V. P. Dokuchayev (ref. 61). It can be concluded from these studies that the drift of meteor trails and ionospheric inhomogeneities in the E region of the ionosphere virtually coincides in direction and velocity with the movements of neutral masses of gas.

This process occurs more complexly in the high regions of the ionosphere. The drift of ionospheric inhomogeneities in the F region cannot be identified fully with the wind. The term "drift" usually is applied to a kinematic process in which a "particle" participates (air particle, smoke cloud, meteor trail) whose dimensions are extremely small in comparison with the scale of circulatory processes. If the particle is of large size (such as the ionized component of gas in the ionosphere filling the entire upper atmosphere), the mass of the drifting particle (such as an ionospheric inhomogeneity) can be extremely small in comparison with the entire mass. From this point of view, the wind can be called a dynamic process in the ionosphere when the measured velocity characterizes the translational movement of the entire medium or the greater part of the mass included in a volume whose size is comparable with the scale of circulatory processes (independently of the mechanism of movement: pressure, hydrothermodynamic, electromagnetic, magnetohydrothermodynamic mechanisms).

In the F region of the ionosphere the ionized gas can move under the influence of electrical and magnetic fields with a different velocity and in a different direction than the neutral gas, which constitutes a large part of the mass in this part of the ionosphere. However, except for measurements of the drift of ionospheric inhomogeneities, for the time being there are no more reliable methods for systematic investigation of atmospheric circulation at heights of more than 150-200 km. At present the drifts of inhomogeneities in the F region are being thoroughly investigated. Extensive investigations were made in the IGY period in the USSR (refs. 40b, 41a, 100b, 177a and 221c). The theory of the movement of ionospheric inhomogeneities will be considered in greater detail in Section 26.3.

Here we will discuss methods for observing the drift of ionospheric inhomogeneities which have directed translational movement in addition to random movements (the latter will not be considered in this book). Measurements of translational movement are the principal source of information on ionospheric winds.

26.1. Fading of Radio Echoes. It was noted long ago, especially during measurements using short waves, that the amplitude of the radio signals reflected from the ionosphere is unstable with time, and that the changes are subject to rapid fluctuations in addition to slow changes (diurnal, seasonal, etc.). This phenomenon, called fading of radio waves, originally was interpreted as primarily the result of interference by the many waves arriving at the point of observation by different paths (ground wave, multiple reflected waves, etc.). However, approximately 10 years ago it was postulated that by its very nature the ionosphere is inhomogeneous. An investigation of the ionosphere, using height-frequency curves, revealed (ref. 233) that in a number of cases ionization inhomogeneities, called clouds, appear in different ionospheric layers. There are fluctuations of electron density in the ionosphere at all times; inhomogeneities ("clouds") statistically appear and disappear. Reflection of radio waves from the ionosphere has a statistical character, i.e., the electromagnetic field at the reception point is a superposing of the signals scattered by inhomogeneities present in the reflecting region (ref. 5). These inhomogeneities are in random motion; the mean square error of the velocity varies in the range 0.5-15 m/sec. In a number of cases this velocity cannot be interpreted as the velocity of movement. Independent or poorly related oscillations of plasma of different frequency apparently can exist in the ionosphere. The experimentally observed changes of the amplitude of a single reflected signal can be caused by oscillations of plasma. In this case the temporal variation of the amplitude would not be determined by the velocity of movement of the clouds, but by the wavelength of plasma waves (ref. 5). However, the role of this mechanism in the described phenomena still remains unclear. It is possible that the principal factor involved is convective instability or turbulent movement (ref. 4).

However, experiments show that in addition to disordered movements in different regions of the ionosphere there also are regular movements which over a prolonged period of time have a definite direction of velocity which varies little. Several methods have been developed for measurement of the velocity and direction of these regular movements.

The first group of methods is based on study of the reflection of signals (echoes) from the ionosphere. If there are several receiving stations situated in an area, simultaneously recording echo signals sent by the same transmitting station, each of these will detect fadings. In a number of cases it is possible to note a similarity between the character of the fadings of the echoes and their alternation recorded by different stations; however, the patterns of the echoes at the different stations are displaced with time in relation to one another. This similarity can be attributed to the fact that the ionospheric inhomogeneities move from one station to another. The time spent in this movement corresponds to the observed lag (shift) in time between the stations.

A reflected wave is formed in the ionosphere by a region containing a great many small-scale inhomogeneities. The echo strength is determined by the interference of individual waves scattered in disorderly fashion by distributed

clouds. If the clouds remained motionless, the strength of the echo received at a certain point would be constant, although it would vary from point to point. In actuality, however, the clouds are in movement. Taking into account the characteristics of this movement, it can be represented graphically as being composed of the disordered movements of individual clouds relative to one another and the drift of the entire layer of clouds as a whole in some direction; any movement of the clouds causes variations (fading) of echo strength. The fadings caused by the regular movement of the cloud layer as a whole are caused by the movement of the diffraction pattern relative to the receiver. The velocity of this movement is equal to double the drift velocity of the scattering clouds (ref. 127).

Three stations situated at the corners of a right-angle triangle (or close to it) (fig. 26.1) are usually used. Inhomogeneities of large or small scale can be investigated, depending on the distances between stations. In 1957 Jones, Landmark and Setty confirmed by careful experiments that data on ionospheric winds obtained by observations of the drift of large- and small-scale inhomogeneities agree with one another (ref. 492). We will now consider these studies in greater detail. This will make it possible for us to become acquainted at once with several methods of wind measurement in the ionosphere. This investigation was made at the Cavendish Laboratory in England.

Signals from the output of three receivers are fed to a central station where instruments simultaneously record the fadings of individual pulses reflected from the ionosphere, received by each of the receivers. The temporal shift between the curves obtained at stations 1 and 2 or 1 and 3 determines the corresponding component of drift velocity of the clouds. By having three stations situated as shown in figure 26.1, it is possible to find the velocity components along the given directions 1-2 and 1-3, and hence determine the velocity and direction of the drift of the scattering inhomogeneities in the ionosphere.

Four methods are used for a detailed comparison of the results of simultaneous observations of small- and large-scale inhomogeneities (ref. 492):

(a) observations using closely spaced receivers (three receivers at a distance of approximately one wavelength λ from one another);

(b) recording of reflection heights as a function of time for widely spaced transmitters (about 200 λ);

(c) recording of amplitude as a function of time for widely spaced stations (about 200 λ);

(d) simultaneous observations of changes of amplitude and phase.

Method (a) can be used to study the movement of inhomogeneities causing rapid changes of amplitude, whereas methods (b)-(d) can be used for determination of movements of large-scale inhomogeneities in the ionosphere.

Three receivers are used in method (a). The transmitting station (common for all receivers) operates at a wavelength of 150 m (for observations of reflections from the E layer) and 75 m (for the F layer). This method was used for the first time at Cambridge by S. N. Mitra (ref. 600) in 1949.

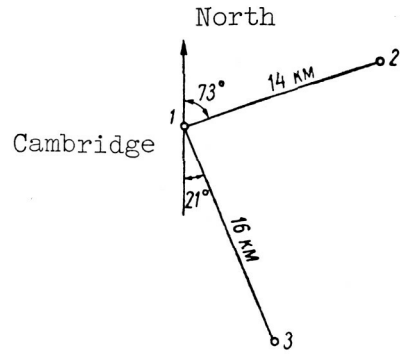

Figure 26.1. Location of stations for measurement of wind in ionosphere (Cambridge).

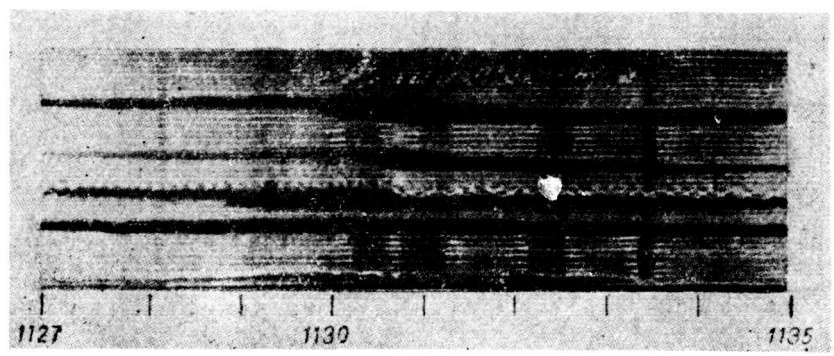

Figure 26.2. Trace of variations of height of reflection of signals transmitted by stations 1-3; location of stations shown in figure 26.1.

Method (b) is based on the use of three transmitters operating at 75 m; these are arranged as shown in figure 26.1. One common receiver is set up at Cambridge where three records of height as a function of time are photographed jointly. Figure 26.2 shows a typical example of the observed variations of height at the time a large-scale inhomogeneity passes over the stations. By measuring the intervals of time between the appearance of characteristics of the same type on the three records, it is possible to determine the direction and the magnitude of wind velocity. If an ionospheric inhomogeneity has an elongated form, the computed velocity does not necessarily coincide with the true velocity; in an extreme case it gives only the drift velocity in the direction of the normal to the line of elongation.

When observations are made by method (b), it sometimes is possible to note a sudden increase of the mean amplitude ("burst") (fig. 26.3). A comparison of the traces in figures 26.2 and 26.3 shows that the time lag at some stations relative to others is identical in both cases. Similar bursts of amplitude are observed more frequently than characteristic changes of height in method (b).

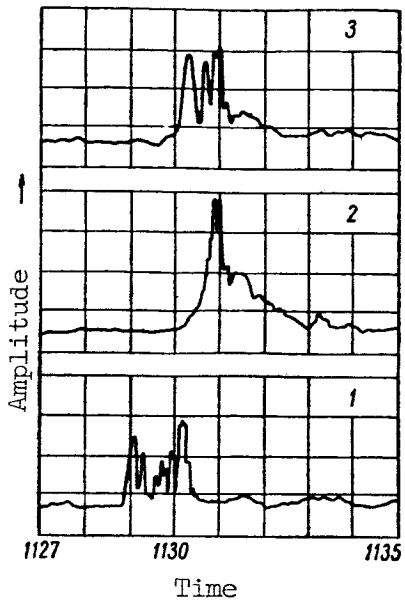

Figure 26.3. Burst of amplitude of reflected wave at stations 1-3 (see fig. 26.1), recorded simultaneously with trace of heights (fig. 26.2).

By recording the times of the bursts of amplitude of the reflected signals it is possible to obtain data for determination of drift velocity. This is the essence of method (c).

Method (d) is based on the relation between amplitude A at the time of a burst and phase P of the signal reflected at height h (this relation was established by Whitehead in 1956)

$$A^2 \sim 1 - \frac{h}{2V^2}\frac{d^2P}{dt^2},$$

where V is the drift velocity of the burst. This method of determining velocity was used in 1956 by Whitehead for the E layer and in 1957 by Landmark for the F layer.

Method (c) is more effective than method (b).

A detailed comparison of the simultaneous readings of all methods revealed that the results agree. This is of great importance for establishing the soundness of the method for measurement of ionospheric winds. In particular, it was established that the movement of large-scale inhomogeneities is identical to the movement of the inhomogeneities causing ordinary fadings. The practical convenience of measurements and the analysis of observations, as well as the accuracy of the results, are most effective when method (c) is used (ref. 492).

In all investigations of the described type it is customary to use three stations (receiving or transmitting), arranged approximately as shown in figure 26.1. In a later study made by M. S. Rao and B. R. Rao (ref. 683) there were four stations, constituting two independent systems of ordinary three-station arrangements, in which the stations were situated at the corners of two identical right angle triangles with sides 108 m in length. The Raos established that the usual three-station method gives a systematic error for wind velocity and direction (up to 10 percent for velocity and up to 27° for direction). They proposed a new method for analyzing observations which increases the accuracy of computation of wind velocity. Improvement of the method was proposed by Court (ref. 340) in 1955. In 1958 Rao and Murty (ref. 684) described a new method in India for using nonattenuating radio waves for study of drifts in the ionosphere; the method is based on the spaced reception of nonattenuating oscillations of radio stations situated at a distance of one hop from the reception point. In this method the ground wave must be completely attenuated.

A new type of recorder of the drifts of ionospheric inhomogeneities has been described by Rao (ref. 688).

26.2. Scintillation of Radio Stars. We will now consider a method for measurement of wind in the ionosphere based on the study of the scintillation of radio stars in the meter wave range. It has been discovered that the radio emission arriving from a source in constellation Cygnus has a variable amplitude. If the fluctuations of a signal from a distant source are caused by the radiation mechanism itself, there should be a total correlation of these fluctuations with time during observation from different stations. But if the source emits with a constant intensity and the fluctuations are caused by the influence of the interstellar medium or the Earth's ionosphere, there can be no total correlation for two points on the Earth's surface. This is what actually occurs. For example, in the case of simultaneous measurements at two points in England at a distance of 210 km apart (Cambridge and Jodrell Bank), no correlation was found between the two records. But with a decrease of the distance between the stations to 4 km there was good, although not total correlation. A careful study of these phenomena established (ref. 111) that the fluctuations of radio emission are associated with its passage through the F layer. Scintillations are caused by electron clouds whose effect is similar to a diffraction screen. The height of the diffraction screens is not known, but apparently they are situated above the ionization maximum of the F2 layer at a height of 400-500 km. These heights are inaccessible to the ordinary pulse method of ionospheric sounding (the radio signals are reflected from the lower layers of the ionosphere, and with an increase of frequency are not reflected at all). For this reason radioastronomical observations assume particular importance. The receiving apparatus consists of movable antenna systems (paraboloids and the Yagi type), receivers with a low noise level and a high response and recorders.

In 1952 Maxwell and Little established that if receiving stations are situated at the corners of an equilateral triangle with sides 2-3 km in length, it is possible to detect a small shift in the time between fluctuations recorded at individual stations. The systematic character of this shift indicates that the diffraction pattern moves on a definite path along the Earth's surface; such movement can be caused by the drift of electron clouds in the ionosphere. By introducing corrections for taking into account the apparent motion of a star,

it is possible to compute the velocity and direction of the drift of ionospheric inhomogeneities (ref. 583). This method gives a velocity of about 340-1,300 km/hour, which increases with an increase of magnetic disturbance in the ionosphere. The dimensions of the ionization clouds were found to be about 2-10 km (ref. 798).

26.3. Theory of the Movement of Ionospheric Inhomogeneities. In a study of the drift of inhomogeneities of the electron concentration it usually is assumed that these inhomogeneities move with the velocity of movement of neutral molecular air masses. However, strictly speaking, this point of view is baseless, because due to the presence of a geomagnetic field a "dynamo field" develops which acts upon the charged particles. An electrical current arises in the medium, and it is acted upon by ponderomotive forces which change the character of the movement.

The character of the movements of inhomogeneities under the influence of the wind has been considered by a number of authors, using an ionized circular cylinder as a model. The most rigorous solution of this problem has been given in a study by V. P. Dokuchayev (ref. 61). This study revealed that, with the exception of a certain part of the E region, the deviations of the velocities of movement of inhomogeneities from the drift velocity of the surrounding ionized medium in the ionosphere are usually insignificant.

This problem has been studied from a somewhat different point of view by Japanese scientists. Maeda (ref. 567) investigated the relationship between horizontal winds (air currents) and horizontal ionization drifts (layer drifts). On the basis of a theoretical analysis of data from the International Polar Year of 1932-1933 he concludes that the drift of ionization inhomogeneities in the F region of the ionosphere is caused mostly by an applied electrical field, and not by a wind in the ordinary sense of this word. In the E and D regions the drift of inhomogeneities caused by electrostatic fields (either induced or applied) has a negligibly small velocity in comparison with wind velocity. In this part of the atmosphere the drift of ionization inhomogeneities for all practical purposes can be identified with an ordinary wind.

The conclusions drawn by Maeda about the F region are in need of further refinement. In particular, it can be noted that Maeda did not take into account the effect of nonelectrodynamic forces (the influence of gravitational forces and the vertical gradient of ionization density), whose influence on the drift of ionization inhomogeneities in the F region can be great.

Matuura (ref. 580) has considered the problem of the relationship between the movement of ionospheric inhomogeneities and the movement of the surrounding ionized gas medium for the two cases when an ionized gas is treated as a hydromagnetic fluid and as a completely ionized gas. In the first case it is assumed that the ratio of the velocity of the neutral particles to the velocity of positive ions is small, which makes it possible to investigate the movement of positive ions, using the ordinary equations of magnetohydrodynamics, assuming the conductivity to be anisotropic. For this case Matuura found that inhomogeneities whose dimensions exceed about 100 km can move with a velocity differing from the velocity of the surrounding medium. The principal role in the formation of such a proper motion of inhomogeneities is played by the magnitude of

the total electrical current. For inhomogeneities of a lesser size the velocity of movement is equal to the velocity of the surrounding positive ions.

When the ionosphere is approximated by a completely ionized gas (this can apply only to the higher regions of the ionosphere, above 200 km), Matuura established that the proper motion of inhomogeneities can be caused by gravitational forces; with inhomogeneities with a scale less than 1,000 km, the velocity of movement is less than 1 m/sec. The direction of movement can be parallel or vertical to the magnetic lines of force.

Tsuda (ref. 771) made an attempt at theoretical determination of the mean velocity of "clouds" in the ionosphere, differing from the surrounding medium with respect to electron density, using a simple theory of turbulent movements. Since kinematic viscosity is much less than magnetic diffusion, it is possible to neglect spontaneous electromagnetic fields Tsuda found that in the E region of the ionosphere, where wind velocity is about 30 m/sec, ionospheric inhomogeneities move with the velocity of the ordinary wind. In the F region, on the other hand, the difference between the movements of ionospheric inhomogeneities, and the movement of the air medium itself becomes extremely great.

These investigations show that observations of the movements of ionospheric inhomogeneities can serve as a method for study of the wind regime in the lower part of the ionosphere in the D and E regions. The use of this method in the F region requires certain precautions and further development of its theoretical basis; this applies in particular to the movement of large-scale inhomogeneities.

Certain anomalies of the drift of large inhomogeneities (apparent drift velocities) have been investigated by V. D. Gusev and S. F. Mirkotan (ref. 46). Their results indicate need for a serious analysis of the correlation method for investigation of ionospheric drifts, when using the spaced reception method for the purpose of developing the method and determining more precisely the conditions under which it is applicable.

CHAPTER 9. DATA ON AIR CURRENTS

27. Wind in the Stratosphere

A great many individual wind measurements have been made in the upper layers of the atmosphere. There is no need to overburden this discussion with summaries of all these observations. We will consider only the most important investigations published in recent years and present results for each of the methods of wind determination in the atmosphere analyzed.

27.1. Drift of Radiosondes and Smoke Clouds. Winds and general circulation of the atmosphere from the Earth's surface to heights of 20-25 km (to approximately the 25 mb level) have been well studied by meteorologists, using data obtained by regular wind sounding. An extensive literature is devoted to the conclusions drawn (e.g., Yeh Tu-chen and Chu Pao-chen, ref. 66a). Therefore, without going further into the investigation of air currents in the lower layers of the stratosphere, we will turn our principal attention to circulation in the higher layers.

Over a period of almost 30 years it was assumed that there was a high-level stratospheric region where an easterly wind prevailed throughout the year, situated above the westerly flow in the troposphere and lower layers of the stratosphere in the temperate and polar latitudes. This assumption was refuted after the results of acoustic wind measurements revealed a well-expressed seasonal wind shift in the stratosphere--from easterly in summer to westerly in winter; it was shown that in this respect the stratospheric wind is monsoon in character (a bibliography of studies in this field is cited in ref. 386). On the basis of daily wind charts for the 41 mb surface over Europe for 1941-1944, Sherhag was able to determine more precisely the seasonal limits of prevalence of an easterly wind in the stratosphere over the middle and high latitudes in summer from May through August. Comparison with improved atmospheric temperature sounding data (after introduction of radiation corrections) led to the conclusion that these winds are of a geostrophic character; this was confirmed by Flohn's conclusions drawn from a comparison of wind measurements over Europe and East Asia.

The lower boundary of easterly flow in the stratosphere initially was assumed to be at a level up to 26 km over the polar and tropical latitudes, rising to 35 km over the middle latitudes, and to lie directly above the zone of maximum velocities of the westerly wind and the maximum rate of decrease of pressure toward the pole over the summer hemisphere. The spatial and temporal boundaries of easterly stratospheric circulation were determined more precisely with increasing improvement of methods and an increase in the volume of wind measurement data.

Barbe (refs. 274 and 275) studied the seasonal changes of stratospheric circulation at Trappe (near Paris). Beginning in October, 1956, he made more than 2,200 soundings exceeding the 20 km level, and thus obtained extensive data for investigation of stratospheric winds at heights from 15 to 30-35 km. Barbe describes atmospheric circulation above the 18 km level as a "stratospheric monsoon." During May the wind assumes a prevailing easterly direction and in September shifts from easterly to westerly. The wind reversal is observed at a height of 18-20 km; the minimum wind velocity also is observed at this level. Wind velocity attains maximum values at the 25-30 km level and is about 70 km/hour in summer and more than 300 km/hour in winter. Both direction and velocity change from day to day, and at times in winter a stratospheric jet stream appears. Repeated soundings (each 5-10 min) reveal the absence of appreciable turbulence at these heights. Barbe postulates that the formation of several daily centers of action occurs in these layers, particularly in winter. Later, Barbe generalized data for four stations located at 50, 32, 27 and 20°N near the Paris meridian (ref. 276). In winter, in the 20-35 km layer in the Paris region, the prevailing wind is westerly (winter stratospheric monsoon). However, in some years for several days or even successive weeks the prevailing wind direction in this same layer is easterly. For example, in January-February 1960, a reversal of the westerly wind to easterly within the 20-30 km layer was observed at all four sounding stations. It is interesting that the wind reversal was observed earlier in the low latitudes and was not noted in the temperate latitudes until several days later. This same phenomenon was also observed in March 1961; in most cases the boundary of the easterly winds attained 35-37 km, and a westerly flow again prevailed farther aloft.

On the basis of an analysis of numerous ascents above 20 km, Faust (ref. 383) investigated the layer of weak winds in the lower stratosphere in the entire northern hemisphere; he regarded this as the zero (boundary) layer. His analysis confirmed the presence of stable layers with extreme wind velocities. The layer of minimum velocities in the lower layers of the stratosphere is situated at an average height of about 19 km. In winter this layer is situated mostly in a westerly flow; Faust regards it as the "zero layer of the second kind." In summer there is no clearly defined velocity minimum at this level, but there is a change of wind direction from westerly below to easterly aloft; in this case Faust regards it as the "zero level of the third kind." Faust computed the isobaric-isometric differences at latitudes 35-55°N between the regions of high and low pressures at the levels from 150 to 11 mb. He found that in winter the zero layer of the second kind is characterized by a change of sign of vertical movements in large volumes of the atmosphere and a dynamic relationship between the upper and lower parts of the layer, with an exceedingly insignificant minimum value of kinetic energy. In a zero layer of the third kind in summer the vertical movements are close to zero, but without a change of sign. The vertical movements are directed upward and downward to this layer, and these movements are not dependent on one another. The dynamic relationship in general is theoretically impossible in this layer. Faust believes that the layer of weak winds at a height of approximately 19 km can be used as one of the principal boundary layers in the general circulation of the atmosphere. Flohn, Holzapfel and Oeckel (ref. 386) obtained interesting conclusions after investigating the easterly flow in the stratosphere of the summer hemisphere. By analysis of available data for the northern hemisphere they concluded that the lower boundary of this flow lies over

the middle latitudes at the 18-20 km level but that it descends considerably toward the pole and toward the equator. The upper boundary of the flow is near the 80 km level. In the middle latitudes it is observed from May to August with some variations from year to year. The wind velocity increases with height at least to the 32 km level.

Systematic wind measurements are made in England by various methods. The seasonal wind variation over England at heights of 35-50 km is characterized by the data in figure 27.1.

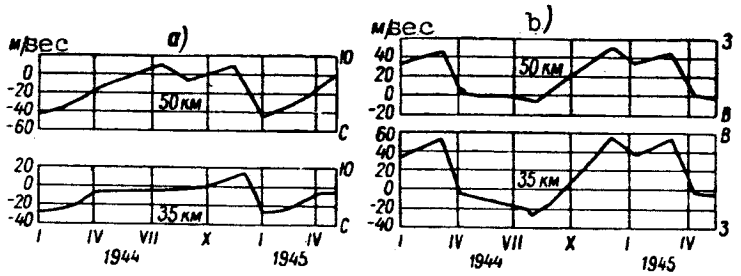

Note: Roman numerals on scale indicate months.

Figure 27.1. Seasonal wind variation in stratosphere over England. a, southerly component (Ю, south; С, north); b, westerly component (В, east; З, west).

Stratospheric circulation in the equatorial region is very unusual. In this part of the atmosphere there is an interaction between the circulatory mechanisms of the northern and southern hemispheres. On the whole, the complex behavior of wind in the stratosphere in the equatorial latitudes still remains inadequately studied.

We will now cite some results of wind measurements at the 60-10 mb levels in 1954-1960 at a number of stations in the equatorial zone: Canton Island (02°46'S, 171°43'W), Christmas Island (02°00'N, 157°23'W) and Nairobi (01°18'S, 36°45'E). The curves of the mean monthly values of the zonal wind component for the 60, 50, 40 and 30 mb levels, published by Ebdon and Veryard (refs. 366-368), show that in some equatorial regions there are stratospheric westerly winds in layers of considerable thickness. The wind direction, once becoming established, prevails for 10-13 months. Change of wind direction occurs in the upper part of the stratosphere and then is propagated into the lower layers. One case was noted where a change of wind direction at the 10 mb level reached the 60 mb surface in approximately one year. If the wind direction changes at the 25 mb level, the corresponding change of wind direction at the 60 mb level occurs 6 months later. There is no appreciable relationship between the processes in the equatorial stratosphere and in the equatorial troposphere. Ebdon and Veryard (ref. 785), after analyzing data obtained by wind sounding of the atmosphere in 1954-1959 in the equatorial (Christmas Island, Canton Island, Nairobi, Singapore and elsewhere) and tropical (San Juan, Khartoum, Bahrein, Aden, Malta) regions, also noted that in the tropical and equatorial regions there are fluctuations of the zonal component of stratospheric winds with periods from 23-29 months. With an increase of height the amplitude of these fluctuations increases, but toward

the pole the amplitude decreases. The most probable value of the period of fluctuations in the equatorial regions is 26 months. There is a close correlation between the mean monthly values of the zonal component at the same level, but at different stations situated at the same latitude in both hemispheres (Christmas and Canton Islands, Christmas Island and Nairobi, etc.).

Reed, Campbell, Rasmussen and Rogers (ref. 694) also concluded that the alternating zones of easterly and westerly winds in the course of time descend from the higher level of observations (30 km). Figure 27.2 shows a cross section which they constructed on the basis of measurements at Canton Island during the period July 1955-February 1960. About one year was required for the subsidence. There is a two-year period of variations of the zonal wind in the equatorial stratosphere. The alternating zones of stratospheric winds over the equator extend over the entire Earth and attain maximum intensity at a height of about 25 km. Thickness of the layers of alternating winds is as great as 10 km and the rate of subsidence is approximately 1 km per month. Near the tropopause the wind zones are attenuated and become unstable. On the basis of ozone measurements the authors concluded that the downward propagation of the alternating winds is a wave movement, not the transport of masses.

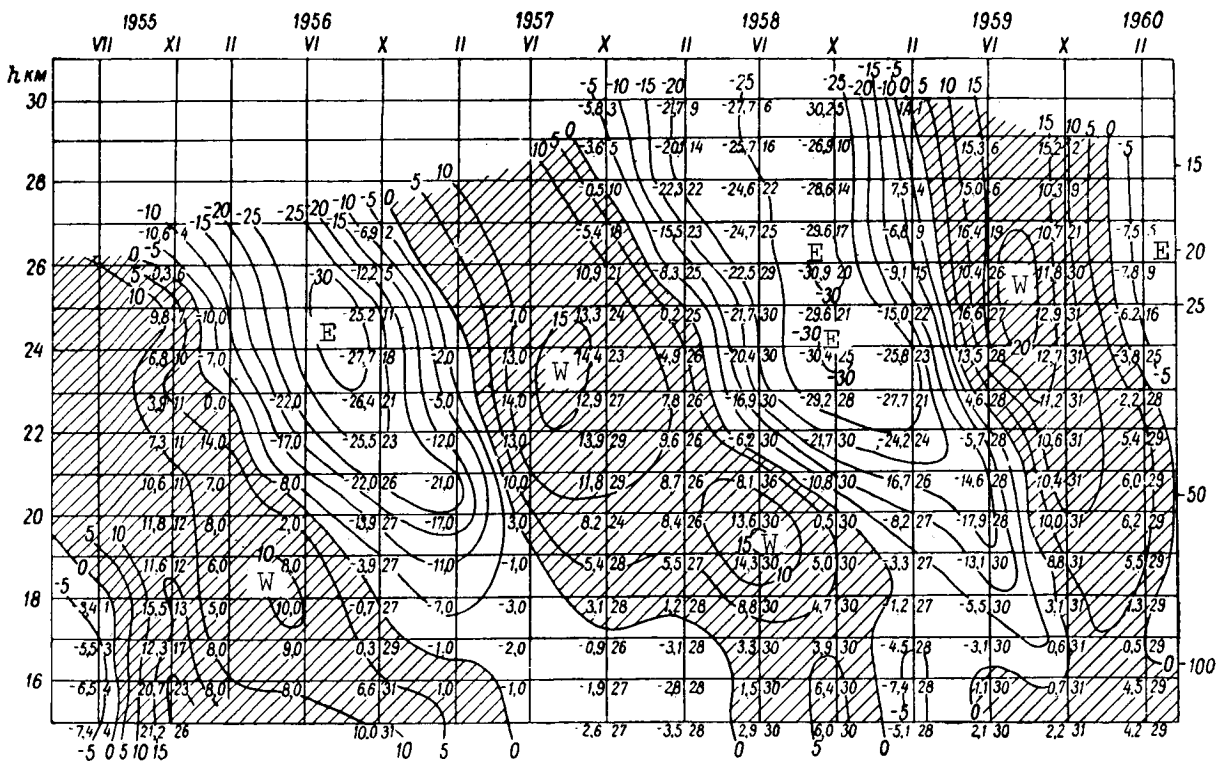

Figure 27.2. Wind in stratosphere over Canton Island (3°S, 172°W). E, easterly; W, westerly.

Finally, we will cite a conclusion drawn by Flohn, Holzapfel and Oeckel (ref. 386) from a study of data on stratospheric winds over the summer hemisphere: over the southern periphery of the large continents of the northern hemisphere there is a tropical jet stream with velocities of 20-50 m/sec.

We have not yet discussed data on air currents in the stratosphere of the western hemisphere. However, systematic investigations of this region of the atmosphere are being made in the United States and other countries.

Since 1948 the United States Army Communications Laboratory has been launching experimental balloons for systematic measurements of air temperature and wind to the greatest possible heights. The objective was to increase the ceiling reached by radiosondes to 50 km, but in actuality the best ascent was only to 42 km. In 1955 Conover and Wentzien summarized the analyzed data for 1948-1952 based on 145 launchings of radiosondes, of which 88 attained heights greater than 30 km (ref. 339). The observations were made at Belmar, New Jersey (20.2°N, 74.1°W). The position of the radiosonde was determined in each 5 min of flight, and the mean velocity of ascent of balloons of this type was approximately 300 m/min. In the analysis the wind was computed from the movement of the balloon in each 10 min. Thus, the derived wind values determined the mean values for a 3 km layer. In a further analysis the wind was determined by graphic interpolation each 2 km.

Figure 27.3 a-d, based on data obtained by Conover and Wentzien, gives the wind velocity values averaged by seasons. These figures show the characteristics of vertical wind distribution: an increase with height in the troposphere, a maximum near the tropopause, a decrease in the lower part of the stratosphere, a wind minimum at the 20 km level or a little higher, a change in direction at this level, and at great heights a new wind intensification.

According to the data in these figures, up to a height of 20 km westerly directions prevail at all seasons. Above this level in autumn and winter the wind has a westerly and southwesterly direction, less frequently northwesterly (not more than 15 m/sec). In summer an easterly wind direction predominates. The maximum wind velocity is observed in winter at all heights.

The patterns of seasonal changes of the stratospheric wind over North America are considered by Belmont (ref. 290) on the basis of observational data for 1957, 1958 and 1959. He believes that over the western hemisphere an easterly flow appears for the first time at higher levels near 55-60°N in early spring and then shifts downward and to the north. The opposite change occurs considerably more clearly and more rapidly; it begins in August at about 55°N and moves upward. By mid-September the wind in the entire stratosphere to the north of 55°N usually becomes changed to westerly. The entire wind reversal process only requires 2 or 3 weeks.

Attmannspacher and Faust (ref. 273) investigated the zero layer constantly observed at the 55-60 km level, a layer of strong winds corresponding to a well-expressed extreme layer, and in the temperature field constituting a zero layer of the first kind. Attmannspacher believes that the reality of this layer is confirmed by measurements made under the IGY program, also by rocket measurements by Kampe in the United States.

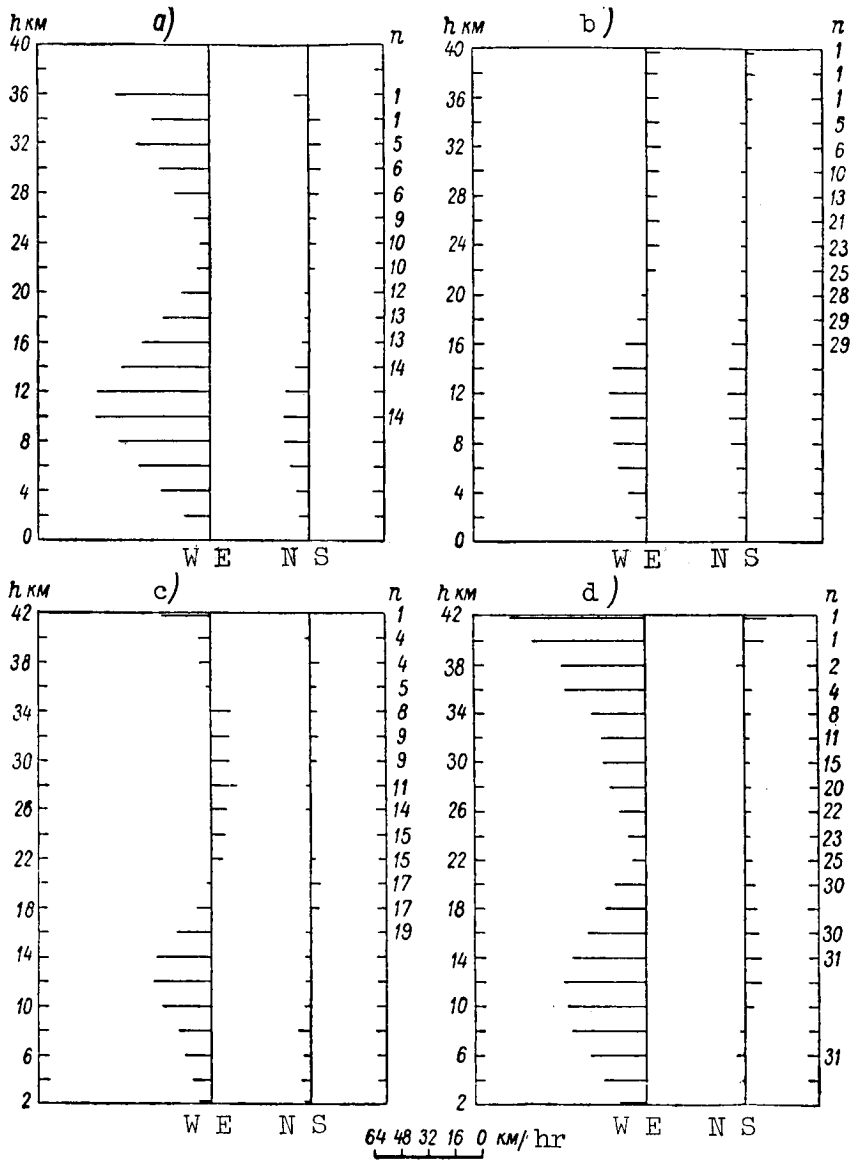

Figure 27.3. Mean wind components. a, January-March; b, April-June; c, July-September; d, October-December; n, number of radiosondes; W-E, N-S, wind direction.

A wind velocity up to 200 m/sec has been repeatedly recorded in this layer.

The rocket measurements by Kampe will be further discussed.

27.2. Measurements by Guided Missiles. This method (Section 24) makes it possible to determine wind velocity and direction to a height of 60 km. Figures 27.4 and 27.5 show the results of measurements by Reisig (ref. 699) in Florida. He obtained 10 wind profiles.

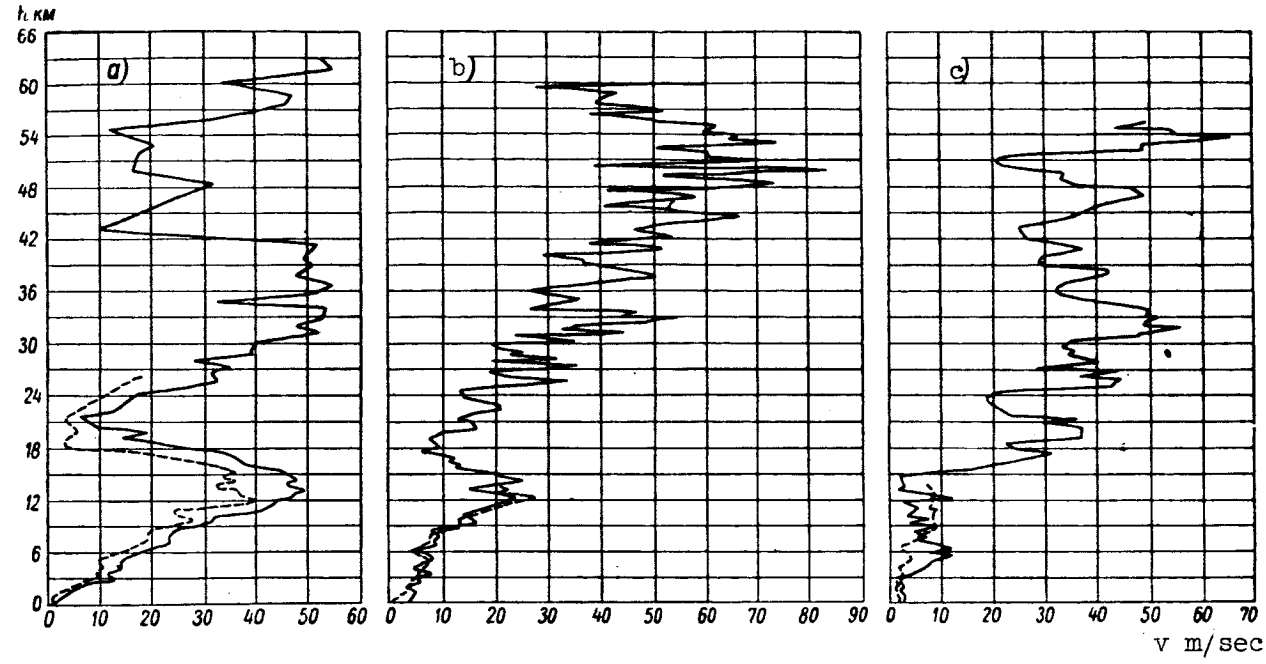

Figure 27.4. Wind velocity v from measurements by guided missiles. a, January 1, 1954; b, April 2, 1955; c, August 3, 1954. Dashed line, measurements using radiosonde.

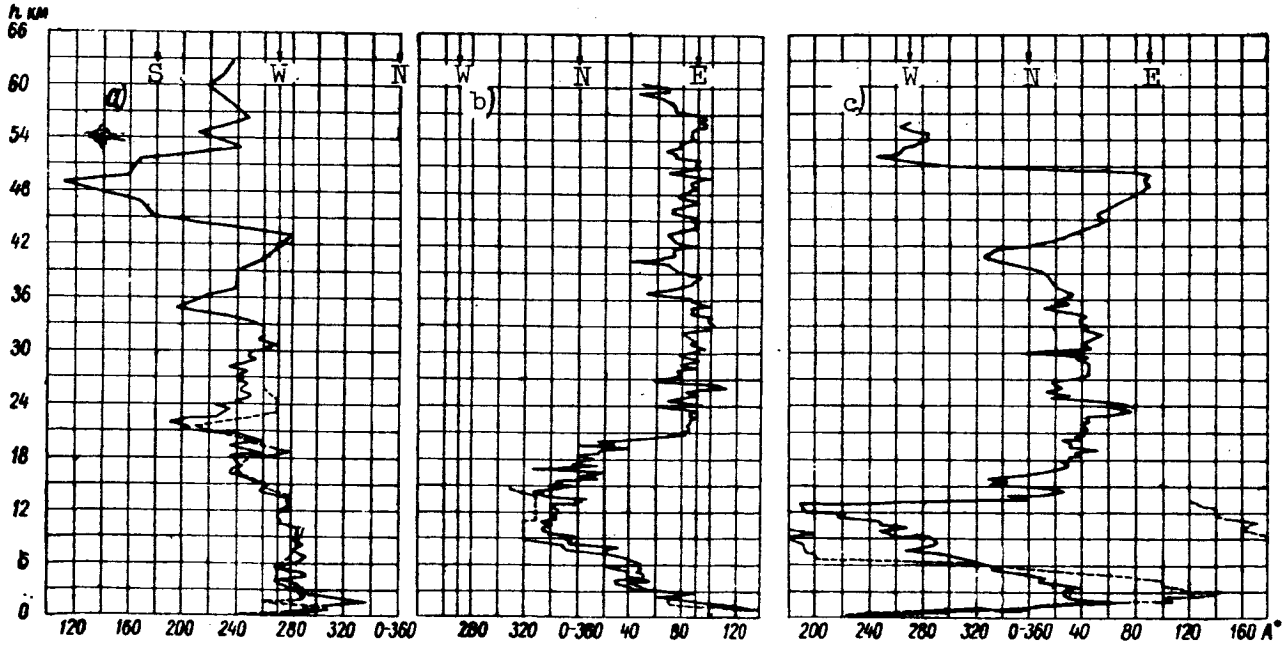

Figure 27.5. Wind direction (N, S, E, W) on basis of measurements by guided missiles. a, January 1, 1954, b, April 2, 1955, c, August 3, 1954. Dashed line, measurements by radiosonde. A, azimuth.

An analysis of these figures reveals the characteristic vertical wind distribution. In the troposphere the wind velocity increases with height, attaining a maximum at the base of the stratosphere. At approximately 20-22 km there is a velocity minimum and sometimes a change of wind direction. At 50-60 km the wind velocity attains 50-70 m/sec.

27.3. Anomalous Propagation of Sound. Regular measurements to obtain information on the seasonal wind variation were made in England in 1944-1945. Figure 27.1 shows the results of observations of the drift of smoke clouds at a height of 30 km and measurements by the acoustic method (anomalous propagation of sound). These data indicate that at a height of 35-50 km, at the latitude of England, a westerly wind predominates in winter and an easterly wind in summer (ref. 613). In winter the westerly component can attain 50-60 m/sec, but in summer the easterly component does not exceed 20-30 m/sec. The northerly and southerly wind components usually are less than the easterly and westerly components. The northerly component appears most frequently in winter and the southerly component in summer.

The results of analysis of acoustic measurements of strong explosions set off on December 15, 1932, in Germany, in accordance with the program of the International Polar Year of 1932-1933, were published in 1954. On the basis of radiosonde data the presence of a first wind maximum of 22 m/sec was established at a height of 10.5 km. Above this level the wind decreased slightly with height, and at 17 km its velocity was 17 m/sec. The azimuth of the predominant direction was 250°. Acoustic data indicated that at great heights the wind velocity increased and at 40 km attained 76 m/sec and at 47 km a maximum value of about 100 m/sec. The wind had an azimuthal direction of 290°.

TABLE 27.1. VELOCITY v AND DIRECTION (AZIMUTH A°) OF WIND FROM OBSERVATIONS OF BOMB BURSTS.

No. of experiment	h km	v m/sec	A°
1-6	30	4	220
	35	5	160
	40	10	150
	45	7	138
7-10	30	14	272
	35	8	292
	40	14	268
	45	14	272

27.4. Explosions of Bombs Dropped from Aircraft. This method of wind measurement was discussed in detail in Section 23. The measurements were made in the region between 38-44°N and 110-120°W. Table 27.1 gives the results presented by Crary and Bushnell (ref. 346). The azimuths indicate the direction from which the wind blows. The relatively small wind velocity, possibly

characteristic of this region and season of the year, should be noted (experiments 1-6 apply to September and experiments 7-10 to October). In general, these data agree with the acoustic measurements of Richardson and Kennedy (ref. 701) made at this same season of the year in eastern Colorado.

Table 27.2 gives data on the wind measurements made by Kennedy, Brogan and Sible (ref. 521) in the period from Oct. 31, 1951-Aug. 28, 1952. In addition, these authors made wind measurements on special "T-days"; these observations were organized by the United States Air Force. Observations of the upper layers of the atmosphere were made on T-days in the southwestern part of New Mexico on a frequent schedule. Observations were made simultaneously by different methods (by different teams of investigators). The wind and temperature were measured on an average of twice a day during the period of T-days from Oct. 20-24, 1952 (ref. 521). The results of observations on T-days are given in Table 27.3. After analyzing these data Kennedy, Brogan and Sible conclude that there is a diurnal wind variation. Between 1,000 and 1,400 hours the changes of wind and temperature occur in opposite phases: the time when wind velocity becomes maximal coincides approximately with the period of minimum temperature.

TABLE 27.2. WIND VELOCITY (M/SEC--FIRST LINE) AND DIRECTION (AZIMUTH--DIRECTION FROM WHICH WIND BLOWS, IN DEGREES--SECOND LINE) FROM OBSERVATIONS OF BOMB BURSTS FROM OCT. 31, 1951 TO AUG. 28, 1952.

	No. of experiment and period of measurements							
h km	33 31/X—6/XI	34 16—19/XII	35 15—17/I	36 16—17/II	37 16—17/IV	39 17—19/VI	40 30/VII—2/VIII	41 26—28/VIII
20	25 300	20 272	8 241	14 268	7 256	8 120	7 94	5 119
25	30 280	20 283	13 263	10 267	18 250	16 118	19 90	10 89
30	31 280	25 323	9 288	2 270	26 246	16 110	30 81	12 89
35	33 280	30 4	11 279	3 258	31 254	20 117	41 79	9 59
40	38 280	33 60	12 290	9 268	21 253	28 102	42 82	11 18
45	45 280	40 70	16 293	25 270	23 104	30		11 50
50	50 280	32 34	19 300	23 270				
55	52 275		31 282					
60			34 284					

Note: Results of experiments Nos. 33 and 39 are rough approximations (obtained from small number of observations).

TABLE 27.3. TEMPERATURE (DEGREES--FIRST LINE), VELOCITY (M/SEC--SECOND LINE) AND WIND DIRECTION (AZIMUTH--FROM WHICH THE WIND BLOWS, DEGREES--THIRD LINE)

No. of experiment, date and average time of measurement

h km	1 and 2 Oct. 20	3 Oct. 21	4 Oct. 21	5 Oct. 22	6 Oct. 22	7 Oct. 23	8 Oct 23	9 Oct.24	10 Oct. 24
	13^h18^m	8^h16^m	14^h20^m	8^h18^m	13^h19^m	17^h47^m	10^h18^m	8^h19^m	13^h18^m
25	—55 2.0 262	—55 3.7 260	—54 2.0 265	—56 5.5 268	—52 2.6 227	—57 3.3 269	—52 0.0	—53 0.0	—55 4.9 252
30	—47 6.5 245	—50 8.6 261	—48 6.4 253	—53 20.2 269	—46 8.4 255	—44 11.4 272	—47 12.2 257	—46 14.1 260	—52 16.3 251
35	—41 16.6 253	—44 22.0 267	—33 13.4 259	—42 30.2 269	—40 21.2 256	—28 20.4 275	—49 34.0 258	—41 30.9 256	—49 31.2 251
40	—27 24.6 266	—30 28.8 270	—12 17.4 269	—22 35.7 260	—22 29.4 256	—5 18.5 278	—35 42.8 260	—20 36.1 260	—37 40.2 252
45	—7 29.4 269	—12 35.6 272	11 20.2 269	—15 46.9 267	4 32.3 260	4 37.5 272	—13 47.8 260		—14 41.6 252
48			23 20.9 268	12 41.9 268	21 33.1 261				—13 51.8 257
50				19 50.7 273					
55				35 60.0 273					

28. Wind in the Mesosphere

28.1. Acoustical Methods. We will now discuss the data presented by Crary and Bushnell (ref. 346). These data were obtained by sound ranging observations of the explosions of bombs and data on wind at a level above 60 km, cited in Table 28.1.

TABLE 28.1. VELOCITY v AND DIRECTION (AZIMUTH A) OF WIND FROM OBSERVATIONS OF BOMB BURSTS.

No. of experiment	Date, time	h km	v m/sec	A°
1	Nov. 27	73	70	291
	18^h15^m	78	95	315
		81	120	326
3	Oct. 1	66	45	285
	6^h15^m	70	75	259
		71	100	258

According to the data in Section 23, the determination of the time and direction of arrival of sound waves from the explosions of grenades ejected from rockets makes it possible to obtain data on the wind at heights of 30-80 km. Table 28.2 gives a summary of 32 wind measurements made at 32°N (rocket test grounds at White Sands, New Mexico), using Aerobee rockets from July 1950 through November 1951. All measurements were made at nighttime (ref. 797). The thickness of the layers and their boundaries are determined by the height of those points at which the grenades ejected from the rockets were exploded.

TABLE 28.2. ACOUSTIC DETERMINATIONS OF WIND OVER WHITE SANDS PROVING GROUND (ROCKET-GRENADE METHOD).

Date and time of rocket launching	Mean height, km	Thickness of layer	Wind velocity, m/sec		Wind azimuth, degrees	
			v	Δv	A	ΔA
July 14, 1950, 1^h37^m	35.4	6.6	19	±3	79	±9
	41.6	5.9	33	4	102	7
	47.3	5.3	46	5	72	6
	56.0	12.1	63	2	75	2
Oct. 16, 21^h00^m	50.0	8,5	46	7	272	9
	57,8	7.1	58	9	277	9
	64.4	6,1	42	11	256	16
	70.1	5,2	35	14	234	24
	75.4	5.6	47	14	217	18
	80.3	4.2	53	20	260	22
Dec. 11, 21^h06^m	35.9	6,5	44	3	269	4
	41,8	5,4	64	4	270	4
	48,1	7.2	83	4	265	2
	54,7	5.9	104	5	272	3
	60.1	4,8	83	7	273	5
	64.5	4,1	68	8	284	7
Dec. 12, 2^h10^m	33,3	12.7	43	1	263	2
	43,5	7,8	74	3	267	2
	53,1	11.3	87	2	286	2
	61.2	4,9	92	6	204	4
June 8, 1951, 23^h11^m	29,6	6.7	12	6	59	29
	38,7	11.5	23	5	96	11
	46,9	4.9	15	13	55	53
	51,5	4,3	61	16	113	16
	55,4	3.6	89	21	66	14
	58,7	3,0	73	22	158	18
	61,9	3,5	30	23	109	46
Nov. 1, 2^h46^m	33,7	7.4	13	6	258	27
	40,5	6.2	71	8	262	7
	46,3	5.4	66	11	268	10
	53,3	8,5	87	8	274	6
	60,5	5.9	64	13	255	12

In Table 28.2 particular attention should be given to the data on seasonal variations of the direction of air flow. In most cases in October, November and December the wind has a westerly direction, whereas in June and July it is easterly. Such seasonal changes also are observed in the middle latitudes (refs. 306, 489, 701 and 722). According to Table 28.2, the wind is characterized by a greater variability over the 60 km level than under it. As pointed out by Weisner (ref. 797), the existence of such deviations from an east to west direction agrees with the wind data for levels above 80 km, obtained earlier from observations of radio echoes from meteor trails (ref. 568). Weisner then notes that the wind over the Bermudas, situated at this same latitude, also has an easterly direction, as was established in experiments by Crary, who studied the anomalous propagation of sound in that area (ref. 345).

Weisner's data permit tracing the pattern of vertical distribution of wind velocity to great heights. The maximum wind velocity, 104 m/sec, was measured at a height of 55 km. Easterly winds have a lesser velocity than westerly winds by an average of 1/3. However, in both cases there is a velocity maximum at a height of 55 km.

Results of measurements made by the rocket-grenade method in later years have been published by Stroud, Nordberg and Walsh (ref. 751). These data are cited in Table 28.3. These measurements confirm the conclusion that there are seasonal changes of wind direction. In the winter months (October-February) the wind has a strictly westerly direction. In summer (April-August) the direction of the air flow is maintained less rigorously, but is mostly easterly. September is transitional; at this time the wind usually is weak and has a northerly direction. No measurements were made in March.

The conclusion that there is a wind velocity maximum in the 50-60 km layer at all seasons is also confirmed. The maximum measured velocity is 104 m/sec; the minimum is 5 m/sec.

In Section 27 we mentioned T-days when air temperature and wind measurements in the upper layers of the atmosphere were made with increased frequency and simultaneously by several independent methods. On the basis of these comparisons it is possible to obtain information on the reliability of wind determinations by the rocket-grenade method. Comparison with simultaneous observations of radiosonde drift gave the following results (first line--data obtained by the rocket-grenade method, second line--data obtained by radiosonde):

Date	h km	v m/sec	A°
Dec. 12, 1950	35	18	263
		25	255
Nov. 1, 1951	34	6	258
		7	258

The results of comparisons with simultaneous observations of the anomalous propagation of sound (these data are given in line 2) reveal the following:

Date	h km	v m/sec	A°
Oct. 2, 1952	47	15	228
		19	266
Oct. 22, 1952	53	34	277
		33	266

Wind measurements by the rocket-grenade method were made regularly in the IGY period. Stroud, Nordberg, Bandeen, Bartman and Titus (refs. 282 and 753) reported the results of wind sounding to a height of 95 km by rockets of the Aerobee type at Fort Churchill, Canada, carried out in November 1956, July, August and December 1957, and January 1958. In summer there is a predominance of easterly winds and their velocity usually is less than 50 m/sec; westerly winds in winter usually had a velocity from 50 to 100 m/sec, but often the velocity exceeded 100 m/sec (fig. 28.1).

TABLE 28.3. ACOUSTIC DETERMINATIONS OF WIND OVER WHITE SANDS PROVING GROUND

Date and time of rocket launching	Mean height, km	Thickness of layer	Wind velocity, m/sec		Wind azimuth, degrees	
			v	Δv	A	ΔA
Sept. 24, 1952, 20^h50^m	42.1	6,3	23	±6	317	±133
	48.2	5,8	14	8	259	33
	54.0	5,6	35	10	314	16
	59,6	5,6	18	10	328	32
	67,3	9,8	23	6	357	15
	76.5	8,6	17	8	201	26
Oct. 22, 20^h45^m	47,3	6,1	33	7	228	13
	53.3	6,0	77	10	277	7
	59.0	5,3	63	11	278	10
	66.6	9,8	15	6	178	13
Feb. 17, 1953, 23^h50^m	48,3	12,1	48	4	290	5
	59,3	9.9	64	5	283	5
	69,0	9.4	54	7	219	7
	77,8	8,2	41	8	335	12
Apr. 24, 3^h19^m	47.1	7.9	30	2	93	4
	54.7	7.3	7	2	61	20
	61.8	6.7	28	3	145	6
	68.1	5.9	43	3	95	5
Aug. 31, 22^h05^m	49.9	8.5	48	6	340	7
	58.1	7.8	57	7	193	7
	65.7	7.3	22	9	340	22
	72.7	6.7	44	5	327	7
Sept. 4, 22^h36^m	58.5	7.7	7	5	46	38
	65.8	7.0	8	6	353	41
	72.5	6.4	30	10	51	20
	78.7	5.8	25	16	344	36

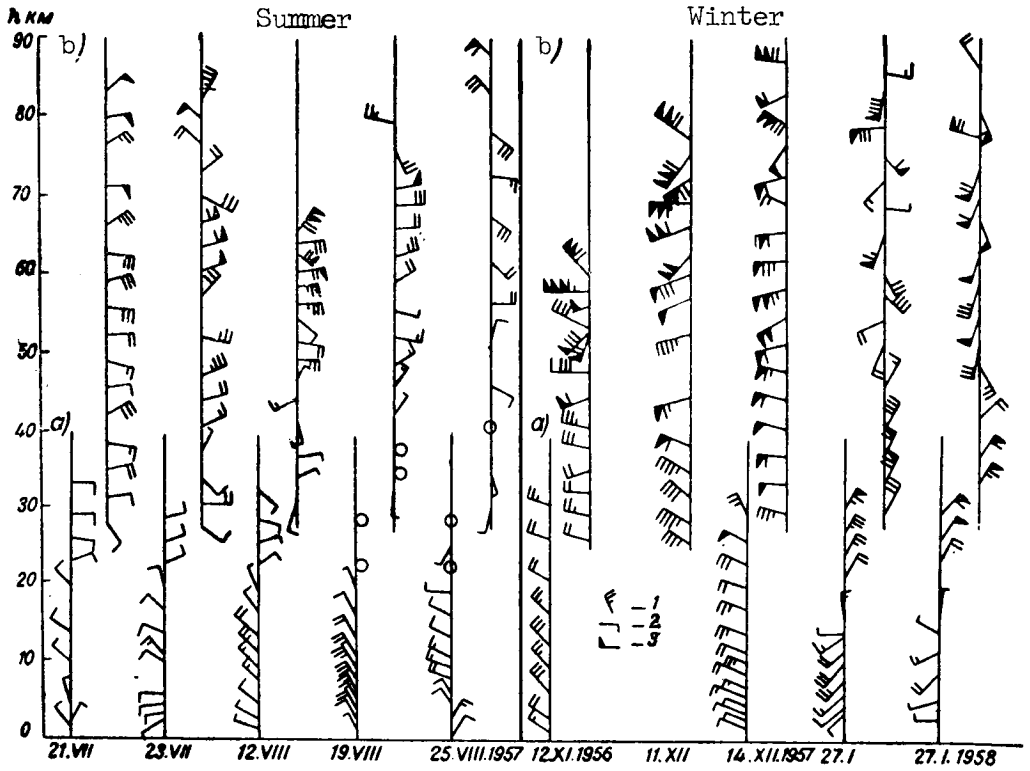

Figure 28.1. Wind velocity and direction from rocket-grenade measurements at Fort Churchill from November 1956 to January 1958. a, radiosonde, b, rocket; 1, 25 m/sec, NW; 2, 10 m/sec, E; 3, 50 m/sec, W.

Nordberg and Stroud (ref. 639) investigated the wind regime of the stratosphere and mesosphere in the equatorial region, and in the IGY period made several soundings in the tropical region (fig. 28.2); these measurements were distinguished by the fact that all were made in a single month (November 1958). Figure 28.2 shows the results. It can be seen that at heights from 35-70 km weak westerly winds predominate (winter circulation). A sudden wind reversal from easterly to westerly was observed at heights between 25 and 35 km. Near the 55 km level the prevailing westerly flow sometimes is disturbed by the appearance of easterly winds. With increase of height, closer to the 70 km level, the prevailing westerly circulation in general is attenuated.

28.2. Relationship Between Wind and Temperature. In Section 28.1, in discussing the results of Kennedy, Brogan and Sible, obtained from observations of the explosions of bombs, we noted a certain kind of relationship between temperature and wind fields, specifically, that during the daytime wind and temperature changes occur in opposite phases. On the basis of their rocket measurements (Tables 28.2 and 28.3), Stroud, Nordberg and Walsh (ref. 751) noted a different relation between temperature and wind. They pointed out the results of two rocket experiments carried out on Dec. 12, 1950, and Aug. 31, 1953. These two flights differed from the others by the occurrence of recorded temperatures deviating sharply from the mean (Table 28.4). In layers in which the air

temperature was anomalously low, the wind direction has an extremely large southerly component in comparison with adjacent layers. However, in layers where the temperature was appreciably above the norm, the wind direction has a strong northerly component. Stroud, Nordberg and Walsh report that an analysis of all collected data confirms the existence of a general relation: with northward shearing of the wind there are higher temperatures. They believe that these phenomena can be caused by dynamic processes in the atmosphere and note that at the time an unusually high temperature was recorded (Aug. 31, 1953), there were disturbances in the ionosphere which can be attributed to dynamic processes.

TABLE 28.4. RELATIONSHIP BETWEEN TEMPERATURE FIELD AND WIND DIRECTION.

Date	Height, km	Wind		Deviation from mean temperature, degrees
		Direction	Azimuth, degrees	
Dec. 12, 1950	33.3	W	263	-2
	43.5	W	267	-2
	53.1	W	268	-2
	61.2	SW	204	-36
Aug. 31, 1953	49.9	NW	340	+16
	58.1	SW	193	-15
	65.7	NW	340	+1
	72.7	NW	327	+22

In the preceding chapters, in discussing the problem of latitudinal variations of pressure and temperature in the stratosphere, we cited the results of rocket measurements in the Arctic (Fort Churchill, Canada) and compared them with measurements in the low latitudes (32°N, White Sands Proving Ground). This demonstrated that the pressure and temperature in the Arctic are appreciably greater than over White Sands Proving Ground. Such a meridional pressure gradient determines the easterly geostrophic wind; this fact, according to the conclusions drawn by LaGow, Horowitz and Ainsworth (ref. 542), generally agrees with the results of wind measurements on the basis of the anomalous propagation of sound and results obtained using "high-altitude balloons."

28.3. Radar Measurements. The method for wind measurements at heights up to 80 km, based on radar tracking of the drift of clouds of fine metal chaff, was discussed in Section 22.2. This method is now being used extensively in the United States for wind measurements in the stratosphere and mesosphere, but publication of the results began only recently. Major work is being done at the United States Army Communications Corps Laboratory (ref. 511).

A communication by Smith (ref. 733) reports that 23 soundings were made in the equatorial part of the Pacific Ocean in the summer months (May, July, and August, 1958). The mean wind was measured at 1 min intervals. A stable easterly flow was discovered at heights of 69-78 km. Below 69 km there is great

increase of turbulence, as indicated by rapid scattering of the cloud and great variability of the observed wind vectors. Observations in Nevada in the United States indicate that such an unstable layer does not exist.

According to measurements in the equatorial part of the Pacific Ocean, the mean wind velocity in the 64-80 km layer is 38 m/sec; the maximum velocity attains 115 m/sec. This velocity was observed at the 69 km level; the wind azimuth was 260°.

Above 78-80 km there was a predominance of meridional winds; this is possibly related to a change in wind direction at great heights.

Definite diurnal wind variations are noted. When sounding is carried out in accordance with a special program, it is noted that there is a 48 hour period of change of the wind vector.

There is regular sounding of the atmosphere with meteorological rockets at Cape Mugu, California (34°07'N, 119°07'W). A parachute and target are ejected from a Loki rocket at a height of about 33 km, and metal chaff is ejected from a Loki II rocket at a height of approximately 65 km. Finally, a parachute and instrument chamber which carries a thermistor for measurement of temperature and a radiotelemetric transmitter are ejected from an Arcas rocket at a height of approximately 60-65 km. All these targets are tracked by radar sets of several types for the purpose of wind measurement. Masterson, Hubert and Thomas reported the results of 106 launchings in which the wind distribution was measured aloft and 34 launchings in which the vertical temperature distribution was measured (ref. 578). The wind sounding extended over a period of 17 months (from Oct. 13, 1959-Feb. 17, 1961).

Circulation over Cape Mugu is characterized by strong westerly winds in winter (from Oct. 15-Mar. 15) with a velocity minimum at a height of approximately 20 km and a maximum at about 60 km. In summer (from May 15-Aug. 15) the winds are easterly and strong and stable in velocity and direction in a broad range of heights. Spring (Mar. 15-May 15) and autumn (Aug. 15-Oct. 15) are transition periods. Masterson, Hubert and Thomas have established the presence of several regions at different heights with a different regime of the meridional component. In the lower region (12-20 km) in winter and spring there is predominance of the northerly component, which in summer and autumn becomes southerly, whereas in the remaining regions meridional circulation has similar characteristics.

Smith and Vaughan (ref. 733a) present the results of wind measurements over Cape Canaveral, Florida, made from April 1959-May 1960 by radar tracking of chaff ejected from a rocket at heights of 20-80 km. The measurement error is 8 km/sec. In summer there is a predominance of easterly winds, and westerly winds predominate in winter. If a westerly wind is observed in summer or an easterly wind in winter, they usually are weak at all these heights. The mean annual wind would have a westerly component, because winter winds have greater velocities than summer winds. Minimum velocities are observed at a height of 23 km and maximum velocities at a height of 70 km; the maximum velocity of 133 m/sec was observed in winter at a height of 71 km. An easterly wind appears for the first time in April at a height of 50 km, and a westerly wind first appears in October. The meridional velocity component indicates some predominance of a southerly direction at heights up to 57 km.

28.4. Dynamics of the Atmosphere in the Region of the Mesopause Determined by Observations of Noctilucent Clouds. Noctilucent clouds permit simultaneous observation of different kinds of movements of the relatively thin layer of the mesopause over an area up to several thousand and sometimes millions of km^2. This circumstance serves as a basis for study of the dynamics of the atmosphere in the zone of the mesosphere on the basis of observations of noctilucent clouds.

The method for making measurements of the movement (also called drift) of noctilucent clouds was discussed in Section 22.4. In this method the specialist selects some morphological formation which is most stable in brightness and configuration or the brightest optical condensation in the field of noctilucent clouds, identified visually or on several photographs; its displacement is measured in a unit time. If there are no such formations, the geometric center or the boundary of the field of noctilucent clouds is used and the displacement of the selected part is determined. A value of 82 km is frequently accepted as the height of noctilucent clouds.

Formerly, observations of the drift of noctilucent clouds were one of the first and principal sources of information on air currents in the upper layers of the atmosphere. Moving at great height (an average of 82 km), these clouds move quite rapidly relative to the observer (up to 1° in a few min), indicating the presence of strong winds. How universal the rapid movement of noctilucent clouds is can be judged from Table 28.5. It was also noted that noctilucent clouds have a predominant direction of movement. As early as the 1930's, Vestine reported that noctilucent clouds over North America mostly move to the west and southwest. As shown by the observations of G. O. Zateyshchikov and V. A. Bronshten in 1936, the movement of noctilucent clouds over the USSR usually occurs to the southwest, west, northwest and north. Data on the direction of movement of noctilucent clouds at different hours of the night indicate a concentration of directions from the east in the morning hours.

TABLE 28.5. WIND VELOCITY AT HEIGHT OF 80-85 KM FROM OBSERVATIONS OF DRIFT OF NOCTILUCENT CLOUDS.

Author	Year	Place of observations	Velocity, m/sec
Jesse	1889	Germany, near Berlin	60-180
Jesse	1890		40-80
S. V. Orlov	1908	Russia, near Moscow	80
Clerk	1908	Australia, Aberdeen	90
V. A. Mal'tsev	1925	USSR, Leningrad	230
I. S. Astapovich	1930	USSR, Eastern Siberia	65-150
C. Störmer	1933-1934	Norway, Oslo	45-80
V. A. Bronshten and G. O. Zateyshchikov	1936	USSR, Moscow	20-135
Vestine	1937	Canada	80 (mean)
V. G. Teyfel'	1951	USSR, Shcherbakov	45-100
Paton	1954	Scotland	50 (mean)

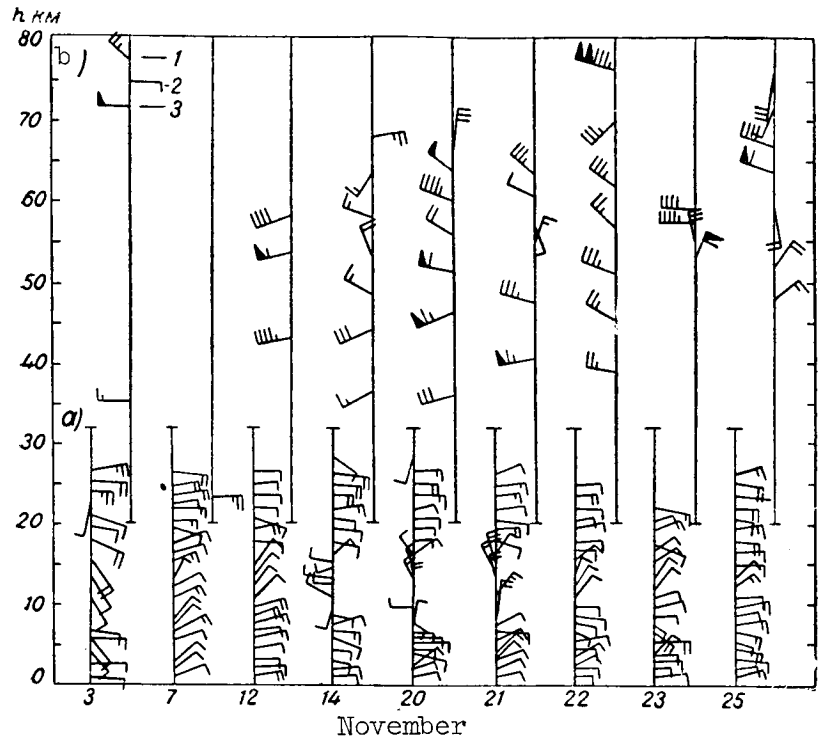

Figure 28.2. Wind velocity and direction determined from rocket-grenade measurements in tropical region (Guam, 13.5°N, 145°E) from Nov. 3-25, 1958. Same notations as in figure 28.1.

The movement of noctilucent clouds from east to west was also observed over the German Democratic Republic (ref. 717). Over Scotland, Paton (ref. 709) on 22 occasions observed noctilucent clouds which all moved from east-northeast with a velocity of about 50 m/sec. According to Stormer's observations, in July 1932, notilucent clouds moved over southern Norway at a height of 81 km in a south-southwest direction at a velocity of 45-55 m/sec.

The accumulation of information on wave formations in the lower atmosphere by scientists of different countries is of great importance for the study of the wave movements of noctilucent clouds. The existence of such phenomena, although transpiring in substantially different regions of the atmosphere, is all the more important because modern "meteorological" knowledge of the upper layers of the stratosphere for the time being remains extremely inadequate. The process of formation of undulating clouds in the troposphere was studied in relatively good detail, and in case of necessity can easily be refined by regular synoptic data, supplemented by ascents, or, finally, by special flights through the particular cloud region by an aircraft carrying measuring instruments. For the time being, not one of these approaches can be used for the study of noctilucent clouds, and the optical method using photographs and movie film at present is

the most objective means for investigation of these extraordinary high clouds. N. I. Grishin successfully has used the technique of slow-motion cinematography, which projects slowly transpiring natural processes onto a screen at greatly accelerated speed.

Preliminary experiments made by N. I. Grishin in 1953 confirmed the possibility of investigation of the movements of noctilucent clouds by use of slow-motion movies (ref. 36). Even the first results revealed definite advantages of the movie-survey method of study of the movements of noctilucent clouds in series of individual photographs. In this case we can observe, on a screen, those movements and changes of configuration of noctilucent clouds which cannot be perceived by visual observations and are not revealed in the development of individual photographs.

In 1954-1955 a movie survey of noctilucent clouds was continued at the Geophysical Institute of the Academy of Sciences USSR in collaboration with the Special Surveys Laboratory of the Moscow Movie Studio for Popular Science Films. General-purpose movie cameras were used in the survey.

Many observers mention the undulating character of certain morphological formations of noctilucent clouds (a classification of morphological formations is given in Section 21).

The large and small crests in the observed fields of noctilucent clouds represent three-dimensional waves, usually occupying a definite, limited region. Within the limits of this wave region there is active movement of these formations. As indicated by the movie survey, the boundaries of such a wave region are in some way the confining boundaries of wave existence and movement. Waves appear at the clearly visible rear boundary, provided this is not the twilight boundary, and disappear after reaching the equally clearly defined frontal boundary. Other morphological forms, existing beyond the confines of these boundaries, apparently are not influenced by these boundaries.

The lifetime and the area of the wave regions vary in broad limits. For example, in the noctilucent clouds of July 20-21, 1954, a small wave region with an area of about 1,000 km^2 developed on a background of bands (IIa) and jets (IIb); after 8 minutes this wave region disappeared completely, leaving behind (as before its appearance) the former arrangement of structural details (ref. 40). There are frequent cases of the appearance of wave regions tens of times greater, occupying a considerable part of the field of usually bright noctilucent clouds with a far greater lifetime.

As pointed out by N. I. Grishin, the nature of the optical condensations is different when formed by intersection with long waves, when there can be changes of the physical properties of the medium facilitating changes of the brightness of noctilucent clouds; when they are formed by intersection with short waves, there apparently is an optical effect due to increase of the linear thickness of the layer when observed at a small angle. However, this problem requires additional study.

The character of the wave movement of notilucent clouds is interesting. A number of authors note a change in the distances between individual crests. The results of investigations by N. I. Grishin (ref. 40) indicate an appreciable increase of velocity and wavelength with time (fig. 28.3). This circumstance, in combination with other characteristics, reveals that the wave formations of noctilucent clouds have much in common with wind waves at sea. We can, therefore, make partial use of the methods employed in investigation of sea waves and their theory for the interpretation of wave phenomena in noctilucent clouds. For example, the formation of small and short-lived wave regions, according to N. I. Grishin, can be attributed to a local wind effect (air flow) on noctilucent clouds, as on some boundary surface, part of which is brought into wave motion. With time the influence of the wind produces an increase of velocity and wavelength. Waves of great length can be caused by other factors, especially pressure.

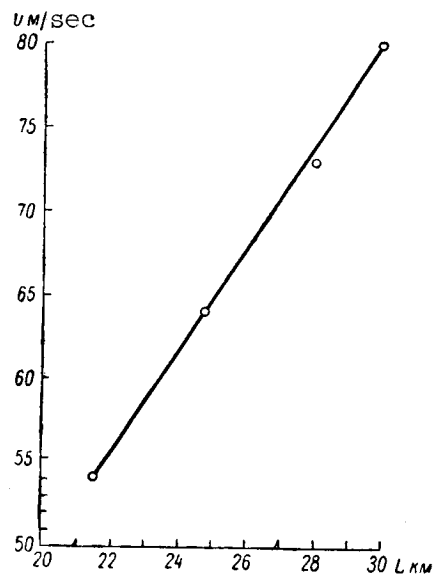

Figure 28.3. Change of velocity v of noctilucent clouds as function of wavelength L of morphological formations of these clouds.

In the case of type-II details, a movie survey in different cases reveals two kinds of movement. The first has definite indications of wave movement. As an example, in the noctilucent clouds of June 30-July 1, 1954, consisting entirely of broad, parallel, poorly defined bands (IIa), there usually was a phase movement to the south, almost precisely in a direction perpendicular to the generating lines of these bands. When projected onto a screen, this resembles the movement of undulating clouds in the troposphere, when new clouds are formed at the front of each wave, while at the rear they disappear, together with the phase shift of the air wave.

In jets (IIb) and certain bands (IIa) of noctilucent clouds, in many cases there is movement of the brightest parts (thickenings) along their generating lines. However, this is a result of the passage of some long wave. Attempts to

find any method for determination of the direction and velocity of movement directly from the jets and bands are unsuccessful at present.

Figure 28.4 shows schematic representations of waves measured from photographs by N. I. Grishin (ref. 40a). The first group of waves with a wavelength L = 5-10 km is characteristic of the small crests, i.e., type-IIIa. They appear to an observer at ground level in the form of small ripples. The velocity of the phase movement of these waves varies between 10 and 30 m/sec. Their height has not been measured, but apparently it is not great and ranges from 0.1-0.3 km.

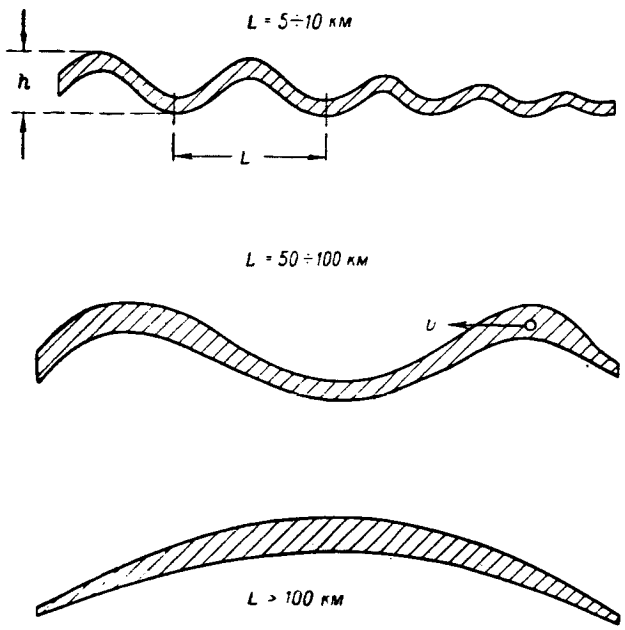

Figure 28.4. Schematic representation of undulating formations in noctilucent clouds.

Waves with L = 50-100 km form crests or type-IIIb. In this case there already is a nonuniform distribution of the cloud mass along the wave surface. In a crest, as in tropospheric clouds, the particles are enlarged and a denser and, therefore, brighter cloud mass accumulates. There is partial or total evaporation of the clouds in the trough of the wave. As revealed by actual data from a movie survey and large-scale photographs, such a picture is a very common occurrence. The height of type-IIIb waves, and especially type-IIIc, for which L > 100 km, on the basis of measurement, is about 3-5 km and possibly more. The velocity of propagation of such waves is 50-150 m/sec. In many cases there are groups of short waves on a long wave surface. This complicates the kinematic picture of phase oscillations and makes their interpretation difficult. For example, two waves (or groups of waves) of different directions of phase oscillation intersect and at this place form a dense and bright condensation of noctilucent clouds (fig. 28.5). The apparent displacement of this condensation

will naturally occur in the direction of the resultant vector $\vec{R}_v$ of the terms of

velocity vectors of two directions: v_1 and v_2. N. I. Grishin discovered the presence of such a combination by analyzing a slow-motion movie survey. Failing to take this phenomenon into account, observers frequently erroneously ascribed the real velocity of the "drift" of a bright, well-defined condensation to the vector $\overrightarrow{R_v}$. Due to this error observers found unreal, exaggerated drift velocities at acute angles of intersection of the components of the vectors.

Several cases of the appearance of single waves in noctilucent clouds have been recorded. The phase movement of such waves occurred in a direction perpendicular to their front.

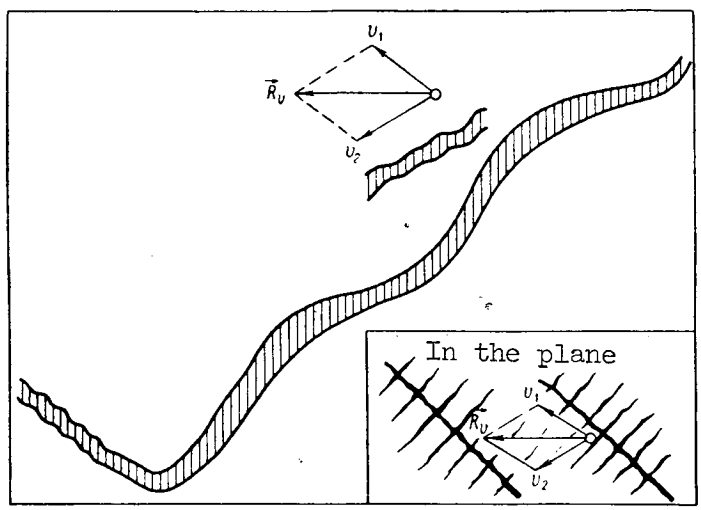

Figure 28.5. Composite apparent motion R_v of noctilucent clouds resulting from wave oscillations of different direction.

Noctilucent clouds, upon entering a region of wave oscillation, like undulating tropospheric clouds develop at the crests and break up in the troughs of the waves. The large scales of wave oscillations and the velocities of their propagation apparently provide the necessary and adequate adiabatic cooling of the volume of air carried to the crest. Movie-survey data confirm the external similarity between the evolution of wave types of noctilucent clouds and the evolution of similar clouds in the troposphere. Parts of noctilucent clouds, not having a wave nature, both externally (statically) and dynamically retain their similarity to the corresponding types of tropospheric clouds. In tropospheric clouds it is also common to observe small eddy formations, but due to observation conditions it is difficult to observe large eddy movements of cyclonic character in them. Preferably observations should be made at a distance of 300-500 km for detection of these movements.

The second characteristic type of movements in noctilucent clouds is eddy formations with movements sometimes resembling "channel flow," but the possibilities of measuring them are limited by the mentioned circumstances.

Small eddy formations, combined into type-IV of the morphological classification, frequently appear in the region of laminar flow of the upper atmosphere. Large eddies (IVc) are formed relatively rarely. On the night of July 1-2, 1956, a movie survey was successful in recording an extraordinarily well-developed vortical rotation (clockwise in projection on the Earth's surface) of the entire field of noctilucent clouds with an area exceeding 500,000 km^2. Small eddies (IVa, b) sometimes are formed near type-II. Their movement in this case (June 25, 26, 1954) occurred along a jet, sometimes coinciding with the direction of phase movement of the closest formations of types-IIIa and IIIb, if the latter were present. The velocity of movement of such eddies, then, was commensurable with the velocity of movement of the crests present (IIIb).

The formation of jets and bands, when the matter of noctilucent clouds is entrained by a current in the direction of flow, in which small eddies develop, apparently is the result of "channel" flow (ref. 40a).

The presence of waves in noctilucent clouds has a natural explanation if it is assumed that noctilucent clouds are similar in composition to ordinary clouds, and, being a product of water vapor condensation, consist of ice crystals. In this case, as for tropospheric clouds, we can invoke the explanation first expressed by Helmholtz: these are waves on a discontinuity where wind and density experience a sharp change. The vertical movements caused by internal waves cause water vapor condensation in the ascending part of the air layer and evaporation of drops in the descending part.

If it is assumed that noctilucent clouds are of a dust origin, then, as pointed out by Haurwitz (ref. 426a), it is difficult to explain the development of the wave structure.

An attempt at such an explanation was undertaken by Ludlam (ref. 101). In this case it must be assumed that the external form of the wave systems (parallel, equidistant bright bands) is caused by an optical effect in the presence of a wave structure of the entire thickness of the cloud layer. Haurwitz computed the difference of the optical paths for the simplified case when alternating linear segments (fig. 28.6) are used to represent the waves instead of sine curves. The distance L between A and B corresponds to the wavelength, 2Z is the doubled amplitude. Distances AA', BB' or CC' are the thickness h of the cloud layer.

If an observer looks at noctilucent clouds in the most "favorable" direction AC', the length of the segment within the cloud along the line of sight will be

$$AC' = \frac{(h + 2Z)}{\sin \beta},$$

and

$$\operatorname{tg} \beta = \frac{2(h + 2Z)}{L}.$$

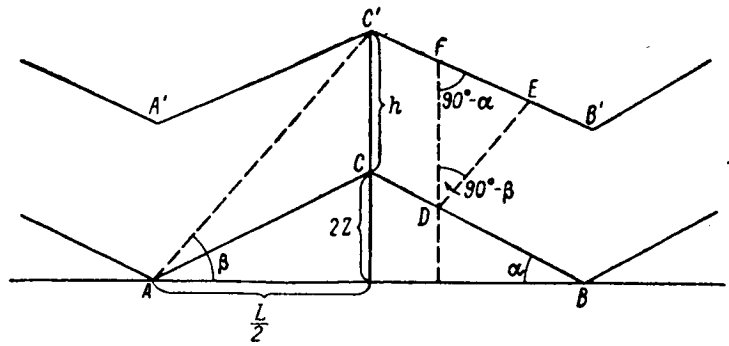

Figure 28.6. Computation of difference of paths of light ray with wave structure of entire thickness of noctilucent cloud.

If the line of sight intersects the cloud in its descending part DE, as a result of the great distance of the cloud from the observer, it can be assumed approximately that AC' is parallel to segment DE. If α is the angle between the base (lower boundary) of the cloud and the horizon AB, then

$$\operatorname{tg}\alpha = \frac{4Z}{L}.$$

If FD is vertical, then

$$\frac{DE}{h} = \frac{\sin(90-\alpha)}{\sin(\alpha+\beta)},$$

hence

$$\frac{DE}{AC'} = \frac{h}{h+4Z}. \qquad (*)$$

It can be assumed that in a general case amplitude Z is small in comparison with cloud thickness h, and therefore ratio (*) is not very small. For example, if h = 4 km, Z = 1 km, the ratio is 1/2.

Taking into account the sinusoidal character of wave surface ACB does not appreciably change the result (ref. 426a).

We will now consider certain problems involved in the theory of waves forming in noctilucent clouds at a discontinuity (Helmholtz waves). We will assume, for simplicity, that two homogeneous incompressible media are in contact, and at the discontinuity lying in plane xy the density changes in a jump from value ρ to value ρ' and the wind velocity from V to V'. The direction of the wind in both cases is identical or mutually opposite. We will assume that the coordinate axis z is directed vertically upward. The wave motion at the discontinuity can be considered two-dimensional, not dependent on coordinate z. Because of the smallness of the scale of the phenomenon, we can neglect the influence of the Earth's rotation. Due to the smallness of amplitude Z, disturbance ξ at the discontinuity can be represented in the form

$$\xi = Z\cos k(x - ct),$$

where k is the wave number $k = \frac{2\pi}{L}$ (L is the wavelength), c is the speed of propagation of the wave. For the potentials of velocity in the lower and upper media we have

$$\varphi = -Vx + (c - V)Ze^{kz}\sin k(x - ct),$$
$$\varphi' = -V'x + (c - V')Ze^{-kz}\sin k(x - ct).$$

From the condition of continuity of pressure at the discontinuity we obtain the following expression for the velocity of wave propagation (ref. 102)

$$\frac{g}{k}(\rho - \rho') = \rho(c - V)^2 + \rho'(c - V')^2,$$

hence

$$c = \frac{\rho V + \rho' V'}{\rho + \rho'} \pm \left\{ \frac{g}{k}\frac{\rho - \rho'}{\rho + \rho'} - \frac{\rho\rho'}{(\rho + \rho')^2}(V - V')^2 \right\}^{1/2}$$

(g is the acceleration of gravity).

The first term on the right-hand side of this equation corresponds to mean velocity weighted proportional to the density of each layer. Due to the small difference of densities this term is virtually equal to the unweighted arithmetical mean. The first term in the parentheses takes into account the stabilizing effect of stratification, because density ρ of the lower medium is greater than ρ'. The second term takes into account instability caused by the wind shear (ref. 426a).

If the wind directions are identical in both layers or mutually opposite, as was assumed, it is natural to assume that the wave crests will be arranged perpendicular to the wind, and that the velocity of propagation of the waves arising at the discontinuity is equal to the mean velocity of the wind in both layers.

On the basis of the last equation Haurwitz (ref. 426a), taking into account atmospheric compressibility, derives an expression for the wavelength

$$L = \frac{\pi}{g} T_m \frac{(V - V')^2}{\left[(T' - T)^2 + (V - V')^2 T_m \frac{(\bar{\varepsilon} - \varepsilon)}{g} \right]^{1/2}},$$

where T_m is the mean temperature at the discontinuity; T and T' are the temperature of the upper and lower layers; ε is the actual vertical temperature gradient,

assumed to be identical in both layers; $\bar{\epsilon}$ is the adiabatic gradient. The second term in the denominator takes into account atmospheric stability because the actual temperature gradient is less than the adiabatic gradient.

If it is assumed that T' = T, it follows from the last equation that

$$|V - V'| = \frac{L}{\pi}\left[\frac{g(\bar{\varepsilon} - \varepsilon)}{T_m}\right]^{1/2}.$$

If it is assumed that L = 10 km, which is frequently observed in wave formations in noctilucent clouds, $T_m = 200^\circ K$, g = 9.8 m/sec, $\epsilon = 0$, then for the wind shear we obtain the estimate

$$|V - V'| = 70 \text{ m/sec}.$$

It has already been mentioned that the presence of a wave structure in noctilucent clouds has a natural explanation, if it is assumed that noctilucent clouds consist of water. Haurwitz tried to explain the development of wave formations in noctilucent clouds by proceeding on the assumption that they have a dust origin (ref. 426a). He demonstrated that the effect of horizontal divergence associated with internal waves can be adequate for the formation of visible wave systems. He considered the changes of horizontal divergence caused by wave motion and their influence on the distribution of density n of dust particles (n is the quantity per 1 cm^3). Consider v, w the horizontal and vertical components of velocity of wave motion. Then for local changes n, the following equation is correct

$$\frac{dn}{dt} = -\frac{\partial}{\partial x}[n(V + v)] - \frac{\partial (nw)}{\partial z}.$$

We first determine the quantity of particles N situated over 1 cm^2 along the line of sight, if the noctilucent clouds are situated over the observer's head. We will assume that the dust is concentrated in a layer with thickness h, situated under the discontinuity. If n is not dependent on z, then

$$N = \int_{-h}^{0} n\,dz = nh.$$

As a result of integration of this expression vertically within the limits of the cloud we obtain

$$\frac{\partial N}{\partial t} + V\frac{\partial N}{\partial x} = -\bar{n}\int_{-h}^{0}\frac{\partial v}{\partial x}\,dz.$$

On the right-hand side of this equation n has been replaced by its mean value $\bar{n}$ (horizontally averaged). Assume

$$N = N_0 + N_1 \cos k(x - ct),$$

where $N_0 = nh$ is the mean value N. Then, using the expression of velocity through its potential $v = -\frac{\partial \varphi}{\partial x}$ we obtain from the preceding equation

$$N_1 = N_0 \frac{Z}{h}(1 - e^{-kh}).$$

For numerical computations Haurwitz assumes the values L = 10 km, h = 4 km, Z = 1 km; hence

$$N_1 = N_0 \frac{0.92}{4} = 0.23N_0.$$

Thus, variations N can attain almost 50 percent.

If the thickness of noctilucent clouds is small in comparison with their wavelength, from the preceding expression for N_1 we obtain the approximate equality

$$N_1 = N_0 2\pi \frac{Z}{L},$$

hence, if the earlier numerical data are accepted,

$$N_1 = 0.63N_0.$$

In both cases the variations of the quantity of particles over a unit surface caused by divergence of wave origin have an identical order of magnitude and are comparable with the perspective effect considered in figure 28.6.

It was assumed that the noctilucent clouds are situated above the observer's head, but in actuality they are usually visible near the horizon. However, the evaluation changes little when this circumstance is taken into account.

On the basis of these computations, Haurwitz concludes that the development of light and dark bands in noctilucent clouds can be explained on the assumption that these clouds are of dust origin, and that the presence of wave formations in noctilucent clouds is no proof of their water composition. However, these computations apply to the case L = 10 km (ref. 426a). According to the observations of N. I. Grishin (ref. 40) and other authors, however, the waves in noctilucent clouds can frequently attain a length of 50-100 km. For such long waves the last of the formulas for N_1 gives extremely small values for the variation of horizontal divergence. In the case of long waves this reasoning cannot explain the origin of wave formations in noctilucent clouds, if these clouds consist of dust particles. But Haurwitz assumes that an allowance for compressibility can give somewhat greater values for horizontal divergence (ref. 426a).

28.5. Wind Field in the Stratosphere and Mesosphere. Murgatroyd compiled an extremely complete generalized summary of the results of wind measurements at heights up to 100 km, published before 1956. The following special characteristics of Murgatroyd's model (fig. 28.7) are noted (ref. 614).

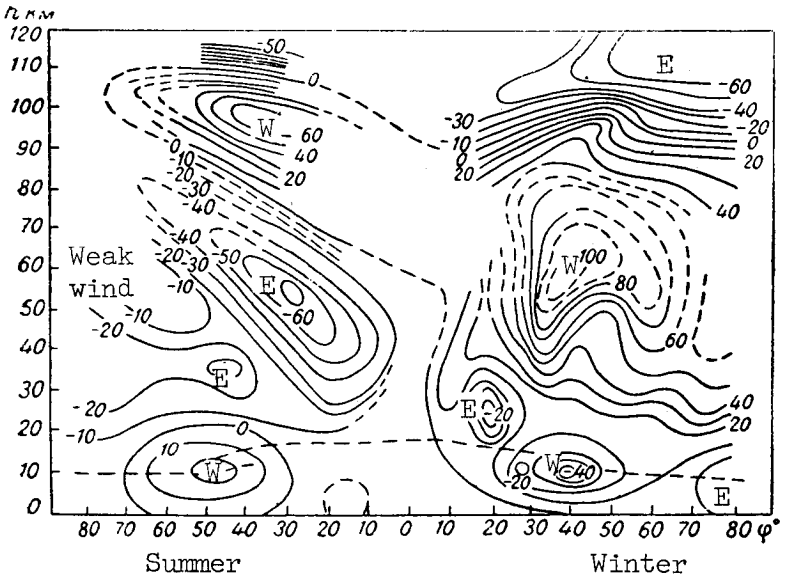

Figure 28.7. Distribution of westerly (W) and easterly (E) components of zonal wind (m/sec).

There are strong westerly winds (particularly strong in winter) in the upper layers of the troposphere. In the higher and lower latitudes the westerly winds are weaker; their direction also changes frequently to easterly. As a result of change of sign of the temperature gradient in the lower layers of the

atmosphere, the velocity of the westerly winds decreases appreciably to the 20 km level. In summer such an attenuation occurs at all latitudes at a height of 20-30 km, but it is particularly noticeable in the subtropics. At great height there is a predominance of westerly winds in winter and easterly winds in summer. The maximum velocities are observed at the 60 km level. Above 70 km, Murgatroyd notes a great wind variability. Above 80 km in summer, the velocity of the westerly winds increases with height almost to the 100 km level.

In the IGY period data on wind in the upper layers of the atmosphere were considerably supplemented by new measurements.

American geophysicists, in developing the standard atmosphere, model 1959 (ARDC-1959), attempted (ref. 418) generalization of available wind measurement data for the upper layers of the stratosphere and for the mesosphere. Figures 28.8a and b give the results for the distribution of zonal wind in winter and summer.

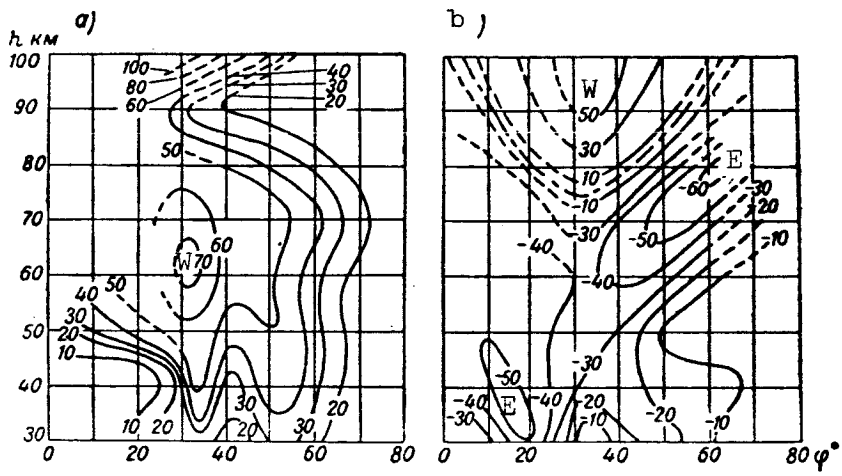

Figure 28.8. Distribution of westerly (W) and easterly (E) components of zonal wind in northern hemisphere (m/sec). a, winter; b, summer.

In 1961 Batten (ref. 286) gave a generalized summary of wind measurements to a height of 100 km, making improvements in Murgatroyd's model shown in figure 28.7. Figure 28.9 shows Batten's model of the mean zonal winds for summer (from May through August) and winter (from November through February). Batten points out that in the equatorial region the wind field changes appreciably from year to year: the dashed lines in the diagram show the results obtained by McCrary in 1959 in the Pacific Ocean Basin.

One of the principal differences between the Batten and Murgatroyd models is in the summer position of the transition zone between the easterly winds in the mesosphere and the westerly circulation in the upper layers of the atmosphere. Measurements at Johnston Island and at Fort Churchill show that the wind reversal occurs near the 80 km level.

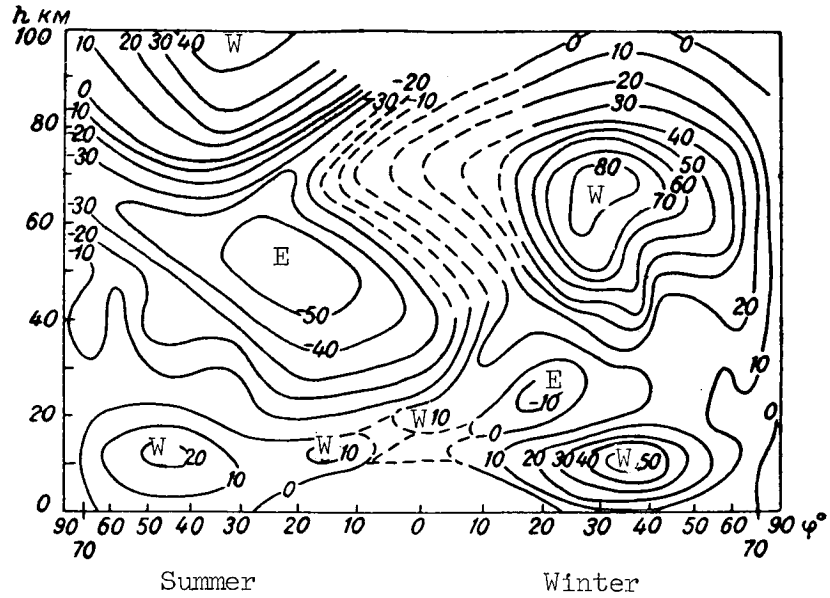

Figure 28.9. Average values of westerly (W) and easterly (E) components of zonal wind (m/sec) according to generalized Batten model.

In the winter hemisphere the principal difference between the Batten and Murgatroyd models is in the position of the center of the westerly winds; according to Batten, this center is situated higher and closer to the equator.

Figure 28.10 shows meridional cross sections of the zonal wind component for the beginning and end of winter, constructed by Batten. In November-December the center of strong westerly winds is situated at a height of about 65 km and latitude 55°. This maximum of the westerly winds extends also into the lower layers of the stratosphere, and gives rise to a jet stream on the edge of the polar night. As is well known, in January-February there are sudden warmings of the stratosphere. This cross section shows a strong westerly flow in the lower part of the stratosphere. Centers of easterly winds appear in the 20-30 km layer.

28.6. Temporal Cross Sections of Wind and Temperature Field to Heights of 80-100 km. Teweles has generalized the results of temperature and wind measurements to a height of 80 km made at Fort Churchill (Canada) by the rocket-grenade method and also by the method of falling spheres (accelerometers) and Pitot tubes. The cross sections which he constructed also include radiosonde data, making it possible to obtain a full picture for an extensive region embracing the entire troposphere, stratosphere and mesosphere (refs. 759 and 760).

Figures 28.11 and 28.12 give cross sections for July and August, 1957. These two cross sections are similar to one another. In both cases tropospheric effects can be noted in the lower layers of the stratosphere: regions of warmth appear there simultaneously with cooling in the troposphere accompanying the passage of a cold front.

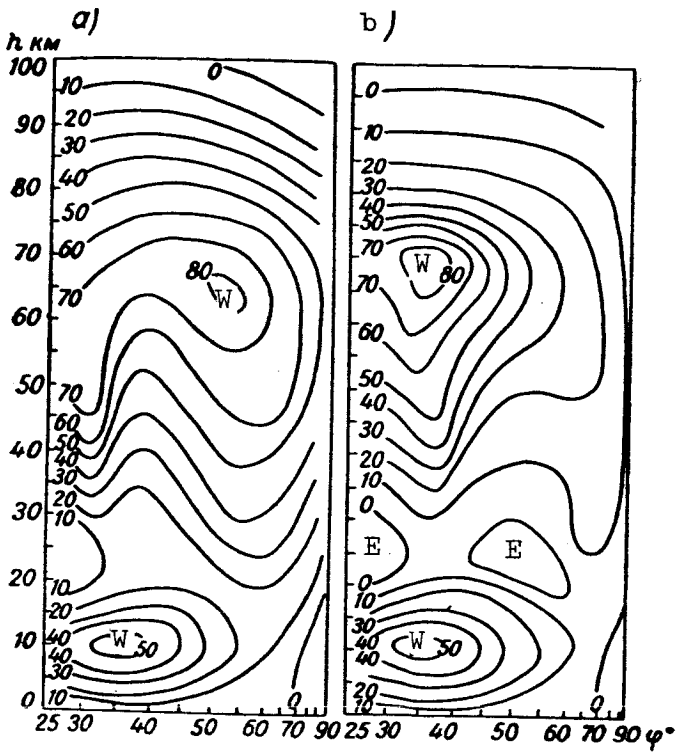

Figure 28.10. Meridional cross section of field of zonal wind (westerly component). a, November-December; b, January-February.

Beginning at the 18 km level and above, as far as the stratopause (the region of maximum temperatures at the 50 km level), the temperature increases approximately from -50-0°. A double temperature maximum at the stratopause was observed on July 29 and again on Aug. 12.

At the end of August (fig. 28.13) the temperature in the troposphere and in the middle layers of the stratosphere decreased by 5° in comparison with July. Cooling was particularly noticeable at the stratopause. However, the temperature of the mesopause increased progressively from July 22-Aug. 25.

If the wind data are compared with the cross sections of the wind field constructed by Murgatroyd for 60°N (ref. 614), it is possible to note the following appreciable differences: the wind measured over Fort Churchill has a greater velocity, exceeding 25 m/sec, in the 60-75 km layer; wind reversal to westerly is observed at the 80 km level, not at 90 km.

Two winter cross sections (figs. 28.13 and 28.14) will now be compared. In December the tropopause was 25° colder than in summer, but the lower layers of the stratosphere had cooled by only 10°. However, the most significant changes occur in the middle layers of the stratosphere: the wind intensifies to 25-50 m/sec (becomes westerly), and the temperature decreases by 30° at a height of 28 km.

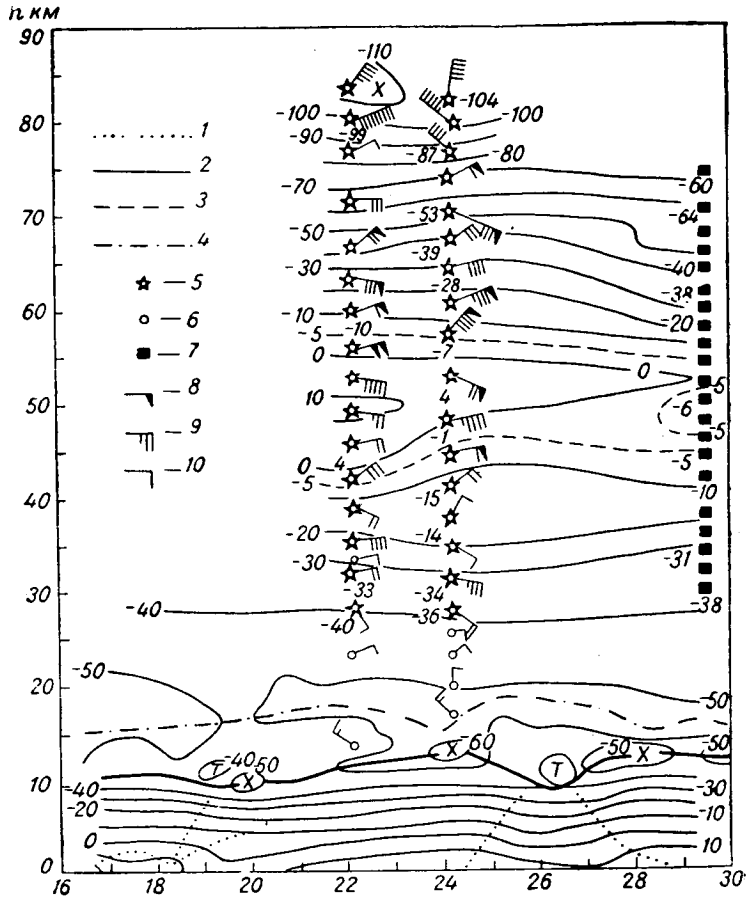

Figure 28.11. Temporal cross section of wind field and temperature field over Fort Churchill on July 17-29, 1957. 1, frontal surface; 2, tropopause; 3, 4, discontinuity of wind and temperature fields; T--region of heat; X--region of cold. Measurement methods: 5, grenades; 6, radiosonde; 7, Pitot tube. Flags indicate wind velocity and direction: 8, 50 m/sec; 9, 25 m/sec; 10, 10 m/sec.

The stratopause, as well as the lower part of the stratosphere, cools by only 10°.

During the period from Dec. 12-14, the temperature at a height of 60 km was subject to considerable change, in contrast to the constancy of the heat regime customary for the summer mesosphere. The wind velocity here approached values of 100 m/sec.

On the January cross section (fig. 28.14) there is an unusually sharp temperature change in the 38-41 km layer during the period from Jan. 25-29: in 4 days the temperature increased by almost 70°.

In contrast to the preceding three cross sections, usually showing the presence of zonal flow, the January cross section of rocket-grenade measurements

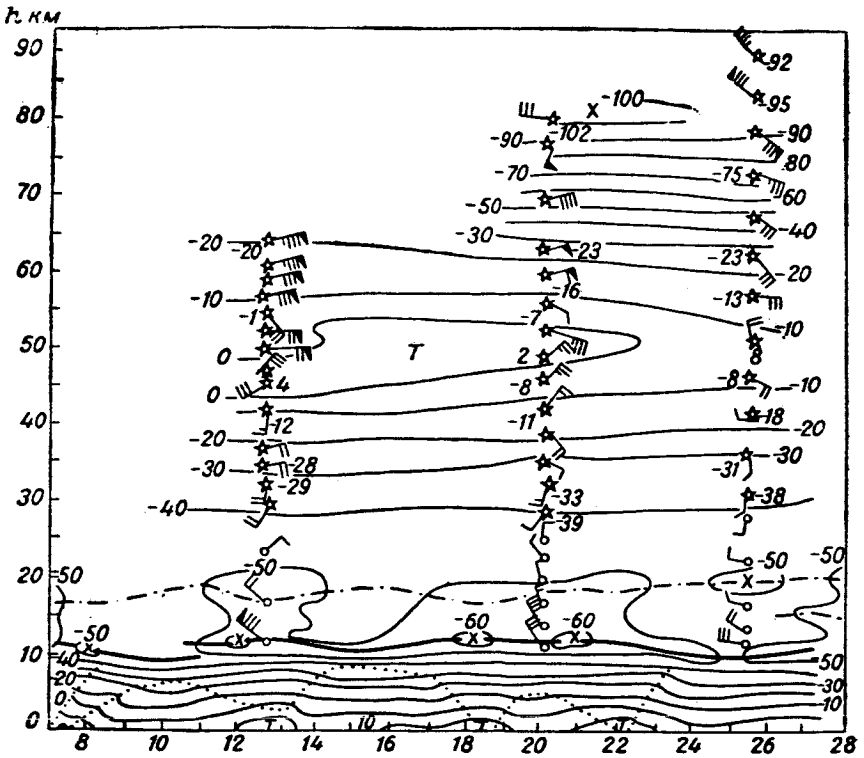

Figure 28.12. Temporal cross section of wind field and temperature field over Fort Churchill on Aug. 8-28, 1957. Same notations as in figure 28.11.

of Jan. 27 reveals a strong meridional wind component in the upper layers of the atmosphere. Between 15 and 45 km the wind blows from the north, and a maximum wind velocity of 75 m/sec was measured at a height of 33 km. Above 45 km there is a wind reversal; at a height of about 63 km a wind blowing from the south has an equally great velocity.

28.7. Wind Field over the United States from Generalized Data from the Rocket Sounding Network. A network of stations for rocket sounding of the atmosphere (12 stations mostly located along the east and west coasts of the North American continent) began to operate in the United States in 1959. The sounding was by light rockets to a height of 60-65 km. The principal objective of the sounding was regular wind measurement in the stratosphere and mesosphere. The publication of the first generalizations of the results of measurements in this network began in 1961. Keegan (ref. 516) prepared a preliminary analysis of wind and circulation in the stratosphere and mesosphere over the United States, based on the results of measurements by this network during the first year of its operation.

Figure 28.15 shows the change of the profile of the mean zonal wind from winter to spring on the basis of measurements at Wallops Island (Virginia, United States). The winter profile was constructed using measurements for January-February and the spring profile using measurements from mid-April to

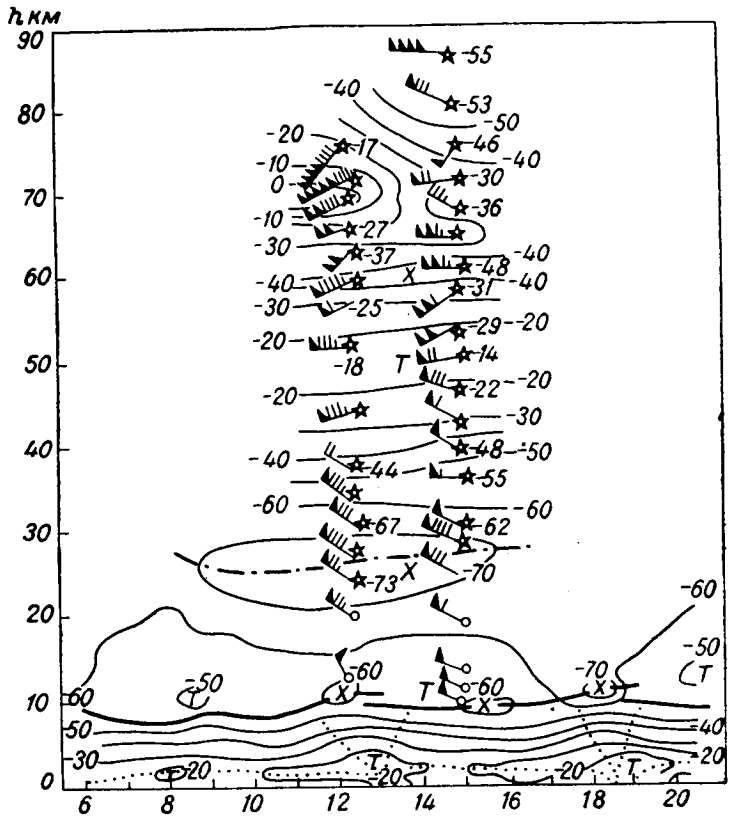

Figure 28.13. Temporal cross section of wind field and temperature field over Fort Churchill on Dec. 6-20, 1957. Same notations as in figure 28.11.

mid-May. Above the winter wind maximum in the troposphere the wind velocity decreases with height to the 25 km level. At great heights the velocity of the westerly wind increases rapidly and attains a maximum at about 50-55 km (more than 60 m/sec). This winter profile agrees well with the section of the zonal wind field constructed by Murgatroyd (ref. 614).

The spring profile shows that the middle and upper layers of the stratosphere are a region of wind reversal from westerly circulation in winter to easterly in summer. A similar result was obtained for a number of other sounding stations, other than Fort Churchill (Canada).

The day-to-day changes of the wind can be judged from the temporal cross sections constructed for the period from the second half of January to the first half of February 1960 for Wallops Island (fig. 28.16), and for August 1960 for Cape Canaveral (Florida, United States, fig. 28.17).

The lower part of the cross section for Wallops Island shows a westerly flow. The maximum of the easterly wind on Jan. 30 at the 30 km level should be noted. Corresponding changes of the wind can be traced clearly to the upper boundary of the stratosphere (50 km).

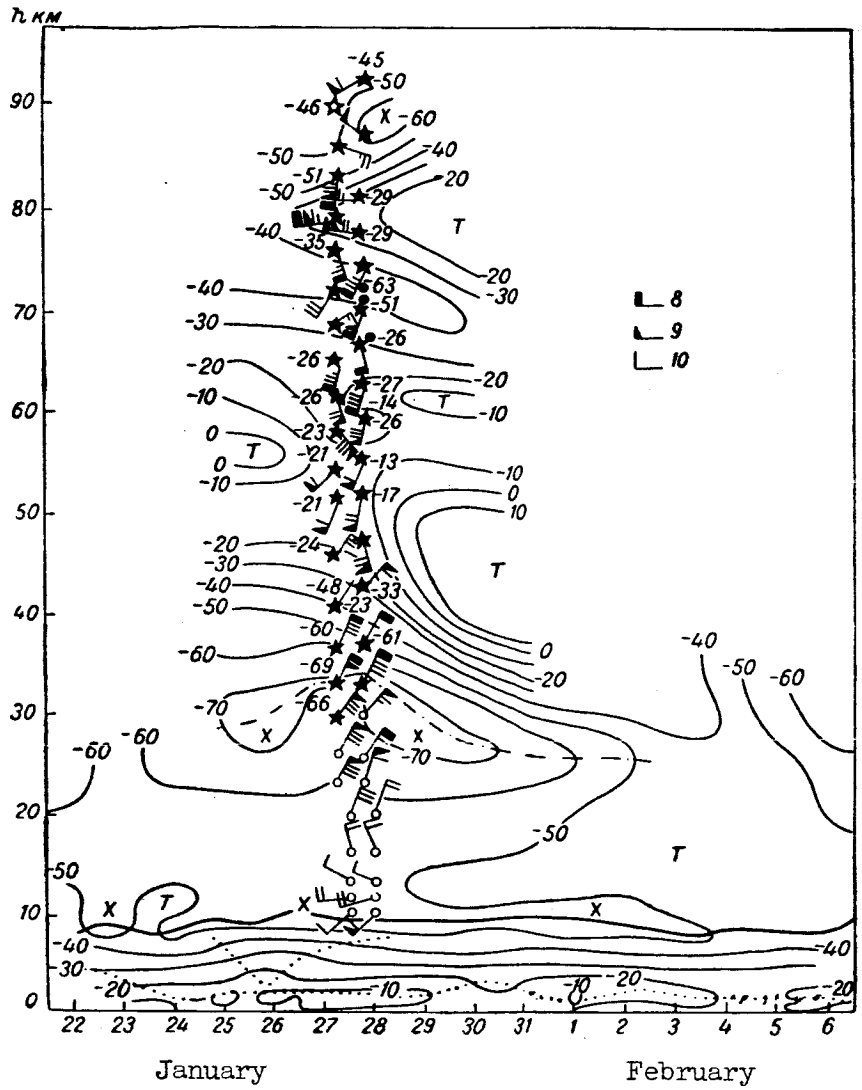

Figure 28.14. Temporal cross section of wind field and temperature field over Fort Churchill, Jan. 22-Feb. 6, 1958. For notations see diagram and annotations to figure 28.11.

The summer stratosphere over Cape Canaveral (fig. 28.17) is subject to clearly expressed day-to-day changes. This is particularly noticeable in the period from Aug. 10-12 at heights from 45-54 km, and also Aug. 22-25 at all levels above 45 km. However, the spatial (vertical) wind changes are still more interesting than the temporal changes. On one of these days, Aug. 25, 1960, three rockets were launched in 40 min. It was established that the zonal wind component changes from easterly (38 m/sec at a height of 51 km) to westerly (28 m/sec at a height of 57 km). This corresponds to a wind shear of about 12 m/sec per 1 km. In the layer between 54 and 57 km this shear increases to 18 m/sec per 1 km.

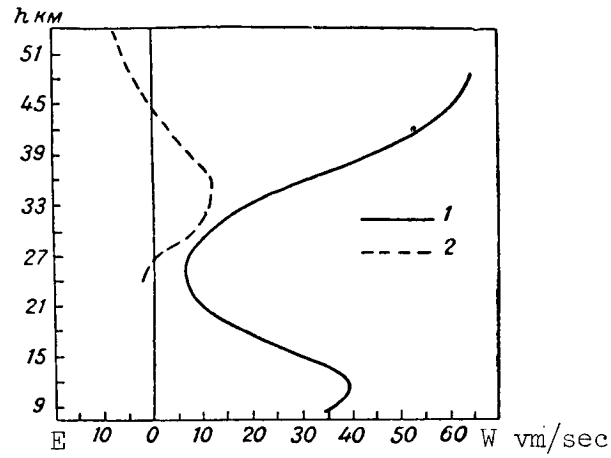

Figure 28.15. Profile of mean zonal wind in winter (1) and spring (2) of 1960.

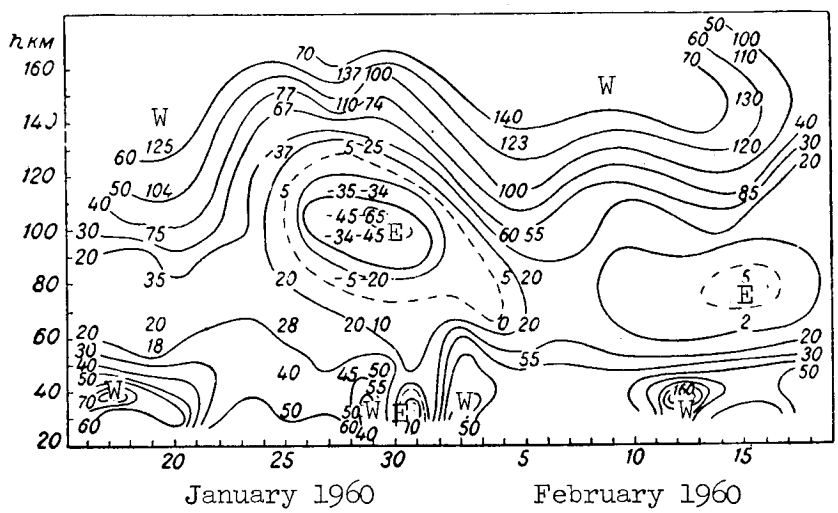

Figure 28.16. Temporal cross section of wind field over Wallops Island.

Batten (ref. 286) has constructed a temporal cross section of the zonal wind field for 30-40°N (fig. 28.18), showing the annual wind variation. This cross section permits tracing the wind reversal process in spring and autumn.

28.8. High-Level Synoptic Charts. The rocket sounding network in the United States operates on a seasonal principle: in one month of each season rockets are launched at all sounding points, insofar as possible on the same days. This makes it possible to compile high-level synoptic charts. The first charts of this kind were published in 1961 (ref. 516).

Figure 28.19 shows a chart of isobars and air currents for the 24 km level, constructed using measurements of Apr. 27, 1960. In general, in the polar region

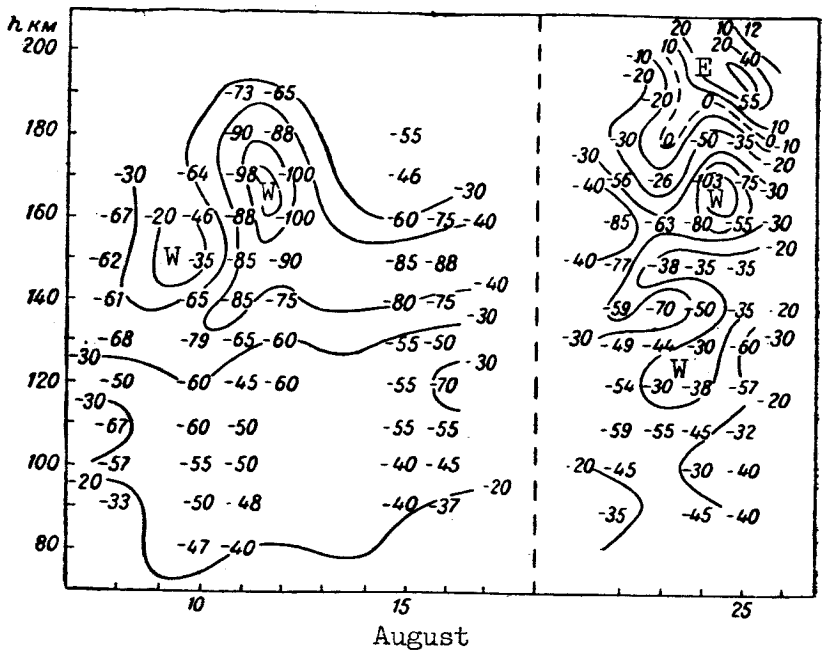

Figure 28.17. Temporal cross section of wind field over Cape Canaveral.

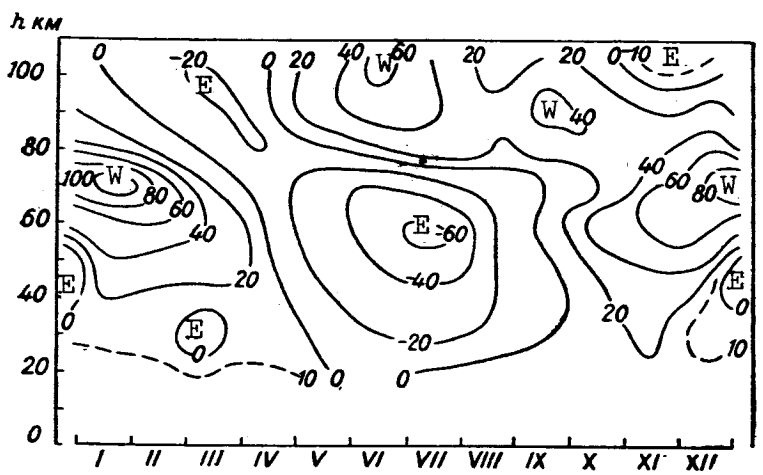

Figure 28.18. Temporal cross section of zonal wind field between 30 and 40°N.

there was easterly circulation, but we can also note a disturbance of zonal flow by a trough situated over the Canadian archipelago to the northwest of a cyclone over the Labrador Peninsula. At the 42 km level the air currents on that day had appreciably different characteristics (fig. 28.20). The easterly circulation is expressed more clearly in this area. The cyclone over Labrador was completely filled by the warm air of the upper layers of the stratosphere, and a polar anticyclone was situated over eastern Canada.

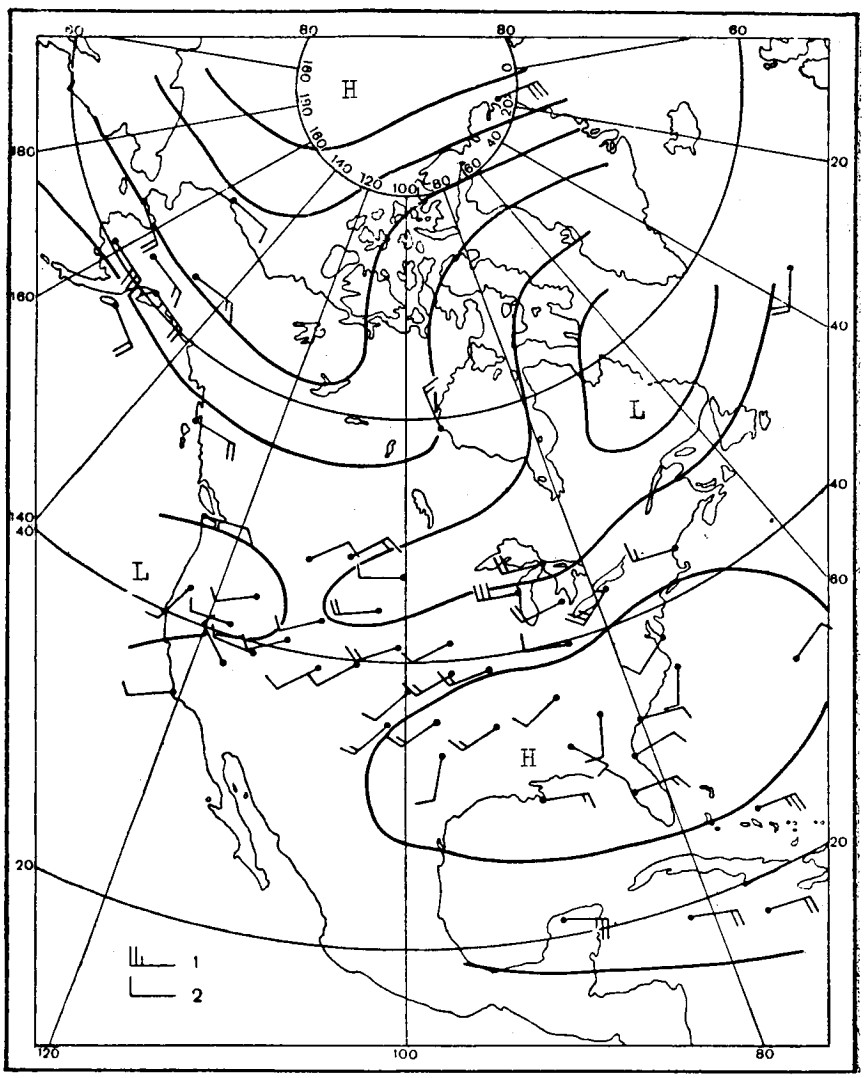

Figure 28.19. Isobars at the 24 km level over North America on Apr. 27, 1960. H = region of high pressure; L--region of low pressure. Wind velocity in knots: 1--25, 2--10 (after division by 2 these values give velocity in m/sec).

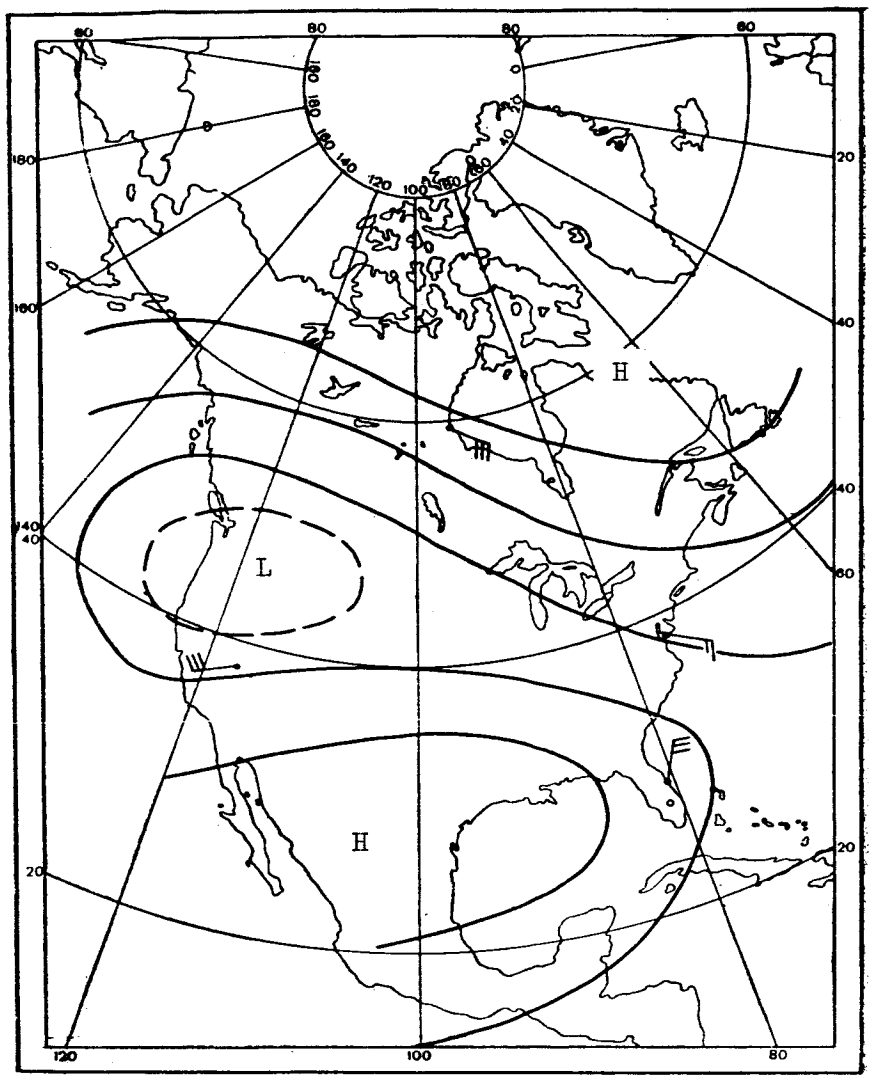

Figure 28.20. Isobars at 42 km level over North America on Apr. 27, 1960. For notations see figure 28.19.

A comparison of these two charts shows that the seasonal wind reversal in the stratosphere is better developed in its higher layers, an important fact observed by the author on the basis of other data as well.

The character of summer circulation at the 24 km level can be judged from the two charts in figure 28.21 (ref. 516). An intercomparison of these charts reveals some attenuation of the winds of Aug. 8 in comparison with those of July 20. At the 48 km level the circulation on Aug. 8 was appreciably weaker than on July 20 (fig. 28.22). These comparisons are also evidence that seasonal reversals are manifested more clearly at greater heights.

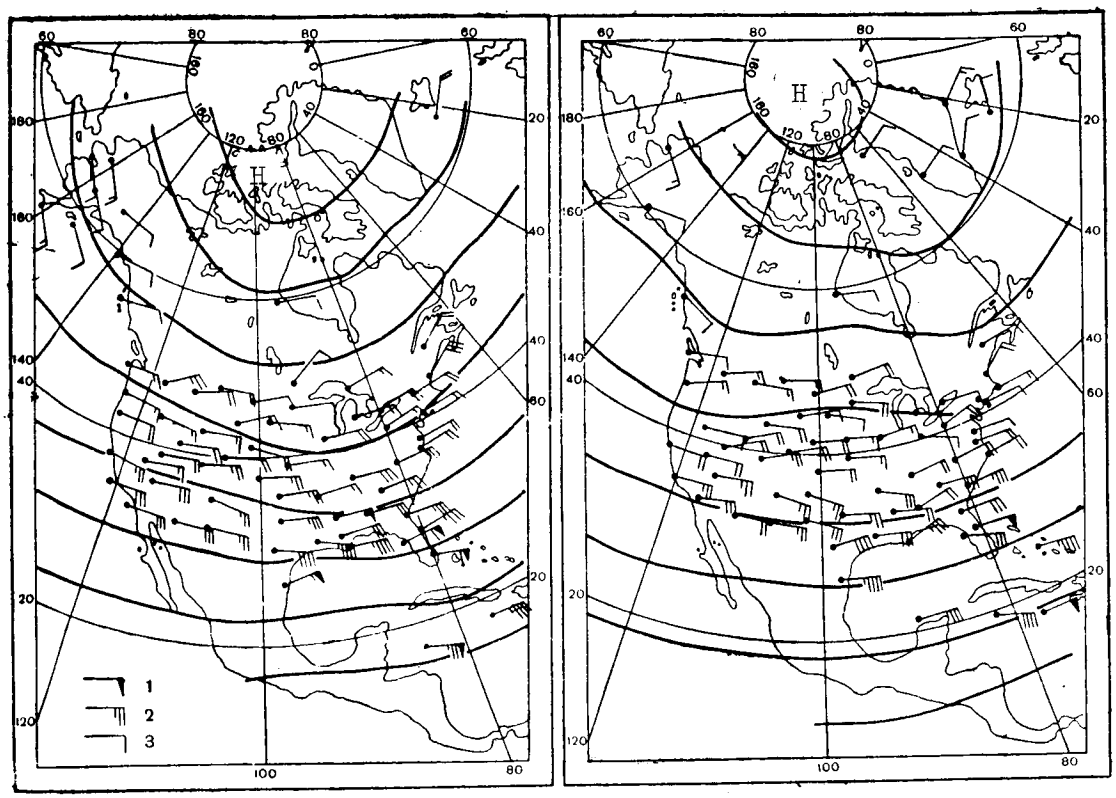

Figure 28.21. Isobars at 24 km level over North America on July 20 (at left), and Aug. 8 (at right), 1960. For notations see figure 28.19. Wind velocity in knots: 1--50, 2--25, 3--10.

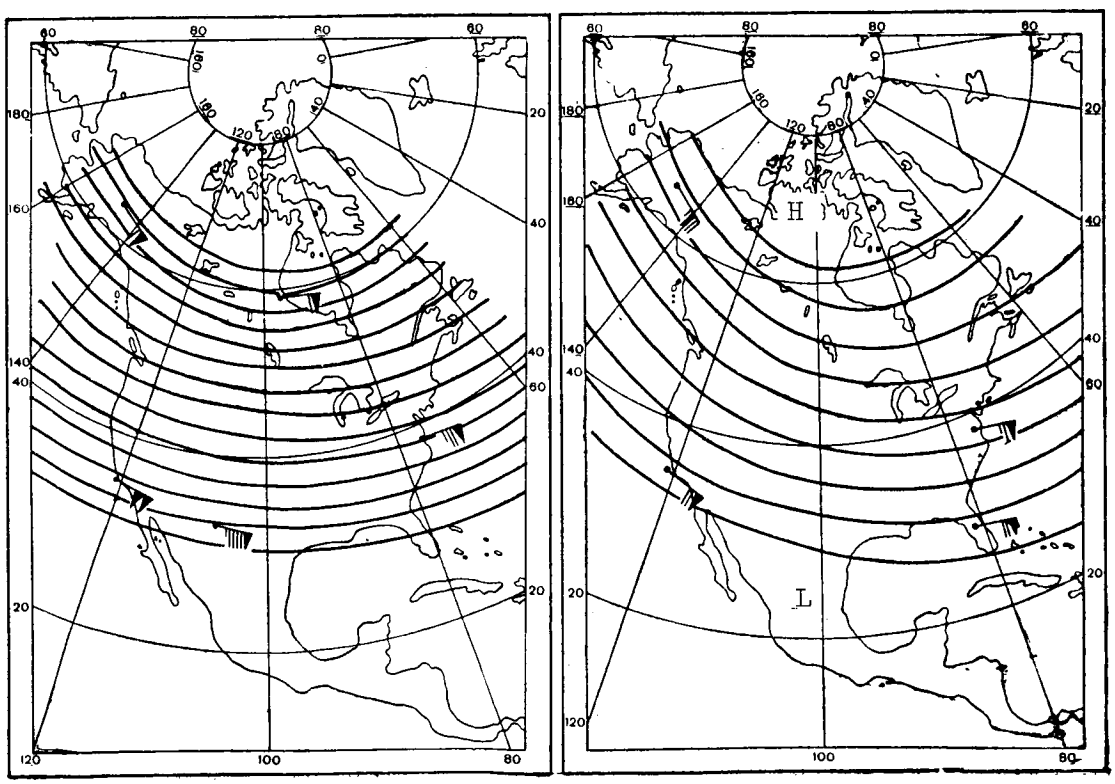

Figure 28.22. Isobars at 48 km level over North America on July 20 (at left), and Aug. 8 (at right), 1960. For notations see figure 28.21.

29. Wind in the Thermosphere

According to the adopted naming of the atmospheric layers, the mesosphere, bounded at top by the mesopause, the layer of minimum temperatures, is followed by the thermosphere. This region is characterized by a well-developed temperature inversion beginning at the 80-85 km level. Temperature increase with height continues to enormous heights, many hundreds of kilometers, and can even extend to the upper boundary of the Earth's atmosphere (thousands of kilometers).

We will now consider data on air currents in the lowest part of the thermosphere, specifically, at heights from 80 to 100 km. This region is characterized by a great singularity of atmospheric circulation. The principal method for wind measurement at these heights is meteor observations.

29.1. Meteor Observations. Regular observations of the drift of meteor trails in air currents in the upper layers of the atmosphere are being made by the Astronomical Observatory of the Academy of Sciences of the Tadzhik SSR. Extensive data on drift at heights of 80-100 km have been obtained by V. V. Fedynskiy (ref. 200) by visual observations made in 1934-1938. Table 29.1 gives statistics on the distribution of trails with respect to the linear velocity of their drift. Drift was estimated for periods of time from 10 to 100 sec. Before midnight lt the velocity distribution curve has two maxima: 130 and 320 m/sec. After midnight the velocity distribution curve acquires a different character with a sharply expressed maximum of about 70 m/sec; there is a rapid decrease with transition to greater velocities.

TABLE 29.1. DISTRIBUTION OF MOVEMENTS OF METEOR TRAILS BY VALUE OF LINEAR VELOCITY.

Time	Linear velocity of movement, m/sec									Total
	0-50	60-100	110-150	160-200	210-250	260-300	310-350	360-400	410	
Before midnight	2	2	4	3	1	1	3	0	3	19
After midnight	7	10	3	2	1	1	0	1	3	28
Total	9	12	7	5	2	2	3	1	6	47

Direction of movement is indicated in Table 29.2. Easterly directions predominate both before and after midnight. The wind rose before midnight gives a predominance of flow to the northeast, east and southwest, and after midnight to the north and east-southeast. Fedynskiy's data agree well with earlier observations made by Kalke over Germany (1921) and Trowbridge over the United States (1907). This is shown in figure 29.1. This made it possible for Fedynskiy to construct a summary wind rose using data from the Astronomical Observatory of the Academy of Sciences of the Tadzhik SSR and Kalke's data, based on 124 determinations. According to this rose, there is a predominance of movement to the north and east-southeast in the 80-100 km level (ref. 200).

TABLE 29.2. DISTRIBUTION OF MOVEMENTS OF METEOR TRAILS BY DIRECTION (V. V. FEDYNSKIY).

Time	Direction								Total
	N	NE	E	SE	S	SW	W	NW	
Before midnight	2	4	3	2	2	5	1	-	19
After midnight	6	1	8	6	1	1	-	5	28
Total	8	5	11	8	3	6	1	5	47

Data on air currents in the layer of luminescence of meteor trails also have been obtained by I. S. Astapovich, A. M. Bakharev, O. V. Dobrovol'skiy, R. L. Khotnik, Whipple and others. In particular, Whipple (ref. 803) obtained a very interesting detailed wind profile on Nov. 23, 1951, at heights of 80-100 km.

Whipple used a telescopic meteor camera at Harvard University for photographing a stable meteor trail. This trail was photographed simultaneously by two other ordinary cameras spaced along a base. This arrangement determined the heights of individual points on the trail. Whipple (ref. 803) discovered thin adjacent layers which differed greatly from one another with respect to wind velocity (in the 87-89 km layer the wind component perpendicular to the direction of the meteor trail intensifies to 30-40 m/sec, but at heights of 90-93 km this velocity component decreases sharply).

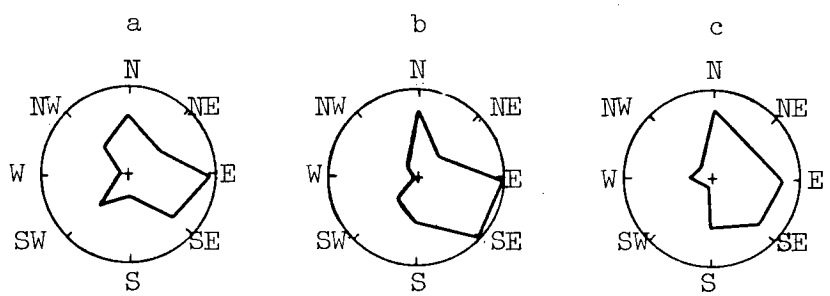

Figure 29.1. Distribution of movements of nighttime luminescent meteor trails by direction (wind roses). Radius of circle corresponds to 25 percent of frequency of directions. a, from Fedynskiy; b, from Kalke; c, from Trowbridge.

More precise information on the drift of meteor trails has recently been obtained by the radar method (ref. 569). Figure 29.2 shows the distribution of frequency of occurrence of winds of different velocities on the basis of observations made by Greenhow (ref. 411) at Jodrell Bank. The most common wind velocity at heights of 80-100 km is 20-40 m/sec; the maximum values attain 80 m/sec (visual observations of the drift of luminescent meteor trails give somewhat exaggerated velocities).

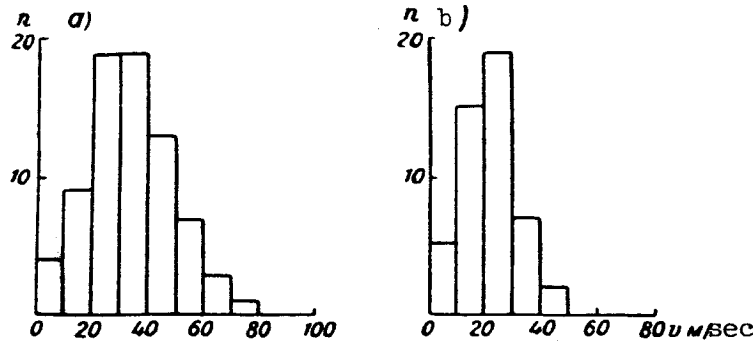

Figure 29.2. Distribution of frequency of occurrence of mean hourly values of wind velocity v. a, September; b, October, 1953.

During the IGY period important investigations of atmospheric circulation were made at Khar'kov by B. L. Kashcheyev and V. N. Lebedinets (ref. 81a). They devised an apparatus for radio observations by the coherent pulse method. Measurements with antennas alternately oriented to the north and south revealed that wind velocity values are described satisfactorily by a Fourier series containing a constant value (prevailing wind direction), 24- and 12-hour components. Amplitudes of the higher harmonics (8- and 6-hour) usually are small in comparison with the second and first.

The large value of the amplitude of the 12 hour component possibly indicates a resonance character of atmospheric oscillations.

If these data are compared with the corresponding results obtained by meteor measurements at Jodrell Bank station (53°N) and ionospheric measurements at Cambridge (52°N), i.e., if we take three points at which latitude is virtually identical (the latitude of Khar'kov is 50°N), we find much in common. In actuality, the phases of the 12 hour component for April and May virtually coincide, much like the N-S component of the prevailing wind, and also the E-W component.

Despite the considerable quantitative agreement of the results obtained both at Khar'kov and in England, and the theory of atmospheric movements, there are significant departures from it. The predicted phase values of the 12 hour component are not satisfied; the amplitude of this component changes considerably in the course of the day.

The described measurements were made in the middle latitudes. Elford and Murray (ref. 374) have studied meteor radar echoes in Antarctica (Mawson, 68°N). According to preliminary data, there is a diurnal variation of the wind which can be represented by three horizontal components: one predominant component and two oscillating with periods of 24 and 12 hours. In this respect the behavior of the Antarctic wind in general agrees with the properties of the wind measured at these same heights (80-100 km) in the zone of low latitudes. The prevailing wind has a strong meridional component (for further details see Section 29.3).

29.2. Artificial Luminescent Sodium Clouds. Bedinger, Ghosh, Manring, Moore and Edwards (refs. 288, 289, 564 and 571), and Pettit and Edwards (refs. 288, 289, 370 and 571), determined the wind in the upper layers of the atmosphere by observing the movement of luminescent clouds of sodium vapor ejected into the atmosphere by rockets. The experiments were carried out in the United States (Holloman Air Force Base, New Mexico). Three luminescent clouds were thus formed during the period 1955-1957: two at evening twilight and one at morning twilight. The results of wind measurements are presented in Table 29.3. At the time of formation of the third cloud (November 1957), a luminescent rocket trail was formed and observed at great heights, making it possible to calculate the wind to the 202 km level.

TABLE 29.3. WIND FROM OBSERVATIONS OF DRIFT OF LUMINESCENT CLOUDS OF SODIUM VAPOR.

Year	Height, km	Wind velocity, m/sec	Wind direction, degrees	Year	Height, km	Wind velocity, m/sec	Wind direction, degrees
1956	77	43	118	1957	114	63	50
	84	175	82		119	36	60
	85	80	320		122	20	120
	92.5	107	47		126	28	155
	93	125	48		132	33	240
	102	100	287		142	40	270
	102.3	91	290		152	30	245
1957	104	125	250		162	20	230
1956	105	179	276		172	40	200
1957	106	115	280		182	41	210
	108	43	360		192	42	220
	109	153	350		202	38	240
1955	110	45	120				
	110	75	30				

Note: 1955--Oct. 12, 1800 hours; 1956--Apr. 11, 1905 hours; 1957--Nov. 12, 0556 hours.

The fourth and fifth experiments were carried out by Manring and Bedinger on Aug. 17 and Nov. 18, 1959 (ref. 570), when a continuous jet of vaporous sodium was ejected into the atmosphere, beginning at a height of 80 km and continuing up to 230 km; in both cases the rockets were launched at dawn, before sunrise, and the sodium vapors were therefore illuminated by the Sun's rays and could be seen clearly against the background of the still dark sky. The vapors were photographed from four stations on the ground.

Air currents of a complex character were recorded at heights of 80-130 km; farther aloft, to 230 km, the wind was northeasterly. On Aug. 17, the velocity attained 220-280 m/sec, but on Nov. 18 was less than 20 m/sec.

The study of luminescent clouds of sodium vapor was begun in 1959 by French geophysicists. Veronique rockets were used for this purpose. There were two launchings in Algeria: on Mar. 10 to a height of 127 km and on Mar. 12 to a height of 180 km. A study was made of cloud luminescence at twilight (ref. 778) and the drift of clouds was measured for the purpose of wind determination (ref. 298). Several additional experiments were carried out in 1960 (in March and June). The observations were made from ground stations supplied with cameras specially adapted for such observations from a base 100 km in length. Wind measurements indicated the existence of different winds, predominantly westerly (ref. 300). The maximum measured velocity at a height of 134 km was 160 m/sec (in June). At heights greater than 140 km there was a predominance of meridional directions--northerly or southerly. A zone of strong turbulence was observed at heights of 100 km and below; the maximum values of the vertical wind gradient occur in this same zone. Vertical movements of about 50 m/sec were observed at a height of about 150 km.

29.3. Diurnal and Seasonal Wind Variations. By observing the radio echoes from ionized meteor trails it is possible to measure the wind 24 hours a day. This has made it possible to study the diurnal variation of the wind.

According to measurements made by Elford and Robertson (ref. 373) at Adelaide (southeastern Australia, 35°S) in October-December, 1952, the wind attained its maximum values in the morning hours (in November-December up to 100 m/sec to the east and in October to 70 m/sec). The mean diurnal velocities were 61 m/sec in November and 64 m/sec in December. The wind direction varies little with height, but velocity increases by approximately 3.6 m/sec per km.

On the basis of a harmonic analysis of data on wind velocity, Elford and Robertson discovered two waves in diurnal wind variation: diurnal and semidiurnal. The diurnal wind component is directed to the north in the evening and to the east in the morning; the semidiurnal component is directed to the north at midday and midnight and to the east in the morning and evening.

Further observations at Adelaide led Elford (ref. 372) to the conclusion that at any time of year the wind can be characterized by three components: some constant number and two periodic components with 12 and 24 hour periods. The wind vector at heights of 75-94 km rotates counterclockwise (this corresponds to tidal movements in the southern hemisphere). The 12 hour wind component at heights of 75-94 km is approximately constant during the year in amplitude, but its phase changes, without conforming to a definite pattern. At the equinoxes this component has a vertical phase gradient of about 5°/km. At heights of 95-104 km its amplitude is considerably greater.

Mean monthly data show that there is always a prevailing wind from east to west; in summer and winter there is a large vertical wind gradient: in summer the wind in the 75-104 km layer decreases with height (gradient 3.3 m/sec per km) and in winter it intensifies (gradient 2.3 m/sec per km). In spring and autumn the wind is virtually free of a dependence on height, but there is a slow decrease of wind velocity with height.

Elford (ref. 372) compared his summer and winter radio meteor measurements of the wind at heights of 75-104 km with a summary of data on the wind at heights

of 0-70 km, presented by Brasefield (ref. 308) approximately at these same latitudes, but in the northern hemisphere (fig. 29.3). Brasefield's data were based on pilot balloon observations to heights of 40 km at 40°N and acoustic measurements (observations of the explosions of grenades ejected from rockets) at heights of 35-75 km at 32°N. The curves for summer in figure 29.3 agree well with one another, indicating a change of the sign of west-east transport at a height of about 70 km. According to meteor determinations the wind in winter is considerably stronger than indicated by rocket data (it must be remembered that the part of the curve in figure 29.3 applying to the 60-70 km layer was constructed solely on the basis of one rocket launching).

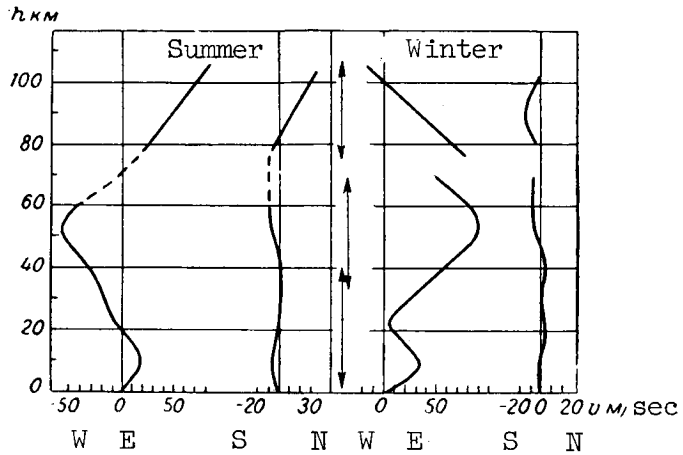

Figure 29.3. Predominant wind component.

Important results were obtained by Greenhow (fig. 29.4) in September 1953 at Jodrell Bank (England). He established the existence of a definite (mean) change of wind direction and velocity with height. Figure 29.5 shows Greenhow's data (ref. 411) for wind velocity (average value for 3 days in September 1953). The wind gradient is positive and in this case is 2.3 m/sec per km. Positive wind gradients of this magnitude apparently are typical for heights of 75-105 km; nearly the same values for the gradient were obtained by Elford and Robertson (refs. 372 and 373).

Greenhow and Neufeld subjected data on the diurnal variation of the wind to harmonic analysis (ref. 412). The W_{NS} and W_{EW} wind components were represented by these authors by the first three terms of a Fourier series in the form

$$W_{NS} = A_1 + B_1 \sin \frac{\pi}{12}(T + t_1') + C_1 \sin \frac{\pi}{6}(T + t_1'), \tag{29.1}$$

$$W_{EW} = A_2 + B_2 \sin \frac{\pi}{12}(T + t_2') + C_2 \sin \frac{\pi}{6}(T + t_2'). \tag{29.2}$$

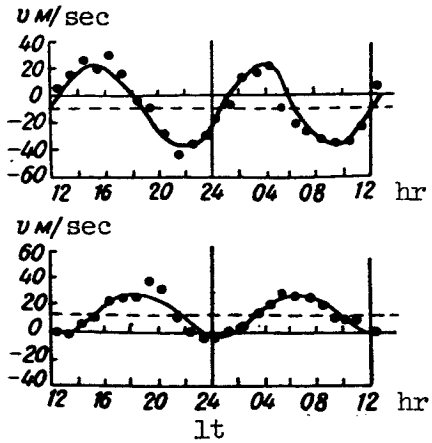

Figure 29.4. North-south and east-west wind components. September 1953.

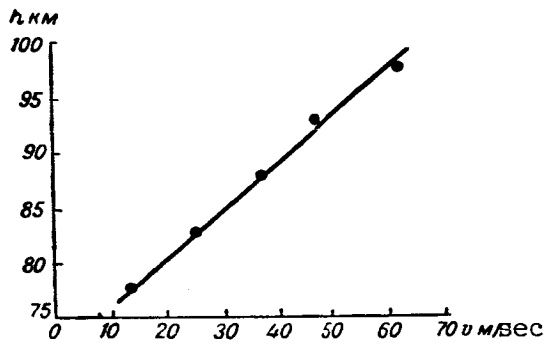

Figure 29.5. Dependence of wind velocity v on height h.

Here A_1 is the mean 24 hour wind velocity in a north-south direction (A_1 indicates the predominant wind component); B_1 is the amplitude of the 24 hour periodic wind component; t_1' is its phase; C_1 and t_1'' are the amplitude and phase of the 12 hour periodic wind component; A_2, B_2 and C_2 are the same for the wind in an east-west direction; T is time in hours, read from midnight. The phases are determined with the condition that the maximum velocity in the direction to north (or east) occurs when T + t = 6 hours for the first harmonic and 3 hours for the second harmonic.

The results of a harmonic analysis for a 24 hour period on a September day in 1954 are shown in figure 29.6. A dependence on height also is indicated by these results. The numerical values of the Fourier coefficients were as follows:

$$100\ \text{км}\ \ldots\ W_{NS} = +1.4 + 6.6 \sin\frac{\pi}{12}(t-2.3) + 40.0 \sin\frac{\pi}{6}(t-0.4)$$

$$W_{EW} = +2.2 + 12.5 \sin\frac{\pi}{12}(t-3.4) + 26.5 \sin\frac{\pi}{6}(t-3.0)$$

$$95\ \text{км}\ \ldots\ W_{NS} = -2.6 + 2.8 \sin\frac{\pi}{12}(t-3.6) + 23.0 \sin\frac{\pi}{6}(t-1.1)$$

$$W_{EW} = +10.7 + 10.9 \sin\frac{\pi}{12}(t-4.9) + 23.0 \sin\frac{\pi}{6}(t-3.2)$$

$$90\ \text{км}\ \ldots\ W_{NS} = +0.2 + 5.1 \sin\frac{\pi}{12}(t-0.4) + 18.1 \sin\frac{\pi}{6}(t-1.5)$$

$$W_{EW} = +8.9 + 1.9 \sin\frac{\pi}{12}(t-3.0) + 16.9 \sin\frac{\pi}{6}(t-4.3)$$

$$85\ \text{км}\ \ldots\ W_{NS} = +1.8 + 4.7 \sin\frac{\pi}{12}(t-3.8) + 15.8 \sin\frac{\pi}{6}(t-2.2)$$

$$W_{EW} = +13.8 + 1.6 \sin\frac{\pi}{12}(t-3.8) + 12.0 \sin\frac{\pi}{6}(t-5.0)$$

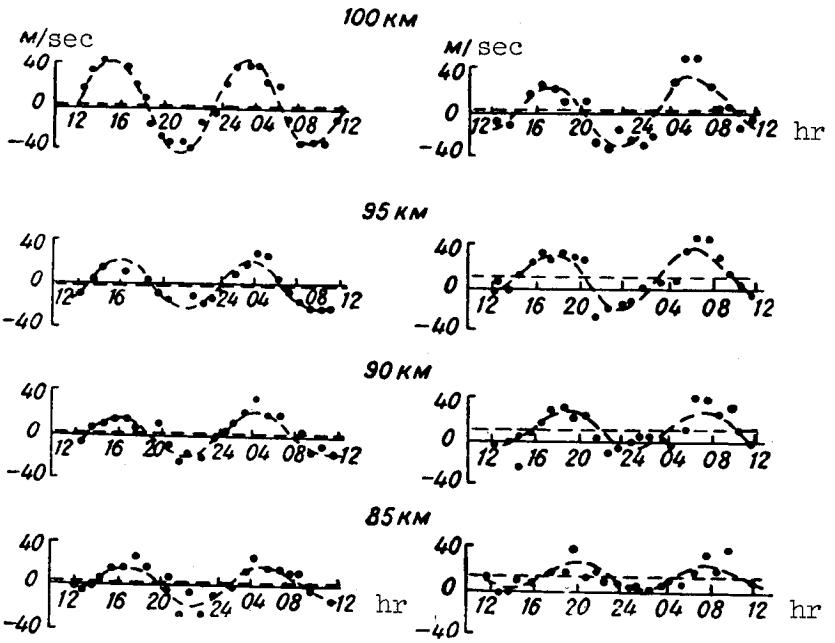

Figure 29.6. Dependence of the north-south and east-west wind components on height, Sept. 16-17, 1954. Dashed lines--constant and sums of two first periodic terms of Fourier series.

The dashed lines in figure 29.6 represent the first three terms of the Fourier series for W_{NS} and W_{EW} (equations (29.1) and (29.2)). We note good correlation between the experimental points and the theoretical (dashed) curves. This indicates that harmonics higher than the first two can be neglected.

Particular attention should be given to the data on the semidiurnal wave. The following table illustrates the change of amplitude and phase of semidiurnal wind components with height.

Height, km	Amplitude		Phase	
	N-S	E-W	N-S	E-W
100	40.0	26.5	-0.4	-3.0
95	23.0	23.0	-1.1	-3.2
90	18.1	16.9	-1.5	-4.3
85	15.8	12.0	-2.2	-5.0

These data show that the amplitudes of the semidiurnal components increase rapidly with height, but the phases (indicating the time of maximum velocity to the north or east, respectively) decrease appreciably; the phases of the N-S (north-south) and E-W (east-west) components differ from one another by three hours.

The 24 hour harmonic does not reveal regular changes of amplitude and phase with height; there is no clear difference between the phases of the N-S and E-W components. In the case of a true rotation of the vector, there should, of course, be a phase difference of 6 hours between the maxima of the northerly and easterly wind components. The mean daily wind velocity for the 24 hour harmonic is only 5 m/sec. Greenhow and Neufeld believe this can be caused by fluctuations of the predominant and semidiurnal wind components (ref. 412).

Neufeld (ref. 620) subjected to harmonic analysis data on the regular wind for a 100 day period from September 1953-August 1957 (Jodrell Bank) and determined more precisely the values of the Fourier coefficients of the series (29.1) and (29.2).

Systematic data from wind measurements made by Greenhow and Neufeld during one year (September 1954-August 1955) gave interesting characteristics of seasonal variations. Figure 29.7a shows the annual variation of the east-west component of the prevailing wind at heights of 85 and 100 km. It is interesting to note that although at a height of 100 km in summer and winter the wind is directed to the east, in spring and autumn it is directed to the west; at a height of 85 km the wind also remains directed to the east in autumn. Figure 29.7b shows the seasonal changes of the vertical gradient of the east-west component of the prevailing wind. Positive values of the gradient correspond to an increase of the east-west component with height if the wind is directed to the east, or to a decrease if the wind is directed to the west. The points for each month were determined from measurements of the wind velocity difference in two 10 km intervals: at heights of 85-95 and 90-100 km. During a large part of the year there are gradients of about 1 m/sec; in February-March and September-October the gradients are negative.

Figures 29.7a and 29.7b are combined in figure 29.7c in order to represent graphically the seasonal variations of wind direction at heights of 85, 90, 95 and 100 km (extrapolation was used to obtain data for 110 and 70 km as well). This diagram was constructed in the following way. As an example, in September the wind blows to the east and its velocity decreases with height by 0.5 m/sec·km,

which decreases velocity to a value of only 2 m/sec at the 100 km level. If the mean value of the gradient, measured in a 15 km interval, is applied to greater heights, beginning at the 104 km level this wind component changes sign to westward. This conclusion is confirmed by October observations, when the change of wind sign occurred directly within the measurement interval. As an additional confirmation of the reality of these wind changes, Greenhow and Neufeld cite the results of measurements on individual days (ref. 412). Although from June through August the mean wind is directed to the east at all heights, on individual days the wind assumes a westward direction at low levels. If we proceed on the basis of an observed decrease of velocity averaging 1 m/sec·km, we find that there is a wind reversal at a height of about 75 km.

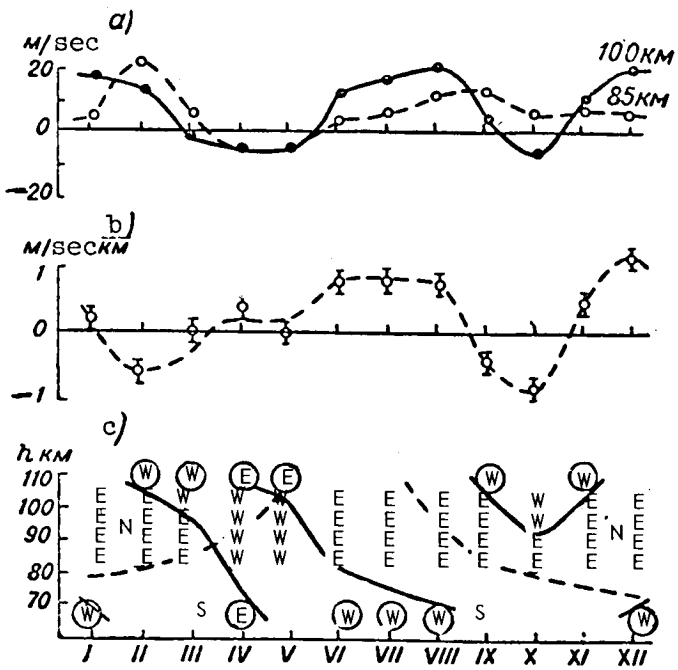

Figure 29.7. Seasonal wind variations.

The seasonal variations of the north-south component of the prevailing wind at heights of 87.5 and 97.5 km are shown in figure 29.8a. At the 87.5 km level this component is close to zero during the greater part of the year, except in May-August, when a strong southerly component is observed. A positive wind gradient of 0.3 m/sec·km (fig. 29.8b) decreases the value of this southerly component during the summer, and causes a small northerly component in the remaining seasons. An indication of the directions for the north-south component is shown on the same diagram as for the east-west component (fig. 29.7c). This composite diagram, e.g., shows that in July the wind vector above 85 km is directed to the southeast.

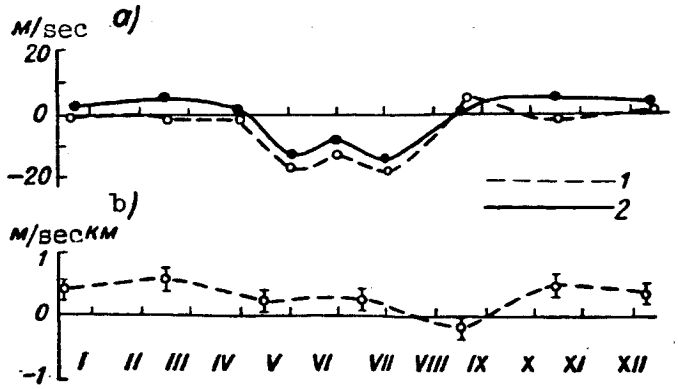

Figure 29.8. Seasonal variations of north-south component of prevailing wind (a) at heights of 87.5 (1) and 97.5 km (2) and its gradient (b).

30. Wind in the Ionosphere

The region of the atmosphere called ionosphere spatially coincides almost completely with the thermosphere. The difference is in the method of definition: the thermosphere is defined on the basis of temperature stratification and the ionosphere on the basis of the presence of appreciable concentrations of charged particles--ions and electrons. The thermosphere begins from the mesopause and its base is a thick temperature inversion over the mesopause. The lower boundary of the ionosphere (D region) is situated 10-20 km below the mesopause, but upward the ionosphere, like the thermosphere and exosphere, extends to the upper boundaries of the Earth's atmosphere.

It can, therefore, be assumed that the data presented in Section 29 also describe wind in the ionosphere. However, this section is presented as a separate discussion, because it includes the results of measurements of such a process as drift of inhomogeneities in the ionosphere, so characteristic of that region, and information on air currents above 100 km. We note that in ionospheric investigations it is customary to indicate the direction in which the wind blows, not the direction from which the wind blows, as is customary in meteorology.

30.1. Drift of Electron Inhomogeneities in the E Region. The ionosphere is a region of strong winds with velocities of 100-200 m/sec. Measurements of movements of small-scale inhomogeneities at the heights of the E region, made at stations in the Soviet Union in the IGY period (ref. 40b), have indicated the presence of a predominance of movements in southwesterly (azimuth 210-250°) and northeasterly (azimuth 40-50°) directions. The velocities vary in the range 18-170 m/sec, with the most probable velocities of 60-80 m/sec. For example, the prevailing wind at Gor'kiy is characterized by the azimuth A = 40° and a velocity v = 120 m/sec; at Simeiz (Crimea) A = 50 and 230°, v = 80 m/sec; at Tomsk A = 45, 135, 230 and 300°, v = 60-80 m/sec; at Khar'kov A = 230 ± 20°, v = 35-55 m/sec.

According to measurements made by S. N. Mitra (ref. 600), the most common wind velocity in the E layer is 50 ± 30 m/sec. Chapman (ref. 321) was one of the first to make systematic wind measurements in the ionosphere over Canada (Ottawa and Montreal) from June 1950 through July 1951. For three days in each month he made continuous observations, and the remainder of the time observations were made episodically. On the basis of 250 determinations he obtained a mean wind velocity in the E layer of about 80 m/sec. Measurements made by Greenstone in Washington indicate that the most common velocity of air currents at the level of the E layer is in the range 50-70 m/sec. The same velocity was recorded over France.

Wind velocity in the ionosphere usually undergoes large, brief changes. Figure 30.1 shows the results of measurements made in a 24 hour period in New Zealand (ref. 341). The mean value of the velocity in this case is also about 80 m/sec. The wind direction is also extremely variable (fig. 30.2), although in general there is a definite diurnal variation. Rawer in Freiburg (ref. 693) frequently observed changes of direction of movement constituting complete reversal in the course of a single observation period (15 min).

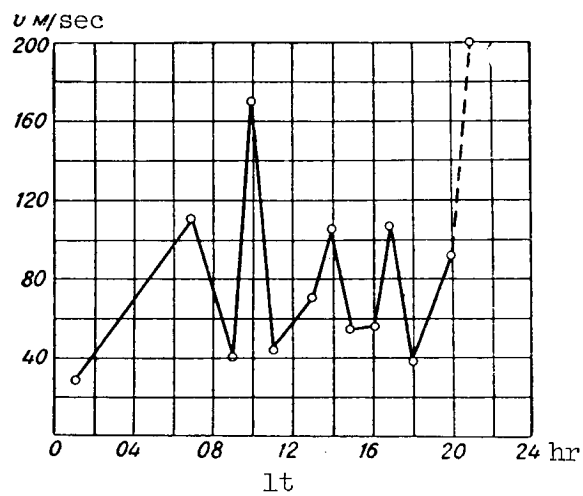

Figure 30.1. Wind velocity in E layer over New Zealand on Jan. 17, 1953.

Systematic measurements of wind in the E layer are being made by Harang and Pedersen (ref. 419) in Norway (near Oslo). On the basis of measurements made from June 1953 through September 1955 by the S. N. Mitra method, they obtained detailed data on the diurnal and annual variation of the wind, which will be discussed later. At this point we will mention the very interesting observational data on wind which they obtained during the total solar eclipse of June 30, 1954. They found that the wind direction was reversed during the time of the eclipse.

30.2. Sporadic E_s Layer. At the time of the sporadic appearance of the E_s layer we can observe the drift of ionospheric inhomogeneities at a height

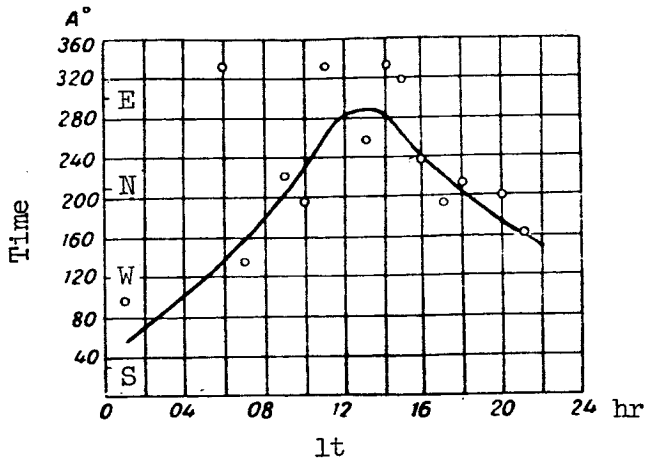

Figure 30.2. Variations of wind direction in E layer over New Zealand on Jan. 17, 1953.

differing somewhat from the height of the normal E layer. Figure 30.3 shows Becker's data (ref. 287) on wind velocity in the E_s layer over the German Demo-

cratic Republic (n is the number of observations in which he recorded velocity in a particular range). Velocities of 75-105 m/sec were observed most frequently. Four years of observations (1949-1952) by Gerson in the United States indicate that the most typical wind component in the E_s layer at the 110 km level is di-

rected from the east; the mean velocity is about 85 m/sec. By using reports by radio amateurs on the audibility of certain stations operating at a frequency of 50 Mc/s (signals of such high frequency are not reflected from the normal E layer), Gerson was able to trace the movement of an ion cloud (i.e., the sporadic E_s layer) in a number of cases at a height of 110 km. In the case shown in fig-

ure 30.4 the E_s layer was traced for a period of 6 hours; the mean velocity of

its drift was 110 m/sec.

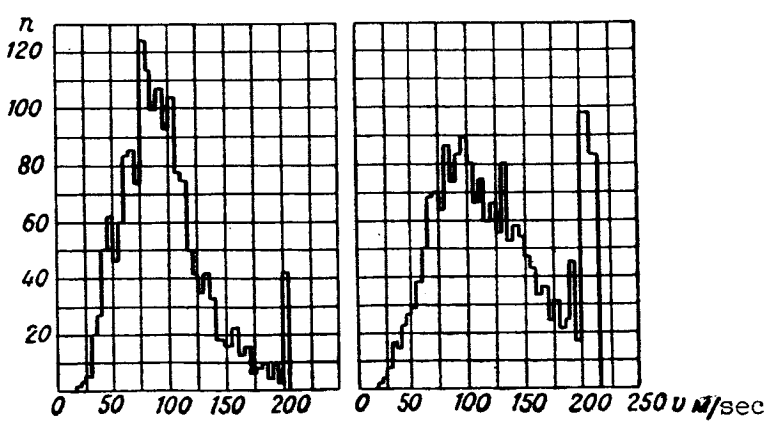

Figure 30.3. Distribution of wind velocity in E_s layer over German Democratic Republic.

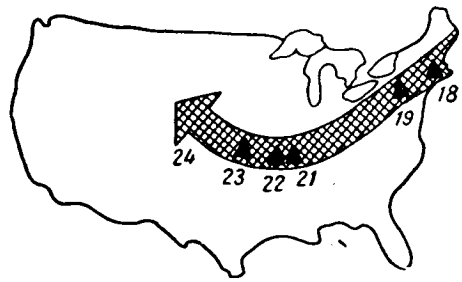

Figure 30.4. Path of sporadic formation of E_s layer over United States on June 11, 1950.

30.3. Diurnal and Annual Wind Variation. An analysis of measurements at Tomsk revealed that in autumn the north-south component has a constant component of 30 m/sec directed northward. The east-west velocity component has a constant component of 25 m/sec directed to the east. The winter months characteristically have a southerly direction of the north-south component with a constant component of about 40 m/sec. The constant part of the east-west component is directed eastward and is 50 m/sec. In spring the north-south component is 30 m/sec and directed to the north; the east-west component is 50 m/sec and directed to the west. Preliminary data from a harmonic analysis confirm the existence of a 12 hour periodicity. The velocity vector makes two complete rotations per day.

According to the measurements made by Harang and Pedersen in Norway (ref. 419), carried out systematically for over two years (1953-1955), the general character of the air currents at the level of the E layer and their diurnal and seasonal variations has much in common with what was obtained from observations of meteor trails (Section 29) at somewhat lower heights. Harang and Pedersen made a harmonic analysis of wind data. Much as was done by Greenhow and Neufeld in formulas (29.1) and (29.2), they represented the W_{NS} and W_{EW} wind components by the first three terms of a Fourier series in the form

$$W = A + C_1(\sin t + \epsilon_1) + C_2(\sin 2t + \epsilon_2), \qquad (30.1)$$

where A is the mean wind velocity in 24 hours in a direction from north to south or from east to west (predominant wind component), C_1 is the amplitude of the 24 hour periodic wind component, ϵ_1 is its phase, and C_2 and ϵ_2 are the amplitude and phase of the 12 hour periodic wind component. They found that the behavior of the true wind is described well by equation (30.1), and the coefficients and phases depend on the season (Table 30.1 and fig. 30.5). In Table 30.1 the minus sign indicates that the drift is directed southward or westward, respectively. In contrast to the results obtained by Greenhow and Neufeld relating to somewhat lower heights (Section 29), where the diurnal component is manifested weakly, the data obtained by Harang and Pedersen show that the 24 hour periodic wind component is an extremely appreciable value.

TABLE 30.1. FOURIER COEFFICIENTS AND PHASES OF DIURNAL AND SEMIDIURNAL WIND COMPONENTS IN E LAYER OVER NORWAY (HARANG AND PEDERSEN).

Season	Wind component	A m/sec	C_1 m/sec	C_2 m/sec	ϵ_1 degrees	ϵ_2 degrees
Summer	W_{NS}	15	15.0	18.2	-90	-45
	W_{EW}	21	67.8	38.2	-95	-103
Autumn	W_{NS}	31	19.1	12.2	154	11
	W_{EW}	-3	17.7	23.2	-72	-59
Winter	W_{NS}	14	19.0	14.1	159	-7
	W_{EW}	-47	18.3	33.1	-146	-106
Spring	W_{NS}	14	5.6	10.8	-104	20
	W_{EW}	-12	19.5	32.6	-99	-104
Mean	W_{NS}	11.8	10.1	12.0	-169	-14
	W_{EW}	-10.5	30.0	31.4	-100	-97

The results obtained by Harang and Pedersen are represented in figure 30.6 in the form of a vector diagram. As a comparison the figure also gives data for Washington as indicated by Gotier (ref. 419).

The periods of observation applying to the right-hand diagram are indicated in the caption of figure 30.6. The radii of the three circles correspond to wind velocities of 25, 50 and 75 m/sec. The figures near the points on the diagram indicate local time (in hours). In the winter months there is great similarity between the diagrams for Oslo and Washington, with respect to both configuration and magnitude. In summer, on the other hand, the similarity is poor and the Oslo diagram clearly indicates a 12 hour rotation as at the principal moment, whereas the Washington diagram has a more complex structure. However, the wind at both Washington and Oslo falls in the same quadrants in both winter and summer.

The observations of Harnischmacher and Rawer (ref. 420) in France also established the presence of a clearly expressed diurnal variation of wind direction in the E layer in winter (including March), not only as a mean but also for individual days. The most characteristic feature of these variations is a clearly expressed semidiurnal component. The wind vector very regularly undergoes 360° rotation between 0800 and 1600 or 1800 hours (lt). About 0800 the wind azimuth (the direction toward which the wind is blowing) is 60°; it increases to 180° (south) between 1000 and 1230 hours, to 270° (west) between 1200

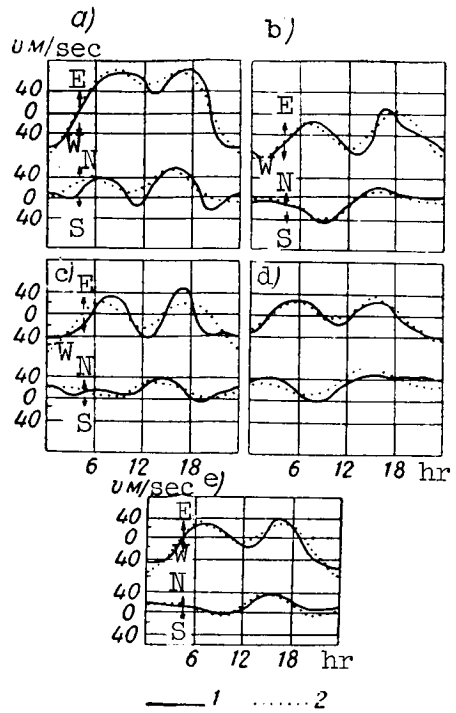

Figure 30.5. Diurnal variation of wind (1) in E layer over Norway at different seasons and during year, and theoretical variation using first three terms of Fourier series (2). a, summer; b, winter; c, spring; d, autumn, e, year.

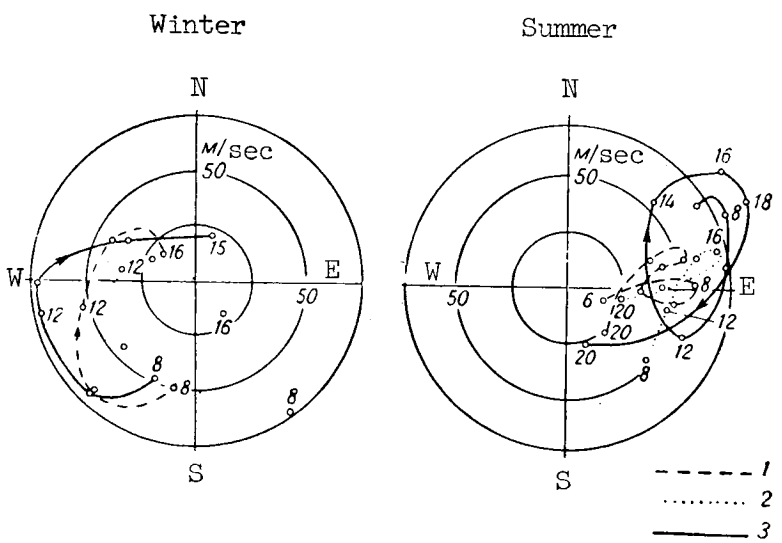

Figure 30.6. Vector diagram of wind in E layer for Norway (Oslo) and United States (Washington). 1, United States: winter (January-February), summer (May-June); 2, United States: winter (November-December), summer (July-August); 3, Norway.

and 1500 hours and to 360° (north) between 1400 and 1700 hours. The days when this pattern is disrupted do not exceed 20 percent of the total number of observations. At nighttime the measurements are less regular (stable reflections of radio waves with a frequency of 2-3 Mc/s are observed only during the daytime), but they indicate a continuing rotation of the wind vector during the night. In the course of 24 hours the wind apparently makes two complete rotations, but more rapidly during the daytime than at nighttime. The wind velocity, whose mean monthly values vary in the 60-100 m/sec range, does not show significant diurnal variations. Harnischmacher and Rawer postulate that there is a wind minimum at about 1400 hours. In summer the variations of wind direction are expressed much less strongly, wind velocities are less and average 40-70 m/sec.

Rawer (ref. 693) used the similar fadings method for measurement of drift in the E layer at Freiburg from October 1955 through February 1957. Rawer detected a 12 hour velocity component corresponding to tidal currents in the atmosphere. It was expressed less clearly in summer, possibly because the E layer is screened by the lower E_s layer. Rapid changes of movement to the opposite direction (in a period of 15 min) suggest the presence of horizontal wind eddies or the existence of vertical movements in the E layer.

In 1955-1957 Sprenger (ref. 737) measured ionospheric drifts at Kühlungsborn (54°N, 18°E) on long waves (245 kc/s). The results of his observations apply to the lower part of the region (height of about 90 km). Due to great absorption during the daytime the measurements were made at night. The velocity vector of the drift has a clockwise diurnal rotation. In addition, Sprenger established the presence of a prevailing drift direction in the evening hours: in summer and winter it was east-northeast, and in spring and autumn it was almost opposite. The mean velocity of drift at all seasons was about 70 m/sec. In periods of magnetic storms there is an increase of drift velocity to 150 m/sec and sometimes more, and there is an additional velocity component in a north-south direction.

Beginning in July 1957, Skinner, Hope and Wright (ref. 730) measured the wind velocity in the E and F regions near the equator (Ibadan, magnetic latitude 2.5°S). They studied the east-west velocity component. It was found from observations in August-September 1957 that this velocity component in the E direction is directed westward during the daytime and eastward during the nighttime. The phase of the east-west component indicates a direction opposite to that obtained for the middle latitudes. It is suggested that there is a wind velocity minimum at about 1400 hours. In summer the variations of wind direction are expressed much less strongly and wind velocity is less, averaging 40-70 m/sec.

30.4. Vertical Variations of Wind in the E Region. Since wind measurements in the ionosphere by radio methods usually are made at a fixed frequency, it is necessary to reckon with the possibility of a change of the height from which radio waves are reflected at different times of day and during the year. Jones, Millman and Nertney (ref. 497) report development of a method permitting simultaneous measurements of the ionospheric wind and determination of the height of reflecting inhomogeneities. According to their observations, made in Pennsylvania in the United States on long waves (frequency 150 kc/s), there is a diurnal variation of the height of reflection. On the basis of 70 daily series of observations, they established that in the course of the day the height of the reflecting

layer varies by 10-25 km (from 74-77 km during the daytime to 83-100 km at nighttime). Measurements made by other authors usually are at higher frequencies (except those of Sprenger, ref. 737); the wind data obtained by these authors therefore apply to somewhat greater heights (about 100 km during the daytime), but a diurnal variation of reflection can occur in all cases. On the basis of the results cited in the preceding section and discussed in this section, it is known that there is a large (of the order of 3 m/sec·km) vertical wind gradient. Therefore, if the diurnal variation of the height of reflection is not taken into account, it can distort the data on the diurnal wind variation. The same consideration applies to the seasonal variation. These effects are not taken into account in most investigations (this requires additional, rather complex measurements). Data on wind and its diurnal and seasonal variations obtained from observations of the drift of ionospheric inhomogeneities, therefore, contain some uncertainty with respect to the height of the drifting object. This uncertainty is particularly significant for wind in the F layer.

Jones (ref. 494) reports measurements of drift velocity in the E region simultaneously at two frequencies: 2.0 and 2.5 Mc/s (using Mitra's method). The drift velocities which he observed differ appreciably from one another. Jones concluded, therefore, that at the level near which the reflecting inhomogeneities are situated, the wind essentially depends on height above sea level. Observations at different frequencies give information on wind at different heights. The velocity vector rotates by 360° in the course of the day. In the winter months the rotation corresponding to reflection at a lower height lags in phase relative to the rotation of the wind vector at a higher level. The rotation of the velocity vector occurs nonuniformly during the course of the day. This nonuniformity is explained by Jones by considering the character of the variations of reflection height a function of the time of day.

Jones compared his observations with the results obtained by Greenhow and Neufeld (ref. 412); the latter measured wind from the drift of meteor trails (Section 29). He found that the phase shift of rotation of the wind velocity vector observed by these two methods can be explained satisfactorily, if the difference in heights at which drift was measured is taken into account. The wind direction changes by 7 or 8° per km of height.

Great wind variability in the autumn months--September and October--was revealed by both methods.

Beynon and Goodwin (ref. 294) studied horizontal drifts in the lower part of the E region at midday hours. They established that the wind velocities are greater in winter than in summer. The velocities of horizontal drifts in the region of height 75-100 km clearly depend on height; the minimum velocities occur in a relatively thin layer between 85 and 90 km. Beynon and Goodwin believe that this wind minimum is not situated randomly near the temperature minimum (mesopause). They point out that observations of bursts of grenades ejected from rockets have demonstrated the existence of a wind maximum in the 50-60 km layer (Section 28), i.e., near (somewhat above) the temperature maximum in the ozonosphere. Temperature measurements in the middle latitudes indicate that in the region of heights 50-80 km the air temperature is higher in winter than in summer. Measurements by Beynon and Goodwin show that wind velocity at heights of 75-100 km

are also greater in winter than in summer. An important factor determining wind velocity is the horizontal temperature gradient. It can, therefore, be assumed that at least at some heights the value of the horizontal temperature gradient depends on the absolute temperature of the atmosphere at this level, and that large gradients are associated with higher temperatures.

30.5. F Region. According to some data there is a tendency to an increase of wind velocity with height in the ionosphere. On the average the wind velocity in the F layer is greater than in the E layer. This is concluded from observations made by Becker over the German Democratic Republic (ref. 287), shown in figure 30.7.

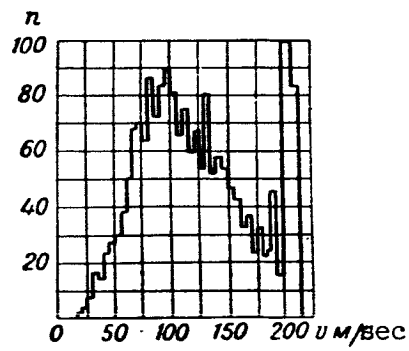

Figure 30.7. Distribution of wind velocities v in F layer over German Democratic Republic.

Comparison of data from this same author for the E_s layer (fig. 30.3) shows a predominance of great wind velocities at great heights. In the F layer, in addition to wind velocities of 60-160 m/sec, which are the most common, velocities of 200-220 m/sec have been recorded in many cases. Chapman (ref. 321), on the basis of 500 measurements in Canada, established that the mean wind velocity in the F layer (100 m/sec) is approximately twice as great as the mean wind velocity in the E_s layer (50 m/sec).

V. V. Tolstov and B. G. Bondar' (ref. 192) measured the drift of ionization inhomogeneities in the F region at frequencies of 1.5-1.7 Mc/s. Observations from October 1955 through April 1956 revealed that the movements of inhomogeneities have velocities from 10 to 200 m/sec, with a most probable value of about 80-100 m/sec. The wind direction before midday is predominantly westward and after midday is eastward. Individual measurements give a scattering around these mean values up to $\pm$ 60°.

Observations of the drift of small-scale inhomogeneities in the F2 region made in the USSR under the IGY program established the most frequently occurring values of the wind azimuth A (the direction in which the wind is blowing) and the velocity v for many stations:

Station	A°	v m/sec	Station	A°	v m/sec
Ashkhabad	240	60-80	Simeiz	220	60-100
Gor'kiy	260	60-80	Tomsk	240	100-120
Moscow	275	50-100	Khar'kov	225	40-60

These data (ref. 40b) indicate that in the F2 region there is a prevailing drift direction A = (260 ± 20)° with a most probable velocity of v = 80-100 m/sec.

The drift of small inhomogeneities in the F2 layer over the USSR has a quite clearly expressed diurnal variation. In the morning hours the prevailing wind direction is westward, but in the evening it is eastward with small deflections to the north or south. There also is some increase of velocity in the evening and nighttime hours. Drift velocity has little dependence on season but it is, nevertheless, possible that there is a predominance of wind to the east in summer and to the west in winter; in equinoctial periods the direction of movement is quite chaotic (ref. 40b).

Mitra, Vij and Dasgupta (ref. 603) measured the horizontal drift in the ionosphere over Delhi in the period from April 1958 through May 1959. They found that in the F region the most probable velocity is 85 m/sec and in the E region is 55 m/sec. The most typical drift azimuths in the F region are 120-240°.

Heisler (ref. 433), in contrast to many other authors, such as Rao and Ramana (ref. 689), did not discover a dependence of velocity on height in the range of heights 160-230 km.

Measurements in New Zealand (ref. 341) indicated a wind velocity in the F layer of 160 m/sec at 0200 hours, decreasing to 60 m/sec at 0500 hours (Jan. 17, 1953).

S. N. Mitra (ref. 602) observed an individual cloud with a diameter of about 1 km at a height of 250 km over England (Cambridge) on Sept. 11, 1948. The cloud drifted to the south-southeast at a velocity of 80 m/sec.

Many determinations of wind in the F layer are based on observations of reflections from large-scale ionospheric inhomogeneities. For example, Munro (ref. 609), who made observations in the eastern part of Australia (Sydney), found a daytime (0900-1700 hours) wind direction in winter (1948-1949) of 20° (azimuth of the direction in which the wind was blowing), and in the summer of 1948 an azimuth of 110°; however, on June 1 and 2, 1950, the azimuth changed during the day from 50 to 15°. Nighttime measurements in 1952 indicated that the wind direction was mostly westward. The wind velocity (during day and night) averaged 80-130 m/sec. Price (ref. 682) reports on measurements in 1950-1952 in the western part of Australia; in these same daytime hours he found a wind direction in winter of 0-60° and in summer of 90-180°; the wind velocity varied in the broad range of 90-320 m/sec. Velocities of about 160 m/sec were observed most frequently. The directions of velocity change during the day and quite frequently there are variations of direction as great as 50°. Price notes that the wind characteristics he found coincide with the results of measurements made by

Munro at Sydney, and he considers probable a constancy of velocities in a zone with a radius up to 3,500 km. Measurements made in England by Bramley and Ross (ref. 583) revealed wind velocities of 35-135 m/sec. In the winter of 1942-1943 Beynon (ref. 293) measured reflections from large-scale inhomogeneities in the F layer at sunrise and found a westward drift with a velocity of 120 m/sec.

Data have also been obtained (ref. 583) from observations of reflection of radio waves from small-scale inhomogeneities in the F layer. On the basis of measurements in 1949-1952 in England, Phillips, Briggs and Spencer found that at nighttime the wind was directed westward and during the daytime was directed eastward; mean wind velocity was 100 m/sec. Nighttime measurements made by Salzburg and Greenstone in the United States in 1949-1951 revealed that the wind has a mean velocity of 100 m/sec and is directed westward.

Data obtained by Rao and Murty (ref. 684) and measurements by Ramakhandra and Bhagiratha Rao (ref. 686), made at Waltair (18°N, 83°E, magnetic latitude 9°30'N) in 1956-1957, indicate that the drift velocity observed most frequently in the F1 region (virtual height 200-240 km) is 60-70 m/sec, without appreciable diurnal and seasonal variations. The drift direction at midday for all seasons is to the southwest; in the morning (0900 hours) it is to the southwest in winter and spring, but to the northwest in summer and autumn; at 1500 hours in autumn and winter the direction is to the southwest, and in spring and summer it is to the northeast.

In the F2 region (virtual heights 280-320 km), the most frequently observed velocity is about 95 m/sec; the velocity vector in the course of the day describes an ellipse which passes twice through the maximum and minimum values. At midnight the drift direction is to the northeast, in the morning and during the daytime to the southwest and in the evening to the northwest (ref. 686).

Measurements made by V. D. Gusev and S. F. Mikrotan (ref. 46) show that movement of large inhomogeneities in the F2 region occurs with a velocity of 120-150 m/sec, sometimes as great as 600 m/sec; velocity increases from nighttime to daytime. The direction of movement has a clearly expressed diurnal variation: at nighttime to the north, during daytime to the south, in the morning to the south with deflection to the east and in the evening to the north with deflection to the west.

According to the measurements made by Thomas (ref. 763), who also investigated the horizontal movements of large-scale inhomogeneities in the F2 region using widely spaced (up to 300 km) observation stations (Slough, Swansea, Bangor), drift occurs with a velocity from 40-280 m/sec, with southeast a predominant direction. Thomas also studied the diurnal and seasonal variations and compared simultaneous drift measurements made from two stations, one of which was situated 650 km to the north of the other: greater drift velocities were recorded over the more northerly station.

In addition, Thomas noted a vertical increase of drift velocity in the F2 region by approximately 1 m/sec·km.

Individual rocket measurements reported in reference 428 indicate that at a height of 200 km over White Sands Proving Ground in the United States the wind is directed toward the southeast and has a velocity of 80 ± 20 m/sec.

Radioastronomical techniques are used for study of wind in the highest part of the ionosphere.

30.6. Radioastronomical Observations. Investigations of the scintillation of radio stars reveal a drift of ionospheric inhomogeneities at extremely great heights, apparently not less than 400-500 km (Section 26). Systematic use of this method at the experimental station at Jodrell Bank (England) has made it possible to obtain important information on air currents in the upper layers of the atmosphere at nighttime. It was found that the wind velocity at this level can attain enormous values, up to 1,200 m/sec, although the predominant velocity is about 100 m/sec (fig. 30.8). The velocity changes considerably from night to night, revealing a close correlation with geomagnetic disturbances. Under stable geomagnetic conditions the wind velocity remains constant during a particular night. Mean data (for several years) on changes of wind velocity v during the night are as follows (ref. 583) (the problem of the relationship to geomagnetic activity will be considered separately):

Time, hr, min	$\bar{v}$ m/sec	Time, hr, min	$\bar{v}$ m/sec	Time, hr, min	$\bar{v}$ m/sec
19.30	159	23.30	183	2.30	288
20.30	187	0.30	161	3.30	268
21.30	181	1.30	286	4.30	172
22.30	231				

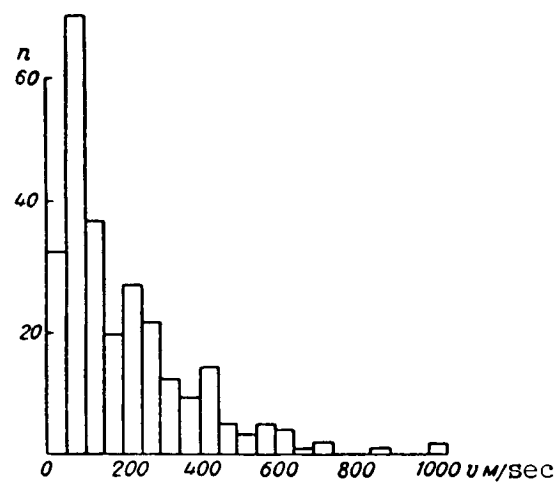

Figure 30.8. Distribution of wind velocity in upper part of F2 region over England. n--No. of observations.

The direction of movement of diffraction screens (ionospheric inhomogeneities) usually differs little from an east-west line, and the north-south component usually is less than 30 m/sec. This can be seen from the polar histograms in figure 30.9; these histograms show the number of cases when the drift direction fell within the limits of a particular 15° sector (the directions show the course of the wind). During the first half of the night, from 1900 hours to midnight, the prevailing direction is toward the west. From 0000-0100 hours the direction is reversed. From 0100-0500 hours the wind is directed mostly to the east (ref. 583).

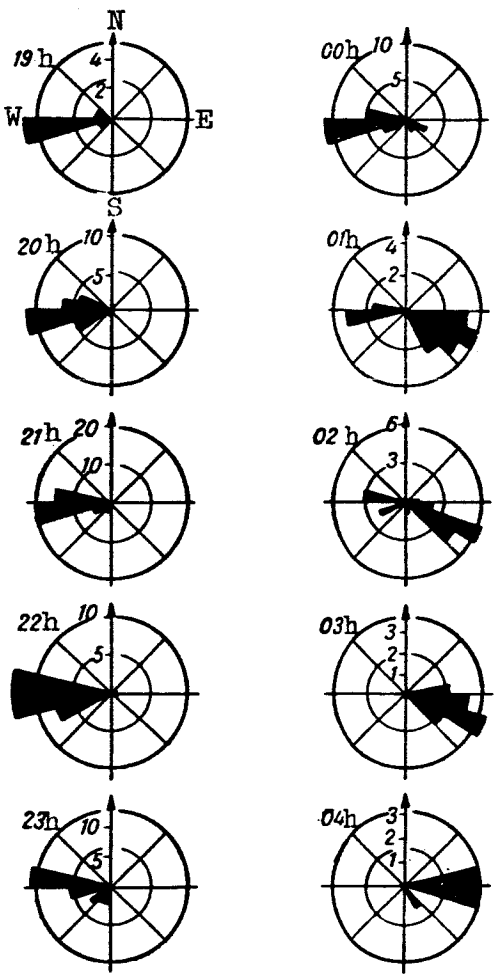

Figure 30.9. Hourly polar histograms of drift direction in F2 layer. Figures along vertical diameters give number of observations.

30.7. Relationship to Geomagnetic Disturbances and Solar Activity. As already mentioned, a close relationship has been found between the drift velocity of inhomogeneities in the upper part of the F region and geomagnetic disturbances.

According to data presented by Lovell (ref. 560), there is a proportionality between drift velocity and the k index characterizing the disturbance of the Earth's magnetic field. The relationship between mean drift velocity $\overline{w}$ and the k index is as follows:

k	0	$\frac{1}{2}$	1	$1\frac{1}{2}$	2	$2\frac{1}{2}$	3	$3\frac{1}{2}$	4	$4\frac{1}{2}$	5	$5\frac{1}{2}$	6	$6\frac{1}{2}$	7	$7\frac{1}{2}$
$\overline{w}$ м/sec	38 ± 4		76 ± 5		110 ± 8		175 ± 12		325 ± 20		472 ± 58		553 ± 48		732 ± 110	

A similar correlation between the k index and drift velocity measured at Delhi (29°N) by reflections from the F region was established by Mitra, Vij and Dasgupta (ref. 603) during magnetic storms; on magnetically quiet days drift velocity remained almost constant with a change of the k index.

Observations at Tomsk established the presence of variations of the velocity vector with a 24 hour and a semidiurnal period. It was found (ref. 40b) that the modulus of drift velocity in the F2 layer (the same as in the E region) is dependent on magnetic activity (fig. 30.10).

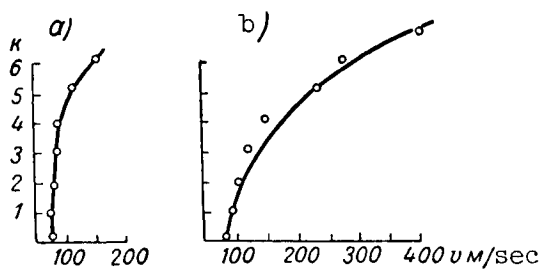

Figure 30.10. Dependence of drift velocity on index of magnetic activity k (on basis of observations at Tomsk). a, for E layer; b, for F2 layer.

This sort of dependence is a very graphic illustration of the well-known conclusion of the theory of geomagnetic variations that a definite part of the disturbances and variations of the Earth's magnetic field is caused by certain systems of electrical currents in the ionosphere: a drifting electron or ion cloud is like some current whose circuit coincides with the drift trajectory of the cloud (e.g., figure 30.4), and the current strength is proportional to the charge of the cloud and the velocity of its drift.

From this point of view it is easy to understand another dependence which has been established by radioastronomical observations of the drift of ionospheric inhomogeneities: the relationship between the drift velocity and velocity (frequency) of fadings (fluctuations). Even in the first radioastronomical investigations it was established that the slowly changing (fluctuating) intensity of a particular radio star with time attains a maximum, on the average, of once a minute, but this frequency of scintillation varies in the range from 0.2

to 10, whereas on individual nights it even reaches 20 maxima per min. Further investigations (ref. 583) show that the frequency of fadings is directly proportional to the drift velocity in the broad range of velocity from 30-1,000 m/sec; the scattering of individual points does not exceed 20 percent. The mean values of the observed drift velocity for the experimental station at Jodrell Bank (ref. 583) were related to the fading frequency as follows:

No. of fadings (max/min)	1	2	3	4	5	6	7	8	9
Drift vel, m/sec	50	120	190	270	330	390	440	480	530

The study by Thomas (ref. 763) also notes a relationship to magnetic activity: in the case of values of the index $k > 2.5$ the drift velocity in the F2 region increases, roughly proportional to k.

B. Rao, E. Rao and Murty (ref. 687), on the basis of observations near the magnetic equator (Waltair, magnetic latitude 9°30'N), obtained an inverse dependence: with an increase of the k index from 1-6 the drift velocity decreases almost linearly, although very insignificantly: from 94-80 m/sec. The maximum change of drift velocity as a function of magnetic activity is observed at midday and at midnight; a less clearly expressed dependence was obtained for 1500 hours. It is important to note that the dependence of drift velocity on magnetic activity can be detected more clearly, if the study of the total velocity vector is replaced by an examination of its components: the north-south component remains more or less constant, but the east-west component decreases with increase of k, even to extremely small values.

Observations made by B. Rao and E. Rao (ref. 685) at this same station indicate that there is also a dependence of drift on solar activity. Whereas on ordinary days the north-south component is directed southward during the daytime and northward at nighttime, on June 6 and 18, 1957, strong solar flares were observed and the behavior of this component changed sharply: on these days it was directed northward during the daytime and only near midnight on June 18 did it assume a southward direction. In addition, drift velocity increased considerably on these days.

Interesting data on the movement of ionized regions of auroras which reflect radio waves, and the relationship between these movements and magnetic disturbance were obtained by Lyon and Kavadas (ref. 564) (Section 30.10, fig. 30.13).

30.8. Radioastronomical Observations in the Auroral Zone. The experimental station at Jodrell Bank, being the principal center of radioastronomical investigations of the upper layers of the atmosphere, is located at 53°14'N and 2°18'W. The observations at this station are made using two very bright radio stars, one in constellation Cassiopeia and the other in constellation Cygnus. In their diurnal apparent motion in the sky neither of these stars dip below the horizon; their zenith distances at upper culmination are 5 and 23° and at lower culmination are 68 and 86°, respectively. Observations of the source in Cassiopeia near its upper culmination provide data on the drift of ionospheric inhomogeneities

virtually over the station. However, the line of sight directed to the source in Cygnus at its lower culmination intersects the ionosphere far to the north of the station: the layer situated at a height of 400 km is intersected by the line of sight in the zone of maximum frequency of occurrence of auroras. Observations of the source of radio emission in constellation Cygnus near its lower culmination make it possible, therefore, to investigate from England that part of the ionosphere situated in the zone of maximum frequency of occurrence of auroras (ref. 583). It was found that the character of the drift movements in the F layer in the auroral zone differs appreciably from the drift in the non-polar part of the ionosphere: the F layer in the auroral zone is considerably more mobile and disturbed.

These differences can be detected at once when observing the appreciable scintillations of radio stars. Whereas in observations at small zenith distances scintillations are noted on only one night in a three-day period throughout the year, in measurements using the source in constellation Cygnus, situated low over the northern horizon, the line of sight intersects the strongly disturbed ionosphere in the auroral zone, and the scintillations can be measured on any day or night.

A histogram of the distribution of the observed drift velocities is shown as figure 30.11. The velocities vary approximately from 50-1,000 m/sec; the mean value is 360 m/sec (only 6 of these observations were made when the value of the geomagnetic index k was greater than 6). In periods of a quiet geomagnetic field the velocities remained constant. The mean drift velocities during 6 hour intervals change little during the course of the day, as can be seen from the following data (ref. 583):

Time period, hr	12-18	18-24	0-6	6-12
Mean drift vel $\bar{w}$ m/sec	365	313	410	487
No. of observations n	36	92	60	9

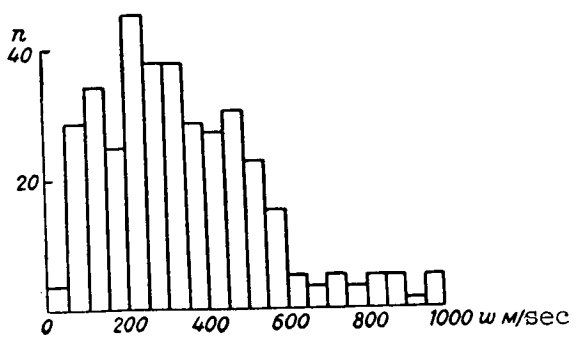

Figure 30.11. Histogram of drift velocities in F2 layer (auroral zone). n--No. of observations.

Between 0900 and 2100 hours the most frequently observed wind direction was westward; from 2100-0600 hours it was southeast or southwest (fig. 30.12). In this case the drift velocity is proportional to the frequency of scintillations, so that an estimate of the wind velocity in the F2 layer for the auroral zone can be made directly by a calculation of the scintillation frequency.

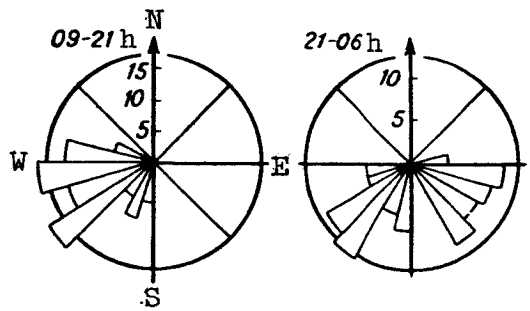

Figure 30.12. Polar histogram of drift directions in F2 layer (auroral zone). Figures along vertical diameters denote number of observations.

30.9. Comparison of Ionospheric Winds at Great Distances. Simultaneous observations of the scintillations of radio stars in constellation Cassiopeia were made in May-June, 1952, from two stations in England 200 km apart: at Jodrell Bank at a wavelength of 3.7 m and at Cambridge at a wavelength of 6.7 m. It was found that the drift directions coincide at the two stations in 90 percent of the cases. Air movements in the F layer, therefore, can be considered similar at distances of about 200 km (ref. 583).

Other experiments at Jodrell Bank demonstrated the existence of such a similarity at a distance of 800 km. This was done by using the same receiving apparatus to observe the scintillations of two different radio stars in different parts of the sky (the source in constellation Cygnus 3 or 4 hours after its lower culmination and the source in constellation Cassiopeia at its lower culmination). This made it possible to compare the drift of ionospheric inhomogeneities at two places in the F layer, situated at an identical geomagnetic latitude at a distance of 800 km apart (the line of sight to Cygnus intersected the F layer over the Shetland Islands and the line of sight to Cassiopeia intersected it over western Norway). The investigation was made on 18 nights in April-June, 1952, and in February-March, 1953. Analysis of the results revealed that in general the velocities agree well with one another (ref. 583). The drift direction was identical to an accuracy of 10°, and the difference of drift velocities on the average was less than 30 percent.

The work of Price (ref. 682) has been mentioned previously. In his study he compared the results of measurements of reflections from large-scale ionospheric inhomogeneities in the eastern and western parts of Australia, and concluded that there is a constancy of velocities within a zone with a radius of 3,500 km (however, the observations for Australia which he compared were not simultaneous).

30.10. Auroras and the Night Airglow. Observations of movements of auroras were discussed in Section 22. A bright aurora observed by McLaughlin (ref. 585) drifted westward before midnight and eastward after midnight. Similar data were obtained by Bless, Hartlein and Kimball, and also by Meinel and Schulte (ref. 595). Meek (ref. 590) observed the movement of auroras at Saskatoon, Canada; the velocity was 200-500 m/sec, and movement was to the east in 19 cases and to the west in 14 cases. In 25 cases he observed north-south movement.

Lyon and Kavadas (ref. 564), making observations at Saskatoon, Canada (52°N), studied the reflections of radio waves at a frequency of 48.2 cps from ionized layers, in which auroras develop (in short, radio echoes from auroras). They discovered systematic movements of reflecting regions. Before local midnight, the movement is to the west and after midnight to the east. In addition, they established the existence of a statistical relationship between mean velocity and direction of movement and variations of the geomagnetic field. Figure 30.13 (curve 1) shows the mean hourly values of the X-component (horizontal component in the north-south direction) of the geomagnetic field; as usual, the vector component directed to the north is considered positive. The value of this vector is read from the level of a quiet day: it usually applies to an undisturbed period at 1200-1400 hours lt. In almost all cases negative disturbances have a greater magnitude than positive disturbances.

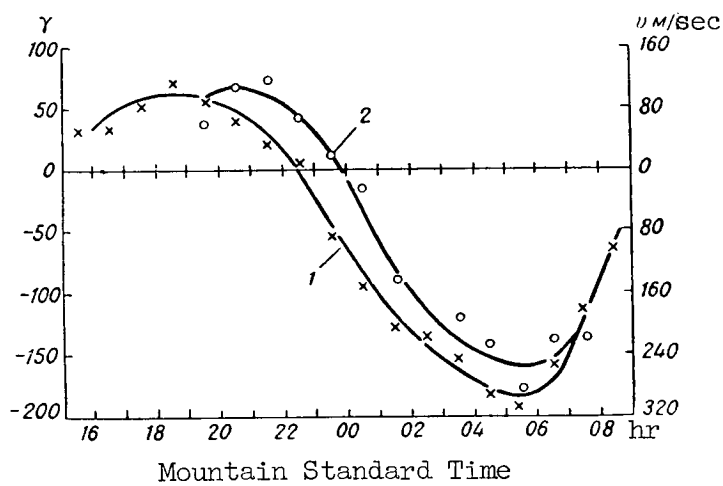

Figure 30.13. X-component of magnetic disturbance γ (1) and radial velocity v (2) of reflecting region (radio echoes) from auroras for antenna directed eastward.

Curve 2 in this same graph shows the diurnal variations of the mean hourly values of the radial velocity of movement of radio echoes from auroras (recorded by an antenna oriented eastward). The shape of this curve is surprising in its similarity to the diurnal variation of the X-component of magnetic disturbance. The reason for the small temporal displacement of one curve relative to the other, according to Lyon and Kavadas, is the fact that the reflecting region was situated at a distance of 250 km to the northeast of the magnetometer.

These curves show that the movement of reflecting ionized regions to the west is associated with a positive magnetic disturbance and movement to the east with a negative disturbance. An exception to this rule was noted by Lyon and Kavadas in only 5 of 122 cases.

It must be remembered that the mentioned relationships are only statistical: Lyon and Kavadas did not find a simple relation between velocity of movement of the reflecting region and the magnitude of the magnetic disturbance for individual radio echoes. It also must be remembered that movement of the reflecting region of auroras is not always observed: in many cases these reflecting regions remain fixed over a long period of time (ref. 564).

Unwin (ref. 774) investigated the movements of ionization of auroras in New Zealand (radio echoes at a frequency of 55 Mc/s). It was demonstrated that the radio signals emitted by a radar set are reflected from a layer with a thickness from several to 25 km; the middle of the layer is situated at a height of 110-120 km. Unwin believes that the ionospheric inhomogeneities detected during the radar observation of auroras can be identified with the system of electrical currents responsible for geomagnetic disturbances.

Kim and Currie (ref. 524) measured the drift of auroral forms at three stations in the west-central part of Canada. These movements coincide in velocity and direction with the movement of ionospheric inhomogeneities recorded using radio waves. The velocities increase with an increase of geomagnetic activity, especially in the east-west direction. Kim and Currie did not obtain definite indications of a reversal of east-west movement near midnight. The direction and velocity of the movements revealed no characteristic dependence on time of night.

Feibelman (ref. 384) reports observation of the movement of an aurora at 40°N, 80°W.

Extensive observations of movements of auroras and the geomagnetic phenomena accompanying them were made in Antarctica by an Australian expedition (ref. 302).

The phenomenon of night airglow will now be considered. Measurements of the redistribution of the brightness of the night sky through the heavens make it possible (as already noted in Section 22) to detect the movement of bright (luminescent) "clouds." Roach, Williams and Pettit (ref. 703), on the basis of simultaneous observations at the observatories Cactus Peak (California, United States, 36°04'N, 117°49'W) and Haut-Provence (France, 43°56'N, 5°43'E), constructed isophote maps of the brightness of the green line $\lambda = 5{,}577$ Å every hour for two nights (January 1951 and November 1952). During the night the regions of enhanced brightness of the luminosity of the night sky move with an average velocity of about 150 m/sec. In both cases the emitting region (a cloud of dissociated oxygen) moves in the first half of the night in a general east to west direction, whereas in the second half of the night there is a small component of movement directed from west to east and a small southern component. In the middle of the night movement ceases.

Data presented by Huruhata, Tanabe and Nakamura (ref. 468) indicate that similar luminescent clouds are observed in Japan in the infrared region of the spectrum (luminescence of molecules of the hydroxyl OH). They move with a velocity of about 100 m/sec in a north-northeast or south-southwest direction.

The height of the hydroxyl luminescence is less than 100 km. The layer emitting the green line of atomic oxygen apparently is situated at a level of about 100 km.

Roach, Tandberg-Hansen and Megill (ref. 704) discovered that at a height of about 100 km bright clouds (emission of the green line) have not only a translational movement with a velocity of about 100 m/sec, but also a rotational movement with a mean period of 5 hours.

30.11. Movement of Extensive Ionospheric Disturbances. Australian scientists discovered the existence of extensive moving ionospheric disturbances, which in the daytime hours of the winter months move from south to north over the eastern coast of Australia. Such disturbances are traced to a distance of 3,000 km without appreciable changes in their intensity. The frontal extent of the phenomenon attains and sometimes exceeds 1,000 km. Such disturbances were also noted in the northern hemisphere. Some of them extended at least from the eastern to the western coast of America and moved a distance of 4,000 km. It was assumed for a long time that this phenomenon exists only in the daytime hours. Heisler (ref. 432) reported that it has also been discovered at nighttime.

Such phenomena are quite rare and it is possible, therefore, reliably to record the occurrence of the same disturbance at several stations. By determining the time difference of the observations, the velocity and direction of movement of this disturbance can be computed.

As examples we mention two such disturbances described by Heisler (ref. 432). They were observed on the nights of June 26 and July 5, 1957, at Brisbane (27°28'S, 153°02'E), Townsville (19°10'S, 146°58'E) and Camden (34°03'S, 150°40'E). In both cases the movements were to the east; the velocity was 260 m/sec in the first case and 130 m/sec in the second. The front of the movement extended for 1,800 km.

CHAPTER 10. VERTICAL AND TURBULENT AIR MOVEMENTS IN THE UPPER LAYERS OF THE ATMOSPHERE

31. Convection in the Ozonosphere

The development of ascending air movements is dependent on vertical distribution of temperature and humidity. The more rapid the decrease of temperature with height, the more probable (all other conditions being equal) is the development of convection and the more intense are the turbulent movements and ascending slippage of warm air on atmospheric fronts. (For further details on the conditions for development of free (thermal) convection see the article by N. V. Lebedeva (ref. 104); a general exposition of the problem of conditions for development of vertical movements in the atmosphere can be found in a study by Kohlsche, ref. 536).

It was formerly assumed that the stratosphere is characterized by total absence of convective movements and turbulence. The basis for this opinion was the existence of isothermal conditions in the stratosphere and even an increase of temperature with height. It was found later that such a concept of the stratosphere fails to correspond to reality in many respects. This can be attributed to the fact that there are strong winds whose velocity changes appreciably with height h in the stratosphere. The stability of atmospheric stratification is dependent not only on the thermal factor, but is determined by the Richardson number as a dimensionless criterion of turbulence

$$\mathrm{Ri} = \frac{g}{T}\frac{\gamma_0 + \frac{\partial T}{\partial h}}{\left(\frac{\partial u}{\partial h}\right)^2 + \left(\frac{\partial v}{\partial h}\right)^2}, \qquad (31.1)$$

where u and v are the horizontal components of wind velocity, g is acceleration of gravity, T is absolute temperature, λ_0 is the adiabatic temperature gradient (in the Richardson approach) or the equilibrium gradient (from the modern point of view), equal to approximately 6-7°/km. The greater the Ri number, the more stable is atmospheric stratification. When Ri > 1, a steady-state turbulent regime is impossible; the thermal factor extinguishes turbulence.

31.1. Vertical Mixing. The constancy of composition of stratospheric air, established for the first time by experiments with the stratospheric balloon "USSR," indicates a relatively strong vertical mixing in the stratosphere. There now is direct proof of the existence of strong stratospheric turbulence. In particular, this is demonstrated by the results of special observations of pilot balloons (refs. 271 and 723), although the method used and the interpretation of the measurements have been subjected to a number of criticisms (ref. 547). Very important information on vertical transport in the atmosphere was obtained

in the study of the ozonosphere, especially investigation of the vertical change of ozone distribution. There are data which suggest that the mentioned processes are characteristic not only of the lower layers of the stratosphere, but also the middle part of the ozonosphere to a height of 50 km, although their intensity possibly is not great.

No further details will be given here on the problem of ascending and descending currents, which are links in the general circulation of the atmosphere. For example, according to Gold's model, meridional circulation consists of an ascending flow in the equatorial zone (for such a type see fig. 17.4) and a descending polar flow. Libby and Palmer (ref. 548) express the opinion that this model is confirmed by numerous observations of world-wide radioactive fallout. Validity of the model is supported by the existence of a spring fallout maximum, and also by the fact that the products of high-latitude nuclear explosions are retained in the atmosphere a considerably shorter time than the products of explosions in the equatorial zone. Figure 17.5 shows the vertical wind component in the lower layers of the stratosphere, computed by Libby and Palmer.

On the basis of different considerations, a similar problem can be considered with respect to the upper layers of the ozonosphere. The literature contains repeated references to the fact that the atmospheric layer at a height of 50-80 km, in which air temperature should decrease rapidly with height, should be unstable and can be characterized by strong turbulence and convective currents. The mentioned phenomena should transpire in this layer approximately the same as in the troposphere, where they are stimulated by an underlying surface heated by solar rays. The role of an "underlying surface" for the 50-80 km layer is played by a layer of warm air at the 50 km level, which is heated by the absorption of solar ultraviolet rays by ozone.

In addition, the ozone layer can possess (at least to a small degree) the properties of a nonhomogeneous underlying surface because there can be local anomalous ozone concentrations (in particular occurring over extratropical cyclones, ref. 721), and there can, therefore, be local disruptions of the temperature regime of the ozonosphere. The problem of the stability of atmospheric stratification at heights of 50-80 km now will be considered in greater detail, although only with the temperature factor taken into account.

31.2. Conditions in the Upper Layer of the Ozonosphere. Due to the low relative air humidity in this part of the atmosphere, in estimating the degree of stability of its stratification we can use as a point of departure the dry adiabatic gradient $\lambda_0 = 9.8^\circ/\text{km}$ (or, if the decrease of acceleration of gravity g with height is taken into account, we can assume in further computations that $\lambda_0 = 9.6^\circ/\text{km}$).

The vertical temperature distribution in this region is subject to changes and depends on latitude. Slater (ref. 731) compared (fig. 31.1) the schematic vertical temperature distribution in the region 35-90 km (on the basis of data

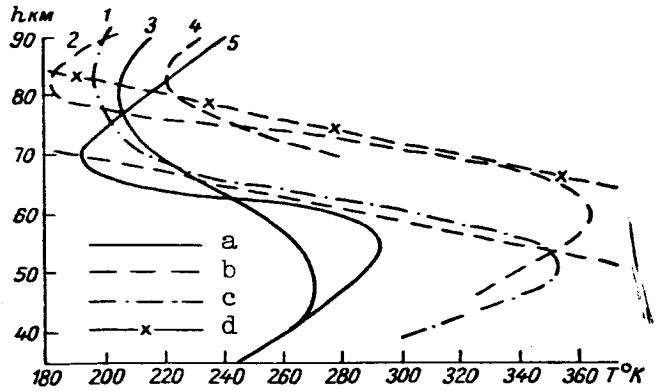

Figure 31.1. Vertical temperature distribution on basis of data from various authors. 1--Jacchia and Kopal; 2--Whipple; 3--United States Rocket Committee (ref. 707); 4--Jacchia (ref. 789); 5--Newell (ref. 622). Observational data: a--rocket; b--meteor; c--atmospheric oscillations; d--computation for dry adiabatic temperature gradient.

from various authors) with the distribution corresponding to $\lambda_0 = 9.8°/km$ (curve d). Comparison of the curves shows that in many cases there are conditions favorable for the development of convective currents.

Some rocket data on temperature will be considered first. Whereas the average curve 3 corresponds to a stable state of this part of the atmosphere, curve 5, constructed from data for January, March and August, indicates instability in the 60-67 km layer.

Temperature curves constructed by Whipple in 1941 on the basis of meteor observations indicate instability in the 67-78 km layer, but according to data obtained later (1952) by Jacchia (ref. 789) this layer is stable. Curve 1, obtained by averaging direct temperature measurements, also agrees with observed tidal oscillations of the atmosphere and shows instability at the 57-63 km level.

Data on atmospheric instability at heights of 50-80 km therefore cannot be regarded as being in full agreement, but in those cases showing indications of instability it involves relatively thin layers.

However, there is other evidence, mostly indirect, confirming the existence of convection. The composition of the air (see Chapter 6) remains virtually constant to a height of 80 km, which indicates the presence of vertical movement (although weak) without which there would be partial separation of light and heavy gases. The development of wind measurement methods makes it possible to undertake direct investigation of turbulence in the mesosphere. Radar on Johnston Island in the Pacific Ocean has tracked the drift of clouds

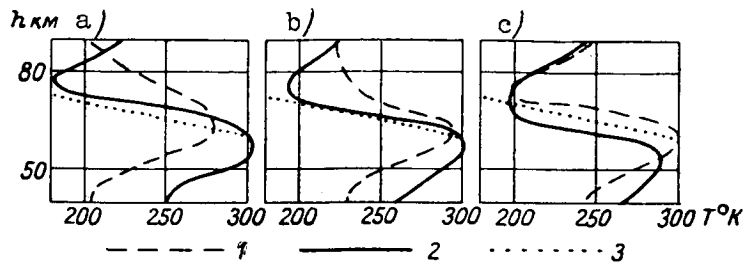

Figure 31.2. Summer and winter temperatures at heights of 40-90 km.
a--poles; b--at latitude 60°; c--at latitude 30°.
1--winter; 2--summer; 3--adiabatic gradient.

of fine metal dipoles ejected from a rocket. Smith (ref. 733) reports the discovery of a stable easterly flow (in summer) at heights of 69-78 km, whereas below 69 km there was strong increase of turbulence, as indicated by the rapid scattering of clouds, and great variability of the observed wind vectors. Meteor observations give some indications of turbulence (Section 32).

Conditions favorable for the development of convective movements in the upper part of the ozonosphere can change depending on the latitude of the place and season. Kellogg, using data on air currents, constructed diagrams (fig. 31.2) showing that at some heights between 60 and 75 km the air is unstable in summer at all latitudes, whereas in winter instability is observed only between latitude 30° and the equator.

The comparison is based on the assumption of an adiabatic change of temperature in the process of convective movements. In general, this is not always the case under real conditions. For example, as a result of radiant heat exchange and heat losses through radiation in the process of ascending movements of an air particle, an equilibrium state can be reached when the actual temperature gradients are superadiabatic. However, when radiation is absorbed, convective currents can develop when the gradients are smaller.

31.3. Character of Convective Currents. Convective currents are classified as regular and irregular. The simplest form of the regular type is related to the Benard cells, in each of which the flow is ascending at the center and descending at the periphery, or vice versa. The ideal Benard cell should be hexagonal, viewed from above; its horizontal diameter should be approximately 2.5 times greater than its vertical extent (thickness), and the latter coincides with the thickness of the convection layer.

Such phenomena are easily reproduced on a small scale in models, and their frequent occurrence in the atmosphere is indicated by clouds of such types as altocumulus and stratocumulus. However, the development of the phenomenon requires complete uniformity of heating of the underlying surface. However, if wind velocity changes with height, which usually occurs in this part of the

atmosphere, the cells are curved and elongated along the direction of wind change. In the lower layers of the atmosphere a similar phenomenon is sometimes observed in the form of parallel "cloud streets," well known to glider pilots (ref. 731).

Chapter 9 gives data indicating relatively rapid changes of wind velocity with height in this region of the atmosphere. For example, according to data published by Kennedy, Crary and Bushnell (ref. 520), who determined the wind regime in the stratosphere from observations of anomalies of sound propagation, an easterly wind in summer over Bermuda had a velocity of 58 m/sec at a height of 50 km and 63 m/sec at a height of 55 km. Wind variations with height, but of opposite sign, also are observed.

The irregular type of convection is constantly observed in the lower layers of the atmosphere. This convection is the result of nonuniform heating of the soil. Warm air particles are moved upward in the form of large "bubbles" with only a short lifetime, because in the process of motion they are mixed with the surrounding air, in most cases from behind and from below, creating small-scale turbulence in this region. The development of such turbulence requires contrasts in heating at the base of the convection layer. Although it is known that such contrasts are encountered below the ozone layer, at the level considered they are much less probable because in the upper part of the ozonosphere photochemical equilibrium is established rapidly (in minutes), and a state close to thermal equilibrium apparently is established with almost the same rapidity. Paton, on the basis of his observations of noctilucent clouds in Scotland, has postulated that possibly there are rapid ascents of large convective "bubbles" of this type (ref. 671). The undulating surface of the clouds which he observed (undulation indicates stability and wind change with height) suddenly was transformed into a disorderly surface (at 0218 lt), as if disturbed by strong convection.

Very interesting data on eddy movements of air at a height of 80 km were obtained by N. I. Grishin (Section 28) from a motion picture survey of noctilucent clouds (refs. 39 and 40).

31.4. Velocity of Ascending Currents. We will examine the problem of the degree of vertical current velocity. A theoretical estimate involves great difficulties because the scale of convective movements is unknown (ref. 721). Some information on this can be obtained from observations of the behavior of meteor trails, noctilucent clouds and inhomogeneities in the lower part of the ionosphere.

It is easy to compute the vertical acceleration of an air particle, dependent on temperature excess, if turbulent viscosity and the mixing of air by penetration from the outside are neglected (ref. 731). At a temperature of 300°K, a rising air particle will experience an acceleration of 0.01 g (g is the acceleration of gravity) if it is 3° warmer than the surrounding medium, or 0.1 g if it is 30° warmer. Long has estimated that in the lower layers of the atmosphere viscosity decreases the velocity of thermal convection currents by 20-30 percent. For comparison it can be pointed out that in the lower layers a velocity of thermal currents of 2 m/sec is an ordinary

phenomenon; a velocity of 5 m/sec is frequent, and currents sometimes are as great at 10 m/sec. Hurricanes have a vertical component of a velocity of 30 m/sec, with a limit of 50 m/sec.

According to a rough estimate by Slater (ref. 731), based on Long's extremely preliminary data on the role of viscosity, an ascending current must be 10° warmer than the surrounding medium to attain a velocity of 100 m/sec and rise to 30 km. However, it would be extremely risky to assume that such conditions can actually be encountered. In an extreme case heating of 1° might occur. In the lower layers of the atmosphere such heating is adequate for the development of thermal convection.

The important study by Murgatroyd and Singleton (ref. 618) appeared in 1961. It was devoted to the problem of meridional circulation in the stratosphere and mesosphere. This problem (which will be discussed in Section 36) is closely related to certain problems of vertical movements in the atmosphere. As the basis of their computations Murgatroyd and Singleton used the concept of heat transport between radiation sources and radiation outlets in the stratosphere and mesosphere. With some simplifying assumptions they computed not only the velocity of meridional currents, but also the velocity of vertical movements at different heights from 15-80 km and at different seasons of the year (fig. 31.3a-d). As shown in figure 31.3, the velocity of vertical movements has a value of the order of mm per sec.

In the lower layers of the stratosphere in midsummer (fig. 31.3a) there is a region of ascending currents near the equator, with a velocity of about 1 mm/sec extending approximately to 30° latitude.

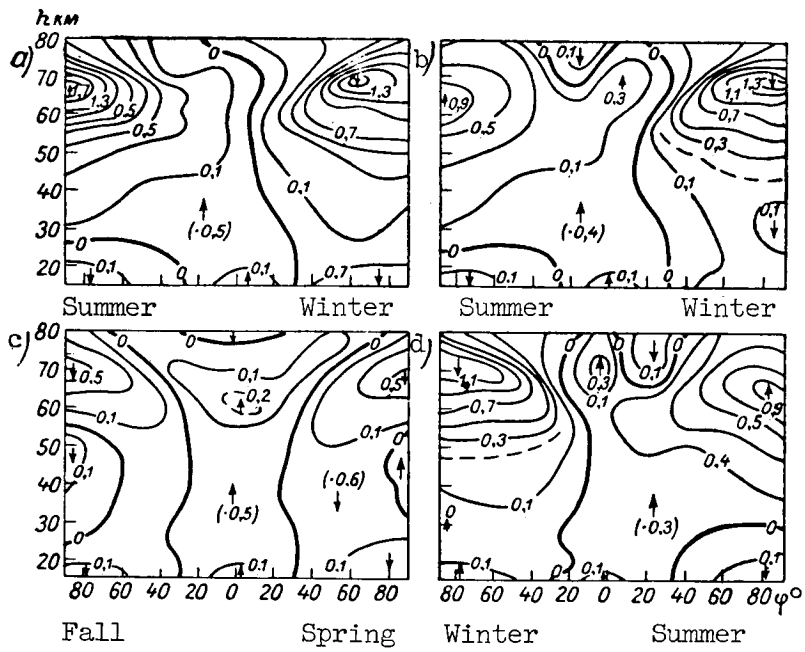

Figure 31.3. Velocity of vertical movements (cm/sec). a--middle of summer and winter; b--end of summer and winter; c--autumn and spring; d--beginning of winter and summer.

There is an extensive region of ascending currents in the summer hemisphere (with the exception of the lower layers of the polar stratosphere) and descending currents in the winter hemisphere. The maximum velocity of ascending currents is about 1.7 cm/sec and is observed at a height of about 70 km near the summer pole; the maximum velocity of descending currents is 1.5 cm/sec and is observed at the same height at a latitude of 65° in the winter hemisphere.

Six weeks later (fig. 31.3b), the maximum velocity of ascending currents was 9 mm/sec over the summer pole, and the maximum velocity of descending movements was 1.3 cm/sec in the winter hemisphere.

In the equinoctial periods (fig. 31.3c) the currents move upward over both poles in the upper part of the stratosphere with a maximum velocity of about 1 mm/sec at a level of 45 km; in the mesosphere, however, the air subsides toward the poles and at a height of about 70 km the velocity attains 5 mm/sec. At heights of about 60 km over the equator there is an extensive region of ascending currents with a velocity of 2 mm/sec.

Murgatroyd and Singleton believe that the mechanism of change of the field of vertical currents shown in figure 31.3b to the form corresponding to figure 31.3c involves the formation and development of a region of ascending currents in the upper layers of the stratosphere in spring, whereas in autumn there is formation and development of a region of air subsidence near the mesopause. Interesting relationships involving vertical movements are shown in figure 36.4.

32. Wind Turbulence as Indicated by Meteor Data

Meteor trails frequently (60 percent of all cases) assume a complex form and experience deflections indicating the existence of air currents of different velocity and direction of movement, resulting in the disruption of the initial linearity of the meteor trail (fig. 32.1). Data presented by N. I. Gur'yev (ref. 200) indicate that in 11 of 24 cases there was such distortion of meteor trails.

It is necessary to distinguish between vertical movements caused by convection and accompanied by atmospheric mixing and wave movements in which the vertical displacements of the air particle occur alternately, first upward and then downward, but in the final analysis its height does not change. Wave movements are possible only in the stable part of the atmosphere and are extremely calm, as is well known to glider pilots. Wave movements sometimes are referred to as "turbulence," which in Slater's opinion can only lead to confusion (ref. 731). For example, Oliver found that almost all meteor trails soon after their appearance become more or less zigzag, indicative of wave movements rather than convection.

Interesting data on wind turbulence in the high layers of the atmosphere were obtained with radio echoes from meteor trails. Greenhow and Neufeld (ref. 412) established, on the basis of observations at Jodrell Bank, that

Figure 32.1. Zigzag meteor trail. Photograph by D. Debabov.

the wind in the lower part of the ionospheric E layer is characterized by "extreme turbulence." The following method is used for such measurements.

Turbulence is investigated by measuring the velocity of "drift" of a meteor trail at two points along it. Greenhow and Neufeld (ref. 412) described the reception of reflected signals at two points (fig. 32.2): at a transmitter (point O) and at a distance of 3.6 or 20 km away (point C). AB is the meteor path. The signals received at points O and C are reflected from the meteor trail at points X and Y. Meteor velocity is

$$V = \frac{XY}{T},$$

where T is the time expended by the meteor in travelling path XY. The difference Δh in the heights of the reflection points and velocity V are related as follows

$$\Delta h = \frac{2(VT)^2}{d} \operatorname{ctg} E,$$

where d and E are notations explained in figure 32.2. Velocity V was determined independently from the rate of increase of the amplitude of the reflected signal, and the height of the reflection point was computed from the time of signal disappearance. A coherent pulse transmitter (carrier frequency 36.3 Mc/s, pulse power 50 kw, pulse frequency 300 cps, pulse duration 30 μ sec) operated using an antenna tilted 45° to the horizon. As a result, the first reflected signal always arrived at transmitter O and the corresponding reflection point was always situated above another. The intermediate frequency and the heterodyne frequency of receiver C were transmitted (through the air) to point O, where the carrier frequency of the reflected

signal arriving at point C was restored. The velocity fluctuations δu_0 and δu_C were determined from the mean hourly radial velocity $\bar{u}_r$ and instantaneous velocities u_0 and u_C as the differences

$$\delta u_0 = \bar{u}_r - u_0,$$
$$\delta u_c = \bar{u}_r - u_c.$$

Greenhow and Neufeld computed the correlation coefficient between δu_0 and δu_C, using formula (ref. 412)

$$g = \frac{\Sigma \delta u_0 \delta u_c}{\left(\Sigma \delta u_0^2 \Sigma \delta u_c^2\right)^{1/2}}, \qquad (32.1)$$

and the experimental error of determination of g, using formula

$$\delta_n = \frac{1 - g^2}{(n-1)^{1/2}},$$

where n is the number of used measurements of the values of the velocity fluctuations δu_0 and δu_C.

The study of radio echoes from persistent meteor trails reveals that the difference in wind velocity at points only 5 km apart can attain 50 m/sec, even in those cases when the wind velocity itself only has a value of this same order of magnitude. For this reason, during wind observations made in a short period of time in a definite part of the sky, it is difficult to detect regular variations of wind velocity because they are masked by wind turbulence. In order to detect regular changes, it is necessary to make at least 100 individual measurements of the drift of meteor trails, responsible for radar echoes, distributed over an area about 200 km in length, 100 km in width and 10 km thick.

Observations of radar echoes from meteor trails reveal large wind variations with height in the region 80-100 km. According to the observations at Jodrell Bank, in many cases there are wind velocity differences up to 50 m/sec at points differing only a few kilometers in height (ref. 411).

Greenhow and Neufeld computed the space correlation functions of the wind velocity field, investigated by simultaneous recording at two stations of radar echoes, from a pair of points in the same meteor trail. They established that the vertical scale of nonuniformities of the velocity field has a value of about 6 km, and the horizontal scale is about 100-200 km (ref. 412). They also observed velocity fluctuations with time at a fixed point of the meteor trail and computed temporal correlation functions. It was established that the temporal scale of velocity fluctuations has a value of the order of 100 min,

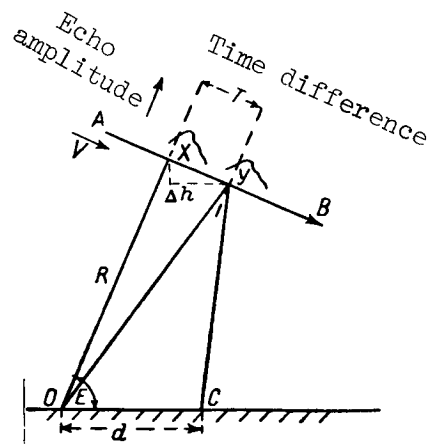

Figure 32.2. Measurement of velocity at two points (O and C) from observation of radio echoes from meteor trail.

Observations made in recent years fully confirm the conclusion drawn by I. S. Astapovich and V. V. Fedynskiy, that in addition to the prevailing winds it is possible systematically to observe currents of the opposite direction, so that the wind roses for the upper layers of the atmosphere resemble a two-bladed fan with unequal blades. The scatter of the observed drift vectors sometimes reaches the opposite direction, which indicates the existence of large deviations of air currents from the main flow. This confirms the turbulent character of air movements in the upper layers of the atmosphere and stratification within the 80-100 km zone; in individual layers there is a change of drift direction and velocity.

Greenhow and Neufeld (ref. 412), using the described method (formula (32.1) and fig. 32.2), investigated the correlation coefficient g between velocity fluctuations at points X and Y as a function of the difference of heights Δh and distance $l = VT$; they used 900 pairs of reflections in this work. They found that with an increase of l the correlation coefficient g decreases to a value $g = 0.2$ when $l = 2$ km, and then changes little. There is a considerably more rapid decrease of g with an increase of Δh. These data are shown in Table 32.1. If curve $g = g(\Delta h)$ is extrapolated, it is found that it intersects the Δh-axis at point $\Delta h = 7$ km. This measurement can be interpreted as the vertical scale of turbulent velocity fluctuations. However, if pairs of reflections corresponding to identical differences of height, but different distances l are compared, it becomes possible to estimate the horizontal dimensions of the turbulent eddies. With a 75 percent probability the computations give a value of more than 60 km, and the most probable dimension of eddies is 150 km. This exceeds by an entire order of magnitude the vertical extent of turbulent formations.

Greenhow and Neufeld (ref. 412) have investigated the diurnal variation of the vertical scale of turbulent fluctuations of velocity. They found that

there is no diurnal variation, and that the scale of turbulence during the day and night is approximately identical. This also applies to the vertical wind gradient.

TABLE 32.1. COEFFICIENT g OF CORRELATION BETWEEN VELOCITY FLUCTUATIONS AS FUNCTION OF DISTANCE l ALONG METEOR PATH AND HEIGHT DIFFERENCE Δh.

l км	Δh км	n	g	$\pm \delta g$
0.6	0.25	39	0.96	0.01
0.67	0.43	319	0.92	0.01
1.5	0.6	76	0.85	0.02
2.5	1.3	88	0.63	0.04
3.5	2.2	101	0.51	0.05
4.5	3.3	104	0.34	0.07
5.5	4.3	86	0.22	0.09
6.5	4.5	44	0.22	0.11
7.8	4.3	72	0.28	0.08

Note: n is the number of observations, δg is the error of g.

The distance l at which the correlation coefficient begins to differ appreciably from unity can serve as a measure of small eddies. In particular, parameter λ, characterizing turbulent diffusion, can be related to g as follows

$$g = 1 - \frac{l^2}{\lambda^2}. \qquad (32.2)$$

Large-scale turbulence is essentially anisotropic, but with a descrease of the size of the eddies the degree of anisotropy decreases. If the smallest eddies of scale λ are isotropic, value λ can be obtained from the dependence of g on l, known from measurements (Table 32.1). However, if there is still partial anisotropy, the value derived in this way can be considered the lower limit for λ.

The parameter λ can be used for determination of the ratio of the minimum scale η of fluctuations to the scale L of the largest eddies. According to Townsend (ref. 768), this dependence has the form

$$\eta^2 = \frac{\lambda^3}{10\sqrt{15}L}. \qquad (32.3)$$

Greenhow and Neufeld (ref. 412) obtained value L = 150 km from their paired observations of radio echoes from meteor trails; from the data cited in Table 32.1 they obtained the estimate λ = 2.4 km. Then, using formula (32.3) they obtained the approximate value 50 m for η.

The velocities of turbulent movements occupy a broad spectrum from large postitive to large negative values. The mean square value V can be computed from the values of the sums

$$\sum \delta u_0^2 \text{ and } \sum \delta u_c^2;$$

it was equal to 28 m/sec for daytime and 23 m/sec for nighttime, a mean value of 25 m/sec. It was also found that the mean velocity of turbulent movements does not depend on the mean wind velocity and the mean vertical wind gradient (from a negative gradient of 1 m/sec·km to a positive gradient of 3 m/sec·km). The mean value of the fluctuations remains unchanged even when the mean wind velocity is equal to zero.

Evaluation of the Reynolds number Re led Greenhow and Neufeld (ref. 412) to the value

$$\mathrm{Re} \simeq \frac{LV}{\nu} = 2 \cdot 10^4.$$

Here ν is the kinematic viscosity which in this region of the atmosphere is equal to approximately 10^5 cm^2/sec. If the turbulence in the upper layers of the atmosphere were isotropic, the Kolmogorov-Obukhov law (2/3 law) should be satisfied. However, an analysis of the dependence of the mean difference $\overline{u_0 - u_c}$ on Δh shows that it does not conform rigorously to this law; this apparently is related to the strongly expressed anisotropic character of the structure of turbulence.

An interesting theoretical analysis of the factors responsible for changes of the Doppler frequency of recorded radio echoes from the Geminids meteor stream, observed by Rao, was made by V. V. Sidorov (ref. 177). This phenomenon can be attributed to the presence of large-scale turbulent formations of the order of 6-10 km at a height of 90 km, without the need for the presence of turbulent movements of a lesser scale, as was indicated in Rao's study.

An investigation of vertical movements is of great interest. Greenhow investigated the degree of horizontality of the wind and demonstrated that at a height of 80-100 km, if there is divergence of the wind from the horizontal, it does not exceed several degrees (ref. 411). Such divergence from the horizontal is too small to permit determining the drift of meteor trails on the basis of observations from a single point in the middle latitudes, the method used by a number of investigators. However, at a wind velocity of 60-80 m/sec, which frequently is observed in the upper layers of the atmosphere, divergence of the wind from the horizontal by only 3-6° would be accompanied by the appearance of a vertical wind component of 3-8 m/sec, which is a large value.

According to measurements made by Greenhow and Neufeld (ref. 412), the mean square values of the vertical component of velocity are 1-2 m/sec.

Thus, according to the results of measurements of reflections of radio waves from meteor trails, the atmosphere in the region of heights 80-100 km is characterized by high turbulence. Large-scale turbulence is anisotropic. The vertical scale is only about 7 km in comparison with 150 km for the horizontal scale.

In this region of heights, air temperature increases rapidly with height. The presence of large positive temperature gradients gives a basis for assuming high stability of the atmosphere at these heights and absence of turbulence. From this point of view the presence of considerable wind irregularities must be considered unexpected. The energy of turbulent movements occurring with a mean square velocity of 25 m/sec is a value of the same order of magnitude as the energy of a homogeneous wind of this same velocity. But in those cases when the mean wind velocity is equal to zero and the mean square velocity of turbulent movements retains its high value of 25 m/sec (it was previously mentioned that from time to time there is such a regime of movements), it is found that all the energy corresponds to turbulent movements. According to measurements made by Greenhow and Neufeld, there is no correlation between the degree of turbulence and the vertical wind gradient, although this could be expected. Greenhow and Neufeld believe that all this indicates an extremely unusual form of turbulence determined by the extremely anisotropic nature of large turbulent bodies. The vertical wind components are extremely small and the mean square values are only 1-2 m/sec. As a result, vertical mixing is extremely difficult, although the wind velocity in two horizontal planes separated by a distance of only 0.4 km can differ by 20 m/sec.

Taking these observations into account, it can be postulated that turbulence at heights of 80-100 km is determined by large plane eddies caused by horizontal disturbances, such as horizontal temperature gradients; in the vertical direction turbulence is greatly suppressed (ref. 412).

33. Turbulent and Vertical Movements in the Ionosphere

The results of experimental investigations of the ionosphere permit us to conclude that the reflecting region is nonhomogeneous; in this region there apparently is a constant replacement of some inhomogeneities by others and their movement (Section 26). The theory of the formation of ionospheric inhomogeneities is extremely complex. The literature describes different mechanisms of the formation of inhomogeneities: instability (turbulent movements) caused by ionospheric winds; convective instability; penetration of interstellar matter, etc. Without considering these mechanisms (several of them will be discussed briefly at the end of the section), we note that for the time being each of them meets with certain objections. The conditions determining the movement of the ionized component of the gas in the ionosphere are of great importance. The clarification of this problem, considered by B. N. Gershman and V. L. Ginzburg (ref. 30), is basic for development of a theory of "ionization winds" and the formation of inhomogeneities in the F region.

Despite the ambiguity of the mechanism responsible for these phenomena, it can be assumed, nevertheless, that the inhomogeneities are caused by isolated electron (or ion) "clouds" moving in a disorderly fashion in different

directions; some clouds are scattered in the ionosphere and others develop in their place. The fading of reflected waves, recorded simultaneously by several surface stations, caused by the movement of clouds, can be related to one another (the pattern of fadings observed at one receiver is repeated at another receiver with some time shift), making it possible to measure the velocity and direction of the drift of the cloud layer as a whole. But a large part of the fadings recorded at different receivers (assuming a sufficiently great distance between them) are completely independent of one another. The latter indicates a disorderly movement of individual clouds relative to one another (movement of a turbulent character). This type of noncorrelating fading curves, obtained at spaced receivers, can be subjected to statistical analysis.

The character of the behavior of the amplitude of a single signal reflected from the ionosphere makes it possible to assume that the electromagnetic field at the point of observation is the result of superposing a mirror-reflected wave and a group of scattered signals. If this supposition is correct, field strength E and the square of the amplitude R can be represented in the form

$$E = a_0 \cos(\omega_0 t - \varphi_0) + \sum_s a_s \cos[(\omega_0 + \Omega_s)t - \varphi_s], \tag{33.1}$$

$$R^2 = \left[a_0 + \sum_s a_s \cos(\Omega_s t - \varphi_s)\right]^2 + \left[\sum_s a_s \sin(\Omega_s t - \varphi_s)\right]^2, \tag{33.2}$$

where $\omega_0 = 2\pi f_0$ is the angular carrier frequency of the incident wave, a_S is the amplitude of the scattered wave, φ_S and Ω_S are its phase and the frequency shift (ref. 3).

In order to check the correctness of the assumption expressed by formula (33.1) it is necessary to compare the distribution curve obtained form observations with the theoretical curve, i.e., to compare the experimentally determined probability density $W_{el}(R)$ of the amplitude R of a signal with the function W(R), computed theoretically for expression (33.1).

As an example figure 33.1 shows a curve illustrating the character of the variability of the amplitude of a single signal reflected from the ionosphere (ref. 3). By reading successive values R_i of signal amplitude from such curves at equal small time intervals τ, it is possible to construct a $W_{el}(R)$ distribution curve. This requires that values R_i be broken down into a finite number of equal intervals ΔR_i and computation of the following ratio for each interval

$$W_{el}(R_i) = \frac{N_i}{\Delta R_i \Sigma N_i}, \tag{33.3}$$

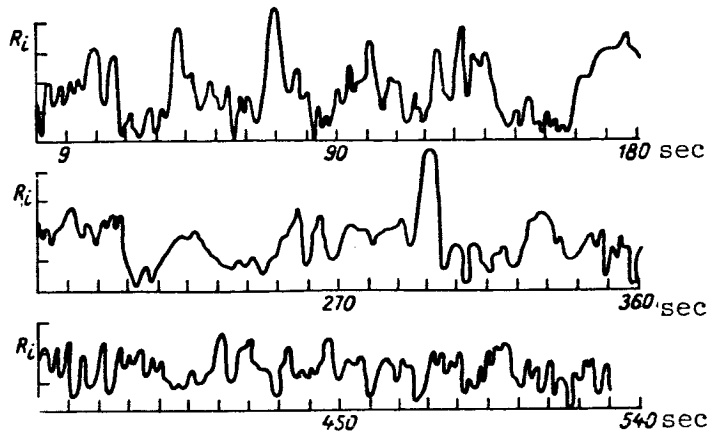

Figure 33.1. Variability of amplitude of single signal reflected from ionosphere.

where N_i is the number of signals having amplitude in the interval $(R_i, R_i + \Delta R_i)$, and ΣN_i is the total number of all measured values R_i. Figure 33.2 (curve 1) shows a $W_{el}(R_i)$ distribution curve constructed by S. N. Mitra (ref. 601).

In the theoretical computation of probability density W(R) it is natural to assume that by virtue of the chaotic character of movements of scattering inhomogeneities the values v_S can have a Gaussian distribution, i.e.,

$$W(v_S) = \frac{1}{\sqrt{2\pi v_0^2}} e^{-\frac{v_S^2}{2v_0^2}}, \tag{33.4}$$

where v_0 is mean square velocity

$$v_0^2 = \overline{v_S^2}. \tag{33.5}$$

The movement of scattering inhomogeneities causes a change of the frequency ω_0 of the incident wave so that the frequency ω_S of a scattered wave has the Doppler shift

$$\Omega_S = \omega_S - \omega_0 = \frac{2\pi v_S}{\lambda}. \tag{33.6}$$

After substituting value Ω_S into (33.4) in place of v_S, it is possible to obtain the energy spectrum of the scattered waves (ref. 5).

The assumption that a group of scattered signals represented by the second term on the right-hand side of formula (33.1) is caused by the effect of scattering inhomogeneities, which experience turbulent movements completely independently of one another, makes it possible to make a theoretical computation of the probability density W(R) by methods well developed in the theory of fluctuating electrical processes. Figure 33.2 shows the theoretical distribution curve of the amplitude of a reflected signal (curve 2), computed by Ratcliffe using formulas from the theory of thermal noise in the resistors of radio receivers with an entrance filter of a certain passband (ref. 690). The good agreement between experimental and theoretical curves confirms the correctness of these initial assumptions. The methods of the theory of fluctuating electrical processes were applied more rigorously for computation of probability density W(R) in a study by Ya. L. Al'pert and A. A. Aynberg (these methods have been discussed most fully in a book by V. N. Bunilovich, ref. 18). This type of computations gives the following formula for probability density (ref. 3)

$$W(R)=\frac{2R}{\sum a_S^2}\,e^{-\frac{R^2+a_0^2}{\sum a_S^2}}\,I_0\left(\frac{2a_0R}{\sum a_S^2}\right), \tag{33.7}$$

where I_0 is a Bessel function of the zero kind, the modified Bessel function

$$I_0(x)=J_0(ix).$$

Analysis of numerous experiments has shown that in most cases the function W(R), computed using formula (33.7), well describes the results of experiments.

On the basis of (33.4)-(33.6) we can write an expression for the total energy of the scattered waves (ref. 3)

$$W_0=\frac{1}{2}\sum a_S^2=\int_0^\infty W(f)\,df \tag{33.8}$$

and for their energy spectrum

$$W(f)=\frac{W_0}{\sqrt{2\pi}\,\sigma_f}\,e^{-\frac{(f-f_0)^2}{2\sigma_f^2}}, \tag{33.9}$$

where

$$\sigma_f^2=(f-f_0)^2=\frac{4v_0^2}{\lambda^2}.$$

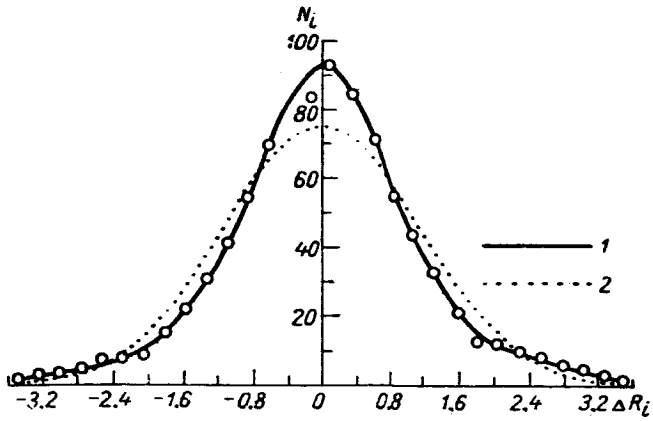

Figure 33.2. Distribution curves of amplitude of reflected signal.
1--computed from observations (fig. 33.1); 2--theoretical.

Determination of the value of the mean square velocity from the results of measurements of the amplitude R of a single signal is possible by several methods. In particular, successive computations of the value $\left(\overline{\frac{dR^2}{dt}}\right)^2$ can be used for this purpose. As pointed out by Ya. L. Al'pert and A. A. Aynberg, the following relation is correct to an accuracy of a factor of the order of $\sqrt{\frac{\pi}{2}}$

$$v_0 = \frac{\lambda \overline{R} \cdot \overline{|\Delta R|_\tau}}{4\pi\tau \sqrt{2W_0^2 + a_0^2 W_0}}, \qquad (33.10)$$

where

$$\overline{|\Delta R|_\tau} = \overline{|R(t) - R(t+\tau)|}$$

is the mean value of the modulus of the difference of successive values of amplitudes R_i and R_{i+1}, measured at any time t and subsequent time $(t + \tau)$.

In those cases when it is possible to neglect the influence of a mirror-reflected wave, we have $a_0 = 0$ and

$$W_0 = \frac{1}{2}\Sigma a_s^2 = \frac{1}{2}\overline{R^2} = \frac{2}{\pi}(\overline{R})^2;$$

from (33.10) we obtain

$$v_0 = \frac{\lambda \overline{|\Delta R|_\tau}}{8\sqrt{2}\tau \overline{R}}. \qquad (33.11)$$

S. N. Mitra, using a formula differing from (33.11) by absence of factor $\sqrt{\frac{1}{2}}$, obtained identical values for v_0 in the E layer and the F layer. These values fell in the range 2-6 m/sec, with an average of 2-3 m/sec. Ya. L. Al'pert and A. A. Aynberg, in analyzing the results of observations using formula (33.10), obtained values v_0 for the F layer varying in the range 0.2-15 m/sec; the most frequently encountered values v_0 apparently were 1-4 m/sec.

The results of recording the phases of reflected signals can also be used for determination of the velocity of turbulent movements in the ionosphere (a discussion of this method can be found in an article by Ya. L. Al'pert, ref. 3). Using this method Findlay (ref. 387) found $v_0 = 0.5$ m/sec for the E layer, and Ratcliffe (ref. 690) obtained $v_0 = 1$ m/sec for the E layer from an analysis of measurements made by Weeks and Brasefield. Mean square velocities of the order of several m per sec have also been obtained by other authors (ref. 287).

Matuura and Nagata (ref. 581) made an attempt to explain the observed properties of ionospheric inhomogeneities from the point of view of turbulence theory. According to their computations, an estimate of the maximum and minimum size of inhomogeneities gives about 1 km and 30 m for the 100 km level, and 30 and 20 km for the 200 km level. The random velocities of the largest and smallest inhomogeneities are about 30 and 8 m/sec for the 100 km level, and about 300 m/sec for large and small inhomogeneities at the 200 km level. Matuura and Nagata believe that these computations agree well with observations, which indicates a possibility of considering the mechanism of formation of ionospheric inhomogeneities on the general background of turbulence of the upper layers of the atmosphere.

Booker (ref. 303) considered in detail the appearance of turbulence in the ionosphere at the meteor level (the principal characteristics of radio echoes from long-lived meteor trails) in the light of the Kolmogorov-Obukhov-Heisenberg turbulence theory. Due to ionospheric turbulence a meteor trail breaks down into eddies of different sizes. The turbulent velocities of large-scale eddies are much greater than the velocities of small-scale eddies, and, therefore, the principal characteristics of the fadings of signals reflected from long-lived meteor trails are determined mostly by movements of large-scale eddies.

Dungey (ref. 364) made a theoretical investigation of the influence of the geomagnetic field on turbulent movements in the ionosphere. The magnetic field acts only on the movement of very large (of the order of 100 km) inhomogeneities of the entire ionospheric plasma as a whole. The geomagnetic field exerts a considerably greater influence directly on charged particles (in particular, on the movement of the electron component of the plasma). On the basis of the equations of motion of charged particles in plasma, Dungey

attempted to estimate the possible relative changes of the electron concentration $\frac{\delta n}{n}$. For the 80 km level he obtained $\frac{\delta n}{n} \approx 4 \cdot 10^{-3}$, and at heights of about 110 km $\frac{\delta n}{n} \approx 5 \cdot 10^{-2}$.

G. S. Golitsin (ref. 408) also investigated the influence of the magnetic field on ionospheric turbulence. Using the equations of magnetohydrodynamics he made estimates showing that at heights of 150-200 km this influence is small, but above 200 km it must be taken into account in a study of dynamic processes.

For the time being very little study has been made of vertical movements in the ionosphere. One of the methods for their investigation is based on the Doppler effect. Ogawa (ref. 640) used this method for determination of velocity of vertical movements in the E region of the order of 0.6-2.5 m/sec. Ratcliffe, Robbins and Thomas (ref. 691), after analyzing vertical ionization distribution curves, discovered no appreciable vertical movements in the F region.

N. M. Boyenkova and Yu. V. Kushnerevskiy (ref. 12a) investigated vertical movements of disturbances in the F2 region, using ionograms obtained at Moscow (Krasnaya Pakhra) and Sverdlovsk stations. They postulate that all vertically moving disturbances in the form of inhomogeneities with a high electron concentration begin at the level of maximum ionization of the F2 layer, or even above this level, and then move downward. But it is less probable that disturbances always reach the level of the E or even the F layer. Boyenkova and Kushnerevskiy note the presence of vertically moving inhomogeneities at all seasons of the year without dependence on the degree of ionospheric disturbance.

CHAPTER 11. THEORY OF AIR CURRENTS

34. Wind in the Stratosphere

34.1. General Patterns of Atmospheric Movements. The wind data discussed in the preceding chapters, obtained by using many independent methods, indicate a complex pattern of air currents in the upper layers of the atmosphere. The character of the prevailing winds is dependent on latitude of the place, height of the layer, season and time of day. In the development of a theory of air currents there are many difficulties involved, particularly those due to the inadequacy of factual data from the upper layers of the atmosphere. Although the study of this problem began recently, there already have been many tens of studies devoted to this problem. However, until now the theory of circulatory processes in the upper layers of the atmosphere essentially remains in its initial stages.

The mechanism of the genesis, development and variations of atmospheric currents in the upper layers has many differences from the mechanisms of wind in the troposphere, but undoubtedly they also have much in common. For this reason we will first mention certain general patterns of atmospheric movements known in meteorology (ref. 67). We will discuss the principal forces acting in the atmosphere.

These forces can be divided into two categories: body or volume forces and surface forces. Whereas in the theory of tropospheric circulation the most important specific body forces to be taken into account are gravity and the deflecting force of the Earth's rotation (ref. 67), tidal forces (lunar and especially solar tides) assume great importance in the thermosphere, and in the ionosphere it is also necessary to consider electrodynamic forces, whose magnitude under certain conditions is comparable to body forces entering into the equations of hydrodynamics. The use of these equations, constituting the basis of the theory of atmospheric currents in the troposphere, is based on the assumption that the atmosphere can be considered a continuous medium (fluid). The validity of applying the equations of hydrodynamics at great heights, where the mean length λ of the free path of molecules is great, should be given special consideration.

Among the most important surface forces acting in the atmosphere is the force of the pressure gradient and viscosity. The principal force leading air masses into movement is the horizontal pressure gradient. Viscosity arises between adjacent layers of a fluid moving at different velocities V. The coefficient of molecular viscosity μ is related to the shearing stress of internal friction τ by the equation

$$\vec{\tau} = \mu \frac{\partial \vec{V}}{\partial z}.$$

In a study of real atmospheric movements, the turbulent character of these movements makes it necessary to replace μ by the coefficient of virtual viscosity A, whose numerical values are tens and hundreds of thousands of times greater than the value of the coefficient of molecular viscosity (ref. 67).

As is known from kinetic theory, the coefficient of molecular viscosity μ is not dependent on density ρ, and therefore its numerical value does not change with height. Accordingly, the kinematic viscosity in the upper layers of the atmosphere (kinematic coefficient of virtual viscosity $k = \frac{A}{\rho}$, the exchange coefficient) considerably exceeds the tropospheric values of kinematic viscosity. According to kinetic theory, the coefficient of kinematic viscosity increases without limit with decrease of ρ. However, this conclusion of kinematic theory cannot be applied to highly rarefied gases, when the length λ of the free path of molecules becomes extremely large. Analysis of data on wind in the ionospheric E and F regions reveals that the coefficient of kinematic viscosity in the ionosphere is appreciably less than can be concluded from kinetic theory, but it is sufficiently great to permit the assumption of the existence in this region of a cellular-meridional structure of general circulation, with a high degree of probability.

Taking into account those forces which were previously considered, we can write the equations of motion. We will introduce a standard coordinate system (the x-axis is directed along a circle of latitude from west to east, the y-axis runs along a meridian from south to north and the z-axis extends vertically upward). The following equations (ref. 67) are correct for the velocity components u, v and w, which are functions of the coordinates x, y, z and of time t

$$\left.\begin{aligned}
&\frac{\partial u}{\partial t}+u\frac{\partial u}{\partial x}+v\frac{\partial u}{\partial y}+w\frac{\partial u}{\partial z}=-\frac{1}{\rho}\frac{\partial p}{\partial x}+(2\omega_z v-\\
&\qquad-2\omega_y w)+\frac{\partial}{\partial z}\left(k_z\frac{\partial u}{\partial z}\right)+k_0\left(\frac{\partial^2 u}{\partial x^2}+\frac{\partial^2 u}{\partial y^2}\right)\\
&\frac{\partial v}{\partial t}+u\frac{\partial v}{\partial x}+v\frac{\partial v}{\partial y}+w\frac{\partial v}{\partial z}=-\frac{1}{\rho}\frac{\partial p}{\partial y}-2\omega_z u+\\
&\qquad+\frac{\partial}{\partial z}\left(k_z\frac{\partial v}{\partial z}\right)+k_0\left(\frac{\partial^2 v}{\partial x^2}+\frac{\partial^2 v}{\partial y^2}\right)\\
&\frac{\partial w}{\partial t}+u\frac{\partial w}{\partial x}+v\frac{\partial w}{\partial y}+w\frac{\partial w}{\partial z}=-\frac{1}{\rho}\frac{\partial p}{\partial z}+2\omega_y u+\\
&\qquad+\frac{\partial}{\partial z}\left(k_z\frac{\partial w}{\partial z}\right)+k_0\left(\frac{\partial^2 w}{\partial x^2}+\frac{\partial^2 w}{\partial y^2}\right)-g
\end{aligned}\right\} \qquad (34.1)$$

Here ω_y and ω_z are the components of the vector $\vec{\omega}$ of the Earth's angular velocity of rotation, directed along the rotational axis from south to north ($\omega_x = 0$, $\omega_y = \omega \cos\varphi$, $\omega_z = \omega \sin\varphi$, where φ is latitude). The solution of the extremely complex system of equations of motion (34.1) involves great difficulties. By using estimates of the order of magnitude of the individual terms and

neglecting the small terms, the system of equations (34.1) can be rewritten in the following simplified form

$$\left.\begin{aligned}
\frac{du}{dt} = \frac{\partial u}{\partial t} + u\frac{\partial u}{\partial x} + v\frac{\partial u}{\partial y} + w\frac{\partial u}{\partial z} = -\frac{1}{\rho}\frac{\partial p}{\partial x} + \\
+ 2\omega_z v + \frac{\partial}{\partial z}\left(k_z \frac{\partial u}{\partial z}\right) \\
\frac{dv}{dt} = \frac{\partial v}{\partial t} + u\frac{\partial v}{\partial x} + v\frac{\partial v}{\partial y} + w\frac{\partial v}{\partial z} = -\frac{1}{\rho}\frac{\partial p}{\partial y} - \\
- 2\omega_z u + \frac{\partial}{\partial z}\left(k_z \frac{\partial v}{\partial z}\right) \\
\frac{dw}{dt} = 0 = -g - \frac{1}{\rho}\frac{\partial p}{\partial z}
\end{aligned}\right\} \qquad (34.2)$$

Estimates (ref. 67) show that the first two equations are satisfied to an accuracy to 0.01 and the third to an accuracy of 0.001.

If for great heights we neglect the influence of internal friction on atmospheric movement and consider the case of a stationary or quasi-stationary linear horizontal movement, when

$$\frac{du}{dt} = \frac{dv}{dt} = 0,$$

equation (34.2) can be replaced by the following system

$$\left.\begin{aligned}
-\frac{1}{\rho}\frac{\partial p}{\partial x} + 2\omega \sin\varphi\, v_g = 0 \\
-\frac{1}{\rho}\frac{\partial p}{\partial y} - 2\omega \sin\varphi\, u_g = 0 \\
-\frac{1}{\rho}\frac{\partial p}{\partial z} - g = 0
\end{aligned}\right\} \qquad (34.3)$$

The first two equations of this system represent geostrophic relationships and determine the geostrophic wind; its components along the coordinate axes will be denoted u_g and v_g. A geostrophic wind occurs when there is an equilibrium between the deflecting force and the pressure gradient. The geostrophic wind blows along the isobars, and its direction is perpendicular to the direction of the pressure gradient. The total velocity of the geostrophic wind

$$V_g = \sqrt{v_g^2 + u_g^2}$$

is determined using formula

$$V_g = \frac{1}{2\rho\omega \sin\varphi}\frac{\partial p}{\partial n}. \qquad (34.4)$$

In the northern hemisphere the deflecting force is directed to the right in relation to the velocity of movement, and therefore the geostrophic wind in the northern hemisphere blows along the isobars in such a direction that the region of high pressure remains to the right of the wind direction. In the southern hemisphere the region of high pressure remains to the left of the direction of movement.

The relationship between the velocity of the geostrophic wind and the slope of the isobaric surfaces is frequently used in computations of wind in the upper layers of the atmosphere. This relationship can be described by a simple expression. For example, if the wind direction coincides with the direction of the y-axis so that $u_g = 0$, from (34.3) we have

$$2v_g\omega \sin\varphi = \frac{1}{\rho}\frac{\partial p}{\partial x},$$

$$-g = \frac{1}{\rho}\frac{\partial p}{\partial z}.$$

By multiplying the first of these equations by dx and the second by dz and combining both equations, we obtain

$$\frac{dp}{\rho} = 2v_g\omega \sin\varphi\, dx - g\, dz.$$

At an isobaric surface the pressure is constant (dp = 0), and therefore the equation for this surface can be represented in the form

$$\frac{dz}{dx} = \frac{2\omega \sin\varphi}{g} v_g. \qquad (34.5)$$

Introducing the dynamic height H of the isobaric surface using formula

$$H = \frac{gz}{10},$$

we obtain as the slope of the isobaric surface

$$\frac{dH}{dx} = \frac{1}{10} 2v_g\omega \sin\varphi,$$

hence

$$v_g = c\frac{dH}{dx}, \qquad (34.6)$$

where $c = \frac{10}{2\,\omega \sin\varphi}$ is a coefficient constant for a particular latitude. Thus, the velocity of the geostrophic wind is directly proportional to the slope of the isobaric surface.

We will not discuss here other aspects (ref. 196) of the problem of the influence of the Earth's rotation on atmospheric circulation.

We now will consider the problem of wind change with height. As is well known, wind change with height is related closely to the presence of a horizontal gradient of temperature T in the layer. After introducing into consideration the mean temperature T_{mean} of a layer of the thickness Δz, the barometric formula (after differentiating it for x and y) and formulas (34.3) and (34.4) for the velocity of the geostrophic wind will easily give the following equations (ref. 67)

$$\left.\begin{aligned}(u_g)_z &= \frac{T}{T_0}(u_g)_{z_0} - \frac{T_g}{2\omega \sin\varphi T_m^2}\Delta z \frac{\partial T_m}{\partial y}\\ (v_g)_z &= \frac{T}{T_0}(v_g)_{z_0} + \frac{T_g}{2\omega \sin\varphi T_m^2}\Delta z \frac{\partial T_m}{\partial x}\end{aligned}\right\} \qquad (34.7)$$

Consequently, the components of the geostrophic wind $(u_g)_z$ and $(v_g)_z$ at the level z are equal to the components of the geostrophic wind at the level z_0, multiplied by the ratio $\frac{T}{T_0}$, plus additional components--the thermal wind components.

On the basis of (34.7) we obtain an approximate formula for the total velocity of the geostrophic wind $(V_g)_z$ at the level z, sufficiently precise for slow changes of temperature with height

$$(V_g)_z \simeq \frac{1}{2\rho\omega \sin\varphi} G_0 + \frac{g\Delta z}{2\omega \sin\varphi T_m}\Gamma_m, \qquad (34.8)$$

where G_0 is the value of the horizontal pressure gradient at the lower level, Γ_{mean} is the horizontal gradient of the mean temperature of the layer. Formula (34.8) can be written as

$$(\vec{V}_g)_z = (\vec{V}_g)_{z_0} + \Delta\vec{V}, \qquad (34.9)$$

where $\Delta\vec{V}$ is the vector of the thermal wind. It is easy to see that the thermal wind in the northern hemisphere is directed at a right angle to the right from $\vec{\Gamma}_{mean}$, i.e., along the mean isotherms of the layer (the region of cold remains to the left). When the isobars and isotherms coincide (i.e., in the absence of an advective transport of heat), the wind intensifies with height without changing direction; in the region of heat advection the geostrophic wind turns to the

right with height, and in the region of advection of cold--to the left. If the horizontal gradient of the mean temperature of the layer $\vec{\Gamma}_{mean}$ is directed opposite to $\vec{G}_0$, and the thermal wind $\Delta\vec{V}$ is directed opposite to the geostrophic wind at the lower level, the geostrophic wind weakens with height, at some level becoming equal to zero; it then assumes an opposite direction, gradually intensifying with height (provided the initial condition relative to the arrangement of vectors $\vec{G}_0$ and $\vec{\Gamma}_{mean}$ is maintained at all these heights). The change of the geostrophic wind in all remaining cases of intermediate positions of $\vec{\Gamma}_{mean}$ relative to $\vec{G}_0$ can easily be explained on the basis of the principal models (ref. 67). These models will be used in a study of the air currents in the upper layers of the atmosphere.

These results of wind measurements at great heights show that the air currents in the upper layers of the atmosphere in many cases have a character close to zonal circulation. It follows from equation (34.7) for the thermal wind that

$$\Delta u = -\frac{Tg\Delta z}{2\omega \sin\varphi T_m^2}\frac{\partial T_m}{\partial y}.$$

If it is assumed that in the upper layers of the atmosphere the temperature as an average increases from the pole to the equator ($\frac{\partial T}{\partial y} < 0$), the thermal wind is directed from west to east. When the temperature gradient has the opposite sign, the thermal wind is directed from east to west. Thus, purely zonal circulation (west-east transport) is a result of the dependence of the quantity of solar heat received by the atmosphere on latitude. In the following sections we will discuss computations of zonal circulation in the upper layers of the atmosphere.

A theory of meridional circulation in the upper layers of the atmosphere is now being developed.

The problem of the statistical distribution of wind velocity is of definite interest in an investigation of the wind field in any region of the atmosphere (in the troposphere, stratosphere and the higher layers). This problem has been studied most fully for the troposphere (ref. 47); its study for the upper layers of the atmosphere is only beginning.

Experiments on rotating models (ref. 775) and comparisons of atmospheric circulation on the Earth with circulation in the atmospheres of other planets--Jupiter, Saturn, Uranus and Neptune (ref. 676)-- are of considerable interest in relation to investigation of the general patterns of atmospheric movements.

34.2. Air Currents in the Lower Part of the Stratosphere. We will now discuss various models of air currents in the upper layers of the atmosphere; many of these models are empirical or semiempirical and only a few are theoretical in the proper sense of the word (wind computations from a given temperature and pressure field).

A thorough theoretical investigation of stratospheric zonal flow to the 25-30 km level, made in 1955-1956 by Kochanski (refs. 534 and 535), is an attempt to generalize available data on temperature and wind for the purpose of determining the structure of the temperature and wind field; his study is typical of many in this field. The geostrophic wind is computed on the basis of the known temperature distribution for supplementing wind data. However, wind data are used for more precise determination of the temperature field; the same relationships for the geostrophic wind are used in the computations.

Kochanski (ref. 534) constructed vertical cross sections of mean zonal flow for four seasons (January, April, July and October) along the meridian 80°W. The velocity of geostrophic zonal flow was computed from the mean monthly pressure pattern charts.

Figure 34.1a-d shows the isotachs of the westerly and easterly components of the mean geostrophic flow. The wind field cross section for January (fig. 34.1a) clearly shows three regions of maximum velocity: (1) a westerly flow in the middle latitudes, associated with the mean position of the polar tropopause; (2) a westerly flow in the stratosphere near 70°N, observed during the polar night, and (3) a subtropical maximum of the easterly wind near 20°N in the lowest part of the stratosphere.

On the cross section for April (fig. 34.1b) the westerly middle-latitude flow has three individual "centers" of maximum wind velocities, situated at 50, 34 and 25°N and at heights of 10, 12 and 13 km, respectively. On the October cross section (fig. 34.1d) there are two such centers, situated at 49 and 37°N and at heights of 10.7 and 11.8 km, respectively. However, as pointed out by Kochanski, the number of centers and their position apparently change from year to year (ref. 534).

The mean flow in July (fig. 34.1c) is characterized by a considerable decrease in the size of the region with prevailing westerly winds and a weakening of the middle-latitude maximum to 25 m/sec.

In 1956 Kochanski and Wasko published a similar investigation for the mean distribution of the wind at the 200, 100, 50 and 25 mb levels for January, April, July and October for North America and the ocean areas adjacent to it (ref. 535). Using data for 85 stations for a four year period, they constructed mean monthly pressure pattern charts for the 200, 100, 50 and 25 mb surfaces. These charts were used to compute the geostrophic wind. Important conclusions were drawn characterizing the general circulation.

It was found that in July over North America there is, on the average, a sharp change from a westerly flow at the 100 mb level to an easterly flow at the 50 mb level. At the 50 and 25 mb levels there are two maxima of the easterly wind: one near the polar region and the other in the subtropics (15-25°N).

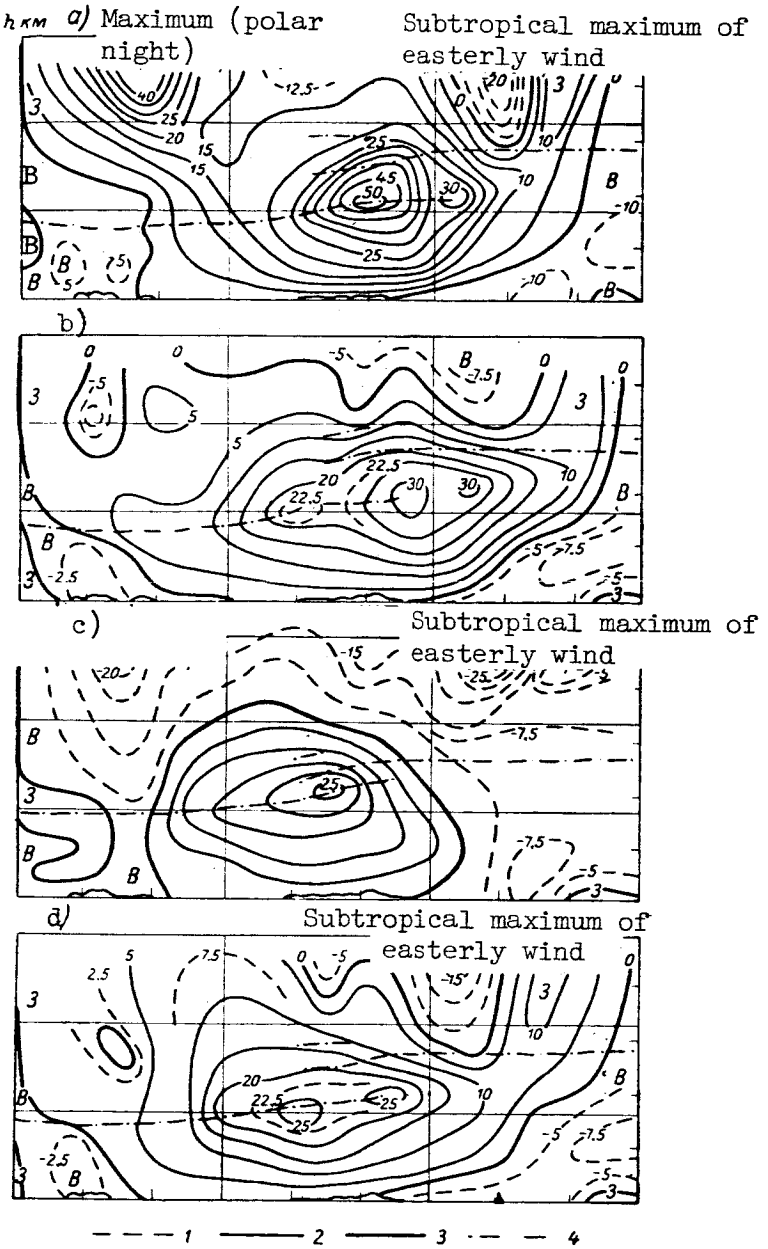

Figure 34.1. Zonal components of the mean geostrophic wind along 80° W. (a) January, (b) April, (c) July, (d) October. Isotachs in m/sec. (1) Easterly wind, (2) westerly wind, (3) region of wind reversal, (4) tropopause. B = E, З = W, C = N and Ю = S in this and following illustrations.

There is a strong mean westerly wind at the 100 mb level in January; however, this wind weakens rapidly with height up to the 25 mb level. At these latitudes the mean flow at the 50 and 25 mb levels have a direction between northerly, westerly and southwesterly. In the polar region or near it (70-80°N), there is a strong maximum of the westerly wind at the 50 and 25 mb levels.

In October the 100 mb surface over the United States has a strong westerly flow, and the 50 mb surface is situated a little below the level at which the flow becomes primarily easterly. The 25 mb surface over the southern United States already shows an easterly wind.

Finally, the wind over the United States in April at the height of the 100 mb surface is westerly, but the transition layer to easterly is lower (ref. 535).

34.3. Cellular Structure of the Atmosphere. A model of vertical circulation in the stratosphere over cyclones and anticyclones, proposed in 1951 by L. R. Rakipova (ref. 164), is of great interest. In 1958 Faust (ref. 382) considered a similar model for the problem of the possible existence of layers in the stratosphere, characterized by high wind velocities. The basic theses of these studies are as follows.

An important problem in the dynamics of the atmosphere is the study of the prerequisite conditions for pressure formations and deviation of the wind from a gradient wind. The spreading of air in the lower layers of the atmosphere from regions of high pressure (anticyclones) should be accompanied by an antigradient influx of air in the higher layers. Similarly, there should be an antigradient outflow of air over a cyclone. Faust attempted to determine the height to which descending movements and adiabatic heating of the air occur in anticyclones and to which ascending movements accompanied by cooling occur in cyclones. Faust found (ref. 382) that at a height of approximately 10 km there is a layer (which he called the "zero layer") without vertical movements. The existence of a zero layer at this level, according to Faust, follows from the fact that, in the course of the day, the heating in anticyclones attains heights of 10.5 km; farther aloft there is cooling of the air, whereas in cyclones the

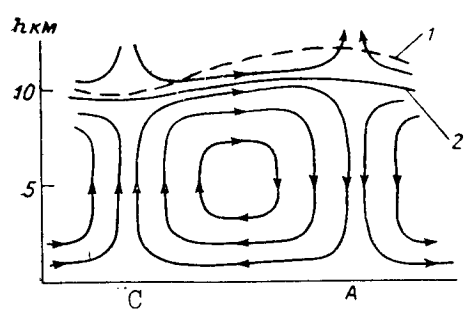

Figure 34.2. Model of vertical and nongradient horizontal circulation over regions of cyclones (C) and anticyclones (A). (1) tropopause, (2) zero layer.

cooling extends to a height of 9.5 km and heating occurs in the higher layers. The maximum horizontal pressure gradients corresponding to maximum wind velocities should occur in the zero layer.

This layer of the wind velocity maximum is situated approximately 1 km below the tropopause. The changes in the height of the tropopause and zero layer as a function of latitude and season of the year occur parallel to one another.

On the basis of such concepts and known meteorological data, Faust (ref. 382) devised a model of vertical and nongradient horizontal circulation over regions of cyclones and anticyclones (fig. 34.2). Extending this model above the tropopause, Faust proposed a model of a cellular structure of the atmosphere to great heights (fig. 34. 3). In this model there is a vertical alternation of regions of high and low pressure. At a height of 20 km there is a layer of minimum horizontal pressure gradients, and at some still greater height it is postulated that there is a second zero layer and a corresponding wind velocity maximum in the stratosphere.

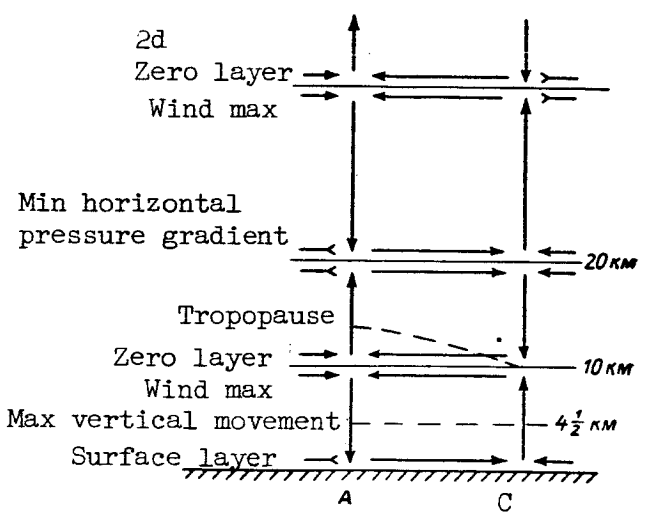

Figure 34.3. Model of cellular structure of atmosphere.

As noted earlier, data on the variability of the curves of the vertical distribution of ozone can be used for determining the position of regions of alternating rising and subsidence of air.

This model of a cellular structure of the atmosphere presented by Faust coincides completely in its basic features with a model of the structure of the atmosphere proposed earlier by L. R. Rakipova (ref. 164) as an explanation of the mechanism of the relationship between the troposphere and the upper layers of the atmosphere.

34.4. Energy of Stratospheric Movements. The general problems of the energy of atmospheric movements were considered in studies by A. A. Dorodnitsin,

V. V. Shuleykin, Kh. P. Pogosyan (ref. 148), L. R. Rakipova, M. I. Budyko and G. V. Gruz (ref. 43), but little attention was given to stratospheric processes in particular.

The distribution of temperature and the movement of the air medium in three-dimensional space is dependent on energy balance. If friction is neglected, this consists of four kinds of energy: solar radiant energy, terrestrial radiant energy, energy from other sources and the energy of motion (advection, convection). The first form of energy is basic and can be evaluated relatively simply. It is more difficult to evaluate the second form of energy, but much research is being done on this problem. The third form of energy, including the latent heat of water vapor condensation, is important for the troposphere, but is unimportant in the stratosphere. At present it is extremely difficult to make a precise evaluation of the energy of motion.

Under certain conditions the last two forms of energy can be neglected in comparison with the first two: under these conditions the temperature of the atmosphere will be close to the temperature of radiant equilibrium. However, such conditions are not frequently encountered in the atmosphere.

We will now consider the results of one of the few studies devoted directly to the energy of stratospheric movements. Starr (ref. 740) made an attempt to explain the processes maintaining the kinetic energy of stratospheric movements.

He writes the energy equation in the following form

$$\frac{\partial}{\partial t}\int \rho \frac{u^2+v^2}{2}\,d\tau = \int \rho \frac{u^2+v^2}{2} V_n\,dS + \int p \operatorname{div} \vec{V}_h - D. \qquad (34.10)$$

Here u and v are the wind velocity components, ρ is density, p is pressure, $d\tau$ is an element of volume, dS is an element of surface of this volume, $\vec{V}_h$ is the vector of the horizontal component of wind velocity, V_n is the normal wind component and D is the dissipation of kinetic energy.

Under the condition that kinetic energy does not change during a sufficiently long period of time, the energy equation can be written in the form

$$D = A + S, \qquad (34.11)$$

where A denotes the first term on the right-hand side of equation (34.10), characterizing the flux of the kinetic energy across the boundary, and S is the second term, characterizing the work of expansion.

The area of the lower base of the stratosphere will correspond to a sufficiently large region of the lower surface of the volume. In this case the

normal velocity component is the vertical velocity component w. We therefore can write

$$A = \int \frac{u^2 + v^2}{2} \rho w \, d\sigma, \tag{34.12}$$

where $d\sigma$ is an element of horizontal area.

For a sufficiently long interval of time

$$\int \rho w \, d\sigma = 0.$$

Under this condition the flux of kinetic energy A will differ from zero only in the case where there is correlation between ρw and $\frac{u^2 + v^2}{2}$. For example, if $A > 0$, ρw should be greater than zero. In addition, it is required that large values of positive w coincide with regions of large values of kinetic energy.

Starr proceeds as follows for evaluation of the expansion S. It can be shown that equation (34.10) is correct only in a case when

$$\int \operatorname{div} p \cdot \vec{V}_h \, d\tau = 0.$$

Under this condition the following equation is correct

$$\int p \operatorname{div} V_h \, d\sigma = -\int V_h \Delta_h p \, d\sigma. \tag{34.13}$$

It is easy to see that for the work of expansion we can write the following expression

$$S = \int p \operatorname{div} \vec{V}_h \, d\tau = \int \left[\int p \operatorname{div} \vec{V}_h \, d\sigma \right] dz.$$

However, it is difficult to compute $\vec{V}_h$, and Starr therefore uses formula (34.13) for estimating S. Proceeding from the Euler formula, we obtain the relation

$$w = \frac{dp}{dt} = \frac{\partial p}{\partial t} + \vec{V}_h \cdot \nabla_h p + w \frac{\partial p}{\partial z}. \tag{34.14}$$

Using equations (34.13) and (34.14) we obtain

$$S = -\int w \, d\tau + \frac{\partial}{\partial t} \int p \, d\tau + \int w \frac{\partial p}{\partial z} \, d\tau. \tag{34.15}$$

The second and third integrals on the right-hand side of equation (34.15) become equal to zero because pressure remains constant over a sufficiently long interval of time. Similarly, the vertical transport of mass in a long interval of time is equal to zero. Therefore

$$S = -\int w\, d\tau = -\int_0^{p_0} \int w\alpha\, d\sigma\, dp,$$

where $\alpha = \frac{1}{\rho g}$, p_0 is pressure at the isobaric surface used as the lower base of the stratosphere and $d\sigma$ is an element of area of this surface.

But from the continuity equation

$$\frac{\partial w}{\partial p} + \operatorname{div} \vec{V}_h = 0$$

it follows that for a particular isobaric surface

$$\int w\, d\sigma = 0,$$

if total divergence is equal to zero. In this case the condition of work of expansion is different from zero only when there is a correlation between α and w. For example, in a case when large values α correspond to negative values w, the work of expansion is positive.

Starr concludes (ref. 740) that the velocity of vertical movements plays a decisive role in the transport of kinetic energy in the stratosphere and in maintaining it (against frictional forces).

35. Air Currents in the Mesosphere and Lower Layers of the Thermosphere

For the most part this section is devoted to the theory of atmospheric circulation in the mesosphere (55-85 km). However, the system of winds in the mesosphere in many respects is closely related to winds in the stratosphere and in the lower layers of the thermosphere. For this reason, while discussing winds in the mesosphere, we will also consider some theoretical problems applying to stratospheric circulation (e.g., the theory of meridional circulation in the stratosphere and mesosphere) and the circulation in the lower layers of the thermosphere (to the 100 km level).

35.1. Empirical Models. The empirical model devised by V. V. Fedynskiy, which is one of the first attempts to generalize data on wind at great heights, and the later empirical model devised by Sheppard for a still greater range of heights, are of great interest.

In 1944 V. V. Fedynskiy proposed a circulation model based on an analysis of observations of meteor trails in Tadzhikistan, and also data on noctilucent and nacreous clouds and auroras (ref. 200). Fedynskiy pointed out the possible existence of independent circulation of the upper layers of the atmosphere, resembling the system of trades and antitrades in the troposphere. The movements in the 30-80 km zone in general have a westward direction (NW-W-SW), and to a certain degree can be compared with the trades in the troposphere. In the higher layers there is a predominance of easterly and northeasterly movements, indicating the reverse movement of air masses rising over the low latitudes, similar to the antitrades of the troposphere. On the whole, the layers of the atmosphere from 30 - 100 km form a thick and complex air circulation system, which can be represented schematically as a system of stratospheric trades and stratospheric antitrades compensating them. The discontinuity between these two prevailing systems of air currents is situated at a height of about 82-83 km.

In addition to the presence of such a general pattern in the high layers of the atmosphere, indicated by V. V. Fedynskiy, there should also be a number of local centers and zones of higher and lower pressure. These local pressure systems give rise to extremely rapid and varied air currents created by large pressure gradients at insignificant distances apart. Centers of high and low pressure are formed under the influence of solar rays in the daytime hemisphere, and gradually break up during the first half of the night.

We will now consider the Sheppard model (ref. 187) proposed in 1949. This rough model of the vertical distribution of zonal winds in the middle latitudes is shown in figure 35.1. The Sheppard model is a generalization of presently available observations of pilot balloons, smoke clouds, meteor trails and noctilucent clouds. On the graph the height is shown at a logarithmic scale to estimate directly the transported air masses. The right part of the graph shows the direction of the meridional temperature gradient computed on the assumption that the observed winds are close to geostrophic.

The models of the distribution of the zonal wind in winter and summer in the northern hemisphere, cited in Section 28 (figs. 28.3 and 28.4), are among the empirical models of circulation in the stratosphere, mesosphere and lower layers of the thermosphere. These models were developed using sounding data generalized in 1960 by American geophysicists (ref. 418).

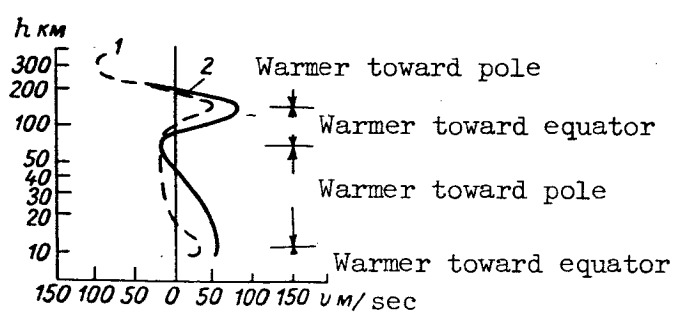

Figure 35.1. Approximate vertical distribution of zonal wind. (1) Summer, (2) winter.

35.2. Temperature Field Determined Using Wind Data. An interesting attempt to devise a model of circulation in the upper layers of the atmosphere was made in 1951 by Kellogg and Schilling. Although with respect to specific content their work now is obsolete in many ways, in methodological respects it still retains its importance. In this model (ref. 517) they generalized various experimental data and applied certain theoretical concepts, and determined vertical distribution of temperature and the zonal wind component for several latitudes (0, 30, 60 and 90°N and S, separately for summer and winter). Information on wind and pressure distribution to a height of 100-120 km, available at that time, was used by Kellogg and Schilling as initial data. These data were used to compute the possible vertical distribution of air temperature at these latitudes, using the formulas discussed in Section 34. They then attempted to use these data to derive a model of a circulatory system which would agree with the maximum range of experimental wind data. As a result, Kellogg and Schilling obtained a conjectural model of the general circulation of the atmosphere at heights up to 120 km, shown in figure 35.2.

Using the method employed by Kellogg and Schilling, we will become acquainted in greater detail with the work of Deb, considered in the next section.

Essentially the same method was used in the work of Pant, which we will now consider.

In 1956 a study by Pant appeared which was devoted to the theory of winds in the upper layers of the atmosphere (ref. 667). Pant's computations apply to the same region of heights (20-100 km) as the model of Kellogg and Schilling,

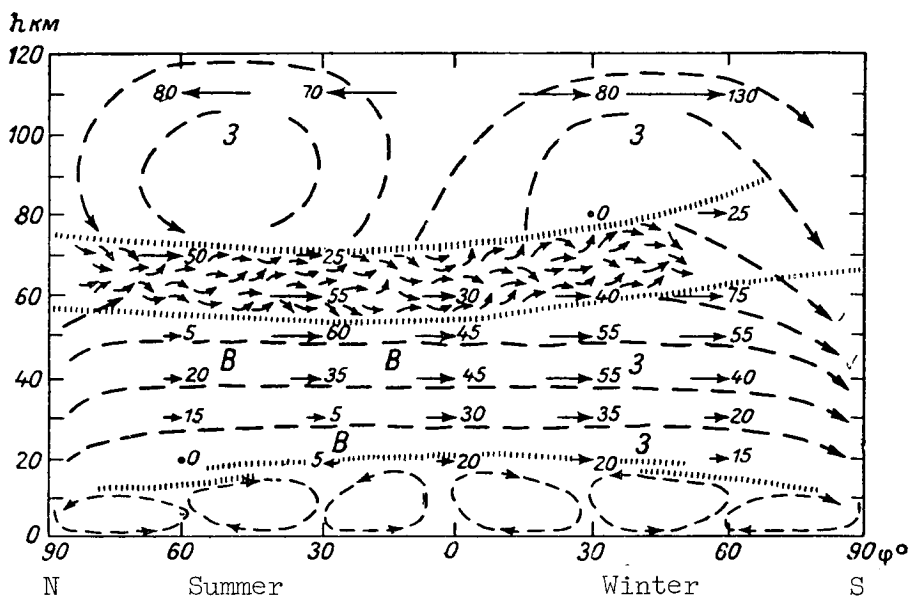

Figure 35.2. Postulated model of general circulation of the atmosphere to a height of 120 km. Size of arrows proportional to wind velocity; figures at arrows denote wind force in m/sec; B--easterly, З --westerly wind.

but they were made five years later, and therefore were based on considerably newer and more complete data. The general approach used in Pant's computations was as follows.

He determined the field of winter and summer temperatures, using wind data and taking into account mean rocket curves of pressure. The computations were based on the assumption that the wind is geostrophic. The temperatures determined by this method agreed well with direct observations. This indicates that there is correlation between observations of the distribution of temperature and wind. The wind cross sections constructed in the process of the study were compared by Pant with wind distributions indicated in earlier published studies and found to be in good agreement. On the basis of the determined wind distributions and certain theoretical concepts, Pant constructed a model of the circulatory system in the stratosphere and above it.

TABLE 35.1. TEMPERATURES (°K) COMPUTED (PANT) FOR 30°N AND OBSERVED (GUTENBERG) FOR 32°N.

Height, km	Summer		Winter	
	comp	obs	comp	obs
15	211	208	211	212
25	229	225	230	221
35	248	245	249	235

TABLE 35.2. TEMPERATURES (°K) AT 40°N COMPUTED (PANT) AND OBSERVED (BRASEFIELD).

Height, km	Summer		Winter	
	comp	obs	comp	obs
15	214	216	215	221
25	231	226	228	221
35	250	243	245	241

Tables 35.1 to 35.3 show the temperatures computed by Pant for different latitudes and heights; these temperatures are compared with observations (the acoustic measurements of Gutenberg and Brasefield, ref. 306) and measurements by Elterman by the searchlight method of sounding the atmosphere, ref. 378). The discrepancy does not exceed 15°, and in many cases it is much less. These data are of interest from the point of view of discussion of seasonal variations of temperature. The results of an analysis of the computed and observed temperatures made by Pant (ref. 667) are shown in Table 35.4.

At heights of 35-45 km the seasonal temperature change (i.e., the difference $T_{summ}-T_{wint}$, where T_{summ} is the summer temperature and T_{wint} is the winter temperature) increases with height at all latitudes, and at a particular level increases with an increase of latitude (at some heights--to 50-60°N and at other heights, to the pole itself). Computations by Pressman (ref. 680) indicate that such variations can be attributed to heating of the atmosphere as a result of absorption of ultraviolet solar radiation by ozone: this absorption also increases with latitude and height. In addition, Pant believes (ref. 667) that the total seasonal change of temperature in this region also depends on absorption by water vapor and carbon dioxide gas, but their influence should be small compared with the influence of ozone.

TABLE 35.3. TEMPERATURES (°K) COMPUTED (PANT) FOR SUMMER AT 30°N AND OBSERVED (ELTERMAN, JUNE 1952) OVER NEW MEXICO IN THE UNITED STATES.

Height, km	Computed	Observed
15	211	205
25	229	219
35	248	248
45	293	285
55	270	280
65	250	235

Table 35.4 also shows that at all latitudes to the north of 10°N and above the 20 km level the summer temperatures are greater than the corresponding winter temperatures. According to Kellogg and Schilling (ref. 517), this can be attributed to seasonal variations of the zenith distance of the Sun, the quantity of ozone and longwave terrestrial radiation.

Other interesting data obtained by Pant (ref. 667) include the seasonal changes of temperature: heating from summer to winter at the 15 km level between 0-50°N and at the 25 km level between 0-10°N. Such a warming of air from summer to winter at a height of 15 km between 0 and 50°N is also shown in data analyzed by Kochanski (ref. 543). The same warming is indicated by the data in Tables 35.1 and 35.2 and by the measurements by Conover and Wentzien (ref. 339). The explanation of this warming can be related to the presence of descending currents from the higher layers in winter. It is also impossible to exclude factors associated with radiation processes. According to Dobson, Brewer and Quaylong (ref. 60), the increase of the percentage of water vapor and carbon dioxide gas in comparison with ozone should lead to a temperature decrease corresponding to radiation equilibrium. The reason for the low temperatures at heights somewhat exceeding the height of the tropopause, therefore,

TABLE 35.4. DIFFERENCES OF SUMMER AND WINTER TEMPERATURES AS FUNCTION OF HEIGHT AND LATITUDE.

Height, km	North latitude, degrees									
	Equator	10	20	30	40	50	60	70	80	North pole
15	−3.4	−2.8	−2.6	−3.6	−3.3	−1.7	+4.1	+9.6	+16.7	+18.8
25	−4.5	−3.5	+0.2	+4.5	+8.9	+14.9	+22.2	+20.9	+14.9	+14.2
35	+7.7	+8.2	+8.6	+8.3	+14.9	+19.8	+21.1	+25.4	+28.0	+30.6
45	+17.0	+25.6	+36.3	+45.2	+57.5	+60.4	+57.4	+54.0	+51.4	+49.0

can be the presence of large quantities of water vapor at the corresponding heights and latitudes. However, such an assumption requires confirmation by observational data.

Possible seasonal variations of temperature at great heights, similar to those determined by Pant (ref. 667), can be judged from figure 35.3. Above the ozonospheric temperature maximum (above 45-50 km) the summer temperatures to the north of 30°N are lower than the winter temperatures (fig. 35.3a and 35.3c). The same result was obtained by Kellogg and Schilling (ref. 517). Brasefield (ref. 308), studying wind data obtained by the acoustic method, drew a similar conclusion: there is warming of the air in winter at heights of 53-73 km in the region between 30 and 40°N. Further confirmation of the reality of such warming is found in the work of Elterman (ref. 378), who obtained, from observations by the searchlight method of sounding the atmosphere, a clear indication of warming from June to October at heights of 45-68 km over New Mexico. All this gave Pant basis for assuming that the temperature increase from summer to winter, which he found in the upper part of the ozonosphere in the middle and high latitudes (fig. 35.3), is real.

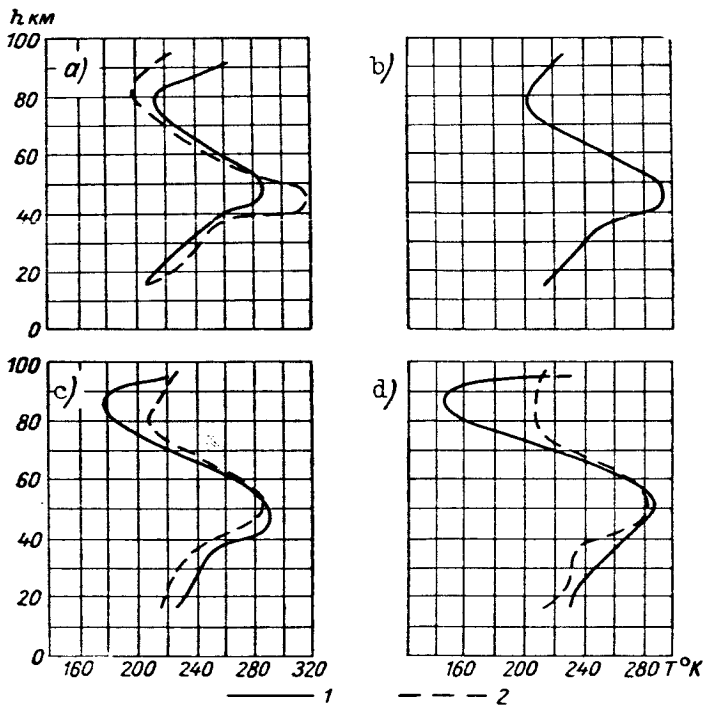

Figure 35.3. Summer and winter temperatures at different latitudes. (a) equator, (b) 30°N, (c) 60°N; (1) summer, (2) winter.

This warming can also be attributed qualitatively to the dependence of the temperature of radiant equilibrium on the quantity of ozone present in the air, in comparison with the quantity of water vapor and carbon dioxide gas (ref. 60). Accordingly, it is postulated that the temperature decrease in summer in the upper half of the ozonosphere is caused either by an increase of the relative content of H_2O and CO_2 molecules or a decrease of the relative content of ozone,

or, finally, the simultaneous effect of both factors. In this connection we note the catalytic effect of water vapor which facilitates the destruction of ozone molecules. It can, therefore, be postulated that a large quantity of water vapor penetrates into the high layers of the ozonosphere in summer (as a result of intensification of vertical mixing with the lower layers), accompanied by decrease of the ozone content. These concepts can be compared with a certain fact concerning noctilucent clouds: these clouds usually appear only in summer in the high latitudes at heights of about 80 km (Section 21). There is a basis for assuming that noctilucent clouds consist of ice crystals. If this assumption is correct, this circumstances can serve as an indication of the presence of a large quantity of water vapor in the upper part of the ozonosphere. In Pant's opinion this supports the explanation of the causes of low air temperatures in the high layers of the ozonosphere in summer (ref. 667).

Pant does not include the value of seasonal temperature variations above 45 km in Table 35.4, because on the basis of data available at that time (1956) it was possible to judge only the sign of these variations, not their magnitude.

Computations of the temperature field, taking into account wind data similar to the computations of Pant, were made by Murgatroyd, who used the more complete data on temperature and wind available by that time (1957). The mean meridional cross sections of the temperature field for summer and winter (Section 14.2) constructed by Murgatroyd have been considered in detail in books by K. Ya. Kondrat'yev and O. P. Filipovich (ref. 91) and I. A. Khvostikov (ref. 233).

35.3. Circulation in the Upper Layers of the Atmosphere According to Pant and Murgatroyd. Applying the computation method described in Section 35.2, Pant determined the wind distribution in summer and winter shown in figures 35.4a and b in the form of zonal flow. As noted by Pant, this distribution agrees with earlier data, i.e., with the geostrophic wind at heights below 45 km, according to Goldie's computations (ref. 406), with the vertical wind distribution determined by Sheppard (ref. 725) for the middle latitudes (fig. 35.1), with Gerson's summaries (refs. 398 and 400) and with the wind cross sections constructed by Haurwitz (ref. 425). There is a discrepancy with Kochanski's computations (Section 34.2): according to his data, at latitudes about 15°N at a level of about 20 km in January, (fig. 34.1) there is a westerly wind not shown on Pant's diagram (fig. 35.4b). Otherwise Kochanski's and Pant's data agree.

An extremely important circumstance is the seasonal reversal of wind direction in the region 20-70 km from easterly in summer to westerly in winter, agreeing with the models of the zonal wind represented in figures 35.4a and b. The existence of such a change in direction has also been noted by other authors: Johnson (ref. 489), Sheppard (ref. 725) and Kellogg and Schilling (ref. 517). The change in wind direction can also be established from the summaries of Gerson (refs. 398 and 400), Haurwitz (ref. 425) and recently generalized data (ref. 418) from rocket sounding represented in figures 28.4 and 28.5. Wind reversal occurs in spring.

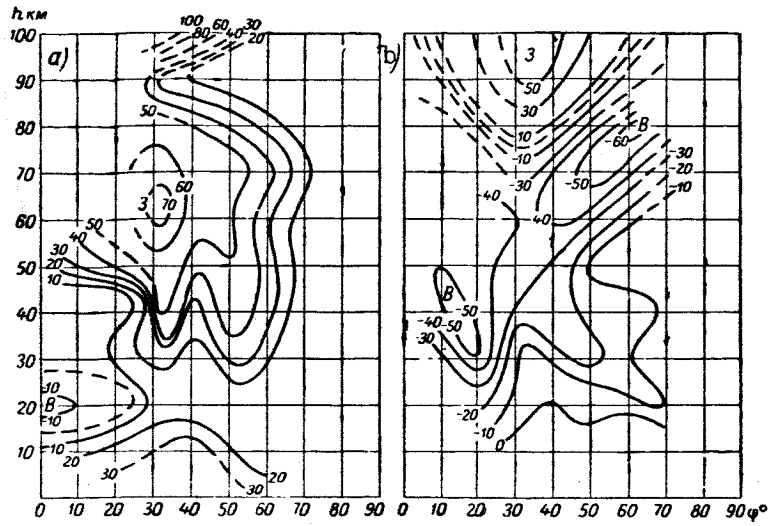

Figure 35.4. Distribution of westerly (3) and easterly (B) zonal wind circulation (in m/sec) in northern hemisphere. (a) summer, (b) winter.

Murgatroyd (ref. 614) investigated the problem of the relation between wind characteristics obtained from observations and data computed from the thermal wind equation. He checked this relationship, using as a basis data on winds for a height of 25 km and the temperature field to a height of 60 km known from observations. By using the thermal wind equation he computed the wind distribution each 5 km. The wind field computed in this way is shown in figure 35.5.

The horizontal temperature gradient exerts a great influence on the results of wind computations. This is shown in Table 35.5, giving the results of computations using the thermal wind equation for a 5 km layer of the atmosphere,

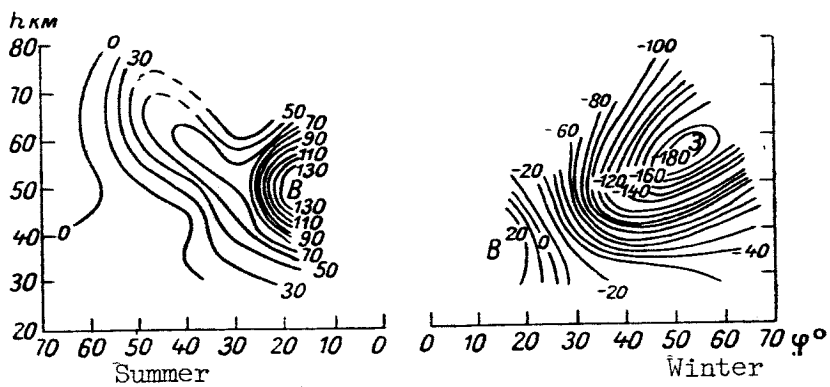

Figure 35.5. Wind field computed by Murgatroyd from temperature field known from measurements. Wind velocity in m/sec, (B)--easterly, (3)--westerly direction.

TABLE 35.5. VERTICAL WIND SHEAR (M/SEC) IN 5 KM LAYER DEVELOPING WITH HORIZONTAL TEMPERATURE GRADIENT OF 1° PER 10° OF LATITUDE (MURGATROYD).

Height, km	Latitude			
	10	30	50	70
30	10	4	2	2
40	8	3	2	2
50	5	2.5	1.6	1.5
60	6	2.5	1.0	0.7

situated at different heights and latitudes. Therefore, if it is assumed, for example, that an error of 1° per 10° of latitude exists in a 30 km layer, this leads to an error in the wind force in the upper part of this layer from 40-50 m/sec at latitude 10° to 10 m/sec at latitude 70°.

On the basis of a study of the horizontal temperature gradient, corresponding to the introduced generalized wind distribution, and taking into account available data on the temperature of the stratosphere and mesosphere, Murgatroyd obtained a "standard" temperature distribution. On the basis of this temperature field he computed the zonal winds, shown in figure 35.6. Comparison with the observed winds (fig. 28.3) reveals, in Murgatroyd's opinion (ref. 614), that for the most part there is agreement, but there are two appreciable differences: (1) very strong easterly winds at a height of 45 km in the low latitudes in summer and (2) very strong westerly winds at a height of about 60 km in the middle latitudes in winter.

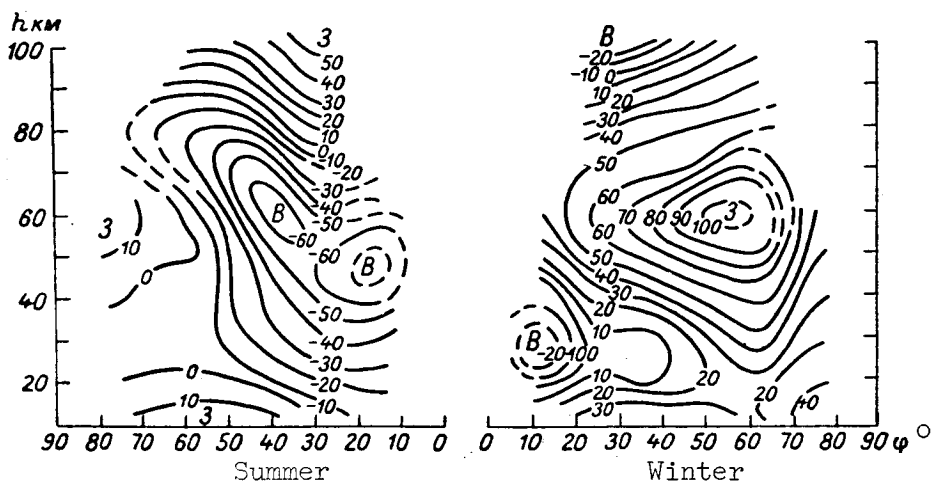

Figure 35.6. Zonal circulation computed from "generalized" temperature field. Notations same as in figure 35.5.

35.4. Batten's Computations. Batten (ref. 286) solved a problem of the same kind as was solved by Pant and Murgatroyd--more precise determination of the measured temperature field, taking into account the measured wind with subsequent computation of a wind field of increased accuracy, using the thermal wind equation. He used data obtained up to 1960. If the geostrophic approximation is correct, the measured temperatures should differ little from the computed temperatures determined from the values of the zonal wind by the thermal wind equation. In those cases when the computed values differ appreciably from the measured values, Batten accordingly corrected the wind data. The wind field generalized by Batten by this method is shown in figure 35.7. The initial wind field corrected by Batten is cited in Section 28 (fig. 28.6). The generalized wind field differs from the initial field (determined from observations) in that the wind field in the upper part of the stratosphere became smoother and the wind shear near the mesopause was determined more accurately.

The generalized wind field in the stratosphere and mesosphere for summer constructed by Batten (fig. 35.7) corresponds (on the average) to the highest degree to actual wind data for the northern hemisphere available to late in 1961.

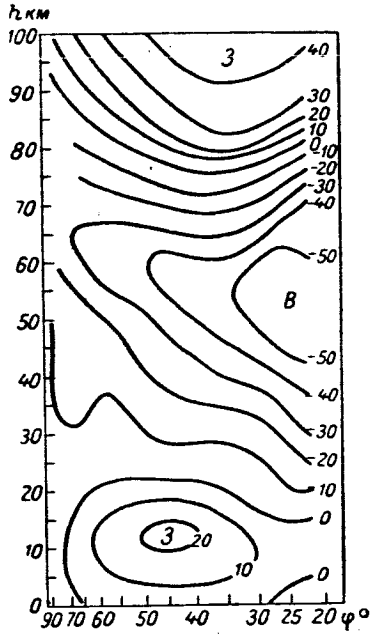

Figure 35.7. Generalized field of zonal circulation in summer. Notations same as in figure 35.5.

36. Meridional Circulation in the Stratosphere and Mesosphere

The problem of the meridional component of the wind is among the least studied problems of atmospheric circulation in the upper layers of the atmosphere. We will now discuss certain data available on this point and attempts at a theoretical evaluation of meridional circulation in the upper layers of the atmosphere.

36.1. Meridional Circulation in the Stratosphere. Many facts indicate the development of a strong meridional circulation in the upper layers of the troposphere and lower layers of the stratosphere under certain atmospheric conditions. A review of these investigations is beyond the scope of this book, and among recently published studies we will cite only an article by A. A. Pavlovskaya (ref. 144), in which she investigated cases of strong warmings of the stratosphere over the Arctic in the cold half-year. A. A. Pavlovskaya established that warming occurs only when there are sharply expressed meridional transformations of the temperature and pressure field in the region of a high-level frontal zone.

The mechanism of development of meridional circulation under certain conditions can be investigated, using model laboratory experiments in rotating vessels with a fluid. For example, Väisänen (ref. 775) studied the three-dimensional structure of water flow in a symmetrical tank and compared the results with corresponding atmospheric processes. In particular, he observed a zone of reversal of flow from easterly near the bottom to westerly at a great distance from the bottom. Väisänen's observations established the existence of almost strictly zonal symmetrical flows with a meridional component whose magnitude is an order of magnitude less than the magnitude of the zonal component. Väisänen mentions two methods for computation of the meridional wind.

We will now cite investigations of a completely different kind. In 1956 Dobson published conclusions drawn from an analysis of data on the vertical distribution of ozone O_3 and water vapor H_2O in the stratosphere (ref. 359).

The Dobson circulation model is shown in figure 36.1. According to this model, describing certain properties of air movements in the lower part of the stratosphere, there is a meridional exchange of air through the stratosphere between the equator and the middle latitudes; at latitudes of about 50° the air subsides (arrows A and B), but near the equator there are ascending currents (arrows C and D).

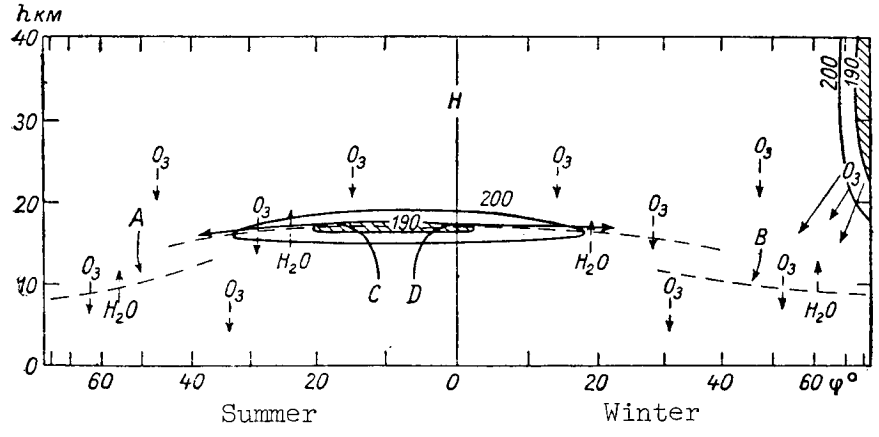

Figure 36.1. Model of meridional circulation. H, approximate level where O_3/air ratio is maximal. Isotherms in °K.

The model of meridional circulation devised by Libby and Palmer on the basis of measurements of the rate of radioactive fallout is of definite interest. This model is shown in Section 17 (fig. 17.4).

36.2. Meridional Circulation in the Mesosphere. In Section 35.3 we considered computations and concluded, in particular, that a comparison of temperatures computed from the wind field and temperatures determined from observations reveals that wind data, in general, agree with the temperature field as determined from observations and from theoretical computations. The same can be said with respect to similar computations made by Murgatroyd and Batten, discussed in Sections 35.3 and 35.4.

In computing temperature from the wind field Pant, Murgatroyd and Batten made the simplifying assumption that the wind is geostrophic at heights from 20-100 km. In the lower layers of the stratosphere the friction is small, but should, nevertheless, create a wind directed across the isobars in the direction of low pressure. Such a wind component along the gradient cannot be great enough to nullify the assumption that there is a geostrophic wind; this is confirmed by the satisfactory agreement of the determined temperature values. During the summer there is an easterly wind in the lower layers of the stratosphere, caused by a decrease of pressure from the pole to the equator. This pressure gradient increases with height. As was just pointed out, meridional movement from high to low pressure develops under the influence of friction and an unbalanced pressure gradient, i.e., from the pole to the equator. There is a westerly wind at these heights in winter, associated with falling pressure from the equator to the pole. The meridional movement caused by these factors is, therefore, directed in winter from the equator to the pole (ref. 667). This type of meridional movement at these heights in winter was also proposed earlier by Wolf and Craig for explanation of variations of the ozone content. These authors also postulated the presence of descending movements in the high latitudes, which Pant took into account in developing a model of winter circulation in the lower layers of the stratosphere.

36.3. Meridional Circulation and the Balance of Angular Momentum in the Stratosphere and Mesosphere. At the beginning of this section we discussed general concepts of the meridional circulation in the upper layers of the atmosphere and certain rough models based on qualitative estimates of certain processes (see Sections 36.1 and 36.2). We will now attempt to make quantitative computations of meridional circulation. Two studies of this type appeared in 1961 (ref. 619).

Murgatroyd and Singleton used as the basis of their computations the concept of heat transport between radiation sources and losses in the stratosphere and mesosphere. They assumed that the principal heat sources are situated in the region of the equatorial tropopause and in the mesosphere over the summer pole, and the principal losses are near the polar tropopause and over the winter pole in the mesosphere; they used this as a basis for computing the principal part of circulation (ref. 619).

The total rate of change of the temperature of moving particle $\frac{dT}{dt}$ can be written in the form

$$\frac{dT}{dt} = \left(\frac{\partial T}{\partial t} + \vec{V} \cdot \nabla_p T + w \frac{\partial T}{\partial p}\right) = \frac{R}{c_p} \frac{T}{p} w + \left(\frac{dT}{dt}\right)_R, \tag{36.1}$$

where T is temperature, t is time, $\vec{V}$ is the vector of horizontal velocity, $\nabla_p T$ is the temperature gradient along a surface of constant pressure p, w is vertical velocity in the pressure coordinates, R is the gas constant, c_p is the specific heat capacity of the air at constant pressure and $\left(\frac{dT}{dt}\right)$ R is the rate of radiation cooling.

If there is no zonal advection, the authors use equation (36.1) to obtain the meridional cross section

$$\left(\frac{dT}{dt}\right)_R = \frac{\partial T}{\partial t} + v \left(\frac{\partial T}{\partial y}\right)_p + wST, \tag{36.2}$$

where v is the desired velocity of meridional circulation--velocity along the direction of the meridian y, $S = \frac{1}{\theta} \frac{\partial \theta}{\partial p}$ is static stability (θ is potential temperature). By neglecting turbulent exchange we can interpret each term on the right-hand side of the last equation as the mean value of a circle of latitude for a particular pressure.

The continuity equation, if it is also applied similarly to the mean meridional cross section, taking into account the Earth's sphericity, can be written in the form

$$\frac{\partial v}{\partial \varphi} - v \operatorname{tg} \varphi = - E \frac{\partial w}{\partial p}, \tag{36.3}$$

where φ is latitude and E is the distance from the center of the Earth to the point considered.

After integrating in the limits between the two latitudes φ_0 and φ, we obtain

$$v \cos \varphi - v_0 \cos \varphi_0 = \int_{\varphi_0}^{\varphi} E \cos \varphi \frac{\partial w}{\partial p} d\varphi. \tag{36.4}$$

For this model (meridional plane through both hemispheres, extending from pole to pole) it must be postulated that v becomes equal to zero near both poles at all levels; consequently, when $\varphi \to \frac{\pi}{2}$ and $\varphi_0 \to \frac{\pi}{2}$

$$\int_{\varphi_0}^{\varphi} E \cos\varphi \frac{\partial w}{\partial p} d\varphi \to 0, \tag{36.5}$$

and this integral becomes equal to zero when $\varphi = \frac{\pi}{2}$ and $\varphi_0 = -\frac{\pi}{2}$.

The initial data used by Murgatroyd and Singleton in their computations were the estimates of the sources and the loss mechanisms of radiant energy of the upper layers of the atmosphere, published by Murgatroyd and Goody and also Ohring; after some refinements of these data they adopted the distribution of sources and losses shown in figure 36.2. Then, proceeding on the basis of the adopted values of temperature and pressure between the tropopause and 100 km level, they computed the potential temperature, stability and horizontal temperature gradient for different latitudes and heights. The computations were made for 10° latitude zones from pole to pole, in other words, for points 85, 75,..., 5, -5,..., -75, -85° for six week intervals, beginning from the solstice, for levels 16, 21, 28, 34, 40, 50, 60, 70 and 80 km.

The results of computations of meridional circulation are shown in figures 36.3a - d. The meridional cross sections were constructed for four periods of the year: solstice and equinox,and also for intermediate periods.

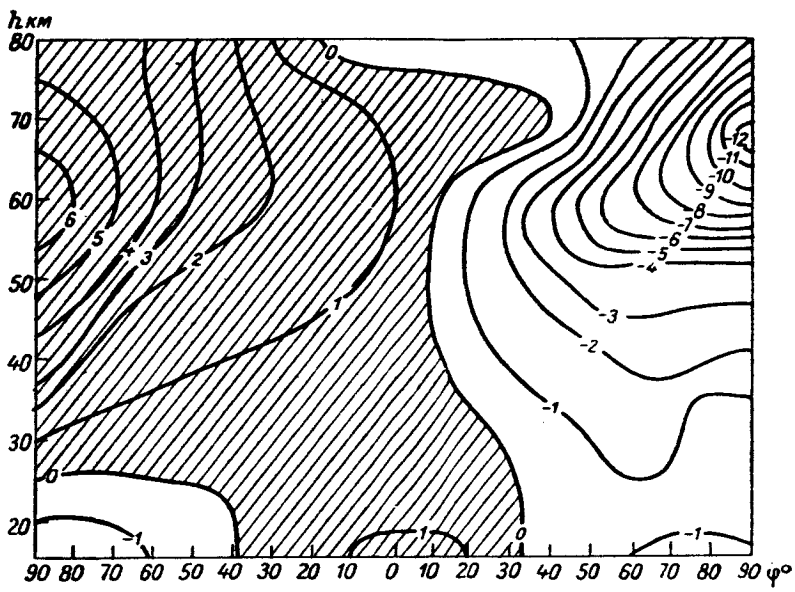

Figure 36.2. Radiation heating (cross hatched) and cooling (°K/day).

As shown by these cross sections, the velocity of meridional flow is centimeters, decimeters and meters per second.

There is a region of ascending currents near the equator with a velocity of 1 mm/sec in the middle of summer in the lower layers of the stratosphere, extending approximately to 30° latitude. These currents then are directed

poleward. Accordingly, at all latitudes the air is moving poleward at a velocity of about 70 cm/sec. In the corresponding season of the southern hemisphere there are similar conditions, but the velocity of horizontal flow attains almost 1 m/sec.

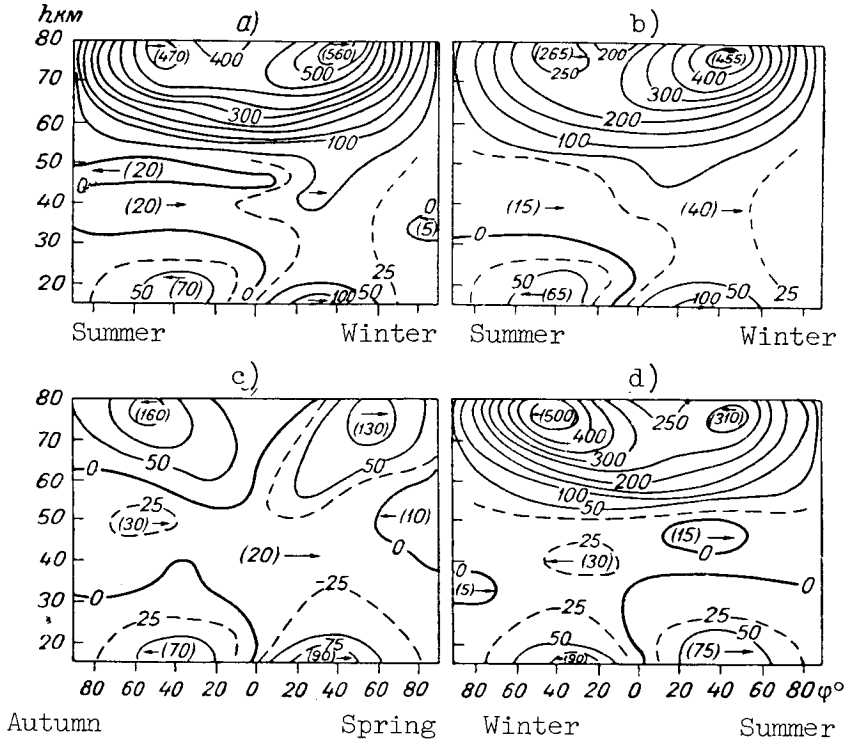

Figure 36.3. Velocity of meridional flow (cm/sec). (a) midsummer and winter, (b) end of summer and winter; (c) autumn and spring; (d) beginning of winter and summer.

At heights from 30-45 km in the summer hemisphere the flow is directed equatorward, but at the level 45-50 km it is poleward. Both flows have a velocity of about 20 cm/sec. In summer, with the exception of a small region near the pole in which weak flow at the 30 km level is directed equatorward, in the larger part of the hemisphere the flow is directed poleward at a velocity of 50 cm/sec at heights up to 50 km. Above the 50 km level and to a height of 80 km (or more) the horizontal flow is directed from the summer to the winter pole and has a velocity up to 5 or 6 m/sec.

The ascending and descending flows corresponding to these conditions have been discussed in Section 31.4 (fig. 31.3).

Six weeks later (fig. 36.3b) the field of meridional circulation has approximately the same general structure, with the exception of the disappearance of the region of flow directed poleward at a level of about 50 km in the summer hemisphere and directed equatorward at a height of about 30 km in the winter hemisphere. The maximum velocity of flow moving toward the winter pole is about 4.5 m/sec.

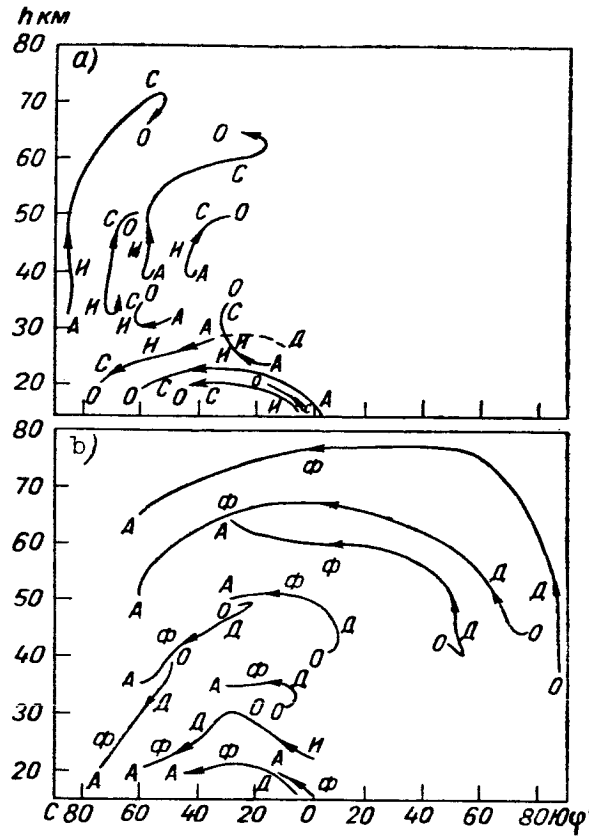

Figure 36.4. Trajectories of motion of air particles in 6 months. (a) From spring to autumn, (b) from autumn to spring. Dashed line shows trajectory for preceding 6 months: Ф = February, А = April, И = July, С = September, О = October, Д = December.

In equinoctial periods (fig. 36.3c) the picture changes primarily above 30 km. The principal circulatory branch above 60 km is divided into two flows directed poleward in both hemispheres. In spring a flow appears at heights of 40-50 km, directed equatorward.

36.4. Air Particle Trajectories. Murgatroyd and Singleton (ref. 618), using this model as a point of departure, computed air particle trajectories for a more complete and graphic investigation of the character of meridional movements. They computed the change in position of particles in six week periods, as mentioned in Section 36.3. Their results are shown in figures 36.4a and b.

These graphs show that both in spring and autumn the air entering the lower layers of the stratosphere between the equator and latitude 50° is always of tropospheric origin. In the polar regions the air enters the lower layers of the stratosphere in spring from the higher layers: during winter it subsides from the 30-40 km level. However, in autumn the air entering the lower layers of the

stratosphere subsides during summer from a level of only 20-28 km. In both cases the reverse extension of the trajectory into the preceding period shows that a large part of the air mass in the lower stratosphere initially had a tropospheric origin and could require 1 or 2 years to reach the lower layers of the polar stratosphere.

Tropospheric air rises into the high layers of the atmosphere only near the equator; the process of subsidence from the upper into the lower layers of the stratosphere occurs only in the high latitudes during the polar night.

Murgatroyd and Singleton conclude that the transfer of air from hemisphere to hemisphere in the lower layers of the stratosphere is either entirely absent or very insignificant (ref. 618). However, much air can enter the mesosphere in spring from the other hemisphere after crossing the equator during the preceding six months, but in autumn the air usually enters the mesosphere from the lower layers of the atmosphere of the same hemisphere.

On the whole, the model of meridional circulation shown in figures 36.3 and 36.4 is in many respects similar to the qualitative models considered in Sections 36.1 and 36.2, based on observations of the distribution of water vapor, ozone and radioactive fallout. It must be noted, however, that none of these models satisfy the conditions of balance of angular momentum. Nonconservation of angular momentum can be the result of turbulent exchange, which was not taken into account in the Murgatroyd-Singleton theory.

36.5. Meridional Circulation and the Balance of Angular Momentum in the Stratosphere and Mesosphere. The theory of meridional circulation proposed by Murgatroyd and Singleton (see Section 36.3) is based on the concepts of heat balance, but does not take dynamic factors into account. Without these factors it is impossible to explain the nonconservation of angular momentum inherent in models of meridional circulation in the stratosphere, based on observations of the distribution of water vapor, ozone and radioactive fallout. It would be of considerable interest to attempt to derive quantitative patterns of meridional circulation from dynamic principles. An attempt of this kind was undertaken recently by Haurwitz (ref. 426).

For a meridional transport of heat or momentum there must be a pressure gradient having a zonal component. In this case the condition of conservation of angular momentum is not satisfied, and the air can move in a meridional direction. Such a meridional transport of an air mass develops as a result of meridional movements caused by the effect of viscosity. Since atmospheric movements for the most part are geostrophic, it can be concluded that the influence of viscosity is small (except in the boundary layer near the Earth's surface). However, the influence of viscosity is a constantly acting factor and therefore, as pointed out by Haurwitz, it can be appreciable despite its smallness.

In the lower layers of the atmosphere the influence of viscosity on real atmospheric movements, as a result of their turbulent character, is manifested through turbulent rather than molecular friction. There is a basis for assuming

that a similar situation occurs in the mesosphere. The shearing stress of turbulent friction with which we are concerned is equal to

$$-\rho\overline{u'w'}$$

and

$$-\rho\overline{v'w'},$$

where u', v' and w' are the three components of the velocity of turbulent movements and ρ is air density. Since there are no direct data available on the velocity of turbulent movements in the upper layers of the atmosphere, Haurwitz finds (as is customary) expressions for the two stresses of internal friction by the components of mean horizontal velocity u, v and w, using for this purpose the Prandtl mixing length theory

$$-\rho\overline{u'w'}=\mu\frac{\partial u}{\partial z};$$

$$-\rho\overline{v'w'}=\mu\frac{dv}{dz}.$$

Here the parameter μ is the coefficient of virtual viscosity. Although μ is not a constant value, due to the lack of appropriate data an attempt can be made to neglect its change.

In making computations to obtain a quantitative estimate of the influence of friction, Haurwitz introduces a coordinate system in which the x-axis is directed south in the direction of increase of θ (θ is colatitude), the y-axis is directed east, in the direction of increase of longitude λ, and the z-axis is directed vertically upward. The wind components used by Haurwitz are u (positive, a northerly wind, directed to the south), and v (positive, a westerly wind, directed to the east). The other notations are: p--pressure, f = 2ω cos θ--Coriolis force, ω--angular velocity of Earth's rotation, r--Earth's radius. All subsequent discussion applies to the northern hemisphere. Haurwitz postulates that there is equilibrium between the Coriolis force, the pressure gradient and friction, so that

$$-fv=-\frac{1}{\rho}\frac{\partial p}{r\partial\theta}+\frac{\mu}{\rho}\frac{\partial^2 u}{\partial z^2}, \tag{36.6}$$

$$fu=-\frac{1}{\rho}\frac{\partial p}{r\sin\theta\,\partial\lambda}+\frac{\mu}{\rho}\frac{\partial^2 v}{\partial z^2}. \tag{36.7}$$

In this problem (determination of friction-induced meridional circulation caused by zonal flow) it can be assumed that the pressure field does not depend on longitude, and the first term on the right-hand side of equation (36.7) therefore becomes equal to zero. Haurwitz assumes that the velocity of the zonal wind is equal to the velocity v_g of the geostrophic wind (which is only approximately true)

$$v = v_g = \frac{1}{f}\frac{1}{\rho}\frac{\partial p}{r\partial\theta} \tag{36.8}$$

and

$$u = \frac{1}{f}\frac{\mu}{\rho}\frac{\partial^2 v_g}{\partial z^2}. \tag{36.9}$$

Equation (36.9) shows that there should be a meridional component of the wind caused by viscosity; the magnitude and direction of this component depend on the curvature of the vertical profile of the zonal wind. Figure 36.5 shows several typical profiles of the zonal wind and the meridional component of the wind caused by curvature of the profile (component caused by viscosity effect).

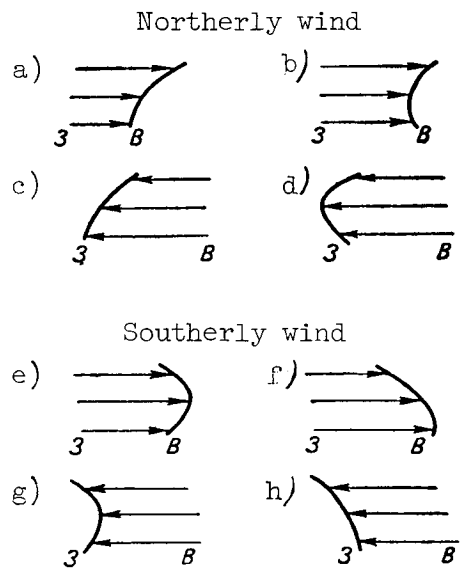

Figure 36.5. Curvature of vertical profile of zonal wind and resultant meridional wind component caused by effect of viscosity.

It is easy to understand the physical sense of these relations. For example, we will consider case a (fig. 36.5a). Intensification of the wind from level 1 to level 2 occurs more slowly than from level 2 to level 3. Consequently, the wind shear directed along the positive y-axis increases with height and intensity of shear, proportional to the vertical velocity of change of shear, accelerates the movement of the medium at level 2 to a supergeostrophic velocity. The air movement at level 2, therefore, becomes too rapid in comparison with the existing pressure gradient, and movement occurs in a southerly direction.

In numerical estimates of the value of the meridional component developing under the influence of viscosity, Haurwitz assumes that

$$\frac{\partial^2 v}{\partial z^2} = \frac{1\ \text{м/ sec}}{(5\ \text{км})^2} = 4 \cdot 10^{-10}\ \text{см}^{-1}\ \text{sec}^{-1} \tag{36.10}$$

(this corresponds to the mean profile of the zonal wind). As a representative value of the Coriolis force we can assume $f = 10^{-4}\ \text{sec}^{-1}$ (this corresponds to a latitude of about 45°). It is more difficult to indicate a representative value for kinematic viscosity $\nu = \frac{\mu}{\rho}$; Haurwitz assumes $\nu = 10^{7}\ \text{cm}^2/\text{sec}$, but indicates that at the heights with which we are concerned this value can be exaggerated by an order of magnitude.

The problem of the dependence of curvature of the profile of the zonal wind (and therefore its determined meridional movement) on the vertical and meridional temperature distribution is of definite interest. This problem can be solved using the equation for the thermal wind

$$f\frac{\partial}{\partial z}\left(\frac{v_g}{T}\right)=\frac{g}{T^2}\frac{\partial T}{r\partial\theta}, \tag{36.11}$$

where g is acceleration of gravity and T is temperature. After differentiation of this equation we obtain

$$\frac{\partial^2 v_g}{\partial z^2}=\frac{v_g}{T}\frac{\partial^2 T}{\partial z^2}+\frac{g}{fT}\frac{\partial^2 T}{r\partial\theta\,\partial z}. \tag{36.12}$$

In further estimates Haurwitz assumes the values:

$$\frac{\partial^2 T}{\partial z^2}=-4\cdot 10^{-11}\ \text{deg}\ \text{см}^{-2},$$

$$\frac{v_g}{T}\frac{\partial^2 T}{\partial z^2}=7\cdot 10^{-1}\ \text{см}^{-1}\,\text{sec}^{-1},$$

$$\frac{\partial}{r\partial\theta}\left(\frac{\partial T}{\partial z}\right)=6.7\cdot 10^{-14}\ \text{deg}\ \text{см}^{-2},$$

$$\frac{g}{fT}\frac{\partial^2 T}{r\partial\theta\,\partial z}=-2.6\cdot 10^{-9}\ \text{см}^{-1}\,\text{sec}^{-1}.$$

Haurwitz made the principal computations of the meridional wind, caused by the forces of internal friction, by using the mean field of the zonal wind; he used Batten's data (Sections 29 and 35). In order to use the results of computations not only for determination of the meridional wind, but also for vertical movements, Haurwitz formulated as his basic problem the investigation of convergence and divergence of masses. In this connection he did not compute the velocity u directly, but instead the product ρu, bearing in mind that it is not particularly difficult to consider the change of atmospheric density with height and to compute the value u later.

On the basis of these concepts Haurwitz determined and constructed the field of the value $\frac{\partial^2 v}{\partial z^2}$. The results of his computations are shown in Figures 36.6-36.8.

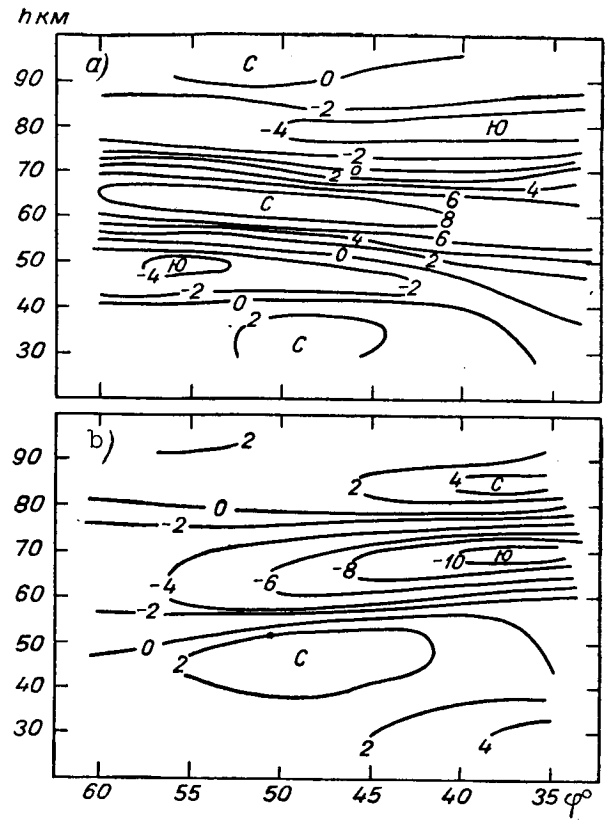

Figure 36.6. Distribution of curvature of vertical profile of zonal wind (in units of $4 \cdot 10^{-10}$ $cm^{-1}sec^{-1}$). a--summer, b--winter, C--southerly wind component, Ю --northerly wind component.

As mentioned above, the unit used in construction of the cross sections was the value $\frac{1 \text{ m/sec}}{(5 \text{ km})^2} = 4 \cdot 10^{-10}$ $cm^{-1}sec^{-1}$, which corresponds to u = 40 cm/sec (if $\frac{\mu}{\rho} = 10^7$ cm^2sec^{-1}, $f = 10^{-4}sec^{-1}$).

The summer situation is shown in figure 36.6a. Strong northerly circulation is observed in the high latitudes at the 60-70 km level. Above this northerly flow, there is a weaker southerly flow. The winter situation (fig. 36.6b) is simpler than the summer situation, and the direction of meridional flow is mostly opposite. In the upper layers of the stratosphere the flow has a northerly direction, in the greater part of the mesosphere there is a predominance of southerly flow, but above this the meridional wind component again assumes a northerly direction. A schematic diagram of winter circulation is shown in figure 36.7. Due to lack of data our ideas concerning circulation to the north of 60°N and to the south of 30°N suffer a certain ambiguity: the corresponding part of the flow lines in figure 36.7 is shown as a dashed line.

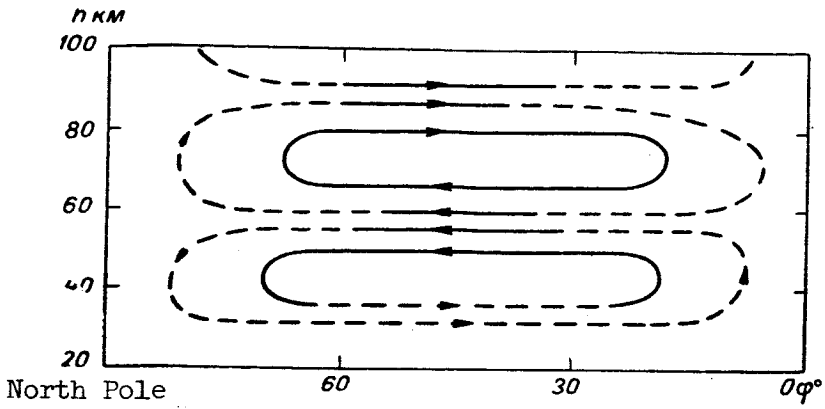

Figure 36.7. Schematic representation of meridional circulation in winter.

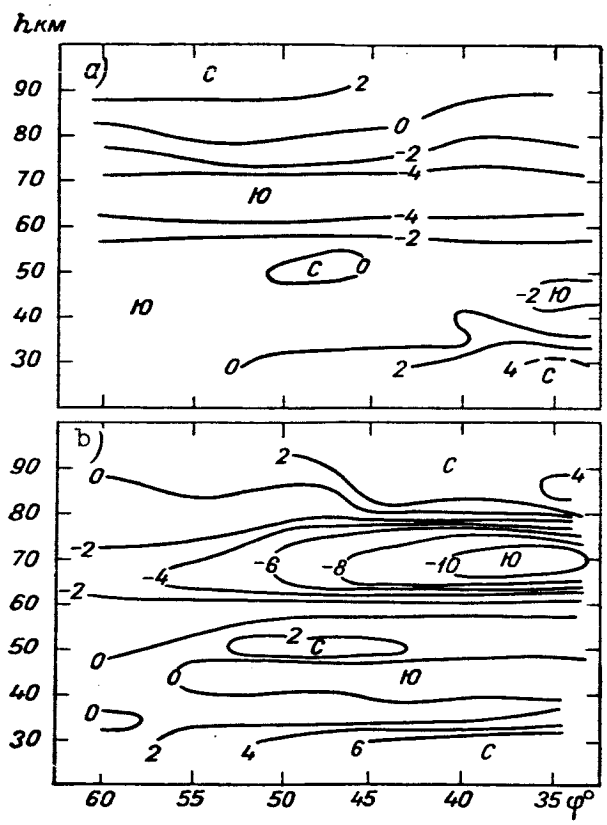

Figure 36.8. Meridional distribution of curvature of vertical zonal wind profile. (a) November-December, (b) January-February. For clarification see figure 36.6.

In Section 17 we discussed a model of meridional circulation devised by Libby and Palmer on the basis of measurements of the rate of radioactive fallout (fig. 17.4). This model gives the same directions of flow (as obtained in the lower part of the cross section in fig. 36.7) by Haurwitz. However, the northern branch of this circulation lies considerably lower. This and certain other differences can be attributed partly to the fact that the model derived by Libby and Palmer was applied to all seasons.

If the periods November-December and January-February are considered separately, the rather simple picture obtained for the entire winter (fig. 36.6b) becomes somewhat more complex. During the first half of winter (fig. 36.8a) the southern component, as determined from Haurwitz' computations, prevails almost throughout the stratosphere and mesosphere, with the exception of that part of the stratosphere which lies to the south of 50°N and below 35 km. In the second half of winter (fig. 36.8b) the northerly flow in the upper layers of the stratosphere enters increasingly northerly latitudes.

36.5 Meridional Circulation in the Ionosphere. In Section 35.3 we discussed computations of circulation in the upper layers of the atmosphere, reported by Pant (ref. 667), and models of zonal flow in the northern hemisphere in summer and winter (figures 35.4 and 35.5). In this same study Pant cites computations of meridional circulation.

As demonstrated in studies by Yerg, with which we are familiar, the value of kinematic viscosity becomes appreciable at a height of 80 km, attains a maximum at heights of about 200 km and then decreases and becomes negligibly small at the 300 km level. The influence of viscosity in this region should give rise to meridional flow directed from north to south in the region of the easterly zonal wind and from south to north in the region of the westerly zonal wind. Pant made an attempt to estimate the meridional wind component caused by the viscosity effect, using as a point of departure the distribution of zonal flow in the region 80-100 km, discussed in Section 35. He found that meridional flow attains appreciable values at a height of about 200 km, where Yerg states that kinematic viscosity is maximal. It naturally follows from the concept of continuity of the medium that a reverse meridional flow should develop in the layer situated above the 200 km level and below 300 km. At heights greater than 300 km the kinematic viscosity becomes negligibly small. In this region there will therefore be shearing, and an easterly wind can prevail at heights greater than 300 km. The models of ionospheric circulation shown in the upper part of figures 36.9a and b are based on these concepts. These models agree with the curves of wind change with height (fig. 35.1) proposed in 1949 by Sheppard (ref. 725), and with data on wind above latitude 50°N at a height of 120 km obtained from the observations of Hoffmeister (ref. 446). These models are also similar to the atmospheric circulation at heights of 100-300 km obtained by Yerg in 1951 on a theoretical basis and used successfully for explanation of the observed longitudinal differences of the electron concentration for the ionospheric layer. These concepts on general meridional circulation in the ionosphere should only be considered extremely simplified models, which must be supplemented, taking into account such effects as periodic tidal winds and aperiodic variations (ref. 667).

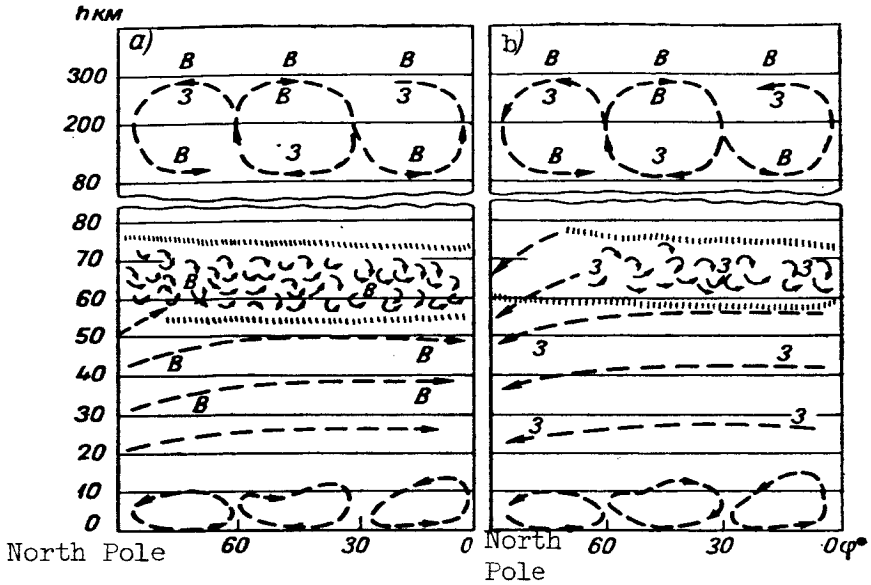

Figure 36.9. Meridional circulation in northern hemisphere. (a) summer, (b) winter.

37. Wind in the Ionosphere

With an increase in height of these layers, there is a gradual change in the degree of influence of different factors on wind velocity and direction. Tidal forces act in the entire thickness of the atmosphere, but at low and even at moderate heights their influence is so small it can usually be neglected. However, at sufficiently great heights the effect of tidal forces becomes considerable. In developing a theory of air currents in different regions of the atmosphere, such as in the lower, middle, high and highest parts, it is necessary to take various additional forces into account. In the ionosphere, in contrast to the lower layers, it is necessary to take into account the influence of kinematic viscosity, the effect of tidal forces and the influence of energy reserves forming as a result of dissociation processes.

Interesting concepts of the character of atmospheric circulation in the region of the ionosphere were expressed by Yerg in 1951-1955 and by Pant in 1956, but the fullest computations of the wind at heights of 100 km or more were made by Deb in 1953 and by Pant in 1956.

37.1. Deb's Computations. The approach to the problem of computing the wind in the ionosphere used by Deb essentially differs little from the method used for the lower layers by Kellogg and Schilling. Deb's work was devoted to an investigation of zonal circulation.

The first stage of the investigation involved obtaining sufficiently complete data on air temperature at different latitudes and heights. Assuming the temperature field at all latitudes to be zonal (dependent only on latitude), Deb

constructed five curves of the vertical distribution of temperature for heights of 100 and 400 km: a mean annual curve for 30°N and winter and summer curves for 45° and 80-90°N (fig. 37.1). The second stage of the computations was the determination of the zonal pressure field for heights of 100-400 km each 20 km (using the equilibrium equation). Since the vertical temperature distribution depends on latitude, the corresponding pressure distribution should also depend on latitude. Thus, in general, the isobaric surfaces should be sloping, relative to the horizontal plane, and an air movement will therefore develop in the direction of the pressure gradient. However, under the influence of the Coriolis force caused by the Earth's rotation, the wind will be deflected to a direction parallel to the isobars. Deb considers the case of stationary circulation when the forces caused by the pressure gradient and the Earth's rotation balance one another (geostrophic wind). Deb computes wind velocity using the formula

$$V_g = \frac{g \operatorname{tg} \theta}{2\omega \sin \varphi} \tag{37.1}$$

(θ is the angle of slope of the isobaric surface relative to the horizon), similar to equation (34.6). When viscosity is present, a wind component appears directed along the normal to the isobars. Viscosity is also a hindrance to development of large wind velocity gradients in adjacent layers.

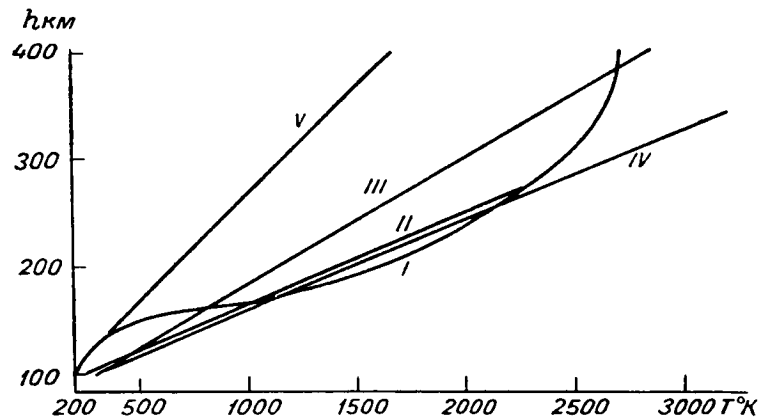

Figure 37.1. Vertical temperature distribution. I, winter, 80°N, II, summer, 80°N, III, winter, 45°N, IV, summer, 45°N, V, mean annual, 30°N.

The following generalized barometric formula can be obtained by integration

$$p = p_0 \exp\left[-\int_0^h \frac{dh}{H}\right], \tag{37.2}$$

which p_0 denotes pressure at the particular level. Deb computes the vertical distribution of pressure by using curves of temperature distribution (fig. 37.1) and the value p_0 for a height of 100 km as initial data and formula (37.2). The mean annual value used by Deb for 30°N is $p_0 = 5.36 \cdot 10^{-4}$ mb and $p_0 = 1.49 \cdot 10^{-3}$ mb for 45°N (for winter and summer), $p_0 = 8.5 \cdot 10^{-4}$ for 80-90°N (summer) and $p_0 = 4.5 \cdot 10^{-4}$ mb (winter). The mean molecular weight m of the air is considered by Deb to decrease with height, i.e., m = 23.95 at heights of 100-200 km and m = 22.28 at heights of 200-400 km.

The gradient wind, computed from the zonal pressure field, is then corrected by Deb for viscosity, using Yerg's computations for this purpose. Yerg's computations show that kinematic viscosity plays a considerable role at heights of 90-300 km, where its value varies in the range 10^6-10^3.

The data on the vertical distribution of pressure at latitudes 30, 45 and 80-90°N, computed by Deb, by no means agree in all respects with one another, and sometimes lead to results for wind velocity and direction which contradict observational data. One of the reasons for such disagreements is the inadequacy of the used initial data on temperature and pressure at different heights and latitudes.

Deb computes the wind in the middle latitudes of the northern hemisphere using the following three differences of the zonal pressure fields for computation of the slope of the isobaric surfaces: (1) pressure at latitude 80-90° minus pressure at latitude 45°; (2) the same for 80-90 and 30°; (3) the same for 45 and 30°.

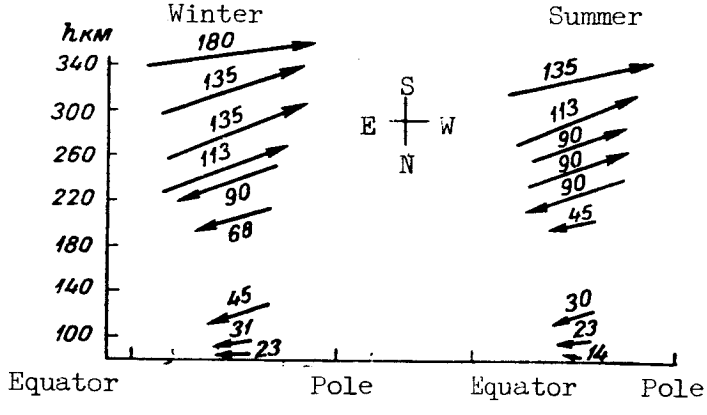

Figure 37.2. Wind in upper layers of atmosphere computed from curves of vertical distribution of temperature at 80-90 and 45°N. Figures along arrows denote velocity in m/sec.

In the case of latitudes 80-90 and 45° he found that the pressure increa[illegible] equatorward, so that the isobaric surfaces slope poleward. For example, at a height of 105 km this slope is $\frac{1}{508.7}$; therefore, using formula (37.1) for 60°N we obtain V_g = 90 m/sec.

The wind data obtained by Deb for this case are shown in fig. 37.2. At a height of 100 km or more there are no seasonal changes of wind direction: in both winter and summer the wind blows from south to north. The wind velocity is appreciably less in summer. For example, at heights of about 100 km the velocity in summer is 25-30 m/sec and in winter about 45 m/sec.

Above the 100 km level there is a tendency to development of a large vertical wind gradient. In winter the wind velocity increases from 45 m/sec at a height of 100 km to 180 m/sec or more at the 120 km level, and at a height of 200 km it attains enormous values (many hundreds of meters per second). However, viscosity also increases to its maximum values precisely in the region 120-200 km, which leads to a considerable decrease of the gradient with height.

One of the results of this northward transport of air and the retarding effect of viscosity can be the development of a reverse flow at high velocity at a height of about 250 km in summer and at somewhat greater heights in winter. Thus, the movement of air in the region of the ionospheric F2 layer apparently occurs from south to north.

Deb's computations revealed that an allowance for the effect of Coriolis force and viscosity leads to the following conclusion: there is a southwesterly wind with a velocity of 25-90 m/sec in the ionospheric E region in the northern hemisphere, whereas in the F region there is a northeasterly wind of a greater velocity (fig. 37.2).

We will now consider the system of winds defined by Deb from an analysis of the vertical distribution of pressure at 80-90 and 30°N. He found indications of the presence of small seasonal variations of wind direction at heights of 100-120 km. In winter the air moves from south to north and in summer in the opposite direction and at a greater velocity (fig. 37.3). However, for the layer above the 150 km level there are no indications of such variations of wind direction, and the wind in this layer always blows from north to south.

At a height of 100 km the wind velocity in winter is less than in summer (in winter about 40 m/sec, and in summer about 18 m/sec). At the heights of the F layer the difference is expressed still more clearly.

The vertical wind velocity gradient at heights of 100-180 km in winter is small, but in summer has moderate values; at great heights the gradient has an appreciable value even in winter, and in summer it is extremely great. However, this tendency is checked at heights greater than 180 km by an appreciable viscosity effect, which has a considerable value at these heights.

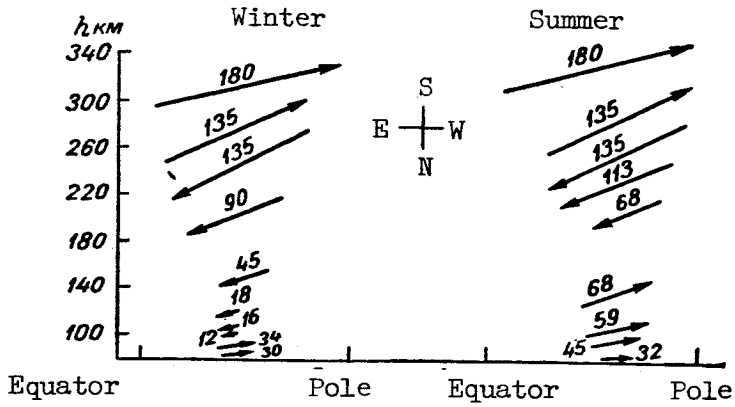

Figure 37.3. Wind in upper layers of atmosphere computed from curves of vertical distribution of pressure at 90-80 and 30°N. Figures along arrows denote wind velocity in m/sec.

As a result of the rapid transport of air in an equatorward direction in this region of latitudes and the retarding effect of viscosity, there apparently can be a development of air currents of opposite direction above a level of about 250 km in winter and at lesser heights in summer. Thus, air movement in the ionospheric F2 layer can be directed from south to north throughout the year. An allowance for the effect of Coriolis force and viscosity leads to the following conclusions: in the E layer in winter there is a southwesterly wind, but this is very weak; in this layer in summer there is a northeasterly wind with a velocity of about 45 m/sec. In the F2 region the wind always is southwesterly or westerly with a velocity of 90-135 m/sec (fig. 37.3).

In addition to these two wind systems, Deb computed air currents on the basis of data on the vertical distribution of pressure at lower latitudes--45 and 30°N. The results which he obtained can be summarized as follows (fig. 37.4).

During the entire year the wind blows from north to south with approximately the same velocity. There are indications of a large value of the vertical wind velocity gradient. At such relatively low heights as 150 km, the wind velocity could attain values of many hundreds of meters per second, if it were not retarded by viscosity. As a result of the equatorward transport of air and the downward slowing of velocity, a reverse flow could possibly form above the 250 km level. Taking into account the effect of Coriolis force and viscosity, Deb obtained the following results: in the E region of the ionosphere there is a northeasterly wind with a velocity of 90 m/sec, and in the F1 region a northeasterly wind with a velocity of 110 m/sec. In the F2 region and above there apparently is a reverse flow which can have a southwesterly direction, or, if the decrease of viscosity in this layer is taken into account, a purely zonal circulation, i.e., from west to east.

The theoretical wind models devised by Deb can make no pretense to complete agreement with the true patterns of atmospheric circulation in its upper layers,

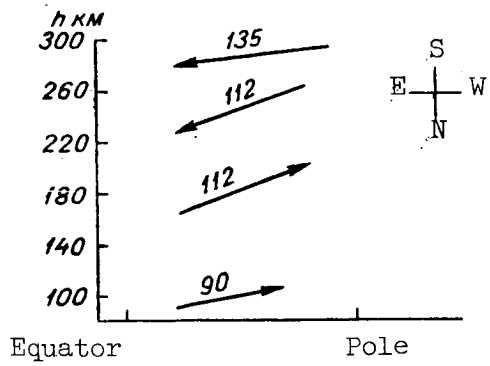

Figure 37.4. Wind in upper layers of atmosphere computed from curves of vertical distribution of temperature at 45 and 30°N. Figures along arrows denote wind velocity in m/sec.

because he failed to take into account many factors on which wind velocity and direction probably depend. We now will mention some of these factors.

1. Tidal air movements.
2. Influence of the geomagnetic field.
3. Pressure changes caused by change of the vertical temperature gradient, which can influence a circulatory system of this same scale.
4. Strong vertical temperature gradients facilitating the development of turbulent and eddy diffusion.

The great importance of taking into account tidal movements in the theory of air currents in the upper layers of the atmosphere will be demonstrated in the following sections. The need for clarification of the possible influence of the geomagnetic field arises, because much information on wind is obtained by sounding the ionosphere with radio waves, and the results of such sounding obviously depend on the influence of the Earth's magnetic field on motion of ions and electrons.

37.2. Comparison of Theoretical Data with Observations. A comparison of the theoretical circulation models (figs. 37.2-37.4) obtained by Debs with observational data reveals that in many respects there is a close similarity, but there also are large differences. In the case of the theoretical wind determined from data for 80-90 and 45°N (fig. 37.2), we can note the following discrepancies in comparison with experimental data. Whereas in summer the observed direction of the prevailing winds is the same as the computed direction, the pattern is completely different in winter. Theoretical computations do not indicate any large-scale diurnal or seasonal changes of the wind to the opposite direction, although observations constantly indicate such reversals.

The theoretical computations based on data for 80-90° and 30°N (fig. 37.3) indicate greater wind velocities in summer than in winter, but measurements indicate the exact opposite. The wind velocity in summer agrees well with observations for the entire ionosphere (E and F regions), but the wind direction is

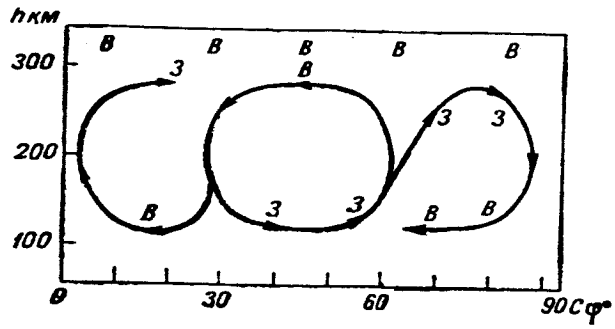

Figure 37.5. Possible circulation system in F1 region of ionosphere when air temperature decreases with latitude.

actually opposite. In this case as well the computations do not indicate the presence of any diurnal or seasonal changes of the wind to the opposite direction.

With respect to data for 45 and 30°N (fig. 37.4), there are no theoretical indications of large-scale differences of wind velocities in winter and summer. In addition, wind direction in the F2 region usually is opposite to the observed direction. As in the two preceding cases, there are no diurnal changes of the computed wind direction in the E region or seasonal changes in the F region.

After studying the seasonal changes of wind in the upper part of this region of heights, it can be concluded from Deb's data that the layer in which the wind direction changes in the F region is situated higher in winter than in summer. This circumstance can be the cause, at least partly, of the change in the 250 km region from an easterly wind in summer to a westerly wind in winter. In the reverse flow over the F1 region, the cold air should move southward, from pole to equator. This can lead to a temperature decrease with height in this region.

Yerg (ref. 814) as early as 1951 postulated that the corresponding vertical temperature gradient can be sufficiently great so that under its influence the unified circulatory system breaks down into three parts (fig. 37.5). As shown by this diagram, in the central part the circulation consists of a westerly wind in the lower part and an easterly wind in the upper part, and the opposite is true in the equatorial and polar parts. However, the development of such a complex circulation, as suggested by Deb, is possible only when there is a sharply expressed temperature decrease poleward. Such a circulation, therefore, is only possible in winter when the entire region near the pole below the 200 km level and around it is plunged into darkness. Deb believes that in the summer months it is more probable that there is a simple circulation extending from the pole to the equator. Transition to such a simple system from the complex system shown in figure 37.5 can give rise to the beginning of a seasonal change of wind direction in the polar and equatorial regions.

At this point it should be emphasized that the vertical temperature distributions at 80-90 and 45°N used by Deb do not fully correspond to the true

situation, and in the polar region the atmosphere in winter is plunged into complete darkness to a height of 300 km at all hours of the day.

The vertical temperature distribution used by Deb for latitude 30° is based on rocket data obtained before 1952. Deb made interesting computations of the vertical temperature distribution over the polar region on the assumption that the temperature profile used for 30°N was reliable and assuming that the observed wind is a gradient wind (caused only by the pressure gradient). Table 37.1 shows the results of his computations. These temperatures for heights of 150-200 km are considerably lower than those which now have been established by measurements on rockets and satellites, which indicates a need for substantial improvements in Deb's computations.

TABLE 37.1. VERTICAL TEMPERATURE DISTRIBUTION IN POLAR REGION DETERMINED FROM ROCKET DATA FOR 30°N AND THE OBSERVED WIND.

Height, km	Pressure, mb	Temperature, °K
100	$4.6 \cdot 10^{-5}$	230
120	$6.0 \cdot 10^{-6}$	248
160	$1.4 \cdot 10^{-7}$	342
200	$1.6 \cdot 10^{-8}$	600

37.3. Pant's Results. In Section 35 we discussed Pant's work (ref. 667) in detail. In that study he made a theoretical investigation of the wind at heights of 20-100 km, but some ideas are also presented on the character of air currents at heights of 100-300 km. Pant's results have been given in Section 35.3 (figs. 35.4 and 35.5) and Section 36.5 (fig. 36.9). It follows from data applying to heights greater than 80 km that in summer (fig. 35.4) there is a westerly wind over the middle latitudes. There also are weighty indications that there is a predominance of easterly flow over the low and high latitudes. Over the middle latitudes at heights greater than 80 km the westerly wind also blows in winter (fig. 35.5); over the high latitudes at this season of the year the wind also is westerly, but has a lesser velocity. There are much fewer wind data at these heights in winter than in summer, and figure 35.5 does not show the presence of easterly winds above the 80 km level in the low and high latitudes. In order to clarify this problem, Pant uses the temperature criterion which he used at lower heights (see Section 35): assuming the wind to be geostrophic, he estimates the temperature distribution in the 80-100 km region over the very low and very high latitudes in dependence on whether the wind is assumed to be westerly or easterly, and then compares the determined distributions with other pertinent data. Pant's computations revealed that the most probable temperatures are obtained by operating on the assumption that there is an easterly wind (ref. 667).

37.4. Some General Problems in the Theory of Ionospheric Winds. Since wind measurements in the ionosphere to a large degree are based on the study of the drift of ionospheric inhomogeneities, the theory of these movements should also take into account the mechanisms of formation of inhomogeneities. A number of problems arise in this connection, with respect to the theory of the movement of an ionized gas in the upper layers of the atmosphere. A detailed review of this problem was published in a study by V. P. Dokuchayev (ref. 426).

A modern theory of ionospheric winds should take into account the results of theoretical investigations of the ionosphere by the methods of magnetohydrodynamics. In actuality, the ionosphere is a partially ionized gas with anisotropic conductivity in the Earth's magnetic field. Movements of the gas induce electromagnetic fields, currents and polarizing charges. The body force acting on the induced currents, as a result of the relatively great strength of the Earth's magnetic field, can exert an appreciable influence on the motion of the gas (especially in the upper layers of the ionosphere). The influence of the geomagnetic field on the geostrophic wind was investigated in the first approximation by V. P. Dokuchayev. A simplified system of equations in magnetohydrodynamics was derived by Ye. A. Novikov (ref. 139).

The fields of wind velocities in the ionosphere are subject to regular short- and long-period disturbances of local or (less frequently) of global character. Important characteristics of ionospheric movements have now been established: tidal movements and large-scale wave movements have been discovered. The theory of the indicated movements should take into account the resonance properties of the Earth's gas envelope and possibly nonlinear effects in the ionosphere (ref. 426). Hines (ref. 441) made a theoretical investigation of internal atmospheric waves, taking into account the effect of gravitational forces and forces of compression. The presence of viscosity leads to an attenuation of waves with dimensions less than several hundred meters. Hines also considered possible mechanisms of excitation of internal atmospheric gravitational waves (ref. 442).

The interesting problem of the influence of light pressure on dynamic processes in the upper layers of the atmosphere was considered by Wojciechowski and Reichart (ref. 812). They conclude that the light pressure produced by solar rays on the upper layers of the atmosphere should excite processes of three types:

(1) specific tides in the atmosphere on the nighttime side of Earth;
(2) a strong westerly wind at very great heights;
(3) vertical variations in the upper layers (periodic vertical redistribution of density).

CHAPTER 12. ATMOSPHERIC TIDES

38. Theory of Atmospheric Tides

Chapter 9 presented experimental data indicating the presence of periodic variations of wind velocity and direction. The diurnal variations of wind in the ionosphere (Section 30), having an obviously tidal origin, are particularly significant. However, in the stratosphere as well, careful analysis of wind data reveal periodic components of flows of tidal origin. For example, Mantis (ref. 572) reported that in an investigation of the trajectories of free balloons, flying at a particular (constant) height, special variations of summer stratospheric easterly currents were found. These variations are caused by fluctuations with a period obviously less than that which can be related to movements of a synoptic scale. An analysis detected diurnal variations of the meridional component of the wind at heights of about 30 km at latitudes less than 20°N, with an amplitude of about 1 m/sec; variations of this same amplitude can also exist at latitudes of about 45°N.

This section will present the principal theoretical computations of tidal winds and the results of comparisons of theoretical and observed data. I presented general information on atmospheric tides and the problems involved in the heat regime of the upper layers of the atmosphere, as related to atmospheric tides in reference 233.

38.1. Lunar and Solar Tides. Twice a day the Earth's oceans rhythmically rise and fall. Each day the highest level of the tide sets in at that time when the Moon is overhead. It is almost obvious that the tide is caused by lunar attraction. But what accounts for the second daily tide, when the Moon is on the opposite side of the Earth? The explanation was found by Newton: the tide on the opposite side is caused by the fact that under the influence of lunar attraction the Earth withdraws from the water. For this reason there are simultaneously two tides on mutually opposite sides of the Earth which follow the motion of the Moon in the heavens. This is how the double tidal wave moving westward around the Earth is formed.

Tidal forces act not only on the Earth's liquid envelope, but also on its solid body. Solid matter cannot flow like the water in the oceans, but the elastic Earth is deformed and is drawn out slightly toward the Moon and in the opposite direction. Twice each day the Earth beneath our feet rises up or falls, but so insignificantly that it cannot be sensed, although it can be detected by precise instruments. Observations reveal that the Earth's elasticity on the whole exceeds the elasticity of steel.

Newton apparently was the first to postulate that there also should be tides in the atmosphere, but he considered them to be too small to be discovered; he was right about their magnitude, but they can be detected.

The tidal rise and fall of the ocean level are visible and easy to measure, because the ocean surface occupies a definite position relative to the shore. Tidal instruments record the changes of water level. But this method cannot be used in the middle of the ocean. The only way to record the rise or fall of level there is to record changes of the weight or pressure of a column of water by manometers installed on the ocean floor. This same method can be used in the atmosphere, and a barometer can be used for this purpose. It was Laplace who made the first systematic attempt to detect lunar tides in the atmosphere by means of barometric measurements. He developed the theory of tides in the oceans and applied it to the air ocean. He calculated that lunar tides should produce an increase and decrease of barometric pressure of 1/4 mm per day in the tropics and less at other latitudes. He analyzed the barometric pressure recorded over an 8 year period at the Paris Observatory. Laplace was unsuccessful in obtaining any indication of lunar variations of pressure, and concluded that at least 40,000 barometric measurements are required to obtain a result.

Other investigators, who continued the work of Laplace, were also unsuccessful, although one of them analyzed 30,000 measurements. The problem is difficult not only because changes of barometric pressure are caused by many factors and therefore have an extremely complex character, but also because, in actuality, the amplitude of atmospheric tides is a whole order of magnitude less than Laplace assumed.

Lunar tides in the atmosphere were discovered for the first time in 1842 by Lefroy by changes of barometric pressure in the tropics. It was found that the amplitude of the tides is only about 0.1 mm Hg. In the extratropical zone, the tides were detected for the first time in the classical study of the outstanding modern geophysicist Sidney Chapman. He studied barometric data from Greenwich Observatory for a 64 year period. The amplitude of the tides at this latitude ($51^{\circ}46'$N) attains scarcely 0.01 mm Hg (to be more precise, 0.00914 mm), i.e., corresponds to the change in height of an air column of only 20 cm. Like the Moon in the sky, tides are observed approximately 1 hour later than on the preceding day. The period of lunar tides is 12 hours 25 min. At present lunar tides in the atmosphere have been discovered and are investigated regularly at more than 60 stations over the Earth.

There also are solar tides on Earth. The tidal force of the Sun is 2.5 times less than that of the Moon. The most important aspect of the problem of atmospheric tides is that, in actuality, solar tides in the atmosphere are not weaker than lunar tides, but contrary to expectations are considerably stronger. Their amplitude attains almost an entire millimeter of a column of mercury (at the equator the amplitude is approximately equal to 0.937 mm). It is natural, therefore, that solar tides were discovered earlier than lunar tides--they already were known for almost two centuries. But many aspects of this phenomenon long remained mysterious. The diurnal variation of pressure has a complex character. When it is expanded into simple harmonic variations, waves of different periods are found. Waves with periods of 24, 12, 8 and 6 hours have been found by harmonic analysis; the most clearly defined of these is the semidiurnal (12 hour) wave. Total change of pressure can be considered as the superposing of a small number of sinusoidal oscillations

$$\sum_n C_n \sin(nt+\varphi_n),$$

where t is time read from midnight (1 hour equals 15°). Individual components differ from one another in amplitude C_n and phase φ_n. The large amplitude of diurnal solar tides in comparison with the amplitude of lunar tides can be attributed to the presence of the thermal influence of the Sun on the Earth's atmosphere (daytime heating and subsequent nighttime cooling). But the thermal effect cannot intensify the semidiurnal wave, as was pointed out for the first time by William Thomson in 1882. However, he made a proposal which was a forerunner of the correct approach to the solution of the problem. Thomson mentioned the resonance phenomenon as a possible cause of intensification of the semidiurnal solar tide.

It has now been established that, whereas the principal cause of lunar tides is gravitational forces, solar "tides" are partially of gravitational origin and partially of thermal origin. Like Chapman (ref. 324), we will use the terms diurnal, semidiurnal, etc., for those variations of pressure or other meteorological elements which are not mandatorily caused by tidal (gravitational) forces. It is customary to use the symbols L and S for the two types of atmospheric tides, lunar and solar, respectively; the semidiurnal tides are denoted L_2 and S_2. The tides are manifested in variations of the different meteorological elements, especially barometric pressure, zonal and meridional wind and heights of the ionospheric layers; they exert appreciably less influence on air temperature, the level of formation of secondary cosmic rays (mesons and neutrons), ascending air movements and other elements (ref. 335). The diurnal solar variations of the meteorological elements are a superposing of the harmonic components S_n, where $n = 1, 2, 3, \ldots$ $S = S_1 + S_2 + \ldots$ Each such harmonic component can be represented in the form

$$S_n = s_n \sin(n\omega t + \sigma_n), \tag{38.1}$$

where t is local mean solar time, s_n is amplitude, σ_n is phase. For example, the lunar semidiurnal tide L_2 can be represented in the form

$$L_2 = l_2 \sin(2\omega\tau + \lambda_2), \tag{38.2}$$

where τ is mean lunar time, read from the lower (or upper) transit of the mean Moon. If more than one meteorological element is considered, the tidal symbol is supplemented by an indicator denoting the particular meteorological element. For example, $l_2(T)$ is the symbol of the amplitude of the lunar semidiurnal tidal wave of pressure and $S_2(T)$ is the symbol of the solar semidiurnal wave of temperature (ref. 335). In his dissertation (ref. 745) Stolov uses the following approach in computing the field of tidal winds in the upper layers of the atmosphere on the basis of the general theory of atmospheric tides: proceeding on the basis of the equation for the tidal wave of pressure at the Earth's surface,

e computes the surface wind field; then, using the theory of atmospheric tides developed by Taylor and Pekeris, he determines the tidal wind field at a height of 100 km.

38.2. Stolov's Investigation. In 1918 Simpson (ref. 728) obtained the following expression for semidurnal oscillations of pressure (in mm Hg), agreeing well with observational data

$$s_2(p)\sin(2t+\sigma_2)=0.937\sin^3\theta\sin(2t+154^\circ)+ \\ +0.137\left(\cos^2\theta-\frac{1}{3}\right)\sin[2(t-\lambda)+105^\circ], \tag{38.3}$$

where θ is colatitude (the angle added to 90° for the geographic latitude of a place) and λ is the longitude of the place to the west of Greenwich. The first term on the right-hand side of this equation is the "equatorial oscillation" (to use Simpson's terminology), because it has a maximum value at the equator. This term must also be assigned the sense of a travelling wave, because it describes a pressure wave which propagates around the Earth parallel to the circles of latitude from east to west (following the Sun). The second term on the right-hand side of equation (38.3) represents the "polar oscillation," because it exerts a predominant influence in the high latitudes. This term also can be assigned the sense of a standing wave, because it describes the meridional oscillation of air with the pressure node

$$(\cos^2\theta = 1/3)$$

at a latitude 35°16' to the north and south of the equator.

The considered second term on the right-hand side of equation (38.3) recently was subjected to criticism by Wilkes (ref. 807); he proposed that it be replaced by a different expression. The purely empirical Wilkes formula agrees better with observational data at latitudes less than 50°, where the error in determination of the standing wave can be considerable, but it is less accurate than the Simpson formula at latitudes exceeding 50°. The role of the standing wave in the total variation of pressure becomes significant only in the high latitudes where the Simpson formula is preferable. Proceeding on this basis, Simpson (ref. 745) uses equation (38.3) as a basis for computing the field of the tidal wind; this equation is rewritten in the form

$$p=A\sin[2(\omega t+\lambda)+154^\circ]+B\sin(2\omega t+105^\circ), \tag{38.4}$$

where ω is the angular velocity of the Earth's rotation, t is Greenwich time and A and B are functions of latitude.

The semidiurnal pressure wave can be regarded as a small disturbance superposed on an undisturbed state. If we neglect the squares of the perturbing values (linearized theory), the equations for slow horizontal air movement on a spherical rotating Earth for a frictionless atmosphere can be represented as

$$\frac{\partial u}{\partial t} - 2\omega v \cos\theta = -\frac{1}{\rho_0 r}\frac{\partial p}{\partial \theta}, \tag{38.5}$$

$$\frac{\partial v}{\partial t} + 2\omega u \cos\theta = -\frac{1}{\rho_0 r \sin\theta}\frac{\partial p}{\partial \lambda}, \tag{38.6}$$

where u is the velocity component directed to the north, v is the velocity component directed to the east, r is the Earth's radius and ρ_0 is the mean density of surface air. After substituting (38.4) into (38.5) and (38.6), Stolov (ref. 745) obtained an equation whose joint solution for u and v, after certain simplifications, was represented in the form of the sum of the general integral of a homogeneous equation and the partial solution of a nonhomogeneous equation

$$u = c_1 \cos(2\omega\cos\theta)t + c_2 \sin(2\omega\cos\theta)t + \tag{38.7}$$
$$+ \frac{f + g\cos\theta}{2\sin^2\theta}\cos[2(\omega t + \lambda) + 154°] + \frac{f'}{2\sin^2\theta}\cos(2\omega t + 105°),$$

$$v = c_2 \cos(2\omega\cos\theta)t - c_1 \sin(2\omega\cos\theta)t - \tag{38.8}$$
$$- \frac{g + f\cos\theta}{2\sin^2\theta}\sin[2(\omega t + \lambda) + 154°] - \frac{f'\cos\theta}{2\sin^2\theta}\sin(2\omega t + 105°),$$

where c_1 and c_2 are constants, and in addition

$$\rho_0 = \frac{p_0}{RT_0}, \tag{38.9}$$

$$f = \frac{RT_0}{p_0 r\omega}\frac{\partial A}{\partial \theta}, \tag{38.10}$$

$$g = \frac{2RT_0 A}{p_0 r\omega\sin\theta}, \tag{38.11}$$

$$f' = \frac{RT_0}{p_0 r\omega}\frac{\partial B}{\partial \theta}. \tag{38.12}$$

The first two terms on the right-hand side of equations (38.7) and (38.8) represent free oscillation with a semidiurnal period, which in this case need not be taken into account. Using the CGS system of units and formulas (38.10)-(38.12), it is possible to find the following numerical values (ref. 745):

$$f = 64.7\sin^2\theta\cos\theta, \tag{38.13}$$

$$g = 43.2\sin^2\theta, \tag{38.14}$$

$$f' = -6.31\cos\theta\sin\theta. \tag{38.15}$$

Substituting these three values into equations (38.7) and (38.8) and dropping the inertial terms, we find that

$$u = 54.0\cos\theta\cos[2(\omega t + \lambda) + 154°] - 3.16\operatorname{ctg}\theta\cos(2\omega t + \tag{38.16}$$
$$+ 105°),$$

$$v = -(21{,}6 + 32{,}4\cos^2\theta)\sin[2(\omega t + \lambda) + 154°] + \\ + 3{,}16\operatorname{ctg}\theta\cos\theta\sin(2\omega t + 105°). \qquad (38.17)$$

In this derivation there is no need to consider the continuity equation, because it is assumed implicitly that small vertical movements and possibly temperature variations are such that they satisfy the continuity equation. Air movement in a pressure wave is very different from what it would be if the pressure distribution were geostrophic or changed slowly. At some points of the pressure wave the wind vector is directed along the gradient and in others perpendicular to it, as in geostrophic movement. Stolov's computations show that wind velocity increases with increase of latitude, despite the fact that the semidiurnal pressure wave decreases with increase of latitude. This is the influence of the Earth's rotation (ref. 745). According to Gold's computations (ref. 404), which apply to a similar problem but with the Earth's rotation neglected, wind velocity decreases with increase of latitude.

38.3. Role of Terms in the Equations of Atmospheric Oscillations Including Viscous Forces. Since the time of Laplace, the theory of atmospheric tides has neglected nonlinear terms and viscous forces in the differential equations of motion. This apparently is admissible only if the nonlinear and viscous terms of the equations actually are small at all heights.

According to the linearized theory of semidiurnal solar oscillations, the velocity of air particles at a height of 100 km is greater by more than a hundred times their velocity at the surface (ref. 673). Such great velocity can be considered adequate for a reliable check of the order of magnitude of earlier dropped squared terms. This problem was considered by Pekeris in 1951. According to his estimate, the squared terms cannot be neglected at heights considerably exceeding 100 km, because there the squared terms become equal to the linear terms remaining in the equations. However, it was later postulated that the influence of nonlinear terms at all heights can be neutralized by viscous forces (ref. 745).

Atmospheric tides can be regarded as long waves propagating horizontally along the X-axis and having a vertical wave front. The periodic factor is used in the form $e^{(\text{int-kx})}$, where n denotes frequency and k is the wave number. In this problem it was possible to neglect the Earth's rotation; the differential equation of motion of a viscous liquid for the u component, according to Lamb (ref. 102), neglecting the value $\frac{d\omega}{dz}$ and the variations in the direction of the Y-axis, can be written in the form

$$\frac{\partial u}{\partial t} + u\frac{\partial u}{\partial x} + w\frac{\partial u}{\partial z} = -\frac{1}{\rho}\frac{\partial p}{\partial x} - \frac{\partial \Omega}{\partial x} + \frac{4}{3}\nu\frac{\partial^2 u}{\partial x^2} + \\ + \nu\frac{\partial^2 u}{\partial z^2}, \qquad (38.18)$$

where $\nu = \frac{\mu}{\rho}$ is the kinematic viscosity and Ω is the field potential creating th

tide. The last two terms on the right-hand side of this equation determine the contribution made by viscous forces. By substituting the corresponding numerical values it can be shown (ref. 745) that the next to the last term is smaller than the last by a factor of 10^4, and in comparison with it can be neglected. Thus, for an estimate of the order of magnitude of the error caused by total neglect of viscous forces it is sufficient to determine the limits within which it is possible to neglect the term $\nu \frac{\partial^2 u}{\partial z^2}$ in comparison with the retained linear term $\frac{\partial u}{\partial t}$.

By virtue of what has been said concerning atmospheric tides, we can write

$$u = u_0 \exp [az + i(nt - kx)],$$

where u_0 is an amplitude value, and, therefore,

$$\frac{\partial u}{\partial t} = inu, \tag{38.19}$$

$$\frac{\partial^2 u}{\partial z^2} = a^2 u. \tag{38.20}$$

Consequently,

$$\frac{\partial u}{\partial t} - \nu \frac{\partial^2 u}{\partial z^2} = inu \left(1 + \frac{\nu a^2}{n} i\right). \tag{38.21}$$

Thus, the ratio of the viscous term in the differential equation, which we neglect, to the retained linear term is a value of the order of $\nu \frac{a^2}{n}$. We are concerned with the change of this value with height. This can be conceived most easily if we consider the case of free oscillations of an atmosphere with constant temperature. According to the linearized Pekeris equation, assuming there is resonance with a semidiurnal solar tide, we have

$$a = \frac{(\gamma - 1)}{\gamma H_0} = \frac{2}{7H_0}, \tag{38.22}$$

$$H = \gamma H_0$$

$$\mu = 1.9 \cdot 10^{-4} \quad \text{(in CGS units)} \tag{38.23}$$

$$\rho(z) = \rho_0 e^{-\frac{z}{H_0}} \tag{38.24}$$

Here H is the depth of the equivalent ocean (ref. 233) with H = 7.87 km, H_0 is the height of the homogeneous atmosphere and γ is the ratio of specific heat capacities. For the ratio

$$\frac{\text{term, including viscosity}}{\text{linear term}} = \frac{\nu a^2}{n} = \frac{\mu a^2}{\rho(z) n} \tag{38.25}$$

this formulation gives the approximate value

$$\frac{3.4 \cdot 10^{-13}}{\rho(z)} \simeq 2.6 \cdot 10^{-10} e^{\frac{z}{5.6}}$$

where z must be reckoned in km. The right-hand side of this expression becomes equal to unity at a height of approximately 125 km. Above this level the viscous term, usually neglected, becomes greater in order of magnitude than the retained linear term. In 1951 Pekeris demonstrated that for this case of an isothermal atmosphere the neglected squared term becomes equal to the retained linear term at the considerably lower height of 40 km.

Wilkes (ref. 807) showed that molecular heat conductivity acquires a value of a substantial factor above the 120 km level, i.e., at the same heights where the role of viscosity becomes large. An indication that both viscosity and heat conductivity begin to play an important role in atmospheric processes approximately at the same heights apparently can be obtained from purely physical considerations, if we take into account the close physical relationship between these two phenomena (ref. 745). Kirchgoff noted that the influence of heat conductivity on sound propagation has the same order of magnitude as the influence of viscosity (ref. 533).

38.4. Relationship between Terms Including Viscous Forces and Nonlinear Terms. With an increase of height there is an increase of the influence on atmospheric processes of both the squared terms in the tide equation and the terms including viscosity. In both cases the decrease of density with height apparently exerts an influence. Investigation of the height dependence of the ratio of the terms including viscosity and nonlinear terms in differential equation (38.18) is of undoubted interest. This would make it possible to determine the region where we could neglect viscosity when developing a nonlinear theory of atmospheric tides. Such a theory was proposed by Pekeris, in 1951, but it soon was subjected to criticism by Wilkes (ref. 808). Later this problem was considered more fully by Stolov (ref. 745).

It is clear that in order to obtain a solution of this problem it is sufficient to compare the terms $\nu \frac{\partial^2 u}{\partial z^2}$ and $u \frac{\partial u}{\partial x}$ in the differential equation (38.18). On the basis of the same considerations used in deriving relations (38.19) and (38.20), it also follows that

$$\frac{\partial u}{\partial x} = -iku, \tag{38.26}$$

$$\frac{\partial^2 u}{\partial z^2} = a^2 u, \tag{38.27}$$

and therefore

$$u\frac{\partial u}{\partial x} - \nu\frac{\partial^2 u}{\partial z^2} = -iku^2\left[1 - \frac{\nu a^2}{uk}i\right]. \tag{38.28}$$

It follows, therefore, that the ratio of the term including viscosity to the squared term has a value of the order of $\nu\frac{a^2}{uk}$. This ratio can be investigated using the same method as was used for the case of free oscillations of an isothermal atmosphere. In this case

$$\frac{\text{term including viscosity}}{\text{squared term}} = \frac{\nu a^2}{uk} = \frac{\nu a^2 V}{un} = \frac{\mu a^2 V}{\rho(z)\, nu}, \tag{38.29}$$

where V is phase velocity (i.e., $\frac{n}{k}$). The ratio $\frac{V}{u}$ of the phase velocity of the wave to the velocity of movement of an air particle is equal, according to Pekeris' estimate, to $1{,}140\, e^{-\frac{z}{5.6}}$. Under conditions corresponding to the presence of resonance with a semidiurnal solar tide the desired ratio (38.29) is not dependent on height, and, according to Stolov's computations (ref. 745), is equal to approximately $3\cdot10^{-7}$. The fact that this ratio is not dependent on height can be attributed to the similarity in the character of increase of both values with decrease of density, but it was difficult to assume that the squared term at any height is millions of times greater than the term including viscosity.

These numerical estimates permit us to come to important conclusions concerning the requirements which the theory of tidal air movements in the upper layers of the atmosphere should satisfy. From ratio (38.25) we obtain an estimate which shows that at a height of 125 km each term including viscosity becomes equal to the linear term retained in the equation. At a height of 125 km the squared term is several million times larger than the term including viscosity. It can, therefore, be concluded that when developing a nonlinearized tidal theory it is possible to neglect viscosity to great heights, including the ionospheric E region.

38.5. Role of Turbulence. Many phenomena observed in the upper layers of the atmosphere (movement of meteor trails, noctilucent clouds, ionospheric inhomogeneities) indicate the presence of well-developed turbulent movements of the medium. However, at present no experimental data have been obtained on the vertical distribution of turbulent viscosity. However, it is extremely desirable to discuss this problem, at least on a preliminary basis, and evaluate the role of the forces of turbulent viscosity in the differential equations of atmospheric tides. Data published by Lettau (ref. 546) can be used for this purpose. Lettau attempted to evaluate vertical variations of the turbulent

viscosity coefficient, proceeding on the basis of the intensity of atmospheric circulation and the vertical temperature stratification of the atmosphere.

If the influence of turbulent viscous forces is included, the following term must be added to the right-hand side of equation (38.18)

$$k\frac{\partial^2 u}{\partial z^2},$$

where k is the kinematic coefficient of virtual viscosity. Accordingly, ν should be replaced by $\nu + k$ in formulas (38.25) and (38.29). The region in which turbulent viscosity exerts an influence on the relation between the term including viscosity and the linear term, and also between the term including viscosity and the squared terms is dependent on the relative values k and ν.

Table 38.1 gives sample values k and ν. Lettau's data are used for k. As shown by this table, with the exception of the troposphere where tidal winds are extremely weak, only the region between 50 and 70 km is different in that an allowance for turbulent friction appreciably influences the earlier evaluations of the relations between linear and squared terms and the terms including viscosity. Here the ratio including viscosity to the squared term is a value of the order of 10^{-3}. This ratio decreases by a factor of 10^4 if turbulent friction is neglected. Thus, even in the region where turbulence exerts a maximum influence the term including viscosity is a thousand times smaller than the squared term (ref. 745).

TABLE 38.1. KINEMATIC COEFFICIENT OF VIRTUAL VISCOSITY (k) AND COEFFICIENT OF KINEMATIC VISCOSITY (ν) AS FUNCTION OF HEIGHT.

h км	k см²/sec	ν см²/sec	h км	k см²/sec	ν см²/sec
0	10^3	10^{-1}	60	10^7	10^3
10	10^5	10^{-1}	70	10^7	10^3
20	10^2	10^0	80	10^6	10^4
30	10^2	10^1	90	10^6	10^4
40	10^3	10^1	100	10^6	10^5
50	10^6	10^2			

The ratio of the term including viscosity to the retained linear term increased with height, and at a height of 50-70 km it is about 10^{-8}, if turbulent friction is neglected. When the latter is included, this ratio in the region indicated increases to 10^{-4}. Thus, even in the region where the influence of turbulent friction is particularly great, the term including viscosity, nevertheless, is ten thousand times smaller than the retained linear term.

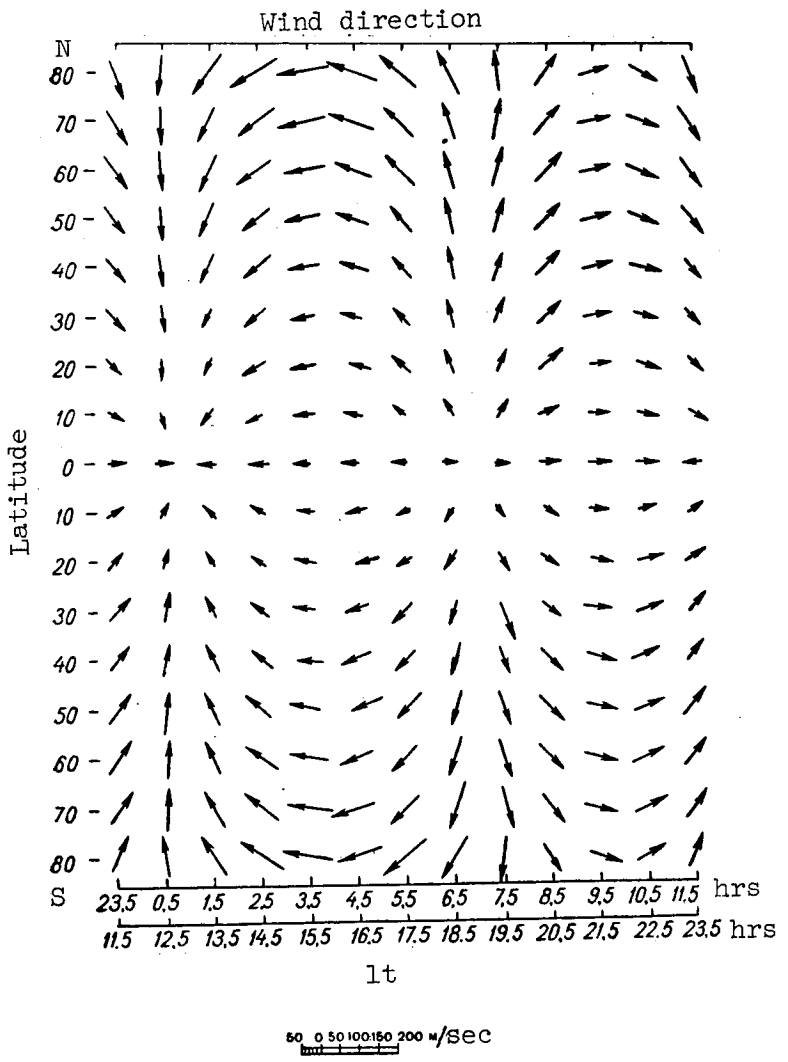

Figure 38.1. Field of tidal wind at 100 km level at 1130 and 2330 lt (total semidiurnal tidal variations).

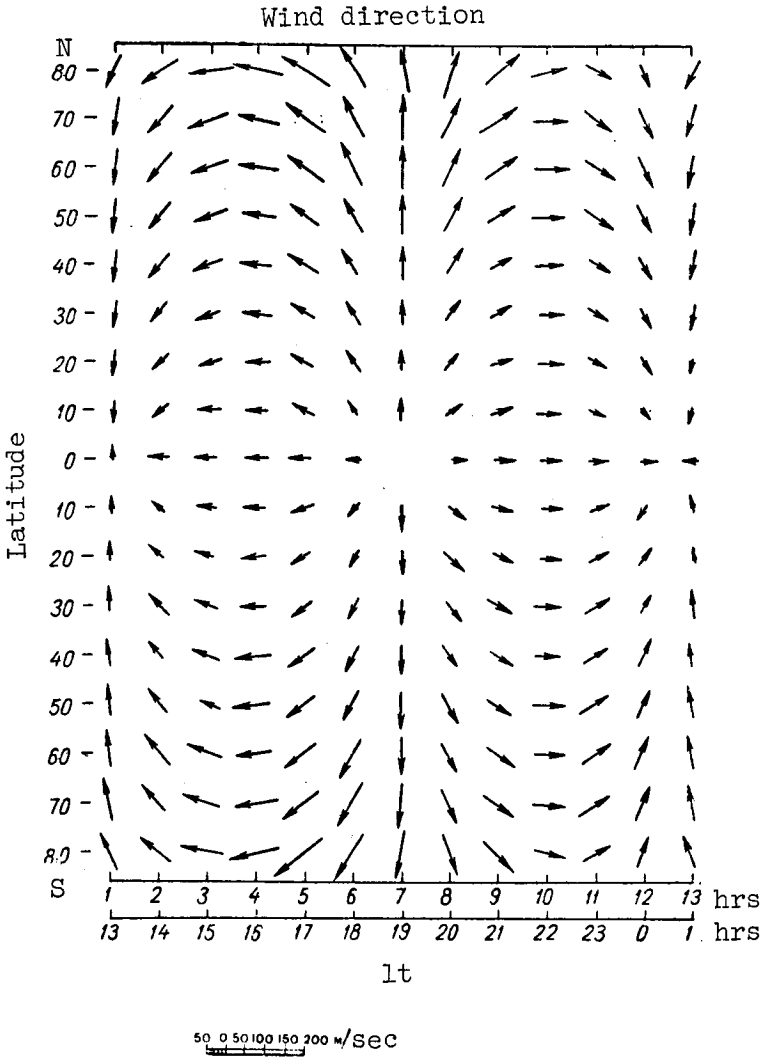

Figure 38.2. Field of tidal wind at 100 km level at 1300 and 0100 lt (total semidiurnal tidal variations).

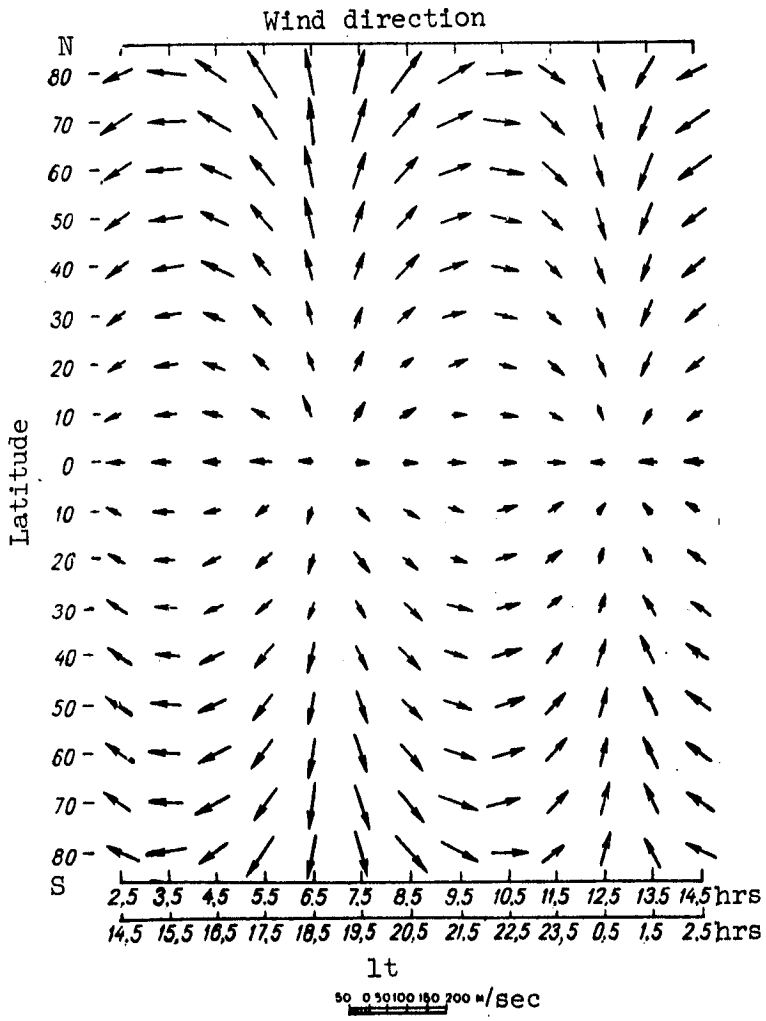

Figure 38.3. Field of tidal wind at 100 km level at 1430 and 0230 lt (total semidiurnal tidal variations).

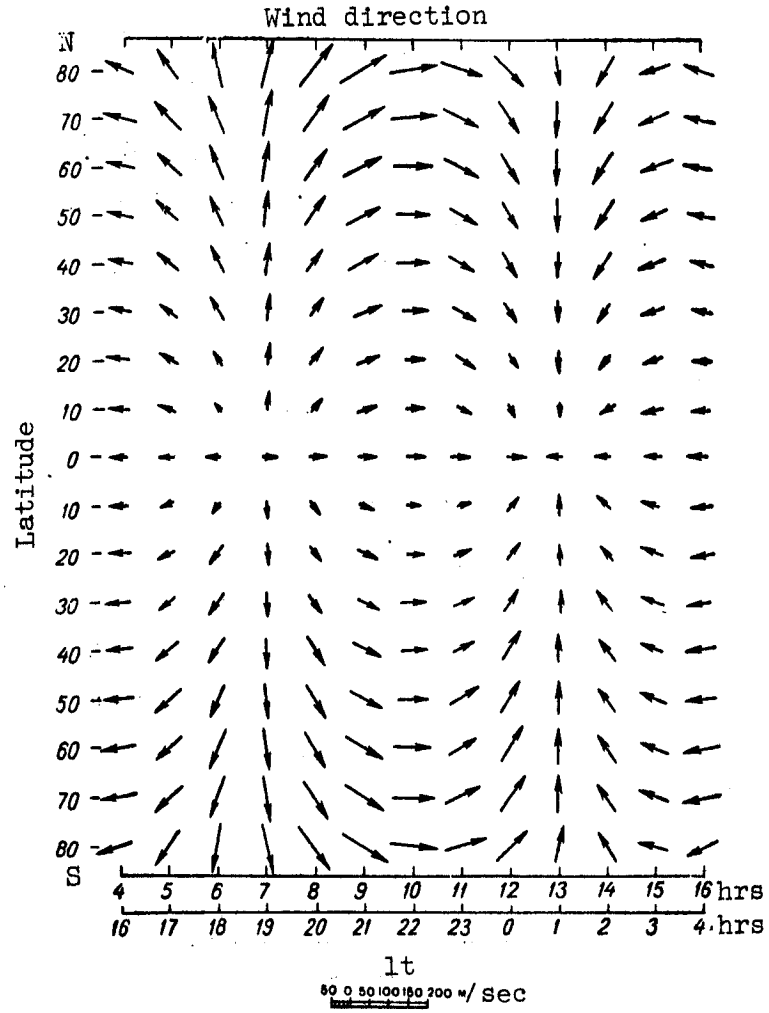

Figure 38.4. Field of tidal wind at 100 km level at 1600 and 0400 lt (total semidiurnal tidal variations).

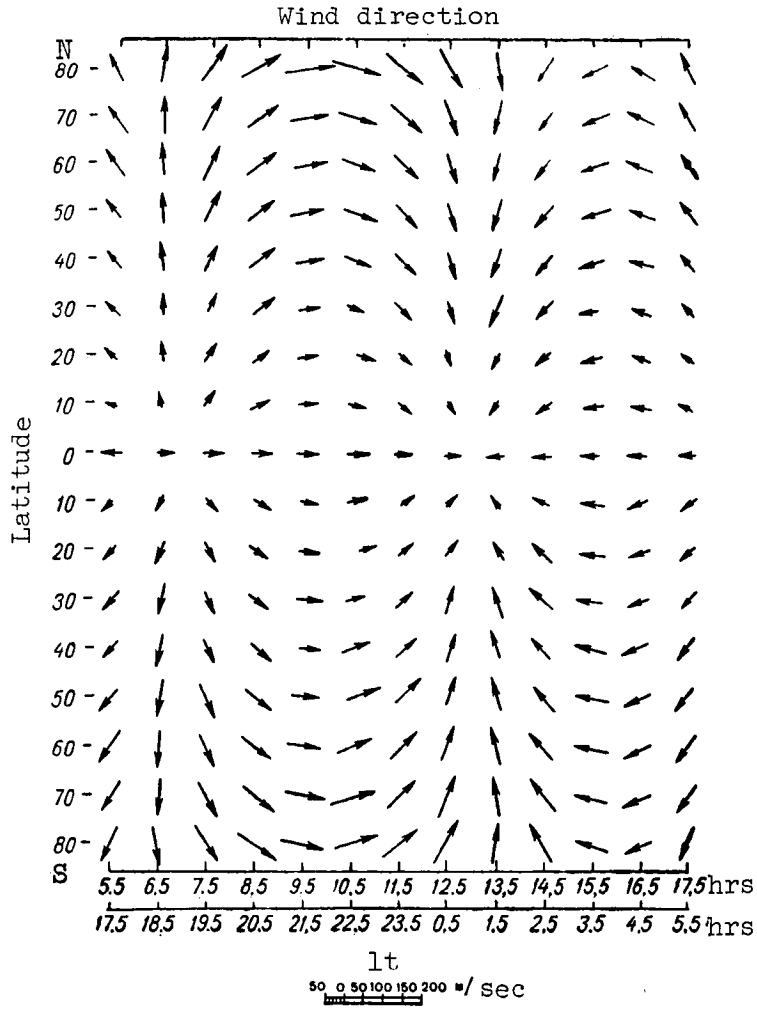

Figure 38.5. Field of tidal wind at 100 km level at 1730 and 0530 lt (total semidiurnal tidal variations).

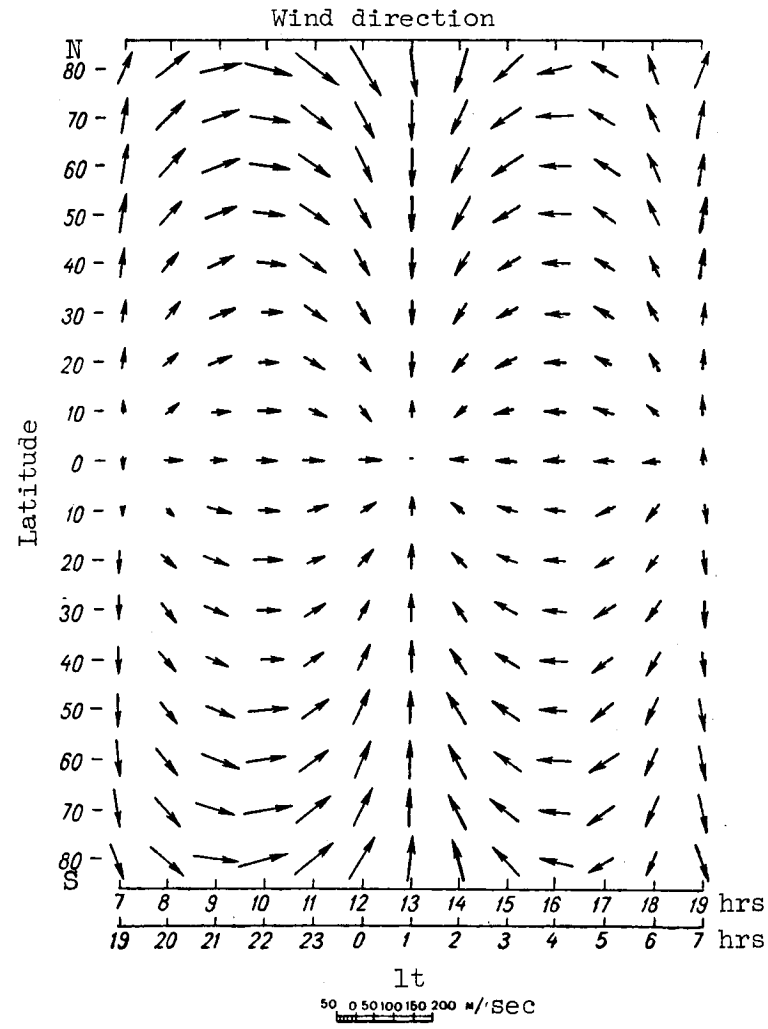

Figure 38.6. Field of tidal wind at 100 km level at 1900 and 0700 lt (total semidiurnal tidal variations).

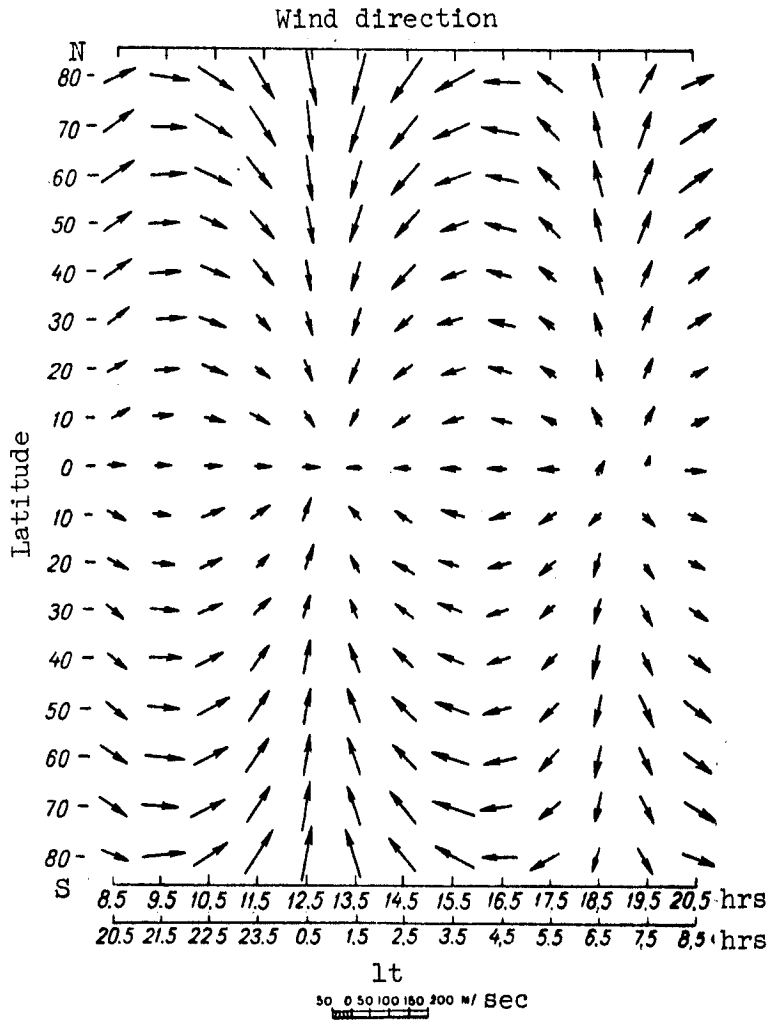

Figure 38.7. Field of tidal wind at 100 km level at 2030 and 0830 lt (total semidiurnal tidal variations).

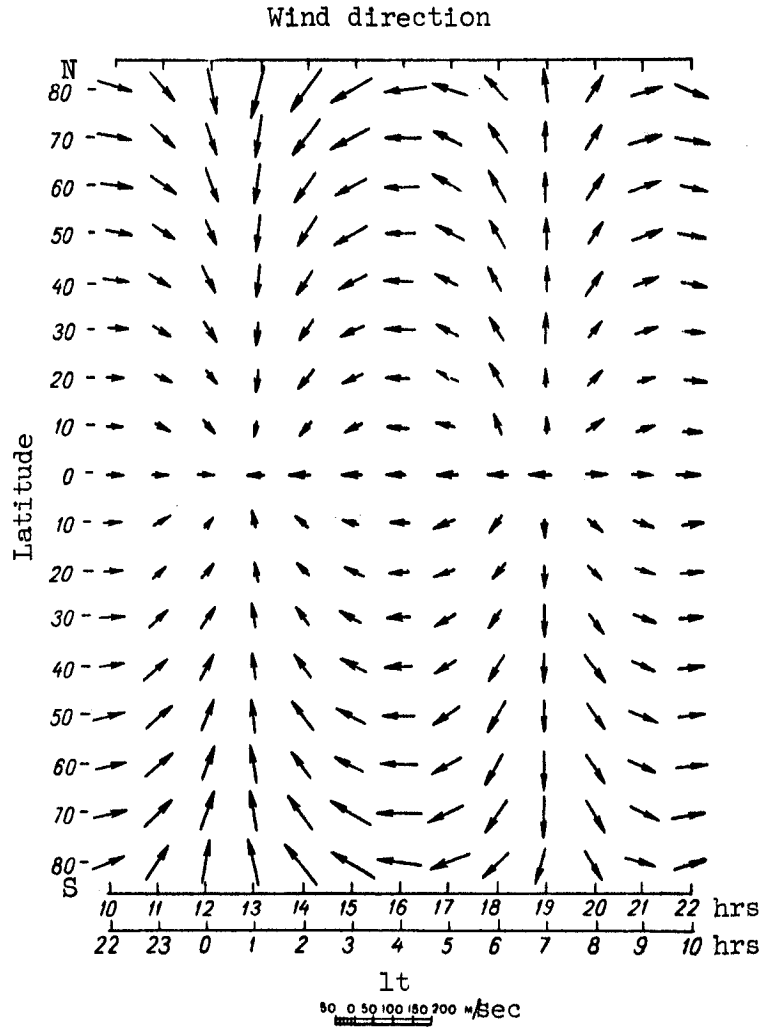

Figure 38.8. Field of tidal wind at 100 km level at 2200 and 1000 lt (total semidiurnal tidal variations).

38.6. Field of the Tidal Wind at the 100 km Level. Proceeding on the basis of these concepts and estimates, Stolov computed the field of the tidal wind in the upper layers of the atmosphere (ref. 745). He assumed that the standing and travelling waves, equation (38.3) experience resonance with oscillation, having a period of 12 hours. Stipulating a condition of a high degree of resonance for the "equatorial oscillation," he adopted a value of 7.9 km for the equivalent height of the atmosphere. The use of the Hoff method gives three free oscillations of other types for an ocean of this depth. In particular, we obtain a $P_2(\cos\theta)$ oscillation with a period of 12 hours 22 min.

If we take into account changes of temperature with latitude, the natural period of a zonal oscillation of this type is 12 hours 10 min, agreeing with the data presented by Chapman, Pramanik and Topping (ref. 332). With such a small difference between the periods of the free and forced oscillations it can be expected that there will be appreciable resonance.

Observational data fully agree with such an assumption. The tidal potential contains no term which could be related to the excitation of this zonal oscillation. Consequently, the disturbing factor is possibly 12 hour temperature variations. In actuality, there should be a harmonic term in 12 hour temperature variations not dependent on local time. A term of this type should be very small, but since a standing wave is regularly observed, the resonance intensification should be considerable.

The Taylor-Pekeris linear theory leads to the conclusion that the tidal wind at a height of 100 km has a phase shift of 180° relative to the surface tidal wind, and at a height of 100 km has a velocity approximately 200 times greater than the velocity of the surface tidal wind. Accordingly, Stolov, after computing the surface tidal wind by the indicated method, obtains from these data a tidal wind at a height of 100 km by a simple change of its direction (reversal), and an increase of velocity by 200 times. Stolov's results are shown in figures 38.1 - 38.8, reproducing his eight world maps of the field of the tidal wind at a height of 100 km for different moments of Universal (Greenwich) Time for each 1 hour 30 min.

39. Comparison of Theory of Tidal Winds and Observations

In Chapter 9 we discussed observations indicating the existence of periodic variations of wind velocity and direction in the upper layers of the atmosphere. The diurnal variations of wind in the ionosphere (Section 30) are particularly well expressed. We will now discuss certain data for the purpose of an intercomparison of experimental investigations and theoretical results. In order to give the full picture we will consider not only the upper layers of the atmosphere, but also observations of tidal movements in the lower part of the atmosphere.

39.1. Tidal Movements in the Lower Part of the Atmosphere. The winds in the troposphere are related to the meridional temperature and pressure gradient and to the movement of large-scale synoptic systems. To all intents and purposes surface tidal winds can be neglected because of their insignificance.

However, by averaging observations for long intervals of time it is also possible to detect from surface data tidal winds superposed on irregular tropospheric winds. Chapman (ref. 324) used a 16 year series of observations at Mauritius (20°18'S, 57°36'E) to find that the velocity of the tidal wind at the Earth's surface is approximately 25 cm/sec, which gives a correct order of magnitude coinciding with theoretical computations (ref. 745).

Tidal movements are more clearly expressed in the lower layers of the stratosphere. Johnson (refs. 484 and 485) discovered and investigated the diurnal and semidiurnal wind variations at the 100 mb surface associated with solar tides in the atmosphere; he used data from the aerological stations of Great Britain for 1950-1951. Johnson considers this height to be convenient for study of tidal air movements in the lower layers of the atmosphere, because there, at least for latitudes 30-60°N, irregular (synoptic) wind variations are considerably smaller than in the upper part of the troposphere. Furthermore, the lower layers of the stratosphere are free of small-scale effects which can mask the variations of the tidal wind.

After analyzing radar observations of the wind, Johnson computed the mean annual divergence of the southerly and westerly wind components at the height of the 100 mb surface (approximately 16 km) for 0300, 0900, 1500 and 2100 hours from the mean annual values of the corresponding wind components. Using harmonic analysis, he obtained the following expressions for the mean annual variations of each component

$$100S = -54\cos(\varphi + 32°14') + 67\cos(2\varphi + 44°24') - \\ - 6\cos(3\varphi + 80°32') + 0.25\cos 4\varphi, \tag{39.1}$$

$$100W = 51\cos(\varphi + 84°24') + 51\cos(2\varphi - 29°3') - \\ - 7\cos(3\varphi - 26°34') + 0.0\cos 4\varphi, \tag{39.2}$$

where S and W are the southerly and westerly wind components in knots (1 knot = 0.51 m/sec) and φ is an angle changing from 0 to 360° with a change of time of 24 hours, beginning at 0300 hours.

As shown by equations (39.1) and (39.2), the first two harmonics considerably exceed the last two in amplitude. The wind variations are explained satisfactorily by a combination of oscillations with a diurnal and semidiurnal period. The description of the results of observations does not require use of harmonics of a higher order.

The diurnal variations of the southerly and westerly wind components are described by the first terms on the right-hand side of equations (39.1) and (39.2). Figure 39.1 is a vector diagram showing the resultant wind velocity causing the diurnal oscillation for any desired time. The wind velocity at any time is determined by the length of the segment (scale is shown on the diagram) connecting the corresponding point of the ellipse with the origin of coordinates (as an example we show such a segment for 0900 hours). The semidiurnal wind variations given by the second terms on the right-hand sides of equations (39.1) and (39.2) are shown in a similar way in figure 39.2. Figure 39.3 shows the result of addition of the diurnal and semidiurnal variations.

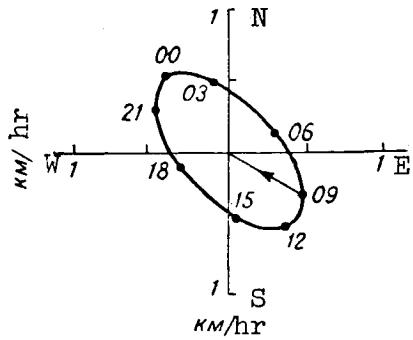

Figure 39.1. Diurnal variations of wind velocity in lower part of stratosphere.

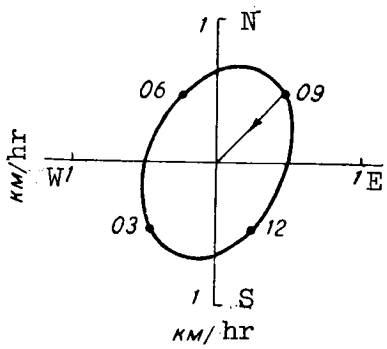

Figure 39.2. Semidiurnal variations of wind velocity in lower part of stratosphere.

If we conceive of an air particle whose movement is determined only by the tidal wind shown in figure 39.3, such a particle would move in a closed curve, as shown in figure 39.4. The maximum movement of the particle to the north occurs at 1700 hours, to the south at 0930 hours, to the east at 0600 hours and to the west at 1330 hours; the entire path of the particle is a few km. This illustrates once again the small magnitude of tidal movements in the lower part of the stratosphere.

To what degree have tidal movements been provided a sound theoretical basis? We will first consider the problem of the phase of tidal winds. As early as 1928 Bartels (ref. 280), proceeding on the basis of Simpson's formula (38.3) for tidal variations of surface pressure (taking into account only the "equatorial oscillation"), obtained the following expressions for the tidal wind

$$\left.\begin{aligned} U &= -54.6\cos\varphi\cos\left[2(\omega t+\lambda)+154^\circ\right] \\ V &= -(21.8+32.8\cos^2\theta)\sin\left[2(\omega t+\lambda)+154^\circ\right] \end{aligned}\right\} \qquad (39.3)$$

where U is the southerly and V the westerly wind component in cm/sec, ω is the angular velocity of the Earth's rotation, t is GMT and λ is the longitude east of Greenwich. It follows from a comparison of equations (39.3) and (38.3) that the variations of pressure and the westerly wind component near the Earth's surface occur with opposite phases; the westerly wind component attains a maximum value at about 0400 and 1600 lt. In the northern hemisphere the southerly wind component assumes its maximum value at approximately 0100 and 1300 lt. Comparison of these data with figure 39.3 leads to the conclusion that the semidiurnal variation in the lower part of the stratosphere approximately coincides in phase with surface tidal variations (ref. 485), which agrees with the conclusions of the theory of atmospheric tides (e.g., see ref. 807).

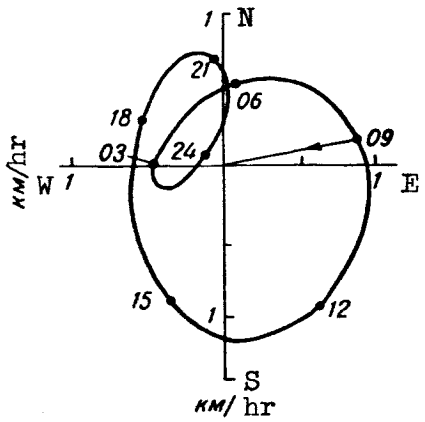

Figure 39.3. Resultant velocity of wind in lower part of stratosphere caused by combination of diurnal and semidiurnal variations.

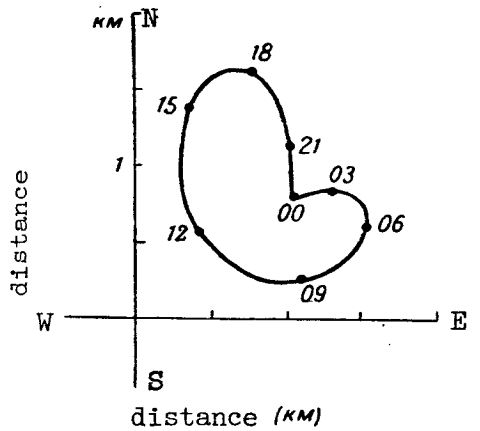

Figure 39.4. Path of particle experiencing tidal motion with velocity indicated in figure 39.3.

According to formula (39.3), at 55°N the amplitude of the tidal surface wind is 1.61 km/hour for the southerly component and 1.57 km/hour for the westerly component. Stolov obtained amplitudes of the same order of magnitude or slightly less (ref. 745). These amplitudes can be compared with those obtained from Johnson's data on tides at the height of the 100 mb surface (fig. 39.2), where the semidiurnal amplitude is 1.24 km/hour for the southerly component and 0.88 km/hour for the westerly component. It can be concluded from this comparison that there are no significant variations of the amplitude of the tidal wind with height in the troposphere and in the lowest part of the stratosphere. Observations show that in the upper layers of the atmosphere the amplitude of the diurnal and semidiurnal variations of wind velocity increase appreciably with height, and in the ionosphere exceed 100 km/hour.

The variations of the surface wind caused by lunar tides are considered by Sawada (ref. 713) on a theoretical basis. The amplitude of these oscillations is relatively small.

39.2. Dependence of Amplitude and Phase of Atmospheric Tides on Height. The semidiurnal wind component is caused by 12 hour oscillations of the Earth's atmosphere, due to the thermal and gravitational influence of the Sun. At the Earth's surface the amplitude of the oscillations is only 0.001 atmospheric pressure, and the wind associated with it theoretically has a velocity of only 0.4 m/sec; this value is also confirmed by observations (see beginning of this Section). However, at great heights the amplitude of variations of atmospheric pressure Δp is increased by many times as a result of resonance. Figure 39.5 shows changes of the amplitude and phase of semidiurnal pressure variations with height on the basis of theoretical (Wilkes, ref. 807) and experimental data.

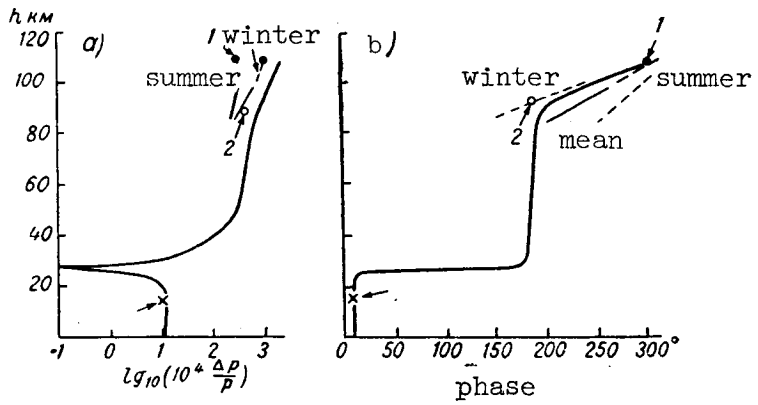

Figure 39.5. Change of amplitude (a) and phase (b) of semidiurnal variations of pressure with height (comparison of experimental data and Wilkes theoretical curve). (a) p, atmospheric pressure, Δp, amplitude of 12 hour variations; (b) scale of degrees constructed in such a way that 10° corresponds to the times 1000 and 2200 hours. 1, Briggs and Spencer; 2, Elford and Robertson; 3, Johnson.

According to the computations of Wilkes, the ratio $\frac{\Delta p}{p}$ increases from 0.001 at the Earth's surface to 0.1 at a height of 100 km; at the 30 km level there is a node. The amplitude obtained by Johnson (see beginning of this Section) (ref. 485) from wind observations in the lower part of the stratosphere agrees well with theory.

The data of Briggs and Spencer and also those of Elford and Robertson (ref. 373) are given for heights of 85-100 km. The latter are based on measurements of the drift of meteor trails. According to the data of these (and other) authors, the semidiurnal variations of wind components at heights of 80-100 km have a value of the order of 110 km/hour. Resonance intensification of the semidiurnal variations of pressure, according to different measurements, is from 20 to 80, which agrees with theory to an accuracy of a factor of 2. On the whole, the observed increase of the amplitude of the wind components with height agrees satisfactorily with theoretical conclusions. The mean value of the vertical wind velocity gradient of 1 m/sec is extremely close to that obtained from computations from the change of ratio $\frac{\Delta p}{p}$ caused by increase of the resonance intensification of atmospheric oscillations with height.

Figure 39.5b shows the theoretically predicted changes of phase of 12 hour pressure oscillations. The maximum of atmospheric pressure at the Earth's surface sets in at 1000 and 2200 lt, which corresponds to the phase $+10^\circ$ on a scale with an arbitrary zero. Pressure variations experience a change of phase to an opposite value at a nodal plane at a height of 30 km. Above this level the pressure maximum sets in at 0400 and 1600 hours. There should be a smooth change of phase by 5° km^{-1} at heights greater than 80 km.

The system of winds associated with the semidiurnal pressure wave in the northern hemisphere is such that the wind vector is directed to the west when pressure is maximal; using this relation, Greenhow and Neufeld determined the phase of pressure variations from the observed time of the maximum of the northerly or westerly wind components (fig. 41.2). These experimental data have been plotted on a graph (fig. 38.5b) for winter, summer and mean annual values. The theoretical curve agrees well with the mean experimental data. The pressure maximum at a height of 80 km is observed at about 0400 and 1600 hours.

The observed change of phase by 5° km^{-1} also agrees with theory.

39.3. Tidal Wind at a Height of 100 km. In Section 38 we presented a detailed exposition of Stolov's theoretical investigation (ref. 745); his results of a study of the tidal wind at the 100 km level are shown in figures 38.1 - 38.8. These maps can be compared with the results of wind measurements by radar echoes made by Greenhow (refs. 411 and 412) at Manchester ($53^{\circ}30'$N, $2^{\circ}15'$W) and Manning (refs. 568 and 569) at Stanford University ($37^{\circ}26'$N, $122^{\circ}10'$W). The agreement between theory and observations is also satisfactory in this case, as shown in Table 39.1. Furthermore, Stolov compared his theoretical results with measurements of the ionospheric wind (from the drift of ionospheric inhomogeneities, Section 30). He used the measurements made at Washington by Salzberg and Greenstone for this purpose. These authors discovered a semidiurnal clockwise rotation of the wind vector.

A similar rotation of the wind was observed by Philipps at Cambridge. It was found that Stolov's computations give approximately the same rotation of the wind, as shown in Table 39.2. The Cambridge data show the presence of a semidiurnal periodicity both for the north-south and east-west components; there is no diurnal component. The amplitude of the solar semidiurnal harmonic attains almost 30 m/sec; at about 0300 lt the wind blows northward and at 0600 to the east (Table 39.2). Whereas Stolov's computations give a close theoretical value for wind velocity, the phase agreement is not so good; according to the computations the wind blows northward at 0700 lt and eastward at 1000 lt.

TABLE 39.1 COMPARISON OF WIND DATA OBTAINED FORM OBSERVATIONS OF DRIFT OF IONIZED METEOR TRAILS AND COMPUTED VALUES OF TIDAL WIND.

Local time, hrs and min	Observation point	Wind observed	Wind computed from tidal theory
2300-2400	Manchester	Northerly wind, 30-60 m/sec	Northerly wind, 63 m/sec
0300-0600	Stanford	Mean velocity 35 m/sec, direction most frequently SSW, but also N	Northerly wind 13 m/sec at 0330 which becomes a southerly wind of 43 m/sec at 0500
0320-0500	Manchester	Southerly wind, 40-60 m/sec	Southerly wind, 11 m/sec at 0400 hours, intensifying to 63 m/sec at 0530

TABLE 39.2. COMPARISON OF MEASURED WIND DIRECTION AND VALUE COMPUTED FROM TIDAL THEORY.

Wind direction	Measured at		Computed (hrs)
	Washington, hrs, min	Cambridge, (hrs)	
N	05 00—06 30	03	07
E	07 00—07 30	06	10
S	10 00—00 00	09	13
W	12 00—13 00	12	16
N	13 30—15 30	15	19
E	15 00—17 30	18	22
S	18 00—19 00	21	01
W	2 00—03 30	24	04

This discrepancy can possibly be attributed to the fact that during the day there is a change of the height of the layer for which wind velocity (drift velocity of ionospheric inhomogeneities) was determined experimentally.

40. Wind in the Ionosphere and Geomagnetic Field Variations

The Earth's magnetic field is subject to changes which are the result of the superposing of a variable field on the permanent geomagnetic field. These changes sometimes occur smoothly, in accordance with some law, but sometimes they have a chaotic character (periods, amplitudes and phases constantly changing in value). In the first case the variations are called quiet or undisturbed, and in the second case they are called disturbed.

The variable geomagnetic field is determined by the vector of magnetic variations, i.e., by the geometric difference between the observed value of field strength and its mean value over a long period of time.

Undisturbed variations are rigorously periodic. Solar-diurnal, lunar-diurnal and annual variations are known. For example, on an undisturbed day a horizontally placed magnetic needle at Leningrad is deflected eastward at its northern end in the morning, and at 0800 hours the deflection becomes maximum. This is followed by a trend to the west, which is completed at 1400 hours. The amplitude of the solar-diurnal variations, having the period of the solar day, does not exceed 16' at Leningrad. Disturbed variations can have a far greater magnitude.

Geomagnetic variations are related closely to other physical processes on Earth and in surrounding space (Earth currents, appearance of active formations on the Sun, and especially phenomena in the upper layers of the atmosphere: auroras, disruptions of radio wave propagation, etc.). When analyzing such relationships it is convenient to characterize the variations by a value showing the degree of magnetic field disturbance. This value is called magnetic

activity or magnetic disturbance. The numerical characteristic δU (the value of variation of magnetic field potential energy U) usually is used as a measure:

$$\delta U = \frac{H\delta H + Z\delta Z}{1000}, \qquad (40.1)$$

where H and Z are the mean monthly values of the horizontal and vertical components of the geomagnetic field, and δH and δZ are the differences between the maximum and minimum values of these elements for a particular period of time (hour, day, etc.). The index k has now been introduced into international practice: it is a numerical characteristic expressed in units. Each unit corresponds to the amplitude of variations of the magnetic elements during a 3 hour period, corrected for quiet diurnal variation.

A special measure of activity u is used as a characteristic of large periods, such as a month or a year. This index represents the mean monthly or annual value of the differences of succeeding mean diurnal absolute values of the horizontal component at the magnetic equator, or near it. It must be remembered that at the time of strong magnetic disturbances the changes of the horizontal component of the magnetic field have the same character over the entire Earth: at the initial time of a magnetic storm the horizontal component decreases everywhere and then slowly returns to a normal state. The measure of activity u is expressed in units 10^{-4} oersted. The measure u_1, related to u as indicated in the following table (ref. 262), is also used

u	0.3	0.5	0.7	0.9	1.2	1.5	1.8	2.1	2.7	3.6 and above
u_1	0	20	40	57	79	96	108	118	132	140

In connection with the problem of air currents in the upper layers of the atmosphere, dealt with in this chapter, we give particular attention to diurnal variations of the geomagnetic field.

40.1. Diurnal Variations of the Earth's Magnetic Field. A characteristic feature of solar-diurnal variations S is that they transpire by local time. Figure 40.1 represents the mean annual variation of declination D of the horizontal H and vertical Z components on the basis of observations at the Pavlovskaya Magnetic Observatory. The horizontal component has a minimum near 1100 hours and a maximum near 2100 hours, and the vertical component, which remains almost constant at nighttime, begins to increase in the morning and attains its maximum value after midday.

Solar-diurnal variations are dependent on the value of magnetic activity on a particular day, and two kinds of variations are therefore distinguished: those of quiet and those of stormy days. The first of these--S_q--are obtained by analysis of observations only for quiet days; disturbed variations--S_d-- are obtained by an analysis of geomagnetic records for stormy days. The difference

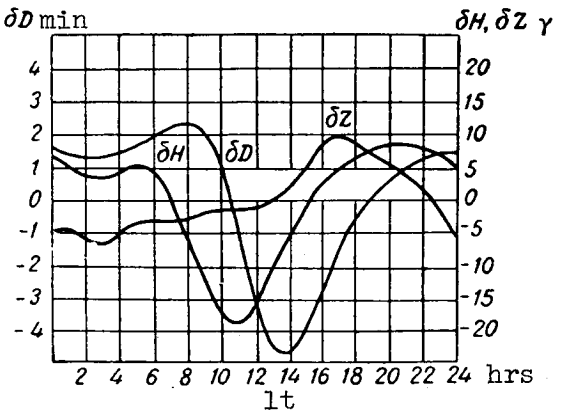

Figure 40.1. Diurnal variation of elements of terrestrial magnetism at Pavlovskaya Magnetic Observatory.

between disturbed variations and S_q is clearly reflected in the curve of variations of the vertical component, where there is a change both of the amplitude and the entire shape of the curve. The amplitudes of quiet diurnal variations S_q change during the year, assuming a maximum value at the time of the summer solstice and a minimum value at the time of the winter solstice. In the equinoctial periods the amplitude has a mean value between the summer and winter values and is the same in both hemispheres.

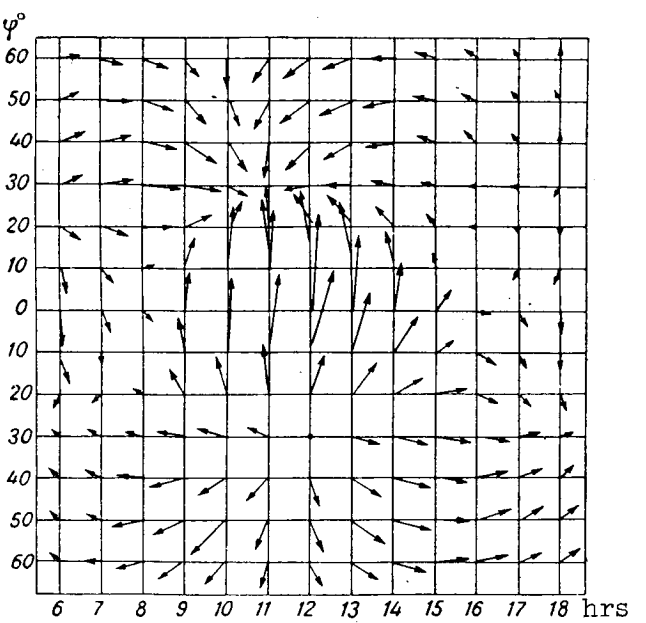

Figure 40.2. Projection of vector of S_q variations onto horizontal plane.

The character of the solar-diurnal variations is different at different points on the Earth's surface. Whereas for points situated on the same parallel the diurnal variation is almost identical, for points situated along the meridian it changes appreciably and in conformity to a definite law. The most graphic representation of the variation of diurnal variations is given by vector diagrams, on which the projections of the vector of S_q variations are plotted on horizontal and vertical planes. Figure 40.2 shows such a diagram of projections on a horizontal plane in equinoctial periods for the daytime and the part of the Earth's surface bounded by the geographic latitudes from 60 to -60° and longitudes from 6^h to 18^h (the longitudes coincide with lt from 0600 to 1800 hours). Figure 40.3 shows diagrams of the projections of the S_q vector onto vertical planes: onto the plane of the midday meridian and onto the plane of a great circle in contact with the 30th parallel at the midday point (ref. 262).

In addition to solar-diurnal variations there are other periodic variations associated with the position of the Moon relative to the horizon. The period of these variations coincides with the interval of time between two successive transits of the Moon across the local meridian, i.e., with lunar half-days (lunar days are equal to 24 hours 50 min 28 sec mean solar time). The principal pattern of these variations is their semidiurnal character: the curves of the changes of all the elements in the course of a lunar day have two maxima and two minima. The mean monthly curve has the form of a regular double wave with maxima at 0600 and 1800 hours lunar time and minima at 0000 and 1200 hours for the northern hemisphere.

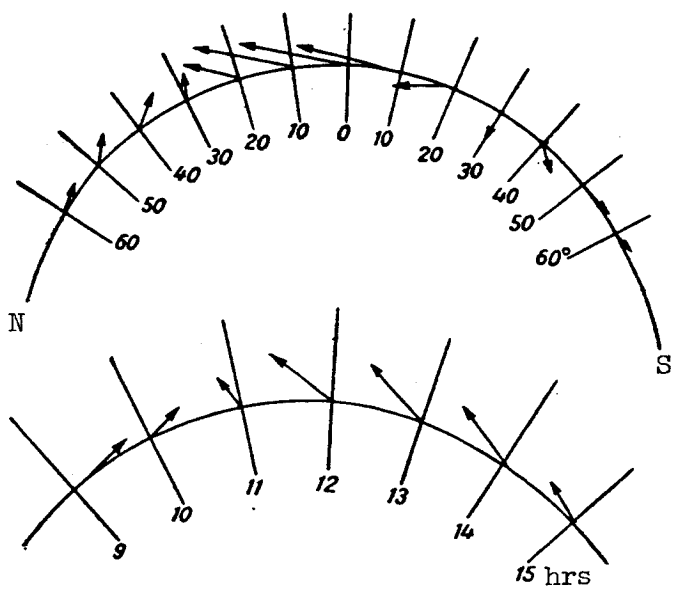

Figure 40.3. Projection of vector of S_q variations onto vertical planes: top, onto plane of midday meridian; bottom, onto plane of prime vertical.

Lunar-diurnal variations have an annual variation depending on the positi of the Sun. At the time of the summer solstice the amplitudes of lunar days attain maximum values in the northern hemisphere and minimum values in the southern hemisphere; at the time of the winter solstice the reverse is true. The maximum amplitudes for the vertical and horizontal components attain no more than 1-2 γ and for declination 40". The dependence of lunar-diurnal variations on latitude and longitude has the same character as for solar-diurnal variations. It is interesting that the amplitude of lunar variations depends on the Moon-Earth distance: the amplitude of the variations changes approximately inversely proportional to the cube of this distance (ref. 262).

40.2. Sources of the Field of Diurnal variations. In a study of the diagram of projections of the vector of S_q variations onto a horizontal plane (fig. 40.2) we clearly note a remarkable characteristic of this diagram: the S_q vector in the northern hemisphere in the daytime hours is always directed toward some center which is situated on the pre-midday meridian at parallel 30°, but in the southern hemisphere it is directed away from the center situated on this same meridian and the parallel -30°. A study of the projections onto vertical planes (fig. 40.3) reveals the presence of a similar characteristic: the S_q vectors are directed toward centers lying above the Earth's surface, approximately over parallels 30 and -30° near the midday meridian.

It has long been speculated that these centers can be identified with the axis of the vortical electrical current whose direction is counterclockwise in the northern hemisphere (if the current is viewed from above) and clockwise in the southern hemisphere. In this case the diurnal variations could be attributed to the existence of systems of closed eddy currents in the atmosphere, which remain fixed in space and within which the Earth rotates; since the maximum values of the vector of variations are in the daytime hours, the maximum current strength should be in the space between the Sun and the Earth. The current system, having a center at latitude 30° and on the midday meridian, remains fixed in the space between the Sun and the Earth, and an observer on Earth, rotating relative to this system, in one day passes through all the values of the vector of field strength of these points, distributed on the observer's parallel.

The electrical current and the magnetic field created by it are unambiguously interrelated (Biot-Savart relation). Therefore, by knowing the field of geomagnetic solar-diurnal variations, it is possible to determine the source of this field, i.e., the system of electrical currents, provided we know the distance between this current and those points at which the field is known. The most important results in solution of this problem were obtained by S. Chapman and N. P. Ben'kova.

In these computations it was convenient to use the equivalence of a closed current and a double magnetic layer which follows from the Biot-Savart relation. By replacing the current system by a double magnetic layer of variable density situated on a sphere, concentric with the Earth's surface and having the radius r ($r > R$, where R is the Earth's radius), it is possible to find the magnetic

potential U of such a layer on the Earth's surface. It is known from potential theory that (ref. 262)

$$U=\iint \mu \frac{\partial}{\partial n}\left(\frac{1}{\rho}\right)dS, \tag{40.2}$$

where μ is the surface density of the magnetic moment of the double layer, corresponding to an element of the surface dS, ρ is the distance to that point of the Earth's surface where the potential U must be determined and n is the direction of the normal to the surface of the sphere coinciding with radius r. Integration is applied to the entire surface of the sphere.

We now transform expression (40.2), using the known results of potential theory. It is easy to see that

$$\rho^2=R^2+r^2-2Rr\cos\gamma,$$

where γ is the angle between R and r; hence

$$\rho^2=r^2\left[1+\left(\frac{R}{r}\right)^2-2\left(\frac{R}{r}\right)\cos\gamma\right].$$

Consequently,

$$U=\frac{1}{r}\iint \mu \frac{\partial}{\partial n}\frac{dS}{\sqrt{1+\left(\frac{R}{r}\right)^2-2\left(\frac{R}{r}\right)\cos\gamma}}.$$

Since r > R, the function

$$\varphi(R,\gamma)=\left[1+\left(\frac{R}{r}\right)^2-2\left(\frac{R}{r}\right)\cos\gamma\right]^{-\frac{1}{2}}$$

can be expanded into a converging series of powers $\frac{R}{r}$, using Newton's binomial theorem

$$\varphi(R,\gamma)=1-\frac{1}{2}\left[\left(\frac{R}{r}\right)^2-2\left(\frac{R}{r}\right)\cos\gamma\right]+ \tag{40.3}$$
$$+\frac{3}{8}\left[\left(\frac{R}{r}\right)^2-2\left(\frac{R}{r}\right)\cos\gamma\right]^2.$$

Removing the brackets and collecting terms $\frac{R}{r}$ with identical powers, we obtain

$$\varphi(R,\gamma)=\sum_{n=0}^{\infty}\left(\frac{R}{r}\right)^n P_n(\cos\gamma), \tag{40.4}$$

where $P_n(\cos\gamma)$ are Legendre polynomials.

Consequently, expression (40.2) for the magnetic potential of a double magnetic layer can be written in the form

$$U = \int\int \mu \frac{\partial}{\partial n} \sum_{n=1}^{\infty} \frac{R^n}{r^{n+1}} P_n(\cos\gamma)\, dS = \tag{40.5}$$

$$= -\sum_{n=1}^{\infty} (n+1) \frac{R^n}{r^{n+2}} \int\int \mu P_n(\cos\gamma)\, dS.$$

The surface density of the magnetic moment μ of a double magnetic layer is dependent on two variables, e.g., on colatitude θ and on longitude λ. It is shown in potential theory that any function of two variables given on a sphere can be expanded uniquely into a series using spherical Laplace functions; accordingly, μ can be represented in the form of the sum (ref. 262)

$$\mu = \sum_{k=1}^{\infty} \mu_k,$$

where

$$\mu_k = \sum_{m=0}^{k} \left(a_n^m \cos m\lambda + b_n^m \sin m\lambda\right) P_n^m(\cos\theta).$$

consequently,

$$U = -\Sigma(n+1) \frac{R^n}{r^{n+2}} \sum_{k=1}^{\infty} \int\int \mu_k P_n(\cos\gamma)\, dS. \tag{40.6}$$

This expression for the magnetic potential of a double layer can be simplified by using the following spherical functions (known from theory) of the relation

$$\int\int \mu_k P_n(\cos\gamma)\, dS = \frac{4\pi r^2}{2n+1} \mu_n,$$

if k = n,

$$\int\int \mu_k P_n(\cos\gamma)\, dS = 0,$$

if $k \neq n$.

Thus,

$$U=-\sum_{n=1}^{\infty}4\pi\frac{n+1}{2n+1}\left(\frac{R}{r}\right)^{n}\mu_{n}. \qquad (40.7)$$

In order to obtain the required result we must become familiar with the conclusions drawn from a spherical analysis of observed geomagnetic variations. We first will consider some theorems of the Gauss theory.

The theory proposed by Gauss in 1838 (ref. 27) in its time was a major step in the analytical representation of the geomagnetic field. This theory was intended to represent the Earth's magnetic field as a function of the coordinates of a particular point, without the physical factors responsible for development of the field being taken into account. As the basis of his investigation Gauss assumed that the geomagnetic field is caused by factors which operate within the Earth and therefore has a potential.

Gauss demonstrated that the magnetic potential U, created at the surface of a sphere by magnetic masses located within it, is expressed by a double sum with an infinite number of terms, each term representing a spherical function

$$P_n^m(\cos\theta)\cos m\lambda$$

of colatitude θ and longitude λ with the constant coefficients g_n^m and h_n^m

$$U=R\sum_{n=1}^{\infty}\sum_{m=0}^{n}\left[g_n^m\cos m\lambda+h_n^m\sin m\lambda\right]P_n^m(\cos\theta), \qquad (40.8)$$

where R is the Earth's radius. For practical purposes it is necessary to limit ourselves to a finite number of terms depending on the degree of convergence of these series (Gauss limited himself to expansion terms of the fourth order of magnitude).

The constant coefficients g_n^m and h_n^m are determined from observations of the geomagnetic elements at the necessary number of points on the Earth's surface. The most recent determinations of the coefficients were made for the epoch 1945 by V. I. Afanas'yeva in the USSR and Vestine in the United States. The coefficients g_1^0 and h_1^1 have the highest values; these correspond to terms of the first order of magnitude, which indicates a dipole character of the geomagnetic field (the first terms of the Gauss expansion (40.8) correspond to the part of the dipole; terms of the second order of magnitude represent the potential of the quadrupole).

An extremely important result of the Gauss theory is that it becomes possible to separate the geomagnetic field into the field caused by internal sources and the field with sources outside the Earth. The expansion of the potential with its sources outside the Earth was performed for the first time by Schmidt (ref. 718) in 1889. If, in addition to magnetic masses localized within the Earth, there are masses outside it, the components X (horizontal component, directed to the north), Y (horizontal, directed to the east), and Z (vertical) of field strength observed at the Earth's surface are expressed as follows (ref. 262)

/54

$$\left.\begin{aligned} X &= -\sum_{n=1}^{\infty}\sum_{m=0}^{n}\left(p_n^m\cos m\lambda + q_n^m\sin m\lambda\right)\frac{dP_n^m(\cos\theta)}{d\theta} \\ Y &= \sum_{n=1}^{\infty}\sum_{m=0}^{n}\left(p_n^m\sin m\lambda + q_n^m\cos m\lambda\right)\frac{mP_n^m(\cos\theta)}{\sin\theta} \\ Z &= \sum_{n=1}^{\infty}\sum_{m=0}^{n}\left(p_n'^m\cos m\lambda + q_n'^m\sin m\lambda\right)P_n^m(\cos\theta) \end{aligned}\right\} \qquad (40.9)$$

where the coefficients p_n^m, q_n^m, $p_n'^m$ and $q_n'^m$ are determined from the relations

$$\left.\begin{aligned} p_n^m &= g_n^m + j_n^m \\ q_n^m &= h_n^m + k_n^m \\ p_n'^m &= (n+1)g_n^m - nj_n^m \\ q_n'^m &= (n+1)h_n^m - nk_n^m \end{aligned}\right\} \qquad (40.10)$$

Here g_n^m and h_n^m are known constant coefficients determining the field potential from internal sources, see equation (40.8), j_n^m and k_n^m are similar coefficients corresponding to the external factors.

With formulas (40.9) we can investigate and separate the external and internal factors causing the observed geomagnetic field. This requires observations of the vertical component Z for determination of the coefficients $p_n'^m$ and $q_n'^m$, and observations of the horizontal component X for determination of the coefficients p_n^m and q_n^m. Then equations (40.10) can be used to determine the coefficients g_n^m and h_n^m, corresponding to the field caused by internal factors, and the coefficients j_n^m and k_n^m, corresponding to external factors.

Analysis of the geomagnetic field reveals that 94 percent of it is caused by the internal field and about 6 percent by the external field.

We now will return to the problem of finding the electrical currents creating solar-diurnal variations of the Earth's magnetic field. A detailed study of the results of a spherical analysis of the field leads to the conclusion that this field is not produced by sources entirely below the Earth's surface (as is the case for the Earth's main magnetic field), and also is not produced by sources entirely above the Earth. It is excited by sources situated partially above and partially below. Analysis revealed that the main part of the S_q field has its source above the Earth and the lesser part of the S_q field (1/4 to 1/3 of the entire field) has its source near the Earth's surface, within the Earth. The horizontal component of the S_q field is intensified by addition of the effect of the internal and external sources, but in the vertical component they are opposite in sign (ref. 244).

It follows from equations (40.9) that the magnetic potential of the field of variations is expressed in the form of a series

$$U = R\sum U_n,$$

where

$$U_n = \sum \left(p_n^m \cos m\lambda + q_n^m \sin m\lambda\right) P_n^m (\cos\theta). \tag{40.11}$$

Here the coefficients p_n^m and q_n^m are known from observations and represent the external part of the potential of variations (ref. 262). Comparing expressions (40.11) and (40.7) we find

$$RU_n = -4\pi \frac{n+1}{2n+1}\left(\frac{R}{r}\right)^n \mu_n,$$

hence

$$\mu_n = -\frac{R}{4\pi}\frac{2n+1}{n+1}\left(\frac{r}{R}\right)^n U_n.$$

Substituting μ_n into equation (40.6) and replacing U_n by its value, we obtain

$$\mu = -\frac{R}{4\pi}\sum_{n=1}^{\infty}\frac{2n+1}{n+1}\left(\frac{r}{R}\right)^n \sum_{m=0}^{n}\left(p_n^m \cos m\lambda + q_n^m \sin m\lambda\right) P_n^m (\cos\theta). \tag{40.12}$$

Thus, the problem of finding the double magnetic layer of variable thickness situated on a sphere, being the source of the observed solar-diurnal geomagnetic variations, has been solved. By using formula (40.12) it is easy to find the corresponding system of electrical currents.

40.3. Electrical Currents in the Ionosphere. Many facts are now known which serve as a basis for assuming that the current system responsible for solar-diurnal variations of the magnetic field is situated in the E layer of the ionosphere. Accordingly, N. P. Ben'kova (ref. 11), in computing the electrical currents in the ionosphere responsible for S_q variations, adopted a mean height of the current-conducting layer of 109 km. If the current strength I is measured in thousands of amperes and p_n^m and q_n^m are measured in gammas, the following formula for the computation of the current system can be derived from expression (40.12)

$$I = -5.0707 \sum_{n=1}^{\infty} \frac{2n+1}{n+1} (1.02)^n \sum_{m=0}^{n} (p_n^m \cos m\lambda + q_n^m \sin m\lambda) P_n^m (\cos \theta). \tag{40.13}$$

N. P. Ben'kova made the most complete analysis of diurnal S_q variations. In making a spherical analysis she used data from 47 magnetic observatories. In order to obtain a better approximation to the theoretical diurnal variation, Ben'kova included observatories situated beyond the polar circle and took into account the dependence of variations on both latitude and longitude; geomagnetic longitude, latitude and time were used (ref. 11).

Diurnal analysis permits expansion of a function depending only on two coordinates. In order to take into account a third coordinate as well, Ben'kova postulated that solar-diurnal S_q variations are the result of superposing of two variations (two functions), of which one S_{q1} is dependent on latitude Φ and local time t, and the others S_{q2} is dependent on longitude λ and latitude, i.e.,

$$S_q = S_{q1}(\Phi, t) + S_{q2}(\Phi, \lambda). \tag{40.14}$$

The expansion was made separately for the functions S_{q1} and S_{q2}. It was shown that the main part of the field of variations is the function S_{q1}, i.e.,

has no dependence on longitude. The influence of longitude is reflected only in the low and middle latitidues. Figure 40.4 represents the current system computed by Ben'kova for the summer months (May-August) for S_{q1} functions. The map shows current isolines (lines corresponding to the direction of flow of a current of a particular strength). The numbers accompanying the isolines indicate the current strength in thousands of amperes, and the difference in the values of current strength between two adjacent isolines is equal to the strength of the current flowing between these isolines.

Figure 40.4 shows that a midday lt in the equatorial latitudes there is a region of a positive current (the solid isolines correspond to a positive direction of the current, counterclockwise; dashed isolines correspond to a negative direction, clockwise). The nighttime region of negative currents breaks down into two clearly defined eddies.

Vestine has done important work in this field. In a study of the influence of ionospheric winds on the development of diurnal (solar and lunar) geomagnetic field variations, he studied the reaction of the radiation belts to magnetic field changes (ref. 786).

With respect to the direct experimental discovery and investigation of the ionospheric current systems corresponding to S_q variations, definite indications of this type were obtained by Appleton, Lyon and Pritchard (ref. 266) from an analysis of data from vertical sounding of the ionosphere by radio waves.

The hypothesis of ionospheric currents flowing at a height of about 100 km received brilliant confirmation from direct measurements in the upper layers of the atmosphere by rocket-borne instruments. Two rockets with magnetometers were launched near the geomagnetic equator (11°S, 89°W) on Mar. 17, 1949; these instruments automatically transmitted radio signals on magnetic field strength at fixed time intervals. The launching time was selected in such a way that one rocket was launched at a time when current density in the ionosphere would be maximal, according to theoretical computations; the other was launched at the minimum of current density.

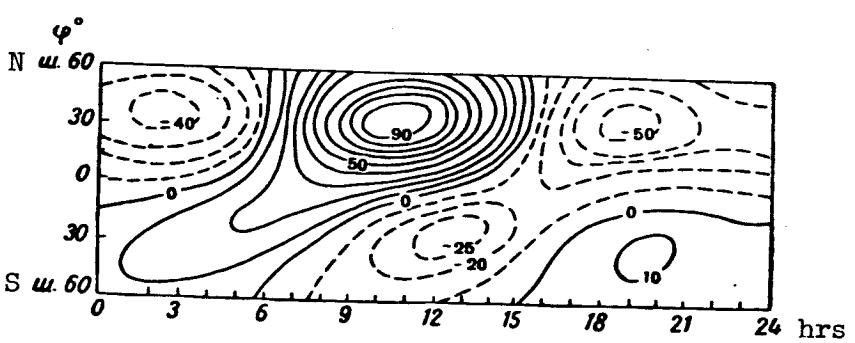

Figure 40.4. Current system in ionosphere in summer.

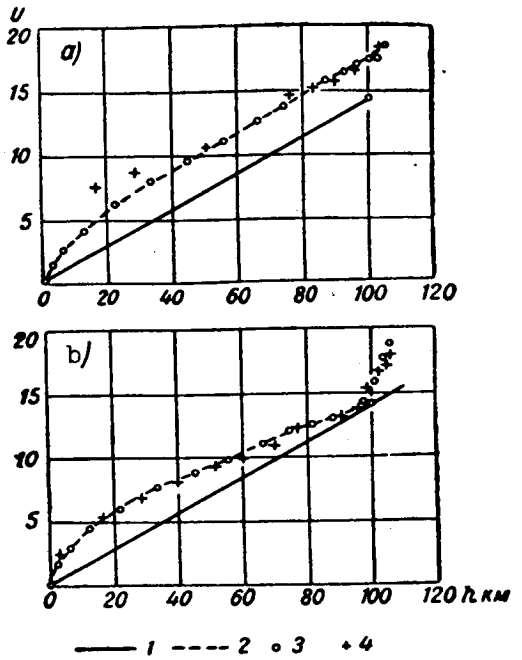

Figure 40.5. Change of strength of geomagnetic field U (milligauss) with height h in km on basis of rocket observations. a, 1720 hours; b, 1120 hours; 1, theoretical curves; 2, observed curves; 3, during rocket ascent; 4, during descent.

The results of the rocket measurements are shown in Figure 40.5. Figure 40.5a applies to observations in the period of the minimum of the ionospheric current; figure 40.5b applies to the period of the maximum. The theoretical curves 1 show a decrease of magnetic field strength with height (in comparison with surface values), computed on the assumption of a uniformly magnetized Earth (i.e., that the Earth's magnetic moment corresponds to the first term of the Gauss expansion, formula (40.8)).

These experiments confirm the presence of currents at a height of 105 km, because at this height in the period of the current maximum (fig. 40.5b) the magnetic field strength experiences a sharp decrease, whereas in the period of the current minimum (fig. 40.5a) there are no such changes.

The more rapid decrease of the geomagnetic field with height recorded at low heights, as indicated by theory, can be attributed to the presence of a magnetic anomaly in the region of rocket launching.

Such rocket measurements of current systems in the ionosphere have been repeated. The State University of Iowa in the United States, in accordance with the IGY program, made a number of magnetic field measurements at great heights, using a nuclear precession magnetometer. This instrument was carried aloft by "Rockoons." The experiments were made in the polar and equatorial latitudes (ref. 315).

In the equatorial latitudes the rockets were launched from a vessel near the Hawaiian Islands in October 1957. The rockets reached heights of 51-129 km. A change of magnetic field strength, indicating that the rocket had entered the layer of the electrical current flowing from east to west at a height of 104 km, was observed on a flight on Oct. 17, at 1244 hours (time at the 165th meridian). A small decrease corresponding to a weak flow of easterly direction was observed at heights of 116 and 123 km.

On Oct. 18 at 1243 hours a rocket passed through two current layers at heights of 100 and 122 km. A similar result was obtained on Oct. 19 at 0750 hours.

Results of magnetic field measurement were used to compute the vertical profiles of current density j. The value obtained for Oct. 17 was $j_{max} = 7$ a/km^2, for Oct. 18 $j_{max} = 6.2$ and more than 7 a/km^2, and for Oct. 19 $j_{max} =$ 19.8 and 22 a/km^2. On the basis of these profiles Cahill (ref. 315) constructed a model of the equatorial electrojet. According to this model the width of the jet is about 300 km, the height of its lower boundary is 97 km and the upper boundary of the lower current layer is 110 km. Cahill assumes that the configuration and intensity of the current system changes from day to day and during the day.

According to Martyn, the most important component of ionospheric conductivity in the equatorial region is directed along the equator, and its vertical distribution has a clearly expressed maximum at the 100 km level. Cahill attributes the existence of two current systems to the presence of a well-developed sporadic E_s layer (ref. 233).

40.4. S_q Variations and Tidal Winds in the Ionosphere. These experimental and theoretical data leave no doubt that solar-diurnal geomagnetic variations are caused mostly by electrical currents in the ionosphere. It must be remembered, however, that up to now there is no certain explanation of the factors responsible for the development of electrical currents in the ionosphere. Existing theories of the diurnal variations in essence can be reduced to the selection of the mechanism of development of these currents. The theory of an atmospheric dynamo and the theory of drift currents merit greatest attention.

The basis for the theory of an atmospheric dynamo, proposed as early as the 1870's and 1880's by Stewart and Schuster (ref. 719), is the principle of electromagnetic induction--the induction of an emf in a conductor during its motion in a magnetic field. Because of the presence of conductivity in the upper layers of the atmosphere during motion, relative to the geomagnetic field H, they propose an electrical field of strength E, perpendicular to H, and the direction of movement

$$\vec{E} = [\vec{u}\,\vec{H}]$$

(Faraday law), where u is the velocity of movement of the ionized layer. The density of the developing induction current is

$$j=\gamma' E,$$

where γ' is the conductivity of the ionized gas in the direction perpendicular to H. The conductivity of a gas in the absence of a magnetic field is

$$\gamma=ne^2\frac{l}{2mv}, \tag{40.15}$$

where n is the quantity of charged particles per cm^3, e is their charge, l is the length of the free path, v is the mean velocity of thermal motion of particles and m is their mass. According to electron theory, γ' is related to γ by the formula

$$\gamma'=\frac{\gamma}{1+\left(\frac{e}{r}\right)^2}, \tag{40.16}$$

where r is the radius of the spiral trajectory of the electron around the lines of force of the magnetic field H, determined from equation

$$r=\frac{mv}{He}. \tag{40.17}$$

After substituting the value of γ' from (40.16) in place of γ' in the formula for current density, we obtain

$$j=\frac{ne^2}{2mv}\frac{l}{1+\left(\frac{e}{r}\right)^2}\left[\vec{u}\,\vec{H}\right]. \tag{40.18}$$

The special importance of the atmospheric dynamo theory, including formula (40.18), for the problem of air currents in the upper layers of the atmosphere, is determined by the fact that velocity u is the velocity of movement of the conducting layer relative to the Earth's magnetic field, i.e., direct wind velocity. In particular, velocity u can be caused by horizontal tidal movements of air in the upper layers of the atmosphere, as postulated by Schuster.

According to the drift current theory, in the process of translational thermal motion, charged particles experience a drift under the influence of ponderomotive forces acting on a moving charged particle from the direction of the magnetic field. In its initial form the drift current theory was proposed by Chapman (ref. 323) and contained a basic error, later pointed out by I. Ye. Tamm (ref. 185). Chapman assumed that in the upper layers of the atmosphere, where l is large, air particles and charged particles seemingly fall in a vacuum and can acquire great vertical velocities under the influence of the Earth's attraction. As a result, the charged particles should have horizontal motion (drift) in a direction mg perpendicular to the force of gravity and the magnetic field H. The velocity of this drift is

$$u = \frac{mg \sin \psi}{eH},$$

where ψ is the angle between H and the vertical.

I. Ye. Tamm pointed out the incorrectness of the concept of ions which are free and independent in their motion, ions which in the absence of a magnetic field can fall downward under the influence of gravity. The fact is that in an equilibrium state of the atmosphere the natural weight of the ions is balanced by the partial pressure of the ion gas $p' = kTn$. Therefore, in an equilibrium state of the atmosphere there can be no drift (ref. 185). However, in this same study Tamm pointed out the possibility of the development of a drift current in the ionosphere as a result of a "nonuniform" density distribution (i.e., densities depending on height, but not conforming to the barometric formula).

The formula for determination of the density of a drift current was derived by Tamm on the basis of a statistical model of the ionosphere by solution of the Boltzmann kinetic equation. The drift current theory, corrected by Tamm, should be adopted, like the dynamo theory, for explaining the system of currents responsible for the diurnal variations of the geomagnetic field. At the same time, as Tamm points out, the drift current theory requires further development.

Not too long ago the atmospheric dynamo theory encountered difficulties in explaining the phases of geomagnetic variations. If we use as a point of departure the times of onset of the maxima and minima of atmospheric pressure in its diurnal (tidal) variations, the extremal times of geomagnetic variations computed on this basis are displaced by several hours relative to the times of the actual maxima and minima of the geomagnetic elements. However, it is now known that the phase of the tides themselves changes with height (fig. 39.5). Furthermore, we now can judge the velocity and phase of tidal movements in the upper layers of the atmosphere directly from the results of wind measurements in the ionosphere. We wonder what relationship exists between data on S_q variations and wind in the ionosphere. This problem has repeatedly been considered in the literature. We will discuss recent studies.

Greenhow and Neufeld, who made a detailed study of the wind in the upper layers of the atmosphere by radio meteor observations, came to the following conclusion in 1956 (ref. 412). In order to explain tidal winds in the ionosphere by quiet solar-diurnal variations of the Earth's magnetic field, the wind vector must be directed north at approximately 1100 and 2300 hours. However, according to the data of these authors on changes of phase of tides with height (fig. 39.5b and its explanation in Section 39.3), the tidal variations of pressure at a height of 85 km have a pressure maximum at 1000 and 2200 lt.

The wind system associated with the semidiurnal pressure wave in the northern hemisphere is such that the wind vector is directed to the west, when the pressure is maximal. Although above the 80 km level the tide phase is displaced somewhat with height, in the range of heights of 85-110 km the

phases of the tidal vectors are such that they cannot be correlated with the phase of the S_q variations: the time when the wind is directed north sets in at this interval of heights between 0730 and 0300 hours. If we extrapolate the curve of the dependence of the tide phase on height (fig. 39.5) to the level at which the wind velocity maximum in the northward direction sets in at 2300 hours, according to the data in reference 412 we obtain a height of approximately 135 km. Following this result and the concepts of the theory of an atmospheric dynamo, it would be necessary to assume that the conducting layer, through which flow the electrical currents responsible for the S_q variations in the middle latitudes, lies at a height of 135 km. This value does not exceed the limits of the heights mentioned in 1952 in the computations of Baker and Martyn, but is considerably greater than indicated by magnetic measurements on rockets (fig. 40.5).

Studies by the Japanese geophysicists Maeda, Kato, Hirono and Kitamura appeared in 1956. They contain a full computation of a system of horizontal winds in the ionospheric E layer, based on the theory of an atmospheric dynamo as related to S_q variations. We will consider these studies.

40.5. Computation of Winds in the E Layer on the Basis of the Dynamo Theory of Geomagnetic S_q Variations. The theory of an atmospheric dynamo presented in Section 40.4 was recently applied in a number of studies of Japanese geophysicists for the computation of horizontal winds in the E layer of the ionosphere on the basis of observed S_q variations (refs. 515 and 565).

Maeda, in solving this problem, took into account the spatial nonhomogeneity and diurnal variation of ionospheric conductivity. In order to simplify the wind computations, he neglected the Earth's rotation, assuming that the field of wind velocities is a potential field (ref. 565). However, Coriolis forces exert a great influence on the diurnal and semidiurnal tidal movements of the upper layers of the atmosphere, and play a significant role in the mechanism of formation of geomagnetic S_q variations. In this connection Kato continued Maeda's investigation, taking into account the effect of Coriolis forces. Since in this case there is no wind velocity potential, Kato made an attempt to find the wind field by solving the equation of motion of the atmosphere for the case of a rotating Earth, jointly with the equation of the atmospheric dynamo (ref. 515).

The system of electrical currents j responsible for the given field of S_q variations can be computed using formulas of the type (40.13). If the atmospheric dynamo is assumed to be the mechanism responsible for the development of the derived current system, it is possible to compute the velocity of movement u of the conducting layer by using formula (40.18). However, using the given field of S_q variations, the corresponding electrical field, rather than the current system can be computed. This was the approach used by Maeda and Kato in development of their theory. We will denote the

total electrical field corresponding to geomagnetic S_q variations by $\vec{E}$. It consists of two parts, i.e., of the electrostatic field $\vec{E}_e$ and the induced electrical field $\vec{E}_i$

$$\vec{E} = \vec{E}_e + \vec{E}_i.$$

Since the electrostatic field is a potential field, curl E_e = 0, and

$$\text{curl } \vec{E} = \text{curl } \vec{E}_i.$$

By virtue of equation (40.18) and Ohm's law, used in differential form, and using electromagnetic units, we can replace $\vec{E}_i$ by the vector product

$$E_i = (\vec{u} \times \vec{H}),$$

and therefore

$$\text{curl } E = \text{curl}(\vec{u} \times \vec{H}).$$

This equation can be rewritten in scalar form (ref. 515)

$$\frac{\partial E_x}{\partial \lambda} - \frac{\partial}{\partial \theta}(\sin \theta E_1) = \frac{\partial}{\partial \lambda}(vH_z) + \frac{\partial}{\partial \theta}(\sin \theta u H_z), \qquad (40.19)$$

where u and v are the wind velocity components directed to the south and east, respectively; θ is colatitude; λ is longitude; E_x and E_y are the components of the E vector directed to the south and east, respectively and H_z is the vertical (directed upward) component of the geomagnetic field. The components of the electrical field were computed by Maeda for a map of S_q variations, constructed on the basis of data from the Second International Polar Year, using as a point of departure available data on air conductivity in the ionosphere. The computations were made using a formula which Maeda derived (ref. 565). H_z was computed using

$$H_z = C \cos \theta,$$

where C is a constant equal to approximately 2/3 gauss (this formula corresponds to the assumption that the Earth's geomagnetic field can be replaced by a dipole field oriented along the Earth's geographical axis). Equation (40.19) also is the equation of the atmospheric dynamo in the form adopted in Kato's study (ref. 515).

The equation of the atmospheric dynamo must be supplemented by equations of atmospheric motion with the Earth's rotation taken into account, see equation (34.1), which in this case can be written

$$\left.\begin{aligned}\frac{\partial u}{\partial t}-2v\omega\cos\theta&=-\frac{1}{R}\frac{\partial}{\partial\theta}\left(\frac{p'}{\rho_0}\right)\\ \frac{\partial v}{\partial t}+2u\omega\cos\theta&=-\frac{1}{R}\frac{1}{\sin\theta}\frac{\partial}{\partial\lambda}\left(\frac{p'}{\rho_0}\right)\end{aligned}\right\} \qquad (40.20)$$

where ρ_0 is the mean value of air density at that height (in the E layer) and p' is the tidally disturbed part of atmospheric pressure. Equations (40.20) were derived on the assumption that this motion of the atmosphere is caused by small disruptions of pressure, and in the equations of motion of hydrodynamics we can, therefore, neglect the terms containing the product of small values of disruptions (ref. 515).

Using these three equations (40.19) and (40.20) we can find the value of the ratio $\frac{p'}{\rho_0}$ in the ionosphere corresponding to geomagnetic S_q variations. This ratio is proportional to pressure changes. If it is known, wind velocity can be computed by use of equations (40.20).

After solving the equation of the atmospheric dynamo (40.19), Kato found the expansion of the functions on the left- and right-hand sides of this equation and presented an expansion of Legendre polynomials. For the left-hand side he obtains

$$\frac{\partial E_x}{\partial\lambda}-\frac{\partial}{\partial\theta}(\sin\theta E_\tau)=\sin\theta\sum_{M=1}^{\infty}\sum_{N=M}^{\infty}F_{N,M}P_{N,M}e^{iM(\omega t+\lambda)}, \qquad (40.21)$$

and for the right-hand side

$$\frac{\partial}{\partial\lambda}(vH_z)+\frac{\partial}{\partial\theta}(\sin\theta uH_z)=\sum_{m=1}^{\infty}\sum_{n=m}^{\infty}L_{n,m}P_n e^{im(\omega t+\lambda)}, \qquad (40.22)$$

where

$$L_{n,m}=\frac{Cm^2\sin\theta}{2af\omega}j\left\{\frac{n-m}{2n-1}\left[n^2+2\frac{m}{f}-1+\right.\right.$$

$$\left.\left.+\frac{2\left(\frac{m}{f}\right)^2}{n(n+1)-\frac{m}{f}}\right]\beta_{n-1,m}+\frac{n+m+1}{2n+3}\left[n^2+2n+2\frac{m}{f}+\right.\right.$$

$$+\frac{2\left(\frac{m}{f}\right)^2}{n(n+1)-\frac{m}{f}}\Bigg]\beta_{n+1,\,m}\Bigg\}. \qquad (40.23)$$

Here $F_{N,M}$ are spherical harmonic coefficients for which Kato found the numerical values (for M = 1, 2 and N = 1, 2, 3, 4); $f = \frac{\sigma}{2\omega}$; σ is angular frequency (tidal variations); $i = \sqrt{-1}$, $P_{n,\,m} = P_{n,\,m}(\cos\theta)$ is the Legendre function of the degree n and the order m, and $\beta_{n,\,m}$ are the coefficients of the expansion. With equations (40.21) and (40.22) we can find the coefficient $\beta_{n,\,m}$ and compute the amplitude and phase of pressure variations using the formula

$$\frac{p'}{\rho_0} = \sum A_{n,m} P_{n,m} \sin(m\omega t + m\lambda + \alpha_{n,m}). \qquad (40.24)$$

In practical computations Kato dropped the expansion terms F_N and $L_{n,\,m}$, except the first four. Kato's study demonstrates the uniqueness of the derived particular integral of the differential equation of the theory of the atmospheric dynamo (40.19).

Table 40.1 gives numerical values of the spherical harmonic coefficients $A_{n,\,m}$ and $\alpha_{n,\,m}$ of the series (40.24) for the ratio $\frac{p'}{\rho_0}$, determining the amplitude and phase of different harmonic components of pressure variations (40.24). The distribution of the computed pressure variations (isobars) and wind velocities corresponding to the computed pressure variations are represented in figures 40.6 and 40.7. These maps are given for the northern hemisphere. The distribution in the southern hemisphere is similar (symmetrical relative to the equator).

TABLE 40.1. SPHERICAL HARMONIC COEFFICIENTS OF SERIES (40.24).

m	n	$A_{n,\,m} \cdot 10^6 \text{cm}^2\text{sec.}^{-2}$	$\alpha_{n,\,m}$ degrees
1	1	114.1	150°30′
	2	33.2	141
	3	3.30	200
2	2	8.79	135°30′
	4	0.567	288
	6	0.00334	152 45

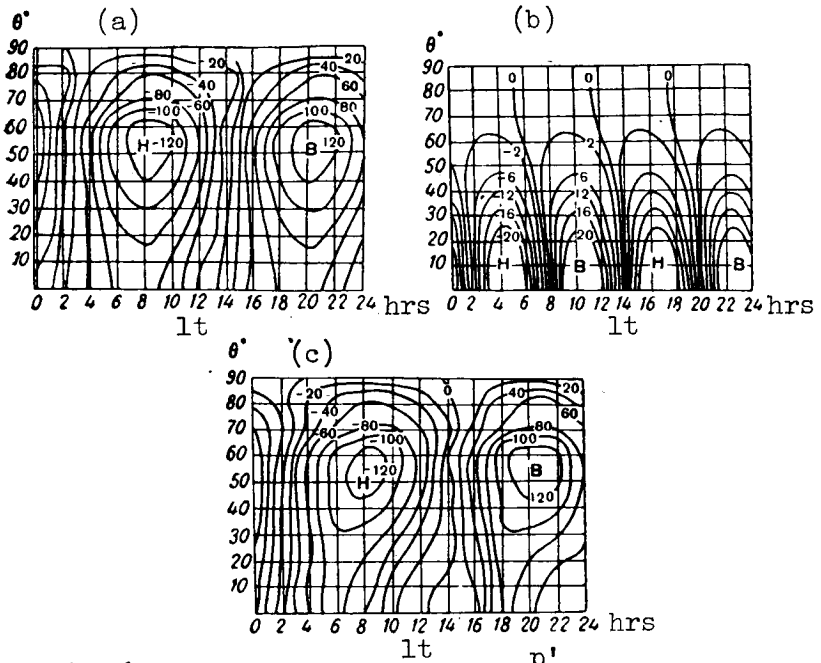

Figure 40.6. Distribution of value $\frac{p'}{\rho_0}$, proportional to pressure variation. Units: 10^6 cm^2 sec^{-2}. a, diurnal component, b, semidiurnal component, c, sum of diurnal and semidiurnal components.

In the results of his computations Kato emphasizes a number of circumstances. First, this applies to the predominant component of pressure variations in the E region, which is diurnal rather than semidiurnal. The diurnal component is almost 3.5 times greater than the semidiurnal component. The semidiurnal variations of pressure at the height of the layer are almost cophasal with variations of surface pressure. A pressure maximum is observed at 1000 and 2200 lt. The maximum of diurnal pressure variations sets in at 1900 hours.

Kato evaluates the intensity of pressure variations using the following relation

$$\frac{\left(\frac{p'}{p_0}\right)_i}{\left(\frac{p'}{p_0}\right)_E} \simeq \frac{\left(\frac{p'}{\rho}\right)_i}{\left(\frac{p'}{\rho}\right)_E} \frac{T_E}{T_i},$$

where p_0 is static pressure and T is static temperature. The molecular weight of air at the Earth's surface and at the level of the E layer can be considered approximately equal. In addition, $T_{ion} \approx T_{Earth}$. At the Earth's surface $\rho_0 = 1.3 \cdot 10^{-3}$ g/cm^{-3}. According to Wilkes (ref. 907) the value p' = 0.937 (in mm Hg) can be used for tidal variations of surface pressure. Then the reduced ratio gives an intensification by a factor of 25-30 for semidiurnal pressure variations in the low latitudes.

Kato's computations give 7-8 m/sec for the velocity of tidal winds (semidiurnal component) and 15-20 m/sec (diurnal component).

As shown in figures 40.6 and 40.7, the daytime system of winds has a cyclonic character in the zone of low pressure and an anticyclonic character in the zone of high pressure (in the northern hemisphere).

Kato compared the results of his computations with wind observations in the ionosphere, cited in the 1954 study of Briggs and Spencer, and found agreement for the semidiurnal tidal winds. However, the results of measurements of ionospheric winds published after 1954 (Sections 28, 30 and 39) contain more complete data, which do not agree in all respects with Kato's computations. It must be remembered that the theoretical and experimental study of tidal winds

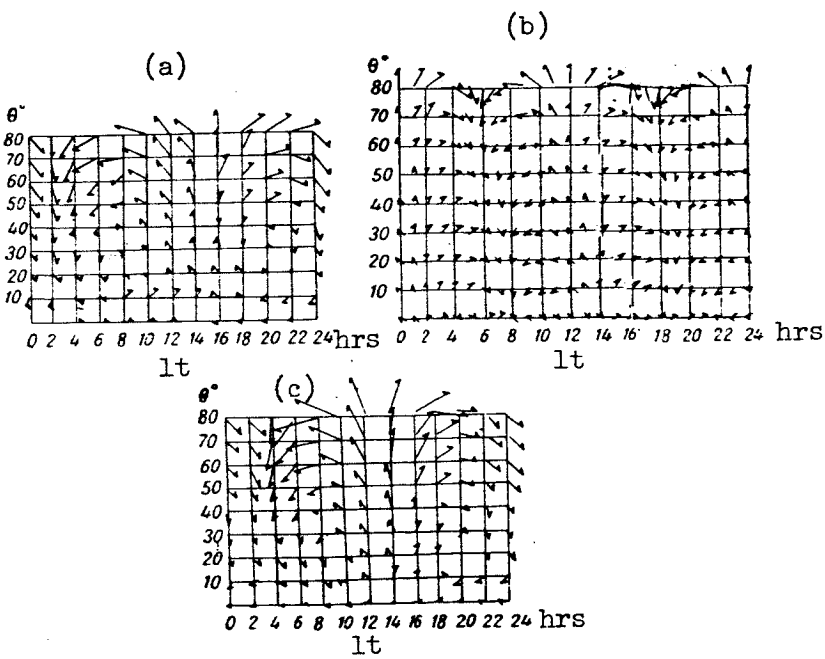

Figure 40.7. Wind velocity distribution corresponding to pressure variations shown in figure 40.6. Scale of arrows: 50 m/sec for length of arrow equal to side of small square. a, diurnal pressure variation, b, semidiurnal pressure variation, c, sum of diurnal and semidiurnal pressure variations.

in the ionosphere began quite recently and additional more systematic experimental and theoretical research is necessary for a sufficiently complete solution of this interesting problem.

Such results were obtained by Maeda and Kato in the first (Maeda, ref. 565)and second (Kato, ref. 515) parts of their joint investigation. In the third part (ref. 565), Maeda used the same method to compute the wind system for the winter and summer hemispheres (for the solstice periods). He found that the winds determined from observed S_q variations have a diurnal component in summer, which is greater in magnitude than in winter. On the other hand, the semidiurnal component is smaller in summer. In the summer hemisphere the diurnal wind component also is larger than the semidiurnal component.

The comparison which Maeda made between computed winds and the air currentsobserved in the ionosphere revealed agreement between them with respect to the direction of rotation of the wind vector and the magnitude of this wind. However, the computed phase of the rotation does not coincide with the observed phase. An analysis of the observed data reveals that the diurnal component is directed southward at 0600 hours in the southern hemisphere, and the semidiurnal wind component is directed northward at about 0600 hours in the northern hemisphere and southward at about 1800 hours in the southern hemisphere. These data were obtained from radar observations of meteors and apply to the region 80-100 km; the reason for discrepancies with theoretical computations can be related to the fact that computations made on the basis of the dynamo theory of geomagnetic S_q variations possibly give a wind which actually is in higher layers.

In the fourth part of the study Kato (ref. 515) took the influence of Coriolis force into account. According to his computations, the diurnal component of wind velocity is greater than the semidiurnal component in summer (by a factor of approximately 2 over the middle latitudes). In summer the diurnal component is greater than in winter.

Maeda (ref. 566) also made an attempt to compute the system of horizontal winds responsible for solar-diurnal magnetic variations on magnetically disturbed days (S_d variations).

CHAPTER 13. ATMOSPHERIC CIRCULATION AS REVEALED BY OBSERVATIONS OF OZONE, ATOMIC OXYGEN AND WATER VAPOR

41. Ozone and Atmospheric Circulation

The problem of atmospheric ozone will not be given particular attention in this book, because it constitutes a field of its own treated elsewhere (refs. 231 and 233). However, in this book a brief discussion is necessary of at least one aspect of the ozone problem related to the investigation of general circulation in the high layers of the atmosphere.

41.1. Time Required for Restoration of a Photochemical Equilibrium Distribution of Ozone. Nicolet (ref. 627), considering the correlations of the photochemical theory of ozone (ref. 233), computed the time t required for restoration of photochemical equilibrium. He found the following values t at different heights h

h km	32	25.5	19	12
t sec	10^3	2.10^3	10^6	10^{10}

According to these data, there is photochemical equilibrium in the layers of the ozonosphere above 25 km, and its disruption is rapidly restored. Below 20 km the disruptions are liquidated so slowly that the vertical ozone distribution should be determined mostly by the character of these disruptions, not by photochemical reactions. The 25 km level is seemingly transitional from one mechanism, regulating vertical distribution, to another ("critical" level).

Other investigators have drawn similar conclusions, but estimates of the level of photochemical equilibrium of the ozonosphere do not always coincide. For example, according to Schroer (ref. 720), photochemical equilibrium is attained only above the 33-35 km level. According to his computations, the time required for the formation (from 0) of an equilibrium concentration (if the photodissociation of ozone is neglected) is

h km	45-50	40-45	35-40	30-35	25-30	20-25
t sec	7.10^3	2.10^4	7.10^4	5.10^5	10^7	10^8

Paetzold (refs. 649 and 650) found similar values. According to his computations, the time required for establishment of photochemical equilibrium is 20 days at a height of 30 km, but increases to 3 years at a height of 20 km. E. Regener gives the following values: below 25 km photochemical equilibrium is attained in weeks or months, at a height of 35 km this process requires days, and in the 45-50 km layer it is about 1 hour. According to Wolf and Deming, the time in which an equilibrium concentration can be half-established is days at a

height of 30 km, and minutes at a height of 60 km. Normand summarizes the available data as follows: there is an equilibrium state of ozone in complete form only above 35 km. Below 35 km the time required for restoration of equilibrium increases rapidly, becoming a week at a height of 27 km.

41.2. Ozone Concentration as a Conservative Property of Atmospheric Masses. Despite the appreciable discrepancy in the results of estimation of the rate of restoration of an equilibrium ozone concentration, obtained by different authors, it is possible to draw some important conclusions. Photochemical equilibrium occurs completely only in the upper part of the ozonosphere, above 30-35 km, where equilibrium is restored rapidly after disruption (in a day or less) under the influence of solar radiation. At lesser heights the time required for restoration of equilibrium becomes extremely great and, beginning approximately at the 27 km level, attains such a large value (a month or more) that any significant disruption of equilibrium is virtually no longer subject to appreciable restoration. As a result, ozone as an "admixture" to the atmosphere acquires a new quality: the greater part of the ozone can be considered "conservative" in the sense that in the process of even slow movements of air masses, the percent content of ozone in a particular air volume remains nearly constant. Accordingly, the ozone problem acquires great importance in meteorology, especially for the study of general circulation of the atmosphere.

It can be concluded from these data on the rate of restoration of an equilibrium concentration that the ozone below the 50 km level (almost all atmospheric ozone is found in this region) cannot react to an intensification (burst) of solar ultraviolet radiation at the time of solar eruptions, since even in the 45-50 km layer the process of restoration of a new equilibrium concentration lasts for hours.

Deviations of the theoretical vertical ozone distribution from the actual distribution, usually observed below the principal ozone maximum ($\sim$23 km), can be the result, strictly speaking, of imperfection of the theory. This does not apply to the basic principles of photochemical theory, which are no longer subject to doubt, but to the lack of final data on the quantum yield and the constants of the corresponding reactions, the extra-atmospheric energy distribution in the spectrum of solar ultraviolet rays and absorption of radiation by oxygen and its dependence on pressure. The computations of different authors lead to results which are by no means in agreement (ref. 233). However, there is an indisputable basis for the assertion that the vertical O_3 distribution in the lower part of the ozone layer is subject to the strong influence of other (disturbing) factors; the existence of considerable fluctuations of this distribution supports this conclusion. This is easily confirmed by all available curves of the vertical distribution of ozone. The discussion of these fluctuations, very common in studies published in recent years, especially during the IGY period, demonstrates beyond doubt that the most important cause of these fluctuations is of a dynamic character and is related to the vertical and horizontal transport of ozone.

41.3. Vertical and Horizontal Movements of Ozone. The ozone balance is dependent on different kinds of vertical movements in the atmosphere. The ozone content increases with subsidence of the upper layers of the atmosphere more abundant in ozone. However, in the upper layers there is rapid photochemical restoration of an equilibrium concentration of ozone, and as a result its total quantity increases when there are descending movements. According to Paetzold's computations, based on analysis of the variability of the curves of the vertical distribution of ozone, the velocity of vertical movements is approximately 1 cm/sec below 35 km, whereas at a level of about 50 km it is several times greater. Very similar values have been obtained by Murgatroyd, Martyn and Brewer (ref. 577). According to Reed's computations, vertical movements have a lesser velocity.

Turbulence can exert an appreciable influence on the vertical redistribution of ozone. Turbulent movement leads to an equalization of the ozone/air ratio. In the troposphere and in the lower layers of the stratosphere this ratio usually increases with height. Turbulent exchange, therefore, results in a transport of ozone into the lower stratosphere and into the troposphere.

Bearing in mind the conservative character of the percent content of atmospheric ozone considered above, it must be pointed out that this conservative character is disrupted somewhat in the lower layers of the atmosphere by processes of ozone destruction. Ozone has a high oxidizability and is easily destroyed by oxidizing particles of organic origin suspended in the air. According to E. Regener (ref. 697), the process of ozone destruction occurs with exceptional rapidity at the surface of the soil due to the effect of easily oxidizing organic matter. Solar radiation also can have a destructive effect. This radiation corresponds to the longwave region of absorption of O_3 molecules.

On the other hand, Frenkiel (ref. 393) points out that to explain the ozone concentration observed in the troposphere we must consider the ozone forming in large quantity in the troposphere, especially near the soil, rather than ozone undergoing destruction. Ozone can be formed as a result of photochemical reactions in an atmosphere containing small quantities of nitrogen dioxide and hydrocarbons. According to Frenkiel's computations, "clouds" of ozone can accumulate over industrial regions under certain meteorological conditions. The reduced thickness of these clouds can become 0.05 mm, (e.g., at Los Angeles). The ozone clouds are later carried away by the wind. Frenkiel believes that almost all ozone observed in the troposphere can be of tropospheric origin, arising from natural or industrial sources.

Renger and Lucke (ref. 700) feel that there is a convective flux of ozone in the troposphere which is generally directed downward; its source is the "parent" ozone layer (the layer of photochemical ozone formation), above 30 km. According to Paetzold's estimate (ref. 650), the vertical ozone flux transports 10^9 tons of ozone earthward annually from the parent layer. The entire quantity of oxygen in the atmosphere passes through the ozone state in 10^6 years.

In the lower layers of the atmosphere there are also ozone-forming processes in the air under the influence of electrical discharges during thunderstorms and the radioactivity of the soil (and also possibly under the influence of the radioactivity of aerosol particles suspended in the atmosphere). In both cases the process apparently begins with the dissociation of O_2 molecules or the formation of excited oxygen molecules (in an electrical discharge or under the influence of radioactive radiations). The phenomenon of ozone formation in the air during electrical storms has long been known. Investigations now have established an increased ozone content for several hours before a thunderstorm. For example, in 1954 A. Vassy recorded thunderstorm discharges simultaneously with measurements of ozone content (ref. 777). The instrument recorded up to 50 percent of the thunderstorms in an 800 km radius. In 82 percent of the cases there was a considerable increase of ozone concentration in the period preceding the thunderstorm. The mean period for 30 storms was 3 1/2 hours. It is still unclear whether there is ozone formation in a cumulonimbus cloud with subsequent earthward transport by descending air currents or whether the appearance of ozone is caused by a higher electrical field near Earth before a thunderstorm.

The relationship between variations of atmospheric ozone content and atmospheric circulation is now being investigated intensively. It has been demonstrated that air influx from the polar regions at heights of about 16 km is the cause of increase of ozone content. This mechanism has been confirmed by other geophysicists, among them Simidziu (ref. 791). He established a relation between the meridional distribution of ozone in Japan along 140°E and the westerly flow at the 200 mb level; this is most effective in spring when the differences between the ozone content in the high and low latitudes are large. On the basis of IGY data, G. P. Gushchin, Normand and others have more precisely determined the seasonal variation of the meridional gradient x of total ozone content. In early spring the ozone content increases with latitude as far as the pole. This explains the close relation between the variations of x and cold intrusions at this season of the year. This relation is disrupted in the months which follow when the maximum is displaced southward near latitude 60°N. The rapid increase of ozone quantity at the end of winter, especially in the polar regions, has been described in detail by Godson (ref. 403). Godson relates the increase of x to the breakup of the winter jet stream "on the edge of the polar night" and the appearance of large baroclinic "long waves" in the general westerly flow of the stratosphere.

There is a basis for assuming that the seasonal and latitudinal variations of the total ozone content in the atmosphere are related to processes of general circulation, vertical movements on a general scale, seasonal and latitudinal turbulence characteristics and certain other phenomena, especially those dependent on solar radiation and its variations (solar activity).

Interesting investigations of atmospheric circulation in relation to ozone variations have been published recently by A. Kh. Khrgian and G. I. Kuznetsov (refs. 100 and 236).

41.4. Models of Meridional Circulation. Problems relating to latitudinal distribution and seasonal variations of ozone are closely associated with processes of interlatitudinal exchange. On the basis of such data many authors have

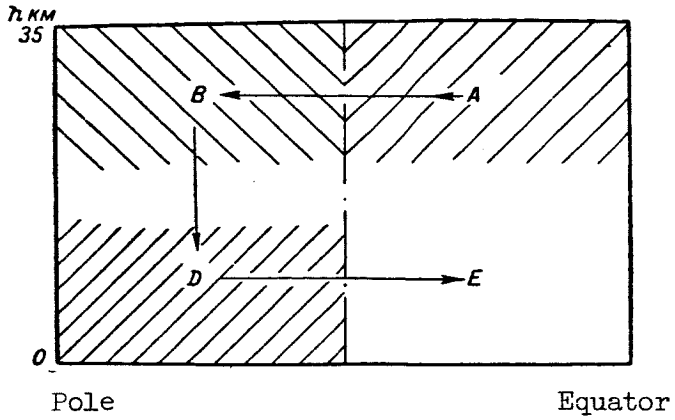

Figure 41.1. Model of meridional circulation.

attempted to develop models of meridional circulation. For example, Paetzold (ref. 658) proposed a meridional circulation between both hemispheres with descending movement in the winter hemisphere and ascending movement in the summer hemisphere, in an attempt to explain the increase of ozone quantity in the winter months beginning in November. Dütsch (ref. 365) postulated the existence of a meridional circulation shown schematically in figure 41.1. Ozone moves northward from region A in the low latitudes into region B, where there is strong vertical mixing. Therefore, part of the ozone enters region D, which is protected from solar radiation and is responsible for ozone dissociation by the ozone layer above.

Figure 36.4 (Section 36.4) shows the paths of air particles computed by Murgatroyd and Singleton (ref. 618). It is possible that this model of meridional circulation, in combination with the conclusions drawn from the photochemical theory of atmospheric ozone, can explain the principal patterns of the latitudinal distribution of ozone and its seasonal variation. In the winter-spring period there are descending currents over the high latitudes accompanied by increase of ozone content at these latitudes; the reverse process occurs in summer.

Important conclusions concerning the general distribution and annual variation of ozone and general circulation of the atmosphere were drawn by A. Kh. Khrgian and G. I. Kuznetsov (ref. 100) after generalization of IGY data.

42. Atmospheric Circulation as Revealed by Observations of Water Vapor in the Stratosphere and Atomic Oxygen

42.1. Figure 36.1 (Section 36) shows a model of meridional circulation proposed by Dobson (ref. 359). This figure shows a section of the atmosphere from the equator to the pole (for winter and summer). It shows the regions of minimum air temperature and the height of the tropopause, the postulated path of air particles penetrating into the stratosphere and escaping from it, and also the ascending and descending diffuse fluxes of water vapor and ozone. The

equatorial zone of very cold air has a maximum thickness and a latitudinal extent of about 20°. During the final winter months there is a cold pole over the winter pole, but its role in drying out the entire stratosphere is possibly insignificant, although it can be the cause of rapid increase of the total content x of atmospheric ozone in the high latitudes in early spring.

Water vapor and ozone should diffuse upward and downward in the atmosphere, as shown schematically in figure 36.1. The decrease of humidity with height in the troposphere is primarily caused by the condensation of vapor and by precipitation. Dobson feels that this factor is lacking in the stratosphere, but the ice point continues to decrease with height, although more slowly. It is difficult to explain this vertical distribution of vapor differently, such as upward diffusion together with the reverse process of slow subsidence of dry air from higher layers, as shown by arrows A and B in figure 36.1.

If there is such slow subsidence of air from the stratosphere into the troposphere in the middle latitudes, it should be balanced by opposite currents from the troposphere into the stratosphere occurring somewhere. The dryness of the stratosphere, in Dobson's opinion (ref. 359), indicates that these currents of opposite direction can occur only in the cold region near the equator. This actually can occur, as shown by arrows C and D in figure 36.1.

The air particle paths, computed by Murgatroyd and Singleton (ref. 618) and shown in figure 36.4, generally correspond to the model of meridional circulation based on data on the distribution of water vapor in the stratosphere. It can be concluded from the arrangement of these paths that the air enters the stratosphere (at least to a height of 25 km) through the equatorial stratosphere (Section 19.3). Murgatroyd and Singleton believe that a considerable part of the stratospheric air follows this path during the preceding year.

42.2. Atomic Oxygen. A region of intensified photodissociation of oxygen under the influence of solar ultraviolet radiation begins at a height of about 100 km. Below the 85-95 km level there is virtually no penetration of solar radiation capable of dissociating oxygen, since it is absorbed in the higher layers. This results in the formation of a certain transitional layer (near 100 km), below which oxygen exists primarily in the form of diatomic molecules. Above this layer a considerable part of the oxygen is in an atomic state (for further details see ref. 233).

Atomic oxygen is manifested actively in the luminescence of the high layers of the atmosphere: the green and red oxygen lines are always present in the spectra of auroras and the night airglow (ref. 233). Attempts have been made to explain the latitudinal variations of the intensity of the green line of the night airglow, observed from the equator to 30°N, using the model of general circulation proposed by Paneth (Section 35.3). According to Paneth, there are three circulation rings in the thermosphere between the equator and the north pole; the base of these rings (direct flow) is situated at the 80 km level and the upper part (reverse flow) is at a height of about 300 km. The transport and interconversion of oxygen atoms and molecules are explained by the diagram in figure 42.1. The O_2 rise near the equator is responsible for the small atomic oxygen content in the upper part of the thermosphere over the

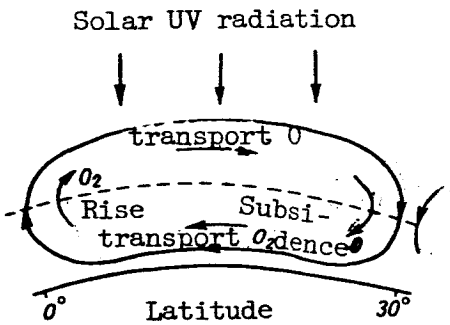

Figure 42.1. Model of general circulation and oxygen transport in the thermosphere.

equator (and accordingly the low brightness of the green line). There is rapid dissociation of oxygen in the high layers of the thermosphere in the process of transport of O_2 from the equator northward. The air subsiding over latitude 30° is relatively rich in atomic oxygen. There is rapid increase in O_2 content as a result of recombination on the reverse path in the "first level" of the thermosphere.

Kellogg (ref. 518) recently attempted to develop a model of meridional circulation over the winter pole, proceeding on the assumption that there are factors causing "warming" of the mesopause in winter. Data on this highly interesting characteristic of the thermal regime of the upper layers of the mesosphere were discussed in detail in Chapter 5, and in relation to the theory of origin of noctilucent clouds (Section 21). Kellogg relates the winter warming of the region of the mesopause in the high latitudes to descending currents which transport atomic oxygen from the thermosphere into the mesosphere; recombination of oxygen in the mesosphere should be accompanied by release of heat. The Kellogg model will now be considered in greater detail.

The oxygen atoms, created continuously in the middle latitudes by the photodissociation of oxygen molecules in the lower layers of the thermosphere, are transported poleward where they are carried downward by subsiding air currents. In the lower layers they recombine, for the most part by triple collision:

$$O + O + M \rightarrow O_2M + 5.1 \text{ ev}, \qquad (42.1)$$

where M is some third particle. In each event of formation of an oxygen molecule by the recombination of two atoms, there is release of a considerable energy of 5.1 ev which can be expended on heating the surrounding medium. Assuming a certain vertical distribution of atomic oxygen, Kellogg has computed the velocity of the descending currents necessary for "chemical" heating of the atmosphere in the reaction (42.1) to be 10°/day. Table 42.1 shows the results of his computations.

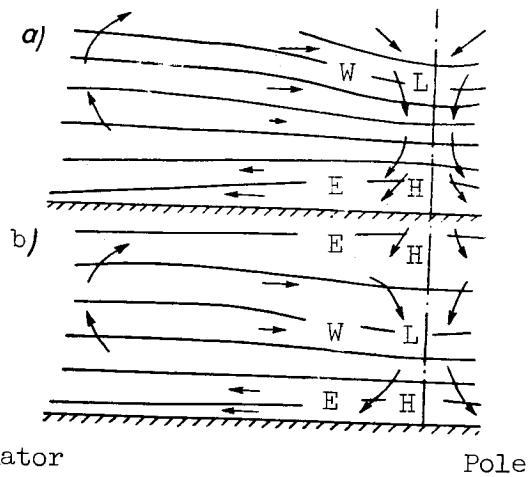

Figure 42.2. Schematic meridional cross section of the atmosphere in the winter hemisphere. The solid lines are isobaric surfaces. L and H, positions of regions of low and high pressure; W and E, westerly and easterly wind directions.

Kellogg schematically relates the development of meridional circulation in the mesosphere and thermosphere in winter to the formation of low and high pressure regions over the pole, as shown in figure 42.2. A cold, low pressure region is formed in the upper layers as a result of winter radiation cooling; at this time a high pressure region is created in the lower layers of the atmosphere. This region is occupied by the continental air masses, which in winter are colder than the oceans. As a result of the gradual development of a cyclonic vortex above the anticyclone, there is a meridional flow across the isobars. According to Kellogg this is the way in which the circulation, shown schematically in Figure 42.2a, is formed.

We can postulate that such meridional circulation takes place in several days. This is sufficient time for a considerable quantity of atomic oxygen to be carried from the thermosphere of the middle latitudes into the region of the

TABLE 42.1 VELOCITY OF DESCENDING CURRENTS OVER THE WINTER POLE AT WHICH "CHEMICAL" HEATING OF THE ATMOSPHERE WOULD BE 10°/DAY.

Height, km	Velocity of descending currents	
	cm/sec	km/day
85	0.7	0.6
90	0.15	0.13
95	0.049	0.042
100	0.074	0.064
110	0.15	0.13

polar mesopause. The heat released as a result of the recombination of oxygen can be more than compensated for in the 80-100 km region by radiation cooling. The general situation, therefore, changes somewhat, as shown in figure 42.2b. The isobaric surfaces are closer together when there is cooling of the atmosphere, whereas, in accordance with the hydrostatic equation, they are farther apart in warm regions.

The interesting problem of the role of atomic oxygen in the heat and circulation regime of the mesosphere and thermosphere has been investigated only inadequately; it can be assumed that further study of this problem will yield many important results.

REFERENCES

1. Alekseyev, P. P., Besyadovskiy, Ye, A., Golyshev, G. I., Izakov, M. N., Kasatkin, A. M., Kokin, G. A., Livshits, N. S., Masanova, N. D., and Shvidkovskiy, Ye. G. Rocket Investigations of the Atmosphere (Raketnyye issledovaniya atmosfery). Meteorologiya i gidrologiya, No. 8, 1957.

2. Alekseyev, P. P., Besyadovskiy, Ye. A., Biryukova, L. A., Golyshev, G. I., Ivanovskiy, A. I., Izakov, M. N., Kokin, G. A., Kurilova, Yu. V., Livshits, N. S., Petrov, A. A., Rozhdestvenskiy, B. G., Solov'yev, N. V., Speranskiy, K. Ye., Khvostikov, I. A., Shvidkovskiy, Ye. G. and Shcherba, I. A. Weather Rocket Investigation of the Upper Layer of the Atmosphere (Izucheniye vysokikh sloyev atmosfery pri pomoshchi meteorologicheskikh raket). Trudy Vsesoyuznogo Nauchnogo Meteorologicheskogo Soveta, Vol. 1. Gidrometeoizdat, Leningrad, 1962.

3. Al'pert, Ya. L. Statistical Character of the Structure of the Ionosphere (Statisticheskiy kharakter struktury ionosfery). Uspekhi Fizicheskikh Nauk (UFN), 49, No. 1, 1953.

4. - - - Contemporary Theories on Radiowave Distribution in the Ionosphere (Sovremennyye predstavleniya o rasprostranenii radiovoln v ionosfere). Izvestiya AN SSSR, No. 11, 1957.

5. Al'pert, Ya. L., Ginzburg, V. L. and Feynberg, Ye. L. Radiowave Distribution (Rasprostraneniye radiovoln). Gostekhizdat, Moscow, 1953.

6. Astapovich, I. S. Noctilucent Clouds (Serebristyye oblaka). Izvestiya Akademii Nauk SSSR, seriya geograficheskaya i geofizicheskaya, 1939.

7. - - - Meteoric Phenomona in the Earth's Atmosphere (Meteornyye yavleniya v atmosfere Zemli). Fizmatgiz, Moscow, 1958.

8. Bagaryatskiy, B. A. Effective Recombination Coefficients in the Ionosphere (K voprosu ob effektivnom koeffitsiente rekombinatsii v ionosfere). Izv. AN SSSR, ser. geofiz., No. 9, 1959.

9. Baum, S. A., Kaplan, S. A. and Stanyukovich, K. P. Introduction to Cosmic Gasdynamics (Vvedeniye v kosmicheskuyu gazovuyu dinamiku). Fizmatgiz, Moscow, 1958.

10. Belekhova, N. G. The Action of Free-Molecular Parameters of the Flow of a Rarefied Gas on Instrument Indications During Rocket Measurement of the Density of the Upper Layers of the Atmosphere (O vliyanii parametrov svobodno-molekulyarnogo techeniya razrezhennogo gaza na pokazaniya priborov pri raketnykh izmereniyakh plotnosti vysokikh sloyev atmosfery). Izv. AN SSSR, ser. geofiz., No. 9, 1959.

10a. Belous, A. T., Gul'medov, Kh. D., Inozemtsev, Yu. A., Lyubarskiy, K. A., Kalyakina, M. I. and Sadykov, Ya. F. Meteor Observations in Ashkhabad (Nablyudeniya meteorov v Ashkhabade). Coll. "Ionosfernyye issledovaniya (meteory)", Izd-vo AN SSSR, Moscow, 1962.

11. Ben'kova, N. P. Daily Variations of the Quiet Sun in Terrestrial Magnetism (Spokoynyye solnechno - sutochnyye variatsii zemnogo magnetizma). Trudy NIU GUGMS, ser. VI, Issue 1, 1941.

11a. Biryukova, L. A. and Kastrov, V. G. Daily Temperature Variations in the Lower and Middle Stratosphere (O sutochnom khode temperatury v nizhney i sredney stratosfere). Trudy Tsentral'noy Aerologicheskoy Observatorii (Tr. TsAO), Issue 45, 1962.

12. Blagonravov, A. A. High-Altitude Rocket Investigations of the Upper Layers of the Atmosphere (Issledovaniye verkhnikh sloyev atmosfery pri pomoshchi vysotnykh raket). Vestnik AN SSSR, No. 6, 1957.

12a. Boyenkova, N. M. and Kushnerevskiy, Yu. V. Vertical Transposition of Ionospheric Disturbances (Vertikal'nyye peremeshcheniya vozmushchennostey v ionosfere). Coll. "Ionosfernyye issledovaniya", No. 9, Izd-vo AN SSSR, Moscow, 1961.

13. Boyd, R. L. F. and Seton, A. J. Rocket Investigation of the Upper Atmosphere (Raketnyye issledovaniya verkhney atmosfery). Translation from English. Izd-vo Inostrannoy Literatury (IL), Moscow, 1957.

14. Bolyunova, A. D. The Construction of Models of the Atmosphere (K voprosu o postroyenii modeli atmosfery). Izv. AN SSSR, ser. geofiz., No. 10, 1960.

15. Borisenkov, Ye. P. Questions on the Energetics of Atmospheric Processes (Voprosy energetiki atmosfernykh protsessov). Gidrometeoizdat, Leningrad, 1960.

15a. Borovikov, A. M., Golyshev, G. I. and Kokin, G. A. Some Characteristics of the Structure of the Atmosphere in the Southern Hemisphere (Nekotoryye kharakteristiki stroyeniya atmosfery yuzhnogo polushariya). Meteorol. i gidrol., No. 3, 1962.

16. Bocharov, Ye. I. Radiation Absorption by Moist Air (Pogloshcheniye radiatsii vlazhnym vozdukhom). Opticheskiy gigrometr. Izv. AN SSSR, ser. geofiz., No. 1, 1959.

17. Budyko, M. I. and Yudin, M. I. Conditions of Thermic Equilibrium of the Atmosphere (Usloviya termicheskogo ravnovesiya atmosfery). Doklady AN SSSR, No. 7, 1946.

18. Bunimovich, V. N. Fluctuation Processes in Radio Receiver Apparatus (Flyuktuatsionnyye protsessy v radiopriyemnykh ustroystvakh). Izd-vo "Sovetskoye Radio", Moscow, 1951.

19. Burov, M. I. Noctilucent Clouds and the Photogrammetric Method of the Determination of their Altitudes (Serebristyye oblaka i fotogrammetricheskiy metod opredeleniya ikh vysot). Trudy Moskovskogo Instituta Inzhenerov Geodesii, Aerofotos"yemki i Kartografii, Issue 39, 1960.

20. Wang Kuei- Ch'in and Gushchin, G. P. Variations in the General Atmospheric Ozone Content in Cyclones and Anticyclones (Kolebaniya obshchego soderzhaniya atmosfernogo ozona v tsiklonakh i antitsiklonakh). Trudy Glavnoy Geofizicheskoy Observatorii (Tr.GGO), Issue 106, 1961.

21. Vasil'yev, O. B. The Calculation of Atmospheric Extinction during Observations of Noctilucent Clouds (Ob uchete atmosfernoy ekstinktii pri nablyudeniyakh serebristykh oblakov). Byulleten' Vsesoyuznogo Astronomo-Geodezicheskogo Obshchestva, No. 25, 1959.

22. - - - Simplified Method for Reduction of Coordinates during Photographic Photometry of Noctilucent Clouds (Uproshchennyy sposob reduktsii koordinat pri fotograficheskoy fotometrii serebristykh oblakov). Byull. Vses. Astron.-Geod. O-va, No. 27, 1960.

23. Vitkevich, V. I. Light Rays as a Method of Investigating the Atmosphere (Zvukovoy luch kak metod issledovaniya atmosfery). Doklad 1-mu s"yezdu Rossiyskoy assotsiatsii fizikov 6 sentyabrya 1920 g, Byull Mosk. Gos. Geofiz. In-ta, No. 6, 1920.

24. Upper Layers of the Atmosphere (Vysokiye sloi atmosfery). Byull. Astronom. In-tov Chekhoslovakii, 6, No. 4, 1955.

25. Marko, V"yelev. Noctilucent Clouds (Srebristi oblatsi). "Priroda" (Bulg.), No. 6, 1959.

26. Gaygerov, S. S. Results of Aerological Observations on the "North Pole 4" Drifting Station in 1955-1956 (K rezul'tatam aerologicheskikh nablyudeniy na dreyfuyuschchey stantsii "Severnyy polyus - 4" v 1955/56 g). Meteorol. i. Gidrol., No. 10, 1957.

27. Gauss, K. F. Selected Works on Terrestrial Magnetism (Izbrannyye trudy po zemnomu magnetizmu). Akad. Perev. A. N. Krylova. Izd-vo AN SSSR, 1952.

28. Georgiyevskiy, Yu. S., Driving, A. Ya., Zolotavina, N. V., Rozenberg, G. V. (ed.), Feygel'son, Ye. M. and Khazanov, V. S. Searchlight Rays in the Atmosphere (Prozhektornyy luch v atmosfere). Issledovaniya po Atmosfernoy Optike. Izd-vo AN SSSR, Moscow, 1960.

29. Gerzon, N. A Critical Survey of Data on the Temperature of the Ionosphere (Kriticheskiy obzor dannykh o temperature ionosfery). 47, Issue 4, 1952.

30. Gershman, B. N. and Ginzburg, V. L. The Formation of Ionospheric Inhomogeneities (Ob obrazovanii ionosfernykh neodnorodnostey). Izvestiya Vysshikh Uchebnykh Zavedeniy. Radiofizika, 2, No. 1, 1959.

31. Ginzburg, V. L. Anomalies of the Polarization of Crepuscular Light (Ob anomaliyakh polyarizatsii sumerechnogo sveta). Dokl. AN SSSR, 38, No. 9, 1943.

32. Ginzburg, V. L. and Sobolev, N. N. Secondary Light Scattering in the Atmosphere and Twilight Polarization Anomalies (O vtorichnom rasseyanii sveta v atmosfere i polyarizatsionnykh anomaliyakh vo vremya sumerek). Dokl. AN SSSR, 40, No. 6, 1943.

32a. Glagolev, Yu. A. Fine Thermometer Temperature Measurement Possibilities in Free Atmosphere of Resistance to Spheres up to Altitudes of 30-35 km (Vozmozhnosti izmereniya temperatury svobodnoy atmosfery s pomoshch'yu tonkogo termometra soprotivleniya na sharakh do vysoty 30-35 Km). Tr. TsAO Issue, 37, 1960.

33. Gol'tsman, M. I. An Objective Method for Determining Dew Points (Ob"yektivnyy metod opredeleniya tochki rosy). Meteorologicheskiy vestnik, No. 3, 1932; Measuring Air Moisture at Low Negative Temperatures (Ob izmerenii vlazhnosti vozdukha pri nizkikh otritsatel'nykh temperaturakh); Problemy Arktiki, No. 1, 1939; Bases of Methodology of Aerophysical Measurements (Osnovy metodiki aerofizicheskikh izmereniy). Gostekhizdat, Moscow-Leningrad, 1950.

34. Gorshkov, G. S. Eruption of the Volcano "Bezymyannaya" (Izverzheniye sopki Bezymyannoy). Byulleten' Vulkanologii stantsii, AN SSSR, No. 26, 1957.

35. Grishin, N. I. Meteorologic Conditions of the Appearance of Noctilucent Clouds (Meteorologicheskiye usloviya poyavleniya serebristykh oblakov). Byull. Vses. Astron.-geod. O-va, No. 15, 1954; Meteorol. i gidrol. No. 4, 1953; Trudy AN Tadzh. SSR, 20, 1954.

36. - - - The Structure of Noctilucent Clouds (O strukture serebristykh oblakov). Astronomicheskiy tsirkulyar, 16 March, No. 147, L'vov, 1954; Byull. Vses. Astron.-Geod. O-va, No. 16, 1955; Meteorol. i Gidrol., No. 1, 1955.

37. - - - Noctilucent Cloud Spectra (O spektre serebristykh oblakov). Astronomicheskiy Tsirkulyar, 10 May, No. 159, L'vov, 1955.

38. - - - The 1957-1958 IGY Program of Observations of Noctilucent Clouds (O programme nablyudeniy serebristykh oblakov v Mezhdunarodnom geofizicheskom godu 1957-1958). Astronomicheskiy Kalendar', 1957, Moscow, 1956.

39. - - - The Study of the Motion of Noctilucent Clouds by Motion Pictures (Izucheniye dvizheniy serebristykh oblakov metodom kinos"yemki). Meteorol. i Gidrol., No. 3, 1957.

40. - - - The Study of the Motion of Noctilucent Clouds (Izucheniye dvizheniy serebristykh oblakov). Byull. Vses. Astron.-Geod. O-va, No. 21, 1958.

40a. - - - Meteorological Conditions for the Appearance of Noctilucent Clouds (K voprosu o meteorologicheskikh usloviyakh poyavleniya serebristykh oblakov). Tr. VI Soveshchaniya po Serebristym Oblakam. Riga, 1961.

40b. Grishkevich, L. V., Gusev, V. D., Kushnerevskiy, Yu. V., Mirkotan, S. F. and Proshkin, Ye. G. Results of Investigations of Atmospheric Disturbances and Their Motion, Obtained by Soviet Stations in the IGY Period (Rezul'taty issledovaniya ionosfernykh neodnorodnostey i ikh dvizheniy, poluchennyye na stantsiyakh Sovetskogo Soyuza za period MGG). Coll. "Issledovaniya ionosfery i meteorov." Izd-vo AN SSSR, Moscow, 1960.

41. Grigorvoskiy, V. M. Changes in the Rotation Period of ISZ-2 (Izmeneniye perioda vrashcheniya ISZ-2). Byull. stants. optich. nablyud. iskusstv. sputnikov Zemli, No. 8, 1960.

41a. Grishkevich, L. V. Some Results of Investigations of Heterogeneities in Ionospheric Structure and Motion in It, Obtained by Spacially-Dispersed, Small-Based Reception (Nekotoryye rezul'taty issledovaniy neodnorodnostey struktury ionosfery i dvizheniy v ney, poluchennyye metodom prostranstvennoraznesennogo priyema s maloy bazoy). Coll. "Ionosfernyye issledovaniya," No. 9. Izd-vo AN SSSR, Moscow, 1961.

42. Gromova, L. F. Some Data on the Frequency of Appearance of Noctilucent Clouds in the Western Half of the USSR (Nekotoryye dannyye o chastote poyavleniya serebristykh oblakov v zapadnoy polovine territorii SSSR). Coll. "Mezhdunarodnyy geofizicheskiy god," Leningradskiy Gosadarstvennyy Universitet (LGU), Leningrad, 1960.

43. Gruza, G. V. Macroturbulence in General Atmospheric Circulation (Makroturbulentnost' v obshchey tsirkulyatsii atmosfery). Gidrometeoizdat, Leningrad, 1961.

44. Gudi, R. M. Physics of the Stratosphere (Fizika stratosfery). Gidrometeoizdat, Leningrad, 1958.

45. Gusev, V. D., Drachev, L. A., Mirkotan, S. F., Berezin, Yu. V., Kiyanovskiy, M. P., Vinogradova, M. B. and Gaylit, T. A. The Structure and Motion of Great Heterogeneities in the Ionospheric Layer (Struktura i dvizheniye krupnykh neodnorodnostey v ionosfernom sloye). Dokl. AN SSSR, 123, No. 5, 1958.

46. Gusev, V. D. and Mirkotan, S. F. Some Anomalies in Investigation of Ionospheric Drift (O nekotorykh anomaliyakh pri issledovanii ionosfernykh dreyfov). Coll. "Issled. ionosfery." No. 3, Izd-vo AN SSSR, Moscow, 1960.

47. Guterman, I. G. Statistical Principles of Wind Velocity Distribution (O statisticheskom zakone raspredeleniya skorostey vetra). Meteorol. i gidrol., No. 9, 1961.

48. Gushchin, G. P. Variations in the Optical Thickness of Aerosols in the Atmosphere (Izmereniye opticheskoy tolshchi aerozoley v atmosfere). Tr. GGO, Issue, 105, 1960.

49. Dandzhi, J. Cosmic Electrodynamics (Kosmicheskaya elektrodinamika). Gosudarstvennoye Izd-vo Literatury v Oblastyakh atomnoy nauki i tekhniki, Moscow, 1961.

50. Danilov, A. D. Molecular Ions in the Upper Atmosphere (Molekulyarnyye iony v verkhney atmosfere). Dokl. AN SSSR, 137, No. 5, 1961.

51. Danilin, B. S., Mikhnevich, V. V., Repnev, A. I. and Shvidkovskiy, Ye. G. The Problem of Measurement of Pressure and Density of the Upper Layers of the Atmosphere with Artificial Earth Satellites (Zadacha izmereniya davleniya i plotnosti vysokikh sloyev atmosfery s pomoshch'yu iskusstvennogo sputnika Zemli). UFN, 63, No. 1b, 1957.

52. Dzhapiashvili, V. P. Diffusion of Brightness in the Earth's Umbra and Penumbra through Electrophotometric Observations of the Full Lunar Eclipse of 8 December 1956 (Raspredeleniye yarkosti v zemnoy teni i poluteni po elektrofotometricheskim nablyudeniyam polnogo lunnogo zatmeniya 8 dekabrya 1956 g.). Byull. Abastumanskoy astrofiz. obs., No. 17, 1954.

53. Deminev, O. V. Some Results of Noctilucent Cloud Studies (Nekotoryye rezul'taty izucheniya serebristykh oblakov). Tr. AN Tadzh. SSR, 20, 1954.

54. Divari, N. B. Light Polarization of the Twilight Sky at the Zenith (O polyarizatsii sveta sumerechnogo neba v zenite). Dokl. AN SSSR, 112, No. 2, 1957.

55. - - - Light Changes in the Twilight Sky (Ob izmeneniyakh tsveta sumerechnogo neba). Dokl. AN SSSR, 122, No. 5, 1958.

56. - - - Zenithal Light of the Twilight Sky (O tsvete sumerechnogo neba v zenite). Izv. Astrofiz. In-ta AN Kaz. SSR, 9, 1959 (1960).

57. Dmitriyev, A. A. The Question of the Speed of Distribution of Fine Cosmic Material from the Upper to Lower Atmospheric Layers (K voprosu o skorosti rasprostraneniya melkoy kosmicheskoy materii iz verkhnikh sloyev atmosfery vniz). Izv. AN SSSR, ser. geofiz., No. 10, 1959.

58. Dmitriyev, A. A., Mishina, M. I., Mikirov, A. Ye, and Cherenkova, Ye. P. The Degree of Influence of Cosmic Dust on Several Actinometric Characteristics of the Atmosphere (O stepeni vliyaniya kosmicheskoy pyli na nekotoryye aktinometricheskiye kharakteristiki atmosfery). Izv. AN SSSR, ser. geofiz., No. 10, 1960.

59. Dobrovol'skiy, O. V. The Explosive Wave Due to the Motion of Meteoric Bodies (Vzryvnaya volna, svyazannaya s dvizheniyem meteornogo tela). Byull. Astronom. Obs. AN Tadzh SSR, No. 6, 1952.

60. Dobson, G. M. B., Bryuyer, A. V. and Kvaylong, B. M. Meteorology of the Lower Layers of the Stratosphere (Meteorologiya nizhnikh sloyev stratosfery). Usp. fiz. nauk, 31, No. 1, 1947.

61. Dokuchayev, V. P. The Theory of the Motion of Ionospheric Heterogeneities (K teorii dvizheniya ionosfernykh neodnorodnostey). Izvestiya Vysshykh Uchebnykh Zavedenyy (Izv.VUZ). Radiofizika, No. 1, 1958.

62. - - - The Action of the Terrestrial Magnetic Field on Wind in the Ionosphere (O vliyanii magnitnogo polya Zemli na vetry v ionosfere). Izv. AN SSSR, ser. geofiz., No. 5, 1959.

63. Dorodnitsyn, A. A. The Theory of Diurnal Temperature Variations in the Mixing Layers (K teorii sutochnogo khoda temperatury v sloye peremeshivaniya). Dokl. AN SSSR, 30, No. 5, 1940.

64. Driving, A. Ya. Nacreous Clouds (O perlamutrovykh oblakakh). Izv. AN SSSR, ser. geofiz., No. 3, 1959.

65. Driving, A. Ya. and Smirnova, A. I. Stratospheric Clouds (Oblaka v stratosfere). Izv. AN SSSR, ser. geofiz., No. 3, 1958.

66. Driving, A. Ya., Zolotavina, N. V., Polozova, M. N. and Smirnova, A. I. Atmospheric Stratification and the Formation of Condensation Products According to Data of Beam Sounding (Stratifikatsiya atmosfery i obrazovaniye produktov kondensatsii po dannym prozhektornogo zondirovaniya). Izv. AN SSSR, ser. geofiz., No. 5, 1958.

66a. E. Tu-Cheng and Chu Pao-Chen. Some Important Questions on General Atmospheric Circulation (Nekotoryye vazhneyshiye voprosy obshchey tsirkulyatsii atmosfery). Gidrometeoizdat, Leningrad, 1961.

66b. Yerofeyev, N. I., Dzhemilev, G. G., Perelygin, V. P. and Petinov, B. P. Initial Results of Radiotechnical Observations of the Motion of Ionospheric (Wind) Heterogeneities over Ashkhabad at Altitudes of 200-300 Km (Pervyye rezul'taty radiotekhnicheskikh nablyudeniy za dvizheniyami neodnorodnostey v ionosfere (vetrov) nad Ashkhabadom na vysotakh 200-300 km). Coll. "Dreyfy i neodnorodnosti v ionosfere," No. 1. Izd-vo AN SSSR, Moscow, 1959.

67. Zverev, A. S., Kiryukhin, B. V., Kondrat'yev, K. Ya., Selezneva, Ye. S., Tverskoy, P. N. and Yudin, M. I. Course on Meteorology (Atmospheric Physics) (Kurs meteorologii (fizika atmosfery). Editor: P. N. Tverskoy. Gidrometeoizdat, Leningrad, 1951.

67a. Zevakina, R. A. The Relation of Ionospheric and Magnetic Disturbances in the Upper Latitudes (Svyaz' ionosfernykh i magnitnykh vozmushcheniy v vysokikh shirotakh). Coll. "Magnitno-ionosfernyye vozmushcheniya, No. 1, Izd-vo AN SSSR, Moscow, 1959.

68. Zonov, Yu. V. The Interaction of Satellites and Earth's Magnetic Field (K voprosu o vzaimodeystvii sputnika s magnitnym polem Zemli). Iskusstv. sputniki Zemli, Issue 2, Izd-vo AN SSSR, Moscow, 1958.

69. Zubyan, G. D. The Interlatitudinal Change of Warm and Cold Stratospheric Air Masses in Winter (O mezhshirotnom obmene teplykh i kholodnykh mass vozdukha v stratosfere zimoy). Meteorol. i gidrol. No. 1, 1959.

69a. Ivanovskiy, A. I. and Repnev, A. I. Density Distribution in a Device with Free-Molecular Flow (O raspredelenii plotnosti v pribore pri svobodno-molekulyarnom techenii). Tr. TsAO, Issue 29, 1960.

69b. Izakov, M. N., Kokin, G. A., Kurilova, Yu. V., Livshits, N. S. and Khvostikov, I. A. Meteorological Rocket Study of the Stratosphere in the USSR (Izucheniye stratosfery pri pomoshchi meteorologicheskikh raket v SSSR). Meteorol. i gidrol., No. 1, 1963.

69c. Izakov, M. N. and Kozlov, L. V. Investigations of Temperature Reduction Coefficients for a Cylinder in the Supersonic Flow of a Rarefied Gas (Issledovaniye temperaturnogo koeffitsiyenta vosstanovleniya dlya tsilindra, obtekayemogo sverkhzvukovym potokom razrezhennogo gaza). Oborongiz, Moscow, 1958.

69d. Izakov, M. N. and Chizhov, A. V. Investigations of Tungsten Temperature Coefficients Obtained by Special CAO Thermometers and Manometers (Izucheniye temperaturnogo koeffitsiyenta vol'frama, primenyayemogo v spetsial'nykh termometrakh i manometrakh TsAO). Trudy Tsentral'noy Aerologicheskoy Observatorii (Tr. TsAO), Issue 25, 1959.

69e. Izakov, M. N. and Kokin, G. A. Atmospheric Temperature, Pressure, and Density Measurements by Rockets (Izmereniye temperatury, davleniya i plotnosti atmosfery s pomoshch'yu raket). Informatsionnyy sbornik No. 4, Komitet po provedeniyu MGG. Gidrometeoizdat, Leningrad, 1957.

70. Istomin, V. G. Rocket and Satellite Investigation of the Ion Content of Earth's Atmosphere (Issledovaniya ionnogo sostava atmosfery Zemli na raketakh i sputnikakh). Iskusstvennyye sputniki Zemli, Issue 2. Izd-vo AN SSSR, Moscow, 1958.

71. - - - A Radio Frequency Mass-Spectrometer for Investigating Ion Content in the Upper Atmosphere (Radiochastotnyy mass-spektrometr dlya issledovaniy ionnogo sostava verkhney atmosfery). Iskusstvennyye sputniki Zemli, Issue 3. Izd-vo AN SSSR, Moscow, 1959.

72. - - - Some Results of Spectral Mass Measurements of Positive Ions on the Third Soviet Artificial Earth Satellite (Nekotoryye rezul'taty izmereniya spektra mass polozhitel'nykh ionov na tret'yem sovetskom iskusstvennom sputnike Zemli). Iskusstvennyye sputniki Zemli, Issue 4. Izd-vo AN SSSR, Moscow, 1960.

73. - - - Investigations of the Ion Content of Earth by Geophysical Rocket in 1957-1959 (Issledovaniya ionnogo sostova atmosfery Zemli na geofizicheskikh raketakh v 1957-1959 gg). Iskusstv. sputniki Zemli, Issue 7. Izd-vo AN SSSR, Moscow, 1961.

74. - - - Mass Spectrometric Measurements of Earth's Atmospheric Gas Content by Rocket and Satellite (Mass-spektrometricheskiye izmereniya gazovogo sostava atmosfery Zemli na raketakh i sputnikakh). Geomagnetizm i Aeronomiya, Vol. 1, No. 3, 1961.

75. - - - Nitrogen Ions in Earth's Upper Atmosphere and Night Ionization in the E Region (Iony azota v verkhney atmosfere Zemli i nochnaya ionizatsiya v oblasti Ye). Dokl. AN SSSR, 137, No. 5, 1961.

76. - - - Changes in Positive Ion Concentration at High Altitudes According to Mass-Spectrometer Measurement Data on the Third Satellite (Izmeneniye kontsentratsii polozhitel'nykh ionov s vysotoy po dannym mass-spektrometricheskikh izmereniy na tret'yem sputnike). Iskusstv. sputniki Zemli, Issue 6. Izd-vo AN SSSR, Moscow, 1961.

77. Kalashnikov, A. G. Observations of the Magnetic Effect of Meteors by the Induction Method (O nablyudenii magnitnogo effekta meteorov induktsionnym metodom). Dokl. AN SSSR, 66, No. 3, 1949; Izv. AN SSSR, ser. geofiz., No. 6, 1952.

78. Kalinovskiy, A. B. and Pinus, N. Z. Aerology, Part I. Methods of Aerological Measurement (Aerologiya, ch. 1. Metody aerologicheskikh izmereniy). Gidrometeoizdat, Leningrad, 1961.

79. Katasev, L. A. Photographic Methods of Meteor Astronomy (Fotograficheskiye metody meteornoy astronomii). Gostekhizdat, Moscow, 1957.

80. Katasev, L. A., Korpusov, V. N. and Orlyanskiy, A. D. Radiolocation of Meteors with Two Receivers of Varied Sensitivities (Radiolokatsiya meteorov s dvumya priyemnikami razlichnoy chuvstvitel'nosti). Astronomicheskiy Zhurnal, No. 1, 1960.

81. Cowling, T. Magnetic Hydrodynamics (Magnitnaya gidrodinamika). Izd-vo inostr. lit., Moscow, 1959.

81a. Kashcheyev, B. L. and Lebedinets, V. N. Radar Investigation of Meteor Phenomena (Radiolokatsionnyye issledovaniya meteornykh yavleniy). Izd-vo AN SSSR, Moscow, 1961.

81b. Kashcheyev, B. L., Dudnik, B. S., Lagutin M. D., Lebedinets, V. N., Luk'yashko, D. N. and Lysenko, I. A. Radar Observations of Meteors at Kharkov (Radiolokatsionnyye nablyudeniya meteorov v Khar'kove). Coll. "Ionosfernyye issledovaniya (meteory)," Izd-vo AN SSSR, Moscow, 1962.

81c. Kashcheyev, B. L. and Lysenko, I. A. Investigations of Atmospheric Circulation at Altitudes of 80-120 Km (Issledovaniye tsirkulyatsii atmosfery na vysote 80-120 km). Coll. "Ionosfernyye issledovaniya." No. 9. Izd-vo AN SSSR, Moscow, 1961.

81d. Kashcheyev, B. L., Tsymbal, N. T. and Proshkin, Ye, G. Atmospheric Investigations over Kharkov During the IGY (Issledovaniya ionosfery nad Khar'kovom v period MGG). Sb. "Dreyfy i neodnorodnosti v ionosfere," No. 1, Izd-vo AN SSSR, Moscow, 1959.

81e. Kerblay, T. S. and Kovalevskaya, Ye. M. The Correlation of f_0F2 with Solar Activity Indexes (Korrelyatsiya f_0F2 s indeksami solnechnoy aktivnosti). Coll. "Issledovaniya ionosfery," No. 3. Izd-vo AN SSSR, Moscow, 1960.

81f. Kessenikh, V. N. Some Features of the Geographic Distribution of Maximal Electron Concentration of the F_2 Layer (Nekotoryye osobennosti geograficheskogo raspredeleniya maksimal'noy elektronnoy kontsentratsii sloya F2). Coll. "Issledovaniya ionosfery," No. 4, Izd-vo AN SSSR, Moscow, 1960.

81g. - - - Possible Mechanisms of Communication Between the Synoptics of the Ionosphere and the Troposphere (Vozmozhnyye mekhanizmy svyazi mezhdu sinoptikoy ionosfery i troposfery). Coll. "Issledovaniya ionosfery i meteorov." Izd-vo AN SSSR, Moscow, 1960.

82. Kiseleva, M. S., Neporent , B. S. and Fusenkova, V. A. Spectral Definition of Air Moisture in the Upper Layers of the Atmosphere (Spektral'noye opredeleniye vlazhnosti vozdukha v verkhnikh sloyakh atmosfery). Izv. AN SSSR, ser. geofiz., 1957; Optika i spektroskopiya, 6, 1959.

82a. Kovshun, I. N. Calculating the Presence of Limiting Masses of Meteors and Radiation Receiver Sensitivity During Detection of the Altitude of the Homogeneous Terrestrial Atmosphere by Data of Meteor Photography (Uchet nalichiya predel'noy massy meteora i chuvstvitel'nosti priyemnika radiatsii pri opredelenii vysoty odnorodnoy atmosfery Zemli po dannym meteornykh fotografiy). Geomagnetizm i aeronomiya, No. 1, 1962.

83. Kokin, G. A. Some Questions on the Nonequilibrium State of Gas in the Upper Atmosphere (O nekotorykh voprosakh neravnovesnogo sostoyaniya gaza v verkhney atmosfere). Tr. TsAO, Issue 29, 1959.

84. Kozik, S. M. The Contour of the Earth's Shadow During Lunar Eclipses (Kontur zemnoy teni pri lunnykh zatmeniyakh). Dokl. AN SSSR, 104, No. 6, 1955.

84a. Kokurin, Yu. L. The Form and Motion of Small Heterogeneities of the Ionosphere (Forma i dvizheniya malykh neodnorodnostey v ionosfere). Coll. "Dreyfy i neodnorodnosti v ionosfere," No. 1, Izd-vo AN SSSR, Moscow, 1959.

85. Komissarov, O. D., Nazarova, T. N., Neugodov, L. N., Poloskov, S. M. and Rusakov, L. Z. Rocket and Satellite Investigations of Micrometeorites (Issledovaniye mikrometeoritov na raketakh i sputnikakh). Iskusstvennyye sputniki Zemli, Issue 2. Izd-vo AN SSSR, Moscow, 1958.

86. Kondrat'yev, K. Ya. Solar Radiant Energy (Luchistaya energiya Solntsa). Gidrometeoizdat, Leningrad, 1954.

87. - - - Radiant Heat Exchange in the Atmosphere (Luchistyy teploobmen v atmosfere). Gidrometeoizdat, Leningrad, 1956.

88. - - - Satellites and Meteorology (Sputniki i meteorologiya). UFN, 74, Issue 2, 1961.

88a. - - - Meteorological Investigation by Rocket and Satellites (Meteorologicheskiye issledovaniya s pomoshch'yu raket i sputnikov). Gidrometeoizdat, Leningrad, 1962.

89. Kondrat'yev, K. Ya. and Nedovesova, L. I. Heat Emission of Carbon Dioxide in the Atmosphere (O teplovom izluchenii uglekislogo raza v atmosfere). Izv. AN SSSR, ser. geofiz., No. 12, 1958.

90. Kondrat'yev, K. Ya. and Filipovich, O. P. The Theory of the Heat Regime in the Upper Atmosphere (K teorii teplovogo rezhima verkhney atmosfery). Meteorol. i gidrol., No. 12, 1959.

91. - - - The Heat Regime of the Upper Layers of the Atmosphere (Teplovoy rezhim verkhnikh sloyev atmosfery). Gidrometeoizdat, Leningrad, 1960.

91a. Kostylev, K. V. Radar Observation of Meteors in Kazan (Radiolokatsionnyye nablyudeniya meteorov v Kazani). Coll. "Ionosfernyye issledovaniya" (meteory). Izd-vo AN SSSR, Moscow, 1962.

91b. Kramer, Ye. N. The Question of Determining Atmospheric Density by Meteor Data. (K voprosu ob opredelenii plotnosti atmosfery po meteornym dannym). Geomagnetizm i aeronomiya, No. 1, 1962.

92. Krinov, Ye. L. Instructions for Observing Noctilucent Clouds (Instruktsiya dlya nablyudeniya serebristykh oblakov). Astronomicheskiy kalendar' Gosudarstvennoye Astronomo-Geodezicheskoye Obshchestvo, Moscow, 1936.

93. - - - Meteorites (Meteority). Izd-vo AN SSSR, Moscow-Leningrad, 1948.

94. - - - The Tungus Meteorite (Tungusskiy meteorit). Izd-vo AN SSSR, Moscow-Leningrad, 1949.

95. - - - Meteorites (Meteority). BSE, Vol. 27, 1954.

96. Kroshkin, M. G. Geophysical Investigations Conducted with Rockets and Artificial Earth Satellites in the USA during the IGY. (Geofizicheskiye issledovaniya, provodimyye pri pomoshchi raket i iskusstvennykh sputnikov Zemli v SShA po programme Mezhdunarodnogo Geofizicheskogo Goda). Inf. byull. MGG, No. 7, Izd-vo AN SSSR, Moscow, 1959.

97. Kryuchkov, S. I. Conditions for Distribution of Short Electromagnetic Waves in the Terrestrial Atmosphere (Usloviya rasprostraneniya korotkikh

elektromagnitnykh voln v zemnoy atmosfere). Zhurnal Prikladnoy Fiziki, 7, Issue 2, 1930.

98. - - - The Structure of the Heaviside Conducting Layer (O strukture provodyashchego sloya Khivisayda). Nauchn-tekhnich. sb. Elektrotekhn. in-ta svyazi, Issue 8, 1935.

99. Kuznetsov, V. V. Cloud Altitude Determination in the Dark Part of the Day by Electric Projection (Opredeleniye vysoty oblakov v temnuyu chast' sutok s pomoshch'yu elektricheskogo prozhektora). Izv. AN SSSR ser. V, Nos. 4 and 5, 1905.

100. Kuznetsov, G. I. Several Relations Between General Circulation and Atmospheric Ozone (O nekotorykh svyazyakh mezhdu obshchey tsirkulyatsiyey i ozonom atmosfery). Izv. AN SSSR, ser. geofiz, No. 3, 1961.

100a. Kushnerevskiy, Yu. V. and Zayarnaya, Ye. S. The Drift of Small-Scale Heterogeneities in the F_2 Layer (Dreyf melkomasshtabnykh neodnorodnostey v sloye F2). Coll. "Dreyfy i neodnorodnosti v ionosfere," No. 1. Izd-vo AN SSSR, Moscow, 1959.

100b. - - - Data on Drift in the F_2 Layer, Obtained through Various Experimental Methods (Dannyye o dreyfe v sloye F2, poluchennyye raznymi metodami obrabotki). Coll. "Ionosfernyye issledovaniya," No. 9, Izd-vo AN SSSR, Moscow, 1961.

101. Ladlam, F. Kh. Noctilucent Clouds (Serebristyye oblaka). Usp. fiz. nauk, 65, No. 3, 1958.

102. Lamb, G. Hydrodynamics (Gidrodinamika). Gostekhizdat, Moscow-Leningrad, 1947.

103. Lebedev, A. A. and Khvostikov, I. A. Visual Photometrics at Dusk (Visual'noye fotometrirovaniye sumerek). Tr. El'brussk. ekspeditsii 1934 i 1935 gg. Izd-vo AN SSSR, 1936.

104. Lebedeva, N. V. Thermic Convection (Termicheskaya konvektsiya). Trudy Tsentral'nogo Instituta Prognozov (Tr. TsIP), Issue 77, 1958.

105. Lebedinskiy, A. I. Radiant Equilibrium of Earth's Atmosphere (Luchevoye ravnovesiye zemnoy atmosfery). Uchennyye zapiski L.G.U., seriya matematicheskaya, No. 31, Issue 3, 1939.

106. - - - Radiant and Arc Forms of Aurora (Luchistyye i dugovyye formy polyarnogo siyaniya). Dokl. AN SSSR, 86, No. 5, 1952.

107. Levin, B. Yu. Elements of the Physical Theory of Meteors (Elementy fizicheskoy teorii meteorov). Astronomicheskiy Zhurnal (A. Zh.) 17, Issue 3, 1940; 18, Issue 4-5, 1941; Dokl. AN SSSR, 25, 1939.

108. - - - Studies of Density of Upper Atmospheric Layers by Meteoric Methods (Izucheniye plotnosti vysokikh sloyev atmosfery meteornymi metodami). UFN, 34, Issue 4, 1948.

109. - - - Physical Theory of Meteors and Meteoric Matter in the Solar System (Fizicheskaya teoriya meteorov i meteornoye veshchestvo v solnechnoy sisteme). Izd-vo AN SSSR, Moscow, 1956.

109a. Lidov, M. L. Determining Atmospheric Density by Observed Braking of the First Artificial Earth Satellites (Opredeleniye plotnosti atmosfery po nablyudayemomu tormozheniyu pervykh iskusstvennykh sputnikov Zemli). Iskusstvennyye sputniki Zemli (ISZ), Issue 1, 1958; Izv. AN SSSR, seriya geofizicheskaya, No. 12, 1957.

110. Lovell, B. Meteor Astronomy (Meteornaya astronomiya). Fizmatgiz, Moscow, 1958.

111. Lovell, B. and Klegg, J. Radioastronomy (Radioastronomiya). Izd-vo inostrannoy literatury (IL), Moscow, 1953.

111a. Logvinov, K. T. (ed.) Materials of the Conference on 1960 IGY Results and Meteorological Study of the Antarctic (1959) (Materialy konferentsiy po itogam MGG (1960) i meteorologicheskogo izlucheniya Antarktidy (1959). Gidrometeoizdat, Moscow, 1961.

112. Martynenko, V. V. and Gapotchenko, A. G. Noctilucent Cloud Observations of June 29, 1957 (Nablyudeniya serebristykh oblakov 29 iyunya 1957 g.). Astronomicheskiy tsirkulyar (ATs), No. 187, Dec. 21, L'vov, 1957.

113. Martynov, D. Ya. Noctilucent Clouds (Svetyashchiyesya nochnyye oblaka). A.Ts., No. 139, June 18, L'vov, 1953.

114. Maeda Ken"iti, Takeya Yosio, Matsumoto Kharuya and Okumoto Takaaki. Study of Air Temperature and Wind Velocity in the Upper Layers of the Atmosphere (Izucheniye temperatury vozdukha i skorosti vetra v verkhnikh sloyakh atmosfery). Seisan kenkyu, Monthly J. Inst. Industr. Sci., Univ. Tokyo, 11, No. 18, 1959.

115. Megrelishvili, T. G. Electrocolorimetry of the Twilight Sky (Elektrokolorimetriya sumerek). Dokl. AN SSSR, 53, No. 2, 1946.

116. - - - The Influence of Twilight Light Changes on the Results of Investigations of the Upper Layers of the Atmosphere by Crepuscular Methods (O vliyanii izmeneniya tsveta sumerek na rezul'taty issledovaniya vysokikh sloyev atmosfery sumerechnym metodom). Dokl. AN SSSR, 55, No. 8, 1947.

117. Megrelishvili, T. G. and Khvostikov, I. A. The Structure of the Upper Layers of the Atmosphere According to Twilight Observations (Stroyeniye vysokikh sloyev atmosfery po sumerechnym nablyudeniyam). Dokl. AN SSSR, 59, No. 7, 1948.

118. Megrelishvili, T. G. Study of Some Physical Characteristics of the Upper Layers of the Atmosphere by the Twilight Electrocolorimetric Method (Izucheniye nekotorykh fizicheskikh svoystv vysokikh sloyev atmosfery metodom elektrokolorimetrii sumerek). Byull. Abastumanskoy astrofiz. obs. 9, 1948.

119. - - - The Question of the Limits of Applicability of the Twilight Method of Atmospheric Study (K voprosu o granitsakh primenimosti sumerechnogo metoda izucheniya atmosfery). Izvestiya AN SSSR, ser. geofiz., No. 8, 1956.

120. - - - The Possibility of Investigating Aerosol Layers by the Twilight Method (O vozmozhnosti issledovaniya aerozol'nykh sloyev sumerechnym metodom). Izv. AN SSSR, ser. geofiz., No. 4, 1958.

121. Megrelishvili, T. G. and Khvostikov, I. A. New Bands in the Twilight Sky Spectrum (Novyye polosy v spektre sumerechnogo neba). A Ts, No. 197, 28 November, 1958.

121a. Mednikova, N. V. Ionospheric Disturbances in the Middle Latitudes (Ionosfernyye vozmushcheniya v srednikh shirotakh). Coll. "Magnitno-ionosfernyye vozmushcheniya," No. 1, Izd-vo AN SSSR, 1959.

122. Mironov, A. V., Khovstikov, I. A. and Shal'nikov, A. I. A Method of Optical Study of the Atmosphere under Diurnal Conditions by Search-light (Metod opticheskogo izucheniya atmosfery v dnevnykh usloviyakh s pomoshch'yu prozhektornogo lucha). Dokl. AN SSSR, 54, No. 6, 1946.

123. Mirtov, B. A. Rocket Investigations of Atmospheric Conditions at High Altitudes (Raketnyye issledovaniya sostava atmosfery na bol'shikh vysotakh). UFN, 63, No. 1b, 1957.

124. - - - Meteoric Material and Some Questions of the Geophysics of the Upper Layers of the Atmosphere (Meteornaya materiya i nekotoryye voprosy geofiziki vysokikh sloyev atmosfery). Iskusstvennyye sputniki Zemli (ISZ), Issue 4, Izd-vo AN SSSR, Moscow, 1960.

125. - - - The Gaseous State of Earth's Atmosphere and Methods of its Analysis (Gazovyy sostav atmosfery Zemli i metody yego analiza). Izd-vo AN SSSR, 1961.

126. - - - Rockets, Satellites and Investigation of the Upper Atmosphere (Rakety, sputniki i issledovaniya verkhney atmosfery). Priroda, No. 10, 1961.

127. Mitra, S. G. The Upper Atmosphere (Verkhnyaya atmosfera). I L, Moscow, 1955.

128. Mikhnevich, V. V. Pressure Measurement in the Upper Atmosphere (Izmereniye davleniya v verkhney atmosfere). UFN, 63, No. 1b, 1957.

129. - - - Preliminary Results of the Determination of Atmospheric Density Above 100 km (Predvaritel'nyye rezul'taty opredeleniya plotnosti atmosfery vyshe 100 km). ISZ, Issue 2. Izd-vo AN SSSR, Moscow, 1958.

130. - - - Some Results of Investigation of the Upper Atmosphere (Nekotoryye rezul'taty issledovaniy verkhney atmosfery). Priroda, No. 5, 1958.

131. Mikhnevich, V. V. and Khvostikov, I. A. Study of the Upper Layers of the Atmosphere (Izucheniye vysokikh sloyev atmosfery). Izv. AN SSSR, ser. geofiz., No. 11, 1957.

132. - - - Atmospheric Sounding by Searchlight to Altitudes of 55 Km (Zondirovaniye atmosfery prozhektornym luchom do vysoty 55 km). Dokl. AN SSSR, 54, No. 3, 1946.

133. Mordukhovich, M. I. The Local Acoustic Method of Air Temperature Measurement (Lokal'nyy akusticheskiy metod izmereniya temperatury vozdukha). Izv. AN SSSR, ser. geofiz., No. 3, 1959.

134. - - - Some Results of Air Temperature Measurement by the Local Acoustic Method to Altitudes of 28 Km (Nekotoryye rezul'taty izmereniya temperatury vozdukha lokal'nym akusticheskim metodom do vysoty 28 km). Izv. AN SSSR, ser. geofiz., No. 1, 1960.

135. Mulyarchik, T. M. Interferometric Measurement of the Width of Line λ = 5,577 A (OI) in Auroras (Interferometricheskiye izmereniya shiriny linii λ = 5577 A (OI) v polyarnykh siyaniyakh). Izv. AN SSSR, ser. geofiz. No. 12, 1959.

136. Myukhkyurya, V. I. The Question of Vertical Distribution of Aerosol-Formed Indicators of Atmospheric Sunlight Weakening (K voprosu o vertikal'nom raspredelenii aerozol'noy sostavlyayushchey pokazatelya oslableniya solnechnogo sveta v atmosfere). Tr. GGO, Issue 105, 1960.

137. The Scientific Use of Artificial Earth Satellites (Nauchnoye ispol'zovaniy iskusstvennykh sputnikov Zemli). I L, Moscow, 1960.

138. Neporent, B. S., Belov, V. F., Dmitriyevskiy, O. D., Zaytsev, G. A., Kastrov V. G., Kiseleva, M. S., Kudryabtseva, L. A. and Patalakhin, I. V. A Test of Direct Measurement of the Vertical Distribution of Atmospheric Moisture by the Spectral Method (Opyt pryamogo izmereniya vysotnogo raspredeleniya vlazhnosti atmosfery spektral'nym metodom). Izv. AN SSSR, ser. geofiz., No. 4, 1957.

139. Novikov, Ye. A. The Magnetic Hydrodynamics of the Ionosphere (O magnitnoy gidrodinamike ionosfery). Izv. AN SSSR, ser. geofiz., No. 11, 1960.

140. Novozhilov, N. I. Noctilucent Clouds over the Karelian Isthmus (Serebristyye oblaka nad Karel'skim peresheykom). Priroda, No. 10, 1960.

141. Okhotsimskiy, D. Ye. and Eneyev, T. M. Some Variation Problems Connected with the Launching of Artificial Earth Satellites (Nekotoryye variatsionnyye zadachi, svyazannyye s zapuskom iskusstvennogo sputnika Zemli). UFN, 63, No. 1a, 1957.

142. Okhotsimskiy, D. Ye, Eneyev, T. M. and Taratynova, G. P. Determination of the Life-Span of Artificial Earth Satellites and the Investigation of Cyclical Disturbances in their Orbits (Opredeleniye vremeni sushchestvovaniya iskusstvennogo sputnika Zemli i issledovaniye vekovykh vozmushcheniy yego orbity). UFN, 63, No. 1a, 1957.

143. Pavlova, T. D. The Visible Frequency of Appearance of Noctilucent Clouds by Observation Stations of the Hydrometeorological Service Network for 1957 and 1958 (Vidimaya chastota poyavleniya serebristykh oblakov po nablyudeniyam stantsiy seti gidrometsluzhby za 1957 i 1958 gody). Coll. "Issledovaniya serebristykh oblakov." Izd-vo Leningradskogo Gosudarstvennogo Universiteta (Izd-vo LGU) Leningrad, 1960.

144. Pavlovskaya, A. A. Interseasonal Changes in Atmospheric Circulation in the Upper Troposphere and Lower Stratosphere (Vnutrisezonnyye izmeneniya atmosfernoy tsirkulyatsii v verkhney troposfere i nizhey stratosfere). Tr. Ts I P, Issue 104, 1961.

145. Pasechnik, I. P. Seismic and Air Waves Arising from the Eruption of the "Bezymyannyy" Volcano on March 30, 1956 (Seysmicheskiye i vozdushnyye volny, voznikshiye pri izverzhenii vulkana Bezymyannyy 30 marta 1956 g.). Izv. AN SSSR, ser. geofiz., No. 9, 1958.

146. Patterson, G. N. Molecular Flow of Gases (Molekulyarnoye techeniye gazov). Fizmatgiz, Moscow, 1960.

147. Perevertun, M. P. Twilight Sky Brightness in the Sun's Vertical Considering Secondary Scattering (Yarkost' sumerechnogo neba v vertikale Solntsa s uchetom vtorichnogo rasseyaniya). Trudy Sektora astrobotaniki AN Kaz SSR, 7, 1959.

148. Pogosyan, Kh. P. General Circulation of the Atmosphere (Obshchaya tsirkulyatsiya atmosfery). Gidrometeoizdat, Leningrad, 1959.

149. - - - The Jet Stream in the Atmosphere (Struynyye techeniya v atmosfere). Gidrometeoizdat, Moscow, 1960.

150. - - - The Geopotential Field in the Stratosphere (Pole geopotentsiala v stratosfere). Meteorol. i gidrol., No. 8, 1961.

151. Polyakov, V. M. Temperature and Gas Density Determination of the Ionospheric Layer Level (Ob otsenke temperatury i plotnosti gaza na vysote ionosfernogo sloya). Trudy nauchno-issledovatel'skogo instituta zemnogo magnetizma, Issue 1, 1955.

152. - - - Temperature and Gas Density Determination in the F Region of the Ionosphere (Ob opredelenii temperatury i plotnosti gaza v oblasti F ionosfery). Trudy Irkutskogo universiteta, 15, 1957.

153. Poloskov, S. M. and Nazarova, T. N. Investigation of the Solid Ingredient Interplanetary Material by Rocket and Artificial Earth Satellite (Issledovaniye tverdoy sostavlyayushchey mezhplanetnogo veshchestva s pomoshch'yu raket i iskusstvennykh sputnikov Zemli). UFN, 63, No. 1b, 1957.

154. Pokhunkov, A. A. Investigation of the Neutral Content of the Upper Atmosphere at Altitudes above 100 Km (Issledovaniye neytral'nogo sostava verkhney atmosfery na vysotakh svyshe 100 km). Izv. AN SSSR, ser. geofiz., No. 11, 1960.

155. - - - Mass Spectrometer Investigation of the Structural Parameters of the Earth's Atmosphere at Altitudes from 100 to 210 Km (Mass-spektrometricheskiye issledovaniya strukturnykh parametrov zemnoy atmosfery na vysotakh ot 100 do 210 km). Iskusstvennyye sputniki Zemli, Issue 7, Izd-vo AN SSSR, Moscow, 1961.

156. Pressman, A. Ya. and Yatsenko, S. P. The Possibility of Measuring the Temperature of the Upper Layers of the Atmosphere by Narrow Tube (O vozmozhnosti izmereniya temperatury verkhnikh sloyev atmosfery pri pomoshchi uzkoy trubki). Geomagnetizm i aeronomiya, 1, No. 1, 1961.

157. Prokudina, V. S. Determining the Rotational Temperature of Hydroxyl in the Upper Atmosphere (Opredeleniye vrashchatel'noy temperatury gidroksila v verkhney atmosfere). Izv. AN SSSR, ser. geofiz., No. 4, 1959.

157a. Pupyshev, Yu. A. Radar Observations of Meteor Activity at the Engelhardt Astronomical Observatory on Aug. 10-17, 1956 (Radiolokatsionnyye nablyudeniya meteornoy aktivnosti na astronomicheskoy observatorii im. Engel'gardta 10-17 avgusta 1956 g.). A Ts, No. 173, Izd-vo AN SSSR, Moscow, 1956.

158. Putilin, I. I. Noctilucent Clouds in 1923 (Nochnyye svetyashchiyesya oblaka v 1923 g.). Mirovedeniye, No. 2, 47, 1924.

159. Raykhl', Ya. Changes in the Front Sections of Meteors (Izmeneniye lobovogo secheniya meteorov). Byull. astronomicheskikh in-tov Chekhoslovakii, 10, Mar. 1, No. 2, 1959.

160. - - - Maximal Brightness and Structure of Meteoric Bodies (Maksimal'naya yarkost' i struktura meteornykh tel). Byull. astron. in-tov Chekhoslovakii, 10, Mar. 1, No. 2, 1959.

161. Rakipova, L. R. The Possible Action of Dust on the Vertical Motion of Air and the Isotherm in the Stratosphere (O vozmozhnom vliyanii pyli na vertikal'nyye dvizheniya vozdukha i izotermiyu v stratosfere). Izv. AN SSSR, ser. geogr. i geofiz., No. 1, 1947.

162. - - - The Vertical Transposition of Air in the Atmosphere and Cosmic Dust (Vertikal'nyye peremeshcheniya vozdukha v atmosfere i kosmicheskaya pyl'). Tr. GGO, Issue 19 (81), 1950.

163. - - - Heat and Moisture Mass Transfer across the Equator (O perenose massy tepla i vlagi cherez ekvator). Tr. GGO, Issue 114, 1960.

164. - - - The Mechanization of Communication Between the Trosposphere and the Upper Layers of the Atmosphere (O mekhanizme svyazi mezhdu troposferoy i verkhnimi sloyami atmosfery). Tr. GGO, Issue 28, 90, 1951.

165. - - - The Heat Regime of the Atmosphere (Teplovoy rezhim atmosfery). Gidrometeoizdat, Leningrad, 1957.

166. - - - The Action of Atomic Explosions on the Atmosphere (Vliyaniye atomnykh vzryvov na atmosferu). Meteorol. i gidrol., No. 6, 1957.

166a. Repnev, A. I. Mass Selection in Tubes Moving in a Rarefied Gas (Massovaya selektsiya v trubkakh, dvizhushchikhsya v razrezhennom gaze). Tr. Ts AO, Issue 29, 1960.

166b. - - - Characteristics of the Upper Atmosphere and Artificial Earth Satellites (Svoystva verkhney atmosfery i iskusstvennyye sputniki Zemli). Tr. Ts AO, Issue 25, 1959.

167. Rozenberg, G. V. Twilight Phenomena, Their Nature and Use for Atmospheric Investigation (Sumerechnyye yavleniya, ikh priroda i ispol'zovaniye dlya issledovaniya atmosfery). UFN, Vol. 79, No. 3, 1963.

168. - - - Polarization of the Secondary Scattering of Light (Polyarizatsiya vtorichnogo rasseyannogo sveta). Izv. AN SSSR, ser. geofiz., 13, 1949.

169. Rozenberg, G. V., Khvostikov, I. A. and Yudalevich, F. F. The Question of the Role of Secondary Light Scattering as a Twilight Effect (K voprosu o roli vtorichnogo rasseyaniya sveta v yavlenii sumerek). Dokl. AN SSSR, 55, No. 8, 1947.

170. Rozenberg, G. V. Twilight (Sumerki). Fizmatgiz, Moscow, 1963.

171. Romantsov, I. I. Tropospheric Investigation by Searchlight (Issledovaniye troposfery s pomoshch'yu prozhektornogo lucha). Izv. AN SSSR, ser. geogr. i geofiz., 12, No. 5, 1948.

172. Romantsov, I. I. and Khvostikov, I. A. Photographing the Tropopause in Polarized Light (Fotografirovaniye tropopauzy v polyarizovannom svete). Dokl. AN SSSR, 53, No. 8, 1946.

173. Rossbi, K. The Nature of Total Circulation in the Lower Parts of the Atmosphere (Priroda obshchey tsirkulyatsii v nizhney chasti atmosfery). Coll. "Atmosfery Zemli i planet" I L, Moscow, 1951.

174. Rubashev, B. M. The Heating of the Atmospheric Layers During Magnetic Storms (O nagrevanii verkhnikh sloyev atmosfery vo vremya magnitnykh bur'). Izv. GGO, 20, Issue 6, 1958.

174a. Rubtsov, L. N. Radar Observations of Meteors at the Dushanbe Astronomical Observatory (Radiolokatsionnyye nablyudeniya meteorov na astronomicheskoy observatorii v Dushanbe). Byull. Astronom. obs. AN Tadzh SSR, Nos. 22 and 23, 1957.

175. Sedov, L. I. Gasdynamics (Gazovaya dinamika). BSE, Vol. 10, 2nd edition 1952.

176. - - - Dynamic Effects in the Motion of Artificial Earth Satellites (Dinamicheskiye effekty v dvizhenii iskusstvennykh sputnikov Zemli). ISZ, Izd-vo AN SSSR, Issue 2, 1958.

177. Sidorov, V. V. The Motion of Deflecting Points along a Meteor Trail (O dvizhenii otrazhayushchey tochki vdol' meteornogo sleda). A. Ts. Izd-vo AN SSSR, Moscow, No. 197, 1958.

177a. Smirnov, V. B. Airplane Measurements of Drift and Dimensions of Irregularities of the E Layer in the Central Arctic (Samoletnyye izmereniya dreyfa i razmerov neodnorodnostey sloya E v tsentral'noy Arktike). Coll. "Ionosfernyye issledovaniya," No. 9, Izd-vo AN SSSR, Moscow, 1961.

178. Smirnov, I. P. Searchlight Probing as a Method of Studying Atmospheric Stratification (Prozhektornoye zondirovanyye kak metod izucheniya stratifikatsii atmosfery). Dokl. AN SSSR, 53, No. 8, 1946.

179. Sosnova, A. K. and Katasev, L. A. Results of Photographic Observations of Meteors in 1952 at the Dushanbe Astronomical Observatory (Rezul' taty fotograficheskikh nablyudeniy meteorov 1952 g. na astronomicheskoy observatorii v Dushanbe). Byull. Astronom. obs. AN Tadzh SSR, No. 11, 1954.

180. Sredinskiy, S. N. Bright Noctilucent Clouds (Yarkiye serebristyye oblaka). Priroda, No. 3, 1960.

181. Stanyukovich, K. P. Elements of the Physical Theory of Meteors and Crater-Forming Meteorites (Elementy fizicheskoy teorii meteorov i krateroobrazuyushchikh meteoritov). Coll. "Meteoritika," 7, Izd-vo AN SSSR, Moscow-Leningrad, 1950.

181a. Stekhnovskiy, D. I. The Barometric Field of Earth's Sphere (Baricheskoye pole zemnogo shara). Gidrometeoizdat, Moscow-Leningrad, 1962.

182. Ston, A. The Motion of a Cone with Supersonic Velocity under Small Angles of Attack (O dvizhenii konusa so sverkhzvukovoy skorost'yu pod malym uglom ataki). Coll. "Gazovaya Dinamika" I L, Moscow, 1950.

183. Syrovatskiy, S. I. Magnetic Hydrodynamics (Magnitnaya gidrodinamika). UFN, 62, No. 3, 1957.

184. Sytinskaya, N. N. A Test of Photographic Photometry of Meteors (Opyt fotograficheskoy fotometrii meteorov). A. Zh., Nos. 174-199, 1935; Uchennyye zapiski LGU, No. 53, 1939; Priroda, No. 4, 1940.

185. Tamm, I. Ye. Ionospheric Flows Causing Variations in Earth's Magnetic Field (O Tokakh v ionosfere, obuslovlivayushchikh variatsii zemnogo magnitnogo polya). Izv. AN SSSR, ser. fizich., No. 2, 1944.

186. Taratynova, G. P. The Motion of Artificial Satellites in Earth's Noncentral Gravitational Field in the Presence of Atmospheric Resistance (O dvizhenii iskusstvennogo sputnika v netsentral'nom pole tyagoteniya Zemli pri nalichii soprotivleniya atmosfery). UFN, 63, No. 1a, 1957.

187. Taylor, G. I. and Makkol, D. V. The Mechanics of Compressible Fluids (Mekhanika szhimayemykh zhidkostey). Coll. "Aerodinamika," Dyurenda, (ed.), Volume 3, Gostekhizdat, Moscow, 1939.

188. Teyfel', V. G. Noctilucent Clouds in 1953 (Serebristyye oblaka v 1953 g.). A Ts, No. 142, 1953.

189. - - - Noctilucent Clouds (Serebristyye oblaka). Tr. Sektora astrobotan. AN Kaz SSR, 5, 1957.

190. Tzyan, Kh. Sh. Problems of Investigation of the Aerodynamics of Rarefied Gases in Tubes (Problemy issledovaniy po aerodinamike razrezhennykh gazov v trubakh). Coll. "Gazovaya dinamika." I L , Moscow, 1950.

191. Tikhomirov, Ye. I. Noctilucent Clouds (Serebristyye oblaka). Meteorol. i gidrol., Nos. 3 and 4, 1935.

192. Tolstov, V. V. and Bondar', B. G. Measuring Drift Velocity of Irregularities in Ionization (Wind) in the F Region of the Ionosphere (Izmereniye skorosti dreyfa neodnorodnostey ionizatsii (vetrov) v oblasti F ionosfery). Inf. byull. Orgkomiteta MGG Prezidiuma AN USSR, No. 1, 1958.

193. Toropova, T. P. Determining Atmospheric Water Vapor Content (Opredeleniye soderzhaniya vodyanogo para v atmosfere). Astrofiz. in-ta AN Kaz SSR, 1, Nos. 1 and 2, 1955.

194. - - - The Application of Exponential Laws to the Water Vapor Absorption Belts (O primenimosti eksponentsial'nogo zakona k polosam pogloshcheniya vodyanogo para). Izv. Astrofiz. in-ta AN Kaz SSR, Issue 10, 1960.

194a. Troitskaya, V. A. Initial Results of the Study of the Microstructure of Very Powerful Magnetic Storms by Short-Period Variations (Predvaritel' nyye rezul'taty izucheniya mikrostruktury krupneyshikh magnitnykh bur' po korotkoperiodicheskim kolebaniyam). Coll. "Magnetno-ionosfernyye Vozmushcheniya," No. 1, Izd-vo AN SSSR, 1959.

195. Transactions of the Conference on Noctilucent Clouds (Trudy soveshchaniya po serebristym oblakam; Tartu), T. I. AN Est SSR, 1959.

196. Usmanov, R. F. The Influence of Earth Rotation on Total Circulation of the Atmosphere (O vliyanii vrashcheniya Zemli na obshchuyu tsirkulyatsiyu atmosfery). Tr. TsIP, Issue 104, 1961.

197. Faraponova, G. P. Studies of Indicators of Weakening Sunlight in the Atmosphere (Izmereniya pokazatelya oslableniya solnechnogo sveta v atmosfere). Tr. TsAO, Issue 23, 1957.

198. Fedorova, N. I. Hydroxyl Illumination of the Upper Atmosphere (Gidroksil'noye izlucheniye verkhney atmosfery). Izv-vo AN SSSR, ser. geofiz. No. 6, 1959.

199. Fedynskiy, V. V. Night Luminous Meteor Trails (Nochnyye svetyashchiyesya meteornyye sledy). Tr. Tadzh. astronom. obs., 2, 1941.

200. - - - Results of Observations of Meteor Trails in Tadzhikistan in 1934-1938 (Rezul'taty nablyudeniy meteornykh sledov v Tadzhikistane, 1934-1938). A. Zh., 21, No. 6, 1944.

201. - - - Meteor Trail Drift (Dreyf meteornykh sledov). Astronom. kalendar', Gos. astr.-geodez. ob-vo, Moscow, 1947.

202. - - - Meteors - Book: Thirty Years of Astronomy in the USSR (Meteory. Kn. "Astronomiya v SSSR za tridtsat' let"). Izd-vo AN SSSR, Moscow-Leningrad, 1948.

203. - - - Meteors (Meteory). BSE, Vol. 27, 1954.

203a. - - - Meteors (Meteory). Gostekhizdat, Moscow, 1956.

204. - - - Comparison of Visual and Radar Determinations of Drift of Meteor Trails (Sopostavleniye vizual'nykh i radiolokatsionnykh opredeleniy dreyfa meteornykh sledov). Byull. astronom. in-tov Chekhoslovakii, 7, No. 3, 1956.

205. Fedynskiy, V. V. and Stanyukovich, K. L. Results of Photographic Study of a Bright Meteor (Rezul'taty fotograficheskogo izucheniya odnogo yarkogo meteora). A. Zh., 12, Issue 5, 1935.

206. Fedynskiy, V. V. and Astapovich, I. S. Meteors (Meteory). Izd-vo AN SSSR, Moscow, 1940.

207. Fesenkov, V. G. The Construction of the Atmosphere (Photometric Analysis of Twilight) (O stroyenii atmosfery (fotometricheskiy analiz sumerek)). Trudy Glavnoy Astrofizicheskoy Observatorii (Tr. GAO), 2, 1923; A. Zh., 7, No. 2, 1930.

208. - - - The Study of the Atmosphere by Photometric Analysis of Twilight (K issledovaniyu stratosfery putem fotometricheskogo analiza sumerek). Izv. AN SSSR, otdelen. mat. i yest. nauk, 1934.

209. - - - The Question of Stratosphere Investigation by Photometric Analysis of Twilight (K voprosu issledovaniya stratosfery putem fotometricheskogo analiza sumerek). Trudy Vsesoyuznoy konferentsii po izucheniyu stratosfery, Moscow, 1935.

210. - - - Investigation of Atmospheric Structure by Photometric Means (Issledovaniye stroyeniya atmosfery fotometricheskim putem). Tr. Gos. astron. in-ta im. Shtenberga, 6, No. 2, 1936; 10, No. 1, 1937.

211. - - - The Earth's Umbra (O teni zemli). A. Zh., 23, No. 3, 1946.

212. - - - Meteor Material in Interplanetary Space (Meteornaya materiya v mezhplanetnom prostranstve). Izd-vo AN SSSR, Moscow-Leningrad, 1947.

213. - - - Thermic Dissipation of the Atmosphere (O termicheskoy dissipatsii atmosfery). A. Zh., 28, Issue 4, 1951.

214. - - - The Question of Micrometeorites (K voprosu o mikrometeoritakh). Meteoritika, Issue 12, 1955.

215. - - - The Theory of Brightness of the Day Sky for Spherical Earth (K teorii yarkosti dnevnogo neba pri sfericheskoy zemle). A. Zh., 32, Issue 3, 1955.

216. - - - The Brightness of the Cloudless Day Sky for Spherical Earth (O yarkosti dnevnogo bezoblachnogo neba pri sfericheskoy zemle). Dokl. AN SSSR, 101, No. 5, 1955.

217. - - - The Question of Investigating Atmospheric Ozone by Photometry of Lunar Eclipse (K voprosu ob issledovanii atmosfernogo ozona putem fotometrii lunnykh zatmenniy). A. Zh., 36, No. 4, 1959.

218. Fialko, Ye. I. Radar Observations of Meteors on the 10 m Wave (Radiolokatsionnyye nablyudeniya meteorov na volne 10 m). Astronomicheskiy tsirkulyar, No. 175, 21 December 1956.

219. - - - Average Characteristic Meteor Altitudes Obtained by Radio (Srednyaya kharakteristicheskaya vysota meteorov, obnaruzhennykh radiosredstvami). A. Zh., 35, No. 6, 1958.

220. - - - A New Method of Determining Radiant Meteoric Flow by Limited-Direction Antenna (Novyy metod opredeleniya radianta meteornogo potoka s ispol'zovaniyem slabonapravlennoy antenny). A. Zh., 36, No. 1, 1959.

221. - - - Some Statistic Characteristics of Meteor Radio Echo (Nekotoryye statisticheskiye kharakteristiki meteornykh radioekho). Byull. Komiss. po kometam i meteoram Astron. soveta AN SSSR, No. 4, 1959.

221a. Some Problems of Radio Meteor Tracking (Nekotoryye problemy radiolokatsii meteorov). Izd-vo Tomskogo un-ta, Tomsk, 1961.

221b. Fialko, Ye. I., Peregudov, F. I., Nemirova, E. K. and Pokrovskiy, L. A. Radar Observations of Meteors in Tomsk (Radiolokatsionnyye nablyudeniya meteorov v Tomske). Coll. "Ionosfernyye issledovaniya (meteory)." Izd-vc AN SSSR, Moscow, 1962.

221c. Filatov, V. V. Drifts of Irregularities in the F2 Layer (Dreyfy neodnorodnostey v sloye F2). Coll. "Ionosfernyye issledovaniya". No. 9, Izd-vo AN SSSR, Moscow, 1962.

222. Filipovich, O. P. Some Types of Equilibrium States of the Atmosphere (O nekotorykh tipakh ravnovesnykh sostoyaniy atmosfery). Vestnik LGU, No. 10, 1959.

223. - - - The Question of Local Thermodynamic Equilibrium in Earth's Atmosphere (K voprosu o lokal'nom termodinamicheskom ravnovesii v atmosfere Zemli). Coll. "Mezhdunarodnyy Geofizicheskiy god". Izd-vo LGU, Leningrad, 1960.

224. Frish, S. E. Qualitative Spectral Analysis of Gaseous Mixtures (Kolichestvennyy spektral'nyy analiz gazovykh smesey). Vestnik LGU, No. 8, 1954.

225. Khvostikov, I. A. Notes on the Physics of Earth's Atmosphere (Ocherki po fizike zemnoy atmosfery). UFN, 19, Nos. 1 and 2, 1938.

226. - - - Investigation of the Atmosphere by Searchlight (Ob issledovanii atmosfery s pomoshch'yu prozhektornogo lucha). Izv. AN SSSR, ser. geograf. i geofiz., 9, Nos. 5 and 6, 1945.

227. - - - Optic Probing of the Atmosphere by Searchlight (Opticheskoye zondirovaniye atmosfery prozhektornym luchom). Izv. AN SSSR, ser. fizich., 10, No. 4, 1946.

228. - - - Structure and Content of the Stratosphere and Ionosphere (Stroyeniye i sostav stratosfery i ionosfery). Vestnik AN SSSR, No. 1, 1948.

229. - - - Night Sky Glow (Svecheniye nochnogo neba). Izd-vo AN SSSR, Moscow-Leningrad, 1948.

230. - - - Noctilucent Clouds and the Structure of the Atmosphere (Serebristyye oblaka i stroyeniye atmosfery. Coll. "Pamyati Sergeya Ivanovicha Vavilova"). Izd-vo AN SSSR, Moscow, 1952.

231. - - - Ozone in the Stratosphere (Ozon v stratosfere). UFN, 59, No. 2, 1956.

232. - - - The Heat Regime of the Atmosphere in the Noctilucent Cloud Zone (Teplovoy rezhim atmosfery v zone serebristykh oblakov). Tr. soveshchaniya po serebristym oblakam (Tartu), T. I. AN Est SSR, 1959.

233. - - - Physics of the Ozonosphere and Ionosphere (Fizika ozonosfery i ionosfery). Izd-vo AN SSSR, Moscow, 1963.

234. - - - Noctilucent Clouds and the Structure of the Upper Layers of the Atmosphere (Serebristyye oblaka i stroyeniye vysokikh sloyev atmosfery). Tr. soveshchaniya po serebristym oblakam (Tallin), Vol. II. AN Est SSR, 1962.

235. Khvostikov, I. A., Sevchenko, A. N. A Polarimetric Method of Studying the Structure of the Upper Layers of the Atmosphere (Polyarimetricheskiy metod izucheniya structury verkhnikh sloyev atmosfery). Dokl. AN SSSR, 4 (13), No. 8, 1936.

236. Khrgian, A. Kh. Atmospheric Physics (Fizika atmosfery). Gostekhizdat, Moscow, 1953.

237. - - - Mother-of-Pearl Clouds (Perlamutrovyye oblaka). Vestn. MGU, ser. matem., mekhan., astron., fiz., khimich., No. 6, 1957.

238. - - - Atmospheric Ozone (Results of the Work of IGY in USSR) (Atmosfernyy ozon (Rezul'taty rabot MGG v SSSR)). Konferentsiya 28-31 Oct. 1959 g. Izd-vo MGU, 1961.

239. Tseraskiy, V. K. Astronomic Photometry and its Application (Astronomicheskiy fotometr i yego prilozheniya). Moscow, 1887.

240. Chernyayev, V. I. and Vuks, M. F. The Twilight Sky Spectrum (Spektr neba v sumerki). Dokl. AN SSSR, 14, No. 2, 1937.

241. Chistyakov, V. F. and Teyfel', V. G. The Visible Limit of Noctilucent Clouds (O vidimoy granitse serebristykh oblakov). A.Ts., 18 June, No. 139, 1953.

242. - - - The Question of the Visible Limit of Noctilucent Clouds (K voprosu o vidimoy granitse serebristykh oblakov). A.Ts.,15 Jan., No. 145, 1954.

243. - - - Some Questions of the Nature of Noctilucent Clouds (Nekotoryye voprosy prirody serebristykh oblakov). Byull. Vses. astron. geod. o-va, No. 19, 1956.

244. Chapman, S. Earth Magnetism. (Zemnoy magnetizm. Translation, editor N. B. Roze) Gidrometeoizdat, Moscow-Leningrad, 1939.

245. Sharonov, V. V. New Data on the Distribution of Noctilucent Clouds (Novyye dannyye o raspredelenii serebristykh oblakov). Priroda, No. 2, 1959.

246. - - - The Dependance of Frequency of Appearance of Noctilucent Clouds on Date and Geographic Latitude (Zavisimost' chastoty poyavleniya serebristykh oblakov ot daty i geograficheskoy shiroty). Inform. Byull. MGG, No. 7, 1959.

247. - - - Photometric Conditions of Visibility of Noctilucent Clouds (Fotometricheskiye usloviya vidimosti serebristykh oblakov). Coll. "Mezhdunar. geofiz. god" Izd-vo LGU, Leningrad, 1960.

248. - - - Determining the Visible and Intrinsic Light of Noctilucent Clouds (Opredeleniye vidimogo i istinnogo tsveta serebristykh oblakov). A.Ts., No. 212, June 5, 1960.

249. Shvidkovskiy, Ye. G. Some Results of Measuring the Thermodynamic Parameters of the Stratosphere by Weather Rocket (Nekotoryye rezul'taty izmereniy termodinamicheskikh parametrov stratosfery pri pomoshchi meteorologicheskikh raket). ISZ, Vol. 2, Izd-vo AN SSSR, Moscow, 1958.

250. - - - Rocket Investigation of the High Layers of the Atmosphere (Raketnyye issledovaniya vysokikh sloyev atmosfery). Tr. TsAO, Vol. 26, 1959.

251. - - - Rocket Meteorological Measurements (Raketnyye meteorologicheskiye izmereniya). Tr. TsAO, Vol. 29, 1960.

252. Shefov, N. N. Determining the Orbital Temperature of the ON Belt (Ob opredelenii vrashchatel'noy temperatury polos ON). Coll. "Spektr. elektrofotometr. i radiolokats. issled. polyarn. siyaniy i svecheniya nochnovo neba," No. 5, Izd-vo AN SSSR, Moscow, 1961.

253. Shklovskiy, I. S. and Kurt, V. G. Determining Atmospheric Density at Altitudes of 430 Km by Sodium Vapor Diffusion (Opredeleniye plotnosti atmosfery na vysote 430 km metodom diffuzii parov natriya). ISZ, Vol. 3, Izd-vo AN SSSR, Moscow, 1959.

254. Shtaude, N. M. Photometric Observations of Twilight as a Method of Studying the Upper Stratosphere (Fotometricheskiye nablyudeniya sumerek kak metod izucheniya verkhney stratosfery). Tr. komis. po izucheniyu stratosfery pri AN SSSR, Vol. I, Moscow-Leningrad, 1936.

255. - - - Bases of the Approximation Theory for Twilight Phenomena (Osnovy uproshchennoy teorii sumerechnykh yavleniy). Izv. AN SSSR, ser. geogr. i geofiz. 11, No. 4, 1947.

256. - - - General Formula for Sky Brightness (Obshchaya formula yarkosti neba). Izv. AN KazSSR, ser. astron. i fiz. No. 12, 1946.

257. - - - Secondary Light Scattering at Twilight under Various Atmospheric Compositions. (Vtorichnoye rasseyaniye sveta vo vremya sumerek pri raznykh stroyeniyakh atmosfery). Dokl. AN SSSR, 64, No. 6, 1949.

258. El'yasberg, P. Ye. Determining the Density of the Upper Atmosphere by Cyclic Measurement of Orbital Elements of the First Two Artificial Earth Satellites (Opredeleniye plotnosti verkhney atmosfery po vekovym izmereniyam elementov orbit pervykh dvukh iskusstvennykh sputnikov zemli). ISZ, Vol. I, Izd-vo AN SSSR, Moscow, 1958.

259. El'yasberg, P. Ye and Yastrebov, V. D. Determining Upper Atmosphere Density Through Observations of the Flight of the Third Soviet Artificial Earth Satellite (Opredeleniye plotnosti verkhney atmosfery po rezul'tatam nablyudeniy za poletom tret'yego sovetskogo iskusstvennogo sputnika zemli). ISZ, Vol. 4, Izd-vo AN SSSR, Moscow, 1960.

260. Eygenson, M. S., Gnevyshev, M. N., Ol', A. I. and Rubashev, B. M. Solar Activity and its Manifestation (Solnechnaya aktivnost' i yeye proyavleniya). Gostekhizdat, Moscow-Leningrad, 1948.

261. Yudalevich, F. F. The Structure of the Theory of Twilight Phenomena, Considering Secondary Scattering (O postroyenii teorii sumerechnykh yavleniy s uchetom vtorichnogo rasseyaniya). Dokl. AN SSSR, 75, No. 6, 1950.

262. Yanovskiy, B. M. Terrestrial Magnetism (Zemnoy magnetizm). Gostekhizdat, Moscow, 1953.

263. Yatsunkiy, I. M. The Influence of Geophysical Factors on Motion of Satellites (O vliyanii geofizicheskikh faktorov na dvizhenii sputnika). UFN, 63, No. 1a, 1957.

264. Adel, A. Seasonal Variation in the Absorption of Solar Radiation by Atmospheric Ozone at 9.6 Microns. Bulletin of the American Meteorological Society, Vol. 35, No. 6, 1954.

265. Allen, W., Rinegart, J. and White, W. Phenomena Associated with the Flight of Ultraspeed Pellets. Journal of Applied Physics, Vol. 23, No. 1, 1952.

266. Appleton, E. V., Lyon, A. J. and Pritchard, A. G. The Detection of S_q Current System in Ionospheric Radio Sounding. Journal of Atmospheric and Terrestrial Physics, Vol. 7, Nos. 4/5, 1955.

267. Appleton, E., Lyon, A. J. and Turnbull, A. G. Distortion of the E Layer of the Ionosphere by Electrical Currents Flowing in it. Nature, Vol. 176, 1955.

268. Armstrong, E. B. A Note on the Diurnal Variation of the OH Emission in the Nightglow. Supplement, J. Atmos. and Terr. Phys., Vol. 5, 1956.

269. --- Width of the Line OIλ 5577 of the Night Sky and Auroras (Largeur de la raie OIλ 5577 du ciel nocturne et des aurores). J. Phys. et Rad., Vol. 19, No. 3, 1958.

270. --- The Temperature in the Atmospheric Region Emitting the Nightglow OI 5577 Line and in Region Above Faint Auroral Arcs. J. Atmos. and Terr. Phys., Vol. 13, 1959.

271. Arnold, A. Turbulence in the Stratosphere. Bull. Amer. Meteorol. Soc., Vol. 35, No. 8, 1954.

272. Arnold, A. and Lowenthal, M. J. A Sixteen-Month Series of Midstratospheric Temperature Measurements. Journal of Meteorology, Vol. 16, No. 6, 1959.

273. Attmannspacher, W. Speed of Winds in the High Stratospheric Zero Layer (Windgeschwindigkeiten in der hochstratospharischen Nullschicht). Meteorologische Rundschau, Vol. 14, No. 4, 1961.

274. Barbe, G. On the Seasonal Variation of Atmospheric Circulation Between the Ground and an Altitude of 30 km at Troppes, near Paris, Between October 1, 1957 and October 1, 1958 (Sur la variation saisonniere de la circulation atmospherique entre le sol et l'altitude de 30 km a Troppes, pres de Paris entre le 1-er Octobre 1957 et le 1-er Octobre 1958). Compte-rendu de l'Academie des Sciences, Vol. 247, No. 22, 1958.

275. --- Atmospheric Circulations at High Altitude. Experimental Study of the Stratospheric Monsoon (Circulations atmosphériques a haute altitude. Etude expérimentale de la mousson stratosphérique). Météorologie, No. 56, 1959.

276. --- On the Sudden Appearance of Eastern Sector Winds in the Mean and Elevated Stratosphere and the Progressive Manifestation of the

Phenomenon Between 20° and 50° Latitude North, in the Vicinity of the Paris Meridian (Sur l'apparition brusque de vents de secteur Est en hiver dans la stratosphere moyenne et elevee et la manifestation progressive de ce phenomene entre le 20-e et le 50-e degré de latitude Nord, au voisinage du méridien de Paris). C. r. Acad. sci., Vol. 252, No. 24, 1961.

277. Barber, D. R. Note on the Seasonal Variation of Sodium D-Line Emission in the Twilight. J. Atmos. and Terr. Phys., Vol. 5, Nos. 5-6, 1954.

278. Barlow, E. W. Krakatau. 1833. Marine Observer, Vol. 25, No. 170, 1955.

279. Barrett, E. W., Herndon, L. R. and Carter, H. J. Some Measurements of the Distribution of Water Vapor in the Stratosphere. Tellus, Vol. 2, No. 4, 1950.

280. Bartels, J. Atmospheric Tides (Uber die atmospharischen Gezeiten). Abhandlungen des Preussischen Meteorologischen Institut, Vol. 8, No. 9, 1927.

281. Bartman, F. L., Chaney, L. W., Jones, L. M. and Liu, V. C. Upper-Air Density and Temperature by the Falling-Sphere Method. J. Appl. Phys., Vol. 27, No. 7, 1956.

282. Stroud, W. G., Nordberg, W., Bandeen, W. R., Bartman, F. L. and Titus, P. Rocket Grenade Measurements of Temperatures and Winds in the Mesosphere Over Churchill, Canada. Space Research, Amsterdam, 1960.

283. Bates, D. R. Proceedings of the Royal Society, London, A. 196, 1949.

284. - - - The Temperature of the Upper Atmosphere. Proceedings of the Physics Society, Vol. 64, No. 381 B, 1951.

285. - - - The Thermosphere. Proc. Roy. Soc., A236, No. 1205, 1956.

286. Batten, E. S. Wind System in the Mesosphere and Lower Ionosphere. J. Meteorol., Vol. 18, No. 3, 1961.

287. Becker, W. Winds and Turbulent Airstreams in the Ionosphere (Winde und turbulente Luftstromungen in der Ionosphäre). Archiv für Meteorologie, Geophysik und Bioklimatologie, A6, Nos. 3 and 4, 1954.

288. Bedinger, J. F., Ghosh, S. N. and Manring, E. R. Emission from Sodium Ejected from Rockets. Threshold Space. Proceedings of the Conference on Chemical Aeronomy, London, Pergamon Press, 1957.

289. Bedinger, J. F., Manring, E. R. and Ghosh, S. N. Study of Sodium Vapor Ejected into the Upper Atmosphere. Journal of Geophysical Research, Vol. 63, 1958.

290. Belmont, A. D. The Reversal of Stratospheric Winds over North America. General Mills, Inc. Minneapolis, Minn., Vol. 42, 1962.

291. Benedict, W. S. Identification of H_2O^{18} and H_2O^{17} Telluric Lines in the Infrared Solar Spectrum. Mem. Soc. roy. sci. Liège, 18, Fasc. uniq., Vol. 41, 1957.

292. Berg, O. E. and Meredith, L. H. Meteorite Impacts to Altitude of 103 Kilometers. J. Geophys. Res., Vol. 61, No. 4, 1956.

293. Beynon, W. J. G. Evidence of Horizontal Motion in Region F_2 Ionization. Nature, Vol. 162, 1948.

294. Beynon, W. J. G. and Goodwin, G. L. Horizontal Drifts and Temperature in the Lower Part of Region E. J. Atmos. and Terr. Phys., Vol. 13, Nos. 1 and 2, 1958.

295. Bhalotra, Y. P. R. Influence of Meteoric Dust on Rainfall. Weather, Vol. 11, No. 2, 1956.

296. Bhattacharyya, B. K. A Study of Auroral Motions from All-Sky Camera Records. Canadian Journal of Physics, Vol. 38, No. 10, 1960.

297. Bigg, E. K. Detection of Atmospheric Dust and Temperature Inversions by Twilight Scattering. Nature, Vol. 177, No. 4498, 1956.

298. Blamont, J. Artificial Sodium Winds. Wind Velocity, Turbulence and Density of the Upper Atmosphere (Nuages artificiels de sodium. Vitesse du vent, turbulence et densite de la haute atmosphere). Space Research, Amsterdam, 1960; Blamont, J. E. and Baguette, J. M. Measurements Deduced from the Deformations of Six Clouds of Alkaline Metals Formed by Rockets in the Upper Atmosphere (Blamont, J. E. and Baguette, J. M. Mesures deduites des déformations de six nuages de metaux alcaline formés par fusees dans la haute atmosphere). Annales géophysique, Vol. 17, No. 3, 1961.

299. Blamont, J. E., Donahue, T. M. and Lory, M. L. Measurement of the Temperature in the Upper Atmosphere to 150 km in a Rocket Experiment. Physical Review, Letters, Vol. 6, No. 8, 1961.

300. Blohinzev, D. I. Journal of the Acoustical Society of America, Vol. 18, 1946.

301. Boclet, D., Jahanno, C., Labeyrie, J. and Boiteux, H. Le. Use of an Experimental Rocket for the Evaluation of Artificial Radioactive Aerosol Concentrations at High Altitudes (Utilisation d'un missile experimental pour l'evaluation des concentrations en aérosols radiactifs artificiels en haute altitude). Space Research. Amsterdam, 1960.

302. Bond, F. R. Motion of the Aurora and Magnetic Bays. Australian Journal of Physics, Vol. 13, No. 3, 1960.

303. Booker, H. G. Concerning Ionospheric Turbulence at the Meteoric Level. J. Geophys. Res., Vol. 63, No. 1, 1958.

304. Bowen, E. G. The Influence of Meteoritic Dust on Rainfall. Austral. J. Phys., Vol. 6, No. 4, 1953.

305. Branscomb, L. M. Phys. Rev., Vol. 86, 1952.

306. Brasefield, C. J. Winds and Temperatures in the Lower Stratosphere. J. Meteorol., Vol. 7, 1950.

307. - - - Measurements of Atmospheric Humidity up to 35 Kilometers. J. Meteorol., Vol. 11, No. 5, 1954.

308. - - - Winds at Altitudes up to 80 Kilometers. J. Geophys. Res., Vol. 59, No. 2, 1954.

309. Bricard, J. and Kastler, A. Research on Radiation D of Sodium in the Brightness of Night and Twilight Sky (Recherches sur la radiation D du sodium dans la lumiere du ciel crepusculaire et nocturne). Ann. Geophys., Vol. 1, No. 1, 1944.

310. Brunner, W. Photometry of the Night Sky, with Special Consideration of the Zodiacal Light and Twilight Phenomena (Photometrie des Nachthimmels mit besonderer Berücksichtigung des Zodiakallichtes und Dämmerungerscheinungen). Publikation der Eidgenössischen Sternwarte in Zürich, Vol. 6, 1935.

311. Buddhue, J. D. Meteoritic Dust. University of New Mexico Publications in Meteoritics, No. 2, Albuquerque, 1950.

312. Bull, G. A. and James, D. G. Dust in the Stratosphere over Western Britain on April 3 and 4, 1956. Meteorol. Mag., Vol. 85, No. 1012, 1956.

313. Burgess, E. Rockets in Investigation of the Ionosphere (Racketen in der Ionosphärenforschung). Vol. 4 of Lehrbucherei der Funk-Ortung, 1956.

314. Byram, E. T., Chubb, T. A. and Friedman, H. The Solar X-ray Spectrum and the Density of the Upper Atmosphere. J. Geophys. Res., Vol. 61, No. 2, Part 1, 1956.

315. Cahill, L. J. Investigation of the Equatorial Electrojet by Rocket Magnetometer. J. Geophys. Res., 64, No. 5, 1959.

316. Casci, C. and Giavotto, V. An Experimental and Indirect Method for Determining the High Atmosphere Density. Nuovo Cimento, Vol. 11, No. 2, 1959.

317. Ceplecha, Zd. Meteor Photographs. I. Air Densities. Bulletin of the Astronomical Institutes of Czechoslovakia, Vol. 4, No. 6, 1953.

318. Chackett, K. F., Paneth, F. A. and Wilson, E. J. The Chemical Composition of the Stratosphere at 70 km Height. J. Atmos. and Terr. Phys., Vol. 1, No. 1, 1950.

319. Chackett, K. F., Paneth, F. A., Reasbeck, P. and Wiborg, B. S. Variations in the Chemical Composition of Stratosphere Air. Nature, Vol. 168, 1951.

320. Champion, K. W. and Minzner, R. A. Atmospheric Densities and Rocket Observation. Planetary and Space Science, Vol. 1, No. 4, 1959.

321. Chapman, J. H. A Study of Winds in the Ionosphere by Radio Methods. Canad. J. Phys., Vol. 31, No. 1, 1953.

322. Chapman, S. The Kinetic Theory of Simple and Composite Monatomic Gases: Viscosity, Thermal Condition and Diffusion. Proc. Roy. Soc. London, A93, 1916.

323. - - - On the Theory of the Solar Diurnal Variation of the Earth's Magnetism, Proc. Roy. Soc., 123A, 1929; 130A, 1931.

324. - - - Atmospheric Tides and Oscillations. Compendium of Meteorology, 1951.

325. - - - Tides in the Atmosphere. Scientific American, Vol. 190, No. 5, 1954.

326. - - - The Molecular Diffusive Rate of Change of Composition in the Atmosphere. J. Meteorol., Vol. 12, 1955.

327. - - - Note on Persistent Meteor Trails. Suppl. J. Atmos. and Terr. Phys., Vol. 5, 1956.

328. - - - Notes on the Solar Corona and the Terrestrial Ionosphere. Smithsonian Contributions to Astrophysics, Vol. 2, No. 1, 1957.

329. - - - Speculations on the Atomic Hydrogen and the Thermal Economy of the Upper Atmosphere. Threshold Space Proc. Conf. Chem. Aeronomy. London, Pergamon Press, 1957.

330 - - - The Outermost Ionosphere. J. Atmos. and Terr. Phys., Vol. 15, No. 1-2, 1959.

331. - - - Interplanetary Space and the Earth's Outermost Atmosphere. Proc. Roy. Soc., A253, No. 1275, 1959.

332. Chapman, S., Pramanik, S. K. and Topping, J. The World-Wide Oscillations of the Atmosphere. Gerlands Beitr. Geophys., 33, 1931.

333. Chapman, S. and Cowling, T. G. Mathematical Theory of Non-Uniform Gases. Cambridge University Press, 1939.

334. - - - The Mathematical Theory of Non-Uniform Gases. 2nd Ed., Cambridge University Press, 1952.

335. Chapman, S. and Westfold, K. C. A Comparison of Annual Mean Solar and Lunar Atmospheric Tides in Barometric Pressure, as Regards their World-Wide Distribution of Amplitude and Phase. J. Atmos. and Terr. Phys., Vol. 8, Nos. 1-2, 1956.

336. Chubb, T. A., Friedman, H., Kupperian, J. B. and Byram, E. T. The Use of Radiation Absorption and Luminescence in Upper Air Density Measurements. Ann. geophys., Vol. 14, No. 1, 1958.

337. Compendium of Meteorology. Edited by Thomas F. Malone. American Meteorological Society, Boston, Massachusetts, 1953.

338. Conover, W. C. An Instance of a Stratospheric "Explosive" Warming. J. Meteorol., Vol. 18, No. 3, 1961.

339. Conover, W. C. and Wentzien, C. J. Winds and Temperatures to 40 Kilometers. J. Meteorol., Vol. 12, No. 2, 1955.

340. Court, G. W. G. Ionospheric Wind Determination from Spaced Radio Receiver Fading Records. J. Atmos. and Terr. Phys., Vol. 7, No. 6, 1955.

341. Court, G. W. G. and Gilfillan, E. S. A Determination of Ionospheric Winds for 24-Hour Period. J. Atmos. and Terr. Phys., Vol. 8, 1956.

342. Cowling, T. G. Magnetohydrodynamics. Interscience Publishers Ltd., New York--London, 1957.

343. Craig, R. A. Radiative Temperature Changes in the Ozone Layer. Compendium of Meteorology, American Meteorological Society, Waverly Press, Baltimore, 1951.

344. Craig, R. A. and Ohring, G. The Temperature Dependence of Ozone Radiational Heating Rates in the Vicinity of the Mesopeak. J. Meteorol., Vol. 15, 1958.

345. Crary, A. P. Stratosphere Winds and Temperatures from Acoustical Propagation Studies. J. Meteorol., Vol. 7, 1950.

346. Crary, A. P. and Bushnell, V. C. Determination of High-Altitude Winds and Temperatures in the Rocky Mountain Area by Acoustic Soundings, October 1951. J. Meteorol. Vol. 12, No. 5, 1955.

347. Curtis, A. R. and Goody, R. M. Thermal Radiation in the Upper Atmosphere. Proc. Roy. Soc., A236, No. 1205, 1956.

348. Dansgaard, W. The Abundance of O^{18} in Atmospheric Water and Water Vapour. Tellus, Vol. 5, No. 4, 1953.

349. Dalgarno, A. The Altitude and Excitation Mechanisms of the Night Air-Glow. Annales Geophysique, Vol. 14, No. 3, 1958.

350. Data from the Sputniks. Time, Vol. 70, Nos. 27 and 35, 1957.

351. Dave, J. V. On the Intensity and Polarisation of the Light from the Sky During Twilight. Part II. Proceedings of the Indian Society of Science, A43, No. 6, 1956.

352. Deb, S. Winds in the Ionospheric Regions. J. Atmos. and Terr. Phys., Vol. 4, 1953.

353. Deirmendjian, D. and Vestine, E. H. Some Remarks on the Nature and Origin of Noctilucent Cloud Particles. Planet and Space Science, Vol. 1, No. 2, 1959.

354. Dessler, A. J. Large Amplitude Hydromagnetic Waves Above the Ionosphere. J. Geophys. Res., Vol. 63, 1958; Phys. Rev., Vol. 1, 1958.

355. - - - Ionospheric Heating by Hydromagnetic Waves. J. Geophys. Res., Vol. 64, No. 4, 1959.

356. Dhari, O. N. Meteoritic Dust and Rainfall. Indian Journal of Meteorology and Geophysics, Vol. 5, No. 4, 1954.

357. Dobson, G. M. B. Ice in the Atmosphere. Quarterly Journal of the Royal Meteorological Society, Vol. 75, No. 324, 1949.

358. - - - Physics and the Atmosphere. Proc. Phys. Soc., Vol. 63, No. 346B, 1950.

359. - - - Origin and Distribution of Polyatomic Molecules in the Atmosphere. Proc. Roy. Soc., A236, No. 1205, 1956.

360. Donahue, T. M. and Resnick, R. Resonance Absorption of Sunlight in Twilight Layers. Phys. Rev., Vol. 98, No. 6, 1955.

361. Dowden, R. L. Ionospheric Thermal Radiation at Radiofrequencies in the Auroral Zone. J. Atmos. and Terr. Phys., Vol. 18, No. 1, 1960.

362. Dubin, M. Direct Measurements of Meteoritic Dust using Rockets and Satellites. Transactions of the International Astronomical Union, Vol. 10, 1958, 1960.

363. - - - Meteoritic Dust Measured from Explorer I. Planet. and Space Sci., Vol. 2, Nos. 2 and 3, 1960.

364. Dungey, J. W. The Influence of the Geomagnetic Field on Turbulence in the Ionosphere. J. Atmos. and Terr. Phys., Vol. 8, Nos. 1 and 2, 1956.

365. Dutsch, H. U. Vertical Ozone Distribution from Umkehr Observations. Archives of Meteorology, Geophysics and Bioclimatology, A 11, No. 2, 1959.

366. Ebdon, R. A. and Veryard, R. G. Fluctuations in Equatorial Stratospheric Winds. Nature (Engl.), Vol. 189, No. 4767, 1961.

367. - - - Notes on the Wind Flow at 50 mb in Tropical and Sub-Tropical Regions in January 1957 and January 1958. Quart. J. Roy. Meteorol. Soc., Vol. 86, No. 370, 1960.

368. - - - Some Notes on the Stratospheric Winds at Canton Island and Christmas Island. Quart. J. Roy. Meteorol Soc., Vol. 87, No. 373, 1961.

369. Eckart C. Hydrodynamics of Oceans and Atmospheres. Pergamon Press, 1960.

370. Edwards, H. D., Bedinger, J. F., Manring, E. R. and Cooper, C. D. Emission from a Sodium Cloud Artificially Produced by Means of a Rocket. Suppl. J. Atmos. and Terr. Phys., Vol. 5, 1956.

371. Ehevarria, B. J. The Atmosphere and the Upper Atmosphere. Physical and Chemical Characteristics (Atmosfera y sobreatmosfera. Caracteristicas fisicas y quimicas). Rev. aeronaut., Vol. 16, No. 182, 1956.

372. Elford, W. G. Winds in the Upper Atmosphere. J. Atmos. and Terr. Phys., Vol. 15, Nos. 1 and 2, 1959.

373. Elford, W. G. and Robertson, D. S. Measurements of Wind in the Upper Atmosphere by Means of Drifting Meteor Trails. I, II. J. Atmos. and Terr. Phys., Vol. 4, Nos. 4 and 5, 1953.

374. Elford, W. G. and Murray, E. L. Upper Atmosphere Wind Measurements in the Antarctic. Space Research., Amsterdam, 1960.

375. Elterman, L. The Measurement of Stratospheric Density Distribution with the Searchlight Technique. Geophysical Research Directorate, Air Force Cambridge Research Center, Geophysical Research Paper No. 10, 1951.

376. - - - The Measurement of Stratospheric Density Distribution with the Searchlight Technique. J. Geophys. Res., Vol. 56, No. 4, 1951.

377. - - - A Series of Stratospheric Temperature Profiles Obtained with the Searchlight Technique. J. Geophys. Res., Vol. 58, 1953.

378. - - - Seasonal Trends of Temperature Density and Pressure to 67.6 km Obtained with the Searchlight Probing Technique. J. Geophys. Res., Vol. 59, No. 3, 1954.

379. Evans, S. Atmospheric Pressures and Scale Heights from Radio Echo Observations of Meteors. J. Atmos. and Terr. Phys., Spac. Suppl., No. 2, "Meteors," 1955.

380. - - - Horizontal Movements of Visual Auroral Features. J. Atmos. and Terr. Phys., Vol. 16, Nos. 1 and 2, 1959.

381. - - - Systematic Movements of Aurorae at Halley Bay. Proc. Roy. Soc., A256, No. 1285, 1960.

382. Faust, G. Strong Wind Zones in the Stratosphere (Starkwindschichten in der Stratosphare)? Racketentechnik und Raumfahrtforschung, Vol. 2, No. 4, 1958.

383. Faust, H. The Weak Wind Zone in the Lower Stratosphere as Zero Layer (Die Schwachwindschicht in der unteren Stratosphäre als Nullschicht). Meteorol. Rundschau, Vol. 13, No. 3, 1958.

384. Feibelman, W. A. Note on Auroral Motion. J. Geophys. Res., Vol. 64, No. 9, 1959.

385. Ference, M., Stroud, W. G., Walsh, J. R. and Weisner, A. G. Measurement of Temperatures at Elevations of 30 to 80 Kilometers by the Rocket-Grenade Experiment. J. Meteorol., Vol. 13, No. 1, 1956.

386. Flohn H., Holzapfel R. and Oeckel, H. Investigations of the Stratospheric East Stream on the Summer Hemisphere (Untersuchungen über die stratosphärische Oststromung auf der Sommerhalbkugel). Beitrage zur Physischen Atmosphäre, Vol. 31, Nos. 3 and 4, 1959.

387. Findlay, J. W. An Investigation of Sudden Radio Fadeouts on a Frequency Near 2 Mc/s. J. Atmos. and Terr. Phys., No. 1, 1951.

388. Fireman, E. L. and Kistner, G. A. The Nature of Dust Collected at High Altitudes. Geochem. et cosmochem. acta, Vol. 24, Nos. 1 and 2, 1961.

389. Foitzig, L. and Heinzpeter, H. Solar Radiation and Turbidity of Air (Sonnenstrahlung und Lufttrübung). Leipzig, Akademische Verlagsgesellschaft Geest und Portig K.-G., 1958.

390. Fowle, F. E. The Spectroscopic Determination of Aqueous Vapor. Astrophysical Journal, Vol. 35, 1912.

391. - - - The Determination of Aqueous Vapor Above Mount Wilson. Astrophys. J., Vol. 37, 1913.

392. - - - The Transparency of Aqueous Vapor. Astrophys. J., Vol. 42, 1915.

393. Frenkiel, F. M. Ozone Theory in the Troposphere. Journal of Chemical Physics, Vol. 23, No. 12, 1955.

394. Gardner, F. F. Ionospheric Thermal Radiation at Radio Frequences. II. Further Observations. J. Atmos. and Terr. Phys., Vol. 5, Nos. 5/6, 1954; Gardner, F. F., Pawsey, J. L., J. Atmos. and Terr. Phys., Vol. 3, 1953.

395. Gates, D. M. Infrared Determination of Precipitable Water Vapor in a Vertical Column of the Earth's Atmosphere. J. Meteorol., Vol. 13, No. 4, 1956.

396. - - - Near Infrared Atmospheric Transmission to Solar Radiation. Journal of the Optical Society of America, Vol. 50, 1960.

397. - - - Spectroscopic Observations of the Stratosphere and Mesosphere. Proceedings of the Instrument Society of America, Vol. 15, Part 1, No. 2, 1960.

398. Gerson, N. C. Seasonal Variations in Wind Velocity. Proceedings of the Conference on Motions in the Upper Atmosphere, Albuquerque, New Mexico, Sept. 7-9, 1953.

399. - - - Sources of Atmospheric and Planetary Energy. J. Atmos. and Terr. Phys., Vol. 5, No. 1, 1954.

400. - - - Sporadic E Movements. J. Meteorol., Vol. 12, No. 1, 1955.

401. Ghosh, S. N. and Sharma, K. D. The Number of N_2 Molecules in Earth's Atmosphere from Rocket Data. Planet. and Space Sci., Vol. 8, No. 1, 1961.

402. Glückauf E. and Paneth, F. A. The Helium Content of Atmospheric Air. Proc. Roy. Soc. (A), 185, 1946.

403. Godson, W. L. Discussion on the Paper: "Total Ozone and the Middle Stratosphere over Arctic and Subarctic Areas in Winter and Spring." Quart. J. Roy. Meteorol. Soc., Vol. 87, No. 374, 1961.

404. Gold, E. The Relation Between Periodic Variations of Pressure, Temperature and Wind in the Atmosphere. Philosophical Magazine, 6th Ser., Vol. 19, 1910.

405. Goldberg, L. The Abundance of Atmospheric Carbon Dioxide and its Isotopes. Vistas in Astronomy, 2, London-New York, 1956.

406. Goldie, A. H. R. The Average Planetary Circulation in Vertical Meridian Planes, Centenary Proceedings of the Royal Meteorological Society, 1950.

407. Goldsmith, P. A Method of Increasing the Range of the Dobson-Brewer Frostpoint Hygrometer in Jet Aircraft. Quart. J. Roy. Meteorol. Soc., Vol. 81, No. 350, 1955.

408. Golitsyn, G. S. On the Influence of the Magnetic Field on the Character of Turbulence in the Ionosphere. J. Geophys. Res., Vol. 64, No. 12, 1959.

409. Goody, R. M. The Physics of the Stratosphere. Cambridge University Press, 1954.

410. Götz, F. W. P., Schein, M. and Stoll, B. Measurements of Groundlevel Ozone in Zurich (Messungen des bodennahen Ozons in Zürich). Gerlands Beitrage zur Geophysik, Vol. 45, 1935.

411. Greenhow, J. S. A Radio Echo Method for the Investigation of Atmospheric Wind at Altitudes of 80-100 km. J. Atmos. and Terr. Phys., Vol. 2, 1952.

412. Greenhow, J. S. and Neufeld, E. L. Diurnal and Seasonal Wind Variations in the Upper Atmosphere. Philos. Mag., Vol. 46, No. 376, 1955; J. Atmos. and Terr. Phys., Vol. 2, Special Suppl., 1955; The Height Variation of Upper Atmospheric Winds. Phil. Mag., Vol. 1, No. 12, 1956; Measurements of Turbulence in the Upper Atmosphere. Proc. Phys. Soc., Vol. 74, No. 1, 1959; Measurements of Turbulence in the 80 to 100 km Region from the Radio Echo Observations of Meteors. J. Geophys. Res., Vol. 64, No. 12, 1959.

413. Grimminger, G. Density of the Upper Atmosphere. Nature (Engl)., Vol. 183, No. 4664, 1959.

414. Groves, G. V. Geometrical Theory of Sound Propagation in the Atmosphere. J. Atmos. and Terr. Phys., Vol. 7, 1955; Introductory Theory for Upper Atmosphere Wind and Sonic Velocity Determination by Sound Propagation. J. Atmos. and Terr. Phys., Vol. 8, Nos. 1 and 2, 1956.

415. - - - Theory of the Rocket Grenade Method of Determining Upper Atmospheric Properties by Sound Propagation. J. Atmos. and Terr. Phys., Vol. 8, Nos. 4 and 5, 1956; Effect of Experimental Errors on Determinations of Wind Velocity, Speed of Sound and Atmospheric Pressure in the Rocket Grenade Experiment. J. Atmos. and Terr. Phys., Vol. 9, Nos. 5 and 6, 1956; A Rigorous Method of Analyzing Data of the Rocket Grenade Experiment. J. Atmos. and Terr. Phys., Vol. 9, Nos. 5 and 6, 1956.

416. - - - Determination of Upper Atmosphere Air Density and Scale Height from Satellite Observations. Proc. Roy. Soc., A252, 16-27, No. 1268; 1959. Methods of Calculating Atmospheric Densities from Satellites Orbit Data. Planet. and Space Sci., Vol. 5, No. 4, 1961.

417. - - - A Theory for Determining Upper Atmosphere Winds from Radio Observations on Meteor Trails. J. Atmos. and Terr. Phys., Vol. 16, Nos. 3 and 4, 1959.

418. Handbook of Geophysics. Revised Edition, New York, MacMillan Co., (USA Air Force, Air Research and Development Command, Geophysical Research Directorate), 1960.

419. Harang, L. and Pedersen, K. Drift Measurements of the E-Layer. Geophysical Publications, Vol. 19, No. 10, 1956.

420. Harnischmacher, E. and Rawer, K. Results of Systematic Observations of Ionospheric Wind in the Region (Résultats d'observations systematiques

du vent ionosphérique dans la région). E. C. r. Acad. Sci., Vol. 243, No. 10, 1956.

421. Harris, I. and Jastrow, R. Density Determinations Based on the Explorer and Vanguard Satellites. Science, Vol. 128, No. 3321, 1958.

422. - - - Upper Atmosphere Densities from Minitrack Observations on Sputnik I. Science, Vol. 127, No. 3296, 1958.

423. - - - An Interim Atmosphere Derived from Rocket and Satellite Data. Planet. and Space Sci., Vol. 1, No. 1, 1959.

424. Haubert, A. On Great Vertical Movements of Region F Observed at Casablanca (A propos des grands mouvements verticaux de la région-F observes a Casablanca). J. Atmos. and Terr. Phys., Vol. 15, Nos. 1 and 2, 1959.

425. Haurwitz, B. The Zonal Wind Field in the Upper Atmosphere. Dept. of Meteorol. and Ocean. New York University, Science Reports, No. 7, 1954.

426. - - - Frictional Effects and the Meridional Circulation in the Mesosphere. J. Geophys. Res., Vol. 66, No. 8, 1961.

426a. - - - Waves Formations in Noctilucent Clouds. Planet. and Space Sci., Vol. 5, 1961.

427. Havens, R. J., Koll, R. T. and LaGow, H. E. A New Vacuum Gage. Review of Scientific Instruments, Vol. 21, No. 7, 1950.

428. Havens, R. J. and Spitz, H. Atmospheric Wind at 200 Kilometers. Transactions of the American Geophysical Union, 33 Abstract, 1952.

429. Havens, R. J., Koll, R. T. and LaGow, H. E. The Pressure, Density and Temperature of the Earth's Atmosphere to 160 Kilometers. J. Geophys. Res., Vol. 57, No. 1, 1952.

430. Havens, R. J., Friedman, H. and Hulbert, E. O. The Ionospheric F2 Region (Report of 1954 Cambridge Conference on Physics of the Ionosphere). The Physical Society, London, 1955.

431. Hawkins, G. S and Whipple, F. L. The Width of Meteor Trails. Astronomical Journal, Vol. 63, No. 7, 1958.

432. Heisler, L. H. Occurrence of Giant Travelling Ionospheric Disturbances at Night. Nature (Engl.), Vol. 183, No. 4658, 1959.

433. - - - Vertical Characteristics of Travelling Ionospheric Disturbances Austral. J. Phys., Vol. 13, No. 4, 1960.

434. Heisler, L. H. and Whitehead, J. D. F-Region Travelling Disturbances and Sporadic-E Ionization. J. Geophys. Res., Vol. 65, No. 9, 1960.

435. Helliwell, N. C., Mackenzie, J. K. and Kerley, M. J. Some Further Observations from Aircraft of Frost Point and Temperature up to 50,000 ft. Quart. J. Roy. Meteorol. Soc., Vol. 83, No. 356, 1957.

436. Heritage, J. L., Weisbrod, S. and Fay, W. J. Experimental Studies of Meteor Echoes at 200 Megacycles. Electromagnet Wave Propagation, London-New York, Acad. Press, 1960.

437. Hesstvedt, E. Note on the Wavelength of Mother of Pearl Clouds. Rapp. Vid-akad. inst. vaer-og klimaforskn., No. 4, 1956-1957, (1957).

438. - - - Mother of Pearl Clouds in Norway. Geophysika. Publikasjoner. Geophysika Norvegica. Vol. 20, No. 10, 1958.

439. - - - Note on the Nature of Noctilucent Clouds. J. Geophys. Res., Vol. 66, No. 6, 1961.

440. - - - On the Physics of Mother of Pearl Clouds. Geophys. publ., Vol. 21, No. 9, 1960.

441. Hines, C. O. An Interpretation of Certain Ionospheric Motions in Terms of Atmospheric Waves. J. Geophys. Res., Vol. 64, No. 12, 1959.

442. - - - Internal Atmospheric Gravity Waves at Ionospheric Heights. Canad. J. Phys., Vol. 38, No. 11, 1960.

443. Hinteregger, H. E. Preliminary Data on Solar Extreme Ultraviolet Radiation in the Upper Atmosphere. J. Geophys. Res., Vol. 66, No. 8, 1961.

444. Hodge, P. W. and Wildt, R. A Search for Airborne Particles of Meteoritic Origin. Geochimie et Cosmochimie Acta, Vol. 14, Nos. 1 and 2, 1958.

445. Hoffmeister, C. Meteors, their Cosmic and Terrestrial Relationships (Die Meteore, ihre Kosmichen und irdischen Beziehungen). Leipzig, 1937.

446. - - - The Currents of the Atmosphere at 120 Km Altitude (Die Strömungen der Atmosphäre in 120 km Hohe). Zeitschrift für Meteorologie, No. 1, 1946.

447. - - - Lucent Night Clouds (Über die "Leuchtenden Nachtwolken"). Mitteilungen der Sternwarte Sonneberg, No. 41, 1953.

448. - - - Atmospheric Turbidity and a Twilight Anomaly. Naturwissenschaft, Vol. 40, No. 12, 1953.

449. - - - Indication of Atmospheric Effects of Interplanetary Matter (Hinweise auf atmospharische Wirkungen interplanetarer Materie). Astronomische Nachrichten, Vol. 283, No. 1, 1956.

450. - - - Ionization by Meteors (Ionisation durch Meteore). Sterne, Vol. 33, Nos. 3 and 4, 1957.

451. - - - The Daytime Meteor of December 6, 1957 (Das Tagesmeteor vom 6. Dezember 1957). Sterne, Vol. 35, Nos. 9 and 10, 1959.

452. Holzman, M. I. A Dark Method for Investigations of the Condensation Requirements of Water Vapor on a Cooled Surface (Eine Dunkelmethode für Untersuchungen der Kondensationbedingungen des Wasserdampfes auf einer abgekuhlten Flache). Physikalische Zeitschrift, Vol. 37, No. 1, 1926.

453. Horn, W. Density of Atmosphere at High Altitudes. Determined from the Trajectory Relations of Artificial Satellites (Die Dichte der Atmosphare in grossen Hohen. Bestimmt aus den Bahnverhältnissen künstlicher Satelliten). Sterne, Vol. 35, Nos. 1 and 2, 1959.

454. Horowitz, R. and LaGow, H. E. Upper Air Pressure and Density Measurements, from 90 to 220 Kilometers with the Viking 7 Rocket. J. Geophys. Res., Vol. 62, No. 1, 1957.

455. - - - Summer-Day Auroral-Zone Atmospheric Structure Measurements from 100 to 210 Kilometers. J. Geophys. Res., Vol. 63, No. 4, 1958.

456. Hitschfeld, W. and Houghton, J. T. Radiative Transfer in the Lower Stratosphere Due to the 9.6 Micron Band of Ozone. Quart. J. Roy. Meteorol. Soc., Vol. 87, No. 374, 1961.

457. Houghton, J. T. and Seeley, J. S. Spectroscopic Observations of the Water-Vapour Content of the Stratosphere. Quart. J. Roy. Meteorol. Soc., Vol. 86, No. 369, 1960.

458. Houghton, J. T., Moss, T. S. and Chamberlain, J. P. An Airborne Infrared Solar Spectrometer. J. Scientific Instrument, Vol. 35, No. 9, 1958.

459. Howkins, G. S and Cook, A. F. Inadequacy of Recombination as the Source of Light from Enduring Meteor Trains. Nature, Vol. 178, No. 4525, 1956.

460. Hulburt, E. O. Observations of a Searchlight Beam to an Altitude of 28 Kilometers. J. Opt. Soc. Am., Vol. 27, No. 11, 1937.

461. - - - Brightness of the Twilight Sky and the Density and Temperature of the Atmosphere. J. Opt. Soc. Am., Vol. 28, No. 7, 1938.

462. - - - Explanation of the Brightness and Color of the Sky, Particularly the Twilight Sky. J. Opt. Soc. Am., Vol. 43, 1953.

463. Humphreys, W. J. Nacreous and Noctilucent Clouds. Monthly Weather Review, Vol. 61, No. 1, 1933.

464. Hunten, D. M. Seasonal Variations of Twilight Sodium Emission. Suppl. J. Atmos. and Terr. Phys., Vol. 5, 1956.

465. Hunten, D. M., Koenig, H. J. and Jones, A. V. Rotational Structure of the 3914 Å N_2^+ Band in Sunlit Aurorae. Nature, Vol. 183, No. 4659, 1959.

466. Hunt, J. N., Palmer, R. and Penney, W. Atmospheric Waves Caused by Large Explosions. Philosophical Transactions, Royal Society of London, A252, No. 1011, 1960.

467. Huruhata, Masaaki. Photoelectric Studies of the Night Sky Light. Annals of the Tokyo Astronomical Observatory, Vol. 3, No. 4, 1953.

468. Huruhata, Masaaki, Tanabe Hiroyoshi and Nakamura Tsuyoshi. Photoelectric Studies of the Night Sky Light. Ionosphere Research Japan, Vol. 9, No. 3, 1955.

469. Hutchinson, G. E. The Biochemistry of the Terrestrial Atmosphere, Chapter 8 of "The Earth as a Planet" (The Solar System, Vol. 2), ed. Kuiper G. P., University of Chicago Press, 1954.

470. Israel, G. Thermal Manometer Used Aboard Rockets from the Ground to 90 Km (Manometre thermique utilisable à bord de fusees depuis le sol jusqu'à 90 km). C. r. Acad. sci., Vol. 251, No. 18, 1960.

471. Jacchia, L. G. A Comparative Analysis of Atmospheric Densities from Meteor Decelerations Observed in Massachusetts and New Mexico. Harvard Reports, Series 11-44, Technical Reports, 10, 1952.

472. - - - A Preliminary Analysis of Atmospheric Densities from Meteor Decelerations for Solar, Lunar and Yearly Oscillations. J. Meteorol., Vol. 14, No. 1, 1957.

473. - - - Two Atmospheric Effects in the Orbital Acceleration of Artificial Satellites. Nature, Vol. 183, No. 4660, 1959.

474. - - - A Variable Atmospheric-Density Model from Satellite Acceleration. J. Geophys. Res., Vol. 65, No. 9, 1960.

475. - - - On the Parameters used in the Physical Theory of Meteors. Smithson. Contribs. Astrophys., Vol. 2, No. 9, 1958.

476. Jacobs, L. Dust Cloud in the Stratosphere. Meteorol. Mag., Vol. 83, No. 982, 1954.

477. Jastrow, R. Geophysical Effects of the Trapped Particle Layer. Reviews of Modern Physics, Vol. 32, No. 4, 1960.

478. Jesse, O. Investigations of the So-Called Lucent Night Clouds (Untersuchungen über die sogenannten leuchtenden Nachtwolken). Sitzungen Berlin, Königliche Preussische Akademie der Wissenschaften, 1890 and 1891.

479. Johnson, F. S. The Telluric Hydrogen Corona and Some of its Consequences. Space Research, Amsterdam, 1960.

480. Johnson, C. Y. Aeronomic Parameters from Mass Spectrometry. Ann. geophys., Vol. 17, No. 1, 1961.

481. Johnson, C. Y. and Heppner, J. P. Night-Time Measurement of Positive and Negative Ion Composition to 120 Km by Rocketborne Spectrometer. J. Geophys. Res., Vol. 60, No. 4, 1955.

482. Johnson, C. Y. and Meadows, E. B. First Investigation of Ambient Positive-Ion Composition to 219 Km by Rocketborne Spectrometer. J. Geophys. Res., Vol. 60, No. 2, 1955.

483. Johnson, C. Y. and Heppner, J. P. Daytime Measurement of Positive and Negative Ion Composition to 131 Km by Rocketborne Spectrometer. J. Geophys. Res., Vol. 61, No. 3, 1956.

484. Johnson, D. H. Solar Tides in the Lower Stratosphere. Nature, No. 4425, 1954.

485. - - - Tidal Oscillations of the Lower Stratosphere. Quart. J. Roy. Meteorol. Soc., Vol. 81, No. 347, 1955.

486. Johnson, E. A., Meyer, R. C., Hopkins, R. E. and Mock, W. H. The Measurement of Light Scattered by the Upper Atmosphere from a Searchlight Beam. J. Opt. Soc. Am., Vol. 29, No. 12, 1939.

487. Johnson, F. S. Temperature Distribution of the Ionosphere Under Control of Thermal Conductivity. J. Geophys. Res., Vol. 61, No. 1, 1956.

488. - - - Pressure and Temperature Equalization at 200 Km Altitude. J. Geophys. Res., Vol. 65, No. 8, 1960.

489. Johnson, N. K. Wind Measurements at 30 Km. Nature, Vol. 157, No. 24, 1946.

490. Jones, A. V. and Harrison, A. W. Rotational Temperatures of the Auroral N_2^+ Bands. J. Atmos. and Terr. Phys., Vol. 6, 1955.

491. Jones, F. E. and Roberts, V. Solar Infrared Spectroscopy from High-Altitude Aircraft. Proc. Roy Soc., A236, No. 1205, 1956.

492. Jones, I. L., Landmark, B. and Setty, C. S. G. K. Movements of Ionospheric Irregularities Observed Simultaneously by Different Methods. J. Atmos. and Terr. Phys., Vol. 10, Nos. 5 and 6, 1957.

493. Jones, L. M. The Measurement of Diffusive Separation in the Upper Atmosphere, Ed, R. L. F., Seaton, M. J., Pergamon Press, London, 1954.

494. Jones, I. L. The Height Variation of Drift in the E Region. J. Atmos. and Terr. Phys., Vol. 12, 1958.

495. Jones, I. M., Peterson, J. W., Schaefer, E. J. and Schulte, H. F. Upper Air Density and Temperature: Some Variations and an Abrupt Warming in the Mesosphere. J. Geophys. Res., Vol. 64, No. 12, 1959.

496. Jones, L. M. Transit-Time Accelerometer. Rev. Scient. Instrum., Vol. 27, No. 6, 1956.

497. Jones, R. E., Millman, G. H. and Nertney, R. J. The Height of Ionospheric Winds as Measured at Long Radio Wavelengths. J. Atmos. and Terr. Phys., Vol. 3, No. 2, 1953.

498. Junge, C. E., Chagnon, C. W. and Manson, J. E. Stratospheric Aerosols. J. Meteorol., Vol. 18, No. 1, 1961.

499. - - - A World-Wide Stratospheric Aerosol Layer. Science, Vol. 133, No. 3463, 1961.

500. Kaiser, T. R. Radio Echo from Meteor Ionization. Advances in Physics, Vol. 2, No. 8, 1953.

501. Kaiser, T. R. and Evans, S. Upper Atmospheric Data from Meteors. Ann. geophys., Vol. 11, No. 2, 1955.

502. Kaiser, T. R. The Incident Flux of Meteors and Total Meteoric Ionization. J. Atmosph. and Terr. Phys. Spec. Suppl., No. 2, "Meteors," 1955.

503. Kaiser, T. R. and Seaton, M. J. Interplanetary Dust and Physical Processes in the Earth's Upper Atmosphere. Memoires de la Societe Royale Scientifique, Liège, Vol. 15, No. unique, 1955.

504. Kaiser, T. R. Radio Investigations of Aurorae and Related Phenomena. Suppl. J. Atmos. and Terr. Phys., Vol. 5, 1956.

505. Kaiser, T. R. and Greenhow, J. S. On the Decay of Radio Echoes from Meteor Trails. Pros. Phys. Soc., B66, Part 2, No. 398, 1953.

506. Kaiser, T. R. The Incidence of Interplanetary Dust. Ann. geophys., Vol. 17, No. 1, 1961.

507. Kallmann-Bijl, H. K. Daytime and Nighttime Atmospheric Properties Derived from Rocket and Satellite Observations. J. Geophys. Res., Vol. 66, No. 3, 1961.

508. Kallmann, H. K. A Preliminary Model Atmosphere Based on Rocket and Satellite Data. J. Geophys. Res., Vol. 64, No. 6, 1959.

509. Kallmann, H. Korf. Upper Atmosphere Properties Based on Rocket and Satellite Data. Physics and Medicine of the Atmosphere and Space, New York-London, John Wiley and Sons, Inc., 1960.

510. Kampe, H. J. Upper Air Wind Measurements with Small Rockets. J. Meteorol., Vol. 13, No. 6, 1956.

511. Kampe, H. J. and Walsh, J. R. USA SRDL Upper Air Research with Rockets. IRE Transactions of Military Electronics, Vol. 4, Nos. 2 and 3, 1960.

512. Kampe, H. J. Meteorological Rocket Network for Measuring Atmospheric Parameters up to 250,000. Weather-Wise, Vol. 13, No. 5, 1960.

513. Karandikar, R. V. Search for Discontinuities in the Brightness of the Twilight Sky. J. Opt. Soc. Am., Vol. 45, No. 5, 1955.

514. - - - Use of a Recording Fabry-Perot Interferometer for the Measurement of 5577 Å Emission Temperatures in the Airglow and Aurorae. The Airglow and the Aurorae. Suppl. J. Atmos. and Terr. Phys., Vol. 5, 1956; Revue d'Optique, Vol. 35, No. 7, 1956.

515. Kato, S. Horizontal Wind Systems in the Ionosphere E-Region Deduced from the Dynamic Theory of the Geomagnetic S_q Variation. Part 2. Rotating Earth. Journal of Geomagnetism and Geoelectricity, Vol. 8, No. 1, 1956; Part 3, Vol. 9, No. 2, 1957; Part 4, Vol. 9, No. 2, 1957.

516. Keegan, T, J. Winds and Circulations in the Mesosphere. ARS Journal, Vol. 31, No. 8, 1961.

517. Kellogg, W. W. and Schilling, G. F. A Proposed Model of the Circulation in the Upper Stratosphere. J. Meteorol., Vol. 8, 1951.

518. - - - Chemical Heating Above the Polar Mesopause in Winter. J. Meteorol., Vol. 18, No. 3, 1961.

519. Kellogg, P. J. and Ney E. P. A New Theory of the Solar Corona. Nature, Vol. 183, No. 4671, 1959.

520. Kennedy, W. B., Crary, A. P. and Bushnell, V. C. Atmospheric Winds and Temperatures at Heights up to 60 Kilometers as Determined by Acoustical Propagation Studies. Proceedings of Toronto Meteorological Conference, Roy. Meteorol. Soc., Vol. 9, 1954.

521. Kennedy, W. B., Brogan, L. and Sible, N. J. Further Acoustical Studies of Atmospheric Wind and Temperatures at Elevations of 30 to 60 Kilometers. J. Meteorol., Vol. 12, No. 6, 1955.

522. Kertz, W. The Thermal Excitant Source of Atmospheric Tides (Die thermische Erregungsquelle der atmosphärischen Gezeiten). Nachrichten der Akademischen Wissenschaft Göttingen. Mathematische-Physikalische kl., lla, No. 6, 1956.

523. Khvostikov, I. A. and Megrelishvili, T. G. The Structure of the Twilight Ray in Different Spectral Regions. Indian J. Meteorol. and Geophys., Vol. 11, No. 4, 1960.

524. Kim, J. S. and Currie, B. W. Horizontal Movements of Aurora. Canad. J. Phys., Vol. 36, No. 2, 1958; Vol. 38, No. 10, 1960.

525. Kimball, D. S. The Duration and Intensity of Twilight. Monthly Weather Rev., No. 9, 1938.

526. King-Hele, D. G. and Leslie, D. C. M. Effect of Air Drag on the Orbit of the Russian Earth Satellite 1957 β: Comparison of Theory and Observation. Nature, Vol. 181, No. 4626, 1958.

527. King-Hele, D. G. Satellite Orbits and their Geophysical Implications. Contemporary Physics, Vol. 2, No. 4, 1961.

528. King-Hele, D. G., Walker, D. M. C. An Irregularity in the Atmospheric Drag Effects in Sputniks 2 and 3 (Satellites 1957 β, 1958 δ1 and 1958 δ2). Nature, Vol. 182, No. 4639, 1958.

529. - - - Irregularities in the Density of the Upper Atmosphere: Results from Satellites. Nature, Vol. 183, No. 4660, 1959.

530. - - - Density of the Upper Atmosphere and its Dependence on the Sun, as Revealed by Satellite Orbits. Nature (Engl.), Vol. 186, No. 4729, 1960.

531. - - - Atmospheric Densities at Heights of 180-700 Km. Ann. geophys., Vol. 17, No. 2, 1961.

532. - - - Density of the Upper Atmosphere Determined from Satellite Orbits, and its Variation During 1957-1961. Nature (Engl.), Vol. 191, No. 4784, 1961.

533. Kirchhoff, G. The Effect of Heat Conduction in a Gas on the Movement of Sound (Uber den Einfluss der Wärmeleitung in einem Gase auf die Schallbewegung). Poggender Annalen, Vol. 134, No. 177, 1868.

534. Kochanski, A. Cross Sections of the Mean Zonal Flow and Temperature Along 80° W. J. Meteorol., Vol. 12, No. 2, 1955.

535. Kochanski, A. and Wasko, P. E. Mean Wind Flow at the 50- and 25-Mb Levels Bull. Am., Meteorol. Soc., Vol. 37, No. 2, 1956.

536. Kohlsche, K. Contribution to the Question of the Source of Vertical Motions (Beitrag zur Frage der Entstehung von Vertikalbewegungen. Z. Meteorol., Vol. 12, Nos. 11 and 12, 1958.

537. Kondratiev, K. Y. and Niilisk, H. I. On the Question of Carbon Dioxide Heat Radiation in the Atmosphere. Geofis. pura e appl., Vol. 46, No. 2, 1960.

538. Kopal. Z. Tables of Supersonic Flow Around Cones. Technical Report, No. 1, 1947; Tables of Supersonic Flow Around Yawing Cones. Tech. Rep. No. 3, 1947; Tables of Supersonic Flow Around Cones of Large Yaw. Tech. Rep. No. 5, 1949; by the Staff of the Computing Section, Center of Analysis, Massachusetts Institute of Technology, Cambridge, Massachusetts.

539. Kroening, J. L. Ion-Density Measurements in the Stratosphere. J. Geophys. Res., Vol. 65, No. 1, 1960.

540. Kviz, Z. and Mrkos, A. Visual and Photoelectric Observations of Noctilucent Clouds. Byull. Astron. In-Tov Chekhoslovakii, Vol. 11, No. 6, 1960.

541. LaGow, H. E. and Ainsworth, J. Arctic Upper Atmosphere Pressure and Density Measurements with Rockets. J. Geophys. Res., Vol. 61, No. 1, 1956.

542. LaGow, H. E., Horowitz, R. and Ainsworth, J. Rocket Measurements of the Arctic Upper Atmosphere. Ann. Geophys., Vol. 14, No. 2, 1958.

543. - - - Results of IGY Atmospheric Density Measurements Above Fort Churchill. Space Research, Amsterdam, 1960.

544. Langer, G. and Stockham, J. High-Altitude Tracking by Chemical Smokes. J. Geophys. Res., Vol. 65, No. 10, 1960.

545. LeGrand, Y. and Lenoble, J. Color of the Twilight Sky at Zenith (Couleur du ciel crepusculaire au zenith). C. r. Acad. Sci., Vol. 238, 1954.

546. Lettau, H. Diffusion in the Upper Atmosphere. Compendium Meteorol., Boston, Am. Meteorol. Soc., 1951.

547. - - - Turbulence in the Stratosphere. Bull. Am. Meteorol. Soc., Vol. 36, No. 4, 1955.

548. Libby, W. F. and Palmer, C. E. Stratospheric Mixing from Radioactive Fallout. J. Geophys. Res., Vol. 65, No. 10, 1960.

549. Lighthill, M. J. Note on Waves Through Gases at Pressures Small Compared with the Magnetic Pressure, with Applications to Upper Atmosphere Aerodynamics. Journal of Fluid Mechanics, Vol. 9, No. 3, 1960.

550. Lindemann, F. A. and Dobson, G. M. B. A Theory of Meteors and the Density and Temperature of the Outer Atmosphere to which it Leads. Proc. Roy. Soc., London, A102, A103, 1923.

551. Link, F. Twilight Glow at the Zenith and Air Density in the Ionosphere (Die Dammerungshelligkeit im Zenit und die Luftdichte in der Ionosphäre). Meteorologische Zeitschrift, Vol. 59, 1942.

552. - - - Twilight Glow in Infrared Light and Air Density of the Ionosphere (Die Dammerungshelligkeit im infraroten Lichte und die Luftdichte der Ionosphare). Meteorol. Z., Vol. 61, No. 3, 1944.

553. - - - Present Situation of Twilight Research (Situation actuelle des recherches crepusculaires). Bull. Astron. Inst. Czechosl., Vol. 1, 1949.

554. - - - Meteoric Dust Layer in the Planetary Atmosphere (Couche de poussières meteoriques dans une atmosphere planetaire). Byull. Astron. In-Tov Chekhoslovakii, Vol. 2, No. 1, 1950.

555. - - - Temporary and Local Density Variations in the Upper Atmosphere (Variations temporaires et locales de la densite dans la haute atmosphere). Bull. Astron. Inst. of Czechoslovakia, Vol. 5, No. 1, 1954.

556. - - - Meteoric Dust in the Earth's Atmosphere (Meteoricky prach v zemske atmosphere). Casop. Ceskosl. ustavu astron., Vol. 4, No. 1, 1954.

557. - - - Lunar Eclipses (Die Mondfinsternisse). Leipzig, Akademische Verlagsgesellschaft Gees and Portig K-G., VIII, 1956.

558. - - - On the Height of Meteoric Dust in the Terrestrial Atmosphere (Sur la grandeur des poussières météoriques dans l'atmosphère terrestre). Byull. Astron. In-Tov Chekhoslovakii, Vol. 7, No. 4, 1956.

559. Lopez, G. A. Winds of the Upper Atmosphere (Vientos de la alta atmosphera). Estudios Geograficos, Vol. 15, No. 56, 1954.

560. Lovell, A. C. B. Radio Astronomy and the Fringe of the Atmosphere. Quart. J. Roy. Meteorol. Soc., Vol. 82, No. 351, 1956.

561. Lowan, A. N. On the Cooling of the Upper Atmosphere after Sunset. J. Geophys. Res., Vol. 60, No. 4, 1955.

562. Lundlam, F. H. Luminous Night Clouds. Weather, Vol. 10, No. 12, 1955.

563. - - - Noctilucent Clouds. Tellus, Vol. 9, No. 3, 1957.

564. Lyon, G. F. and Kavadas, A. Horizontal Motions in Radar Echoes from Aurora. Canad. J. Phys., Vol. 36, No. 12, 1958.

565. Maeda, H. Horizontal Wind Systems in the Ionospheric E-Region Deduced from the Dynamic Theory of the Geomagnetic S_q Variation. Part 1. Non-rotating Earth Ionosphere. Research Japan, Vol. 10, No. 4, 1956; Part 3, J. Geomagn. and Geoelectr., Vol. 9, No. 2, 1957.

566. - - - Wind Systems for the Geomagnetic Sd Field. J. Geomagn. and Geoelectr., Vol. 9, No. 2, 1957.

567. - - - Horizontal Winds and Ionization Drifts in the Ionosphere. Reports of the Ionosphere and Space Research Japan, (formerly Rept. Ionosphere Res. Japan), Vol. 13, No. 1, 1959.

568. Manning, L. A., Villard, O. G. and Peterson, A. M. Meteoric Echo Study of Upper Atmosphere Winds. Proceedings of the Institute of Radio Engineers, Vol. 38, 1950.

569. Manning, L. A. Meteoric Radio Echoes. Transactions IRE, AP-2, No. 2, 1954.

570. Manring, E. and Bedinger, J. Winds in the Atmosphere from 80 to 230 Km. Space Research, Amsterdam, 1960.

571. Manring E., Bedinger, J. F., Pettit, H. B. and Moore, C. B. Some Wind Determinations in the Upper Atmosphere Using Artificially Generated Sodium Clouds. J. Geophys. Res., Vol. 64, No. 6, 1959.

572. Mantis, H. T. On a Diurnal Variation of Stratospheric Winds. J. Meteorol., Vol. 17, 1960.

573. Marks, S. T. What's up there? Ordnance, Vol. 45, No. 243, 1960.

574. Marmo, F. F., Aschenbrand, L. M. and Pressman, J. Artificial Electron Clouds. III. Planet. and Space Sci., Vol. 1, 1959.

575. - - - Artificial Electron Clouds. V. Morning Twilight Study, Release of Cesium and Sodium at 128 and 116 Km. Planet. and Space Sci., Vol. 2, Nos.2 and 3, 1960.

575a. Martyn, D. F. The Physics of the Ionosphere. London, 1955.

576. Martyn, D. F., Pulley, O. O., Walter, B. E. and Hall, E. The Temperatures and Constituents of the Upper Atmosphere. Proc. Roy. Soc. 154A, No. 881, 1936.

577. Manley, G. Solar Variations, Climatic Change and Related Geophysical Problems. Nature (Engl.), Vol. 190, No. 4780, 1961.

578. Masterson, J. E., Hubert, W. E. and Thomas, R. Wind and Temperature Measurements in the Mesosphere by Meteorological Rockets. J. Geophys. Res., Vol. 66, No. 7, 1961.

579. Mathur, S. B. and Mitra, A. P. The Upper Atmosphere and Outer Space. Part 1. Densities, Temperatures and Concentrations of Atmospheric Constituents from 130 to 1000 Km. Journal of Scientific and Industrial Research, A19, No. 7, 1960.

580. Matuura, N. Some Remarks on Motion of Ionospheric Irregularity. Rept. Ionosphere and Space Res. Japan (formerly Rept. Ionosphere Res. Japan). Vol. 13, No. 1, 1959.

581. Matuura, N. and Nagata, T. Turbulence in the Upper Atmosphere. Rept. Ionosphere Res. Japan, Vol. 12, No. 2, 1958.

582. Maxwell, A. and Litlle, C. G. A Radio Astronomical Investigation of Wind in the Upper Atmosphere. Nature, 169, 1952.

583. Maxwell, A. and Dagg, M. A Radio Astronomical Investigation of Drift Movements in the Upper Atmosphere. Phil. Mag., Vol. 45, No. 365, 1954.

584. McCrosky, R. E. A Suggested Rocket Experiment for Determination of Atmospheric Densities and Winds at Extreme Heights. Special Report, Astrophysical Observations, Smithsonian Institution, No. 20, 1959.

585. McLaughlin, D. B. A Note on the Motion of Auroral Streamers. Astrophys. J., Vol. 120, No. 1, 1954.

586. McLennan, J. C. and Shrum, G. On the Origin of the Auroral Green Line 5577 Å and Other Spectra, Associated with Aurora Borealis. Proc. Roy. Soc., Vol. 108, 1925.

587. Meadows, E. B. and Townsend, J. W. Neutral Gas Composition of the Upper Atmosphere by a Rocketborne Mass Spectrometer. J. Geophys. Res., Vol. 61, No. 3, 1956.

588. - - - Diffusive Separation in the Winter Night Time Arctic Upper Atmosphere 112 to 150 Km. Ann. Geophys., Vol. 14, No. 1, 1958.

589. - - - IGY Rocket Measurements of Arctic Atmospheric Composition Above 100 Km. Space Research, Amsterdam, 1960.

590. Meek, J. H. East-West Motion of Aurorae. Astrophys. J., Vol. 120, No. 3, 1954.

591. Meinel, A. B. Origin of the Continuum in the Night-Sky Spectrum. Astrophys. J., Vol. 118, No. 2, 1953.

592. - - - O_2 Emission Bands in the Infrared Spectrum of the Night Sky. Astrophys. J., Vol. 112, No. 3, 1950.

593. - - - Astrophys. J., Vol. 112, 1950.

594. Megrelishvili. T. G. The Possibility of Investigation of Aerosol Layers by Twilight Method. Indian J. Meteorol. and Geophys., Vol. 9, No. 3, 1958.

595. Meinel, A. B. and Schulte, D. H. A Note on Auroral Motions. Astrophys. J., Vol. 117, No. 3, 1953.

596. Migeotte, M., Neven, L. and Swenssen, J. Interpretation of the Solar Spectrum Observed at the Jungfraujoch from 2.8 to 23.7 Microns (L'interpretation du spectre solaire observe au Jungfraujoch de 2.8 a 23.7 microns). Experientia, Suppl., No. 6, 1957.

597. Miller, L. E. "Molecular Weight" of Air at High Altitudes. J. Geophys. Res., Vol. 62, No. 3, 1957.

598. Miley,H. A., Cullington, E. H. and Bedinger, J. F. Day-Sky Brightness Measured by Rocketborne Photoelectric Photometers. Trans. Am. Geophys. Union, Vol. 34, No. 5, 1953.

599. Millman, P. M. Visual and Photographic Observations of Meteors and Noctilucent Clouds. J. Geophys. Res., Vol. 64, No. 12, 1959.

600. Mitra, S. N. A Radio Method of Measuring Winds in the Ionosphere. Proceedings of the Institute of Electrical Engineers, Vol. 96, 1949.

601. - - - Statistical Analysis of Fading of a Single Downcoming Wave from the Ionosphere. Proc. Inst. Elec. Eng., Vol. 96, 1949.

602. - - - Motion of Single Cloud in the Ionosphere. Indian Journal of Physics, Vol. 27, No. 11, 1953.

603. Mitra, S. N., Vij, K. K. and Dasgupta, R. Horizontal Drift in the Ionosphere over Delhi. J. Atmos. and Terr. Phys., Vol. 19, Nos. 3 and 4, 1960.

604. Mosetti, F. Consideration of the Geophysical Application of Periodic Analysis (Considerazioni sulle applicazioni geofisiche dell'analisi periodale). Geofis. e meteorol., Vol. 8, Nos. 5 and 6, 1960.

605. Mother-of-Pearl Cloud in the Antarctic. New Scientist., Vol. 3, No. 59, 1958.

606. Morozov, V. M. Nonmolecular Light Scattering in the High Atmospheric Layers. Mem. Soc. roy. sci. Liège, Vol. 18, Fasc. uniq., 1957.

607. Moore, J. G. and Odencrantz, F. K. The Height and Geographical Position of the Red Auroral Arc of April 1-2, 1960. J. Geophys. Res., Vol. 66, No. 7, 1961.

608. Murcray, D. G., Murcray, F. H., Williams, W. J. and Leslie, F. E. Water Vapor Distribution Above 90,000 Feet. J. Geophys. Res., Vol. 65, No. 11, 1960.

609. Munro, C. H. Travelling Disturbances in the Ionosphere: Diurnal Variation of Direction. Nature, Vol. 171, No. 4355, 1953.

610. Murgatroyd, R. J. The Audibility of the Burton-on-Trant Bomb-Dump Explosion. Meteorological Research Paper, London, No. 284, 1946.

611. - - - Anomalous Sound Reception Experiments. Meteorol. Res. Pap., London, No. 346, 1947.

612. - - - Anomalous Sound Reception Experiments, April 1944- April 1945. Meteorol. Res. Pap., London, No. 611, 1951.

613. - - - Wind and Temperature to 50 Km over England. Geophysical Memoirs, Vol. 12, No. 95, 1955.

614 - - - Winds and Temperatures Between 20 Km and 100 Km. A Review. Quart. J. roy. meteorol. soc., Vol. 83, 1957.

615. Murgatroyd, R. J. and Clews, C. J. B. Wind at 100,000 ft. over Southeast England. Geophys. mem., Vol. 10, No. 83, 1949.

616. Murgatroyd, R. J., Goldsmith, P. and Hollings, W. E. H. Some Recent Measurements of Humidity from Aircraft up to Heights of about 50,000 ft over Southern England. Quart. J. Roy. Meteorol. Soc., Vol. 81. No. 350, 1955.

617. Murgatroyd, R. J. and Goody, R. M. Sources and Sinks of Radiative Energy from 30 to 90 Km. Quart. J. Roy. Meteorol. Soc., Vol. 85, 1958.

618. Murgatroyd, R. J. and Singleton, F. Possible Meridional Circulations in the Stratosphere and Mesosphere. Quart. J. Roy. Meteorol. Soc., Vol. 87, No. 372, 1961.

619. Nagata, T. and Kaneda, E. A Photoelectric Analyzer of all Sky Cameras Auroral Photographs. J. Geophys. Res., Vol. 66, No. 7, 1961.

620. Neufeld, E. L. A Fourier Analysis of Winds in the Lower E-Region. Astronomical Contributions of the University of Manchester, Ser. I, Vol. 1, No. 6, 1960.

621. Neumann, J. Fluctuations of Long-Period Accumulations of Daily Rainfall Amounts. Austral. J. Phys., Vol. 7, No. 3, 1954.

622. Newell, H. E. A Review of Upper Atmosphere Research from Rockets. Trans. Amer. Geophys. Union, Vol. 31, (1), 1950.

623. - - - High Altitude Rocket Research, 298 p., Academic Press, Inc., New York, 1953.

624. - - - Rockets and the Upper Atmosphere. Scientific Monthly, Vol. 78, No. 1, 1954.

625. - - - Rockets Data on Atmospheric Pressure, Temperature, Density and Winds. Ann. Geophys., Vol. 2, No. 2, 1955.

626. - - - (Compil.) Sounding Rockets. New York-Toronto-London, McGraw-Hill Book Co., Inc., VIII, 1959.

627. Nicolet, M. Ozone and its Relation to the Atmospheric Situation (L'ozone et ses relations avec la situation atmosphérique). Institut Royal Météorologique de Belgique, Misc., 19, 1945.

628. - - - Dynamics of the Upper Atmosphere. In "The Earth as a Planet" (Kuiper, G., Ed.), Univ. of Chicago Press, 1954.

629. - - - The Aeronomic Problem of Oxygen Dissociation. J. Atmos. and Terr. Phys., Vol. 5, 1954.

630. - - - Helium in the Terrestrial Atmosphere (L'hélium dans l'atmosphère terrestre). Bulletin des classes de Sciences. Académie Royal de Belgique, Vol. 42, No. 9, 1956.

631. - - - The Aeronomic Problem of Helium. Ann. Geophys., Vol. 13, No. 1, 1957.

632. - - - Temperature at the Boundary of the Thermosphere (Température à la limite de la thermosphere. Bull. cl. sci. Acad. roy. Belgique, Vol. 43, No. 10, 1957.

633. - - - Dissociation of Oxygen in the Upper Atmosphere (La dissociation de l'oxygène dans la haute atmosphère). Arch. Meteorol. Geophys. und Bioklimatol., A 10, No. 4, 1958.

634. - - - Atomic Nitrogen in the Thermosphere. J. Scient. and Industr. Res., A 17, No. 12, Suppl. 36, 1958.

635. - - - High Atmosphere Densities. Science, Vol. 127, No. 3310, 1958.

636. - - - The Thermosphere (La thermosphere). Ann. de Geophys., Vol. 15, No. 1, 1959.

637. - - - Aeronomy (Preprint: will be Published in the Handbuch der-Physik, Geophysik, Band 49. Springer Verlag, Berlin), 1962.

638. Nicolet, M. and Mange, P. The Dissociation of Oxygen in the High Atmosphere. J. Geophys. Res., Vol. 59, No. 1, 1954.

639. Nordberg, W. and Stroud, W. G. Results of IGY Rocket Grenade Experiments to Measure Temperatures and Winds above the Island of Guam. J. Geophys. Res., Vol. 66, No. 2, 1961.

640. Ogawa, T., Ando, S. and Yoshida, A. Vertical Incident Doppler Ionogram. Proc. IRE, Vol. 49, No. 3, 1961.

641. Ohring, G. The Radiation Budjet of the Stratosphere. J. Meteorol., Vol. 15, 1958.

642. Oliver, M. B. and Oliver, V. J. Rainfall and Stardust. Bull. Am. Meteorol. Soc., Vol. 36, No. 4, 1955.

643. Opik, E. J. Meteors and the Upper Atmosphere. Irish Astronomical Journal, No. 6, 1955.

644. - - - Artificial Satellites. Irish Astron. J., Vol. 4 Nos. 7 and 8, 1957.

645. - - - Physics of Meteor Flight in the Atmosphere. New York-London Interscience, VIII, 1958.

646. Otterman, J., Sattinger, I. J. and Smith, D. F. Analysis of a Falling-Sphere Experiment for Measurement of Upper Atmosphere Density and Wind Velocity. J. Geophys. Res., Vol. 66, No. 3, 1961.

647. Paetzold, H. K. Optical Phenomena During a Lunar Eclipse (Die optischen Erscheinungen bei einer Mondfinsternis). Zeitschrift fur Astrophysik, Vol. 30, 1952.

648. - - - Visual Boundary of the Shadow of the Earth During Lunar Eclipses (Über die visuelle Erdschattengrenze bei Mondfinsternissen). Z. Astrophys. Vol. 32, No. 4, 1953.

649. - - - Vertical Distribution of Atmospheric Ozone According to the Photochemical Equilibrium (Die vertikale Verteilung des atmospharischen Ozons nach dem photochemischen Gleichgewicht). Geofisica pura e appl., Vol. 24, 1953.

650. - - - Ozone Layer and Air Movements in the Stratosphere (Ozonschicht und Luftbewegungen in der Stratosphare). Naturwissenschaften, Vol. 41, No. 14, 1954.

650a. Paetzold, H. K. and Zschorner, H. Optical Temperature Measurements of Atmospheric Ozone (Zur optischen Temperatur-messung des atmospharischen ozons). Meteorol. Rundschau, Nos. 5 and 6, 1955.

651. Paetzold, H. K. Some Results from Observations of the First Russian Earth Satellites (Einige Ergebnisse aus den Beobachtungen der ersten russischen Erdsatelliten). Raketentechn. u. Raumfahrtforsch., Vol. 2, No. 2, 1958.

652. - - - The Highest Earth Atmosphere According to Satellite Measurements (Die oberste Erdatmosphare nach Satelliten-Messungen). Naturwissenschaften, Vol. 46, No. 13, 1959.

653. - - - The Fluctuations of the Acceleration of Satellites. J. Atmos. and Terr. Phys., Vol. 16, Nos. 3 and 4, 1959.

654. - - - Vertical Atmospheric Ozone Distributions. Ozone Chemistry and Technology, Washington, D. C., American Chemical Society, 1959.

655. - - - Density and Structure of the Highest Atmosphere (Dichte und Struktur der hochsten Atmosphare). Schweizerische Mech. Zeitschrift, Vol. 31, No. 17, 1960.

656. - - - Yearly Variation of Density of the Highest Earth Atmosphere (Über eine jährliche Variation der Dichte der hochsten Erdatmosphare). Zeitschrift für Naturforschung, 16a, No. 1, 1961.

657. - - - A Preliminary Model for the Variations of Upper Air Densities. Nature, (Engl.), Vol. 190, No. 4770, 1961.

658. Paetzold, H. K. and Piscalar, F. Meridional Ozone Distribution and Stratospheric Circulation (Meridionale Ozonverteilung und stratospharische Zirkulation). Naturwiss., Vol. 48, No. 13, 1961.

659. Paetzold, H. K. and Zschorner, H. An Annual and a Semiannual Variation of the Upper Air Density. Geofis. pura e appl., Vol. 48, No. 1, 1961.

660. Paneth, F. A. Chemical Exploration of the Stratosphere. Nature, Vol. 139, 1937.

661. - - - The Chemical Exploration of the Stratosphere. Journal of the Chemical Society, 1952.

662. - - - The Chemical Exploration of the Stratosphere. Bull. Soc. Chim. France, Vol. 20, 1952.

663. - - - Microanalysis of the Inert Gases. Endeavor, Vol. 12, 1953.

664. - - - The Chemical Exploration of the Stratosphere. Proceedings of the Royal Institute of Great Britain, Vol. 35, No. 4, 1955.

665. Paneth, F. A., Chackett, K. F., Reasbeck, P. and Wiborg, B. S. Variations in the Chemical Composition of Stratospheric Air. Nature, Vol. 168, 1951.

666. Pant, P. S. Circulation in the Upper Atmosphere. Scientific Report No. 1: Contract No. AF19 (604)-1006, New York University, May, 1955.

667. - - - Circulation in the Upper Atmosphere. J. Geophys. Res., Vol. 61, No. 3, 1956.

668. Parkin, D. W. and Hunten, W. Cosmic Dust in the Atmosphere. Nature (Engl.), Vol. 183, No. 4663, 1959.

669. Parkyn, D. G. Atmospheric Tides and Earth Satellite Observations. Nature (Engl.), Vol. 183, No. 4667, 1959.

670. Paton, J. Luminous Night Clouds. Meteorol. Mag., Vol. 79, No. 933, 1950.

671. - - - Direct Evidence of Vertical Motion in the Atmosphere at Height of about 80 Km. Provided by Photographs of Noctilucent Clouds. Proceedings of Toronto Meteorological Conference, Roy. Meteorol. Soc., Vol. 31, 1954.

672. Pava, R. Contributions to the Investigation of Atmospheric Tides (Beiträge zur Forschung der atmospharischen Gezeiten). Acta agron. Acad. sci. hung, Vol. 5, Nos. 1 and 2, 1955.

673. Pekeris, C. L. Atmospheric Oscillations. Proc. Roy. Soc., A158, No. 895, 1937.

673a. Petit, M. Notes on Thermometers with Vibrating Wire for Stratospheric Soundings (Notes sur les thermomètres à fil vibrant pour sondages stratospheriques). Journal de mécanique et de physique de l'atmosphère, Vol. 1, No. 4, 1959.

674. Phillips, J. G. The Determination of the Widths of the Airglow and Twilight Flash. The Airglow and the Aurorae. Suppl. J. Atmos. and Terr. Phys., Vol. 5, 1956.

675. Phillips, H. Determination of Density in the Upper Atmosphere by Observations of Artificial Satellites (Bestimmung der Dichte in der hohen Atmosphäre mittels Beobachtungen an künstlichen Erdsatelliten).

Abhandlungen des Meteorologischen und hydrologischen Dienstes, DDR, Vol. 8, No. 55, 1960.

676. Planetary Atmospheres and Convection in Rotating Fluids. A Symposium held jointly by the Roy. Meteorol. Soc. and Roy. Astron. Soc., Burlington House, 1957, May 23 and 24. Observatory, Vol. 77, No. 900, 1957.

677. Plass, G. N. The Influence of the 9.6μ Ozone Band on the Atmospheric Infrared Cooling Rate. Quart. J. Roy. Meteorol. Soc., Vol. 82, 1956.

678. - - - The Influence of the 15μ Carbondioxide Band on the Atmospheric Infrared Cooling Rate. Quart. J. Roy. Meteorol. Soc., Vol. 82, 1956.

679. Poloskov, S. M. and Mirtov, B. A. The Study of the Upper Atmosphere by Means of Rockets, at the Academy of Sciences USSR. Journal of the British Interplanetary Society, Vol. 16, No. 2, 1957.

680. Pressman, J. Seasonal and Latitudinal Temperature Changes in the Ozonosphere. J. Meteorol., Vol. 12, No. 1, 1955.

681. Pressman, J. and Marmo, F. F. Measurement of Air Density at 430 Km by Sodium Resonance Cloud Techniques. ARS Journal, Vol. 31, No. 6, 1961.

682. Price, R. E. Travelling Disturbances in the Ionosphere. Nature, Vol. 172, No. 4368, 1953.

683. Rao, M. S. and Rao, B. R. Analysis of Fading Records from Four Spaced Receivers for Ionospheric Wind Measurements. J. Atmos. and Terr. Phys., Vol. 10, Nos. 5 and 6, 1957.

684. Rao, B. R. and Murty, D. A New Continuous Wave Radio Method for the Study of Ionospheric Drifts. J. Scient. and Industr. Res., A17, No. 12, 1958.

685. Rao, B. R and Rao, E. B. Effect of Enhanced Solar Activity of the F2 Region Drifts at Waltair. J. Scient. and Industr. Res., A17, No. 12, 1958.

686. Rao, B. R. and Bhagiratha E. Rao. Study of Horizontal Drifts in the F1-F2-Regions of the Ionosphere at Waltair. J. Atmos. and Terr. Phys., Vol. 14, 1959.

687. Rao, B. R., Rao, E. B. and Murty, Y. V. Ramana. Effect of Magnetic Activity on Drifts of the F2-Region. Nature (Engl.), Vol. 183, No. 4662, 1959.

688. Rao, B. R. and Rao, R. R. A New Type of Ionospheric Drift Recorder. J. Atmos. and Terr. Phys., Vol. 21, Nos. 2 and 3, 1961.

689. Rao, B. R. and Ramana, K. V. V. Variation in Height of Anisotropy and Random Drift Velocity of the Irregularities in the Ionosphere. Nature (Engl.), Vol. 190, No. 4777, 1961.

690. Ratcliffe, J. A. Diffraction from the Ionosphere and the Fading of Radios Waves. Nature, Vol. 162, 1948.

691. Ratcliffe, J. A., Robbins, A. R. and Thomas, J. O. Movements in the Quiet F-Layer over Slough. J. Atmos. and Terr. Phys., Vol. 15, Nos. 1 and 2, 1959.

692. Rawer, K. Irregularities and Movements in the F-Region. J. Atmos. and Terr. Phys., Vol. 15, Nos. 1 and 2, 1959.

693. - - - Drift in the E-Region. J. Atmos. and Terr. Phys., Vol. 15, No. 1, 1959.

694. Reed, R. J., Campbell, W. J., Rasmussen. L. A. and Rogers, D. G. Evidence of a Downward-Propagating, Annual Wind Reversal in the Equatorial Stratosphere. J. Geophys. Res., Vol. 66, No. 3, 1961.

695. Rense, W. A. Solar Ultraviolet Spectroscopy and Applications to Problems of the Upper Atmosphere and the Solar Corona. Space Research. Amsterdam, 1960.

696. Reeger, E. Atmospheric Aerosol. A Review (Das atmospharische Aerosol. Ein Überblick). Acta physica Austriaca, Vol. 13, Nos. 2 and 3, 1960.

697. Regener, E. Ozone Layer and Atmospheric Turbulence (Ozonschicht und atmospharische Turbuletz). Forschungs- und Erfahrungsberichte des Reichswetterdienstes, A,No. 9 (Berlin), 1941; Berichte des Deutschen Wetterdienstes in der US-Zone, "Ozone", No. 11, 1949.

698. Regula, H. Temperatures and Winds in the Ozone Layer at the Time of the Oldebroek Explosion (Temperaturen und Winde in der Ozonschicht zur Zeit der Oldebroek-sprengung). Meteorol. Rundschau, Nos. 3 and 4, 1954.

699. Reisig, Gerhard, H. R. Instantaneous and Continuous Wind Measurements up to the Higher Stratosphere. J. Meteorol., Vol. 13, No. 5, 1956.

700. Renger, F. and Lucke, O. Meteorological Conditions of Ozone Density in Air at Groundlevel (Uber die meteorologischen Bedingungen der Ozondichte in bodennaher Luft). Abh. Meteorol and Hydrol. Dienst. DDR, Vol. 2, No. 13, 1953.

701. Richardson, J. M. and Kennedy, W. B. Atmospheric Winds and Temperatures to 50-Kilometers as Determined by Acoustical Propagation Studies. J. Acoust. Soc. Am., Vol. 24, 1952.

702. Rinegar, J., Allen, W. and White, W. Phenomena Associated with the Flight of Ultra-Speed Pellets. J. Appl. Phys., Vol. 23, No. 3, 1952.

703. Roach, F. E., Williams, D. R. and Pettit, H. Diurnal Variation of (01) 5577 in the Nightglow. Astrophys. J., Vol. 117, No. 3, 1953; J. Geophys. Res., Vol. 58, No. 1, 1953.

704. Roach, F. E., Tandberg-Hansen, E. and Megill, L. R. Movements of Airglow Cells. J. Atmos. and Terr. Phys., Vol. 13, 1958.

705. Robley, R. Multiple Scattering in the Atmosphere Inferred from Twilight Observations (La diffusion multiple dans l'atmosphere déduite des observations crepusculaires). Ann. de Geophysique, Vol. 6, No. 3, 1950.

706. Rocket Exploration of the Upper Atmosphere. Ed. Massey Harry, Stewart Wilson. Pergamon Press, London, 1954.

707. Rocket Panel. Pressures, Densities and Temperatures in the Upper Atmosphere. Phys. Rev., Vol. 88, 1952.

708. Roesler, F. L., Fan, C. Y. and Chamberlain, F. W. Interpretation of Rotational Temperatures of Auroral N_2^+ Bands. I. Proton Impact at Intermediate Energye. J. Atmos. and Terr. Phys., Vol. 12, 1958.

709. Royal Meteorological Society. Colloquium on the Upper Atmosphere. Edinburgh, July, 16, 1954. Meteorol. Mag., Vol. 83, No. 989, 1954.

710. - - - Measurement of Humidity at High Altitudes. Meteorol. Mag., Vol. 85, 1956.

711. - - - Measurement of Water in the Stratosphere (Discussion Meeting, Feb. 15, 1956). Quart. J. Roy. Meteorol. Soc., 82, Nos. 353 and 355, 1956.

712. Sato, T. Studies on the Twilight by the Scattering. The Science Reports of the Tohoku Univ., Ser. 5, 1951, Vol. 3, No. 3; Meteorol. Soc. of Japan, Vol. 30 (1), 1952.

713. Sawada, R. The Atmospheric Lunar Tides. Meteorol. Papers New York: Univ. Press, 2, No. 3, 1954; On the Role of Thermal Excitation in the Atmospheric Tides. Tyuo Kiseday Obun Ikho, Geophys. Mag., Vol. 26, 1955; The Atmospheric Lunar Tides and the Temperature Profile in the Upper Atmosphere. Tyuo Kiseday Obun Ikho, Geophys. Mag., Vol. 27, No. 2, 1956.

714. Sawada, R. and Haurwitz, B. The Lunar Air Tides. Ann Geophys., Vol. 11, No. 2, 1955.

715. Schiff, H. I. Rocket Experiments to Determine the Composition of the Upper Atmosphere. Chemistry in Canada, Vol. 11, No. 2, 1959.

716. Schilling, G. F. and Sterne, T. E. Density and Temperatures of the Upper Atmosphere Inferred from Satellite Observations. J. Geophys. Res., Vol. 64, No. 1, 1959.

717. Schindler, G. Lucent Night Clouds on June 30, 1953. (Leuchtende Nachtwolken am 30 Juni 1953). Annalen der Meteorologie, Vol. 6, Nos. 3 and 4, 1953/54.

718. Schmidt, Ad. Mathematical Contribution to the General Theory of Terrestrial Magnetism (Mathematische Entwicklungen zur allgemeinen Theorie des Erdmagnetismus). Hamburg. Aus d. Ach. Seewarte, Vol. 12, 1889.

719. Schuster, A. The Diurnal Variation of Terrestrial Magnetism. Phil. Trans. Roy. Soc. (London), Ser. A, No. 180, 1889.

720. Schroer, E. Theory of Origin Disintegration and Distribution of Atmospheric Ozone. (Theorie der Entstehung, Zersetzung und Verteilung des atmospharischen Ozons). Ber. Deutsch. Wetterdienst US-Zone, No. 11, 1949.

721. Scorer, R. S. Air Motion in the Upper Atmosphere. Nature, Vol. 172, No. 4369, 1953.

722. Scrase, F. J. Radiosonde and Radar Wind Measurements in the Stratosphere Over the British Isles. Quart. J. Roy. Meteorol. Soc., Vol. 77, No. 3, 1951.

723. - - - Turbulence in the Upper Air as Shown by Radar-Wind and Radiosonde Measurements. Quart. J. Roy. Meteorol. Soc., Vol. 80, No. 345, 1954; Vol. 81, No. 347, 1955.

724. Scrimger, J. A. and Hunten, D. M. Observation of Atmospheric Sodium in Absorption. Nature, Vol. 178, No. 4536, 1956.

725. Sheppard, P. A. The Exploration of the Upper Atmosphere. Science Progress (London), Vol. 37, 1949.

726. Sicinski, H. S., Spencer, N. W. and Dow, W. G. Rocket Measurements of Upper Atmosphere Ambient Temperature and Pressure in the 30 to 75 Kilometer Region. J. Appl. Phys., Vol. 25, No. 2, 1954.

727. Siebert, M. Solar Tides on the Barogram of July 1959. (Die solaren Gezeiten im Barogramm des Juli 1959). J. Geophys., Vol. 25, No. 2, 1959.

728. Simpson, G. C. The Twelve-Hourly Barometer Oscillation. Quart. J. Roy. Met. Soc., 44, 1918.

729. Siry, J. W. Satellite Orbits and Atmospheric Densities at Altitudes up to 750 Kilometers Obtained from the Vanguard Orbit Determination Program. Trans. Internat. Astron. Union, 10, 1958 (1960).

730. Skinner, N. J., Hope, J. and Wright, R. W. Horizontal Drift Measurements in the Ionosphere Near the Equator. Nature, No. 4646, 1958.

731. Slater, A. E. Turbulence Above the Ozone Layer. J. Brit. Interplanet. Soc., Vol. 15, No. 1, 1956.

732. Smith, H. The Physical Theory of Meteors. V. The Masses of Meteor-Flare Fragments. Astrophys. J., 119, 1954.

733. Smith, L. B. The Measurement of Wind Between 100,000 and 300,000 ft by use of Chaff Rockets. J. Meteorol., Vol. 17, No. 3, 1960.

733a. Smith, J. W. and Vaughan, W. W. High Altitude Wind Observations above Cape Canaveral. Aerospace Engineering, Vol. 20, Nos. 10, 16 and 17, 1961.

734. Sounding Rockets. New York-Toronto-London, McGraw-Hill Book Co., 1959.

735. Spencer, N. W., Schulte, H. F. and Sicinski, H. S. Rocket Instrumentations for Reliable Upper Atmosphere Temperature Determination. Proc. IRE, Vol. 42, No. 7, 1954.

736. Spencer, N. W, Boggess, R. L., Lagow, H. E. and Horowitz, R. On the Use of Ionization Gage Devices at Very High Altitude. ARS Journal, Vol. 29, No. 4, 1959.

737. Sprenger, K. Measurements of Ionospheric Drift in the Area of Longwaves as Contribution to the Problem of General Circulation of the Upper Atmosphere (Ionospharendriftmessungen im Langwellenbereich als Beitrag zum Problem der allgemeinen Zirkulation der Hochatmosphare). Z. Meteorol., Vol. 12, No. 7, 1958.

738. Sterne, T. E. High-Altitude Atmospheric Density. Physics of Fluids, Vol. 1, No. 3, 1958.

739. - - - The Density of the Upper Atmosphere. Spec. Rept. Astrophys. Observ. Smithsonian Inst., No. 11, 1958.

740. Starr, V. P. Questions Concerning the Energy of Stratospheric Motions. Arch. Meteorol., Geophys. und Bioklimatol., A12, No. 1, 1960.

741. Sterne, T. E. The Effect of the Rotation of a Planetary Atmosphere upon the Orbit of a Cloud Satellite. Astron. J., Vol. 64, No. 1267, 1959.

742. Sterne, T. E. and Schilling, G. F. Some Preliminary Values of Upper Atmosphere Density from Observations of USSR Satellites. Smithsonian Contribs. Astrophys., Vol. 2, No. 10, 1958.

743. Stewart, K. H. Air Waves from a Volcanic Explosion. Meteorol. Mag., Vol. 88, No. 1039, 1959.

744. Stoffregen, W. The East-West Drift of Auroral Forms Determined from All-Sky Camera Films. J. Atmos. and Terr. Phys., Vol. 21, No. 4, 1961.

745. Stolov, H. L. Tidal Wind Fields in the Atmosphere. J. Meteorol., Vol. 12, No. 4, 1955.

746. Stone, A. H. On Supersonic Flow Past a Slightly Yawing Cone. J. Mathematical Physics, Vol. 27, 1948; Vol. 30, 1952.

747. Stormer, C. Height and Velocity of Luminous Night Clouds Observed in Norway 1932. Univ. Observatory, Oslo, publication, No. 6, 1933; Measurements of Luminous Nightclouds in Norway 1933 and 1934. Astrophysica Norwegia, Vol. 1, No. 3, 1935.

748. - - - Mother-of-Pearl Clouds. Weather, 3, 1948.

749. Stroud, W. G., Terhune, E. A., Venner, J. H., Walsh, J. R. and Weiland, S. Instrumentation of the Rocket Grenade Experiment for Measuring Atmospheric Temperatures and Winds. Rev. of Scient. Instr., Vol. 26, No. 5, 1955.

750. Stroud, W. G. Meteorological Rocket Soundings in the Arctic. American Rocket Society, Preprints, No. 637, 1958; Jet Propulsion, Vol. 28, No. 12, 1958.

751. Stroud, W. G., Nordberg, W. and Walsh, J. R. Atmospheric Temperatures and Winds Between 30 and 80 Km. J. Geophys. Res., Vol. 61, No. 1, 1956.

752. Stroud, W. G., Nordberg, W., Bandeen, W. R., Bartman, F. L. and Titus, P. Rocket Grenade Observation of Atmospheric Heating in the Arctic. J. Geophys. Res., Vol. 64, No. 9, 1959.

753. - - - Rocket Grenade Measurements of Temperatures and Winds in the Mesosphere over Churchill, Canada. IAS Paper, No. 47, 1960.

754. Synge, E. H. A Method of Investigating the Higher Atmosphere. Phil. Mag., Vol. 9, 1930.

755. Swestka, Z. The Problem of a Meteoritic Dust Layer in the Earth Atmosphere. Byull. Astron. In-tov Chekhoslovakii, Vol. 5, No. 5, 1954.

756. Swinbank, W. C. Comments on a Paper by E. G. Bowen Entitled. The Influence of Meteoritic Dust on Rainfall. Austral. J. Phys., Vol. 7, No. 2, 1954.

757. Taylor, G. I. and Maccoll, J. W. The Air Pressure on a Cone Moving at High Speeds. Proc. Roy. Soc. (London), 139A, No. 2, 1933; Maccoll, J. W., Proc. Roy. Soc. (London), 159A, 1937.

758. Taylor, H. A. and Brinton, H. C. Atmospheric Ion Composition Measured above Wallops Island, Virginia. J. Geophys. Res., Vol. 66, No. 8, 1961.

759. Teweles, S. Meteorological Analysis of Churchill Rocket Sounding Data. ARS Journal, Vol. 31, No. 6, 1961.

760. - - - Time Section and Hodograph Analysis of Churchill Rocket and Radiosonde Winds and Temperatures. Monthly Weather Review, Vol. 89, No. 4, 1961.

761. The Eruption of Krakatoa. Report of the Krakatoa Committee of the Royal Society, 1888.

762. The Upper Atmosphere. Nature, Vol. 174, No. 4425, 1954.

763. Thomas, L. Some Measurements of Horizontal Movement in Region-F2 using Widely Spaced Stations. J. Atmos. and Terr. Phys., Vol. 14, 1959.

764. Thrane, P. The Filt of a 12 Hourly Atmospheric Tidal Wave. Quart. J. Roy. Meteorol. Soc., Vol. 81, No. 347, 1955.

765. Tohmatsk, Takao. The Dynamical Effect on the Intensity of Nightglow 5577. Rept. Ionosphere Res. Japan, No. 3, 1958.

766. Tolefson, H. B. and Henry, R. M. A Method of Obtaining Detailed Wind-Shear Measurements for Application to Dynamic Response Problems of Missile Systems. J. Geophys. Res., Vol. 66, No. 9, 1961.

767. Tónsberg, E., Langlo, K. and (Olsen, K. L.). Investigations on Atmospheric Ozone at Nordlysobservatoriet, Tromso. Geophys. publ., Oslo, Vol. 13, No. 12, 1944.

768. Townsend, A. A. The Structure of Turbulent Shear Flow. Cambridge, University Press, 1956.

769. Townsend, J. W. and Meadows, E. B. Density of the Winter Night Time Arctic Upper Atmosphere 110 to 170 Km. Ann. Geophys., Vol. 14, No. 1, 1958.

770. Townsend, J. W., Meadows, E. B. and Pressly, E. C. Rocket Exploration of the Upper Atmosphere, Edited by Boyd, R. L. F. and Seaton, M. J., Interscience Publishers, Inc., New York, 1954.

771. Tsuda, T. The Motion of Irregularities in the Ionosphere. Report. Ionosphere and Space Res. Japan (formerly Rept. Ionosphere Res Japan), Vol. 13, No. 1, 1959.

772. Tuomikoski, P. Pressure and Molecular Scale Temperature in the Upper Atmosphere. Geophysica, Vol. 7, No. 1, 1959.

773. Tuve, M. A., Johnson, E. A. and Wulf, O. R. A New Experimental Method for Study of the Upper Atmosphere. Terrestrial Magnetism and Atmospheric Electricity, Vol. 40, 1935.

774. Unwin, R. S. Movement of Auroral Echoes and the Magnetic Disturbance Current System. Nature (Engl.), Vol. 183, No. 4667, 1959.

775. Vaisanen A. A Study of the Symmetrical General Circulation by the Aid of a Rotating Water Tank Experiment. Geophysica, Vol. 8, No. 1, 1961.

776. Vanderschmidt, G. F. Using Isotopes to Measure Low Pressures. Electronics, Vol. 32, No. 25, 1959.

777. Vassy, A. Relations Between Atmospheric Ozone and Thunderstorms (Relations entre l'ozone atmospherique et les orages). C. r. Acad. Sci., Vol. 239, No. 20, 1954.

778. - - - Spectroscopic Study of Sodium Projected in the Upper Atmosphere by Rockets (Etude spectroscopique du sodium projete dans la haute atmosphère à l'aide de fusees). Space Research, Amsterdam, 1960.

779. Vassy, E. C. r. Acad. Sci., Vol. 202, No. 1426, 1936.

780. - - - C. r. Acad. Sci., Vol. 214, No. 219, 1942.

781. - - - Interpretation of Danjon's Law (Interpretation de la loi de Danjon). Journal Scientifique et Meteorologique, Vol. 8, No. 29, 1956.

782. Vaucouleurs, G. de. and Jacobs, L. Dust Clouds in the Stratosphere. Meteorol. Mag., Vol. 83, No. 988, 1954.

783. Vaucouleurs, G. de. Total Eclipse of the Moon of July 26, 1953. (L'éclipse totale de lune du 26 juillet 1953). Documents Observations, Paris, Vol. 7, No. 3, 1954.

784. Verniani, F. The Deceleration of Meteors During their Passage through the Earth's Atmosphere. Nuovo cimento, Vol. 14, No. 5, 1959.

785. Veryard, R. G. and Ebdon, R. A. Fluctuations in Tropical Stratospheric Winds. Meteorol. Mag., Vol. 90, No. 1066, 1961.

786. Vestine, E. H. Geomagnetism in Relation to Aeronomy. Ann. Geophys., Vol. 17, No. 2, 1961.

787. Vigroux, E. Atmospheric Ozone (L'ozone atmosphérique). Ciel et Terre, Vol. 77, Nos. 7 and 8, 1961.

788. Wager, J. H. Electronic Equipment for In-Flight Processing of Rocket-borne Mass Spectrometer Data. Journal of Electronics and Control, Vol. 8, No. 3, 1960.

789. Waite, C. S. and Benson, O. O. (Editors). Physics and Medicine of the Upper Atmosphere (A Study of the Aeropause). University of New Mexico Press, Albuquerque, 1952.

790. Wallace, L. Note on Airglow Temperature Determination from OH Spectra. J. Geophys. Res., Vol. 65, No. 3, 1960.

791. Walshaw, C. D. The Accuracy of Determination of the Vertical Distribution of Atmospheric Ozone from Emission Spectrophotometry in the 1.043^{-1} Band at High Resolution. Quart. J. Roy. Meteorol. Soc., Vol. 86, No. 370, 1960.

792. Wan-Cheng Chiu. The Diurnal Temperature Variation of the Lower Stratosphere over the United States. J. Meteorol., Vol. 16, No. 4, 1959.

793. Ward, F. and Shapiro, R. Atmospheric Temperatures and Solar Activity. J. Meteorol., Vol. 18, No. 2, 1961.

794. Wark, D. Q. A Determination of the Linewidth of the λ6,300 of Oxygen in the Twilight Sky. Nature, Vol. 178, No. 4535, 1956.

795. Weeks, K. and Wilkes, M. V. Atmospheric Oscillating and the Resonance Theory. Proc. Roy. Soc., A192, 1947.

796. Wegener, A. Thermodynamics of the Atmosphere (Thermodynamik der Atmosphare). Leipzig, 1928.

797. Weisner, A. G. Measurement of Wind at Elevations of 30 to 80 Kilometers by the Rocket Grenade Experiment. J. Meteorol., Vol. 13, No. 1, 1956.

798. Wells, H. W. Upper Atmospheric Winds, Absorption and other Special Projects in the U. S. Program in Ionospheric Physics. Geophys. and IGY. (Proc. Sympos., Washington, D. C. June 28-29, 1957). Washington, D. C., Amer. Geophys. Union, 1958.

799. Whipple, F. L. The Theory of Micro-Meteorites. Part I: In an Isothermal Atmosphere. Proceedings of the National Academy of Sciences, Vol. 36, No. 12, 1950.

800. - - - The Theory of Micro-Meteorites. Part II: In Heterothermal Atmosphere. Proc. Nat. Acad. Sci., Vol. 37, No. 1, 1951.

801. - - - On Meteor Masses and Densities. Astrophys. J., Vol. 57, No. 1, 1952.

802. - - - Results of Rocket and Meteor Research. Bull. Amer. Meteorol. Soc., Vol. 33, No. 1, 1952.

803. - - - Winds in the Upper Atmosphere by Meteortrain Photography. J. Meteorol., Vol. 10, No. 5, 1953.

804. Whitney, C. A. Atmospheric Conditions at High Altitudes from Satellite Observations. Amer. Rocket. Soc., (Preprints), No. 779, 1959.

805. - - - The Structure of the High Atmosphere I. Linear Models. Spec. Rept. Astrophys. Observ. Smithsonian Inst., Nos. 21, 1 and 12, 1959. II. A Conduction Model. Astrophys. Observ. Smithsonian Inst., Nos. 25, 1 and 6, 1959.

806. - - - Determination of Atmospheric Densities from Satellite Observations. Ann. Geophys., Vol. 17, No. 2, 1961.

807. Wilkes, M. V. Oscillations of the Earth's Atmosphere. Cambridge, Univ. Press, 1949.

808. - - - World-Wide Oscillations in the Earth's Atmosphere. Quart. J. Roy. Meteorol. Soc., Vol. 78, 1952.

809. Wilkins, E. M. Seasonal Variations in Atmospheric Carbon Dioxide Concentration. J. Geophys. Res., Vol. 66, No. 4, 1961.

809a. Witt, G. Noctilucent Cloud Observations. Tellus, Vol. 9, No. 3, 1957.

810. - - - A Note to the Paper by G. Witt, Polarizations of Light from Noctilucent Clouds. Geophys. Res., Vol. 65, No. 7, 1960.

811. - - - Polarization of Light from Noctilucent Clouds. J. Geophys. Res., Vol. 65, No. 3, 1960.

812. Wojciechowski, K. and Reichart, S. Some Remarks on Light Pressure in Atmosphere. Geofis. pura a. appl., Vol. 47, No. 3, 1960.

813. Wright, J. W. Comment on Models of the Ionosphere above h_{max} F_2. J. Geophys. Res., Vol. 65, No. 9, 1960.

814. Yerg, D. G. Ionospheric Wind Systems and Electron Concentrations in the F-Layer. J. Meteorol., Vol. 8, 1951.

815. Yonezawa, T. On the Physical Properties and Composition of the Upper Atmosphere Between 100 and 400 Kilometres above Ground in Middle Latitudes. Journal of Radio Research Laboratories, Vol. 7, No. 30, 1960.

816. Zito, G. V. An Ion Altimeter for Pressure-Altitude Measurements. IRE Internat. Convent. Rec., No. 8, 1960.

817. Frith, R. Meteorological Satellites. Times Sci. Rev., No. 50, 1963.

818. King-Hele, D. G. Variations of Scale Height in the Upper Atmosphere. Nature (Engl.), No. 4823, 1962.

819. - - - Geophysical Measurements in the Upper Atmosphere. Nature (Engl.), No. 4810, 1962.

820. King-Hele, D. G. and Rees, J. M. The Decrease in Upper-Atmosphere Density Between 1957 and 1963, as Revealed by Satellite Orbits. J. Atmos. and Terr. Phys., No. 9, 1963.

821. Khvostikov, I. A., Izakov, M. N., Kokin, G. A., Kurilova, Gu. V. and Livshitz, N. C. Investigation of the Stratosphere by Means of Meteorological Rockets in the USSR. Proceedings of the First International Symposium on Rocket and Satellite Meteorology (Washington, D. C., April 23-25, 1962), Amsterdam, 34-41, 1963.

Translated for the National Aeronautics and Space Administration by John F. Holman and Co. Inc.